

PETROGENESIS OF THE TERTIARY-RECENT VOLCANIC
COMPLEX OF JEBEL MARRA, SUDAN

IAN RICHARD WILSON

Submitted in fulfilment of the requirements
for the degree of Doctor of Philosophy

Department of Earth Sciences
The University of Leeds
November, 1983

**PAGE NUMBERS ARE
CLOSE TO THE EDGE OF
THE PAGE.**

SOME ARE CUT OFF



IMAGING SERVICES NORTH

Boston Spa, Wetherby

West Yorkshire, LS23 7BQ

www.bl.uk

**VOLUME CONTAINS
CLEAR OVERLAYS**

**OVERLAYS HAVE BEEN
SCANNED SEPERATELY
AND THEN AGAIN OVER
THE RELEVANT PAGE**



IMAGING SERVICES NORTH

Boston Spa, Wetherby

West Yorkshire, LS23 7BQ

www.bl.uk

**CONTAINS
PULLOUTS**

Volcanoes can be beautiful, informative, and both beneficial and dangerous. They serve as windows through which we can dimly perceive the interior. (Press and Seiver, 1974).

ABSTRACT

Jebel Marra is a Tertiary-Recent volcanic complex located in the Darfur Province of Western Sudan. The complex is associated with a negative Bouguer anomaly and domal uplift of the metamorphic basement but not with rifting.

The volcanic products chiefly consist of lavas from the alkali olivine-basalt - trachyte/phonolite series although thick sequences of pyroclastic rocks are also present. Field mapping and photo-interpretation has enabled the suite to be divided into an Old Series and a New Series of rocks.

Trace element and Nd-Sr isotopic compositions of primitive basalts from Jebel Marra are sufficiently similar to alkali basalts from ocean islands and other continental provinces to suggest that the mantle source is chemically and isotopically similar and probably sub-lithospheric. Isotopic and trace element data for the primitive basalts are consistent with their derivation from a mantle source which has either been recently metasomatised by a LILE and LREE enriched fluid or by melting of a depleted source in which highly incompatible elements are fractionated from slightly less incompatible elements.

In general, there is a good correlation between decreasing $^{143}\text{Nd}/^{144}\text{Nd}$, increasing $^{87}\text{Sr}/^{86}\text{Sr}$ and increasing fractionation indices. This indicates that contamination and fractionation are coupled (AFC). The New Series basic rocks trend towards a low $^{143}\text{Nd}/^{144}\text{Nd}$ and relatively low $^{87}\text{Sr}/^{86}\text{Sr}$ contaminant which is characteristic of lower crustal granulite facies rocks. Examination of

$^{143}\text{Nd}/^{144}\text{Nd}$ vs. incompatible elements and $^{143}\text{Nd}/^{144}\text{Nd}$ vs $^{87}\text{Sr}/^{86}\text{Sr}$

indicates that the processes of AFC have given rise to two groups of rocks. These two groups are the result of AFC processes in which the ratio of the rate of assimilation to the rate of fractional crystallisation (r) is different. The New Series rocks and some Old Series rocks comprise a group in which r is high. Some Old Series rocks including rocks from the Pyroclastic Sequence comprise a group in which r is low.

A granulite facies contaminant and high r value of the former trend is compatible with contamination in the lower crust. Kinked trends on $^{143}\text{Nd}/^{144}\text{Nd}$ vs incompatible elements plots may indicate that a decrease in r occurred between basic and acidic rocks which may be evidence for a change in contamination environment to the upper crust at this stage.

Other factors such as a heterogeneous mantle, variable degrees of partial melting or other contamination mechanisms have undoubtedly contributed to some of the variation and scatter of the elemental and isotopic data but their effects have been overshadowed by processes of AFC.

CONTENTS

	<u>Page</u>
TITLE PAGE	i
ABSTRACT	iii
CONTENTS	vii
LIST OF PLATES	viii
LIST OF TABLES	ix
LIST OF FIGURES... ..	xii
ABBREVIATIONS	ixv
ACKNOWLEDGEMENTS..	
CHAPTER ONE : INTRODUCTION	2
1.1 Regional Setting.	2
1.2 Field Work and Sampling	2
1.3 Previous Work	4
1.4 Aims... ..	4
1.5 Geophysical/Tectonic Setting	7
1.6 Conventions	11
CHAPTER TWO : PRE-VOLCANIC ROCKS	12
2.1 Introduction	12
2.2 Basement Rocks... ..	14
2.2.1 Granitic Gneisses... ..	14
2.2.2 Pelitic Schists	14
2.2.3 Amphibolites	15
2.2.4 Quartzites	15
2.3 Granite Intrusions	15
2.4 Quartz Veins and Pegmatites	16
2.5 "Dykes"	16
2.6 Sedimentary Cover	16
2.7 Age	16
2.8 Structure	18
2.9 Domal Uplift	20
2.10 Post-Orogenic Structures... ..	20
2.11 Geochemistry of the Crust..	22
2.12 Conclusions	26
CHAPTER THREE : VOLCANICS	28
3.1 Introduction	28
3.2 Topography and Exposure	30
3.3 Geological History	31
3.3.1 Old Series	31
3.3.1.1 Extrusive and Intrusive Rocks	31
3.3.1.2 Pyroclastic Sequence	34
3.3.2 New Series Rocks	40
3.4 Lithologies	44
3.4.1 Old Series Extrusive and Intrusive Rocks	44
3.4.2 Pyroclastics	46
3.4.3 New Series	47
3.5 Conclusions	48

Contents (Continued)

	<u>Page</u>
CHAPTER FOUR : PETROGRAPHY	50
4.1 Introduction ...	50
4.2 Petrography ...	50
4.2.1 Basalts...	50
4.2.2 Hawaiites.	52
4.2.3 Mugearites	54
4.2.4 Megacrysts	54
4.2.5 Trachytes	54
4.2.6 Phonolites	57
4.2.7 Ignimbrites	59
4.3 Conclusions ...	61
 CHAPTER FIVE : MINERAL CHEMISTRY	 64
5.1 Introduction ...	64
5.2 Olivine ...	64
5.3 Clinopyroxene ...	64
5.4 Plagioclase ...	68
5.5 Potassium Feldspar	71
5.6 Opaque Minerals..	71
5.7 Accessory Phases	73
5.8 Nodules ...	74
5.9 Conclusions ...	74
 CHAPTER SIX : MAJOR ELEMENTS	 75
6.1 Introduction ...	75
6.2 Classification...	75
6.3 'Silica Gap' ...	77
6.4 Overall Variations	78
6.4.1 General Considerations	90
6.5 Temporal Variations	91
6.5.1 Basic Rocks	91
6.5.2 Acidic Rocks	96
6.6 Interpretation..	97
6.7 Conclusions ...	100
 CHAPTER SEVEN : TRACE ELEMENTS	 102
7.1 Introduction ...	102
7.2 Definitions ...	102
7.2.2 Distribution Coefficient (Kd)	102
7.2.3 Bulk Distribution Coefficient (D)	103
7.2.4 Classification ...	103
7.3 Overall Variations	104
7.3.1 Introduction	104
7.3.2 Scatter	104
7.3.3 'Incompatible' Elements	117
7.3.4 'Compatible' Elements	117
7.3.5 'Incompatible/Compatible' Elements	124
7.3.6 Interpretation ...	124

Contents (Continued)				<u>Page</u>
7.4	Temporal Variations	133
	7.4.1 Basic Rocks	133
	7.4.2 Acidic Rocks...	133
7.5	Rare Earth Elements (REE's)	139
	7.5.1 General Features	141
	7.5.2 New Series Variations	141
	7.5.3 Old Series Variations	147
7.6	Discussion and Conclusions	153
CHAPTER EIGHT : ISOTOPIC EVIDENCE				156
8.1	Introduction	156
8.2	Mantle Heterogeneity.	159
8.3	Variation	162
	8.3.1 $^{87}\text{Nd}/^{144}\text{Nd}$ vs $^{87}\text{Sr}/^{86}\text{Sr}$	162
	8.3.2 $^{143}\text{Sr}/^{86}\text{Sr}$ vs Major and Trace Elements	163
	8.3.3 $^{143}\text{Nd}/^{144}\text{Nd}$ vs Trace Elements	170
8.4	Crustal Contamination	170
	8.4.1 End-Members	178
	8.4.2 Simple Mixing (Bulk Assimilation)..	184
	8.4.3 Qualitative Assessment of Simple Mixing	185
	8.4.4 Combined Assimilation and Fractional Crystallisation (AFC)	188
	8.4.5 AFC Parameters	189
	8.4.6 Qualitative Assessment of AFC	190
	8.4.7 Selective Contamination..	196
	8.4.8 Assimilation of Crustal Partial Melts	197
8.5	Sources for Alkali Basalts	199
8.6	Discussion and Conclusions	206
CHAPTER NINE : MODELLING				209
9.1	Introduction	210
9.2	Least-Squares Modelling on Major Elements	211
	9.2.1 Method	211
	9.2.2 Results	213
	9.2.3 Assessment of Least-Squares Results	220
9.3	Trace Element Modelling	221
	9.3.1 Introduction	221
	9.3.2 Results	226
	9.3.3 Deviations from the Fractional ... Crystallisation Model	228
	9.3.4 Fractionation versus Enrichment/ Depletion Diagram	229
	9.3.5 Rare Earth Modelling	231
	9.3.6 Normalised Trace Element Diagrams..	237
	9.3.7 Behaviour of Zr	242
9.4	Crustal Contamination	244
9.5	Simple Mixing (Bulk Assimilation)	245
	9.5.1 Simple Mixing Results	248
	9.5.1.1 New Series	248
	9.5.1.2 Old Series	253

Contents (Continued)

	<u>Page</u>
9.6 Combined Assimilation and Fractionation (AFC)	254
9.6.1 AFC Equations	254
9.6.1.1 Elemental Concentrations	254
9.6.1.2 Isotopic Ratios ...	256
9.6.2 AFC Modelling	257
9.6.3 Application (Determining r)...	264
9.6.3.1 Results	266
9.6.4 $^{143}\text{Nd}/^{144}\text{Nd}$ vs Incompatible Elements	267
9.6.4 $^{143}\text{Nd}/^{144}\text{Nd}$ v $^{87}\text{Sr}/^{86}\text{Sr}$...	271
9.7 Conclusions	274
CHAPTER TEN : CONCLUSIONS	276
REFERENCES	281
APPENDICES	294
A Powder preparation	294
B Electron microprobe	295
C X.R.F. Analysis	305
D Isotopic Analysis	332
E Isotope Dilution	338
F K-Ar dating	347
G Age Corrections to $^{87}\text{Sr}/^{86}\text{Sr}$	348
H Thin-Section Description... ..	350
I Sample locality map	353
J Field number - thin section	354
number equivalence	
K Computer programs used in this thesis	355
L Geological map of southern part of Jebel Marra volcanic complex	Pocket

LIST OF PLATES

Page

CHAPTER THREE

Plate 3.1	Waterfall at Galol...	...	29
Plate 3.2	Trachyte intrusion, J. Koron...	...	29
Plate 3.3	Trachyte intrusion, J. Koron...	...	35
Plate 3.4	Part of Pyroclastic Sequence, near Suni	35
Plate 3.5	Ignimbrites, south from J. Korongtong	39
Plate 3.6	Cinder cones, Torra Tonga	...	39
Plate 3.7	Aerial View of Deriba Caldera..	...	41
Plate 3.8	Trachyte dome at Tereng	...	41

CHAPTER FOUR

Plate 4.1	Primitive basalt	51
Plate 4.2	Less primitive basalt	51
Plate 4.3	Old Series basalt	53
Plate 4.4	Hawaiite	53
Plate 4.5	Mugearite	55
Plate 4.6	Megacryst olivine in basalt	...	55
Plate 4.7	Megacryst plagioclase in basalt	...	56
Plate 4.8	Caldera trachyte	56
Plate 4.9	Mafic bearing trachyte	58
Plate 4.10	Phonolite	58
Plate 4.11	Nepheline bearing phonolite	...	60
Plate 4.12	Ignimbrite	60

LIST OF TABLES

CHAPTER T/0	<u>Page</u>	
Table 2.1	Description and localities of basement samples	22
Table 2.2	Major, trace and isotopic data for basement samples	23
CHAPTER THREE		
Table 3.1	Volcanic/basement contact heights	30
Table 3.2	K-Ar dates for selected samples	32
Table 3.3	Geological History	33
CHAPTER SEVEN		
Table 7.1	Distribution coefficients for transition elements	127
Table 7.2	Geochemical characteristics of acidic rocks	151
CHAPTER EIGHT		
Table 8.1	Geochemical characteristics of end-members	179
CHAPTER NINE		
Table 9.1	Least-squares regression (PETROMIX) results for New Series rocks	216
Table 9.2	Least-squares regression (PETROMIX) results for Old Series rocks	218
Table 9.3	Distribution coefficient data for elements in basic and acidic liquids	223
Table 9.4	Results of trace element modelling using Rayleigh fractionation equation	224
Table 9.5	Results from NLMLAFC	266
APPENDICES		
Table B1	Standards used for calibration of major elements	295
Table B2	Analyses of mineral phases	296
Table C1	Comparison of X.R.F. results with international standards	312
Table C2	Major and trace element analyses of volcanic samples	313
Table D1	$^{87}\text{Sr}/^{86}\text{Sr}$ and $^{143}\text{Nd}/^{144}\text{Nd}$ isotopic data	336
Table E1	Rare earth element analyses	339
Table E2	REE chondrite normalising values of Nakamura (1974)	345
Table E3	Mantle normalising values of Thompson (1982) and Wood (1979)	345
Table E4	Rb and Sr ID data	346
Table G1	Age corrections to $^{87}\text{Sr}/^{86}\text{Sr}$ data	349
Table H1	Thin-section descriptions	351
Table J1	Field-number - thin-section number equivalence	354

LIST OF FIGURES

	<u>Page</u>
CHAPTER ONE	
Figure 1.1 Location map of Jebel Marra in Darfur	1
Figure 1.2 African Cainozoic volcanism	3
Figure 1.3 Area of Jebel Marra studied	5
Figure 1.4 Position of triple junction in Darfur	8
Figure 1.5 Bouguer anomaly map and gravity sections for Jebel Marra region	10
CHAPTER TWO	
Figure 2.1 General geology map of Darfur region	13
Figure 2.2 Structural trends in basement	19
Figure 2.3 Fault trends in basement	21
Figure 2.4 REE patterns for 'lower crustal' rocks	24
Figure 2.5 REE patterns for 'upper crustal' rocks	25
CHAPTER THREE	
Figure 3.1 Sections through Pyroclastic Sequence	36
Figure 3.2 Geology of Deriba caldera	43
CHAPTER FOUR	
Figure 4.1 Modal mineralogy of major and accessory phases throughout the volcanic suite	62
CHAPTER FIVE	
Figure 5.1 MnO vs forsterite content of olivine	65
Figure 5.2 Pyroxene triangle showing pyroxene core and composition	66
Figure 5.3 Al_2O_3 vs Mg number for pyroxene crystals	67
Figure 5.4 Feldspar triangle showing feldspar core and rim compositions	69
Figure 5.5 K_2O vs anorthite content of feldspar	70
Figure 5.6 TiO_2 vs ulvospinel content of titanomagnetite	72
CHAPTER SIX	
Figure 6.1 Alkalis vs silica - classification scheme	76
Figures 6.2a Major elements vs SiO_2	80
-i	
Figures 6.3a CaO , K_2O , Al_2O_3 and P_2O_5 vs MgO	92
-d	
CHAPTER SEVEN	
Figures 7.1 Selected incompatible elements vs SiO_2	107
a-j	
Figures 7.2 Cr, Ni, Sc, Co and Cu vs MgO (basic rocks only)	118
a-e	
Figure 7.2f Zn vs SiO_2	123

List of Figures (Continued)

	<u>Page</u>
Figures 7.3 1-b Sr and Ba vs SiO ₂	126
Figures 7.4 a-d Cr, Sc, Co and Cu vs Ni (basic rocks only)	128
Figure 7.5 CaO vs Nb	134
Figures 7.6 a-b Ba and Sr vs CaO (acidic rocks only)	136
Figure 7.7 Rb vs Nb	138
Figure 7.8 Zr vs Nb	140
Figure 7.9 REE patterns for selected basic rocks	142
Figure 7.10 REE patterns for selected Dariba trachytes	145
Figure 7.11 REE patterns for selected mafic bearing trachytes	148
Figure 7.12 REE patterns for selected Old Series acidic rocks	149
Figure 7.13 REE pattern for 24030	152
 CHAPTER EIGHT	
Figure 8.1a ¹⁴³ Nd/ ¹⁴⁴ Nd vs ⁸⁷ Sr/ ⁸⁶ Sr plot showing isotopic composition of several oceanic and continental primitive basalt provinces	157
Figure 8.1b ¹⁴³ Nd/ ¹⁴⁴ Nd vs ⁸⁷ Sr/ ⁸⁶ Sr plot showing isotopic composition of a variety of mantle nodules	158
Figure 8.2 ¹⁴³ Nd/ ¹⁴⁴ Nd vs ⁸⁷ Sr/ ⁸⁶ Sr plot showing isotopic composition of volcanic suite	161
Figure 8.3 a-c ⁸⁷ Sr/ ⁸⁶ Sr vs SiO ₂ , Zr and Nb	164
Figure 8.4 a-b ⁸⁷ Sr/ ⁸⁶ Sr vs MgO and Sc	167
Figure 8.5 ⁸⁷ Sr/ ⁸⁶ Sr vs Sr	169
Figure 8.7 εNd vs εSr diagram showing isotopic composition of crustal samples	183
Figures 8.8 a-b Simple mixing curves plotted on Nb and Y vs SiO ₂ diagrams	186
Figures 8.9 1-b ¹⁴³ Nd/ ¹⁴⁴ Nd vs Rb and Y (for basic rocks only)	192
Figure 8.10 Spidergrams for Jebel Marra primitive basalt and other continental oceanic provinces	200
Figure 8.11 ¹⁴³ Nd/ ¹⁴⁴ Nd vs ⁸⁷ Sr/ ⁸⁶ Sr for primitive basalts	204
Figure 8.12 Sm/Nd vs Rb/Sr for primitive basalts	205
 CHAPTER NINE : MODELLING	
Figure 9.1 Enrichment/depletion diagram for evolved rocks relative to primitive basalt	230

List of Figures (Continued)

	<u>Page</u>
Figure 9.2 Measured and calculated REE patterns for some basic rocks	232
Figure 9.3 REE patterns for phase calculated from a mugearite liquid and also mugearite and trachyte calculated REE patterns	236
Figure 9.4 Measured and calculated REE patterns for some caldera trachytes	238
Figure 9.5 Spidegrams for primitive basalt, mugearite and lower crust	241
Figure 9.6 Patterns of various rock types normalised to primitive basalt	243
Figure 9.7 Range of hyperbolae for simple mixing	247
Figure 9.8 Simple mixing curves for New and Old Series rocks	249
Figure 9.9 Simple mixing curves for New Series rocks contoured in terms of R	252
Figure 9.10 AFC plots on incompatible vs incompatible a-g element diagrams	259
Figure 9.11 AFC plots on $^{143}\text{Nd}/^{144}\text{Nd}$ vs $^{87}\text{Sr}/^{86}\text{Sr}$ a-c diagram	268
Figure 9.12v AFC plots for $^{143}\text{Nd}/^{144}\text{Nd}$ vs $^{87}\text{Sr}/^{86}\text{Sr}$	273
 CHAPTER TEN	
Figure 10.1 Cartoon synthesising main conclusions	280
 APPENDICES	
Figures C1 I.D. vs X.R.F. diagrams for La, Ce, a-e Nd, Rb and Sr	308
Figure I1 Sample locality map	353

ABBREVIATIONS

A	assimilation
Ab	albite
AFC	combined assimilation and fractional crystallisation
An	Anorthite
BP	before present
cm	centimetre
cpx	clinopyroxene
D	bulk distribution coefficient
DSr	bulk distribution coefficient for a given element (e.g. Sr)
EDS	energy dispersive system
En	Enstatite
F	amount of magma remaining
FC	fractional crystallisation
Fig	figure
Fo	Forsterite
Fs	Ferrosilite
g	gram
G.yrs	giga years 10^9 years
HREE	heavy rare earth element
ID	isotope dilution
Kd	distribution coefficient
kG	kilogauss
KSr	distribution coefficient for a given element (e.g. Sr)
kV	kilovolt
LILE	large ion lithophile element
LRREE	light rare earth element
λ	radio-active decay constant
M	molar
mA	milliamps
ma	million years, 10^6 years
mL	millilitre
mm	millimetre
mol	mole
mol%	mole percent
MREE	middle rare earth element

mt	magnetite
ol	olivine
Or	orthoclase
plag	plagioclase
ppm	parts per million
r	ratio of the rate of assimilation to the rate of fractional crystallisation
REE	rare earth element
Wo	Wollastonite
wt	weight
wt%	weight percent
X	weight proportion
X.R.F.	X-ray fluorescence

ACKNOWLEDGEMENTS

Firstly, my thanks goes to my supervisor, Dr. B.M. Wilson, for initiating the project and supplying continual advice and encouragement thereafter.

I am also particularly indebted to Dr. R. Powell for placing a pool of elegant computer programs at my disposal and for discussions on various aspects of the study.

Special thanks are due to Drs. M. F. Thirlwall and R.A. Cliff for skilful instruction on the machinations of isotope geochemistry. Phil Guise and Dave Rex are also thanked for help in the lab. Mr. D.C. Rex is again thanked for K-Ar dating which he performed.

Sound advice and tuition on microprobe and X.R.F. work was respectively provided by Dr. E. Condliffe and Mr. Alan Grey and Dr. G. Hornung.

Drs. B.M. Wilson, R. Powell and M.F. Thirlwall read various parts of this thesis and provided constructive comments for which I am grateful. Helpful discussions were also engaged with Drs. R.A. Cliff and J.D. Fairhead as well as Messrs. Palacz, Davidson, Birmingham, Robinson and Jones.

It is also appropriate to thank Dr. R. Thorpe and Kevin Smith for providing access to unpublished data as well as for advice on field work strategy.

The geophysical contingent who accompanied me to 'Darkest Africa' are warmly thanked for an enjoyable field season and especially to Derek Fairhead who brought Creme Eggs to Sudan when they were most needed.

Mr. T.F. Johnson and his colleagues are sincerely thanked for providing an efficient service over the past three years.

Mrs. Margaret Mason is thanked for undertaking to do the typing at such short notice.

During my time in Leeds I have made a number of friends and I shall fondly remember some memorable times.

I am also in debt to Jean (a friend of mine) for reading the manuscript, adding some commas and for supporting me over the past year.

The award of a N.E.R.C. studentship is gratefully acknowledged.

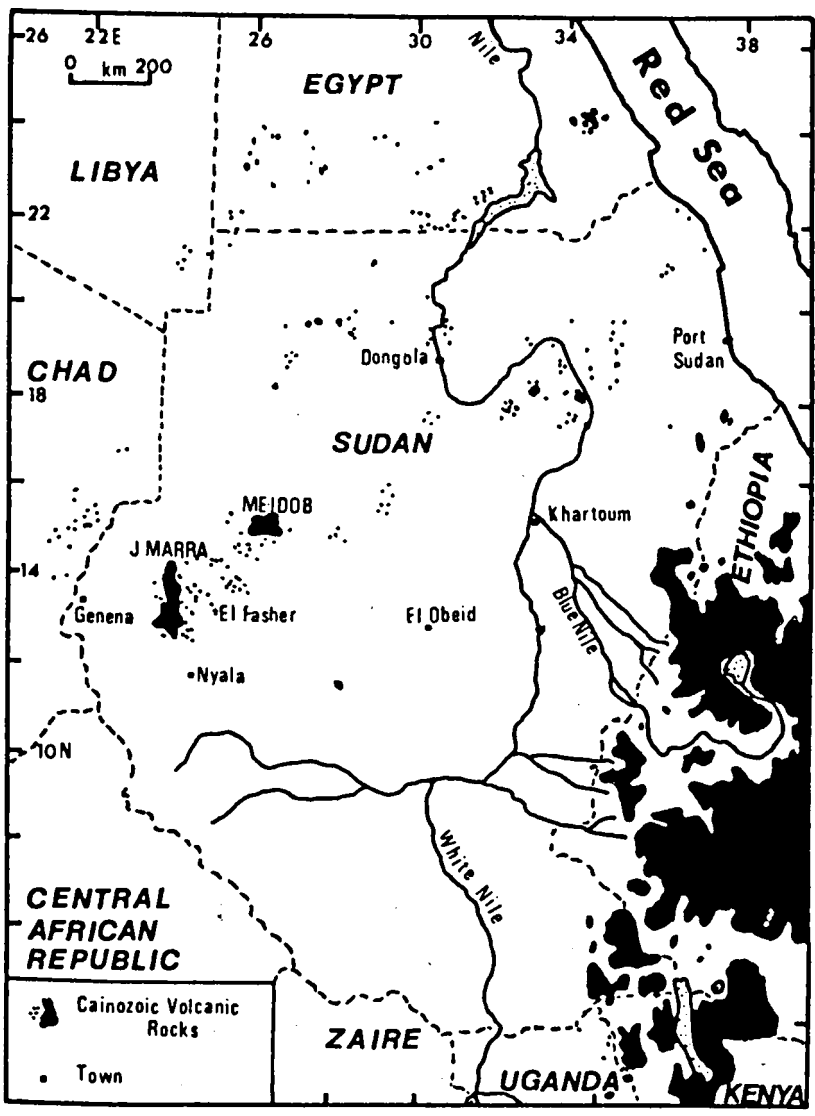


Fig. 1.1 Location map showing the position of Jebel Marra and the Meidob and other north-eastern Cainozoic volcanic centres. (Redrawn after Vail, 1978).

CHAPTER ONE

Introduction

1.1 Regional Setting

Jebel Marra is a continental, intra-plate volcanic complex located in the Darfur province of western Sudan (Fig. 1.1). It consists of a Tertiary-Recent alkali-olivine basalt - trachyte/phonolite series of rocks, including both lavas and pyroclastics. These volcanic products have covered an area of some 13,000 sq. km. (Francis et al., 1973) and have been erupted onto a domally uplifted basement.

In common with many other areas of Cainozoic volcanism in Africa, the complex is situated in an inter-cratonic region (Thorpe and Smith, 1974). This is illustrated in Fig. 1.2, taken from Thorpe and Smith (1974), which shows the distribution of African Cainozoic volcanic fields. The two major cratonic Cainozoic volcanic fields that are present are themselves anomalous. The first is in the Igwisi Hills of Tanzania and probably represents an extrusive kimberlite (Dawson, 1970) and may therefore have a deep sublithospheric origin. The others lie on the Western Rift in the Congo craton which has been affected by Pan African thermal activity (Thorpe and Smith, 1974) and may therefore have lost its cratonic identity. The major significant difference between cratonic and inter-cratonic regions which may help explain the virtual restriction of Cainozoic volcanism to inter-cratonic areas is that the latter have a relatively higher geothermal gradient.

1.2 Field Work and Sampling

The field work was conducted during a 6 month field season between Nov. 1980 and May 1981. The size of the area coupled with

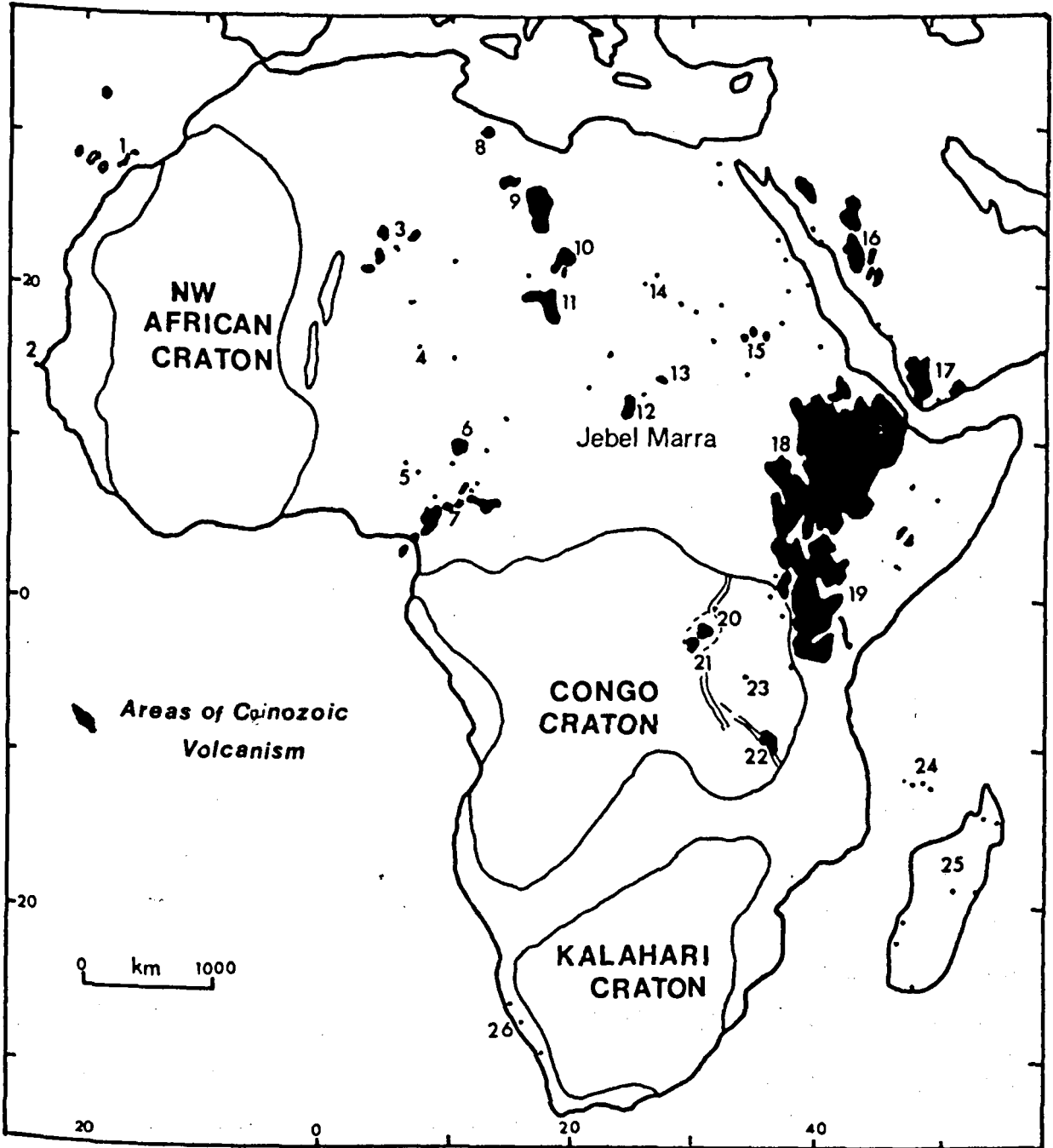


Fig. 1.2 Cretaceous volcanism and structural units of Africa. Note the virtual restriction of Cretaceous volcanic areas to inter-cratonic regions. Individual volcanic areas as follows:- 1 = Canary Islands; 2 = Dakar; 3 = Hoggar; 4 = Air; 5 = Jos; 6 = Biu; 7 = Cameroon Line; 8 = Tripolitania; 9 = Jebel Haruj; 10 = Eghei; 11 = Tibesti; 12 = Jebel Marra; 13 = Meidob; 14 = Jebel Uweinat; 15 = Bayuda; 16 = West Arabia; 17 = South Arabia and Aden; 18 = Ethiopia; 19 = East African Rift; 20-22 = West African Rift with 20 = Birunga; 21 = Kiva; 22 = Rungwe; 23 = Igwisi Hills; 24 = Comores; 25 = Madagascar; 26 = Southwest Africa (Drawn from Thorpe and Smith, 1974, Fig.1, p.92).

the inhospitable terrain restricted mapping and sampling to a self-contained area in the south of the complex (Fig. 1.3). The northern area is described by Coulon and Reyres (1968). The area chosen for detailed study is however the most variable and permits greater access to Recent lavas and pyroclastic rocks. Regrettably however, other areas were necessarily neglected such that a collection of a complete suite of older rocks has not been possible. Nevertheless, inspection of the sample/locality map (Appendix I) reveals that the most geologically interesting area of the complex has been well covered.

1.3 Previous Work

Owing to the remote position of Jebel Marra very little work on the volcanics or the basement rocks has been done. Reconnaissance work by Lebon and Robertson (1961) and Vail (1971; 1972a; 1972b) principally using aerial photographs coupled with some ground traverses have outlined the main components of the geology of the Jebel Marra complex; for example the outline of the volcanic complex in Fig. 1.3 is redrawn from Vail (1972a). A later expedition by Francis et al. (1973) described the tectonic setting and significance of Jebel Marra and has provided some stimulus for this study. Unpublished work by K. Smith has also been useful in this respect. Until now no detailed geochemical study has been made. In conjunction with the present geochemical study there is also a detailed seismic and gravity study being conducted. Results from this work will be discussed later in this Chapter.

1.4 Aims

The main aim of this study is to present a detailed description of the Jebel Marra volcanics in terms of their petrography, major

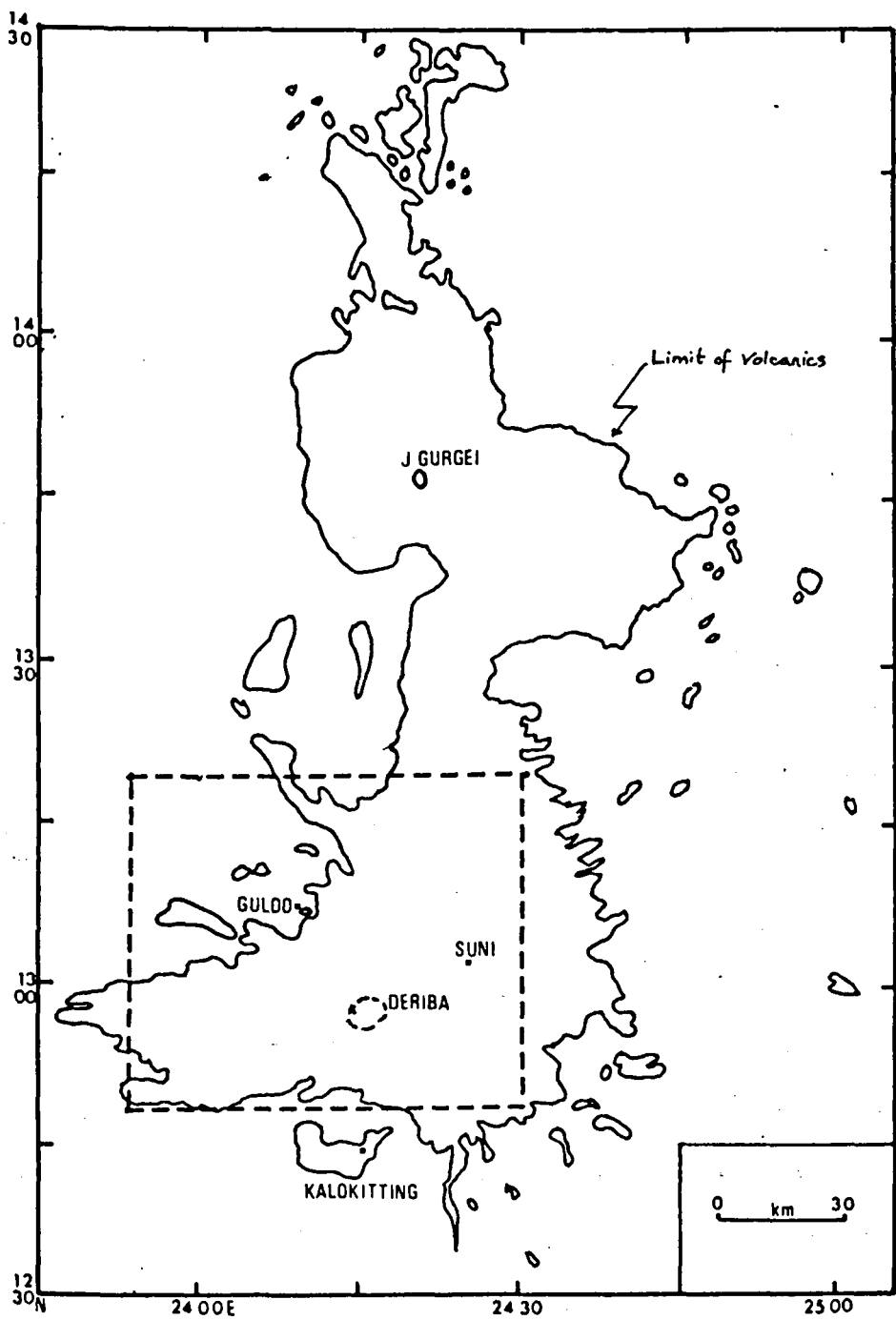


Fig. 1.3 Sketch map of the Jebel Marra volcanic complex after Vail, 1972a. Enclosed region shows area of study.

and trace element and Nd and Sr isotope geochemistry. Field interpretations provide the basis for the classification of the volcanic rocks into older series rocks, which include large pyroclastic sequences, and a newer series of rocks. On the basis of these subdivisions the geochemistry of the suite and variations between the series are considered in Chapters 6, 7 and 8. Although the geology of the volcanics is very important and naturally provides the means to investigate the geochemistry it is the latter which comprises the bulk of this study. Firstly, the major and trace element variations are described in Chapters 6 and 7. Following this in Chapter 8 evidence obtained from Nd-Sr isotopic studies is discussed. Throughout these sections compelling evidence emerges which suggests that the large compositional and isotopic variations that are present are primarily the result of assimilation of continental crust combined with the effects of fractional crystallisation on parental alkali basalt magmas. In Chapter 9 geochemical modelling techniques are employed to strengthen the qualitative arguments that are made in Chapters 6, 7 and 8.

The Jebel Marra volcanic rocks with their wide range in chemistry afford an excellent opportunity to describe the effects of crustal contamination in this intra-plate continental environment. In studying this, it has been necessary to understand other processes, particularly fractional crystallisation, which have also modified the chemistry of these rocks. The emphasis placed on contamination and fractional crystallisation throughout this study is additionally justified because the vast majority, if not all, of the samples from elemental and isotopic considerations demonstrably show the effects of these processes.

Although crustal contamination has been recognised for some time (e.g. Bowen, 1928), it still remains a contentious issue. There are many suggestions from mantle nodules and basalts alike that the sub-continental mantle is an interesting and variable area of the Earth. If it is a goal of geochemistry to make cogent comments about the nature of the sub-continental lithosphere and asthenosphere, then processes which modify primary magmas, principally crustal contamination, must be well understood. Consequently, studies such as this and from other continental terrains therefore assume considerable importance. This is particularly true as it is becoming evident that contamination may occur via a different array of mechanisms in different circumstances, and may show subtly differing effects. The two most viable contamination mechanisms, combined assimilation and fractional crystallisation (DePaolo, 1981) and mixing with crustal partial melts (Patchett, 1980) are discussed at length in Chapter 8.

1.5 Geophysical/Tectonic Setting

The association of Cainozoic volcanism, negative Bouguer anomalies, and domal uplift has long been recognised in Africa (Fairhead, 1978) although its relation to rifting is not unanimously agreed upon (Le Bas, 1971, 1980). The negative Bouguer anomaly is thought by many (e.g. Fairhead, 1978; Fairhead et al., 1981) to be the result of an intrusion of low density, low velocity asthenospheric material into the lithosphere, resulting in an upward migration of the asthenosphere-lithosphere boundary. If this interpretation is correct then this is likely to be in some way responsible for the surface volcanism.

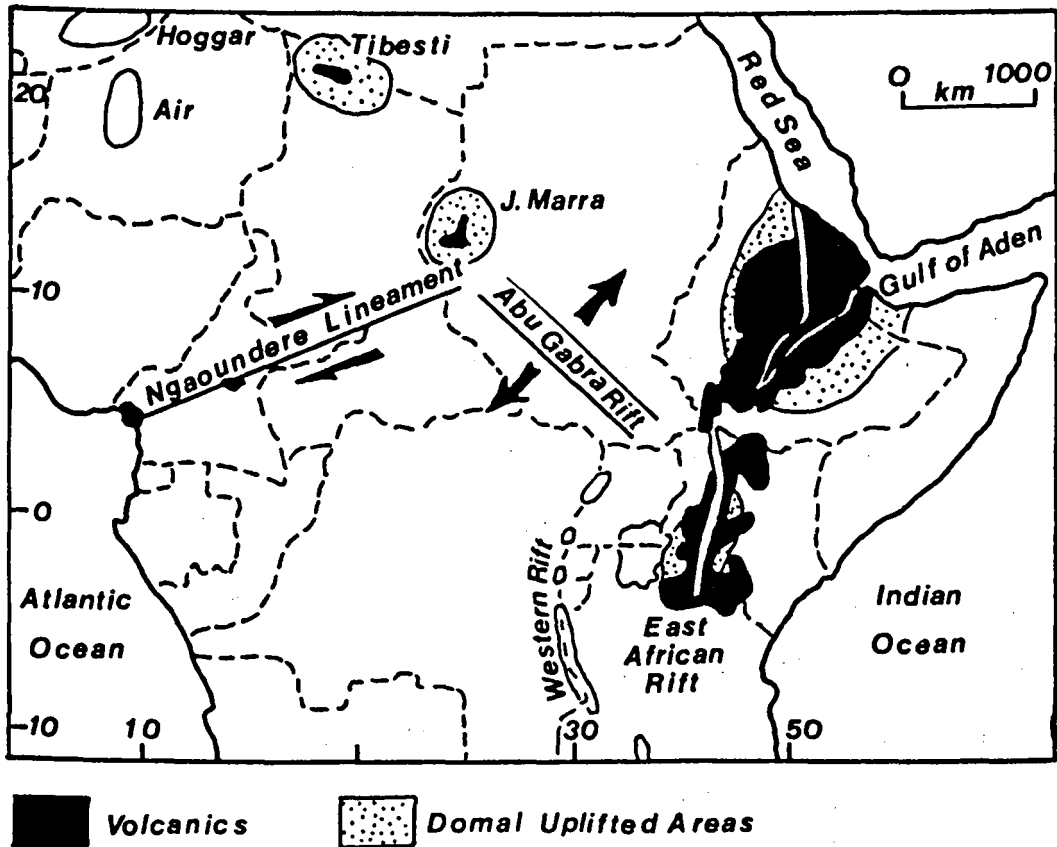


Fig. 1.4 Map of central Africa showing the possible location of a triple junction centred on Jebel Marra. Note the correlation between Cainozoic volcanism and domal uplift (after Fairhead et al. 1981).

Fairhead et al., (1981) interpret the gravity data for Jebel Marra in terms of a triple junction using the East African/Arabian Rift system as a more evolved precedent. The WSW Ngaoundere Lineament and the SE trending Abu Gabra rift system are considered to represent subsiding rift arms while the third and failed arm consists of the domally uplifted area which includes the Jebel Marra volcanic complex (Fig. 1.4). The comparison with the East African/Arabian Rift System is clear (Bermingham et al., 1983): the Red Sea and Gulf of Aden arms represent the rifting arms and the Ethiopian/Kenyan dome and their attendant volcanics represent the failed arm.

Gravity and seismic modelling (Bermingham, unpublished) has led to the following conclusions:-

1) Gravity modelling suggests that domal uplift is associated with a negative Bouguer anomaly approximately 700km in diameter. A Bouguer anomaly map of the Darfur region and selected gravity profiles taken across the area are presented in Fig. 1.5.

2) Three-dimensional gravity modelling (using the method of Cordell and Henderson, 1968) and constraints from seismic observations suggests that the data are consistent with the occurrence of a low velocity, low density body within the mantle part of the lithosphere compensating for the swell; this is interpreted to be either:-

- i) a region of partial melt
- or ii) athenospheric material from the low density zone.

3) Residual gravity studies, i.e. after regional gravity has been removed, reveal a positive anomaly, 50-100km wide, beneath Jebel Marra interpreted to represent a basic body located at base or mid-crustal levels.

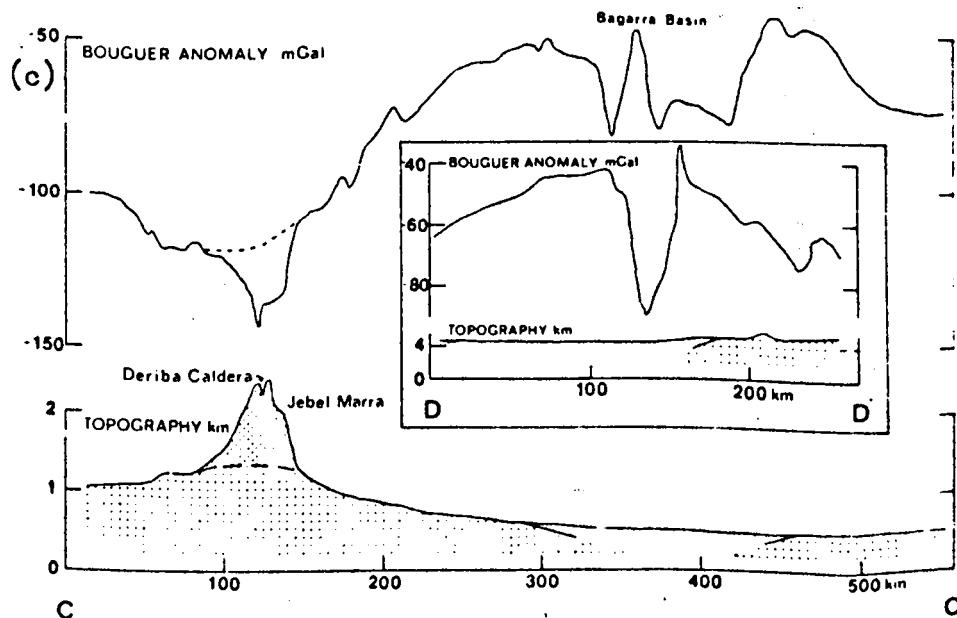
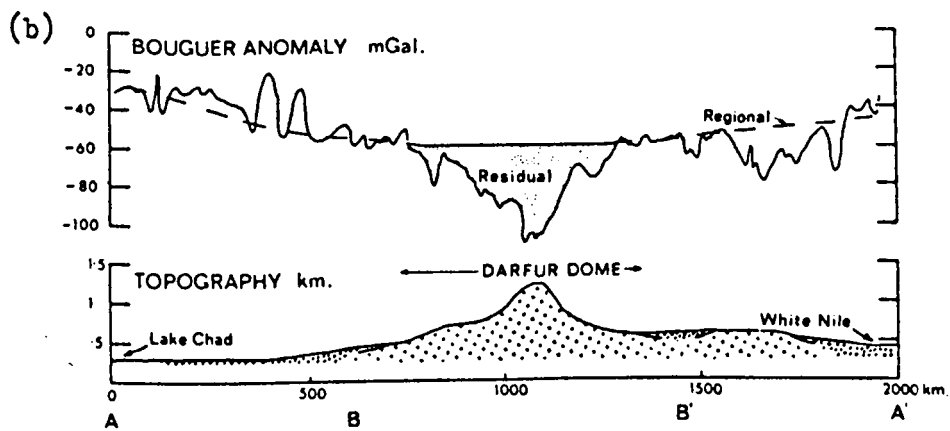
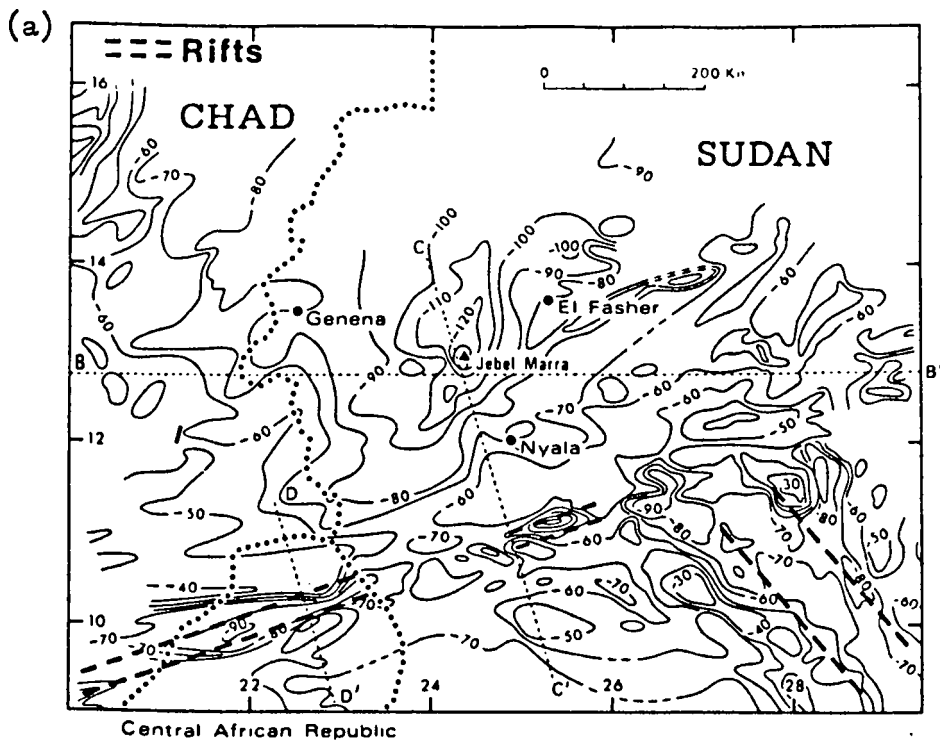


Fig. 1.5a Bouguer anomaly map of the Jebel Marra region. Note the association of large negative Bouguer anomalies with rifting areas.

Figs. 1.5b-c. Profiles across Bouguer anomaly map. (after Bermingham et al., 1983).

1.6 Conventions

The terms 'basic' and 'acidic' rocks are continually used in the text. In the context of the volcanic rocks, basic rocks refer to basalts, hawaiites and mugearites while acidic rocks refer to trachytes, rhyolites and phonolites. Confusion may arise because in describing the geological history basalts, phonolites, ignimbrites etc., from the Pyroclastic Sequence are considered to belong to the Old Series rocks whereas in many of the variation diagrams they are treated separately. This is done to illustrate geochemical differences and should not be taken to infer that they constitute a series of their own. Also throughout the text reference is made to basement samples being either 'upper' or 'lower crustal' in character. This only refers to their isotopic and elemental characteristics as all these samples were collected from surface outcrops around Jebel Marra.

CHAPTER TWO

PRE-VOLCANIC ROCKS

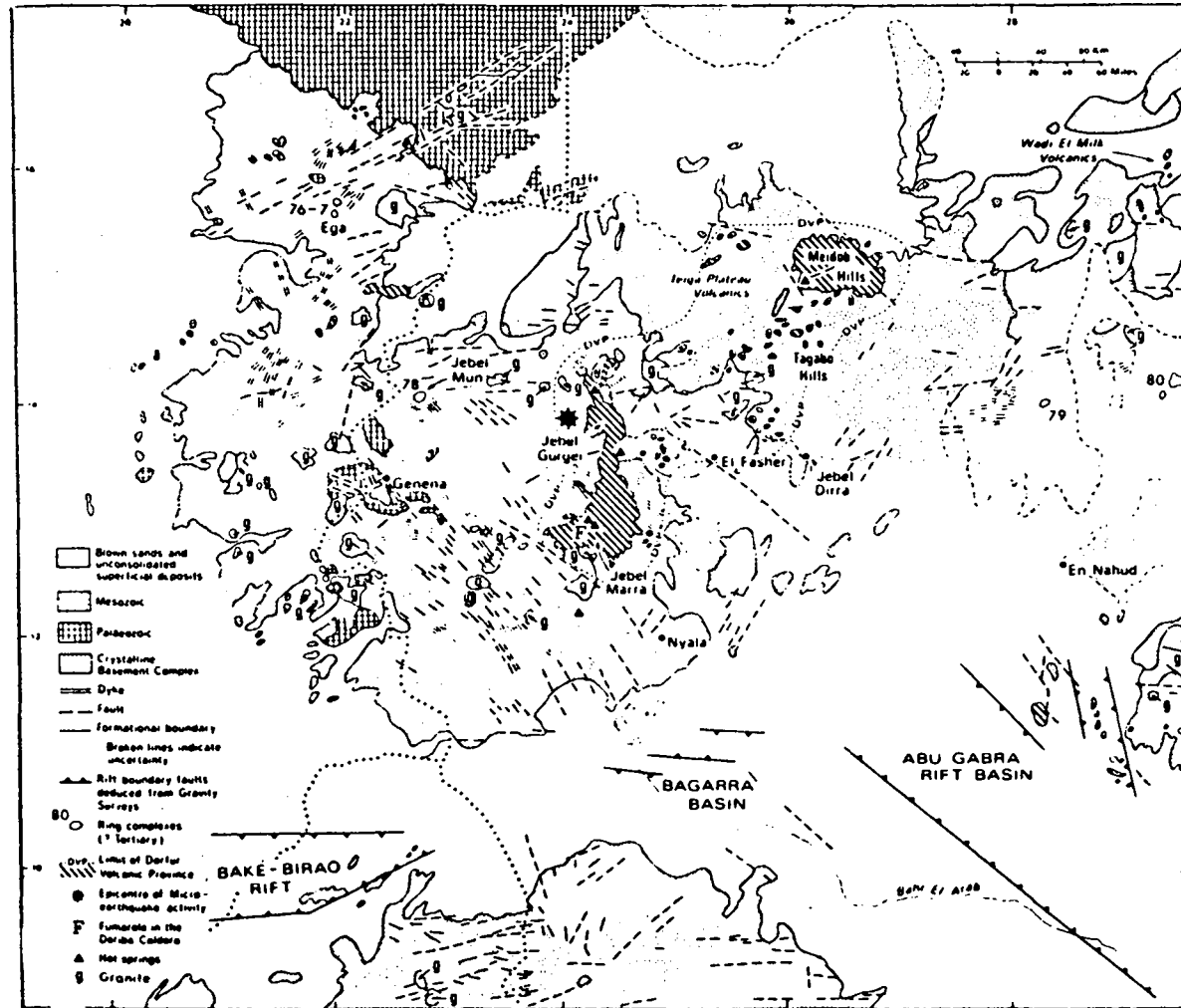
2.1 Introduction

This Chapter gives a general review of the basement and sedimentary cover which exists around the volcanic complex of Jebel Marra. This is an important consideration because magmas originating in the mantle and erupting as lavas will traverse the crust and therefore have the opportunity to assimilate any crustal rocks which they pass through. The consequence of this may be that the chemistry of the magma may be modified en route to the surface of the Earth. To understand some of the effects and processes of contamination it will help to have an idea about the structure, lithology and composition of the basement. To this end, first the general geology of the basement around Jebel Marra and then the geochemistry of selected crustal samples is described.

Rather little, in detail, is known about the pre-volcanic geology of the rocks in Darfur region of Sudan. No structural study on a small scale has been attempted. Only large scale mapping from aerial photographs has been done, by Vail (1972b) and from Landsat imagery (1:2,000,000; Geological map of Sudan, 1981). In Fig. 2.1 a general geology map of the area is presented which illustrates some of the features to be discussed in the following sections.

To the east and south, exposure of the basement is often poor although on the western flank it is extremely good. Unexposed areas are commonly covered in sands or reworked pyroclastic material from Jebel Marra. The basement rock is mainly composed of granitic gneisses which are often badly weathered, particularly the felds-

Fig. 2.1 Geological sketch map of Darfur region (after Bermingham et al., 1983).



pathic component. They are intruded by granite and covered in part by sediments (Vail, 1972b).

2.2 Basement Rocks

In describing the lithologies of the Darfur area, emphasis will be placed on those rocks which outcrop near to the volcanic complex. The basement rocks consist of a variety of gneisses and schists which have been intruded by granite, dykes, pegmatites and quartz veins. On the basis of aerial photogeological interpretation and some field traverses, the basement rocks have been subdivided into four groups (Vail, 1972b).

2.2.1 Granitic Gneisses

Granitic gneisses comprise the dominant member of the basement rocks. They show mineral banding and are well foliated. Feldspar and quartz are the characteristic minerals although biotite is often present. At Gubbo, Kalokitting and Nyertete granitic gneisses of this type are well exposed.

2.2.2 Pelitic Schists

These can occur interbedded with the granitic gneisses where quite often they will stand out as a result of differential erosion. All are mica rich but vary from those at Gubbo, in which mica is subordinate to felsic minerals, to those at Zalingei, in which mica is the dominant phase with respect to felsic minerals. In these micaceous rocks garnet, alkali feldspar and kyanite can coexist with biotite. The 1981 Geological map of Sudan (1:2,000,000), based on recent Landsat imagery, delineates an area of 14,000 sq. km to the south of

Zalingei which is described as "Undifferentiated Schists" (Fig. 2.2). These are elsewhere volumetrically unimportant.

2.2.3 Amphibolites

These are relatively rare around Jebel Marra but they are found interbedded amongst granitic gneisses. For example, at Gubbo a 20m wide sheet of amphibolite is exposed. These tend to be highly weathered and chloritized. Exposures of amphibolite have been reported north of Jebel Marra but, in general, are not as widespread as in other parts of basement Sudan.

2.2.4 Quartzites

These are again rare in the Jebel Marra region but do, however, form extensive ridges in the Zalingei region. They are described by Vail (1972b) as orthoquartzites containing quartz and some muscovite.

2.3 Granite Intrusions

There are a number of granite intrusions close to the complex of Jebel Marra (Figs. 2.2-3). The most notable of these are at Kas, Kutum, and Nyala. There are also a number of smaller bodies which are exposed near Zalingei. They may be conveniently divided on the basis of whether they possess a pervasive fabric or not. For example, the granites of Nyala and Zalingei display a weak foliation, whereas those of Kas and Kutum are largely unfoliated. This observation may enable them to be distinguished as late or post-orogenic respectively. The late-orogenic granites tend to be elongate whereas the post-orogenic ones are more commonly irregular in outline. Mineralogically

they are typically leucocratic containing quartz, feldspar and some biotite.

2.4 Quartz Veins and Pegmatites

Quartz veins and pegmatites are widespread throughout the basement rocks and show varied cross-cutting relationships. The pegmatites consist primarily of quartz and feldspar and sometimes contain white mica. Examples are found well exposed at Gubbo and Nyertete.

2.5 "Dykes"

Dyke like features are found within the basement and are readily identified from aerial photographs sometimes extending for many kms. Their orientation is closely allied to the direction of faults within the basement and many undoubtedly represent intrusion along fault zones.

2.6 Sedimentary Cover

The Nubian Sandstone Formation is a vast succession of deposits of Cretaceous age, which occupies much of Egypt and extends into large areas of N and NW Sudan. It outcrops, intact, to within 30km of the complex. In the NW a supposed outlier of the formation is, in part, overlain by Jebel Marra volcanics. A further smaller outlier has been mapped adjacent to volcanics in the extreme north of complex. Similar deposits also occur near Genena which are described as being of Devonian and Silurian age (Williams et al. 1980). In the N they consist of a variety of continental clastic rocks including sandstones, siltstones, mudstones, and conglomerates and are generally flat lying.

2.7 Age

Very little is also known about the age of the prevolcanic rocks, other than in relative terms. Two K-Ar dates are available from the

area (Vail and Rex, 1971). From the basement a sample of mica schist from the Zalingei area gave an apparent mineral age of 604 ± 24 ma. This age is in general agreement with an average date gathered from much of basement Sudan, which points to an event at around 550 ± 100 ma. This corresponds to a Pan African orogenic event outlined by Kennedy (1965).

A Pb/Pb age derived from galenas from veins in the basement near Kutum place a further constraint on the age. Coomer and Vail (1974) obtain a Holmes Houtermans age (Russell and Farquhar, 1960) of 1100 ± 200 ma from two samples using parameters of Cooper et al (1969). The data lie outside the Russell-Stanton-Farquhar model. This implies that the age obtained must be considered a minimum age. Despite reservations there may be for this as an absolute age, it does suggest that the basement rocks of Darfur are of Archaean age.

The largely undeformed granite at Kas yields a K-Ar age of 230 ± 10 ma. Vail (1972b) considers the date to be anomalous presumably because of the disparity between this and other basement dates. In order to account for this he invokes argon loss through weathering or by heating by overlying basalts. The granite in question is actually quite fresh in thin section, more so in fact than the majority of the basement rocks, and this, coupled with the overall unfoliated nature of the intrusion may actually support a post-tectonic age. If this is correct then a Permian age for the granite would not be unreasonable.

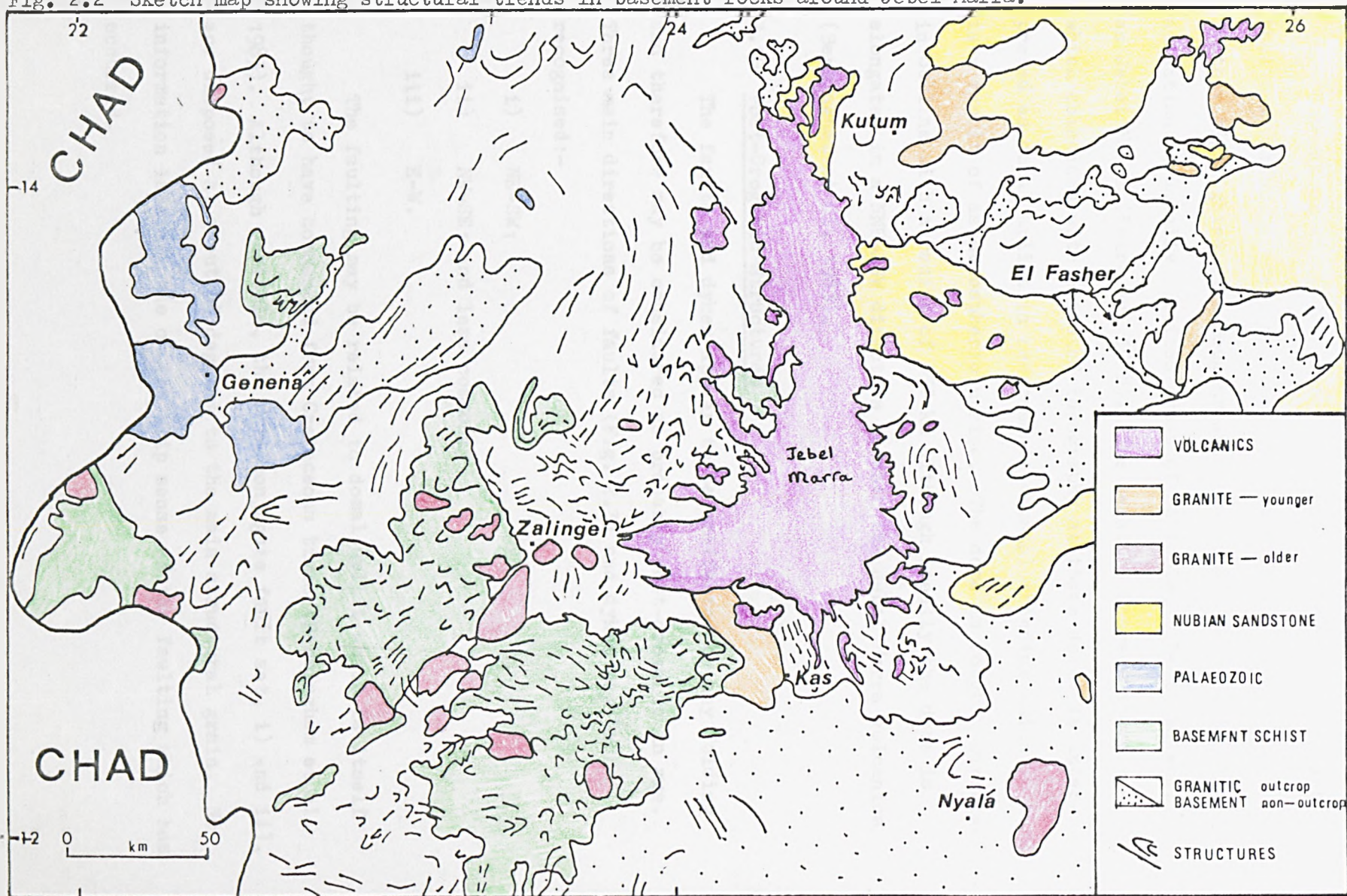
An indication of the old ages of some of the basement samples is given in Fig. 8.7 in which some samples have very low $^{143}\text{Nd}/^{144}\text{Nd}$ ratios.

2.8 Structure

No detailed structural investigation has been carried out on the basement rocks of Sudan. Most of the discussion in this section is based on photogeological interpretation coupled with some ground traverses of Vail (1972b). Exposure of the basement surrounding Jebel Marra is in places extremely good which has enabled structural trends and faults to be mapped with some confidence.

The regional trend appears to be NNE-SSW (Fig. 2.2) although there are departures away from this locally. For example, down the east side of the complex the trend runs N-S from Kutum to Nyala. At Nyala, however, the trend swings to a NW-SE direction. The schists south of Zalingei seem to have preserved trends from other phases of folding and are consequently more variable. Vail (1978) visualizes a complex tectono-thermal history involving at least three phases of folding. The second, and major, phase of folding is seen to run NE-SW which refolds folds of the first phase. Whilst NW-SE trending folds testify to the existence of a third phase of folding. The late-orogenic granites of Nyala, El Fasher and Zalingei, in general, outcrop with their long axes parallel to the local grain. This effect could be caused by the intrusion being more easily accommodated in a direction parallel to the grain or by the intrusion itself, in part deforming the fabric so that it becomes parallel to the long axis of the intrusion. A more likely alternative is that if the granites in question are in fact late-tectonic, then any later deformational event will deform the relatively incompetent gneisses and schists around the relatively competent massive granite body and produce the trends described above.

Fig. 2.2 Sketch map showing structural trends in basement rocks around Jebel Marra.



Redrawn from Geological Map of Sudan, 1981.

2.9 Domal Uplift

Francis et al, (1973) made the first reference to the fact that the Darfur basement has been domally uplifted. This was further highlighted by a Bouguer anomaly map of Africa which drew attention to domally uplifted areas of Ethiopia, Tibesti as well as Jebel Marra (Fairhead, 1978). The negative Bouguer anomaly which coincides with elevated topography at these domes is interpreted as domal uplift in response to crustal thinning which in turn is a result of asthenospheric uprise. The dome is roughly circular in outline with a radius of 350 km although locally the dome is elongated in a NNE-SSW direction beneath the Jebel Marra volcanics (Birmingham et al. 1983).

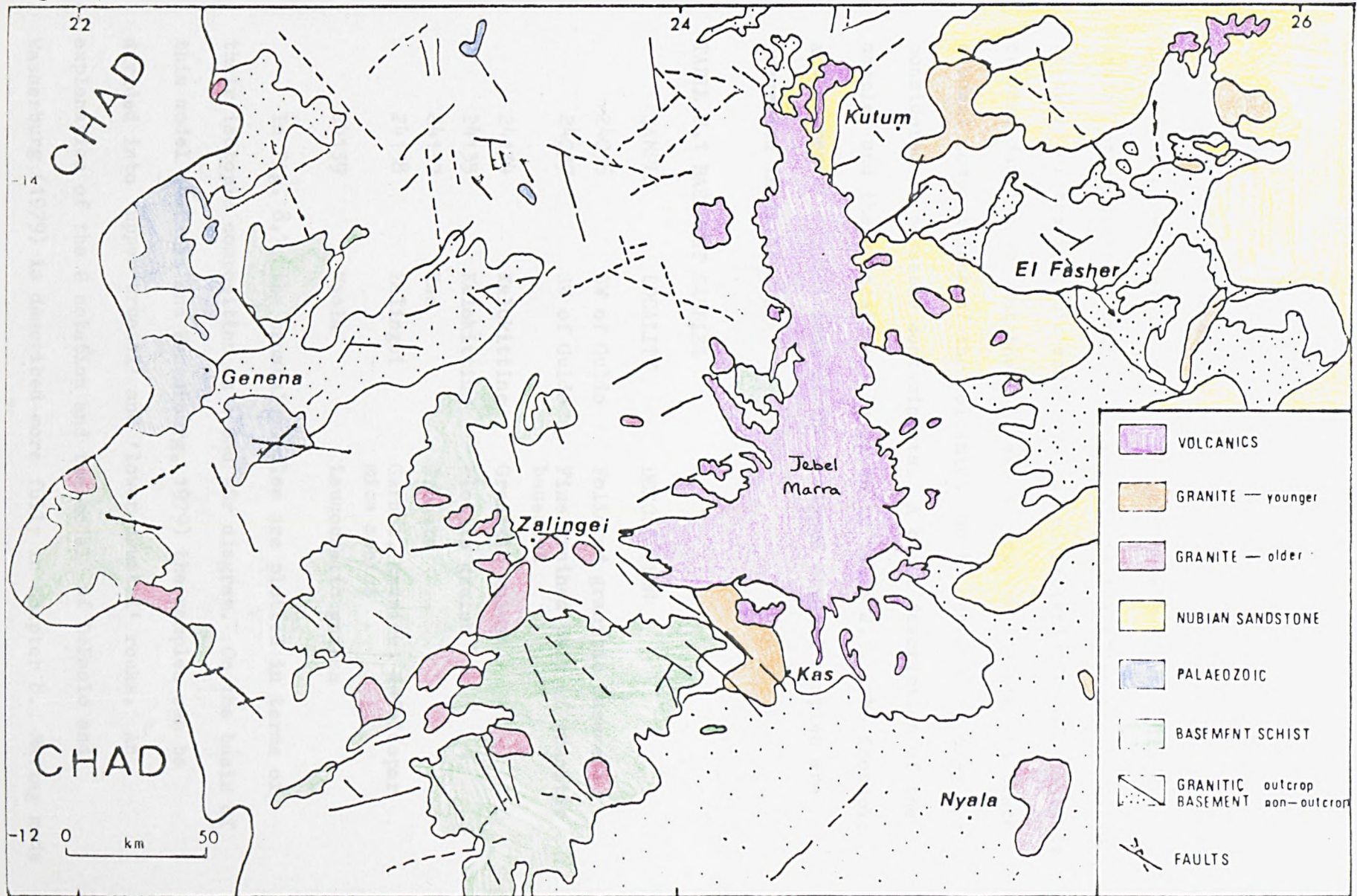
2.10 Post-Orogenic Structures

The faults and dykes appear to be unaffected by any folding and therefore may be considered as probably post-orogenic in age. Three main directions of faults (Fig. 2.3) and dykes may be recognised:-

- i) NE-SW;
- ii) NW-SE; and less commonly
- iii) E-W.

The faulting may be related to domal uplift which is itself thought to have commenced from Cretaceous times (Birmingham et al. 1983). Although variable, the main conjugate fault set, i) and ii), are disposed at about 45 degrees to the main structural grain. No information is available on the slip sense of the faulting which has occurred.

Fig. 2.3 Sketch map showing fault trends in basement rocks around Jebel Marra.



Redrawn from Geological Map of Sudan, 1981.

2.11 Geochemistry of the Crust

It is now proposed to briefly describe the geochemical characteristics of basement samples which were collected from outcrops around the Jebel Marra volcanics. In subsequent Chapters it will be shown that the volcanic rocks have been variably contaminated by continental crustal rocks. It is therefore necessary to be aware of the isotopic and elemental characteristics of available crustal samples so that their likely effects on isotope and trace element compositions of the volcanics can be assessed if they are considered as possible contaminants. A brief description of the samples and their localities is given in Table 2.1. The isotopic and elemental compositions of the analysed crustal samples are presented in Table 2.2

TABLE 2.1 BASEMENT SAMPLES

SAMPLE	LOCALITY	DESCRIPTION
24036	SW of Guldo	Foliated granitic basement
24037	SW of Guldo	Fine grained part of granitic basement
24134	Kalokitting	Granitic gniess
24135	Kalokitting	Biotite gneiss
24137	Kas	Granite
24138	Zalingei	Garnet, kyanite, K-feldspar mica schist
24139	Nyala	Leucocratic gniess

In Fig. 8.7, the crustal samples are plotted in terms of their isotopic composition on a ^{60}Nd ^{87}Sr diagram. On the basis of this model (DePaolo and Wasserburg, 1979) the samples can be divided into 'upper crustal' and 'lower crustal' rocks. An explanation of the ϵ notation and the model of DePaolo and Wasserburg (1979) is described more fully in Chapter 8. Having made

Table 2.2 Geochemical Data for Basement Samples

Basement	24037	24135	24137	24036	24134	24139	24139
SiO ₂	67.16	74.04	70.09	72.04	75.01	72.22	64.69
TiO ₂	0.46	0.30	0.31	0.03	0.62	0.16	0.81
Al ₂ O ₃	15.28	14.73	14.98	13.07	13.33	14.10	17.57
Fe ₂ O ₃ T	2.30	2.53	2.10	0.45	0.74	1.00	8.77
MnO	0.05	0.07	0.66	0.09	0.04	0.05	0.16
MgO	1.20	0.77	0.63	0.20	0.10	0.26	2.48
CaO	2.53	2.23	1.97	0.67	0.55	1.15	0.49
Na ₂ O	5.08	4.09	4.86	4.38	3.55	3.92	1.17
K ₂ O	2.35	3.22	3.69	4.41	5.73	4.81	3.36
P ₂ O ₅	0.14	0.10	0.14	0.04	0.02	0.04	0.09
LOI	0.20	0.28	2.68	4.37	1.12	3.02	0.96
Total	97.93	102.76	101.51	93.75	100.26	100.73	150.57
Th	16	29	11	10	7	34	16
Pa	16	5	9	7	15	12	13
Ud	39	34	33	14	13	27	35
Ce	63	69	49	14	9	51	70
La	47	45	39	7	1	30	37
Pr	6	7	6	7	3	5	20
Cr	6	0	0	0	0	1	77
Co	24	32	30	43	26	38	45
Ni	10	6	2	1	1	2	29
Cu	21	14	13	8	11	13	17
Zn	59	41	52	12	12	32	53
Rb	55	104	67	147	150	198	149
Sr	672	353	814	69	105	220	54
Y	5	7	6	26	12	11	34
Zr	217	140	156	35	34	33	220
Nb	7	5	10	18	25	2	16
Pd	14	23	30	42	64	67	0
Ba	2043	1075	2468	208	315	982	499
⁸⁷ Sr/ ⁸⁶ Sr	0.7066	0.7306	0.705	0.7645	0.7524	0.7271	0.6552
¹⁴³ Nd/ ¹⁴² Nd	0.5114	0.5107	0.5113	0.5114	0.5116	0.5121	0.5116
ε _{Sr}	53.62	370.3	64.27	251.4	679.2	320.3	2138
ε _{Nd}	-24.81	-36.33	-26.72	-24.23	-19.37	-11.47	-19.74
K ₀ /Sr	0.06112	0.2971	0.08477	2.13	1.423	0.9	2.759
K/Rb	0.04497	0.03049	0.04439	0.0245	0.03193	0.02016	0.01972
Zr/Nb	31	28	15.6	1.944	3.36	11.63	13.75
alkalis	6.08	7.31	7.55	8.75	7.33	4.73	4.53
Mg ₀	51.53	43.02	42.67	52.44	25.11	34.21	41.23

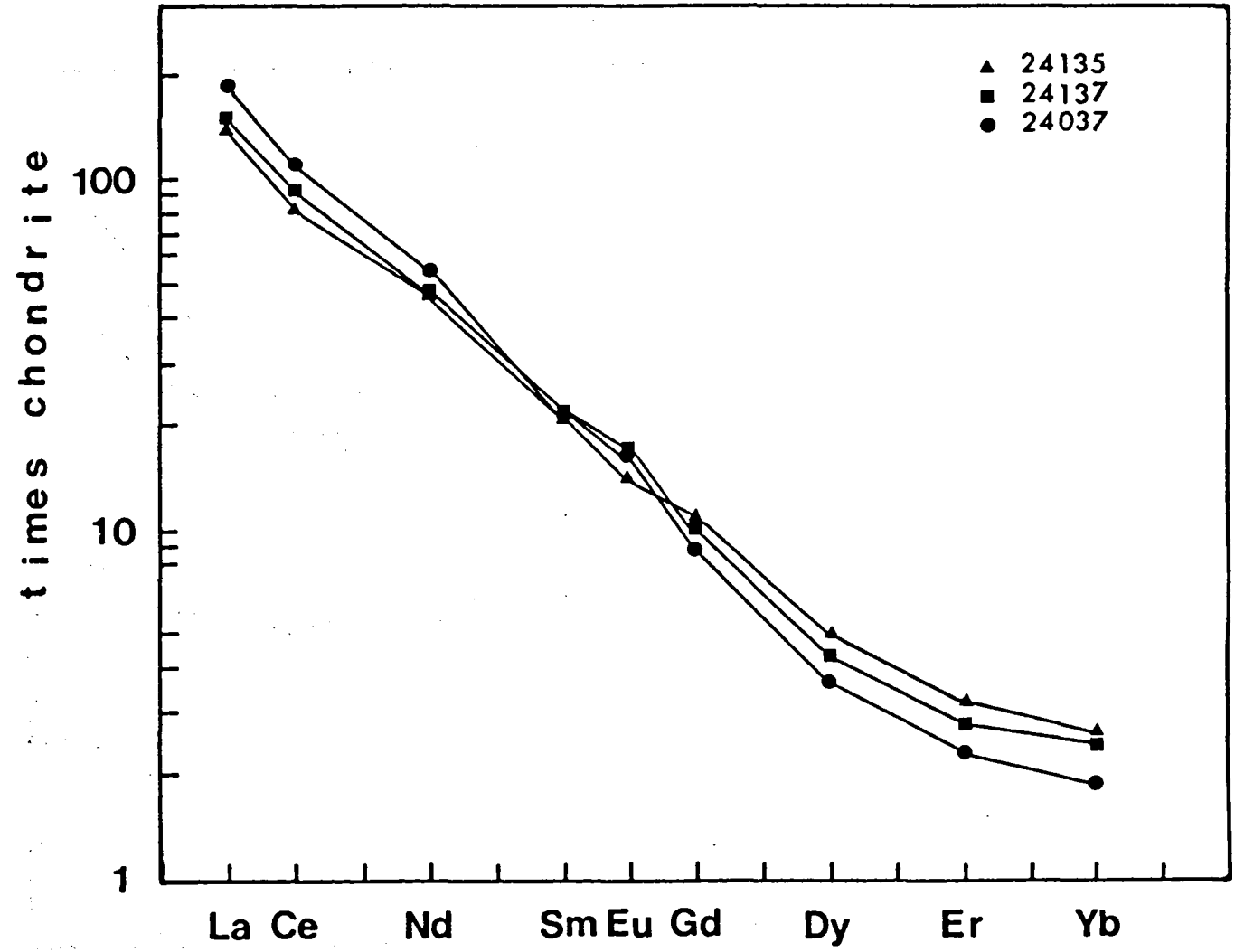


Fig. 2.4 REE patterns for 'lower crustal' samples.

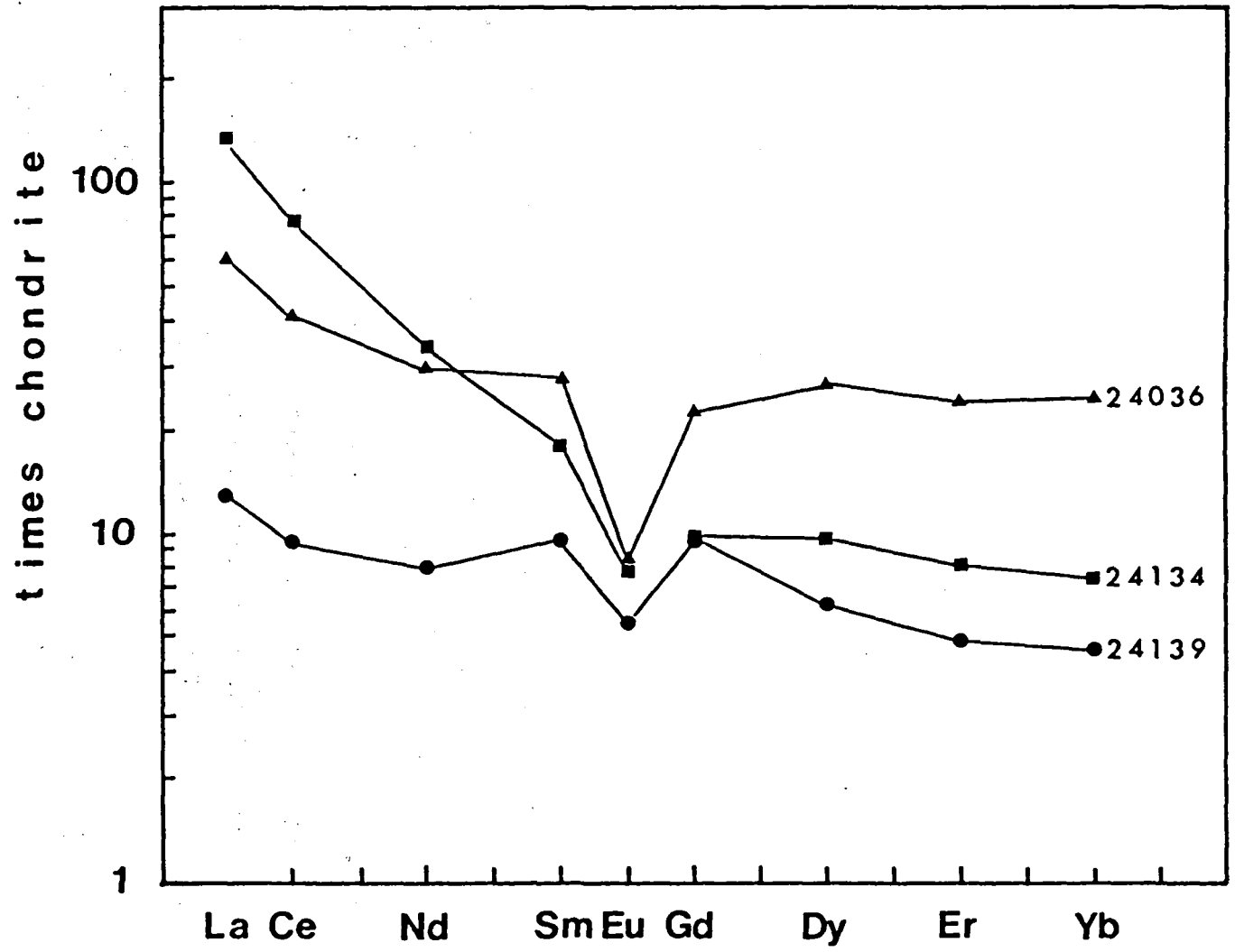


Fig. 2.5 REE patterns for 'upper crustal' samples.

this division on the basis of isotopic compositions it becomes evident that there are also significant elemental differences. This is most strikingly illustrated by the rare earth element (REE) patterns (for explanation of REE patterns see Chapter 7). In Fig. 2.4 patterns for the 'lower crustal' samples are drawn. These have steep light REE enriched patterns and flatter heavy REE patterns. 24135 is considered to have 'lower crustal' characteristics despite plotting in the 'upper crustal' field in Fig. 8.7. These contrast markedly with the typical 'upper crustal' patterns which are mostly flat (Fig. 2.5). Sample 24139 appears to be intermediate between the two groups. Other trace elements also show systematic differences between the two groups. For example, Rb and Pb are lower whereas Sr and Ba are higher in the 'lower crustal' rocks than the 'upper crustal' rocks. The major elements also show systematic differences for example, K₂O is lower whereas CaO and Na₂O are higher in the 'lower crustal' rocks compared with the 'upper crustal' samples. Table 2.2 illustrates the isotopic and geochemical differences between the two groups. The low ¹⁴³Nd/¹⁴⁴Nd and relatively low ⁸⁷Sr/⁸⁶Sr and the low Rb, Pb and K₂O concentrations observed in the 'lower crustal' rocks are characteristic of granulite facies rocks. These are features which are all related to the relative loss of heat producing elements associated with the formation of granulite facies rocks.

2.12 Conclusions

The basement rocks in Darfur have undergone polyphase deformation and metamorphism up to amphibolite grade which has imparted a NNE-SSW regional trend. Late-orogenic and post-orogenic granites have been intruded into the basement rocks. Continental clastic

deposits of Cretaceous age probably covered much of the area which were since removed, apart from two outliers in the north. A set of conjugate faults exist in the basement rocks and may have developed in response to stresses created during doming.

Geochemical analysis has uncovered marked differences in isotopic and trace element compositions within the crustal samples which enables them to be loosely classified as having 'lower' and 'upper crustal' characteristics. Given that assimilation of crust has occurred in the volcanic rocks, then these marked differences should make it possible to discern which of these chemically different groups is responsible for the contamination.

CHAPTER THREE

VOLCANICS

3.1 Introduction

The Jebel Marra volcanic complex is aligned in a N-S direction and is approximately 200km in length and 80km wide at its broadest part in the south. It covers an area of about 13,000 sq. km and the volume of material erupted before erosion is estimated to be 8,000 cubic km (Francis et al., 1973). The volcanic rocks which make up the complex belong to the alkali olivine-basalt - trachyte/phonolite association. They were produced in Miocene to Recent times.

On the basis of field mapping and photo-interpretation it has been possible to divide the volcanics into an Old Series and a New Series. Radiometric data and independent geological evidence (Andrews, 1931) indicate that widespread volcanism in the area began in Miocene times at around 13-14ma ago.

The fact that most of the flows can be traced to discrete vents, combined with the lack of dykes and faults can be used as compelling evidence to suggest that the volcanism is of 'central type' rather than fissure type volcanism (Francis et al., 1973).

The information contained in this Chapter is important because it establishes a framework within which to consider the geochemical data. In any area it is desirable to be able to relate geochemical characteristics, particularly spatial and temporal variations, to features which emerge from the field geology. The geological map of Jebel Marra which accompanies this Chapter (Appendix L) was constructed from mapping and photo-interpretation on 1:40,000 aerial



Plate 3.1 Waterfall
at Suni.



Plate 3.2 Trachyte intrusion at Jebel Koron.

photographs; the absence of the central portion of the map is regretted but was due to unavailability of the necessary photographs.

The rock types described in the following sections are based on a classification which is explained in Chapter 6.

3.2 Topography and Exposure

The height of the contact between the volcanics and the basement has been measured at a number of sites by barometric means (Bermingham, unpublished). The heights are variable but they show that the contact starts at around 1200m. In Table 3.1 the contact height has been measured at these villages which are located on the geological map:-

Gubbo	1291m
Nyertete	1214m
Guldo	1264m
Turra	1432m

Table 3.1 Showing basement/volcanic contact heights above sea level (Bermingham, unpublished).

The volcanic pile rises to a maximum height of 3042m, at a peak adjacent to the caldera at Deriba. Thus a 1800m thick pile of volcanic material is present.

The topography of the Jebel Marra volcanic complex has been strongly influenced by rock type, for example, poorly consolidated pyroclastic deposits, susceptible to erosion, have been deeply dissected to produce incised valleys with spectacular gorges and waterfalls (Plate 3.1). This is especially the case on the east and

west flanks of the central area where thick pyroclastic deposits are exposed. Elsewhere the topography is less severe, typified by trap features and lava fields cut by wadis. In the north the panorama is altered by the appearance of spires and inselbergs (Plate 3.2) of trachyte.

The exposure tends to be very good in the south becoming moderate towards the north, with most of the best exposures being found in wadi cuttings.

3.3 Geological History

A summary of the geological history based on K-Ar data (Table 3.2) and field interpretations is presented in Table 3.3.

3.3.1 Old Series

3.3.1.1 Extrusive and Intrusive Rocks

Based on photo-interpretation and K-Ar radiometric dating, Smith (unpublished) identified that the earliest volcanic complex was established around Jebel Donsa which cut the earliest products at Turra. Whereupon a broad chain of vents emitting lavas developed and extended SE to Suni and continued on towards Melem. Basaltic scoria from Suni, for example, gave a K-Ar age of 14.30 ma which is considered by Smith (unpublished) to occur just after inception of volcanism in the area. Following the construction of this early lava shield, subsequent volcanism persisted as basalt flows but these were constrained to wadis cut in the lava pile.

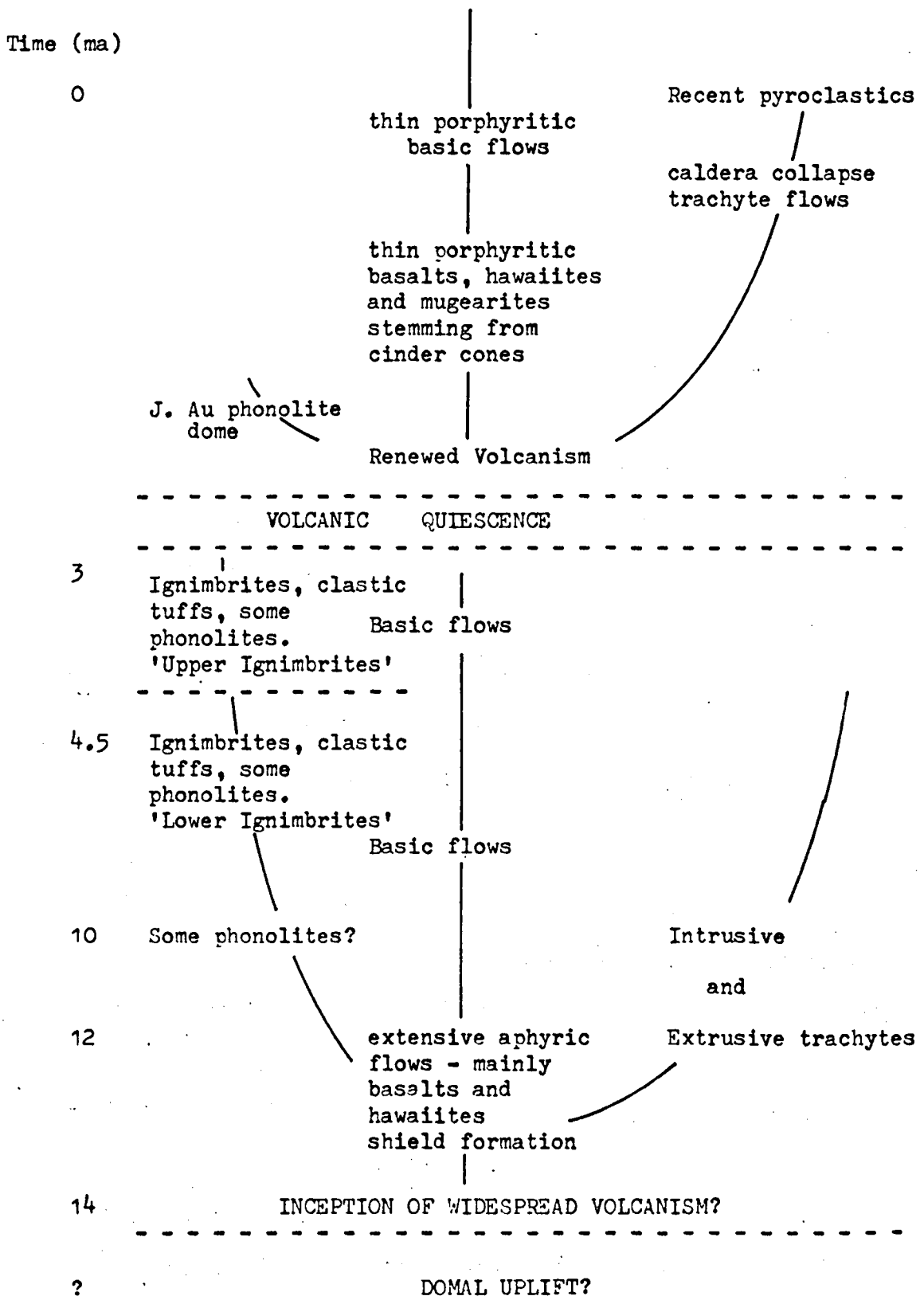
Between 12-10 ma there was a phase of widespread trachytic intrusion. Jebel Kirgo, for example, at Deribat was dated at 10.25 ma (Smith unpublished). A date of 11.6 ma was obtained.

Table 3.2 K-Ar Dates

<u>New Series</u>		<u>Old Series</u>	
24020	trachyte	0.06	ma
24025	trachyte	0.06	ma
Golo	basalt*	0.9	ma
24049	basalt	1.07	ma
Suni	basalt*	1.44	ma
24131	basalt	2.78	ma
24099	hawaiite	3.34	ma
24114	phonolite	3.00	ma
24015	phonolite	4.35	ma
24013	phonolite	2.50	ma (sill?)
24130	trachyte*	10.25	ma
24130	trachyte	11.60	ma
24090	hawaiite	11.20	ma
24059	trachyte	12.10	ma
Turra	trachyte	12.81	ma
Suni	scoria	14.30	ma

* data unpublished by K. Smith

Table 3.3 Geological History of Volcanism
at Jebel Marra



from the same body (at Leeds) which would indicate that there was, at least, more than one phase of intrusion. This would not be in contradiction with the field evidence as other trachyte intrusions in Jebel Marra display cross-cutting relationships.

Jebel Barra at Golo is a composite volcano which has alternating trachyte and basalt lavas. The rocks here tend to be weathered. However, an age was determined on a relatively fresh trachyte gave ages of 12.00 and 12.10 ma. A trachyte lava collected east of Turra has been dated at 12.81 ma (Smith, unpublished). Thus the age data so far suggests that the extrusive and intrusive trachytes are penecontemporaneous. Jebels Nima, Foga and Burie east of Dire and Jebel Ko (Plate 3.3) south of Turra occur as horizontal sill like trachyte masses about 50m in thickness which are present at roughly the same altitude. They are similar in petrography being microphyric with phenocrysts of alkali feldspar. The similarity may not be coincidental and they may well represent a major phase of trachyte intrusion.

3.3.1.2 Pyroclastic Sequence

The end of the Old Series of volcanism is marked by a period of intense pyroclastic activity producing approximately 1km of largely pyroclastic material and associated volcanics (Plate 3.4). Two main phases of pyroclastic activity are responsible. The first phase produced a succession of pyroclastics (Fig. 3.1) which extends from the Jebel Donsa area south and SE towards Gubbo. The regional dip of these deposits



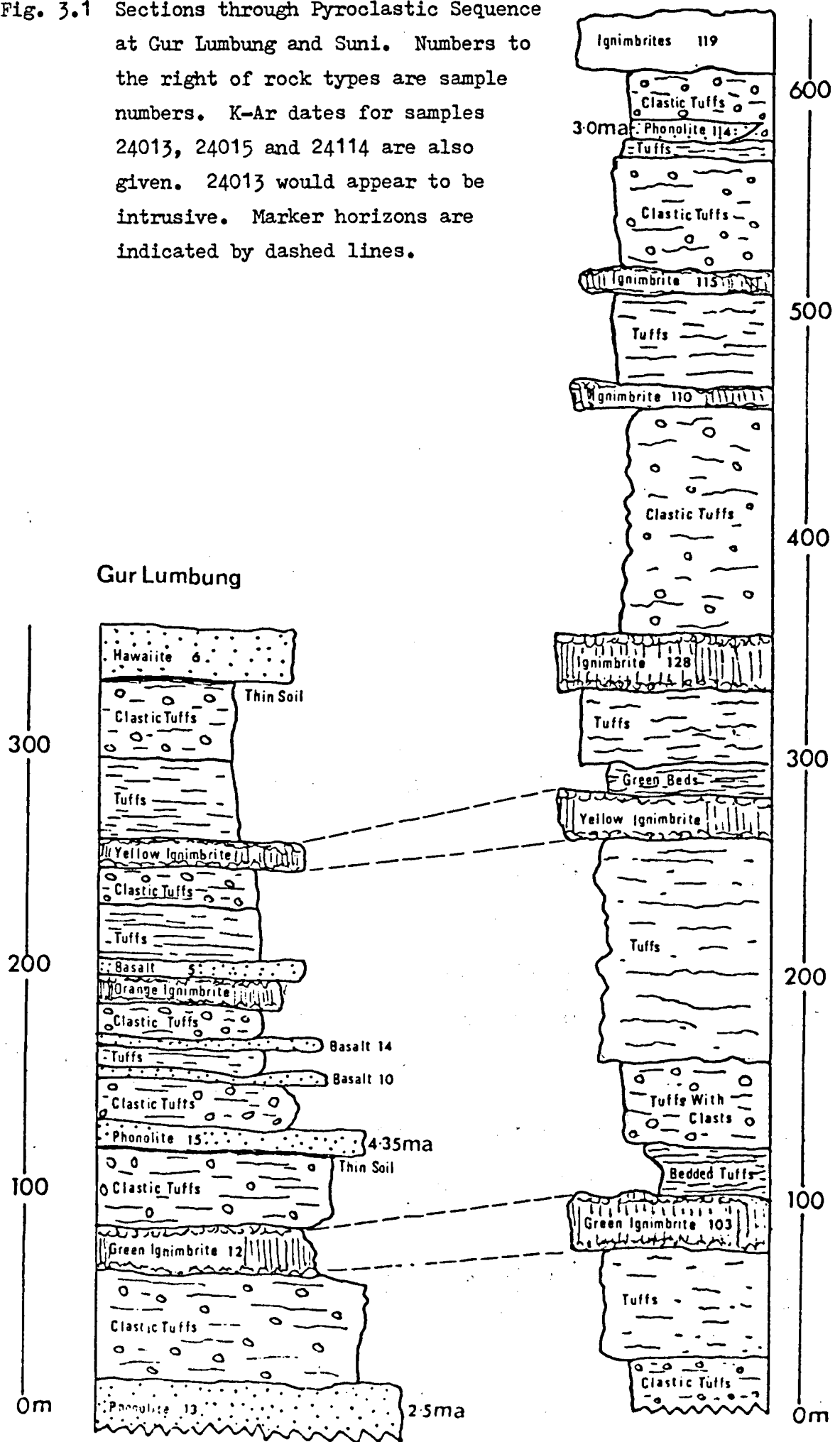
Plate 3.3 Trachyte intrusion at Jebel Ko.



Plate 3.4 Section of Pyroclastic Sequence near Suni.

Suni

Fig. 3.1 Sections through Pyroclastic Sequence at Gur Lumbung and Suni. Numbers to the right of rock types are sample numbers. K-Ar dates for samples 24013, 24015 and 24114 are also given. 24013 would appear to be intrusive. Marker horizons are indicated by dashed lines.



is also in this general direction. Barometric determinations of heights (Bermingham, unpublished) indicate that in the Gur Lumbung section the pyroclastics reach a thickness of about 400m. In the Gur Lumbung section (Fig. 3.1) the succession contains localised phonolites and thin basalts. This may suggest that the restricted distribution of these phonolites may be explicable in terms of a nearby centre. A maar like structure occurs just north of Gur Lumbung and may be a possible focus of activity but appears to be associated with more recent basaltic scoria volcanism. The dip and trend of the pyroclastics point to a centre in the north. Smith (unpublished) tentatively suggests a caldera like structure near Jebel Donsa. This comprises a 2km wide circular depression which is bounded to the north by trachyte intrusives and to the south by pyroclastics. There is a recent basaltic flow which stemmed from a cinder cone in the centre of the depression but this is unrelated temporally to the pyroclastics. This depression would pose a more likely candidate for a centre on both geographical as well as geomorphological grounds. If this is the case then the absence of phonolites in the Suni section implies that the Gur Lumbung phonolites although contemporaneous with the pyroclastics, in which they are interbedded, are indeed from a different local centre.

Following this early pyroclastic phase the locus of volcanism shifted (Smith, unpublished) southward to an area near Jebel Korongtong. This is based on the fact that the deposits are at their thickest here. The pyroclastic deposits, which are about 700m thick west of Suni, overlie the earlier

deposits with a shallow unconformity. These pyroclastic deposits dip E and NE and are largely restricted to central areas to the west of Suni. Plate 3.5 is taken from 1km south of Jebel Korongtong and may show one of the possible vents to these ignimbrites. The ignimbrites towards Uwo Fugo show a noticeably higher degree of welding than their Gur Lumbung counterparts which may also be indicative of a proximal source. However in this context, none of the lag breccias associated with near to source ignimbrite eruptions are observed (Druitt and Sparks, 1982).

In order to obtain an idea of the age and range of the Pyroclastic Sequence some selective age determinations were conducted on the interbedded phonolites. The results are presented in Table 3.2. It is apparent from Table 3.2 and Fig. 3.1 that the phonolite 24013 is intrusive. In fact it bears a close chemical resemblance to 24002 which occurs as a phonolite flow close to Gur Lumbung and may well be related.

The soil horizons discussed later in Section 3.4.2 are relevant in that they may point to breaks in activity hitherto only surmised from the angular unconformity observed between the main pyroclastic episodes. Also noted in the section are the occurrence of basic rocks which with 24099 and 24131 dated at 3.43 and 2.78 ma respectively indicates that basic volcanism is contemporaneous with the acidic pyroclastic activity.

After the pyroclastic activity there was a period of volcanic quiescence. During this time deep dissection of the erosively susceptible tuffs occurred, producing deep valleys



Plate 3.5 Two ignimbrites south from Jebel Korongtong.



Plate 3.6 Cinder cones near Torra Tonga.

and gorges. Reworked material forms poorly consolidated deposits west of Nyertete and south of Kalokitting much of which will have been the products of such erosion. Where more resistant layers occur, such as welded ignimbrites, plateaux have been left.

3.3.2 New Series Rocks

Following the volcanic hiatus activity was renewed giving rise to the New Series rocks. The form of the renewed volcanism was mainly basic flows which can usually be traced to individual vents mostly in the form of cinder or scoria cones (Plate 3.6).

Clearly, the movement of these lava flows would have been considerably influenced by the drainage pattern developed during the erosive phase. For instance, a cinder cone at Uwo Fugo near the top of the pyroclastic pile produced an extensive basalt flow which extends down about 600m before spreading out onto the 'old' lava shield plains east of Suni. The basic flows tend to be relatively narrow and are roughly disposed radially to the complex. There is a concentration of flows in the central and SW areas although examples are widespread over the area except for in the NW. Well over fifty cinder cones and vents have been identified from aerial photographs throughout the area which again underlines the widespread nature of the volcanism. The very existence of these unresistant cinder cones in itself points to eruptions in relatively recent times. For example, at Jebel Kertum there is preserved a tuff cone, which is very similar to very recent documented occurrences in Iceland (Leys, 1982). It is composed largely of unconsolidated scoria and ash.



Plate 3.7 Aerial view of Deriba caldera.



Plate 3.8 Trachyte dome at Tereng.

Some of the lavas of this series have been dated by K-Ar methods. A basalt lava NW of Suni is dated at 1.44 ma (Smith, unpublished) while another lava at Golo has an age of 0.9 ma (Table 3.2).

The volcanism later changed to a more acidic type as is illustrated by the caldera at Deriba and the trachyte volcanoes east of Nyertete. The caldera at Deriba represents the most spectacular feature on Jebel Marra (Plate 3.7). The caldera is 5km in diameter with its walls rising unevenly between 300 and 800m above the floor at 1200m above sea level. The collapse of the caldera is undoubtedly responsible for much of the surrounding pyroclastics which extend south and west for several km. They are principally air fall deposits and recent erosion has created a 'badland' topography. Ignimbrites are less common than in the earlier pyroclastics but are reported near the caldera wall (Williams et al., 1980). The floor of the caldera is occupied by two lakes (Fig. 3.2). The larger lake is saline and shallow, the smaller lake is less saline deep and circular in shape. The latter is set in an explosion crater in which at least five nested cones have been recognised (Williams et al., 1980).

Eruptions from the caldera are thought to be of a Plinian nature (Francis et al., 1973) and consist of airfall pumice deposits which contain accretionary lapilli. Such deposits have been reported (Francis et al., 1973) 20m in thickness, 5km away. Proximally the pumice deposits contain clasts as well as feldspar phyric glass. On the floor of the caldera and in some of the nearby fall deposits there are some cobbles and boulders of gneiss and granite, which may, as Francis et al., (1973) suggest, mean that the basement is not too far below. The floor of the caldera is covered in Pleistocene and Recent alluvium as well as lacustrine deposits (Williams et al., 1980).

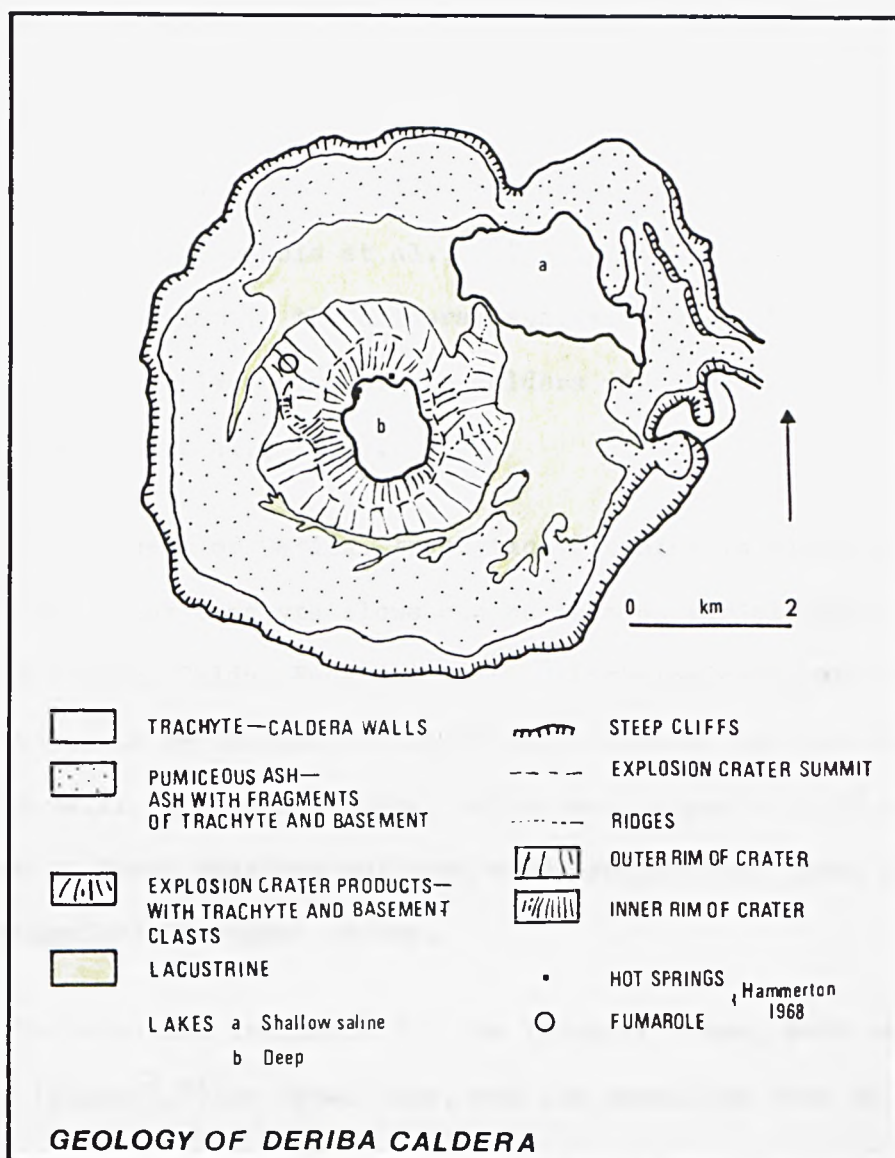


Fig. 3.2 Geology of Deriba caldera (redrawn from Williams et al., 1980).

A K-Ar date from a plug like feature on the north side of the caldera wall gave an age of 0.06 ma. A piece of carbonised wood recovered from the tuffs outside the caldera gave a radiocarbon age of 3520 yrs B.P. (Francis et al., 1973) and may represent the last phases of volcanism in the caldera associated with the inner cone. This would also place some of the caldera volcanism in historic times (Francis et al., 1973).

To the west of Deriba, trachytic volcanism is also evident. Short, but thick trachyte flows can be seen on aerial photographs of Jebels Gaur, Daldu, Fada and Gulbu. Lithologically and spatially, they appear to be related to the Deriba volcanics and probably temporally as well. A date from Jebel Daldu gave an age of 0.06 ma. The volcano at Jebel Fada has suffered more erosion than Jebel Daldu and may, therefore, be older in age.

No dates are available for the trachyte domes, such as at Tereng (Plate 3.8) or Jebel Toba, but the phonolite dome at Jebel Au has been dated at 2.35 ma and in fact may be more closely related to similar rocks from the Pyroclastic Sequence than to the New Series rocks.

3.4 Lithologies

3.4.1 Old Series Extrusives and Intrusives

The Old Series rocks, which comprise most of the area of the complex, are in general poorly exposed and variably weathered. The erupted products belong to the alkali olivine-basalt - trachyte series. Some phonolites are also present. Intermediate rocks occur in the form of hawaiites and mugearites.

The basalts tend to be black in colour and either aphyric or microphyric. Phenocrysts of olivine, clinopyroxene and plagioclase can be identified in hand specimen. In outcrop they are often exposed as rubbly lava fields covered in detritus, wind blown material or soil. They are sometimes veined with calcite and are well jointed. Some of the jointing is clearly related to cooling such as at Nyertete where the basalts display beautiful columnar joints. Although the map reveals an extensive area of Old Series rocks, the presence of good fresh exposure is unfortunately rare.

To the north of the map, in particular, the basic lava shield has been punctured by trachytic intrusions (Plates 3.2-3). Their positions in the pile, coupled with their cross-cutting relationships with other trachytes, as well as their outcrop patterns, which often are in the form of dykes, ring dykes or sills, are suggestive of high level intrusion. The most extensive exposure of trachyte is north of the pyroclastic complex where there is a 6km ridge of trachyte which passes through Jebel Tila in a N-S direction. Some of the trachytes, curiously, occur as hexagonal 'ring dykes' such as at the nested intrusions south of Jebel Burei. The intrusions of Jebels' Nima, Foga and Burie east of Dire and Jebel Ko (Plate 3.3) south of Turra occur as horizontal trachyte masses about 30m in thickness outcropping at roughly the same altitude. They are, also, all microphyric containing phenocrysts of alkali feldspar. Trachyte plugs and spines also appear partly covered by later pyroclastic rocks and New Series rocks. Some of the trachytes are extrusive such as at Jebel Barra and also east of Turra. In some isolated outcrops, however, where contact and chilling relations are absent and weathering and erosion have been active it is difficult to distinguish between intrusive and extrusive trachyte.

3.4.2 Pyroclastics

The pyroclastic deposits represent a thick succession of rocks in the central and southern part of the area and were produced at the end of the Old Series period of volcanism. They comprise a 1000m section of welded and unwelded ignimbrite deposits and clastic pumice tuffs. Locally they are interbedded with feldspar phyric phonolites and thin basic flows. Two sequences have been recognised (Smith unpublished) which dip at shallow angles but show a slight angular unconformity with respect to each other.

The lower ignimbrite sequence (Fig. 3.1) at Gur Lumbung reveals that the sequence is composed of thick clastic pumice deposits interbedded with ignimbrites and phonolites. The clastic pumice tuffs are white deposits containing unwelded pumice fragments and clasts of various lithologies. These clasts are mainly of trachyte, phonolite, glass or sometimes of basement rock. Although variable, the clasts tend only to be a few cm in size. In this section there are two ignimbrites which are characterised by having a rubbly base, which grade into more massive ignimbrite, which in turn, grade into bands containing glass. The glassy bands typically contain phenocrysts of feldspar. These grade into massive ignimbrite before again developing a rubbly top. The massive ignimbrite contains pumice fragments which are usually flattened and streaked out but some remain unflattened. Small clasts of trachyte are often present. Commonly, the ignimbrite displays crude columnar jointing. The two ignimbrites in this section both have distinctive colours which made them particularly useful as marker horizons (Fig. 3.1).

Within the sequence there are several phonolites which are feldspar phyric and extremely fresh. Some of the lavas (24015 and 24006) are underlain by a thin red crumbly deposit which is probably a soil formation. Thin weathered aphyric basalt flows are also present within the section.

In the Suni section (Fig. 3.1) the distinctive ignimbrites of the Gur Lumbung section are picked up again at the same relative positions. The upper ignimbrite section is seen here although its precise contact with the lower deposits is obscure. The upper pyroclastics are largely restricted to central areas. The 300m thick section of upper ignimbrite also contain similar clastic pumice tuffs, but differ from the lower series in that the ignimbrites show a higher degree of welding and are less structured than the less welded equivalents, notwithstanding the similarity in the rubbly base. Another important difference is that there are fewer phonolites than in the lower section.

3.4.3 New Series

The alkali olivine-basalt - trachyte suite of the Old Series is again repeated in the New Series rocks, although there are more examples of hawaiites and mugearites and much fewer phonolites.

Cinder cones, flows, pyroclastics and vents are present throughout the area although they are more common in southern, south-western and central areas. In contrast to the basic flows of the Old Series the New Series lavas are usually more porphyritic. The most primitive lavas, for example, possess phenocrysts of olivine, while slightly more evolved lavas typically contain clinopyroxene as well. Hawaiites and mugearites, however, contain plagioclase and clino-

pyroxenes and less olivine. Basic lavas, such as at Suni, are occasionally very porphyritic and can also contain large megacrysts of intergrown clinopyroxene and feldspar. A feature of the New Series basic lavas is that they are extremely fresh and only rarely vesiculated.

The caldera wall at Deriba is composed of trachyte. The trachyte is porphyritic, containing large phenocrysts of alkali feldspar. In fresh samples the groundmass is lilac in colour becoming yellow to orange with increasing degrees of weathering. The feldspars are commonly coloured yellow although they are still apparently fresh. Ignimbrites are reported in the vicinity of the caldera wall (Williams et al., 1980) but are overshadowed by the volume of airfall pyroclastics. Pumiceous tuffs occur extensively around the caldera, some of which contain accretionary lapilli. The trachytes to the west of the caldera are in general lithologically similar to those at Deriba except at Jebel Fada where the trachytes are only microphyric with respect to feldspar. The trachytes which form the domes also tend to be microphyric as indeed is the phonolite dome at Jebel Au.

3.5 Conclusions

The geology of the Jebel Marra volcanic complex may be conveniently divided into Old Series and New Series rocks. The end of the Old Series culminated with a period of intense pyroclastic activity. Prior to New Series volcanism there is a period of quiescence in which extensive erosion occurred.

In conclusion, it is worth noting the striking array of cinder cones and volcanic vents which trend in a NW-SE direction and include

Jebels Kertum, Kirsin Tonga and Jebel Kuro and which are cross-cut by a NE-SW trending volcanic line which include the cones at Queer, the caldera east of Jebel Umar, through Kertum and the Deriba caldera. Such a surface expression of volcanism cannot be coincidental and must relate to major structures in the crust.

CHAPTER FOUR

PETROGRAPHY

4.1 Introduction

In this Chapter the petrography of the Jebel Marra suite will be briefly described and illustrated with photomicrographs. Petrographic differences between the Old and New Series will be highlighted where it is appropriate. It is intended to document those features of the petrography which can be drawn upon in later geochemical Chapters. Details of individual specimens are presented in tabulated form in Appendix H.

4.2 Petrography

Petrographical descriptions will be given under rock type headings. Classifications of the rock types are given in Chapter 6.

4.2.1 Basalts

The New Series primitive basalts characteristically contain about 10% microphenocrysts which are dominantly olivine. Sometimes the olivines are slightly corroded or rounded and occasionally they possess orange alteration rinds. Clinopyroxene phenocrysts do occur but plagioclase is rare. The groundmass tends to be dominated by clinopyroxene, plagioclase and opaques although olivine is always present. The groundmass is usually microlitic and sometimes interstitial glass is present. Plate 4.1 shows a typical primitive basalt.

Although there is no sharp boundary, less primitive basalts tend to contain proportionally less phenocrysts of olivine and more phenocrysts of plagioclase and particularly clinopyroxene (Plate 4.2). The phenocryst content and grain size is variable. The groundmass grain size is also variable from microlitic to coarse grained.

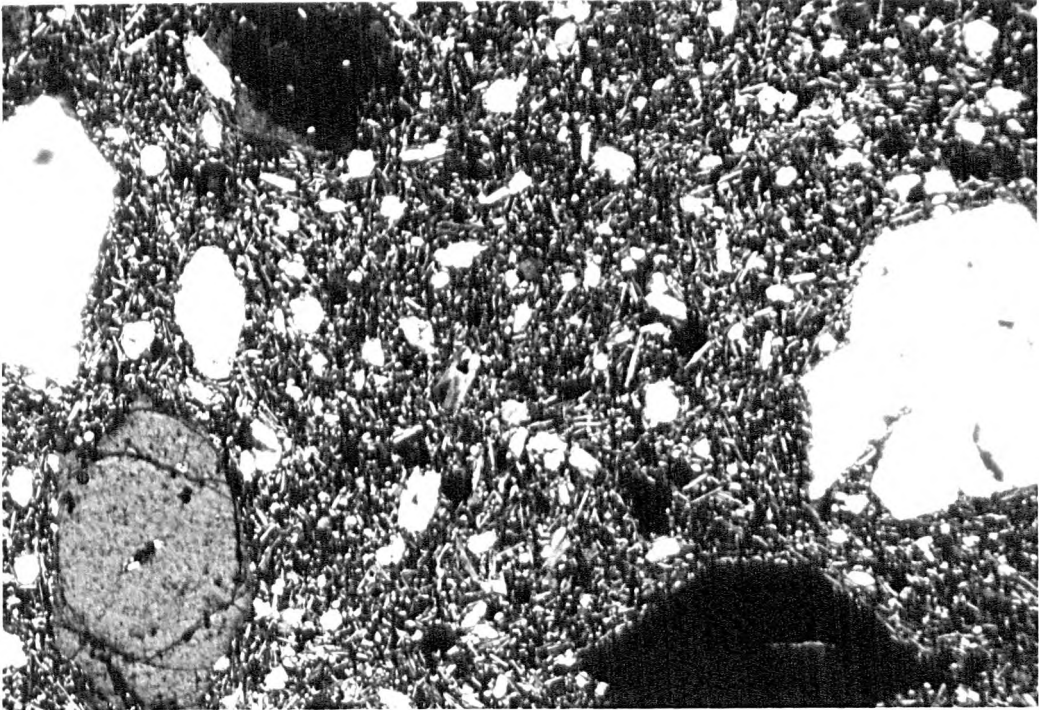


Plate 4.1 Primitive basalt (24088). Note presence of idiomorphic olivine phenocrysts, zoned clinopyroxene bottom right. Crossed nicols, X 40.

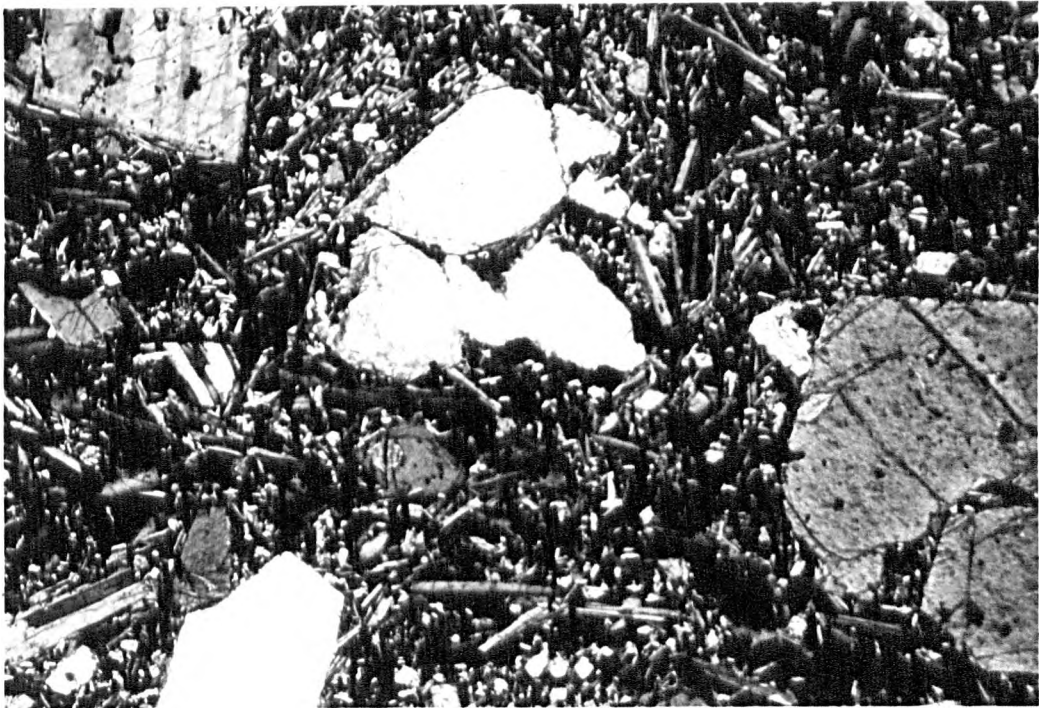


Plate 4.2 Basalt (24001). Idiomorphic olivine phenocrysts. Plagioclase phenocryst top left. Crossed nicols, X40.

Usually, more evolved basalts tend to be more porphyritic as opposed to the more microphyric primitive basalts.

The Old Series basalts show many of the features of the New Series basalts and are similarly variable in mineralogy, mineral proportion and grain size. In general, they are more aphyric with smaller phenocrysts contained in a finer groundmass. The groundmass often shows preferential alignment of plagioclase laths. Plagioclase and olivine in particular, appear to have been affected to a greater extent by alteration (Plate 4.3).

4.2.2 Hawaiites

The hawaiites are much more variable in mineral morphology and mineral proportion ranging from about 30% phyrlic to 5% microphyric. Plagioclase becomes more important modally but clinopyroxene and olivine are still important phenocryst phases. In some hawaiites plagioclase phenocrysts dominate over clinopyroxene phenocrysts, whilst in others clinopyroxene is more abundant. Some of the phenocrysts especially plagioclase, are rounded and partly resorbed. Plagioclase crystals sometimes have digested cores. Zoning in plagioclase and clinopyroxene is commonly observed. The groundmass tends to be dominated by plagioclase and opaques and preferred orientations of plagioclase laths are common (Plate 4.4). Groundmass clinopyroxene and olivine tend to be less abundant.

It is difficult to contrast hawaiites of the Old Series with the New Series because the latter are so variable. However, in general, Old Series hawaiites are less porphyritic and often have a finer groundmass.

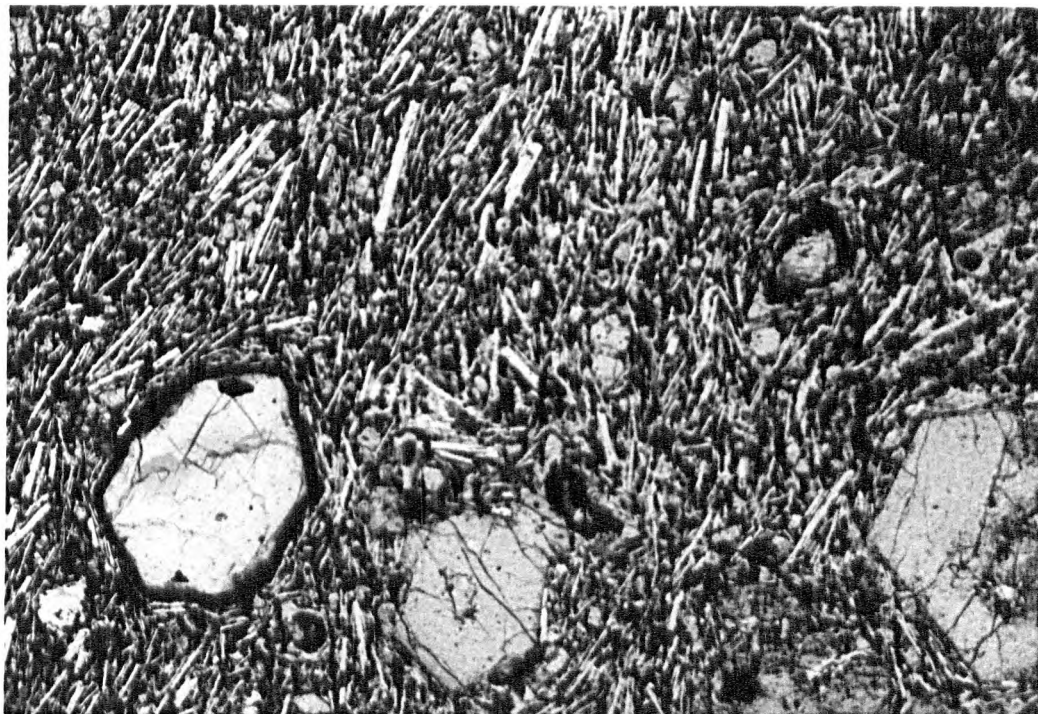


Plate 4.3 Old Series basalt (24029). Note rinds to olivine microphenocrysts, also feldspathic matrix shows preferential alignment of laths. Crossed nicols, X40.

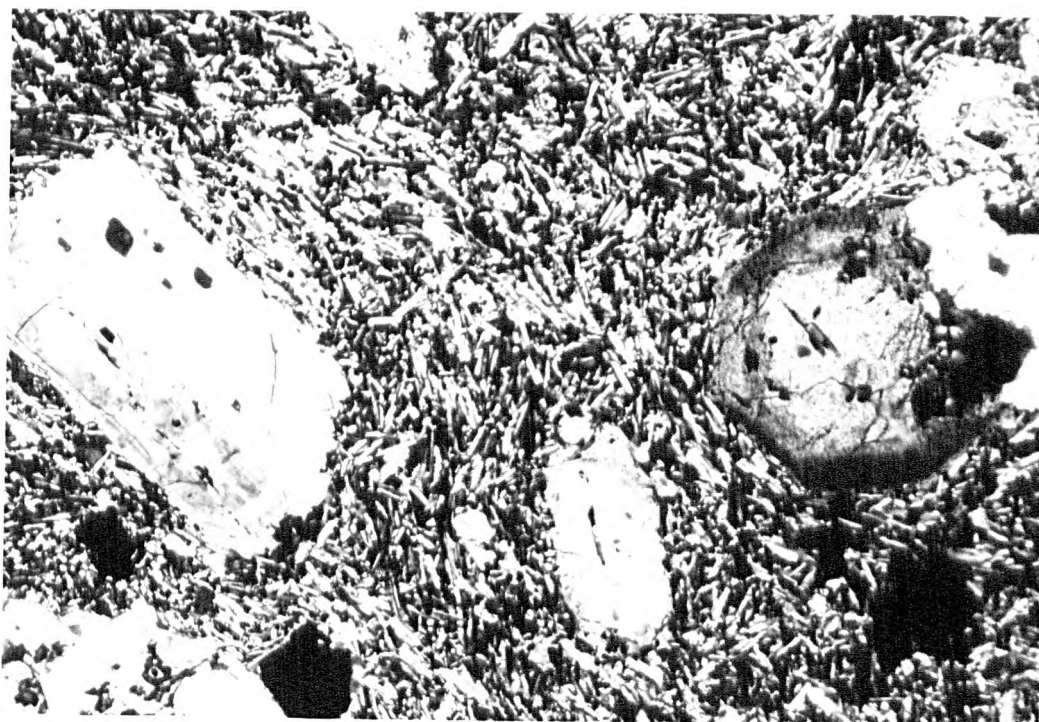


Plate 4.4 Hawaiite (24118). Phenocrysts: plagioclase left, zoned clinopyroxene right and olivine in centre. Crossed nicols, X40.

4.2.3 Mugearites

Mugearites are typically about 20% phyrlic although again they vary in phenocryst content and grain size (Plate 4.5). The phenocryst mineralogy is dominated by plagioclase which can be up to 1cm in length. Phenocrysts of clinopyroxene and less commonly olivine occur, but these are usually smaller than the plagioclase grains. Microphenocrysts of magnetite can occur and small prismatic crystals of apatite are also readily identifiable.

The mugearite members of the Old Series are, in many respects, similar to New Series mugearites but additionally contain microphenocrysts of pale green clinopyroxene rather than light brown clinopyroxene. The groundmass is fine grained and is dominated by plagioclase and opaques: clinopyroxene and olivine are less common. One sample (24061) contains numerous crystals of iron oxide rimmed kaersutite. These appear to represent the disaggregated remains of a kaersutite-plagioclase nodule.

4.2.4 Megacrysts

Throughout all of the above rock groups large xenocrysts (Plate 4.6-7) of clinopyroxene, olivine and plagioclase are sometimes seen. They are characteristically larger than phenocryst phases, often highly resorbed and digested and often carry inclusions of other minerals. They also sometimes show strain features such as shadowy extinction and fractures.

4.2.5 Trachytes

1) New Series caldera trachytes

These occur in and around the Deriba caldera. They are typically highly porphyritic with potassium feldspar comprising 95% of the

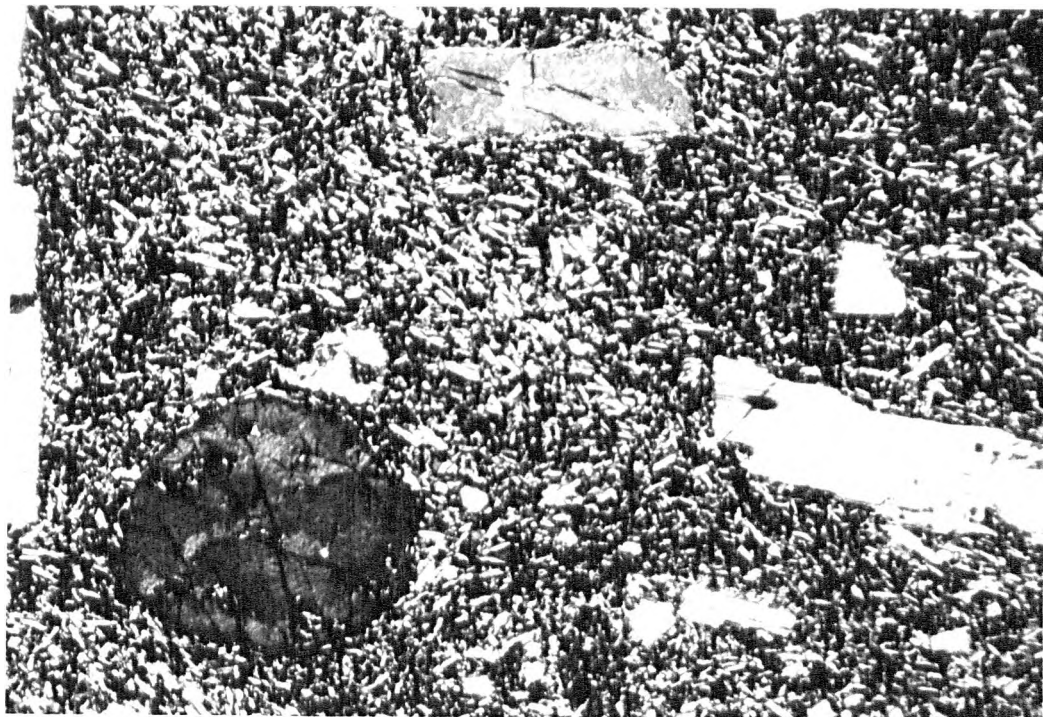


Plate 4.5 Mugearite (24104). Note zoned clinopyroxene on left , plagioclase on right and olivine phenocryst in centre. Crossed nicols, X40.

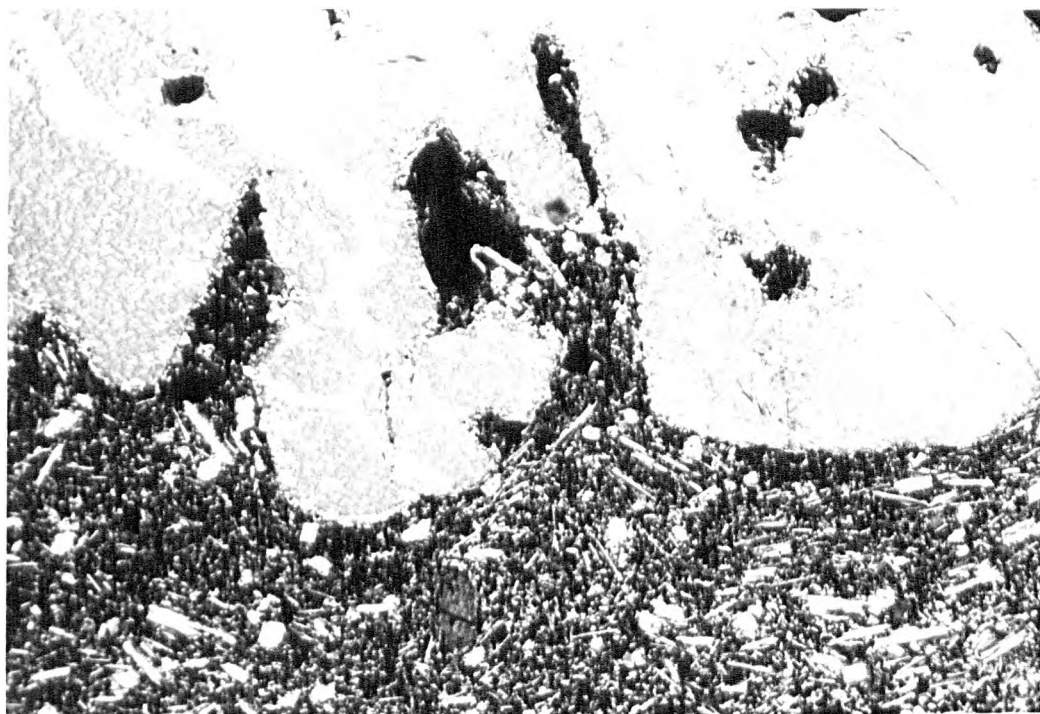


Plate 4.6 Partly resorbed olivine megacryst in basalt (24045). Crossed nicols, X40.

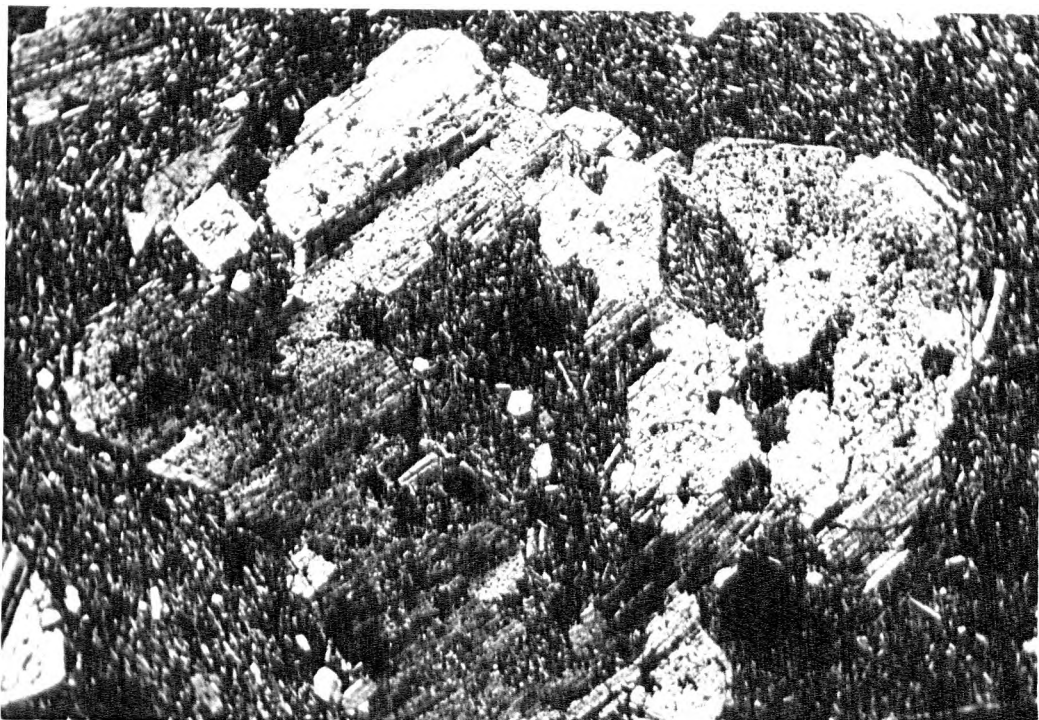


Plate 4.7 Partly digested plagioclase megacryst in basalt (24014).
Crossed nicols, X10.



Plate 4.8 Caldera trachyte (24016). Note twinned anorthoclase
set in typical 'trachyte' groundmass.
Crossed nicols, X40.

phenocrysts. The phenocrysts tend to be very fresh and only occasionally show resorption features. Also they commonly contain a few pale green microphenocrysts of light green clinopyroxene. The groundmass is composed predominantly of coarse grained feldspar displaying good 'trachytic' texture (Plate 4.8). Opaques are also important in the groundmass.

ii) New Series mafic bearing trachytes

These trachytes (Plate 4.9) typically contain plagioclase, potassium feldspar, clinopyroxene and olivine as phenocrysts. Sometimes the plagioclase phenocrysts are rimmed by potassium feldspar. Most often the mafic minerals are heavily resorbed and altered and perhaps 'xenocryst' would be a more appropriate term than 'phenocryst'. In more altered samples pseudomorphs after clinopyroxene and olivine can be recognised. The groundmass is principally composed of feldspar but does not possess the 'trachytic' texture noted in the caldera trachytes.

iii) Old Series trachytes

These bear a close resemblance to the caldera trachytes. They are typically porphyritic containing predominantly potassium feldspar phenocrysts. Again the groundmass feldspars display a 'trachytic' texture. Opaques and aenigmatite are also present in some samples. In general, they contain less clinopyroxene crystals and sometimes contain a deep green mineral in the groundmass which is probably an alkali amphibole.

4.2.6 Phonolites

i) Old Series phonolites

The phonolites (Plate 4.10) of the Pyroclastic Sequence contain extremely fresh phenocrysts of potassium feldspar which may comprise

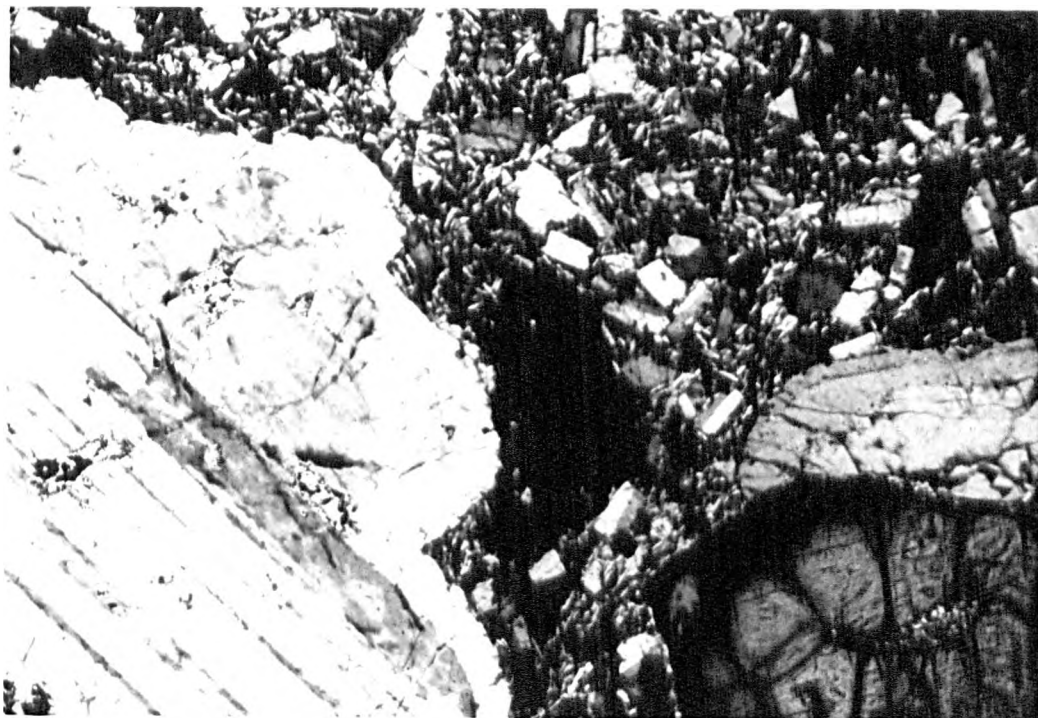


Plate 4.9 Mafic bearing trachyte (24031). Note altered olivine, bottom right, and presence of plagioclase xenocryst rimmed with anorthoclase. Crossed nicols, X40.

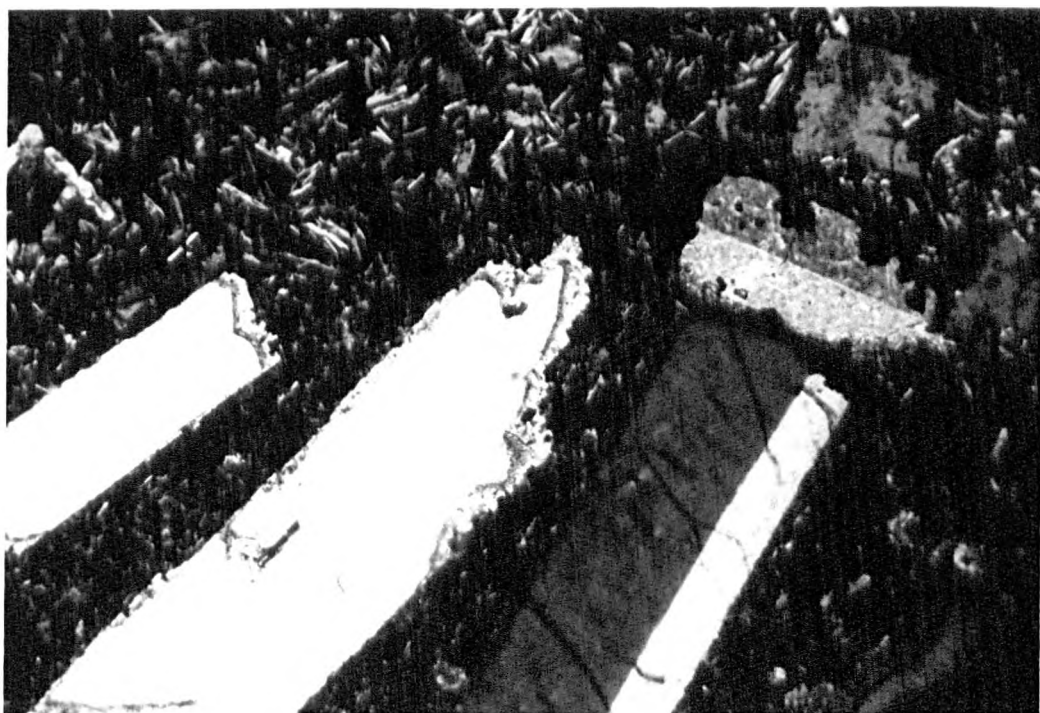


Plate 4.10 Phonolite (24114). Note twinned salite microphenocryst above three anorthoclase phenocrysts. Crossed nicols, X40.

up to 20% of the rock. These are often resorbed sometimes to a high degree. Pale green, often zoned, light green clinopyroxene microphenocrysts are present as well as microphenocrysts of biotite and opaques. Feldspar laths usually exhibit a 'trachytic' texture. The groundmass is fine grained containing feldspar and alkali amphibole, but very few opaque minerals are present. The most evolved phonolite (Plate 4.11) contains microphenocrysts of nepheline surrounded by a late stage development of aenigmatite.

Older, Old Series phonolites, not belonging to the Pyroclastic Sequence, are similar but tend to have a more altered groundmass than the above phonolites.

ii) New Series phonolite

The one example of a phonolite in the New Series shows more signs of alteration than the above phonolites, particularly in the groundmass. Phenocrysts of potassium feldspar are predominant with some opaque microphenocrysts. Pseudomorphs probably after biotite are also present. The feldspar dominated groundmass displays a 'trachytic' texture.

4.2.7 Ignimbrites

Sections of these vary according to where in the unit it had been collected from. Typically, the glassier portions contain flame, flattened and unflattened pumice fragments, crystals of potassium feldspar, light green clinopyroxene, biotite and opaques as well as containing xenoliths which are mainly either of trachyte or phonolite. Eutaxitic texture (Plate 4.12) is typically very well displayed.



Plate 4.11 Nepheline phonolite (24015). Note aenigmatite sheaths growing around nepheline microphenocrysts. Plane polarised light, X40.

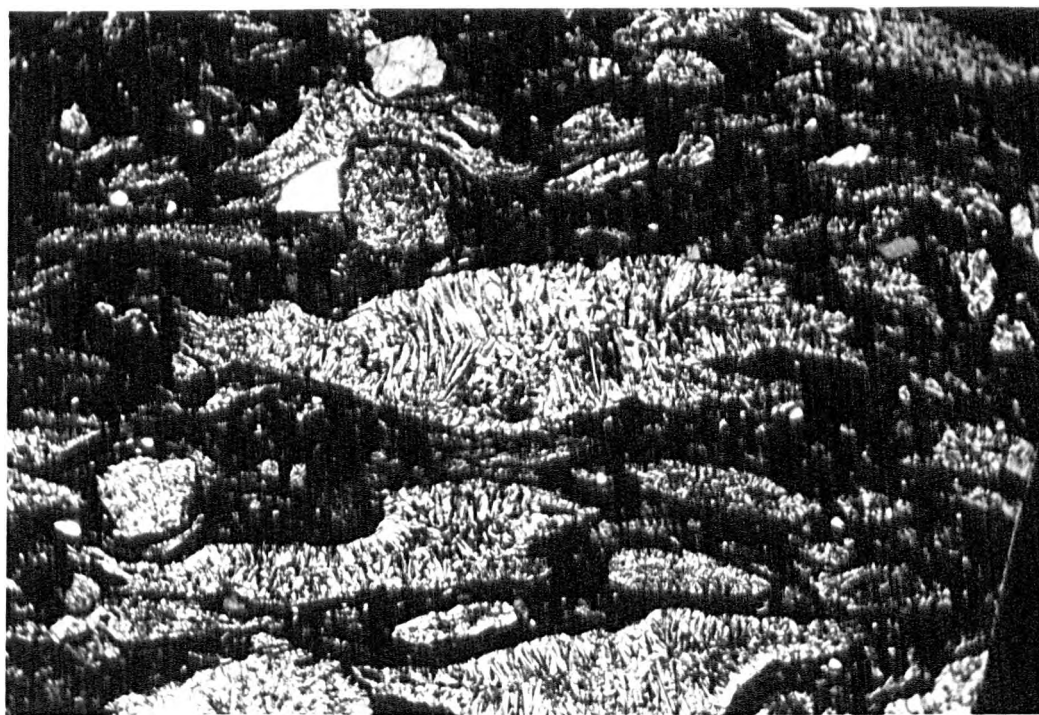


Plate 4.12 Eutaxitic texture in ignimbrite (24012). Crossed nicols, X10.

4.3 Conclusions

Despite the great diversity in petrography of the Jebel Marra volcanics, there are systematic changes in mineralogy and mineral proportions which can be correlated with rock compositions. For example, from basalts to mugearites there is a general decrease in olivine phenocryst content, an increase in plagioclase phenocryst content and an increase in clinopyroxene phenocrysts from primitive basalts to rocks of approximately hawaiite composition which is followed by a decrease to mugearitic rocks. This is schematically illustrated in Fig. 4.1 where the approximate modal % of phenocrysts is plotted against rock composition. Abundances of olivines, clinopyroxene and plagioclase in the groundmass, to some extent, mirror these trends. Opaque minerals comprise the remainder of the groundmass minerals. Only rarely is it possible to discern the order of crystallisation from textural evidence.

The mafic bearing trachytes contain partly resorbed mafic minerals. The occurrence of olivine, clinopyroxene and particularly plagioclase rimmed by potassium feldspar in these trachytes could be interpreted as evidence for mixing of a basic magma with a more acidic magma. The other trachytes are generally dominated by potassium feldspar both as phenocrysts and in the groundmass and also commonly exhibit a 'trachytic' texture which is not present in the mafic bearing trachytes. The differences between these two groups of trachytes will be considered further in later Chapters. Phonolites differ from trachytes in containing less opaques and also by having more microphenocrysts of biotite and more rarely nepheline.

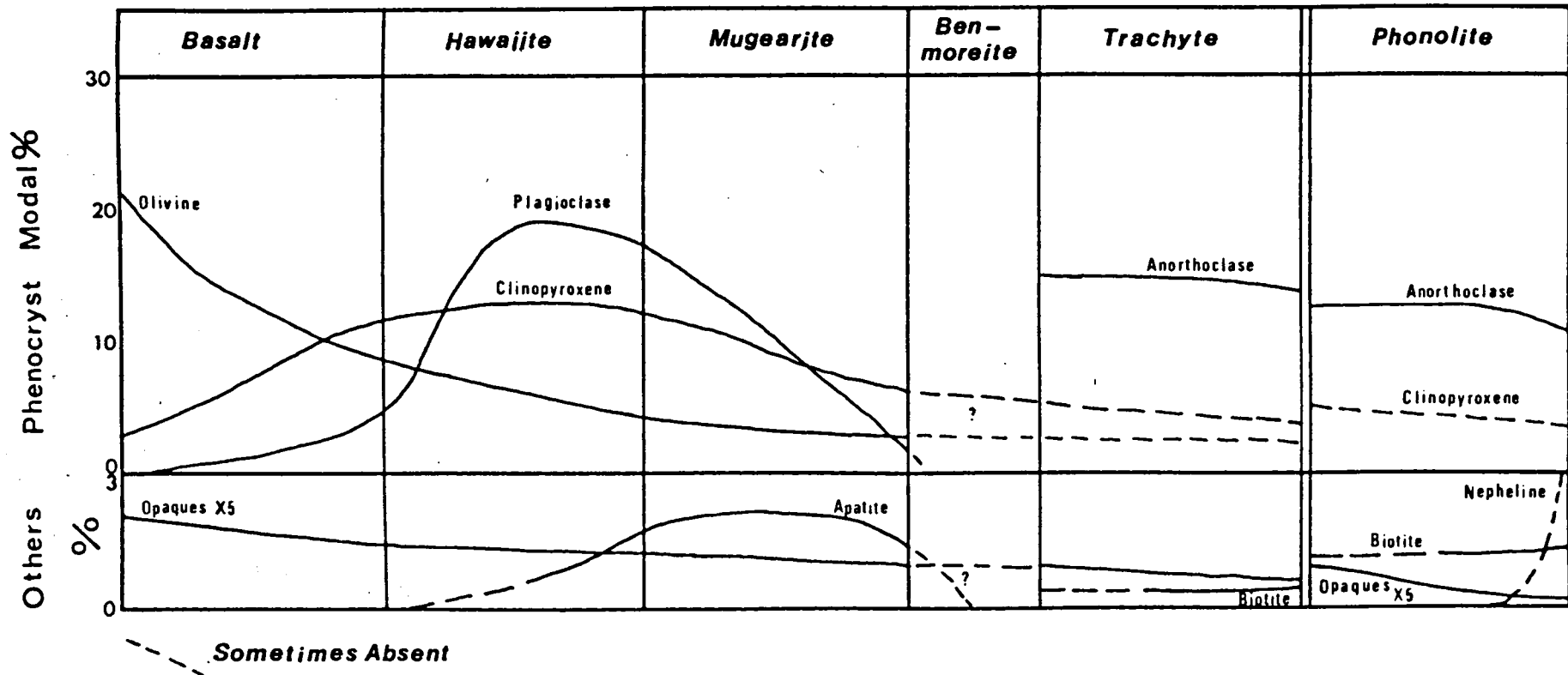


Fig. 4.1 Diagram illustrating the approximate variation of phenocryst modal proportions and other phases with changing rock type. Dashed lines indicate that a given phase may or may not be present.

Petrographic differences between Old and New Series rocks are mainly reflected in a tendency for the former to be less porphyritic and also to be slightly more altered.

CHAPTER FIVE
MINERAL CHEMISTRY

5.1 Introduction

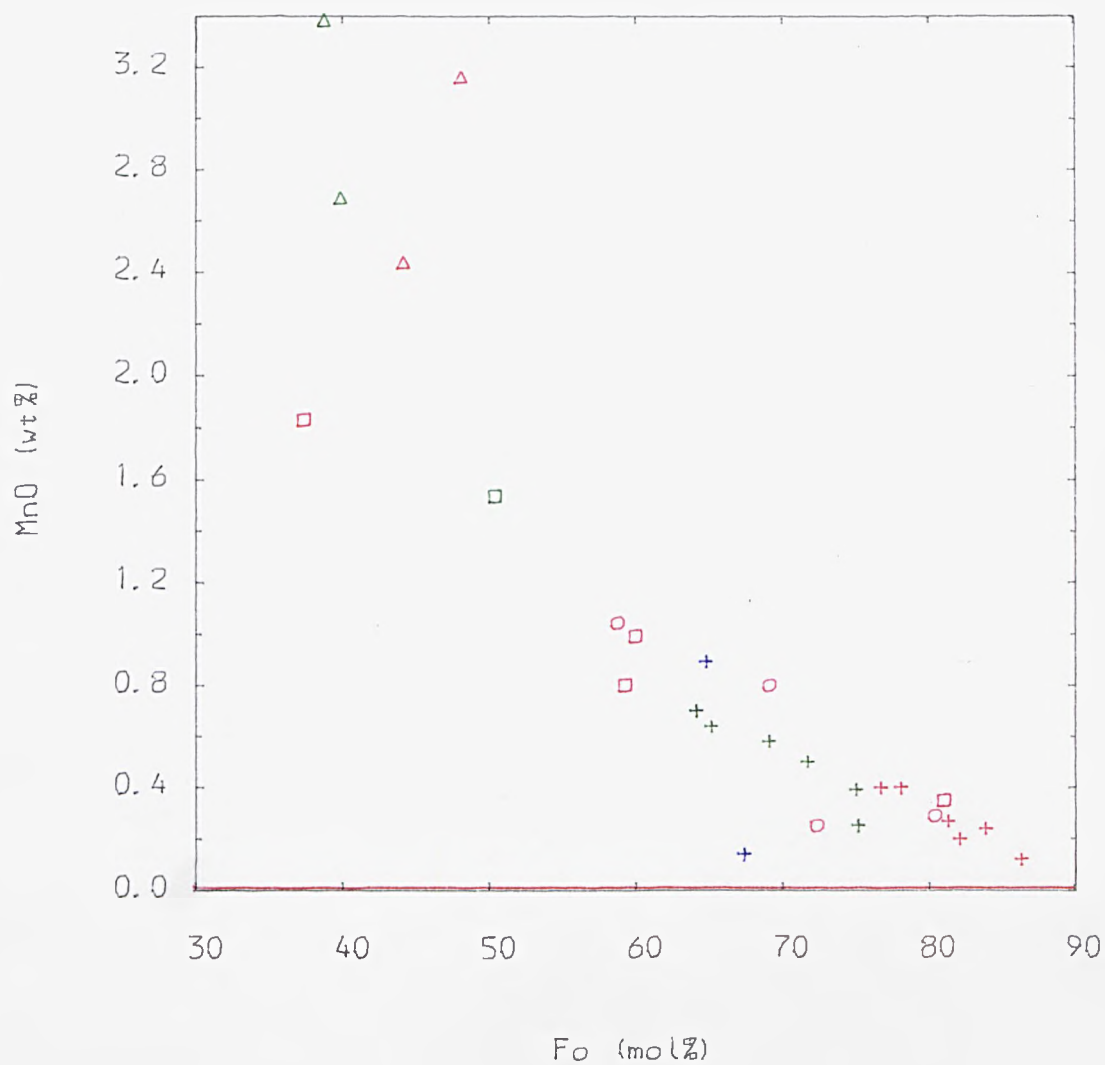
Analyses of the phenocryst phases throughout the suite have been primarily obtained for use in modelling calculations (Chapter 9). As a result the data set is not sufficiently complete to allow detailed study of the possible differences in Old and New Series mineral chemistry. Nevertheless, it is possible to present an overall view of the mineral chemistry of the major phases and the changes in mineral composition that occur as whole rock composition changes. The mineral analyses were performed on an electron microprobe using an E.D.S. system: the analyses and method of analysis are documented in Appendix B.

5.2 Olivine

Olivine is present in all the rock types apart from phonolites, although it is uncommon in trachytes. It is most abundant in primitive basalts. The mineral occurs as euhedral phenocrysts, partly resorbed phenocrysts, anhedral groundmass crystals or as megacrysts. The phenocrysts are invariably zoned towards more fayalitic compositions at the rim. The overall compositional range is from Fo₈₆ to Fo₃₇ in basalts to trachytes respectively. MnO shows a good negative correlation with Fo content (Fig. 5.1). Some of the more fayalitic phenocrysts, particularly in the trachytes, are unusually rich in MnO (up to 3.5 wt%).

5.3 Clinopyroxene

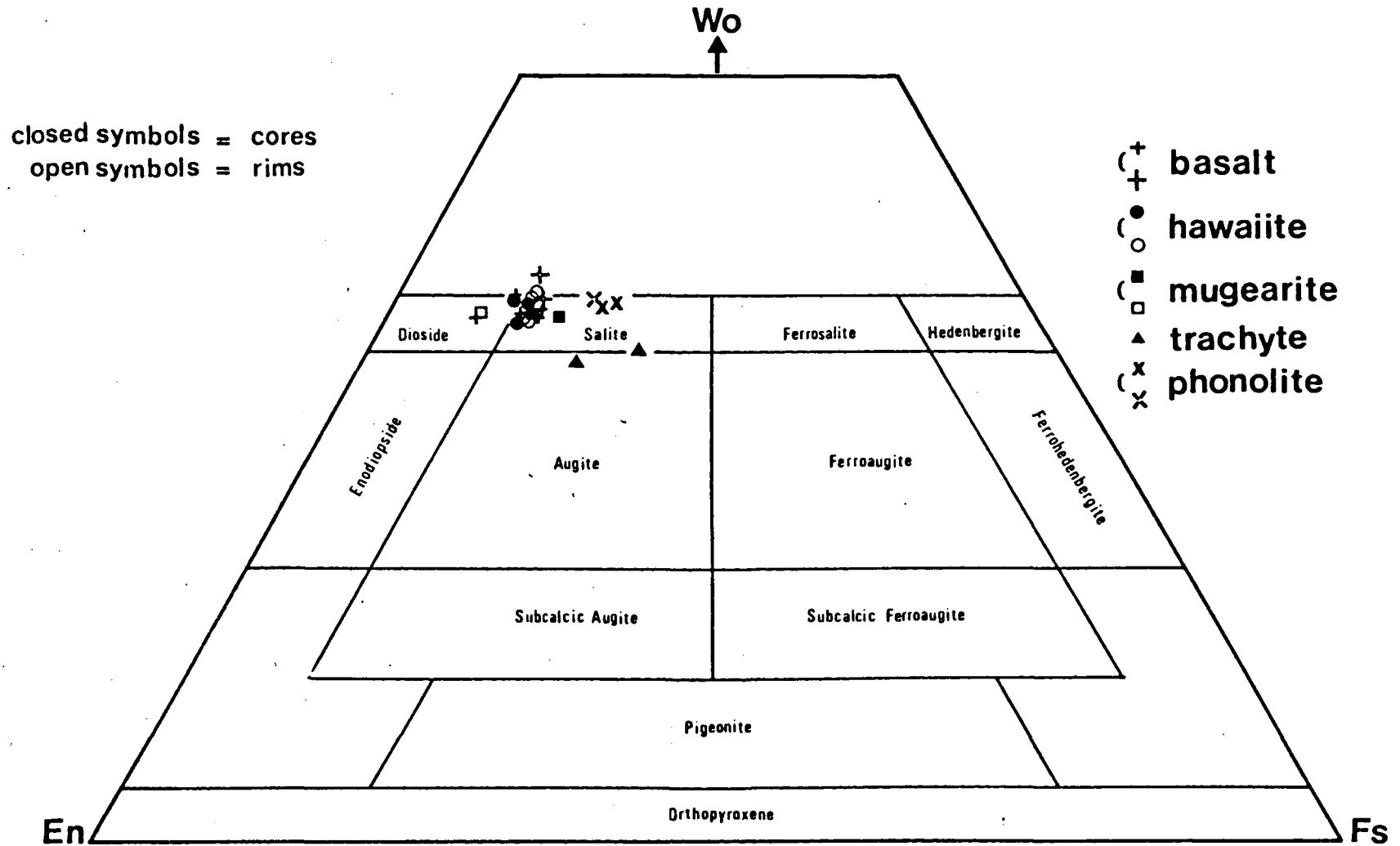
Clinopyroxene is present in all the rock types and is also present in the glassy parts of ignimbrites. In acidic rocks the clino-

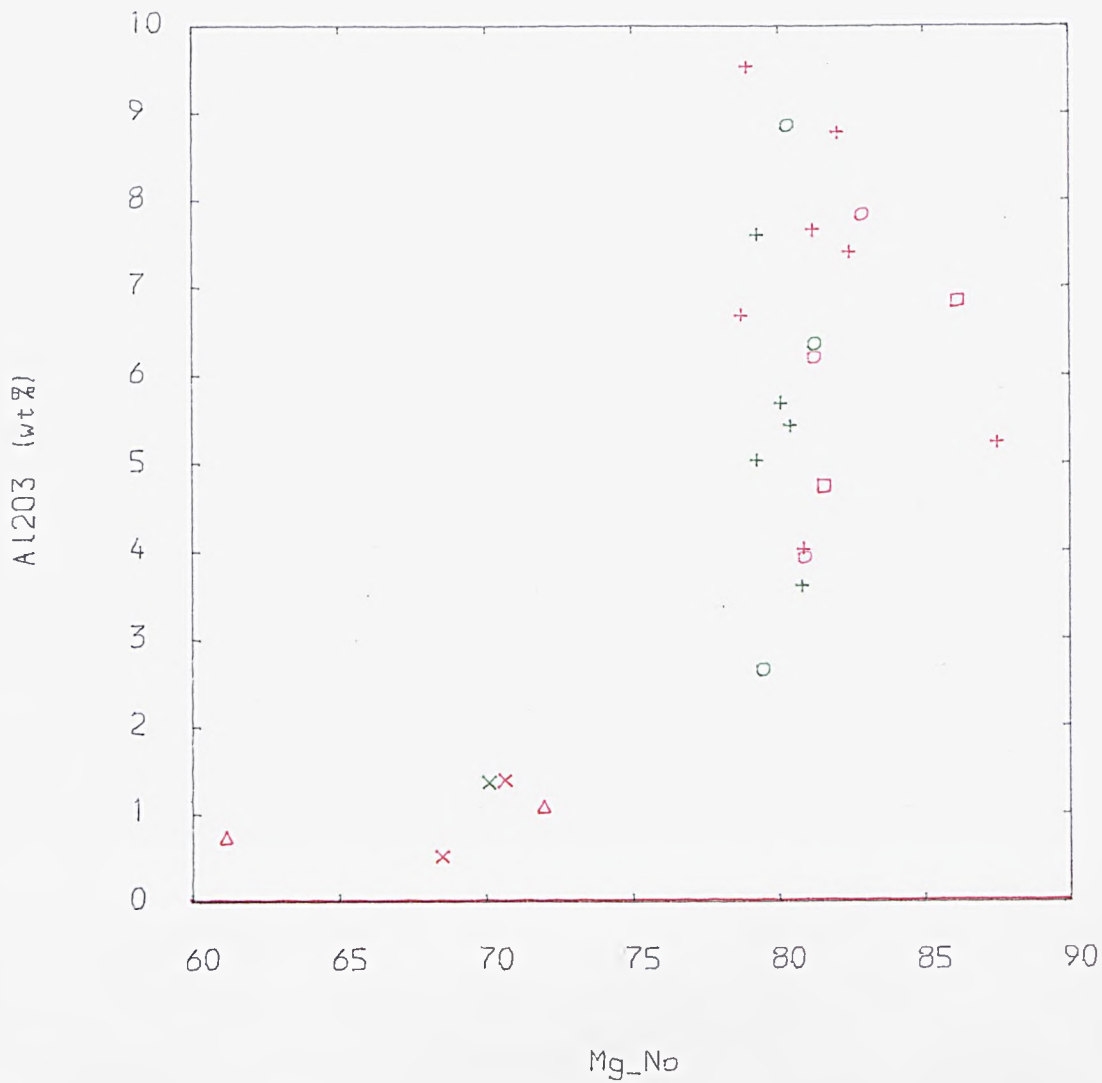


TITLE : Fig : 5.1 MnO vs Fo mol% in olivine

CORE = red
 RIM = green
 GMASS = blue

Fig. 5.2 Core and rim analyses of clinopyroxenes plotted on wollastonite–enstatite–ferrosilite triangle. (Classification after Poldervaart and Hess, 1951).





TITLE : Fig : 5.3 Al₂O₃ vs Mg No. in cpx

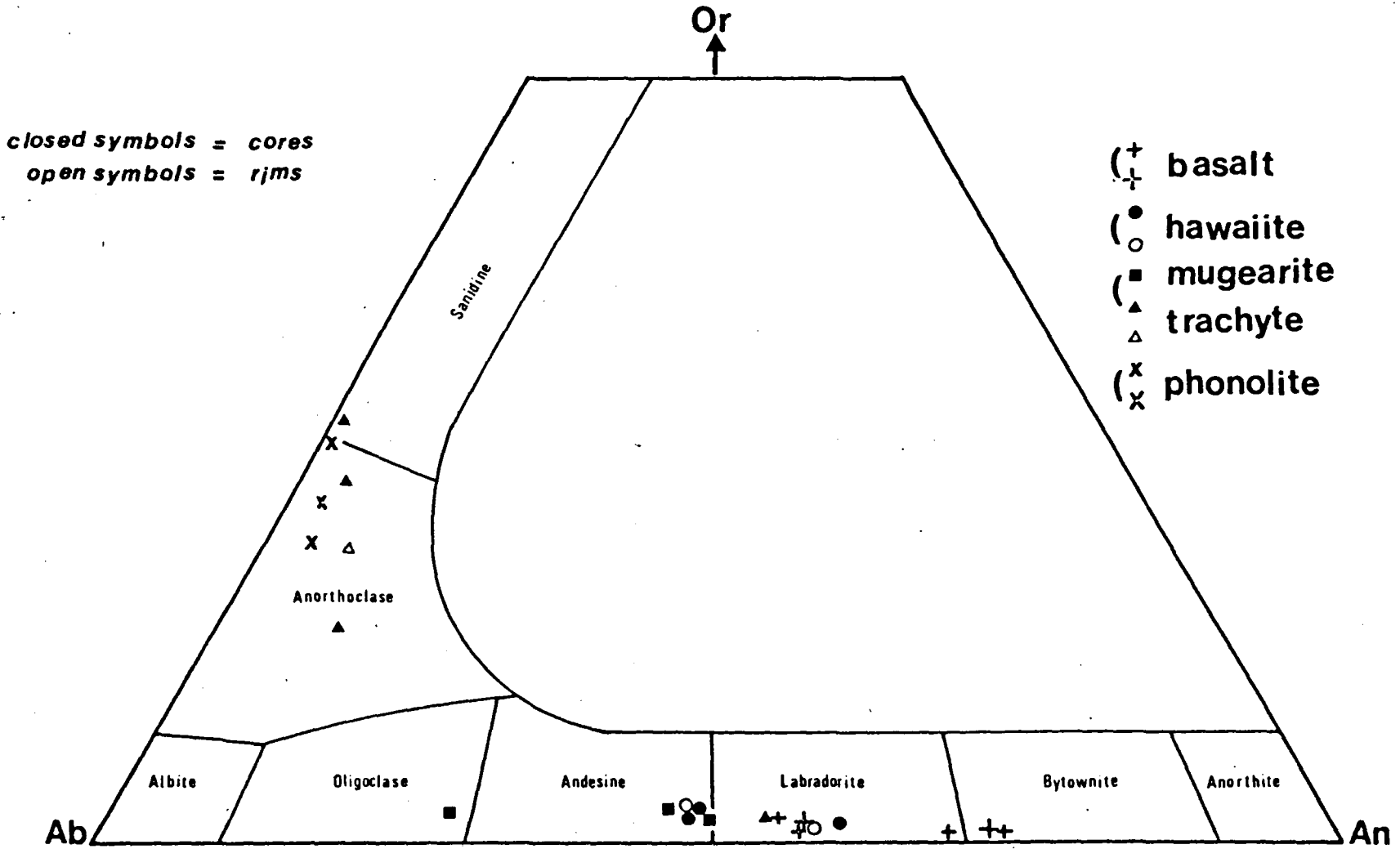
CORE = red
RIM = green

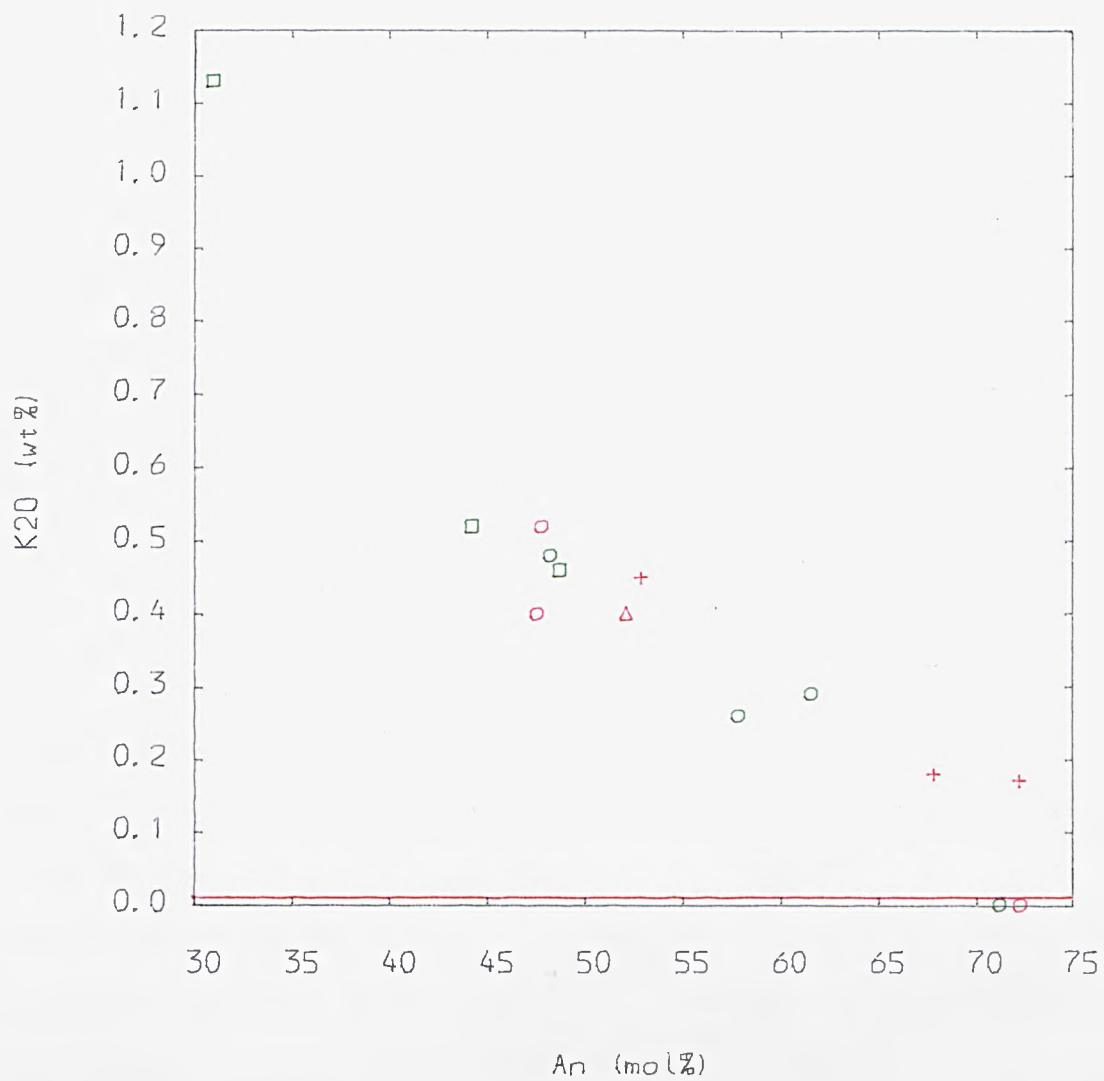
pyroxene differs from the light brown clinopyroxenes in basic rocks by being pale green in colour. This colour change reflects a gradual compositional change from Mg rich salite to more Fe and Na rich salite. As with the olivines, they occur as euhedral or resorbed phenocrysts, groundmass crystals or as megacrysts. Sometimes excellent hourglass zoning may be observed although ordinary zoning is more common. From the core to the rim the clinopyroxenes tend to become less Mg rich and more Ca and Fe rich. The range in composition of clinopyroxenes in basalts to clinopyroxenes in phonolites is from $En_{45}Fe_{07}Wo_{48}$ to $En_{31}Fe_{24}Wo_{45}$. The pyroxenes mainly plot in the salite field (Fig. 5.2) although some additionally plot in the diopside field while the megacrysts tend to plot in the augite field (Smith, pers. comm.). In Fig. 5.3 a good correlation between clinopyroxene composition, expressed as Mg number, and Al_2O_3 can be seen.

5.4 Plagioclase

Plagioclase is present as a phenocryst phase in basic rocks primarily in hawaiites and mugearites. It is also present as a groundmass mineral which becomes increasingly more abundant in rocks of mugearitic composition. In the mafic bearing trachytes, sodic plagioclase is sometimes present often rimmed by anorthoclase. The phenocrysts in the basic rocks commonly show signs of resorption and may also have corroded cores. The phenocrysts are usually normally zoned although reverse and oscillatory zoning is also present. The range in plagioclase composition is from An_{72} to An_{29} (Fig. 5.4) which corresponds to compositions in basalts and mugearites respectively. The gradual change in composition is illustrated in Fig. 5.5 by K_2O vs An mol%. Megacrysts of plagioclase occur in the basic rocks and are typified by showing extreme degrees of resorption.

Fig. 5.4 Core and rim analyses of feldspars plotted on orthoclase-albite-anorthite triangle.
 (Classification after Deer et al., 1966).





TITLE : Fig : 5.5 K20 vs An mol% in feldspar

CORE = red
RIM = green

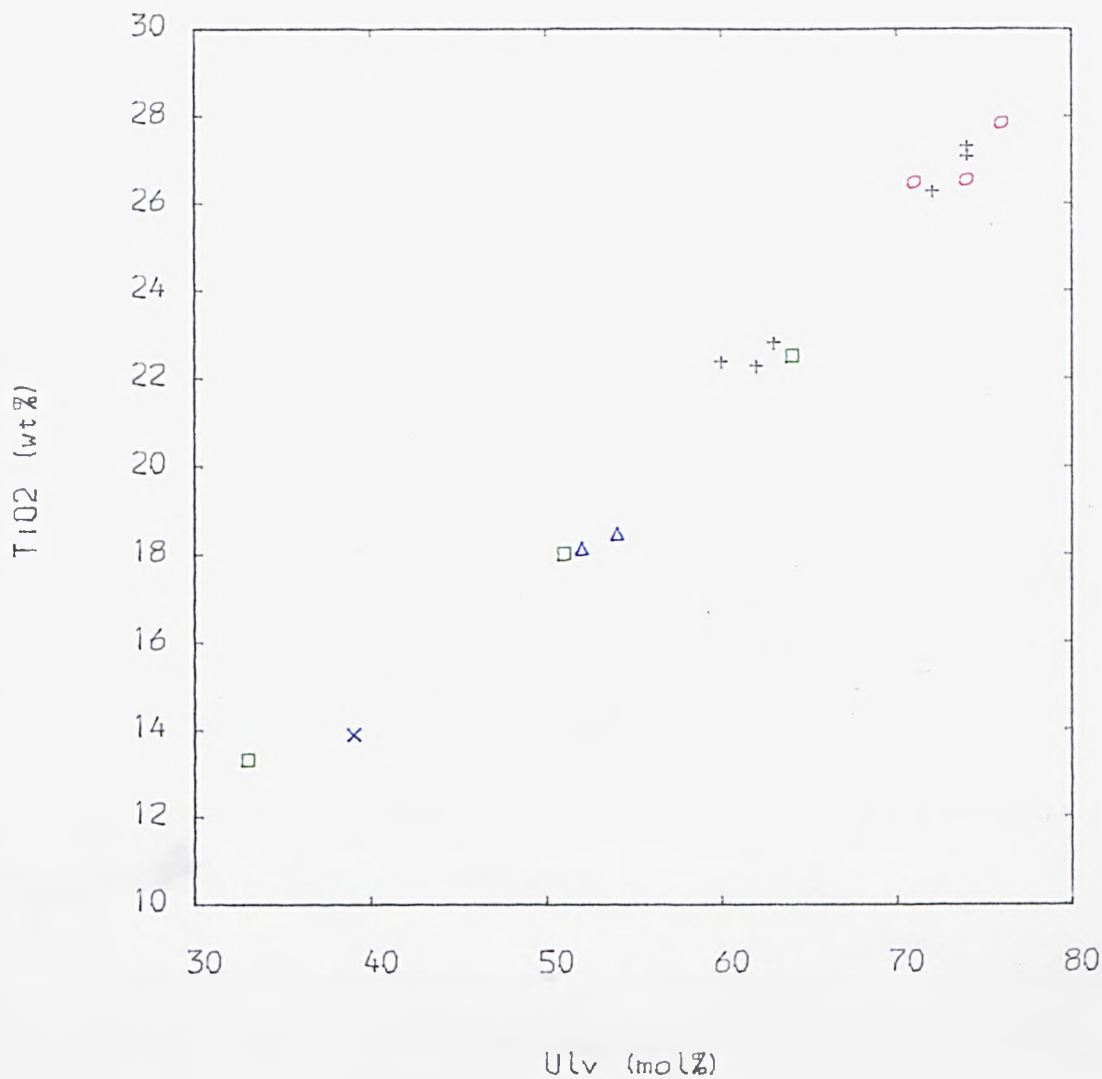
Unpublished work by Smith (pers. comm.) on megacrysts of olivine, clinopyroxene and plagioclase in the Jebel Marra basic lavas has identified compositional differences between these and the corresponding phenocryst phases. Megacryst olivines and clinopyroxenes tend to be more Mg rich than the phenocrysts and also do not show a correlation between mineral chemistry and whole rock composition. Megacryst plagioclase tends to have a restricted composition near An50 whereas phenocryst plagioclase shows much greater range in composition.

5.5 Potassium Feldspar

Anorthoclase first appears in the groundmass of evolved mugearites (cf 24019). In trachytes and phonolites it comprises the bulk of the rock as it is the predominant phenocryst and groundmass mineral. In phonolites, anorthoclase phenocrysts tend to be more rounded than phenocrysts in trachytes. The range in composition is from Ab19 to Ab42 (Fig. 5.4) although more commonly their composition is around Ab35. Some of the high K phenocrysts are strictly sanidinitic in composition.

5.6 Opaque Minerals

Titanomagnetite is overwhelmingly the most abundant oxide phase in the lavas and is present in all rocks although it is conspicuously less abundant in phonolites. It mostly occurs just as a groundmass phase but in some mugearites and trachytes it is present as microphenocrysts as well. Fig. 5.6 shows that, in general, TiO_2 and Ulv content decrease as the rocks become more evolved.



TITLE : Fig . 5.6 TiO2 vs Ulv mol% in opaques

Basalts = black
 Hawaiiites = red
 Mugearites = green
 Acids = blue

5.7 Accessory Phases

Kaersutite occasionally occurs as an accessory mineral mainly in mugearites but in specimen 24061 numerous kaersutite crystals rimmed with iron oxide are present. These are zoned with increasing Fe/Mg ratio towards the rim.

Small prismatic grains of apatite are most common in mugearites but are also present in some of the more basic rocks. Apatite has not been identified in acidic rocks.

Biotite occurs as microphenocrysts in trachytes and phonolites where they are sometimes zoned. In more altered samples, biotite is partly replaced by opaque minerals.

In some under-saturated trachytes and phonolites, nepheline and aenigmatite have been identified and analysed.

Although in general the rocks are extremely fresh, some rocks are partly altered to secondary minerals; these secondary minerals include serpentine, iddingsite, calcite, and various clay minerals. Zeolites occasionally occupy vesicles.

5.8 Nodules

In some of the basic lavas, nodules were found. These are predominantly mono-mineralic olivine nodules which are commonly altered. In addition to these there are some clinopyroxene-plagioclase nodules. Although evidence for their origin is sparse, they most likely represent cumulate nodules accidentally incorporated into the rising magma.

5.9 Conclusions

The volcanic rocks of the Jebel Marra show a wide range in mineral chemistry of the major phases. The most important conclusion

from the mineral analyses is the progressive change in composition which, by and large, correlates with changes in whole rock chemistry. This is best illustrated by feldspar and olivine which show a particularly wide range in composition: clinopyroxene shows a more restricted variation. Megacrysts of olivine, clinopyroxene and plagioclase also show a restricted range in chemistry which do not appear to be related to the composition of the whole rock. (Smith, per. comm.).

CHAPTER SIX
MAJOR ELEMENTS

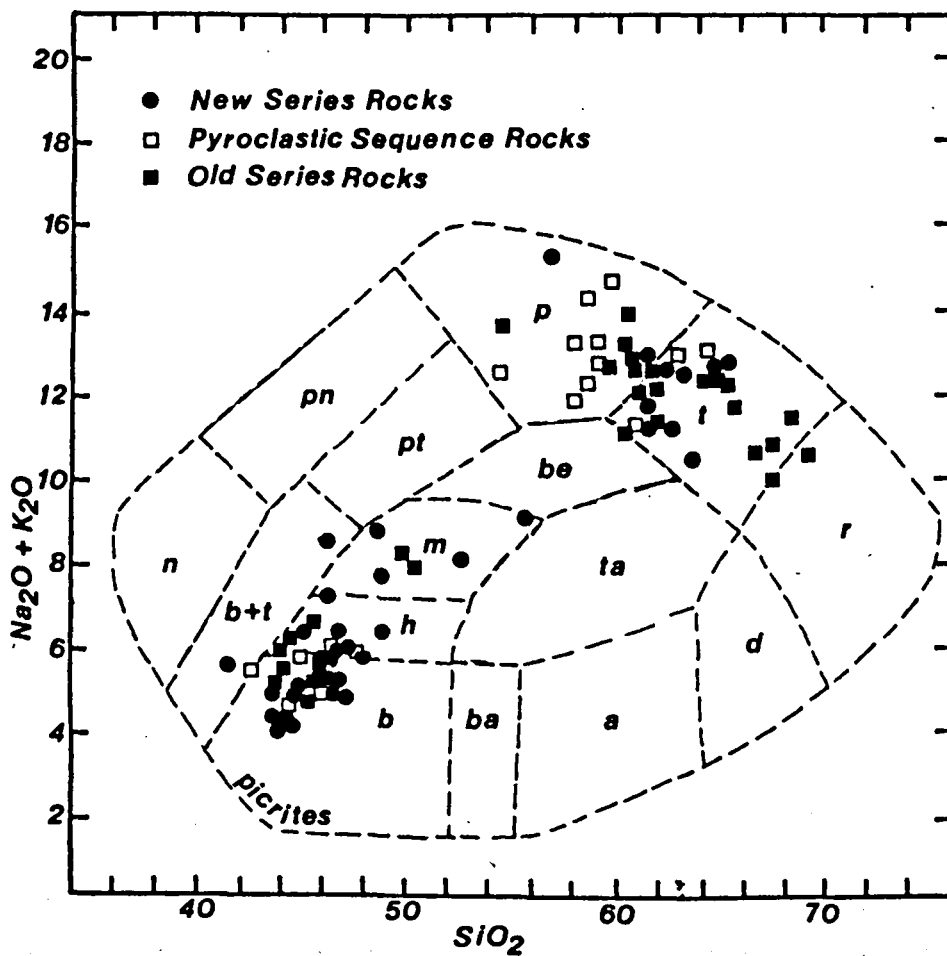
6.1 Introduction

This Chapter documents the variations in major element chemistry throughout the Jebel Marra volcanic suite and explores the temporal variations in the Old and New Series rocks. Nearly 100 whole rocks have been analysed by X.R.F. methods (see Appendix C). Si, Ti, Al, Fe, Mn, Mg, Ca, Na, K and P were measured routinely on all of the samples. The results are presented in Appendix C. Major elements are usefully examined because, in principle, they bear a simple relationship to differentiation processes, such as fractional crystallisation, partial melting and crustal assimilation. Interpretations made on the basis of major elements provide a starting point from which the isotopic and trace element data can be interpreted.

6.2 Classification

Most classification schemes for igneous rocks are based on the major element compositions of the rocks (Le Maitre, 1976).

The volcanic rocks of Jebel Marra form a virtual continuum in composition, broken by a 'silica gap' (see next section). A simple approach to classification has been used which incorporates the total alkalis ($\text{Na}_2\text{O} + \text{K}_2\text{O}$) vs silica diagram (Cox et al., (1979), Fig.6.1). This diagram is useful also in the context of magma series. A basaltic parental liquid, which is slightly over-saturated, could give rise to a trachytic residue at which stage fractionation of anorthoclase would decrease the alkali content and give rise to rhyolites. An under-saturated basaltic parent, however, could be expected to yield



- | | | |
|----------------------|-----------------------------|----------------------------------|
| <i>b</i> basalt | <i>ba</i> basaltic andesite | <i>b+t</i> basanite & tephrite |
| <i>h</i> hawaiite | <i>ta</i> trachyandesite | <i>pt</i> phonolitic tephrite |
| <i>m</i> mugearite | <i>a</i> andesite | <i>n</i> nephelenite |
| <i>be</i> benmoreite | <i>d</i> dacite | <i>pn</i> phonolitic nephelenite |
| <i>t</i> trachyte | | |
| <i>r</i> rhyolite | | |
| <i>p</i> phonolite | | |

Fig. 6.1 Alkalis versus silica diagram. The rocks have been classified according to divisions outlined in Cox et al., 1979. For simplicity the samples that plot in the basanite and tephrite field are classified as basalt and mugearite. (redrawn from Cox et al., 1979, p14, figure 2.2).

a trachytic residue which with continued fractionation could yield phonolitic liquids. This dichotomous behaviour is thought to be due to the presence of a thermal divide (at least at 1-atmosphere and in anhydrous conditions), which separates over-saturated and under-saturated liquids on the diagram (see Cox et al., 1979, Fig. 9.6 p237; Upton, 1974). In the Jebel Marra suite, phonolitic and trachytic-rhyolitic rocks could be interpreted to be derived from basaltic parents whose compositions span the divide. This divide can break down, however, if the conditions of 1-atmosphere and dryness are not met or, alternatively, if the under-saturated liquid is contaminated with SiO₂ rich crust. If crustal assimilation is responsible for a shift from under-saturated to over-saturated rocks then this can be theoretically identified from isotopic evidence (Chapter 8).

Fig. 6.1 shows that the rocks belong to the alkali basalt - hawaiite - mugearite - trachyte - rhyolite/phonolite series. Rocks which strictly plot in the basanite and tephrite fields are instead described as either basalts, hawaiites or mugearites, depending on which field they approach most closely. The higher degree of under-saturation of these rocks is regarded as natural scatter (see section 7.3.2) about the main trend. This seems justified, as there are few petrographic, or any other geochemical reasons to warrant further subdivision.

6.3 'Silica Gap'

One of the major features of Fig. 6.1 is the apparent bimodality of the data. This is a feature recurrent in most of the variation plots. It is not possible to account for the 'silica gap' (approx-

imately 52-55 wt% SiO_2), which coincides with rocks of benmoreite composition, by sampling bias because, in the same field, special emphasis was placed on collecting basic and intermediate rocks, in preference to the more easily obtained acidic rocks. It is therefore considered a real phenomenon.

6.4 Overall Variations

Before describing detailed variations, it is thought worthwhile to examine the variations of the major elements vs SiO_2 individually (Figs. 6.2a-1), in order to develop a general understanding of their behaviour. The symbolism used is also explained in Fig. 6.2a. Throughout the following discussion, reference will be made to rocks being more 'differentiated' or 'evolved' than others, because of having, for example, higher SiO_2 and lower MgO. It is proposed later that the main cause of the differentiation is fractional crystallisation.

SiO_2

Silica shows a large range from just over 40% to 70% from basalts to rhyolites. Silica increases with differentiation throughout the series, except in the phonolites, where the increase in SiO_2 is retarded and then later reversed in the more evolved members.

TiO_2

The range in TiO_2 is considerably smaller (0-4%) than for SiO_2 . The larger analytical error associated with TiO_2 is over a much smaller range, which means that the relative error, and hence the scatter, is much greater. It is suggested that the coherence with other elements is poor for this reason. However, it does decrease, in general, from basalts through hawaiites and mugearites to trachytes and phonolites.

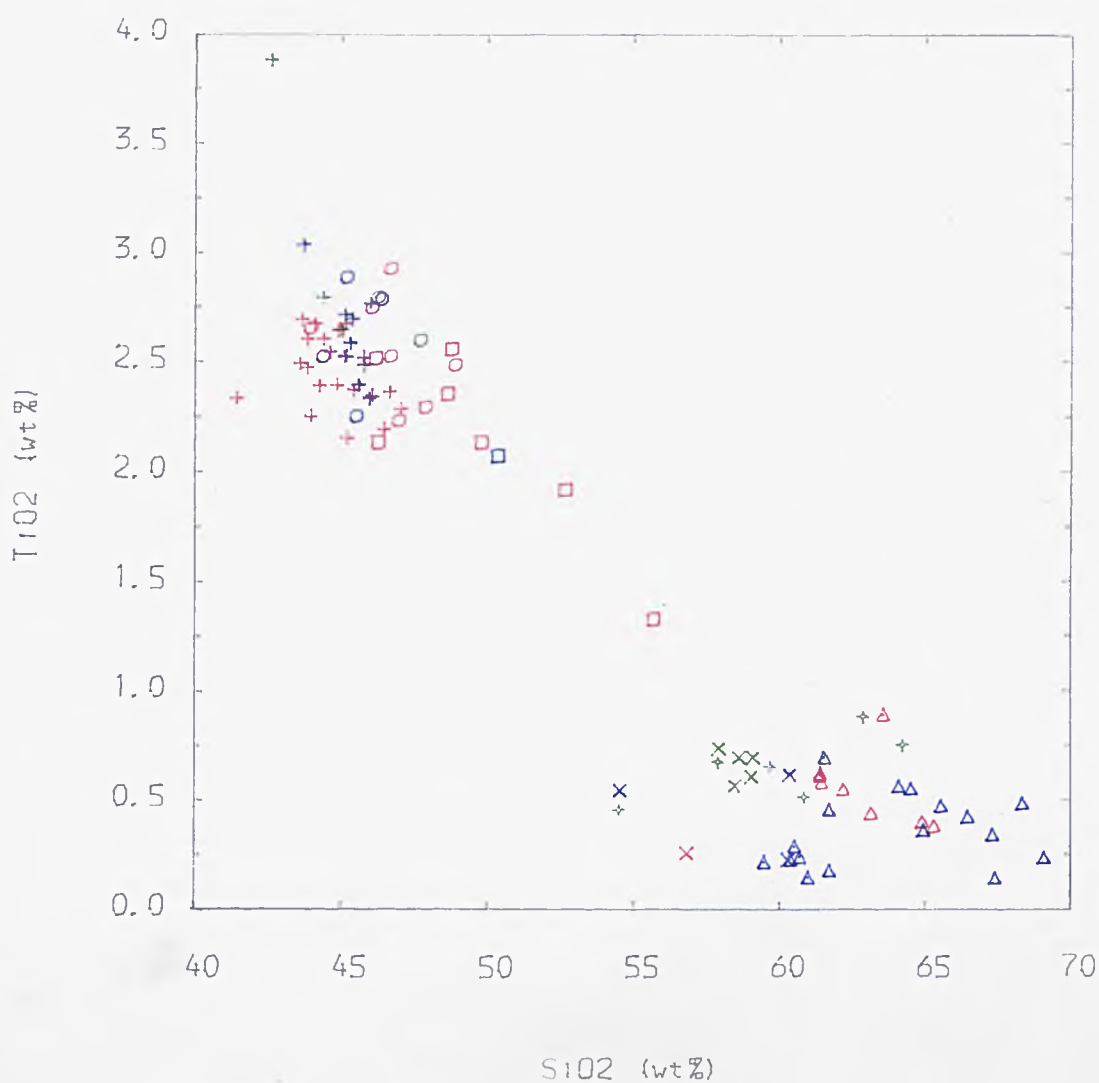
EXPLANATION OF SYMBOLS USED

Red Symbols	New Series Rocks
Green Symbols	Pyroclastic Sequence Rocks
Blue Symbols	Old Series Rocks

+	BASALT
○	HAWAIIITE
□	MUGEARITE
△	TRACHYTE
x	PHONOLITE
⊕	IGNIMBRITE

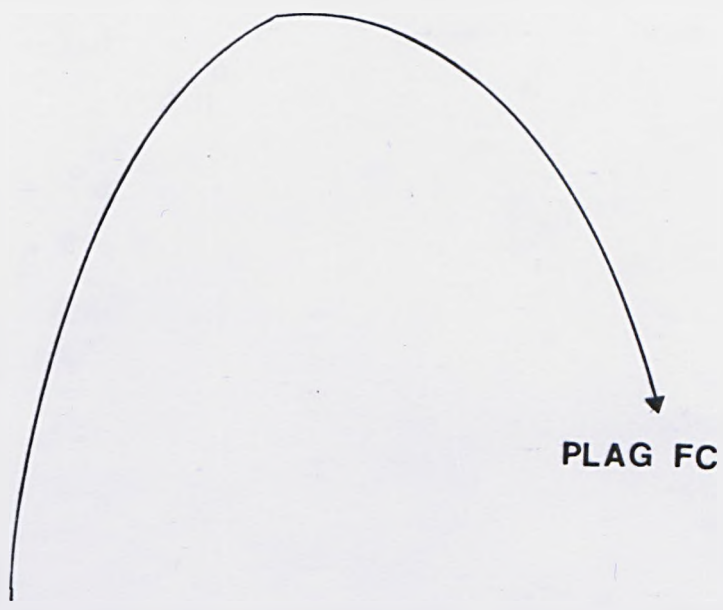
TRACHYTE SUB-DIVISION

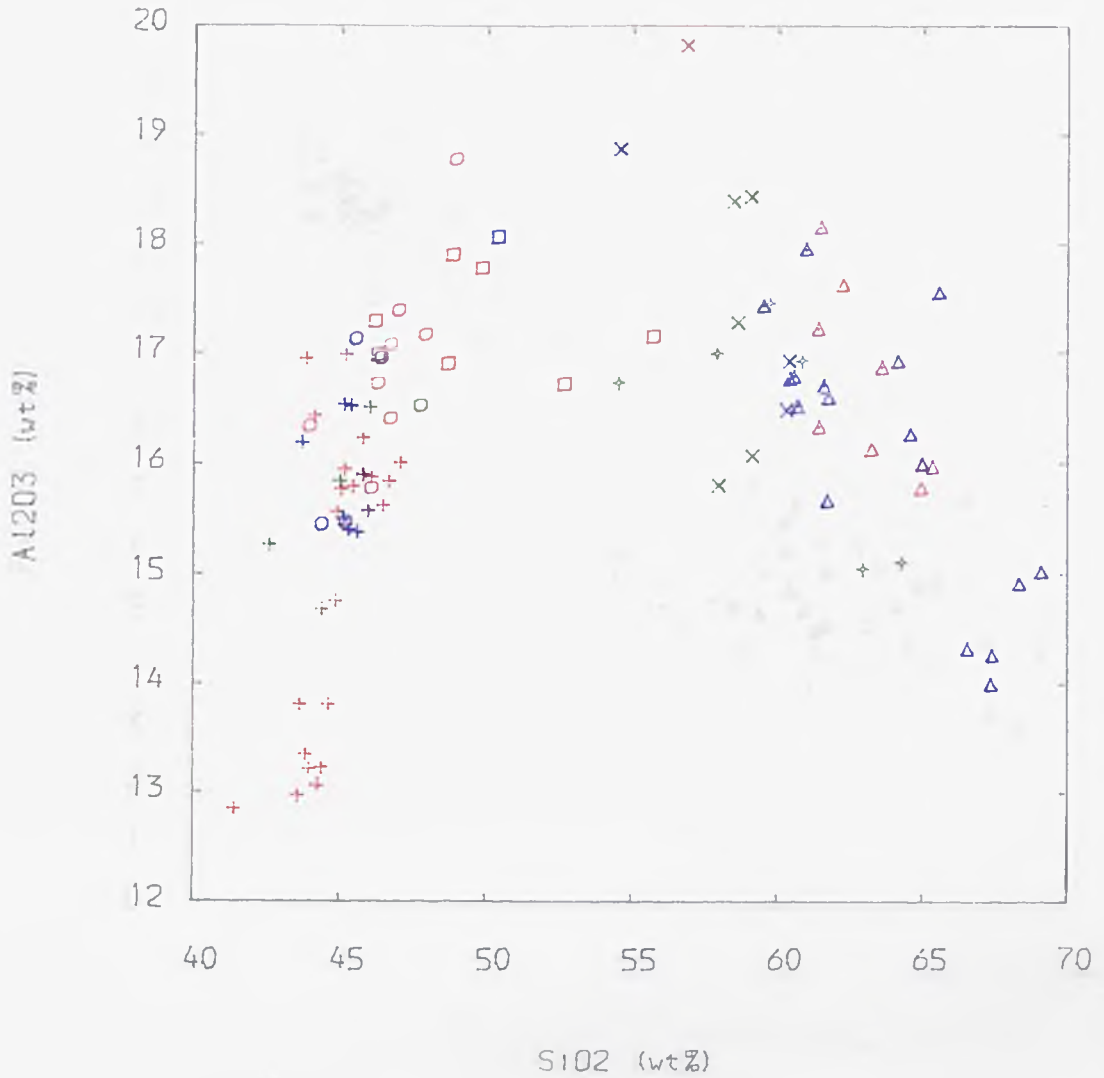
New Series	-	△	<i>caldera trachyte</i>
	-	△	<i>mafic bearing trachyte</i>
Old Series	-	△	<i>'contaminated' trachyte</i>
	-	△	<i>'uncontaminated' trachyte</i>



TITLE : Fig : 6.2a-i Major Elements vs SiO2

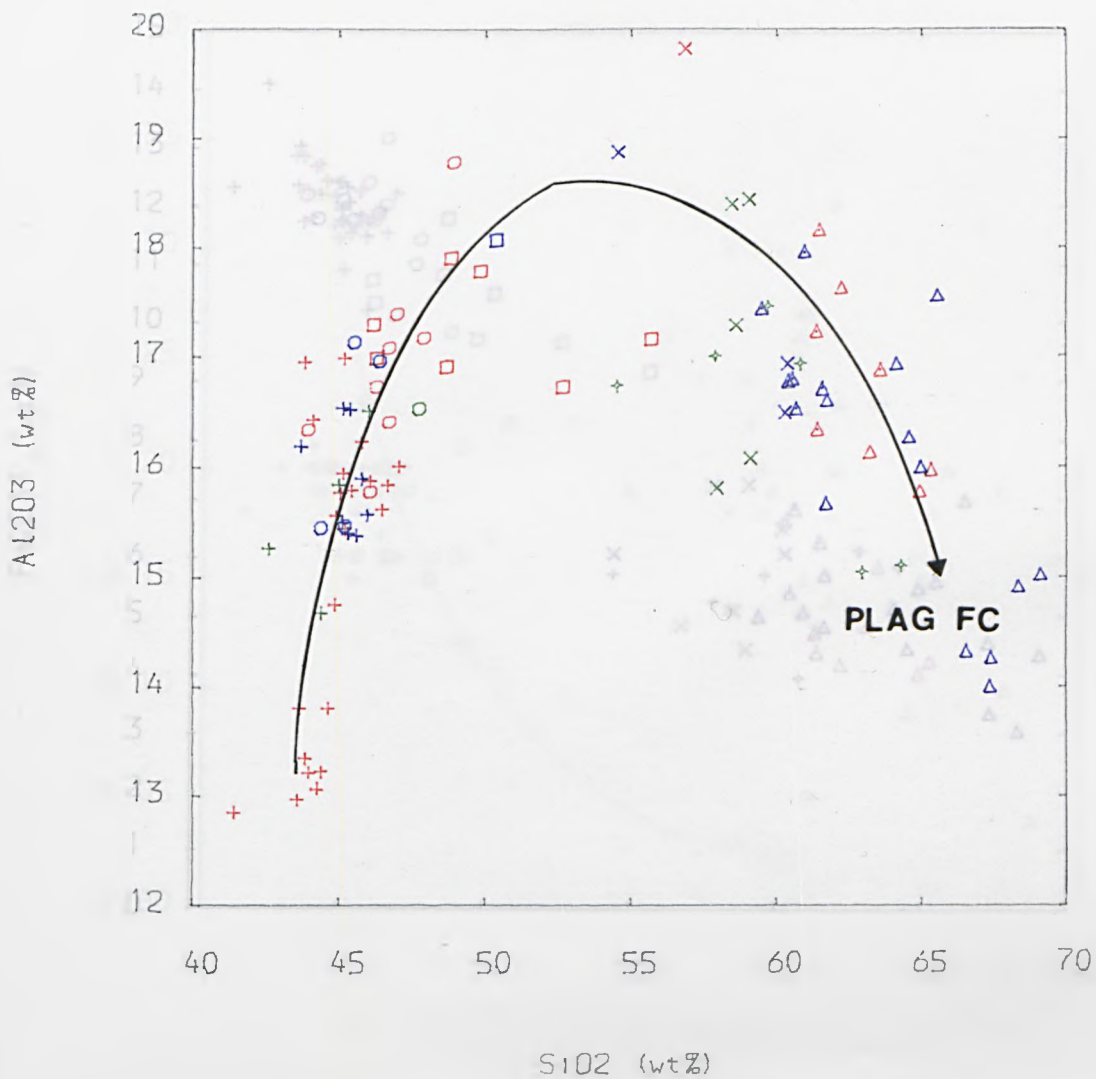
BASEMENT ROCKS	= black
NEW SERIES ROCKS	= red
PYROCLASTIC SEQUENCE ROCKS	= green
OLD SERIES ROCKS	= blue





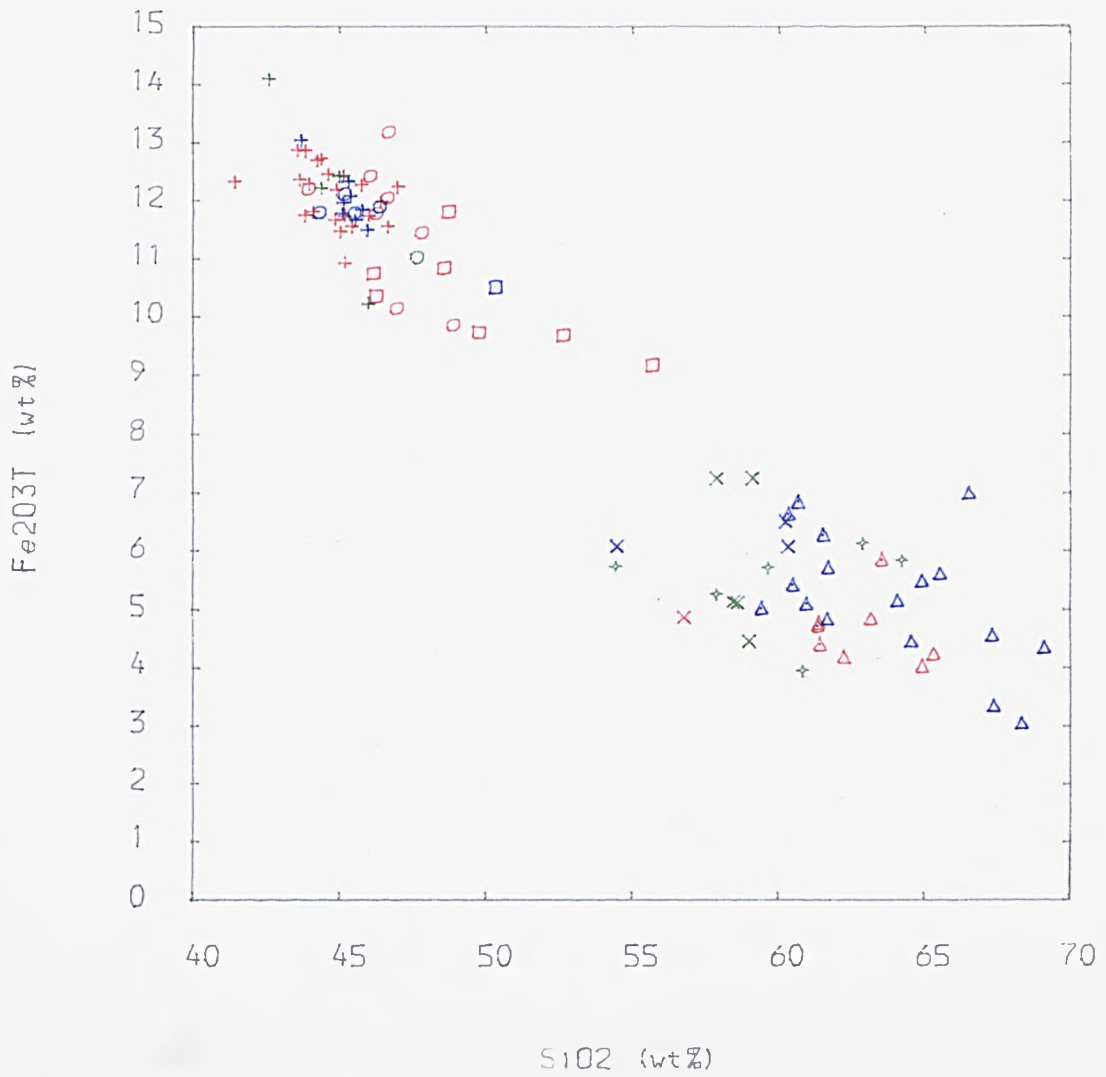
TITLE : Fig : 6.2a-i Major Elements vs SiO₂

BASEMENT ROCKS	= black
NEW SERIES ROCKS	= red
PYROCLASTIC SEQUENCE ROCKS	= green
OLD SERIES ROCKS	= blue



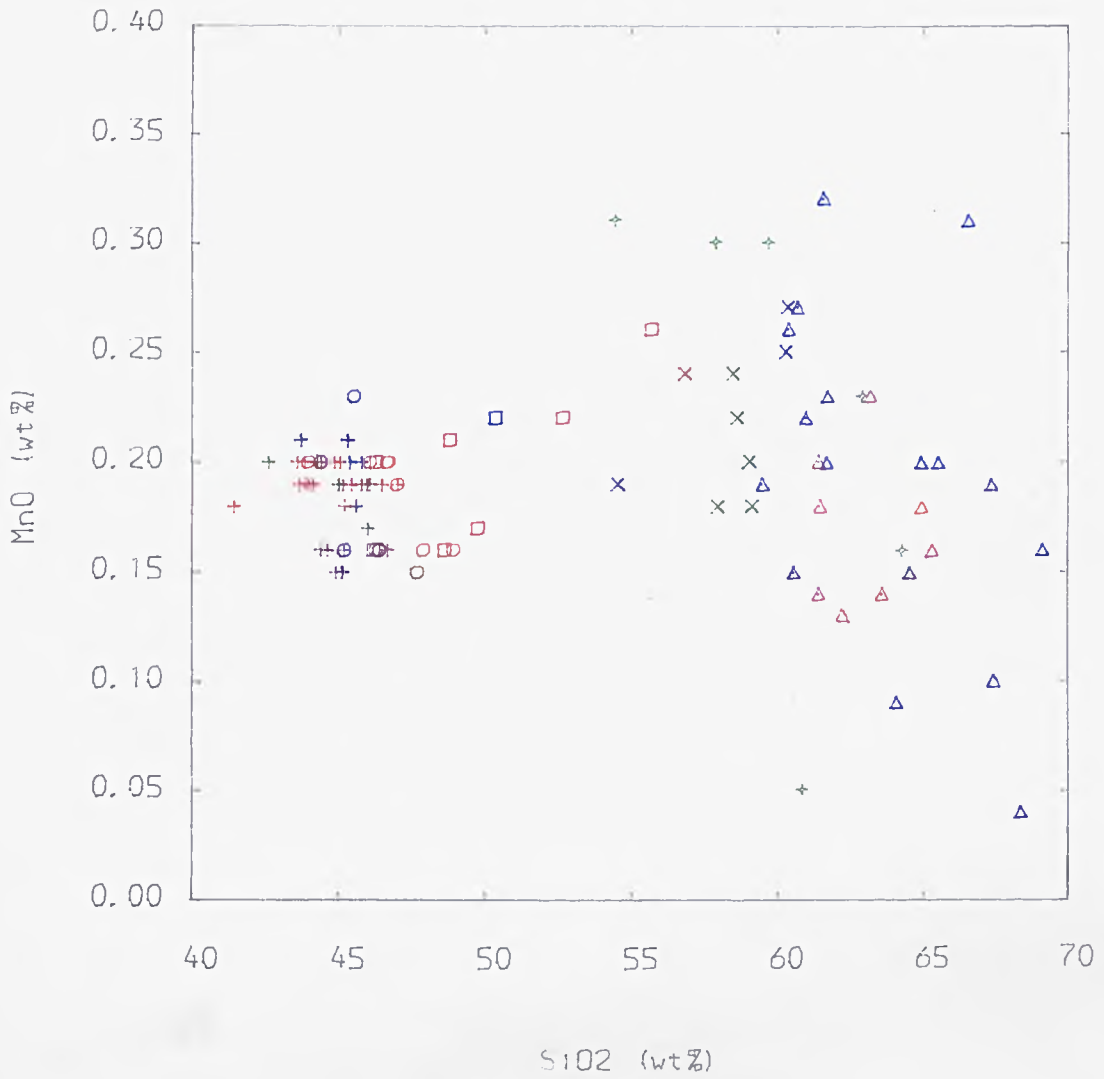
TITLE : Fig : 6.2a-i Major Elements vs SiO2

BASEMENT ROCKS	= black
NEW SERIES ROCKS	= red
PYROCLASTIC SEQUENCE ROCKS	= green
OLD SERIES ROCKS	= blue



TITLE : Fig : 6.2a-i Major Elements vs SiO₂

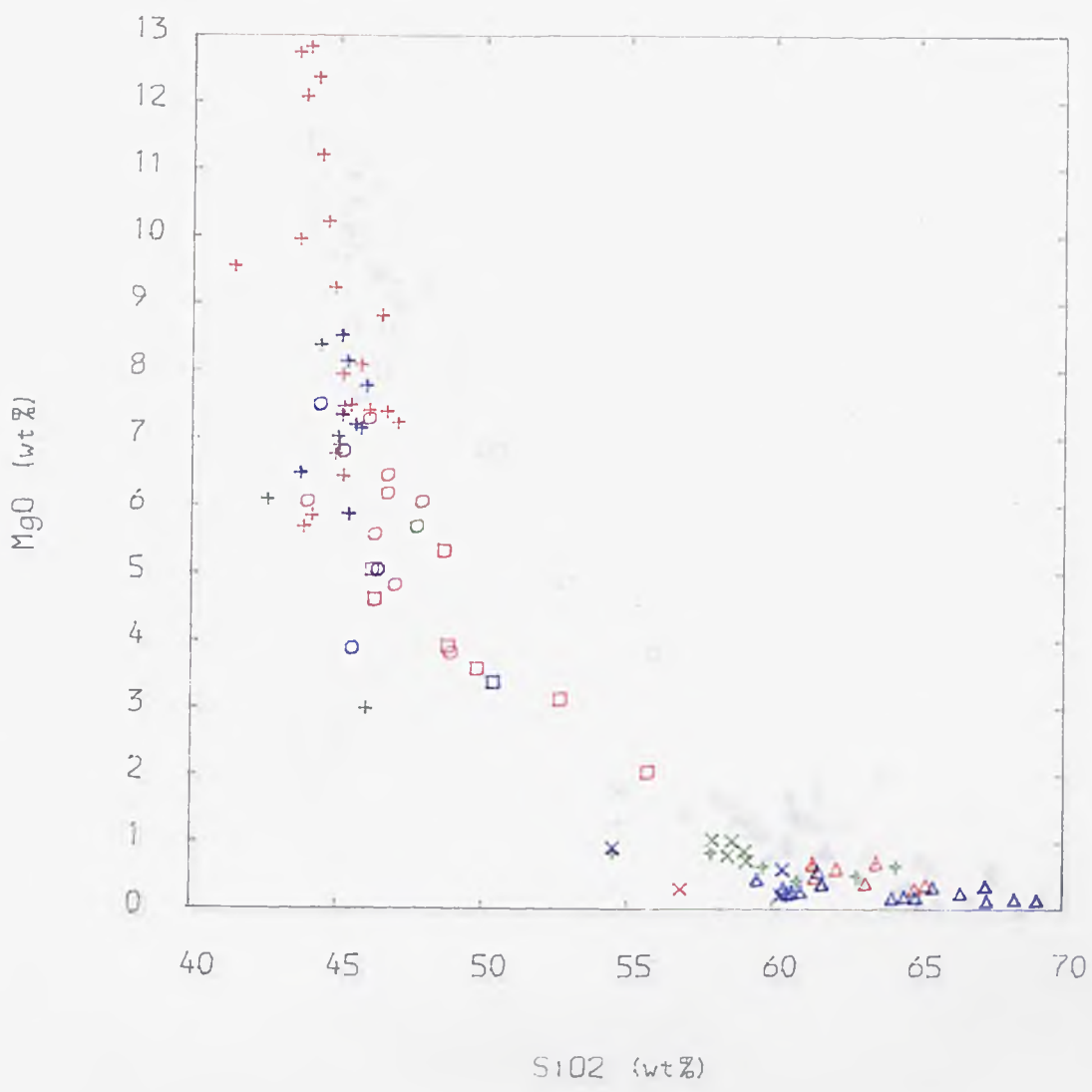
BASEMENT ROCKS	= black
NEW SERIES ROCKS	= red
PYROCLASTIC SEQUENCE ROCKS	= green
OLD SERIES ROCKS	= blue



TITLE : Fig : 6.2a-i Major Elements vs SiO2

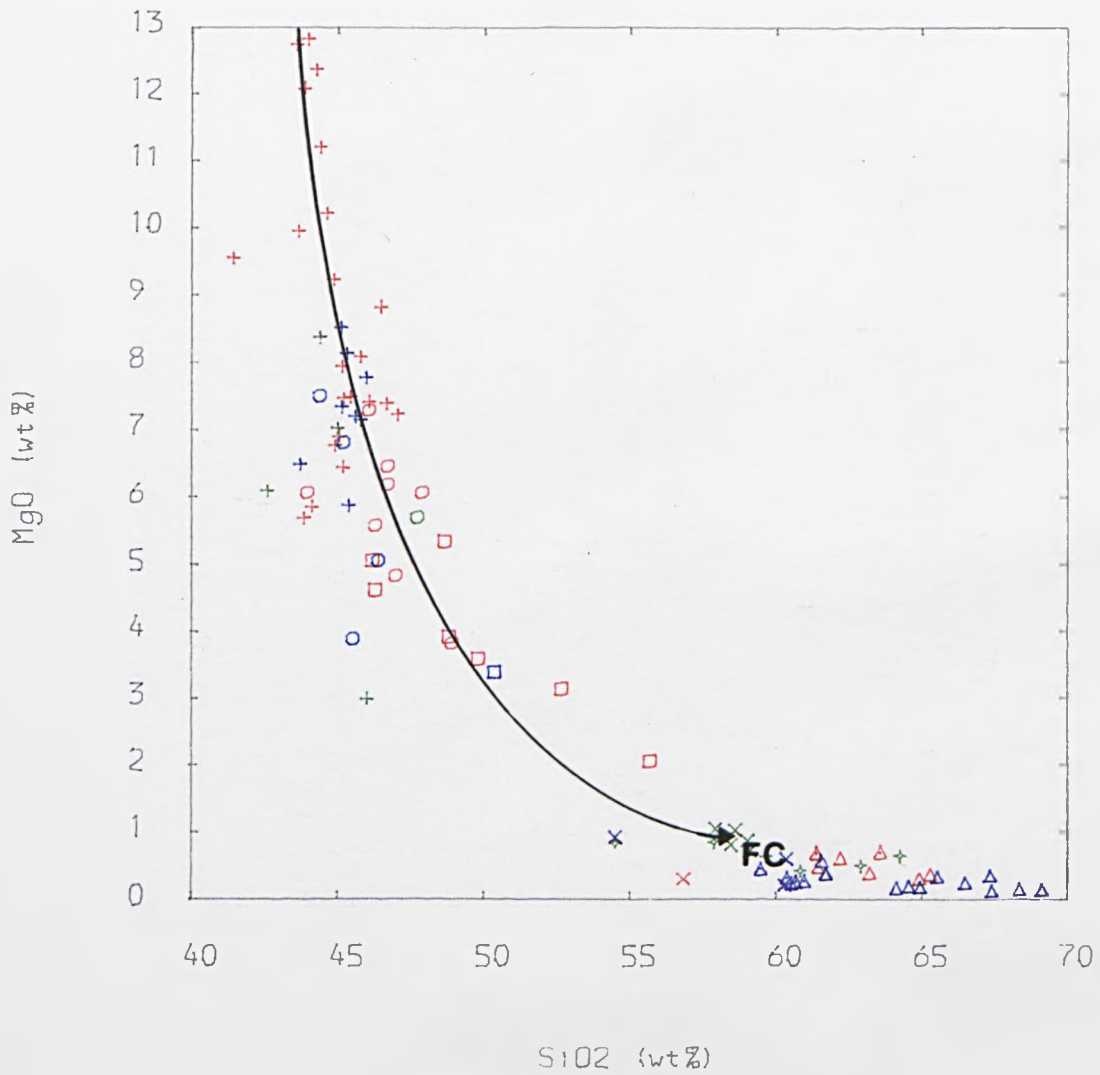
BASEMENT ROCKS	= black
NEW SERIES ROCKS	= red
PYROCLASTIC SEQUENCE ROCKS	= green
OLD SERIES ROCKS	= blue





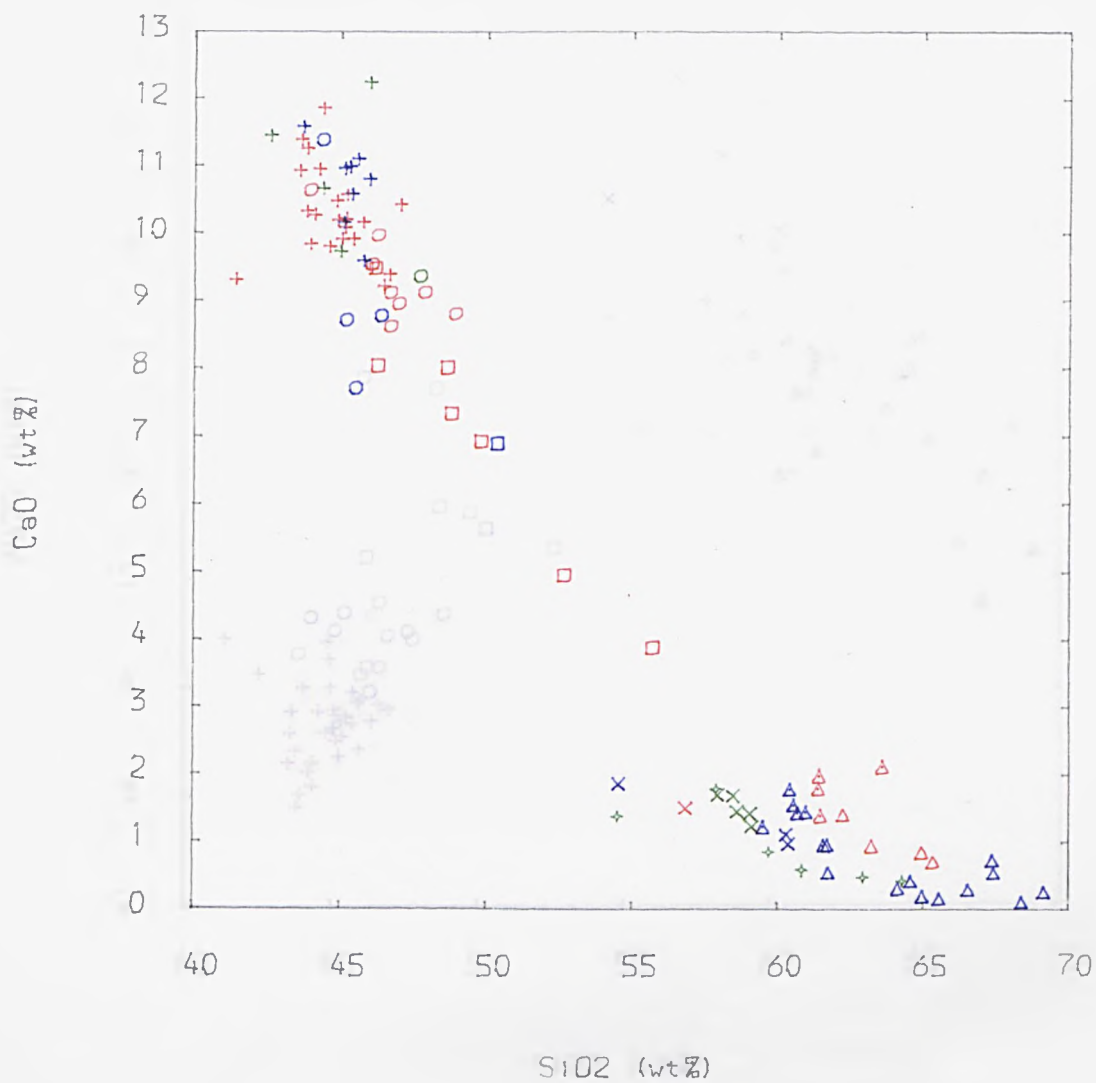
TITLE : Fig : 6.2a-i Major Elements vs SiO2
(see text for explanation)

- BASEMENT ROCKS = black
- NEW SERIES ROCKS = red
- PYROCLASTIC SEQUENCE ROCKS = green
- OLD SERIES ROCKS = blue



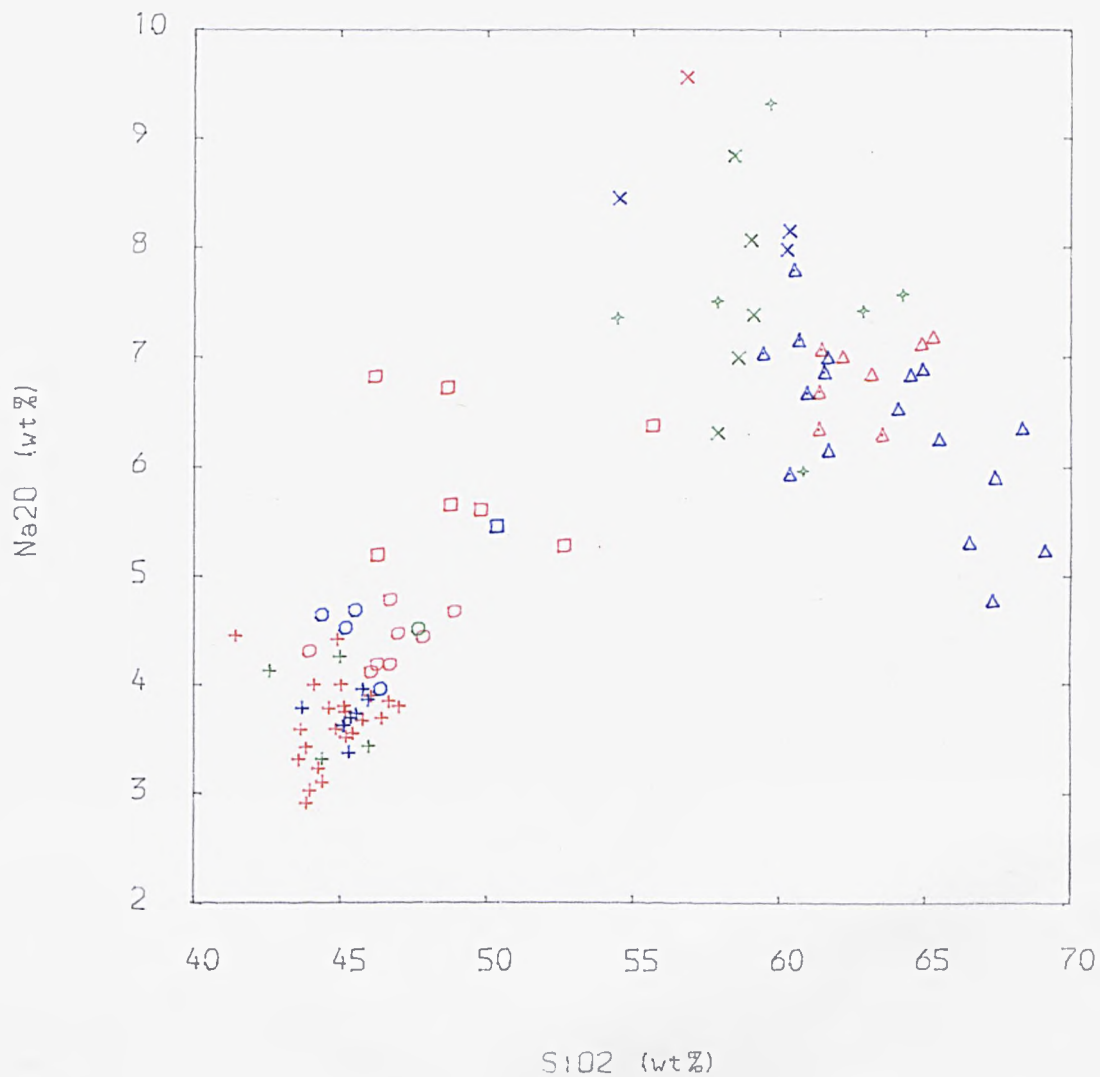
TITLE : Fig : 6.2a-i Major Elements vs SiO2
(see text for explanation)

BASEMENT ROCKS	= black
NEW SERIES ROCKS	= red
PYROCLASTIC SEQUENCE ROCKS	= green
OLD SERIES ROCKS	= blue




TITLE : Fig : 6.2a-i Major Elements vs SiO2

BASEMENT ROCKS	= black
NEW SERIES ROCKS	= red
PYROCLASTIC SEQUENCE ROCKS	= green
OLD SERIES ROCKS	= blue

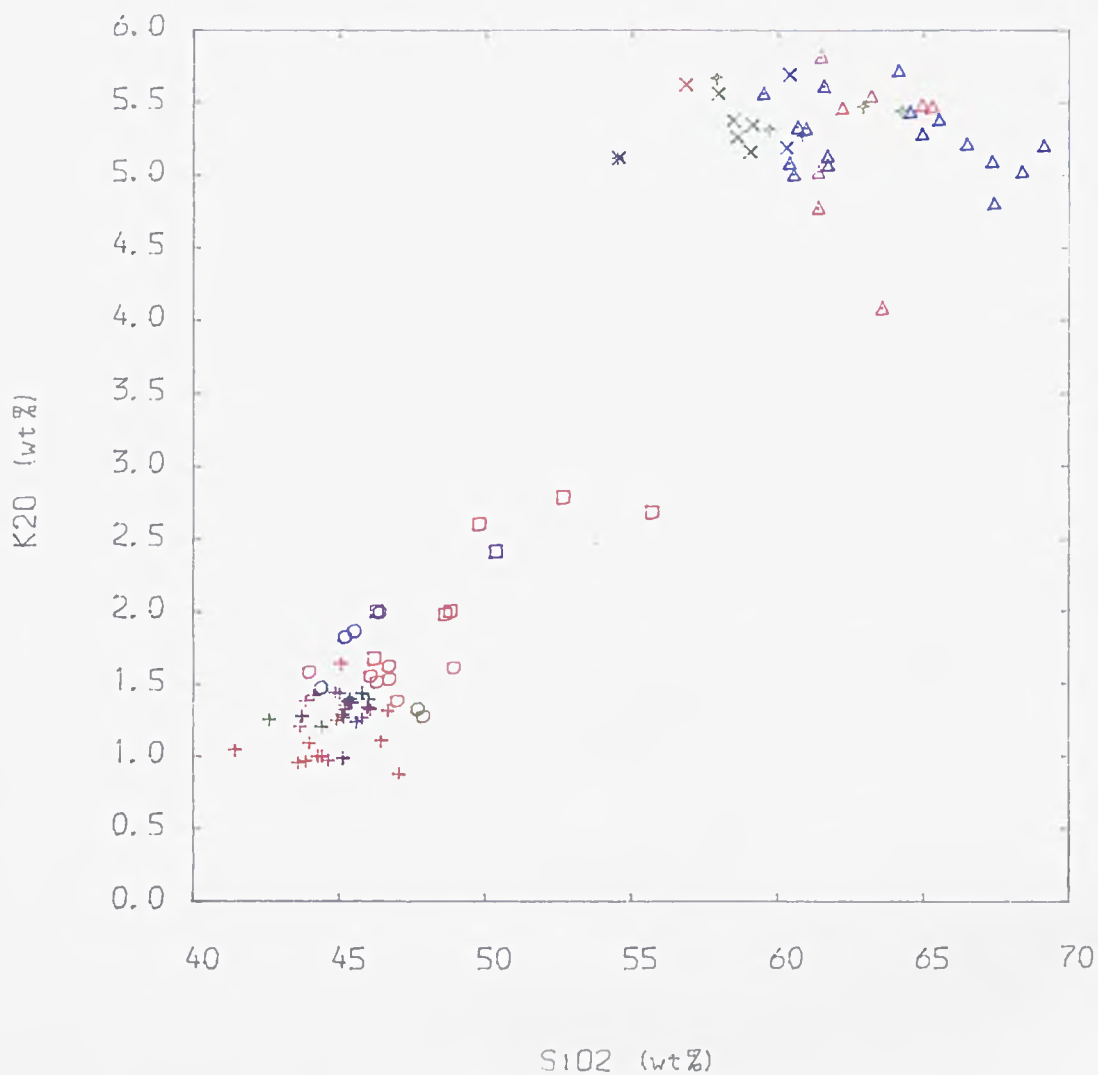


TITLE : Fig . 6.2a-i Major Elements vs SiO₂

BASEMENT ROCKS	= black
NEW SERIES ROCKS	= red
PYROCLASTIC SEQUENCE ROCKS	= green
OLD SERIES ROCKS	= blue

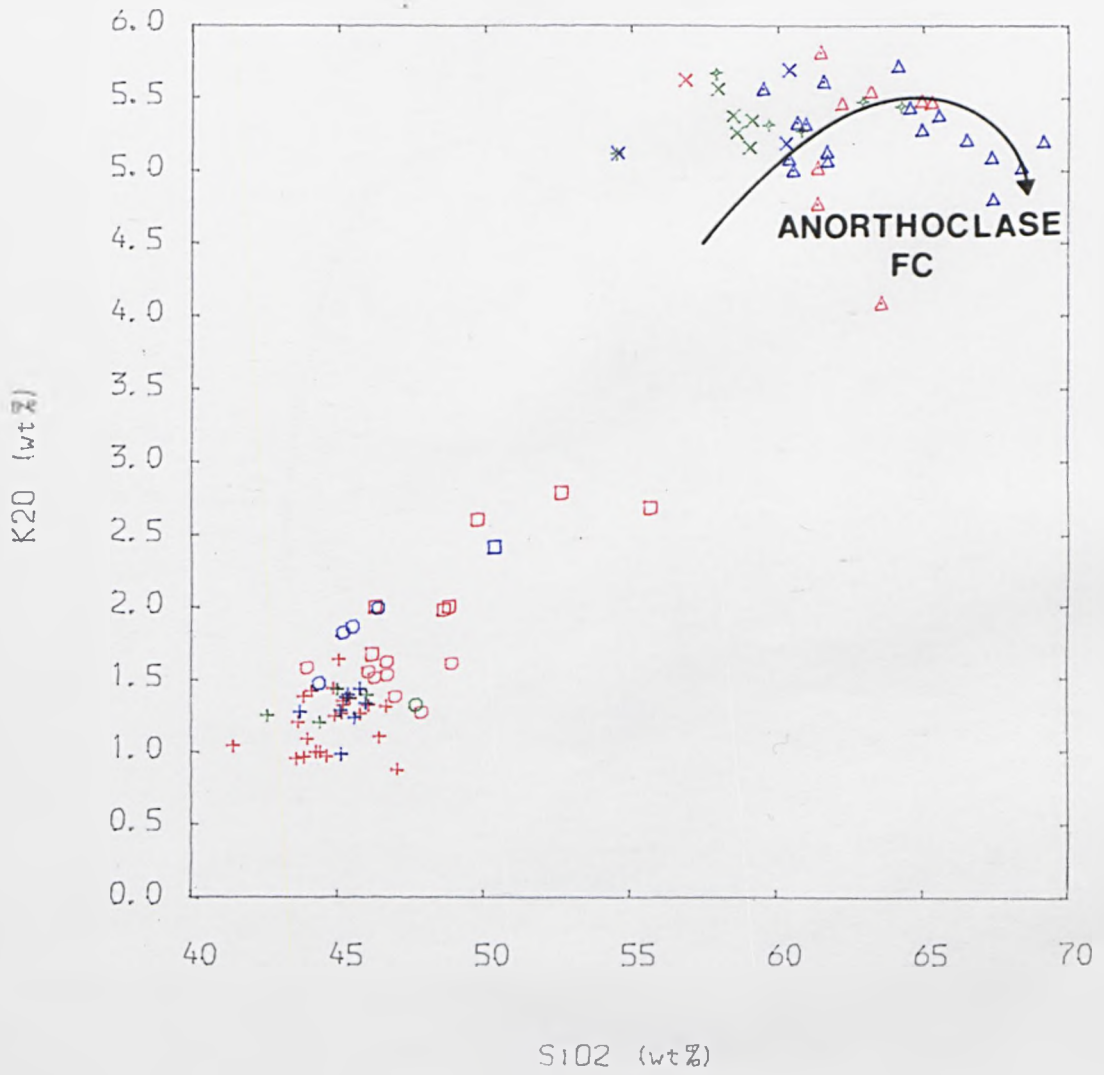


ANORTHOCLASE
FC



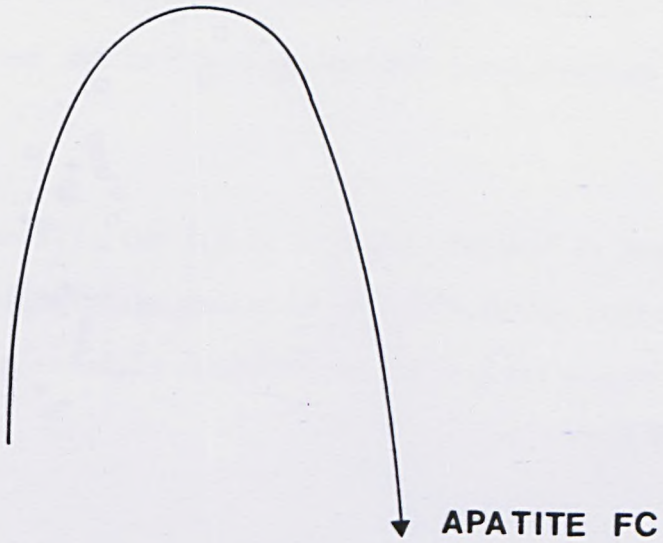
TITLE : Fig : 6.2a-i Major Elements vs SiO2

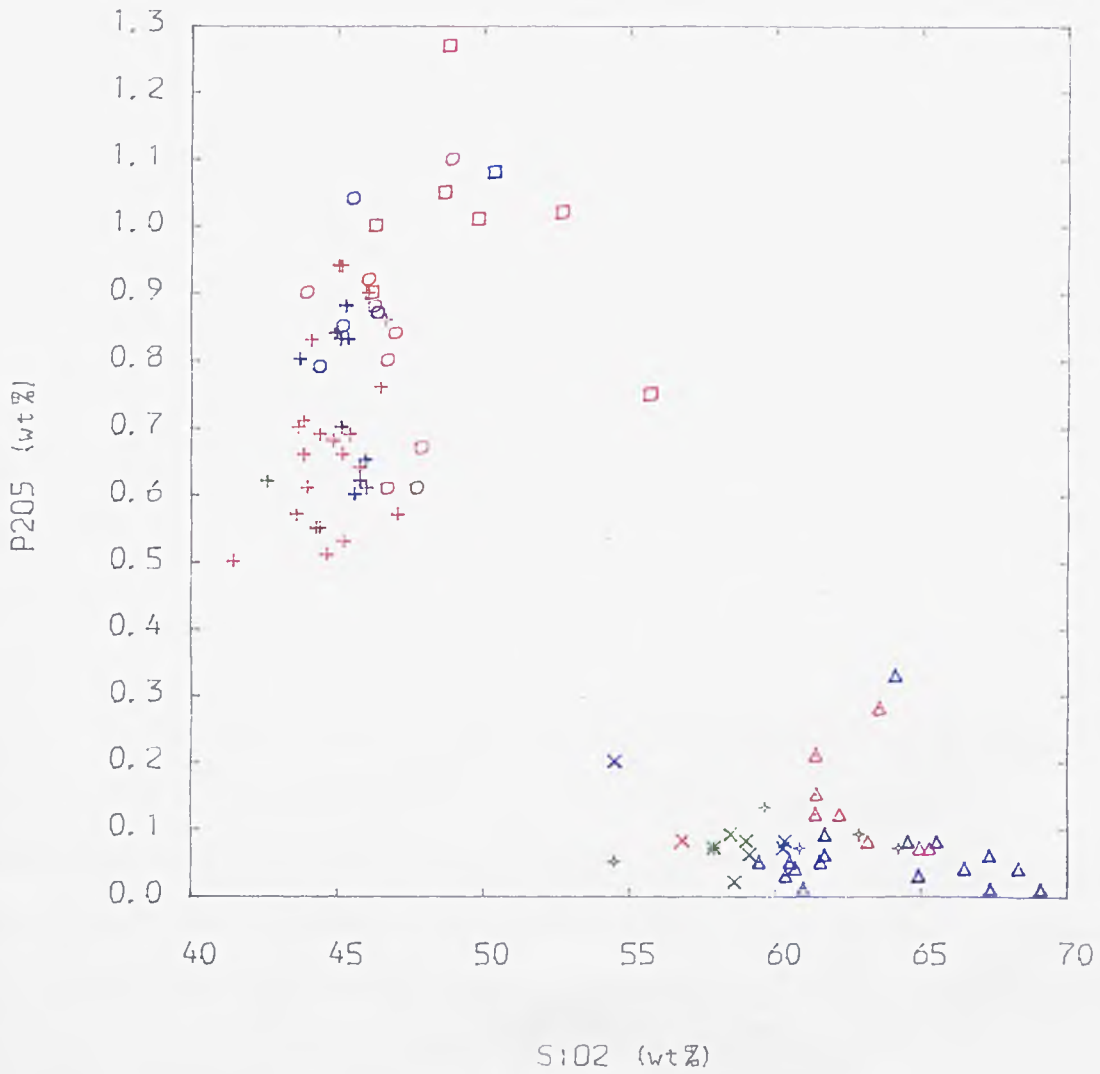
BASEMENT ROCKS	= black
NEW SERIES ROCKS	= red
PYROCLASTIC SEQUENCE ROCKS	= green
OLD SERIES ROCKS	= blue



TITLE : Fig : 6.2a-i Major Elements vs SiO2

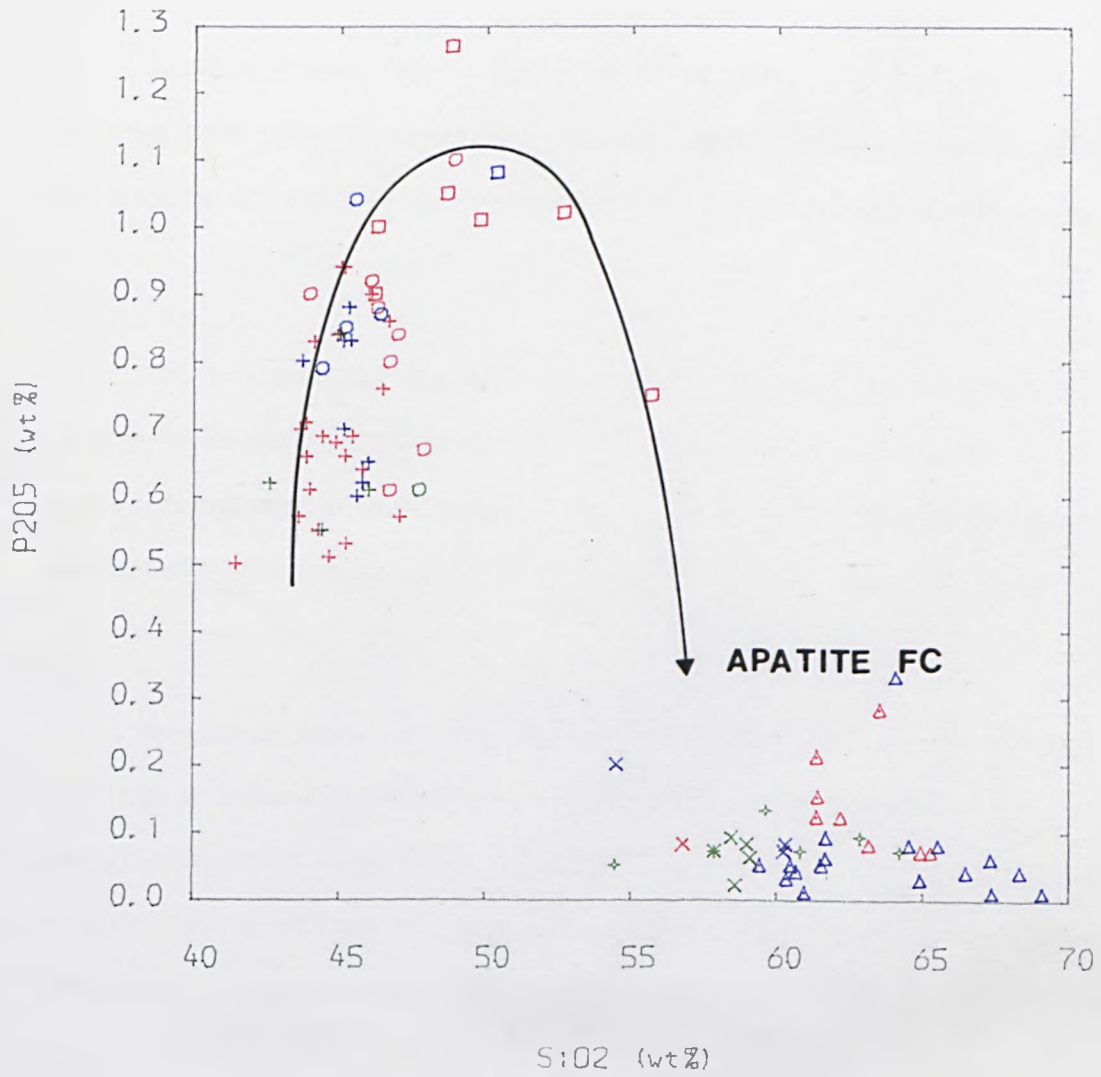
BASEMENT ROCKS	= black
NEW SERIES ROCKS	= red
PYROCLASTIC SEQUENCE ROCKS	= green
OLD SERIES ROCKS	= blue





TITLE : Fig : 6.2a-i Major Elements vs SiO2

BASEMENT ROCKS	= black
NEW SERIES ROCKS	= red
PYROCLASTIC SEQUENCE ROCKS	= green
OLD SERIES ROCKS	= blue



TITLE : Fig : 6.2a-i Major Elements vs SiO2

BASEMENT ROCKS	= black
NEW SERIES ROCKS	= red
PYROCLASTIC SEQUENCE ROCKS	= green
OLD SERIES ROCKS	= blue

Al₂O₃

Alumina rises from a value of about 13% in basalts to a maximum near 20% at mugearitic compositions, before generally falling to around 14% in the more evolved trachytes and phonolites.

Fe₂O₃T

Conventionally, the X.R.F. analysis assumes Fe resides entirely in the 3+ oxidation state and so Fe₂O₃T is used to indicate total Fe. Fe₂O₃T decreases steadily from 13% in basalts, to almost 0% in trachytes.

MnO

Manganese shows a very restricted range, but nevertheless displays a coherent variation. It suffers less markedly from analytical error than TiO₂. MnO is fairly uniform at roughly 0.2% in basalts, hawaiites and mugearites, but concentrations in the phonolites begin at about 0.3% and decrease to 0.05% in the trachytes.

MgO

The range in MgO is from 13% to about 0%. It decreases from the most primitive basalts through to hawaiites, before decreasing less sharply through mugearites. Acidic rocks show uniformly low concentration of MgO.

CaO

CaO decreases uniformly from basalts to mugearites. The trend through phonolites, trachytes and rhyolites decreases less steeply. The overall range is from 12% to about 0%.

Na₂O

Na₂O shows a general increase from basalts (3%) through to phonolites (9%). However, the trachytes and rhyolites depart from the phonolites by showing either only a slight increase, or a decrease in Na₂O.

K₂O

K₂O behaves in a similar way to Na₂O, except that there is less divergence between phonolites and trachytes and rhyolites. The variation is from about 1% in basalts to nearly 6% in the most evolved trachytes.

P₂O₅

P₂O₅ increases from 0.5% in basalts to over 1.2% in mugearites before dropping to much lower amounts, 0.3%, in acidic rocks.

6.4.1 General Considerations

- i) A 'silica gap' is obvious in all diagrams.
- ii) Variation diagrams involving basalts, hawaiites and mugearites generally display coherent patterns in all diagrams.
- iii) Variation diagrams involving phonolites and trachytes are coherent in all diagrams vs SiO₂ except for Na₂O where the two groups diverge.
- iv) Al₂O₃ and P₂O₅ show trends which are first enriched towards mugearite and then become depleted towards rocks of acidic composition.
- v) There is generally more variation amongst the rocks of acidic composition.

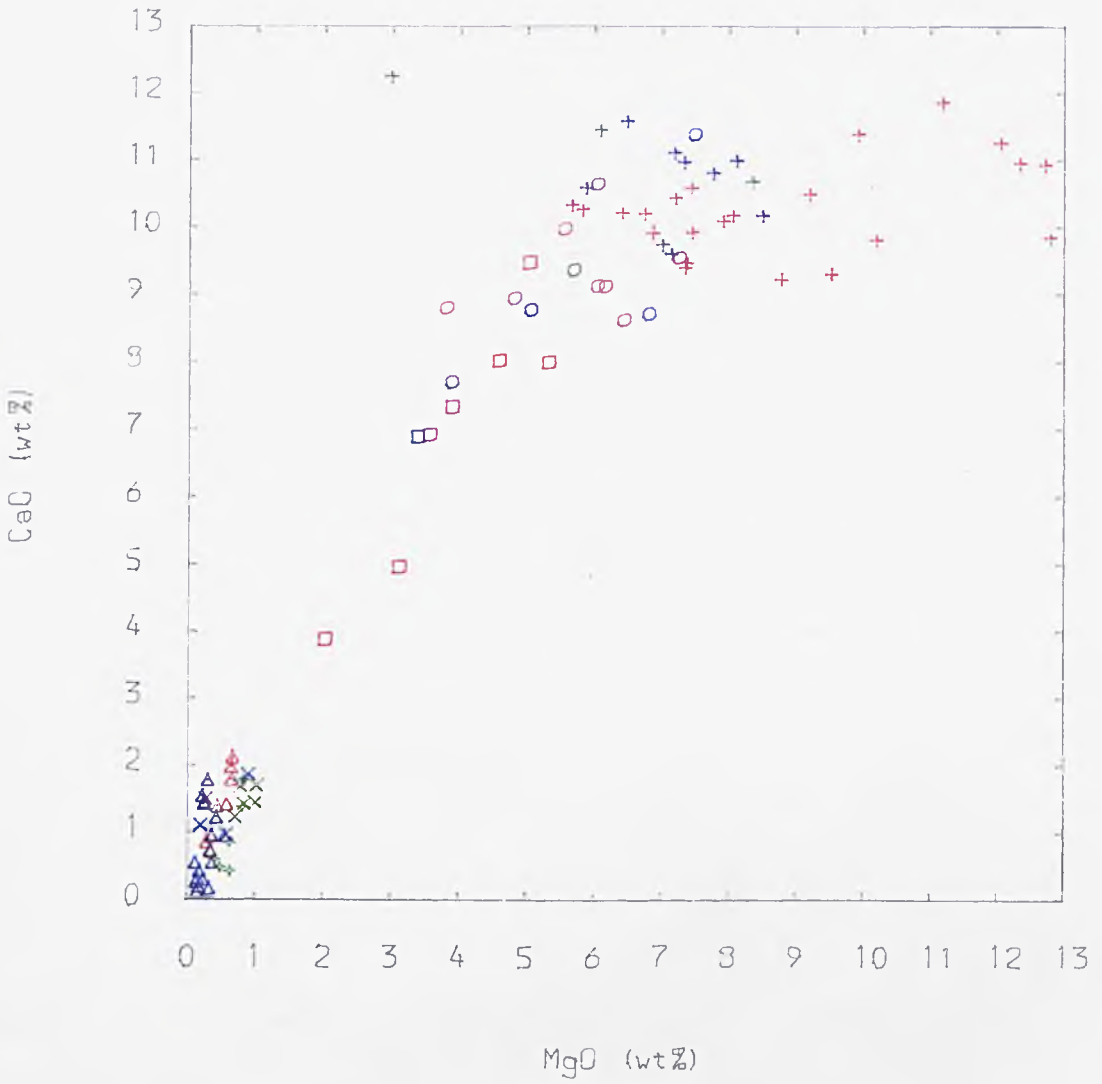
6.5 Temporal Variations

It is convenient for discussion purposes to divide the suite into basic rocks (basalts, hawaiites and mugearites) and acidic rocks (trachytes, rhyolites and phonolites). The ignimbrites of the Pyroclastic Sequence are phonolitic in composition. This division of basic and acidic rocks will recur throughout the text. In order to magnify the possible differences which exist, the data will be discussed in two parts.

6.5.1 Basic rocks

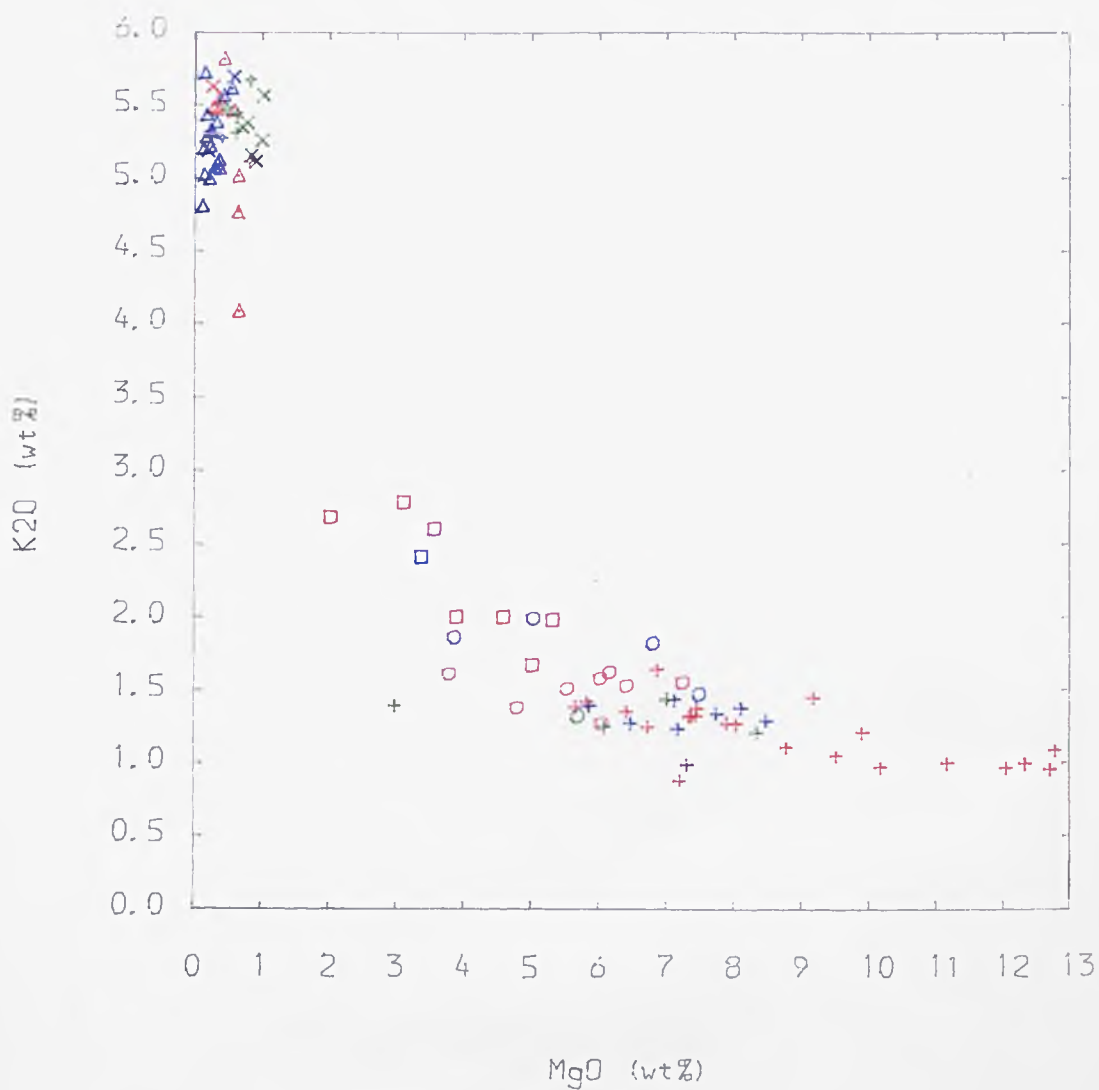
In Figs. 6.3a-d some of the major elements in the basic rocks are plotted against MgO, which is used in the sense of a differentiation index. There are good positive correlations of MgO against Fe_2O_3^T and CaO (Fig. 6.3a), while good negative correlations exist with Na_2O , K_2O (Fig. 6.3b) and SiO_2 . MnO behaves relatively uniformly. TiO_2 in general decreases with MgO but, owing to its large analytical error, the correlation is poor. The trends observed in Al_2O_3 vs MgO (Fig. 6.3c) and P_2O_5 vs MgO (Fig. 6.3d) are discussed below.

Several points emerge from studying the above diagrams. The range in wt% oxide for New Series rocks, in general, encompasses and extends the range in wt% oxide in Old Series rocks. The data for the New Series tends to show a greater coherency than does those for the Old Series rocks. There appears to be no striking differences between Old and New Series rocks, although in detail the Old Series rocks for a given silica concentration, on average contain less MgO. There is also a tendency for members of the Old Series to be slightly more under-saturated (Fig. 6.1). Finally, in the diagram of Al_2O_3 and P_2O_5 vs MgO (Figs. 6.3c-d), as well as in Al_2O_3 and P_2O_5 vs SiO_2 (Figs. 6.2b and 1), it can be seen that the two



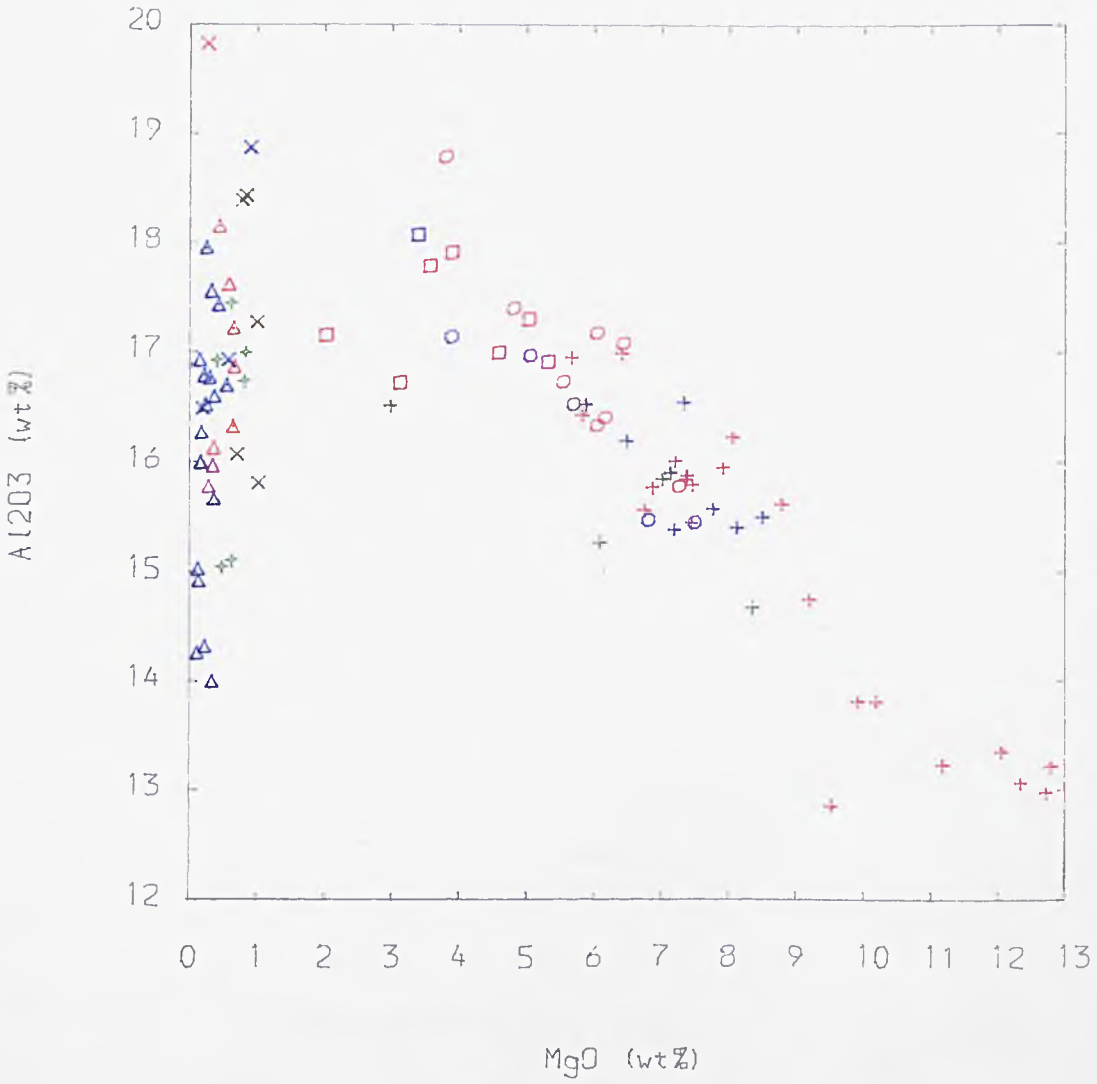
TITLE : Fig : 6.3a-d Selected Majors vs MgO

NEW SERIES ROCKS = red
 PYROCLASTIC SEQUENCE ROCKS = green
 OLD SERIES ROCKS = blue



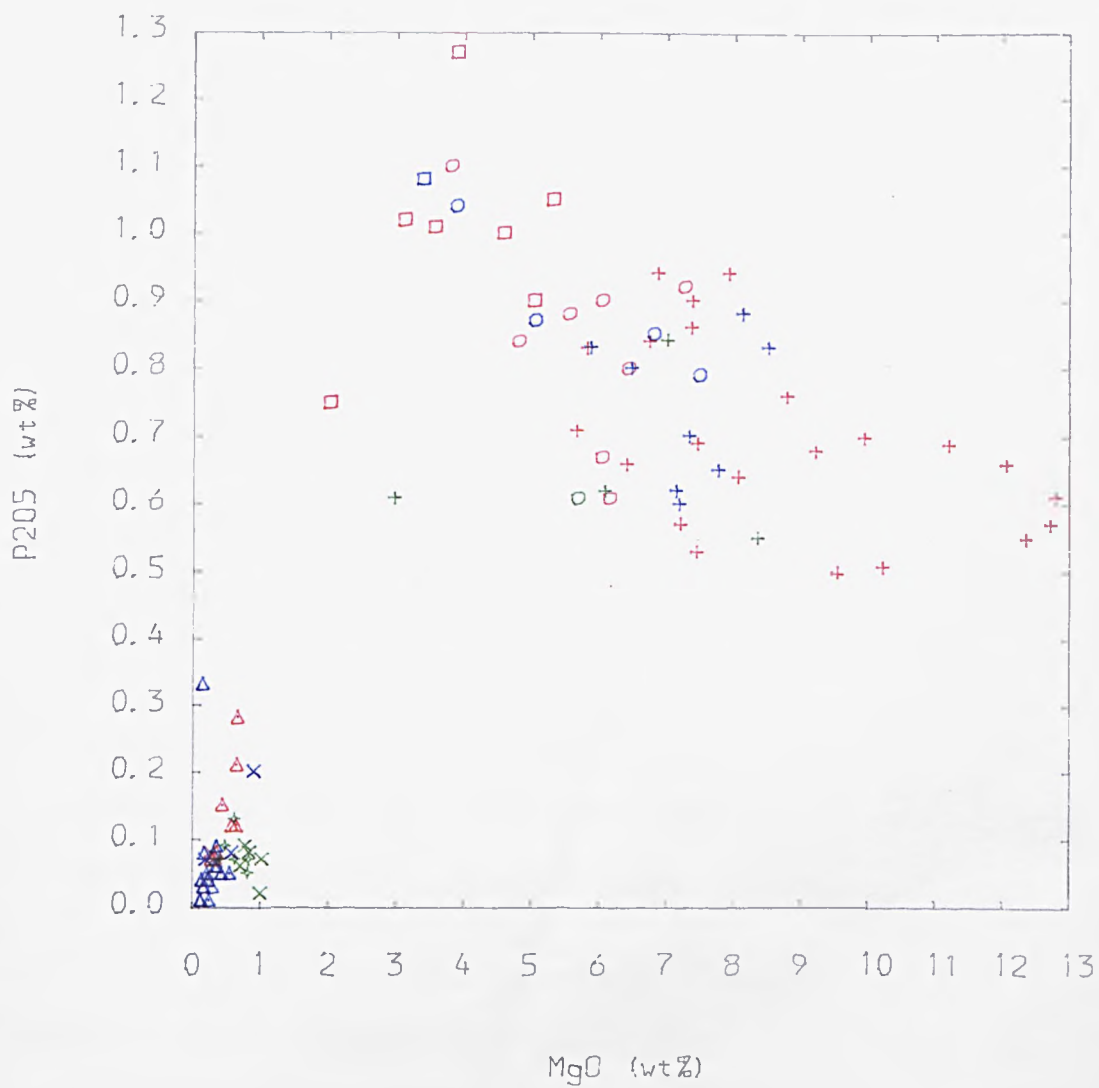
TITLE : Fig : 6.3a-d Selected Majors vs MgO

NEW SERIES ROCKS = red
 PYROCLASTIC SEQUENCE ROCKS = green
 OLD SERIES ROCKS = blue



TITLE : Fig : 6.3a-d Selected Majors vs MgO

NEW SERIES ROCKS = red
PYROCLASTIC SEQUENCE ROCKS = green
OLD SERIES ROCKS = blue



TITLE : Fig : 6.3a-d Selected Majors vs MgO

NEW SERIES ROCKS = red
 PYROCLASTIC SEQUENCE ROCKS = green
 OLD SERIES ROCKS = blue

most evolved mugearites (24026 and 24019) of the New Series show a decrease in Al_2O_3 and P_2O_5 relative to the trend established in the more primitive basic rocks.

6.5.2 Acidic rocks

Although the temporal differences amongst the basic rocks could be considered slight, such differences that exist may have given rise, with continued differentiation, to the much greater differences in major elements that occur in the acidic rocks. This is illustrated in Figs. 6.2a-1, where the major elements are plotted against SiO_2 . Silica is considered preferable to MgO as an index of differentiation, as the latter is considered less suitable in acidic rocks where the concentrations are less than 1% and thus have an inherently larger relative error. Silica, on the other hand is protected from this problem through its large range and high concentration.

Again some important points emerge. Firstly, in most of the diagrams, Old and New Series rocks are relatively distinct. Furthermore, phonolites particularly from the Pyroclastic Sequence are also generally distinct from other Old Series rocks. In the Old Series rocks, not necessarily rocks from the Pyroclastic Sequence, there are reasonable correlations of CaO , K_2O , Na_2O , and $\text{Fe}_2\text{O}_3\text{T}$ vs SiO_2 . Alkalis and TiO_2 , on the other hand, appear to show two trends and thus possibly two evolution paths. Phonolites from the Pyroclastic Sequence show a good trend to under-saturation (cf alkalis vs SiO_2 , Fig. 6.1). In other plots, despite good correlations, the order of rocks is sometimes altered. The New Series rocks show very coherent patterns in all diagrams except those involving Al_2O_3 and MnO . In diagrams of CaO , TiO_2 , $\text{Fe}_2\text{O}_3\text{T}$, Na_2O and K_2O vs silica two separate, and sometimes opposing, paths of evolution are present. In all the

Both the Old Series and the New Series acidic rocks are divisible into groups on the basis of their trace element and isotopic characteristics. The division in the Old Series is based largely on the extent to which they have been contaminated by basement rocks. While this effect is perceptible in the major elements, such that the same groups can be recognised, it is felt inappropriate to make the distinctions at this stage. This is primarily because the fine structure of the groups is much more apparent when the trace element data can also be examined.

6.6 Interpretation

Having presented the major element data in the previous sections, it is now proposed to go some way towards explaining it. A significant observation to be made from the data is that both series constitute a coherent suite of rocks, broken by a 'silica gap'. These coherent trends are indicative of the rocks being cogenetic, such that the trachytes and phonolites have evolved by some differentiation process from a primitive magma or magmas.

Two differentiation processes, fractional crystallisation and variable degrees of partial melting were advocated by Bowen (1928), which, in principle, can produce coherent chemical variation diagrams. Variable degrees of partial melting could account for the major element data of the basic rocks, but it is extremely unlikely, under any circumstance, that trachytes or phonolites could be produced directly by such a mechanism. It would also be difficult to explain the behaviour of alumina and P_2O_5 , without invoking contrived conditions. Moreover, trace element and isotopic data will be presented that would make variable partial melting untenable as an important process in the variation of basic, as well as the acidic,

rocks of each series. It is recognised that differences observed between more basic members of the Old and New Series may be the result of variable partial melting and may also contribute to some of the major element scatter. Clearly, evidence from other sources is required to demonstrate this.

If variable degrees of partial melting is rejected as a major within - series differentiation process, this then leaves fractional crystallisation as a major process to be considered.

Before discussing which phases may have fractionated, it is important to bear in mind the petrographic evidence (Fig. 4.1). This provides important constraining information on which phases are present as phenocrysts in a given rock type, and in what modal proportions they occur and are therefore available for fractionation. In Chapter 4, it was discussed that in primitive basalts, olivine is the dominant phenocryst phase. Its modal proportion decreases from basaltic rocks to acidic rocks, where it rarely occurs. Phenocrysts of clinopyroxene are relatively uncommon in primitive basalts, but they become increasingly dominant in basalts and particularly hawaiites, before decreasing in modal proportion in more evolved rocks. Plagioclase phenocrysts are rare in basalts but become modally important in hawaiites and mugearites. In general, plagioclase is not present in acidic rocks. Phenocrysts of anorthoclase are only found in acidic rocks where they are modally predominant. Opaques are present throughout the suite and apatite is present in small modal proportions, primarily in mugearitic rocks.

In Figs. 6.2a, c, e and f, for TiO_2 , Fe_2O_3 , MgO , and CaO vs SiO_2 , it is seen that these oxides all decrease from primitive basalts.

Their depletion is consistent with the fractionation of olivine, clinopyroxene + magnetite. The fractionation of magnetite is more difficult to establish, however, from major elements alone. The petrographic observations suggest that olivine is more likely to have fractionated first and is later joined by clinopyroxene. In Figs. 6.2a, a fractionation vector corresponding to the removal of the above assemblage is schematically drawn.

In Figs. 6.2b and i, both alumina and P_2O_5 increase to rocks of mugearitic composition and then fall in concentration towards trachytic rocks. Such a feature is consistent with the fractionation of plagioclase and apatite, both of which reach a peak in modal proportions in hawaiitic and mugearitic rocks. The fractionation vector in these diagrams shows the expected effect of significant amounts of plagioclase and apatite fractionation occurring at the mugearitic stage. In fact some of the evolved mugearites, e.g. 24019 and 24026, begin to show depletions in alumina and P_2O_5 , and may indicate the stage at which this process began to operate. For all other oxide plots, these two mugearites continue the enrichment or depletion established in the basic rocks, and so these departures are unlikely to be anomalous. Identifying the cusp of such a trend enables the magma compositions at which plagioclase and apatite begin to fractionate in significant proportions to be pinpointed. Further trace element evidence will be used to support this contention (Chapter 7). Interestingly, it may not be coincidental that the onset of significant plagioclase and apatite fractionation also effectively marks the beginning of the silica gap. In this connection Sparks (1983), stated that significant plagioclase fractionation leads to a decrease in density. The absence of benmoreite rocks could be

explained by this effect if the higher density of these liquids inhibited their eruption. Continued plagioclase fractionation could lower the density of more evolved magmas and perhaps facilitate their eruption. Other factors less tangible than this, such as the position of the magma in the crust and therefore the density contrast between magma and wall-rock and the viscosity of the magma may have also contributed to this effect. Among acidic rocks, the fractionation of anorthoclase could explain the trends that are observed, particularly illustrated by K_2O vs SiO_2 (cf Fig. 6.2h). Na_2O , K_2O and SiO_2 all increase in concentration in early stages of fractionation and are consistent with the fractionation of olivine, clinopyroxene and plagioclase. The retardation, and in some cases the decrease, of these oxides is similarly consistent with the fractionation of anorthoclase at late stages of differentiation. A schematic line representing anorthoclase fractionation is shown on Fig. 6.2h.

6.7 Conclusions

On the basis of major element variations, the Jebel Marra volcanics can be classified as belonging to the alkali basalt - trachyte/phonolite suite. In acidic rocks, differences between the Old and New Series are recognised. Among basic rocks differences are much less apparent. In both series, a 'silica gap' corresponding to rocks of benmoreite composition is present. It would seem improbable that the variations in major elements could be solely explained by variable degrees of partial melting. However, some of the scatter observed in the variation diagram is likely to be the result of variable degrees of partial melting and slight variations in the composition of the mantle source. However, most of the variations in major elements can be explained by fractional crystal-

lisation. The data are consistent with the fractionation of olivine and clinopyroxene in basic rocks, the fractionation of plagioclase and apatite from mugearites to trachytes and the fractionation of anorthoclase in acidic rocks. At this stage it is difficult to make valued statements on the extent to which other processes, such as crustal assimilation, or variable degrees of partial melting have occurred. Answers to questions such as these are more tractable using trace element and isotopic evidence.

CHAPTER SEVEN

TRACE ELEMENTS

7.1 Introduction

The aims of this Chapter are first to document the variations in trace elements which occur throughout the Jebel Marra suite, and to relate these to the magmatic processes which may have operated such as fractional crystallisation and crustal assimilation.

An important advantage of trace elements over major elements, from a point of view of understanding the processes of magma generation is that their range invariably shows a manifold increase in concentration from basic to more evolved rocks. Related to this, is the amount with which different minerals incorporate a trace element, which often varies by orders of magnitude. It is primarily these differences which enable trace elements to be used as such powerful tools in petrogenetic modelling.

7.2 Definitions

7.2.1 Trace Element

An element can be considered to be a trace element if it approximates to the relationship of Henry's Law (for a more detailed discussion see Powell, 1978, pp.46-53). In general, this will apply to concentrations which are approximately less than 1% by weight (Cox et al., 1979).

7.2.2 Distribution Coefficient (Kd)

The following expression is used:-

$$Kd = \frac{\text{Concentration in mineral}}{\text{Concentration in liquid}} \quad \text{Eqn. 7.1}$$

Where the K_d for a given element is a constant, known as the distribution or partition coefficient for a crystal in equilibrium with its host liquid.

7.2.3 Bulk Distribution Coefficient (D)

It is often necessary to consider the distribution of an element over more than one phase, and this is described by the bulk distribution coefficient, D .

$$D = \frac{\sum_{i=1}^n w_i K_{D,i}}{\sum_{i=1}^n w_i} \quad \text{Eqn. 7.2}$$

where w_i represents the weight proportion of the phases in the given assemblage.

7.2.4 Classification

Using K_d 's it is convenient to divide trace elements into those which are compatible, where $D > 1$, and those which are incompatible, where $D < 1$ (and usually $\ll 1$).

Note that the behaviour of an element can change dramatically during fractionation. For example, in some volcanic suites (including Jebel Marra) Sr is incompatible amongst basic rocks until plagioclase begins to fractionate in significant proportions (about 50%) so as to then render it compatible.

A group of trace elements are additionally classified as large ion lithophile elements (LILE): these include K, Sr, Rb, Ba, Th and light rare earth elements (LRRE's). They may be thought of as those elements which are incompatible with regard to 'common mantle' minerals i.e. olivine, pyroxenes, spinel and garnet. However, for simplicity the rare earth elements (REE's) will be regarded as a group on their own. A further useful subdivision can be made for those incompatible elements which have a high field strength (Pearce and

Norry, 1979), a property which has the effect of making them immobile in most weathering processes. These include Zr, Y, Ti and Nb. Unless specified, 'compatible' elements may be assumed to refer to the elements Sc, Cr, Co, Ni, Cu and Zn.

7.3 Overall Variations

7.3.1 Introduction

Trace element abundances were measured in parts per million (by weight) by X.R.F. techniques for 99 rocks for all the elements mentioned above, as well as for La, Ce and Nd. (see Appendix C). In addition, REE's were measured by stable-isotope dilution (ID) techniques (Thirlwall, 1982; Appendix E) on selected rocks.

In Chapter 6 it was considered that much of the major element data is consistent with fractional crystallisation. The variation of the compatible elements can be used as further evidence against variable degrees of partial melting being an important affect. Given that melting occurs in the mantle in which olivine is a residual phase, then elements compatible in olivine, such as Ni and Co, will be buffered and should remain reasonably constant in rocks which are primitive. It is observed however, that Ni and Co are both depleted in more evolved rocks which is consistent with a regime of fractional crystallisation of an assemblage in which olivine is involved, although it is emphasised that variable degrees of partial melting will have some influence on the variations in composition of parental magmas.

7.3.2 Scatter

Inspection of variation diagrams in Chapters 6 and in this Chapter reveal that, although biaxial plots commonly show coherent

trends, they also exhibit a significant degree of scatter. It is unlikely that any suite of rocks will have been melted from a perfectly homogenous source and fractionated to produce lavas whose measured compositions precisely conform to a single line on a variation diagram. In reality a suite of rocks is more likely to result from fractionation of several primary magmas which may have been derived from a homogenous or heterogeneous source, possibly by variable degrees of partial melting. Even the fractionation of the primary magmas may also proceed in differing ways, depending on composition, depth and temperature of the magma for different magma batches. These and other possible factors contributing to the scatter will be discussed separately.

Analytical Error - Some of the observed scatter is inevitably due to analytical error. Regarding the data analysed by the Leeds X.R.F. spectrometer, Downes (1983) considers the relative errors in major elements to be less than 1%, whereas trace elements for the most part are thought to be in the order of 5% relative error (A. Grey, pers. comm., also see Table C2).

Partial Melting - Assuming that the Jebel Marra suite of rocks is derived by differentiation from a number of primary magmas, then they are unlikely to be the result of exactly the same amount of partial melting. The effect of variable degrees of partial melting may be evident in diagrams where elements are plotted against isotopic ratios (Figs. 8.9a-b) for primitive basalts. In this instance, assuming a homogenous source, variable degrees of melting will give rise to differing elemental concentrations, prior to fractionation, but relatively constant isotopic ratios. Once such differences are

established they will largely be maintained by fractionation processes. This may have some relevance to the existence of under-saturated and over-saturated rocks discussed in Section 6.2.

Homogeneity of Source - This is discussed in Section 8.2 which considers isotopic evidence for primitive basalts and concludes that isotopic composition of Nd and Sr in the source region appears to be relatively homogenous.

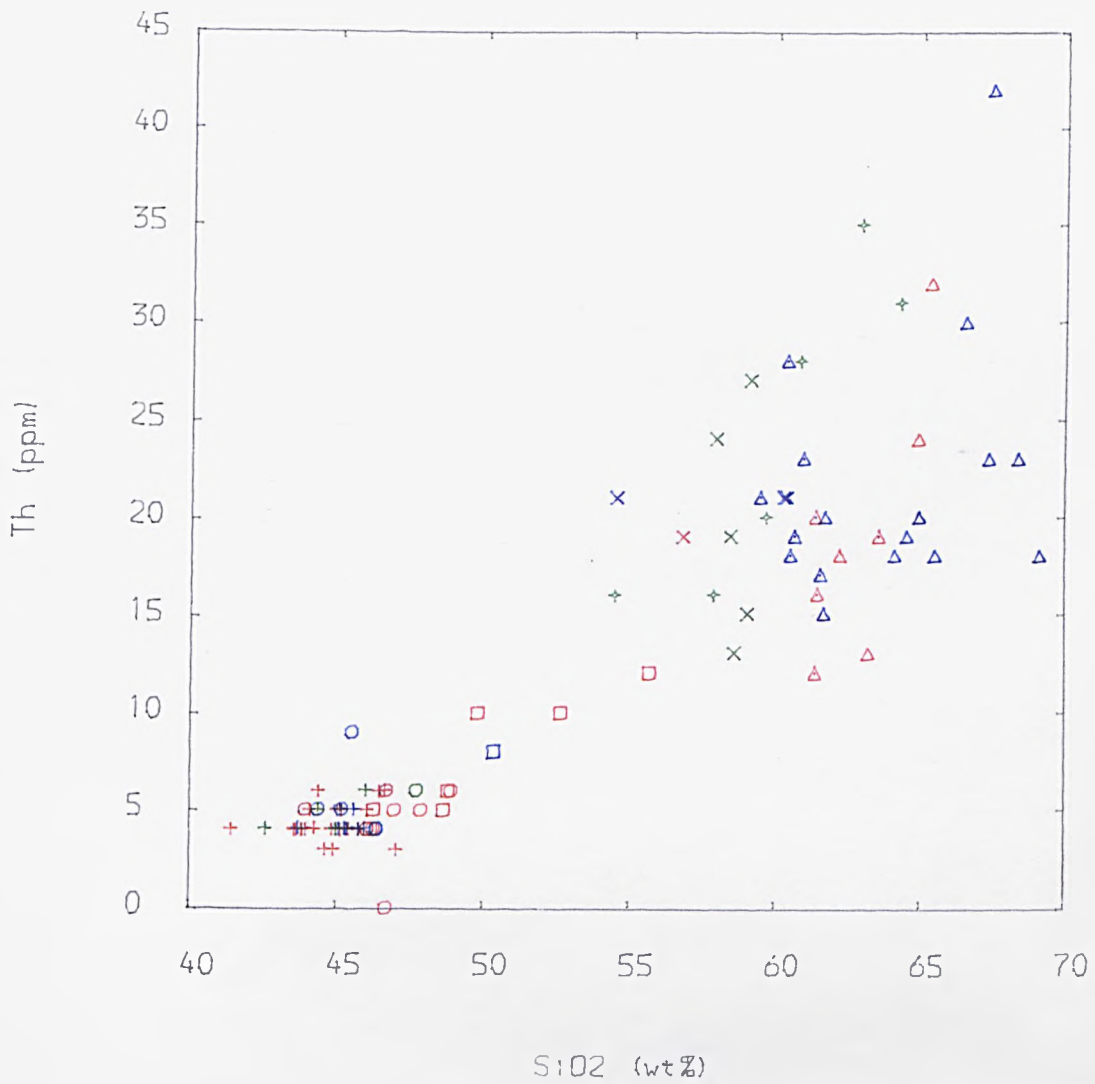
Differentiation Processes - A major influence on the chemistry of the rocks is fractional crystallisation. Scatter may well result from different magma batches evolving slightly differently by fractional crystallisation or by involvement of other differentiation processes (see Section 9.2).

Contamination - Cox and Clifford (1982) have demonstrated that second order processes such as contamination, because they operate less precisely, will contribute, in general, to poor inter-element correlations - or more scatter (see Section 7.6).

Accumulation of Crystals - Inspection of Table H1 reveals that the majority of the Jebel Marra volcanics are porphyritic and in some cases they are highly so. Downes (1983) pointed out that the ubiquity of porphyritic lavas in suites, such as from Jebel Marra, cannot be satisfactorily explained by accumulation of phenocrysts, for if this were the case then there should be an approximately equal number of aphyric lavas present. However, because fractional crystallisation appears to be an integral part of the evolution of these lavas then the relative loss or gain of crystals is inevitable and will result in increased scatter on variation diagrams. For example, diagrams

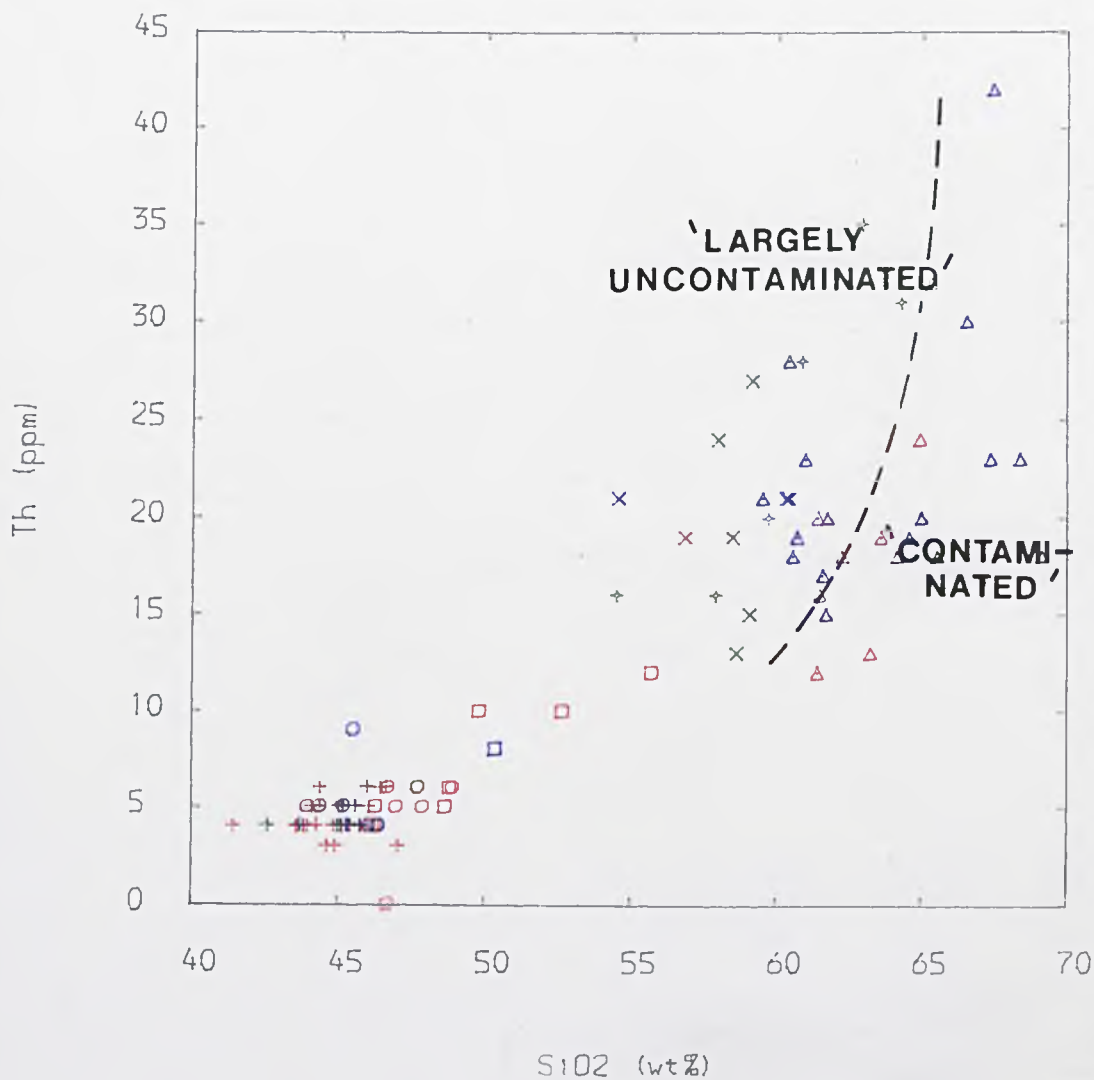
LARGELY
UNCONTAMINATED

CONTAMI-
NATED



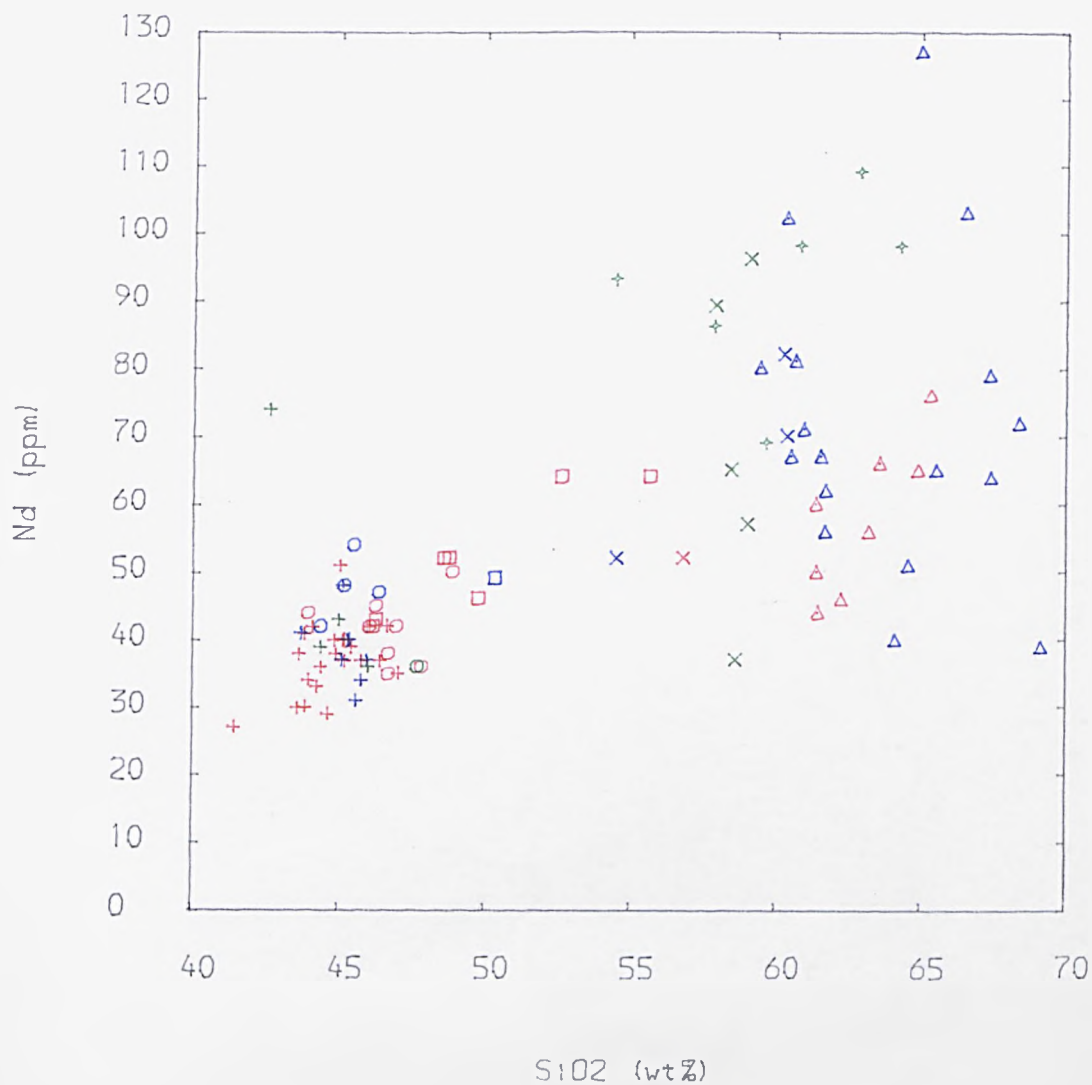
TITLE : Fig : 7.1a-j 'Incompatibles' vs SiO₂
(see text for explanation)

BASEMENT ROCKS	= black
NEW SERIES ROCKS	= red
PYROCLASTIC SEQUENCE ROCKS	= green
OLD SERIES ROCKS	= blue



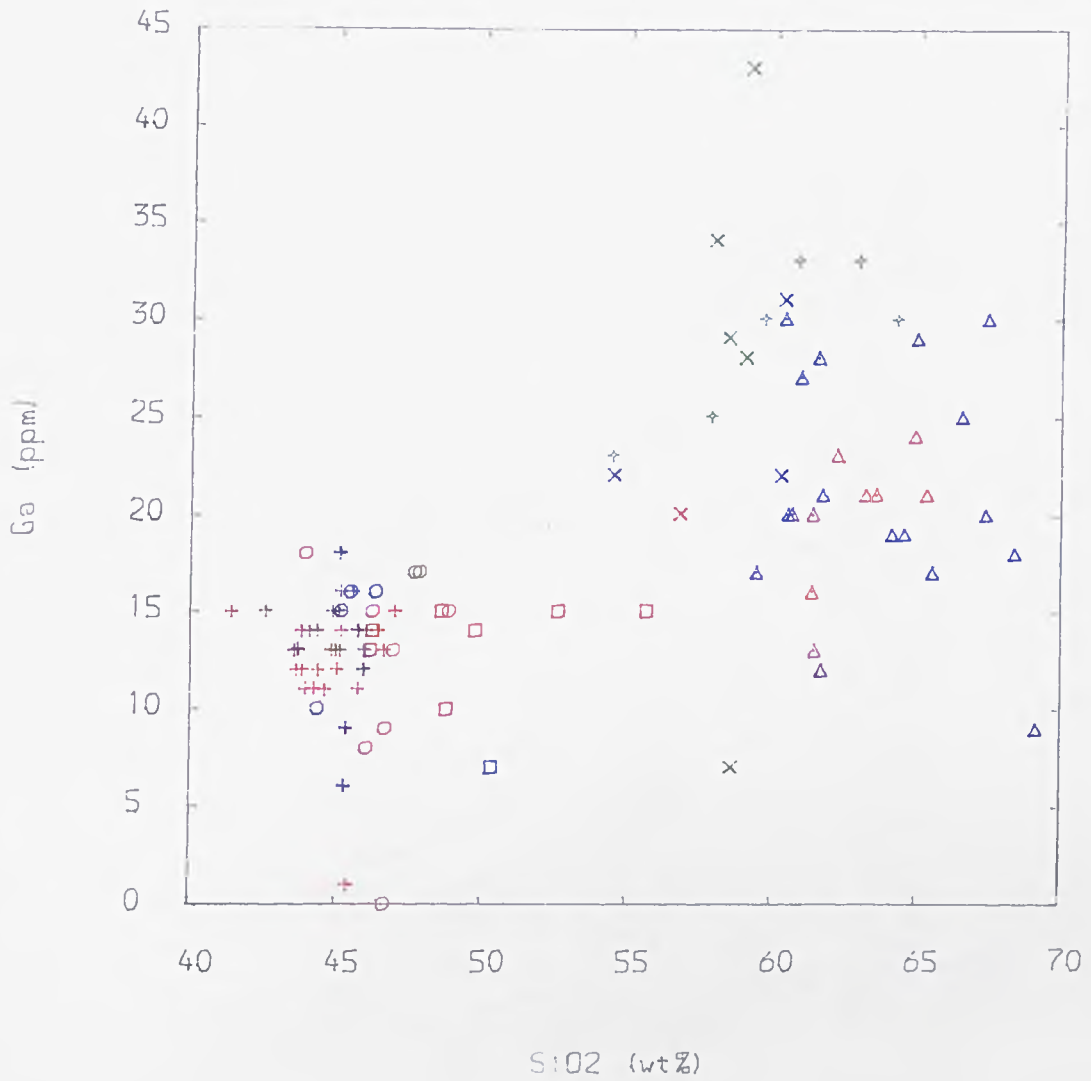
TITLE : Fig : 7.1a-j 'Incompatibles' vs SiO₂
(see text for explanation)

BASEMENT ROCKS	= black
NEW SERIES ROCKS	= red
PYROCLASTIC SEQUENCE ROCKS	= green
OLD SERIES ROCKS	= blue



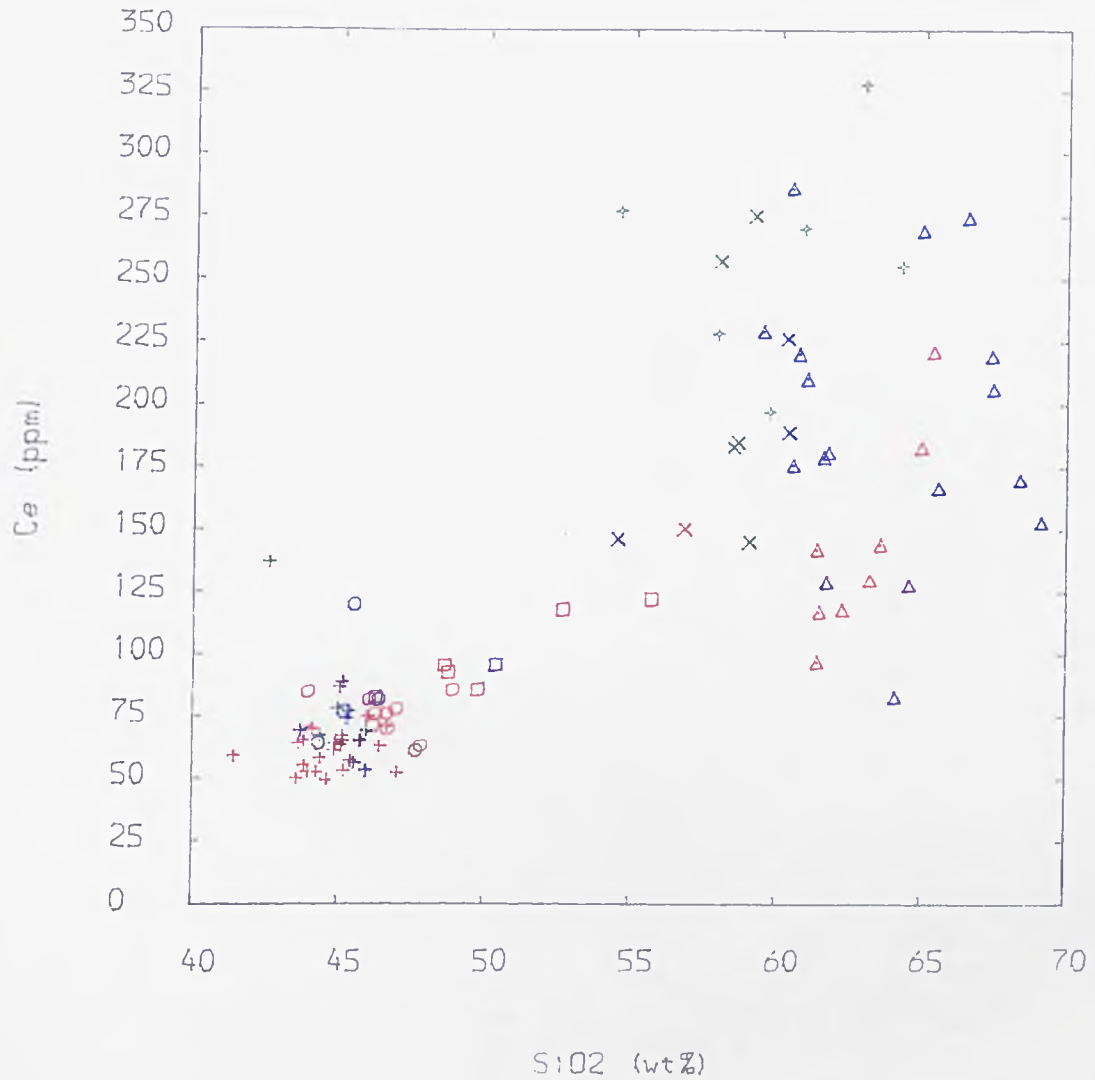
TITLE : Fig : 7.1a-j 'Incompatibles' vs SiO₂

BASEMENT ROCKS	= black
NEW SERIES ROCKS	= red
PYROCLASTIC SEQUENCE ROCKS	= green
OLD SERIES ROCKS	= blue



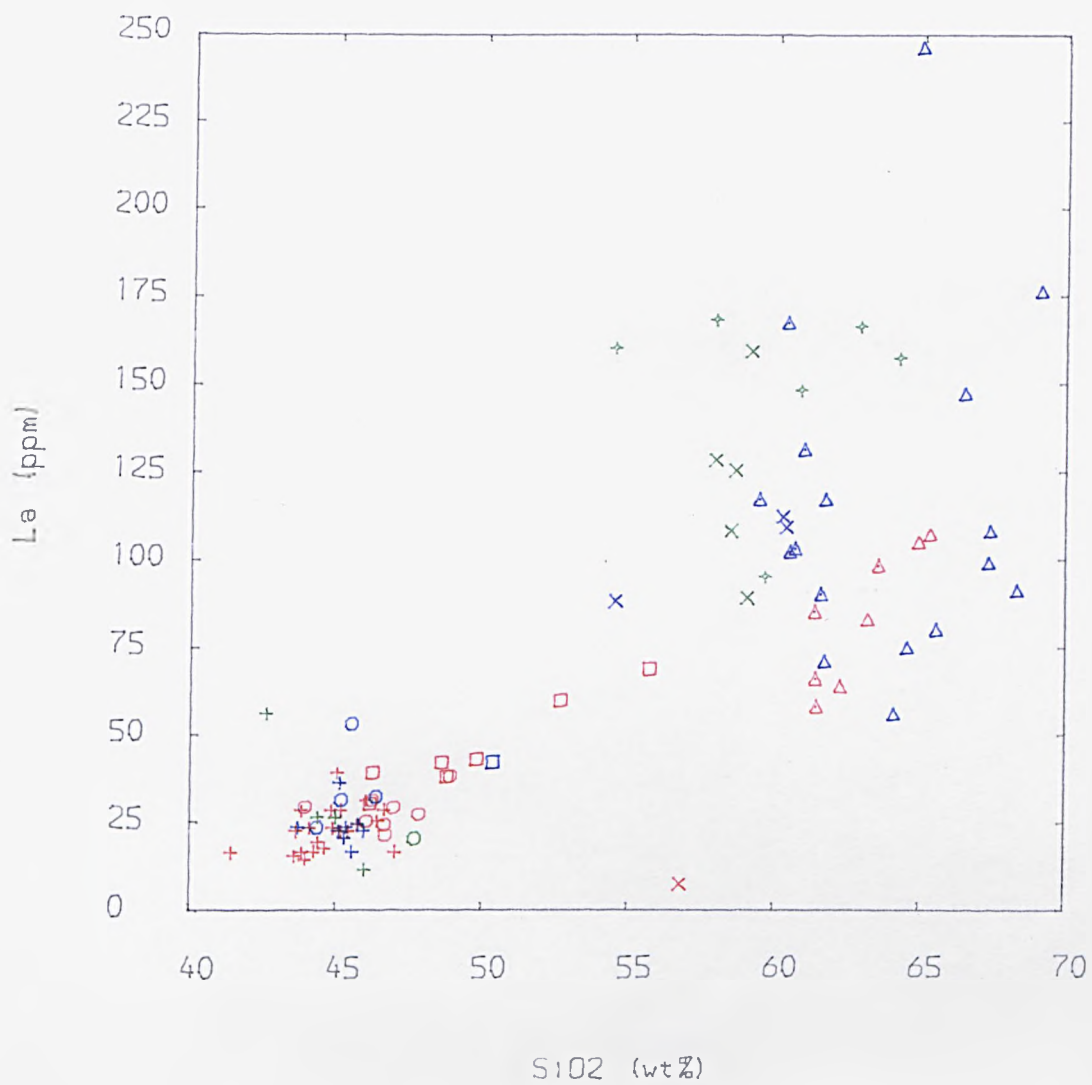
TITLE : Fig : 7.1a-j 'Incompatibles' vs SiO₂

BASEMENT ROCKS	= black
NEW SERIES ROCKS	= red
PYROCLASTIC SEQUENCE ROCKS	= green
OLD SERIES ROCKS	= blue



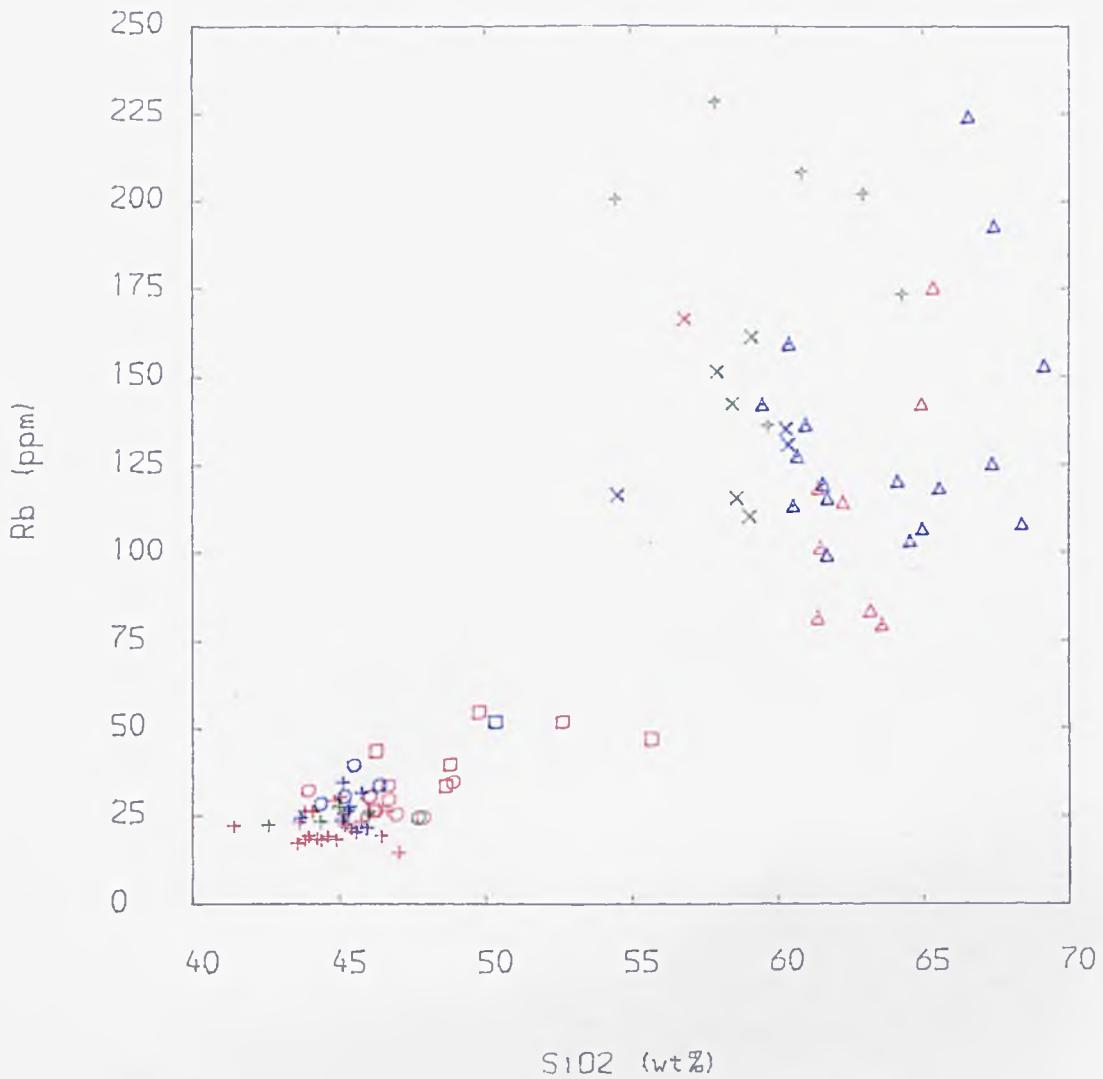
TITLE : Fig : 7.1a-j 'Incompatibles' vs SiO₂

BASEMENT ROCKS	= black
NEW SERIES ROCKS	= red
PYROCLASTIC SEQUENCE ROCKS	= green
OLD SERIES ROCKS	= blue



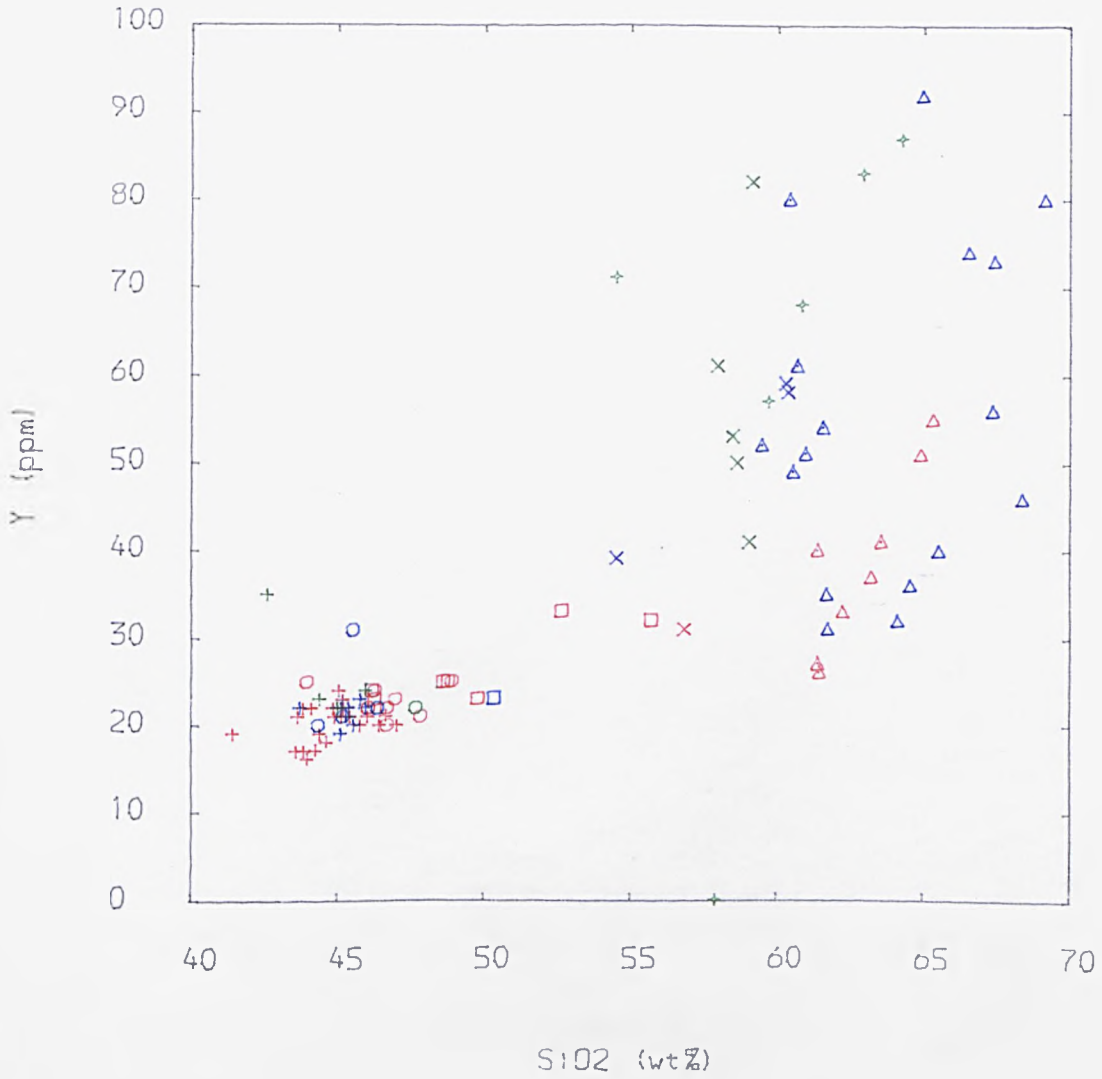
TITLE : Fig : 7.1a-j 'Incompatibles' vs SiO₂

BASEMENT ROCKS	= black
NEW SERIES ROCKS	= red
PYROCLASTIC SEQUENCE ROCKS	= green
OLD SERIES ROCKS	= blue



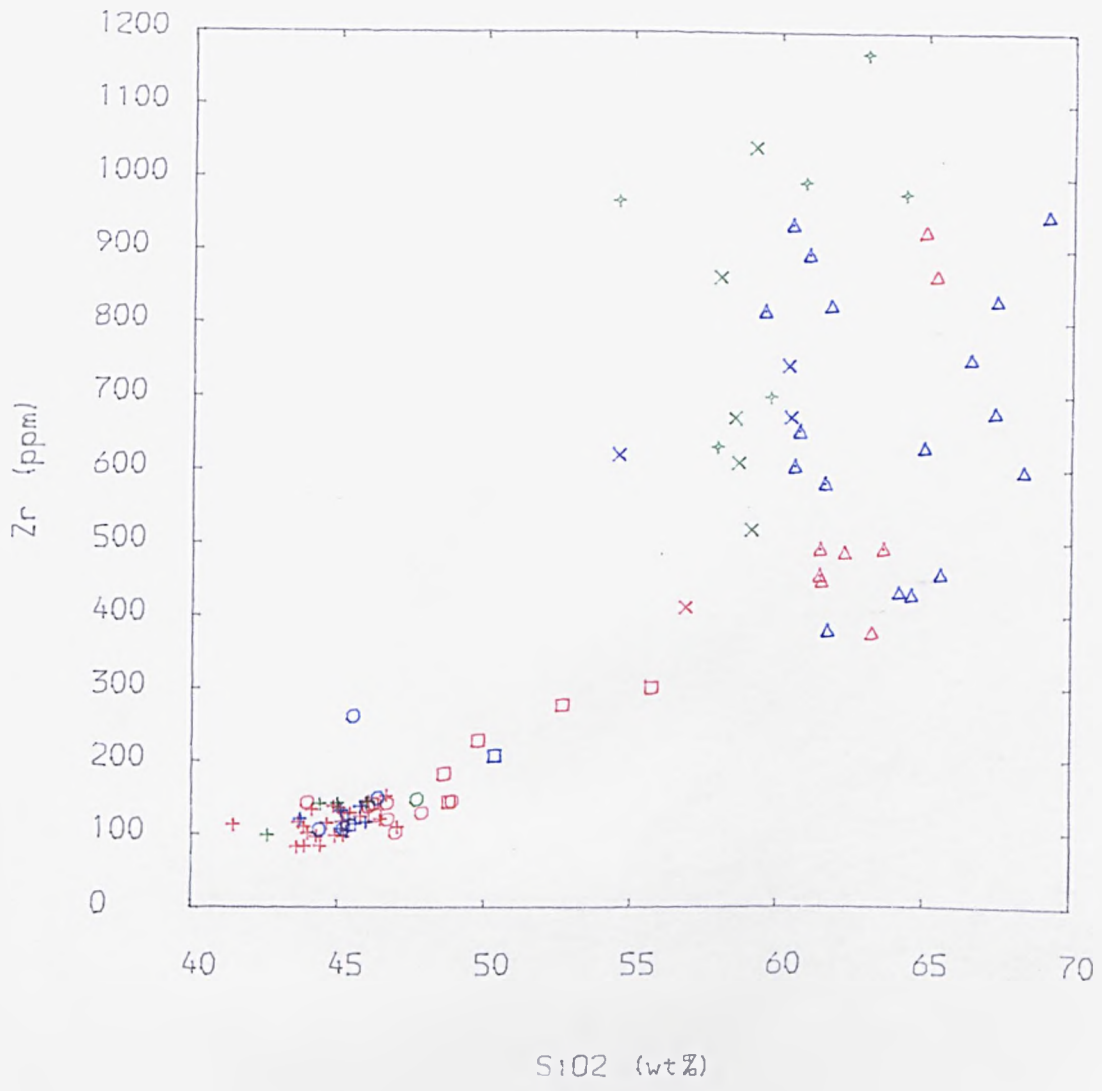
TITLE : Fig : 7.1a-j 'Incompatibles' vs SiO₂

BASEMENT ROCKS	= black
NEW SERIES ROCKS	= red
PYROCLASTIC SEQUENCE ROCKS	= green
OLD SERIES ROCKS	= blue



TITLE : Fig : 7.1a-j 'Incompatibles' vs SiO₂

BASEMENT ROCKS	= black
NEW SERIES ROCKS	= red
PYROCLASTIC SEQUENCE ROCKS	= green
OLD SERIES ROCKS	= blue

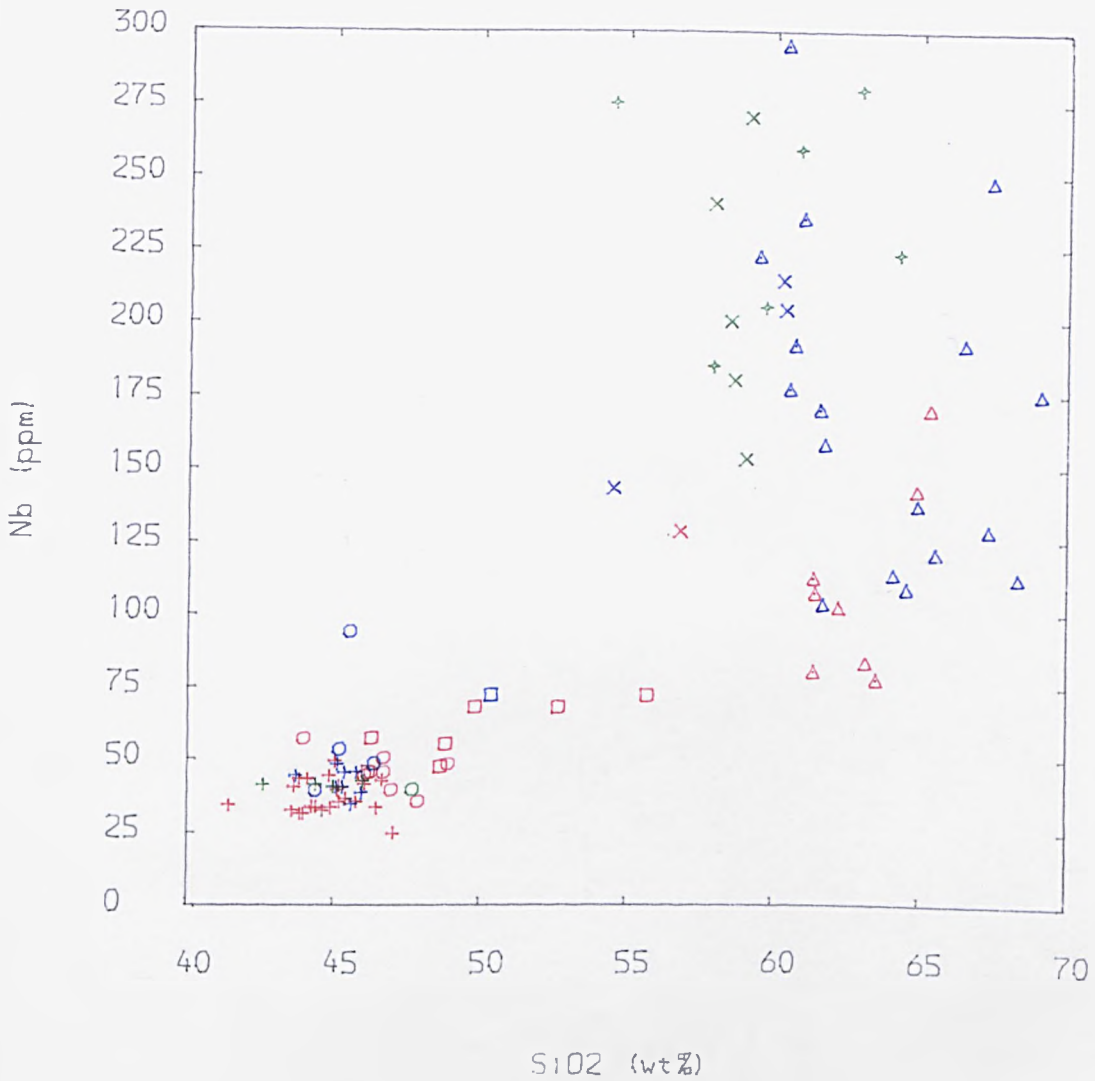


TITLE : Fig : 7.1a-j 'Incompatibles' vs SiO2

- BASEMENT ROCKS = black
- NEW SERIES ROCKS = red
- PYROCLASTIC SEQUENCE ROCKS = green
- OLD SERIES ROCKS = blue

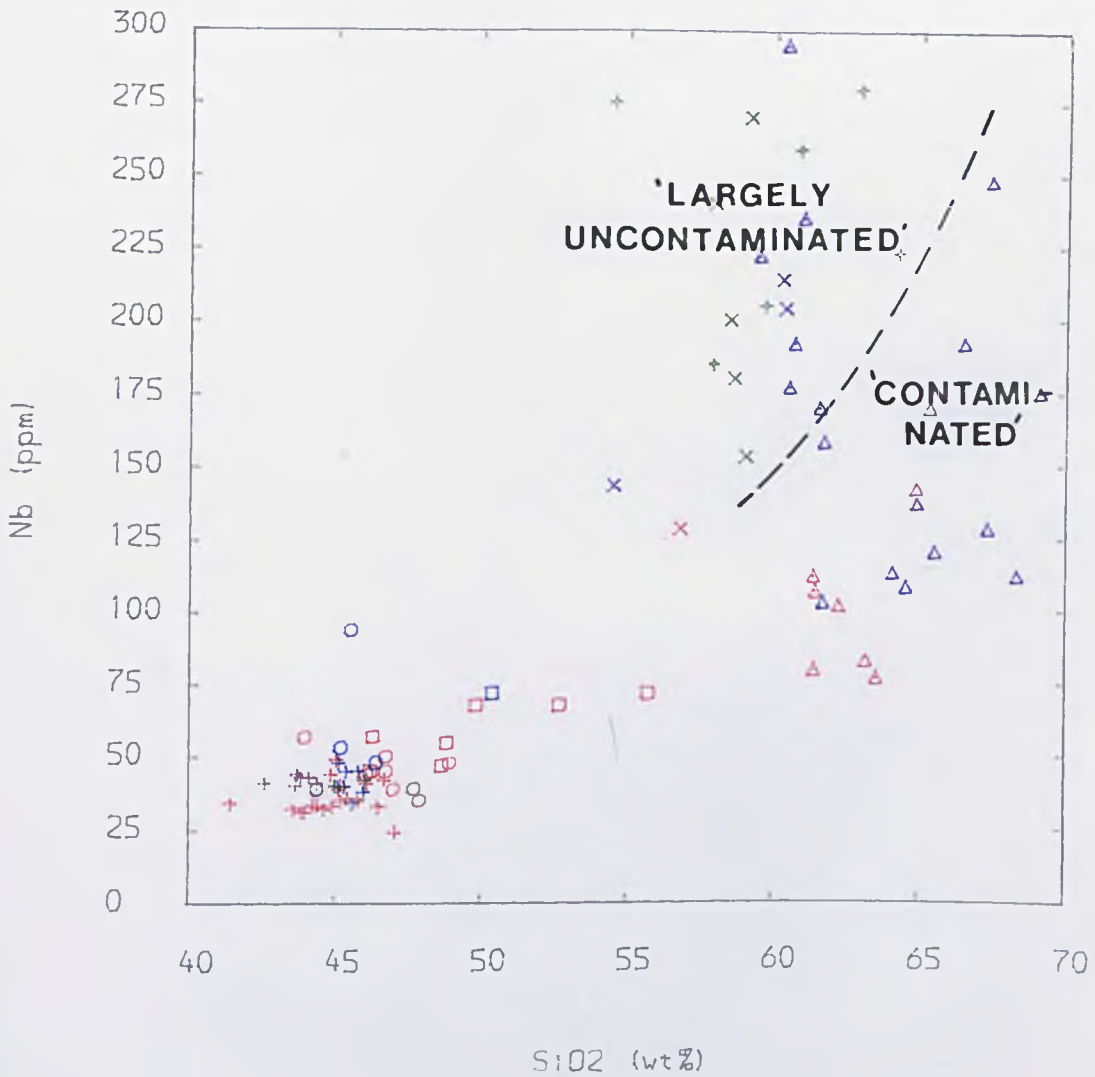
'LARGELY
UNCONTAMINATED'

'CONTAMI-
NATED'



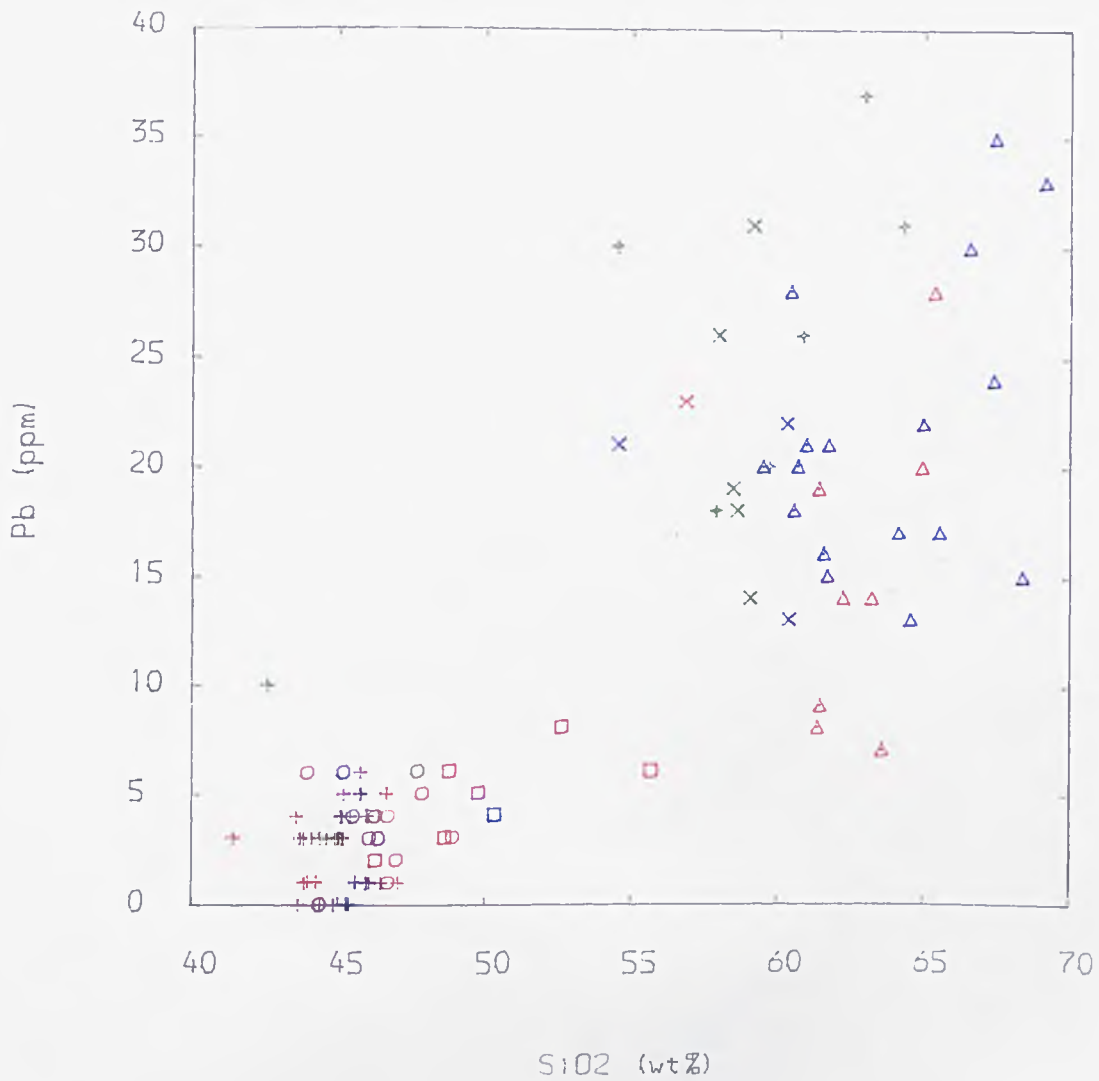
TITLE : Fig . 7.1a-j 'Incompatibles' vs SiO₂

BASEMENT ROCKS	= black
NEW SERIES ROCKS	= red
PYROCLASTIC SEQUENCE ROCKS	= green
OLD SERIES ROCKS	= blue



TITLE : Fig : 7.1a-j 'Incompatibles' vs SiO₂

BASEMENT ROCKS	= black
NEW SERIES ROCKS	= red
PYROCLASTIC SEQUENCE ROCKS	= green
OLD SERIES ROCKS	= blue



TITLE : Fig : 7.1a-j 'Incompatibles' vs SiO₂

BASEMENT ROCKS	= black
NEW SERIES ROCKS	= red
PYROCLASTIC SEQUENCE ROCKS	= green
OLD SERIES ROCKS	= blue

in Chapters 6 and 7 involving Al_2O_3 , CaO and Sr, in which plagioclase bearing samples plot on the high side of the observed geochemical trends could be explained by the accumulation of some plagioclase.

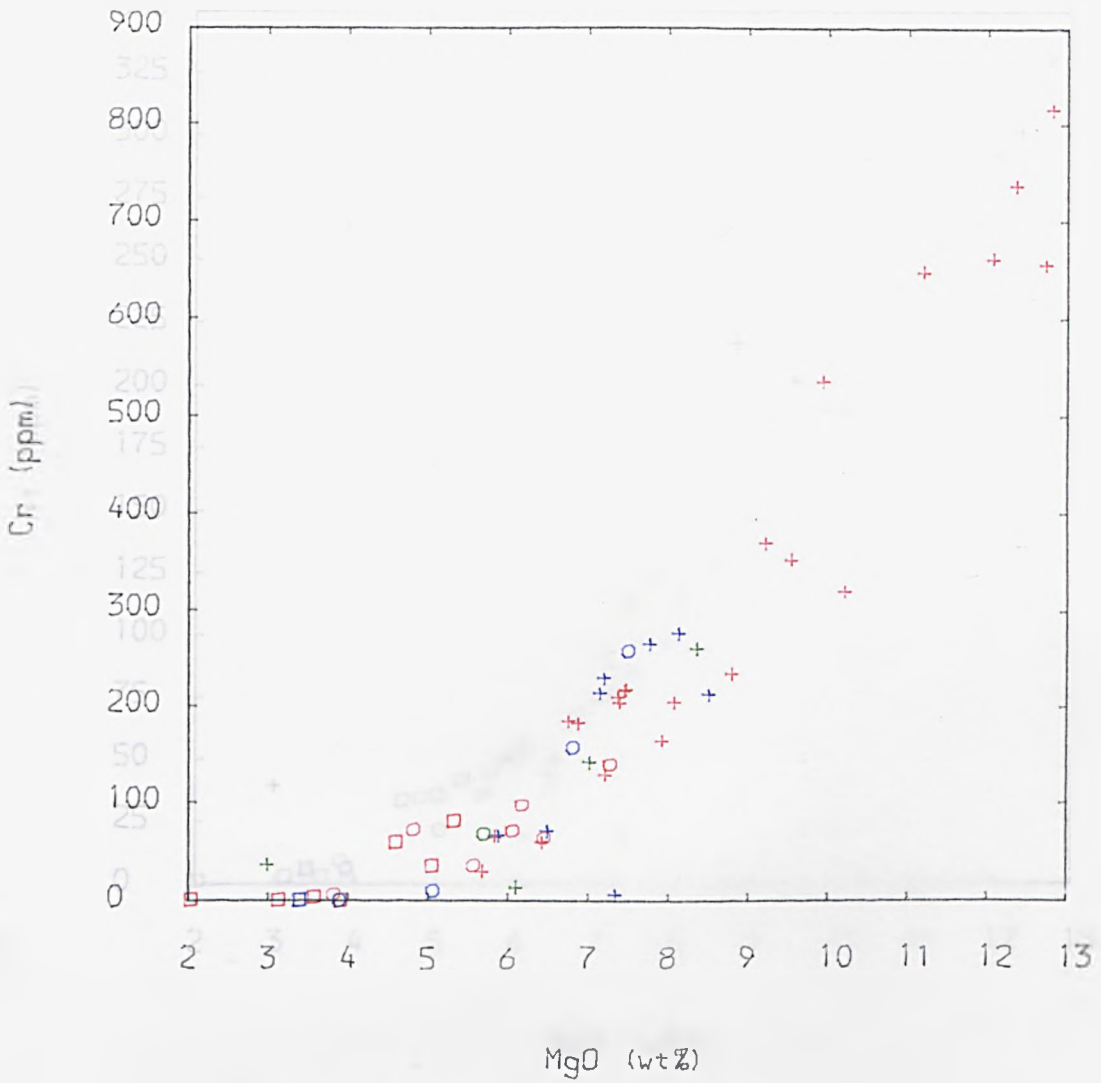
Owing to the behavioural similarities of many of the trace elements it is convenient to deal with them in groups.

7.3.3 'Incompatible' Elements

The elements La, Nd, Nb, Pb, Zr, Th, Ga, Ce, Rb and Y show remarkably similar patterns when plotted against SiO_2 (Figs. 7.1a-j), SiO_2 is used as an index of fractionation as it proves a more illustrative than MgO when the variations across the whole suite are viewed. In these diagrams the trace elements increase with differentiation from basalts through mugearites to trachytes and to more evolved rocks.

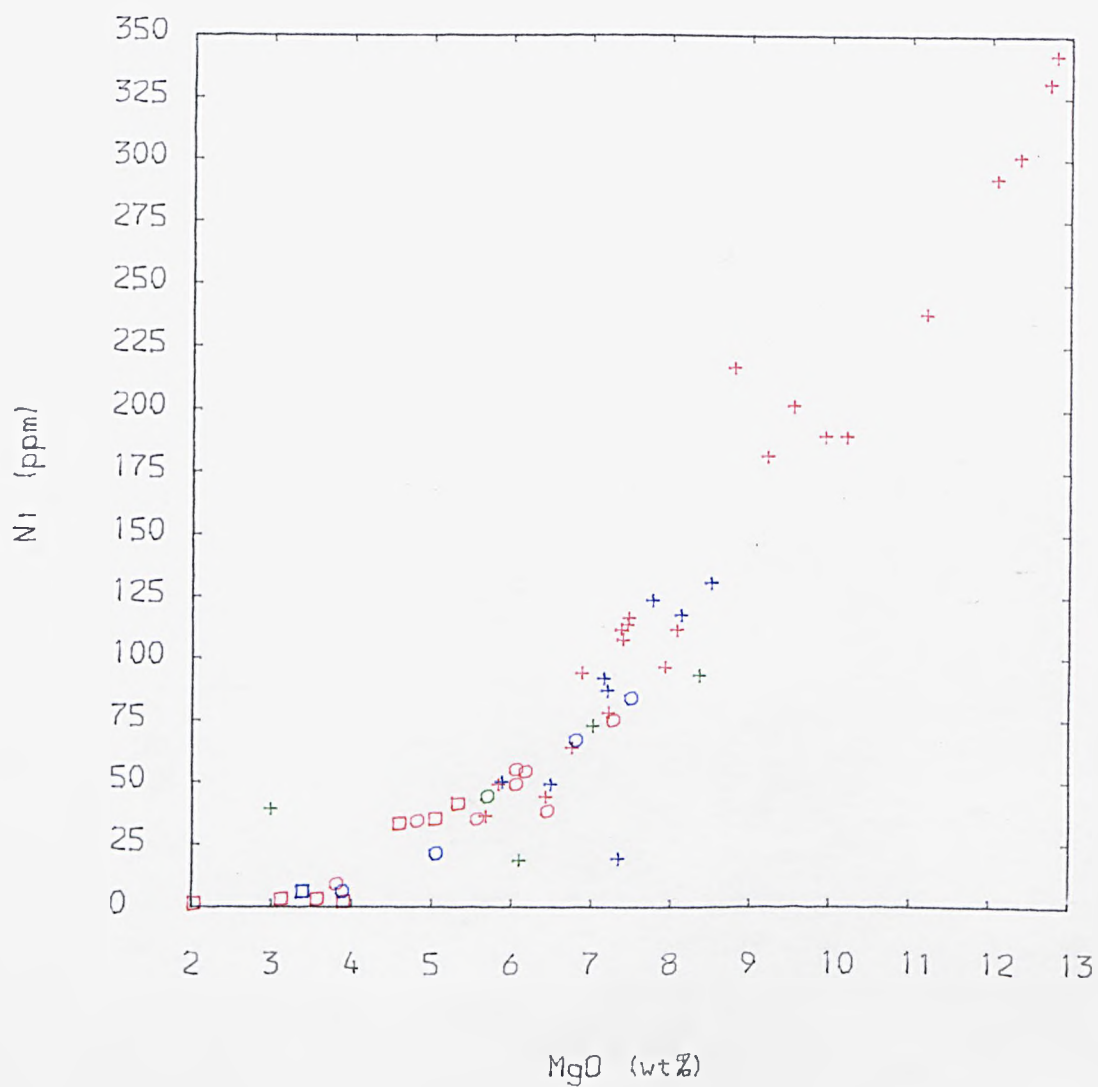
7.3.4 'Compatible' Elements

Because of the marked depletions of these elements they are more profitably viewed plotted against MgO, for basic rocks only. Cr and Ni show very marked depletions from the most primitive basalts to rocks of about 4% MgO where they contain negligible amounts of these elements (Figs. 7.2a-b). At about 6% MgO there may be evidence for an upward inflexion in the trend which is more clearly seen in Fig. 2a. Sc and Co also show similar patterns to each other vs MgO (Figs. 2c-d). With these elements the depletion is less marked and also worth noting is the downward inflexion in the trend which occurs at around 9% MgO. Cu, on the other hand, shows an approximately linear trend when plotted against MgO (Fig. 2e). Zn, plotted against SiO_2 (Fig. 2f), behaves more variably. Its concentration appears to decrease from basalts to primitive mugearites prior to generally increasing through trachytes and on to more evolved rocks.



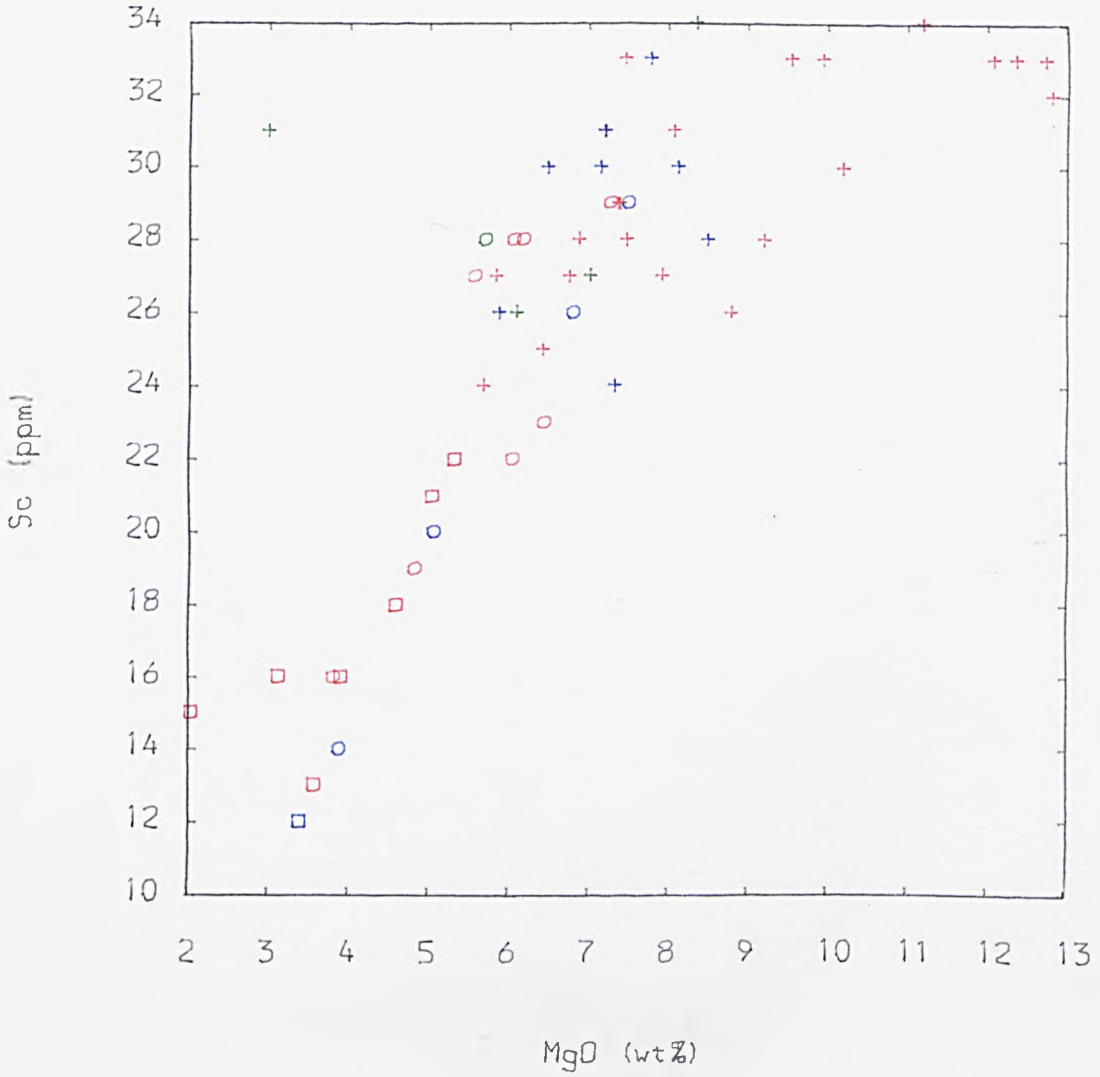
TITLE : Fig : 7.2a-d 'Compatibles' vs MgO

NEW SERIES ROCKS = red
 PYROCLASTIC SEQUENCE ROCKS = green
 OLD SERIES ROCKS = blue



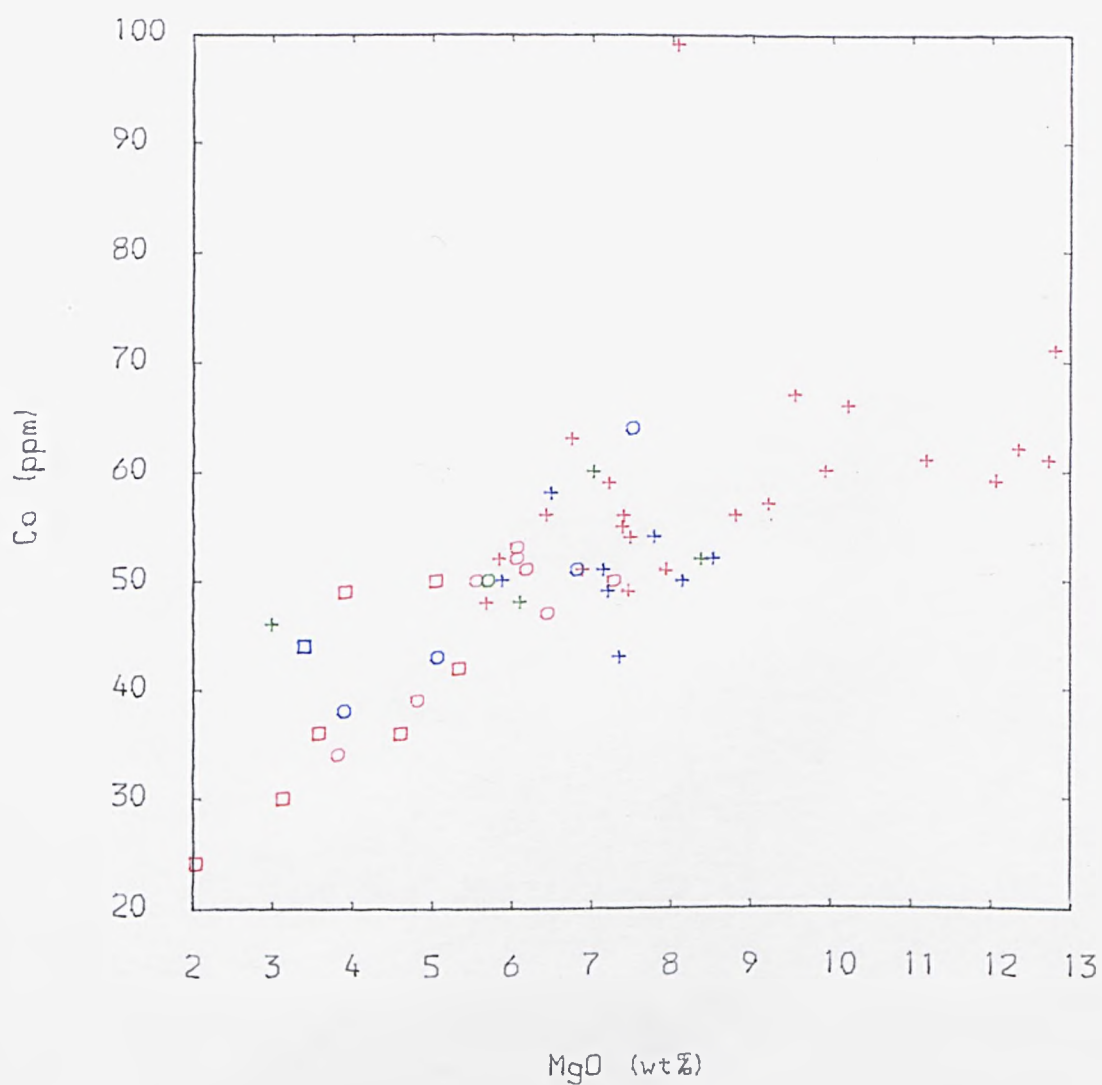
TITLE : Fig : 7.2a-d 'Compatibles' vs MgO

NEW SERIES ROCKS = red
 PYROCLASTIC SEQUENCE ROCKS = green
 OLD SERIES ROCKS = blue



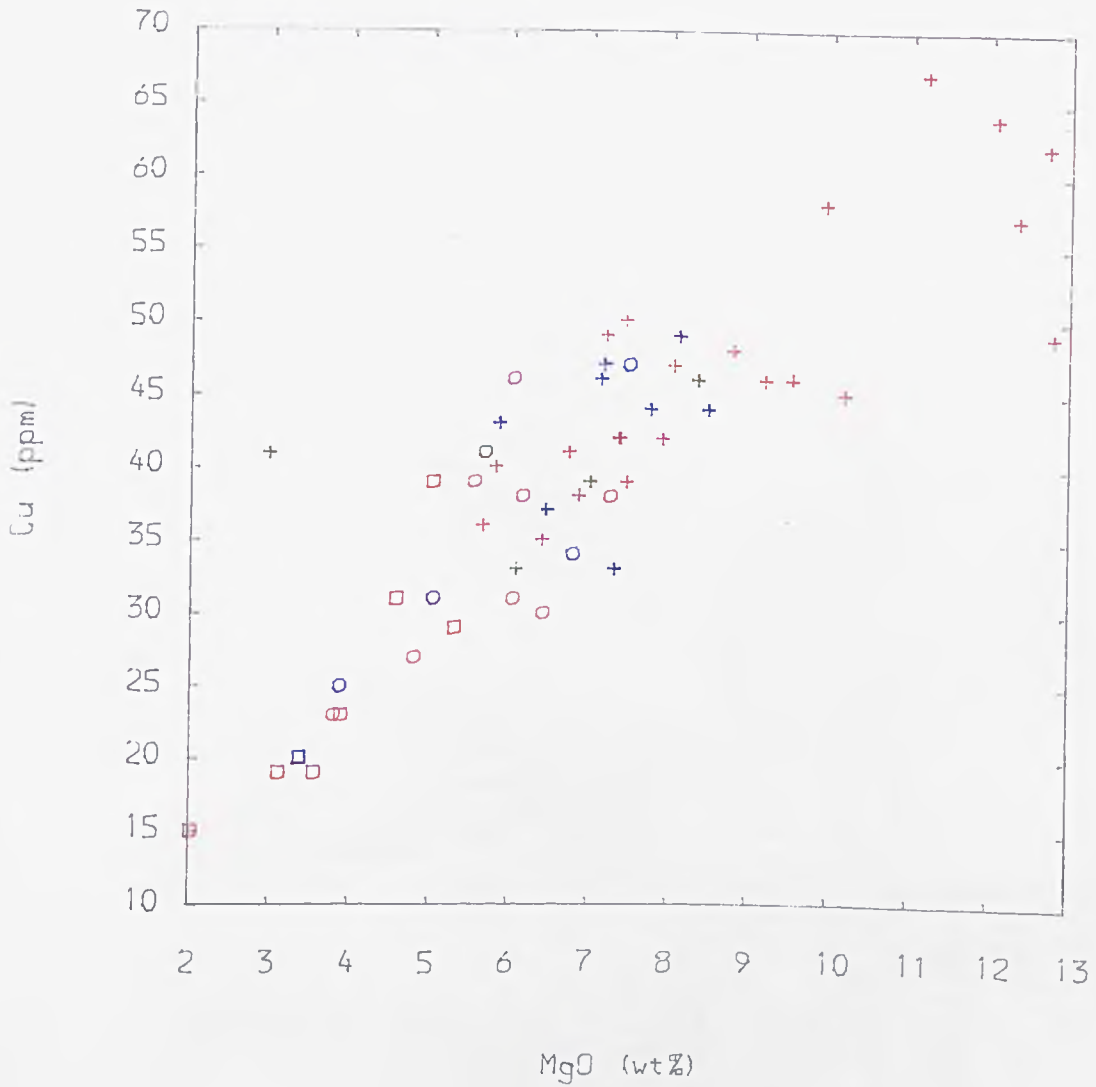
TITLE : Fig : 7.2a-d 'Compatibles' vs MgO

NEW SERIES ROCKS = red
 PYROCLASTIC SEQUENCE ROCKS = green
 OLD SERIES ROCKS = blue



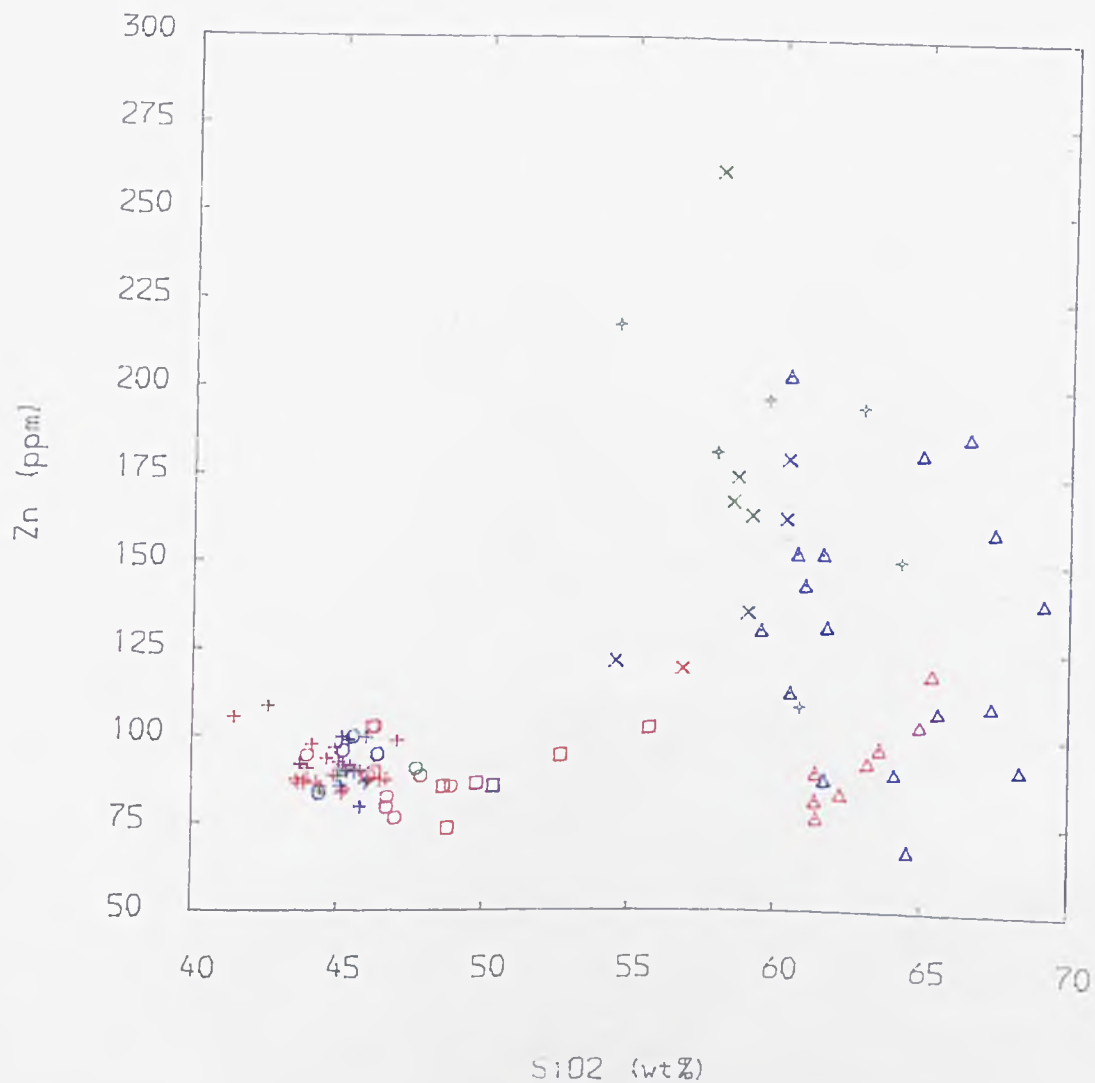
TITLE : Fig : 7.2a-d 'Compatibles' vs MgO

NEW SERIES ROCKS = red
 PYROCLASTIC SEQUENCE ROCKS = green
 OLD SERIES ROCKS = blue



TITLE : Fig : 7.2e Cu vs MgO

NEW SERIES ROCKS = red
 PYROCLASTIC SEQUENCE ROCKS = green
 OLD SERIES ROCKS = blue



TITLE : Fig : 7.2f Zn vs SiO₂

BASEMENT ROCKS	= black
NEW SERIES ROCKS	= red
PYROCLASTIC SEQUENCE ROCKS	= green
OLD SERIES ROCKS	= blue

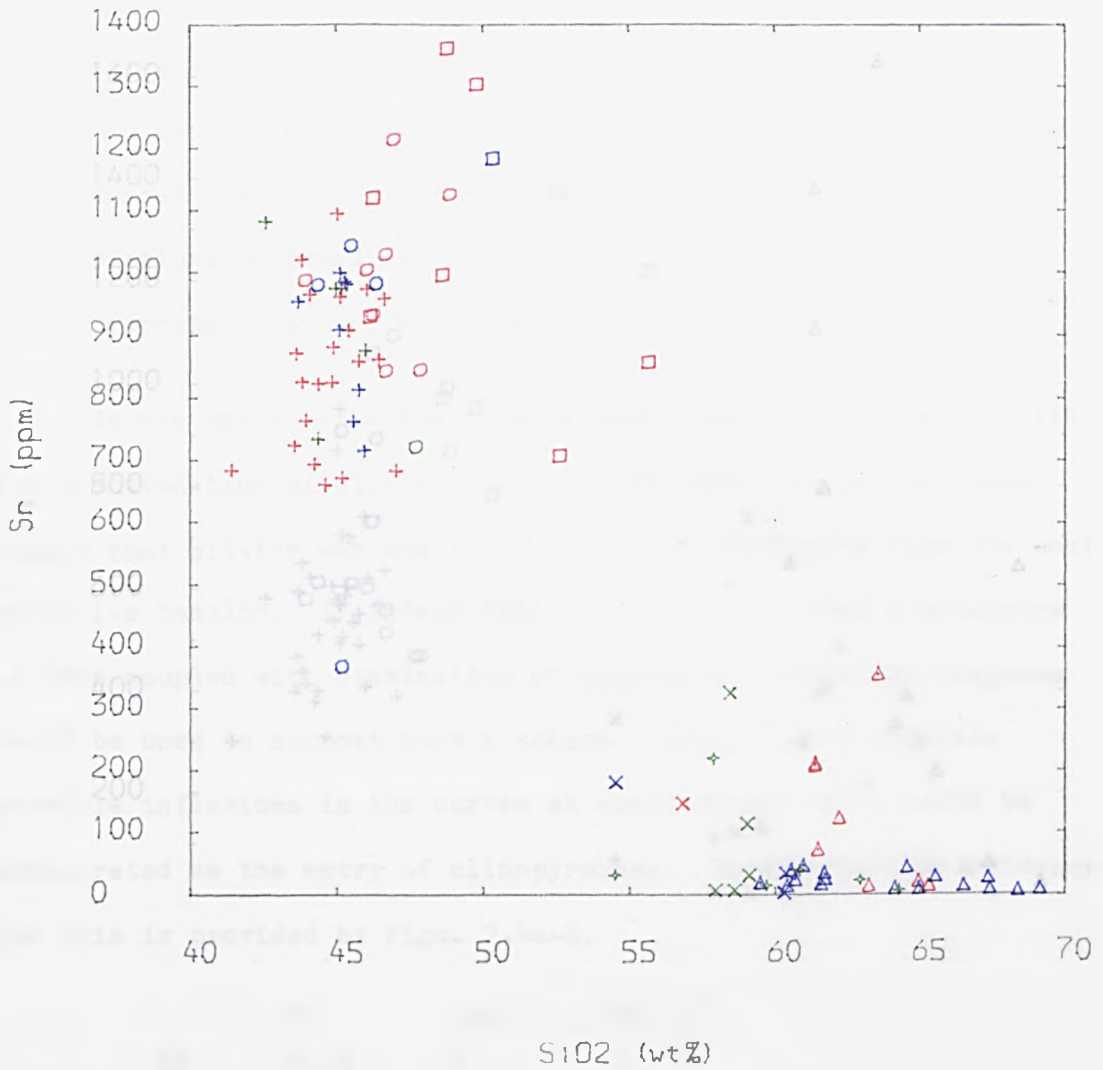
7.3.5 'Incompatible/Compatible' Elements

Both Sr and Ba change from being incompatible to becoming compatible as fractionation proceeds (Figs. 7.3a-b). Firstly, they show an increase in concentration from basalts to mugearites. More evolved mugearites show a depletion in Sr but not Ba. Secondly, in evolving to acidic rocks the concentration of Sr is dramatically reduced. This is also in part the case for Ba although some rocks are in fact enriched (See Section 7.4 for discussion on temporal variations).

The cusp in trends involving alumina (Section 6.6) is also apparent in plots involving Sr. Specimens 24019, 24026, 24061 and 24118 all appear to have lost Sr relative to other incompatible elements which can be attributed to the onset of significant plagioclase fractionation in evolved mugearites.

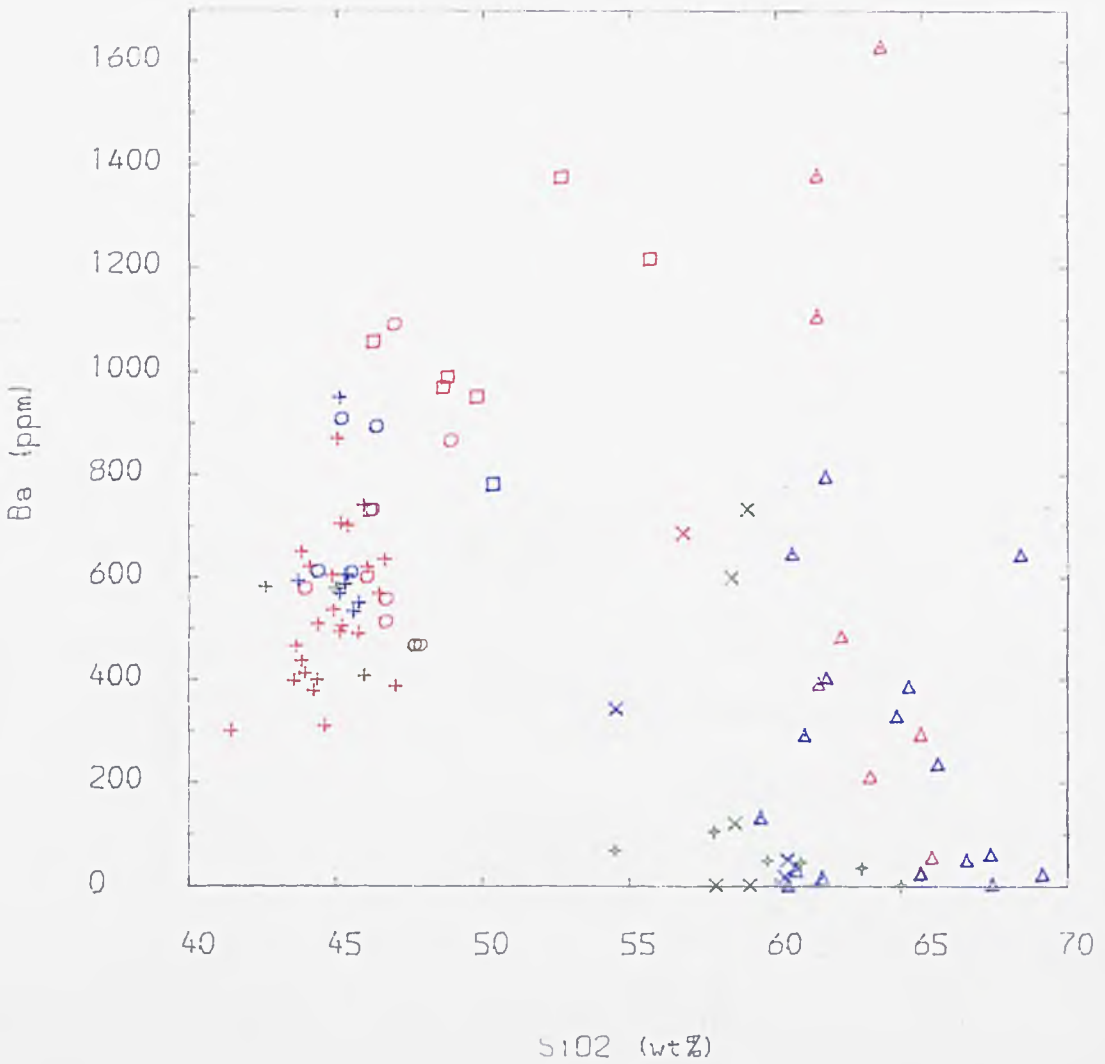
7.3.6 Interpretation

The equation for Rayleigh fractionation is given in Chapter 9. Essentially, the concentration of an element in a magma will increase, with fractionation, if D is < 1 and will increase more rapidly as D tends to zero. Conversely, compatible elements with a $D > 1$ will become depleted in the magma, with fractionation; the greater the D value the greater the degree of depletion expected (see Cox et al., 1979, Fig. 14.1). In order to interpret the data it becomes necessary to understand how trace elements behave with fractional crystallisation (or indeed partial melting). Models which are applicable are derived in Wood and Fraser (1976, Chapter 6). In general these models tend to reflect end-member situations which nevertheless probably serve as good approximations to most natural systems.



TITLE : Fig : 7.3a Sr vs SiO₂

BASEMENT ROCKS	= black
NEW SERIES ROCKS	= red
PYROCLASTIC SEQUENCE ROCKS	= green
OLD SERIES ROCKS	= blue



TITLE : Fig : 7.3b Ba vs SiO₂

BASEMENT ROCKS = black
 NEW SERIES ROCKS = red
 PYROCLASTIC SEQUENCE ROCKS = green
 OLD SERIES ROCKS = blue

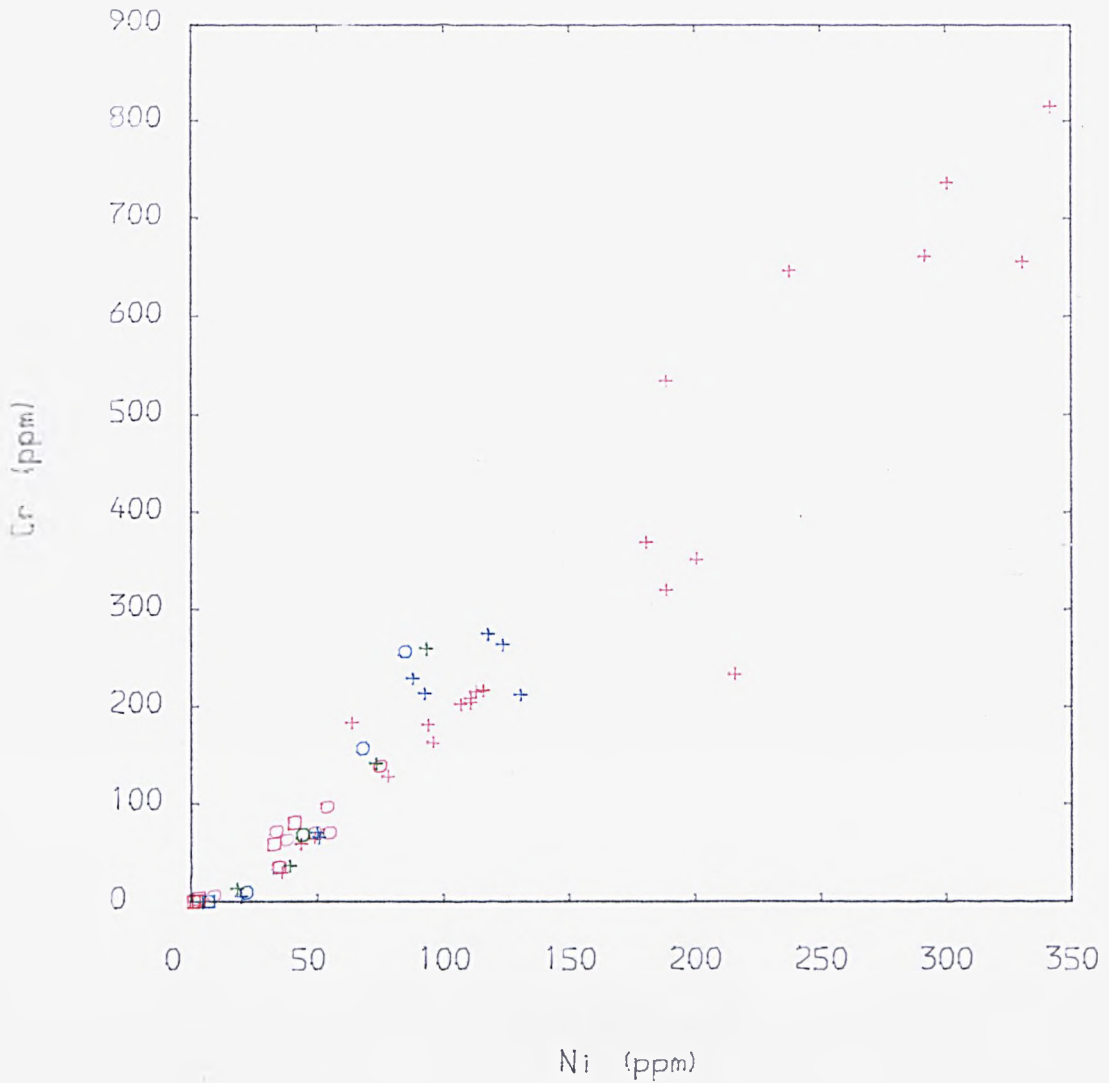
In Figs. 7.1a-j, the trace elements Nb, Pb, etc., are all progressively enriched in the more evolved rocks and can be interpreted in terms of Rayleigh fractional crystallisation. It may be assumed that the D's for these elements are < 1 . In Figs. 7.2a-e the depletions observed are consistent with D's > 1 . Moreover, it can be expected that $D_{Ni} > D_{Sc} > D_{Zn}$.

In the basic rocks the major element data are consistent with the fractionation of olivine and clinopyroxene. It is also more likely that olivine was the first phase to fractionate from the most primitive basalts. If indeed this were the case, then a knowledge of Kd's coupled with examination of appropriate variation diagrams could be used to support such a scheme. Figs. 7.2c-d indicate possible inflexions in the curves at about 9% MgO which could be interpreted as the entry of clinopyroxene. More compelling evidence for this is provided by Figs. 7.4a-d.

	Ol	Cpx	Mt
Sc	0.15	3	1
Ni	12	2	5
Cr	1	10	10
Co	3	1.3	5.8-17
Cu	0.47-2.7	1.5-2.4	?

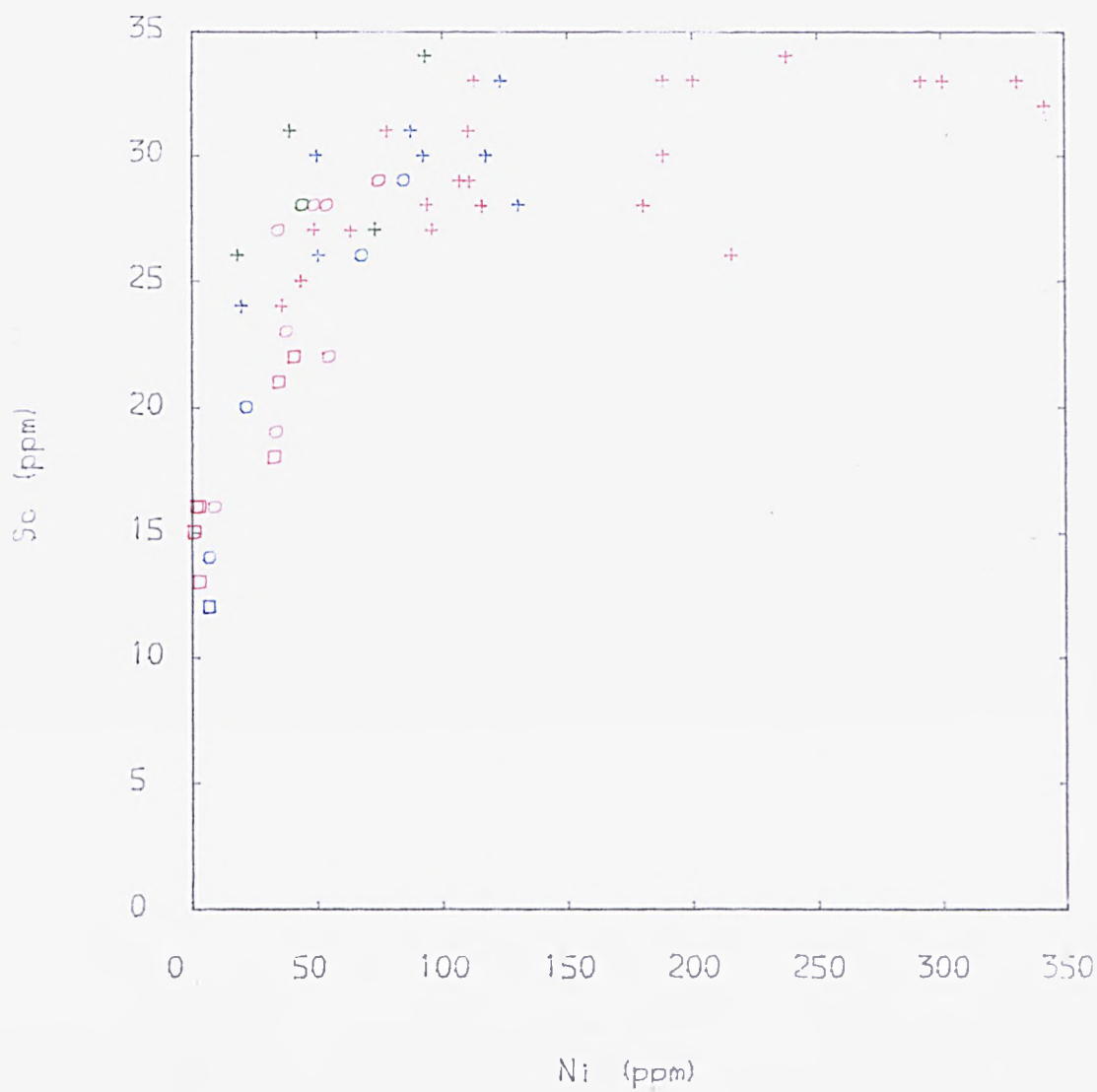
Table 7.1 Distribution Coefficients for transition elements. Data from Sun and Hanson (1979). Irving (1978), and Cox et al., (1979)

Table 7.1 is a compilation of distribution coefficients of transition elements (Sun and Hanson, 1979). Irving, 1978 and Cox et al., 1979). If olivine fractionated first and was then joined by clinopyroxene, from Table 7.1, one would expect curved trends (strictly dog-leg trends) for plots of Cr, Sc, Co and Cu vs Ni



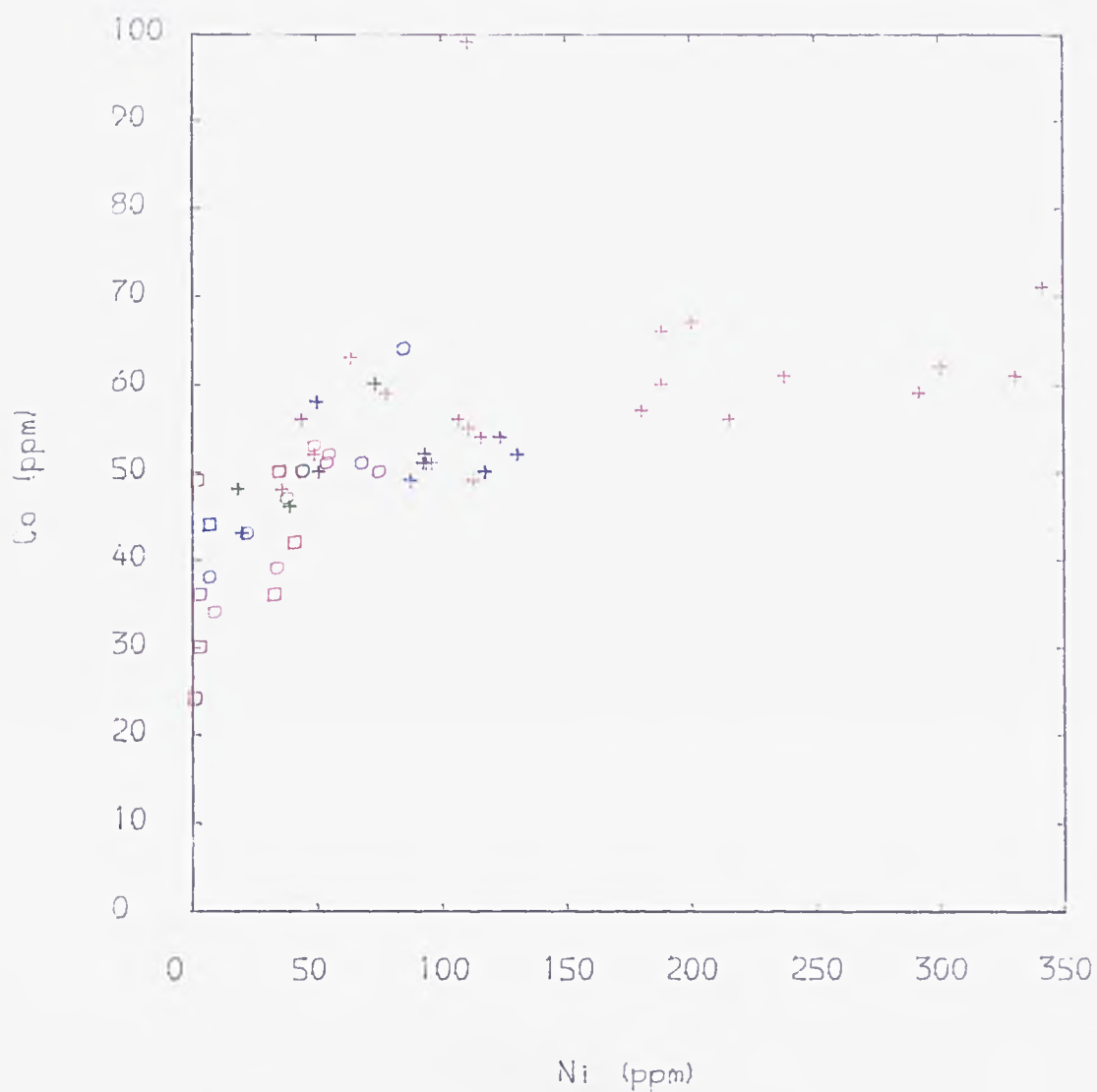
TITLE : Fig : 7.4a-d 'Compatibles' vs Ni

NEW SERIES ROCKS = red
 PYROCLASTIC SEQUENCE ROCKS = green
 OLD SERIES ROCKS = blue



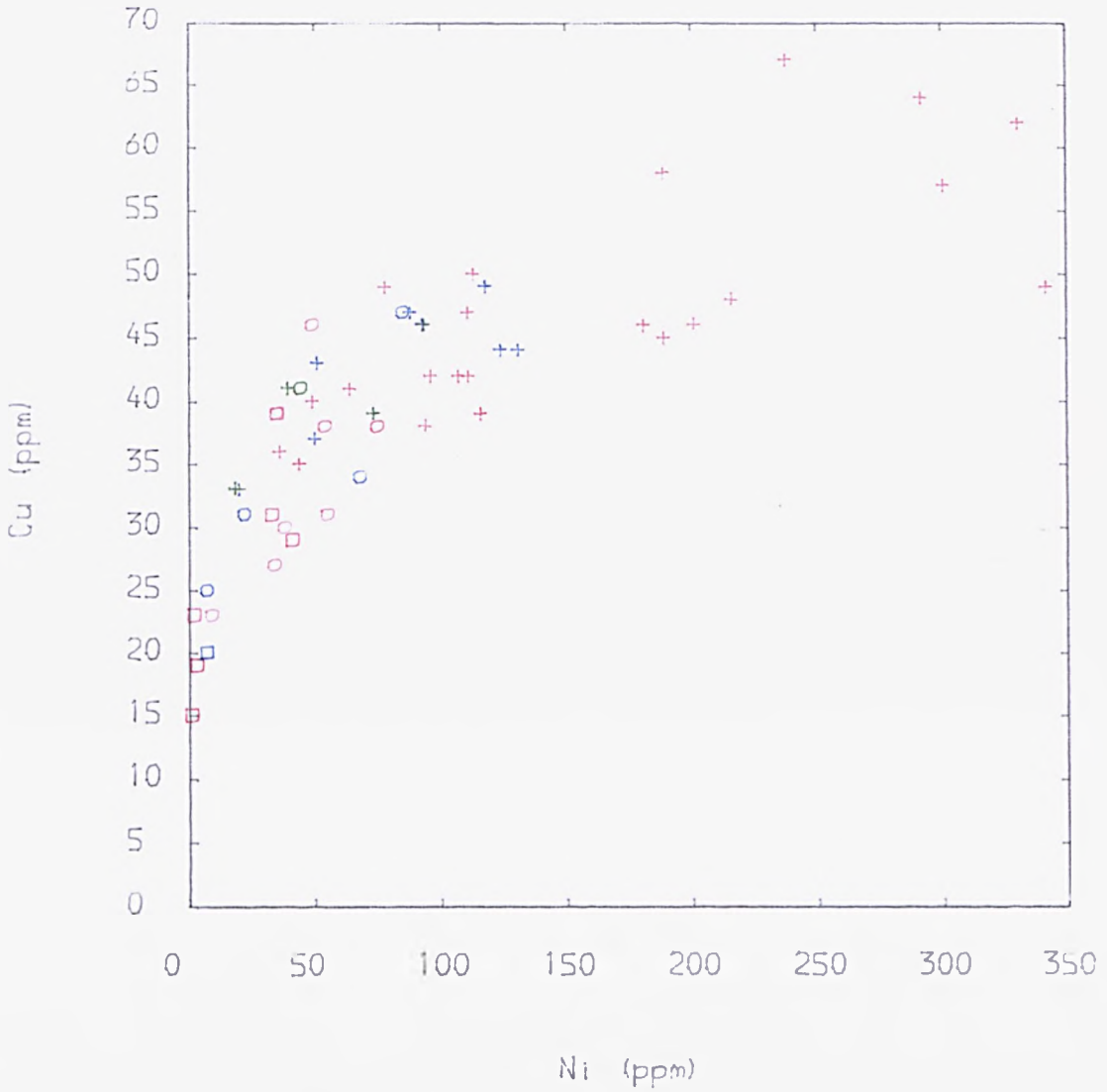
TITLE : Fig : 7.4a-d 'Compatibles' vs Ni

NEW SERIES ROCKS = red
 PYROCLASTIC SEQUENCE ROCKS = green
 OLD SERIES ROCKS = blue



TITLE : Fig : 7.4a-d 'Compatibles' vs Ni

NEW SERIES ROCKS = red
 PYROCLASTIC SEQUENCE ROCKS = green
 OLD SERIES ROCKS = blue



TITLE : Fig. 7.4a-d 'Compatibles' vs Ni

NEW SERIES ROCKS = red
 PYROCLASTIC SEQUENCE ROCKS = green
 OLD SERIES ROCKS = blue

(Figs. 7.4 a-d). This seems to be the case for Sc, Co and Cu but not for Cr vs Ni which has an effectively linear trend. This apparent contradiction may be reconciled if one accepts that a certain amount of magnetite accompanied the olivine fractionation until it was joined by clinopyroxene. The effect could be to make DCr/DNi equivalent in both situations. The amount of magnetite removed need only be small in view of the large KCr involved. In further support of this Fig. 7.4b shows that Sc vs Ni has the greater curvature than either Figs. 7.4c or d. This is in accordance with the Kd 's for Sc and Ni in clinopyroxene and olivine respectively, having a greater difference than either KCu or KCo in clinopyroxene does with KNi in olivine. It will therefore show the largest inflexion at the onset of significant clinopyroxene fractionation. Taking this logic further, in the absence of any data, one would also predict from Figs. 7.4b-d that the KCu in magnetite lies somewhere between that for Co and Cr.

It is also suggested (Chapter 6) that plagioclase becomes a major fractionating phase in evolved mugearitic rocks to trachytes. Sr is compatible in plagioclase and the marked depletion that is observed in the trachytic rocks is consistent with this contention. Also the presence of the possible inflexion noted in Figs. 7.2a-b occurring at low MgO could reflect a change towards a fractionating assemblage dominated by plagioclase. Similarly, anorthoclase fractionation is suggested in the acidic rocks. Ba is compatible in potassium feldspar and depletions in Ba in some of the trachytes would concur with a scheme of anorthoclase fractionation.

7.4 Temporal Variations

The temporal variations of the Old and New Series will be discussed under basic and acidic rock headings.

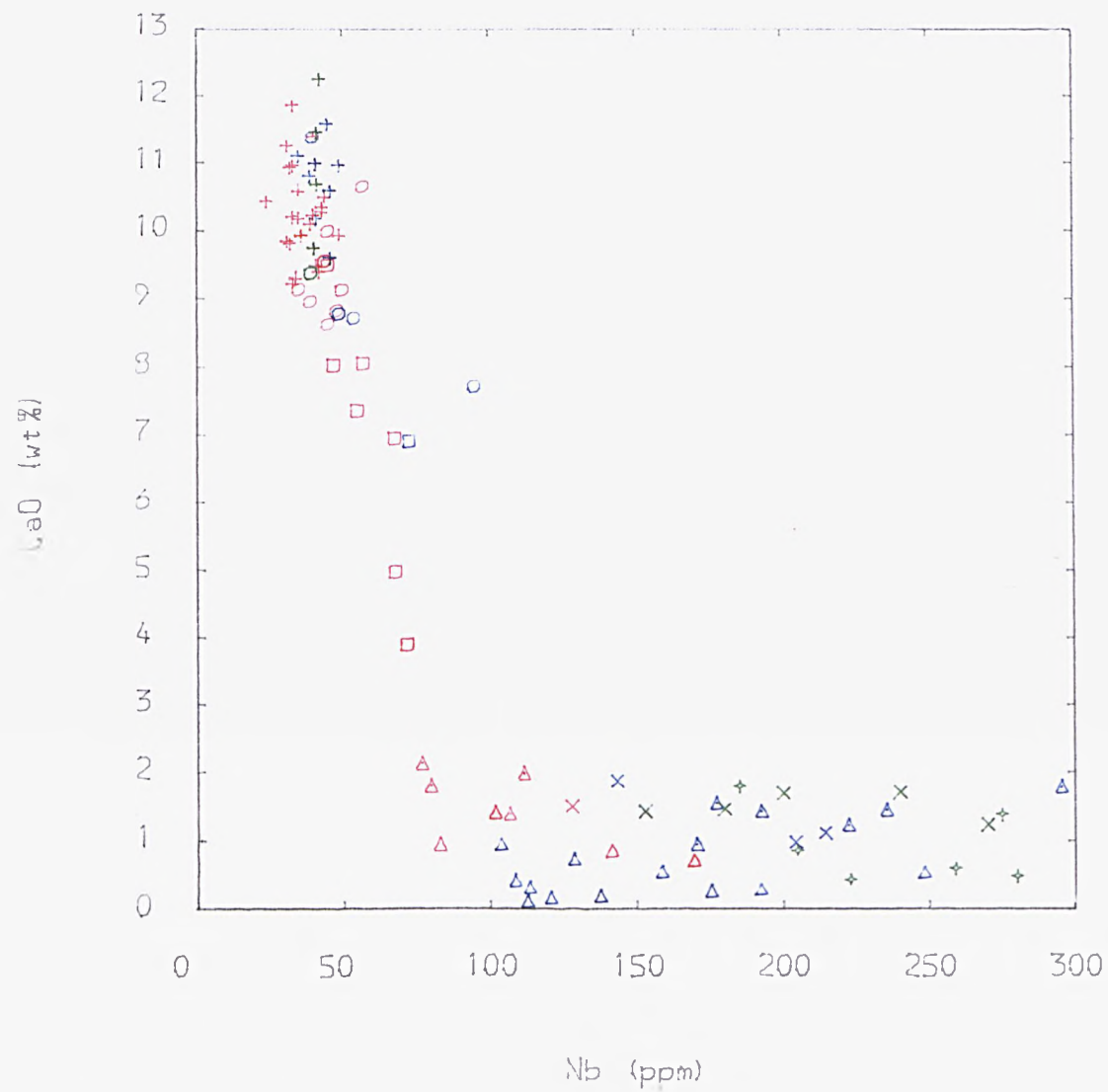
7.4.1 Basic Rocks

In Figs. 7.1a-j there is no major difference between the two Series. The New Series rocks, as with the major element data, encompass the variations of the Old Series in which they show a reasonable coherence. Subtle differences may be perceptible in plots such as CaO vs Nb (Fig. 7.5) in which the Old Series data generally show higher CaO concentrations.

7.4.2 Acidic Rocks

It is immediately evident from Figs. 7.1a-j, La, Nd, Nb, Pb, Zr, Th, Ga, Ce, Rb and Y vs SiO₂, that much greater variation is present amongst the acidic rocks.

These differences are most apparent in a plot of Nb vs SiO₂ (Fig. 7.1i) although any plot of incompatible element vs SiO₂ shows the same relations. In this diagram, coupled with information from isotopic evidence, it is possible to divide the Old Series rocks into a 'largely uncontaminated' group and a 'contaminated' group. The phonolites and the silica poor trachytes of the Old Series belong to the 'largely uncontaminated' group. The silica rich trachytes and rhyolites of the Old Series comprise some of the 'contaminated' group. The New Series trachytes also belong to the 'contaminated' group but can be further subdivided into the caldera trachytes and the mafic bearing trachytes. The caldera trachytes occur in and around Deriba and are petrographically and geochemically distinct (Chapters 4 and 6) from the mafic bearing trachytes, which

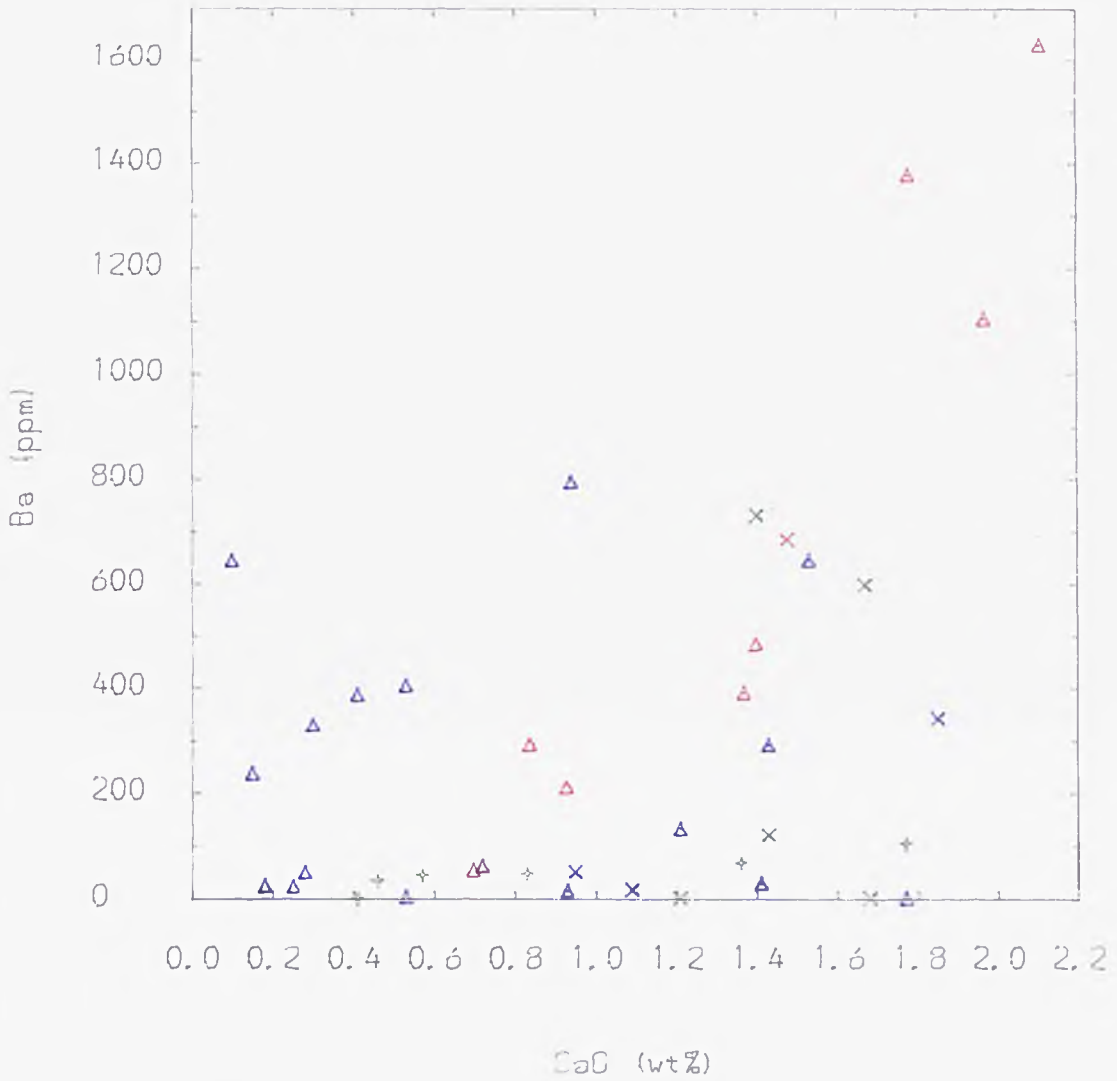


TITLE : Fig : 7.5 CaO vs Nb

BASEMENT ROCKS	= black
NEW SERIES ROCKS	= red
PYROCLASTIC SEQUENCE ROCKS	= green
OLD SERIES ROCKS	= blue

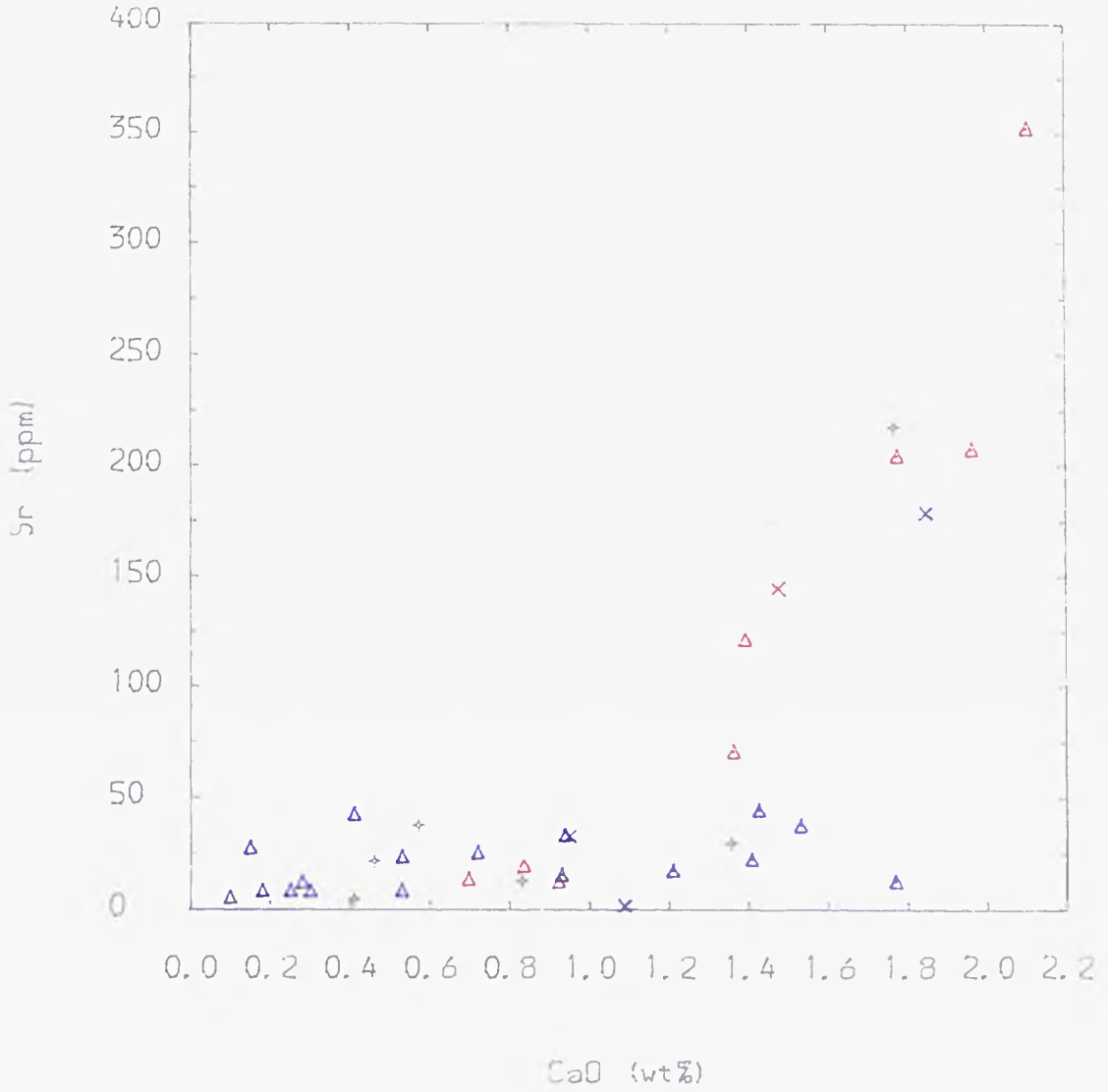
commonly contain clinopyroxene, olivine and plagioclase sometimes rimmed with anorthoclase. The geochemical difference is illustrated in Figs. 7.6a-b. The mafic bearing trachytes trend to rocks rich in Ba, Sr and CaO (in fact they are also relatively richer in TiO_2 , MgO , P_2O_5 and Fe_2O_3) while the caldera trachytes are poor in these components. Any explanation which can account for these features must also explain the highly contaminated nature of some of these rocks, e.g. 24087 ($^{87}Sr/^{86}Sr = 0.7059$; $^{143}Nd/^{144}Nd = 0.5121$). One possibility is that mixing of a basic magma with an acidic magma has occurred. While this could account for the elemental and petrographic features noted above it would not satisfactorily explain the isotopic evidence. For this reason, mixing of a crustal melt, probably granulitic, with a basic magma is preferred. Bulk assimilation of crust by a basic magma is considered unlikely in view of the extent of contamination particularly indicated by the highly unradiogenic $^{143}Nd/^{144}Nd$ ratio in 24087. Trace element concentrations support the notion that 24016 and 24113 are the most primitive members of the two trachyte sub-groups. The above groups which have been identified on the basis of trace elements and isotopic evidence are also apparent, albeit with a greater degree of overlap, in the major elements. Whole rock ignimbrites from the Pyroclastic Sequence are much more variable in composition.

Other trace element - trace element plots reveal information of considerable significance. To illustrate some of the differences Fig. 7.7 shows a plot of Rb vs Nb. Two distinct trends are present in the acidic rocks. The first trend, comprising the main body of the data, reveals that the increase in Rb relative to Nb is retarded. This trend is comprised of Old Series rocks including phonolites from



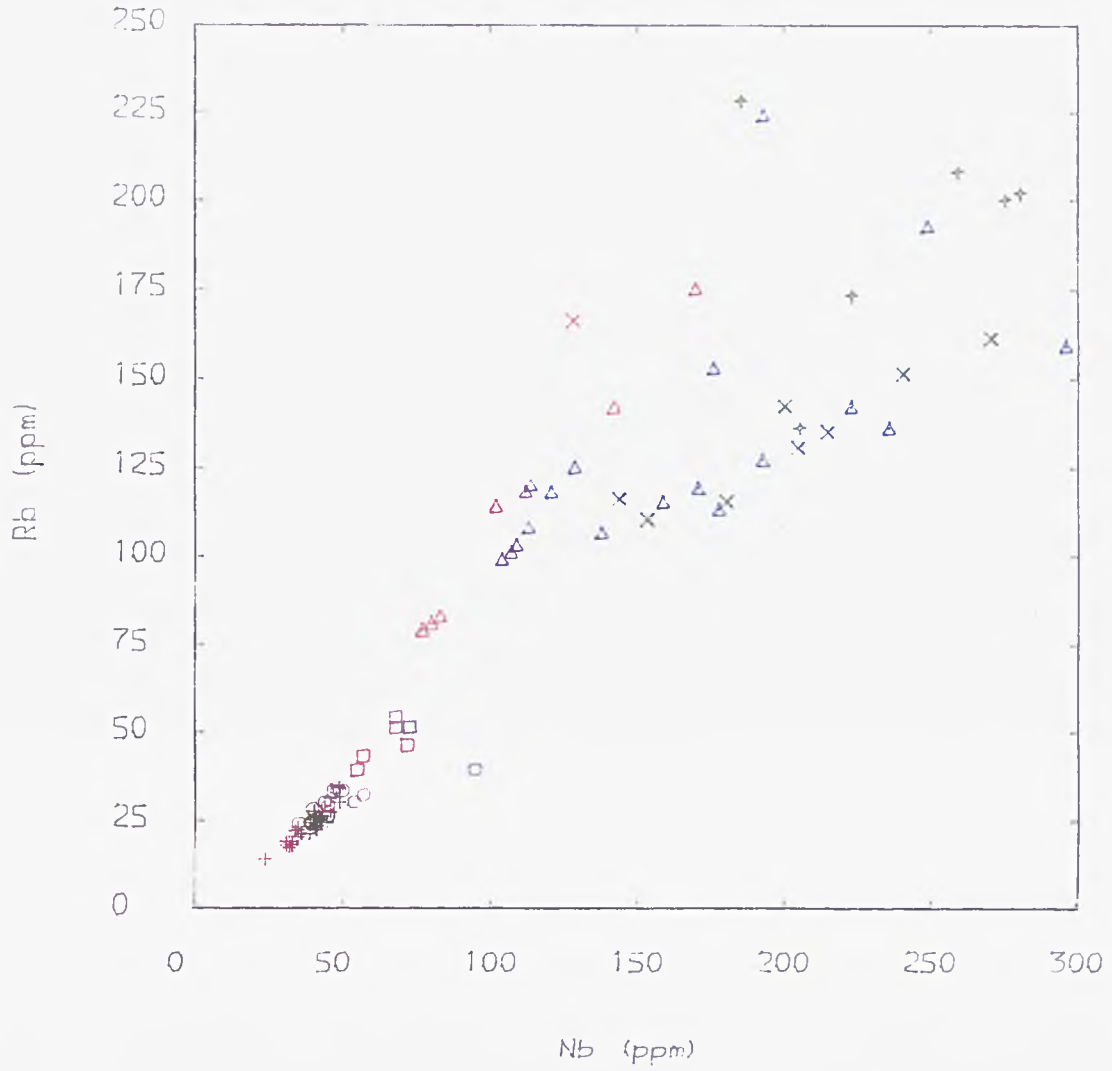
TITLE : Fig : 7.6a Ba vs CaO

NEW SERIES ROCKS = red
 PYROCLASTIC SEQUENCE ROCKS = green
 OLD SERIES ROCKS = blue



TITLE : Fig : 7.6b Sr vs CaO

NEW SERIES ROCKS = red
 PYROCLASTIC SEQUENCE ROCKS = green
 OLD SERIES ROCKS = blue



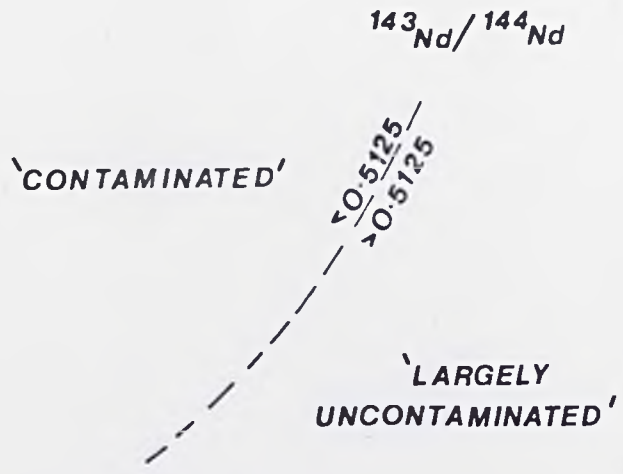
TITLE : Fig : 7.7 Rb vs Nb

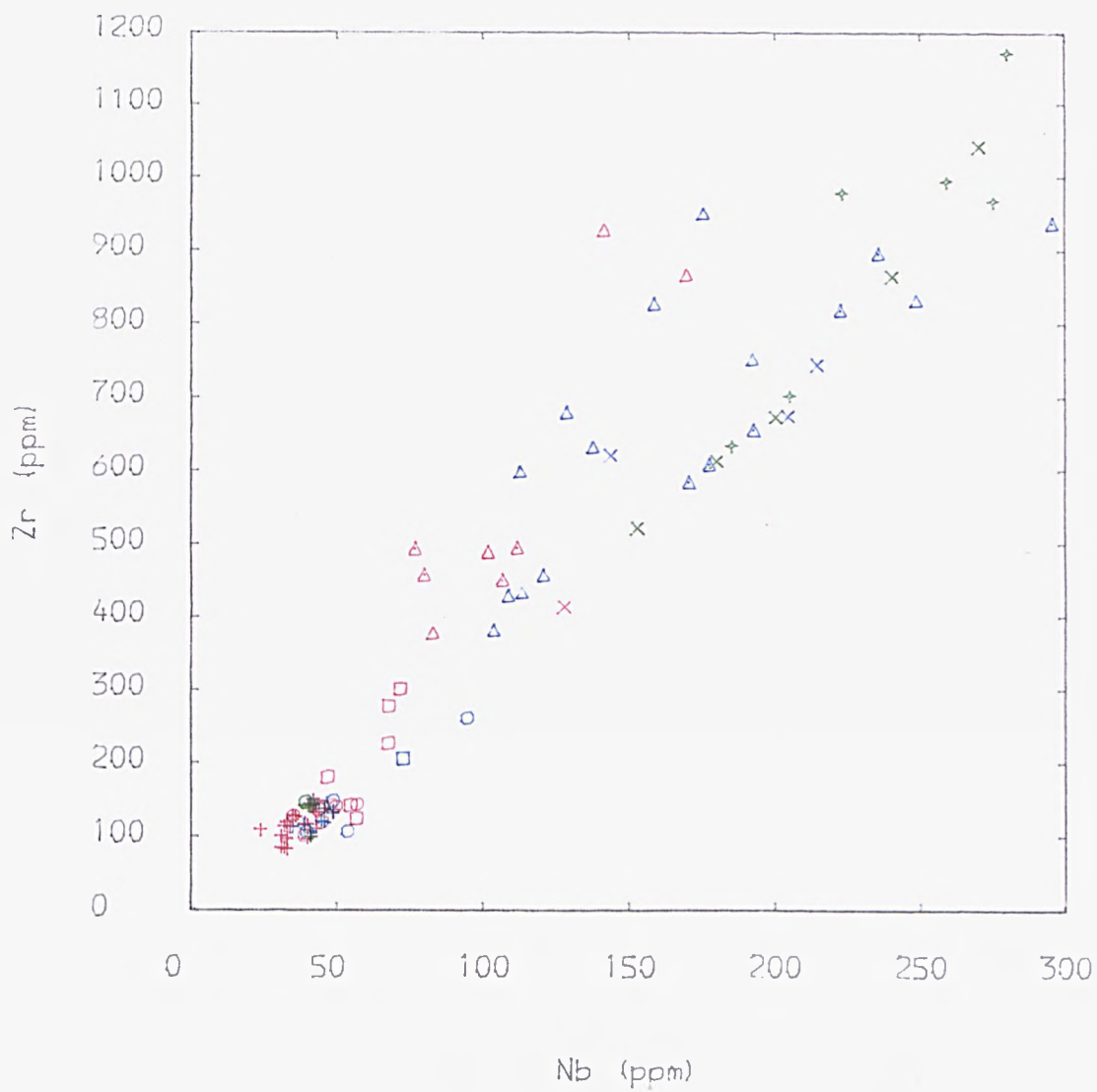
BASEMENT ROCKS	= black
NEW SERIES ROCKS	= red
PYROCLASTIC SEQUENCE ROCKS	= green
OLD SERIES ROCKS	= blue

the Pyroclastic Sequence. This retardation is almost certainly due to the fractionation of a phase in which Rb is more compatible. Biotite may be rejected on the basis of its rarity in these rocks and therefore anorthoclase, which is abundant in the trachytes, and has been suggested as a probable fractionating phase previously, is a more plausible candidate. The second trend does not show the above effect and only contains the mafic bearing New Series trachytes and some Old Series acidic rocks. Plotted in Fig. 7.8 is Zr vs Nb. Amongst the acidic rocks two trends are apparent; one with a higher Zr/Nb ratio which corresponds to the 'contaminated' group of rocks and one with a lower Zr/Nb ratio which corresponds with the 'largely uncontaminated' group. But as the model requires isotope evidence to substantiate the argument, explanations for these effects will be also left until Section 8.4.

7.5 Rare Earth Element's (REE's)

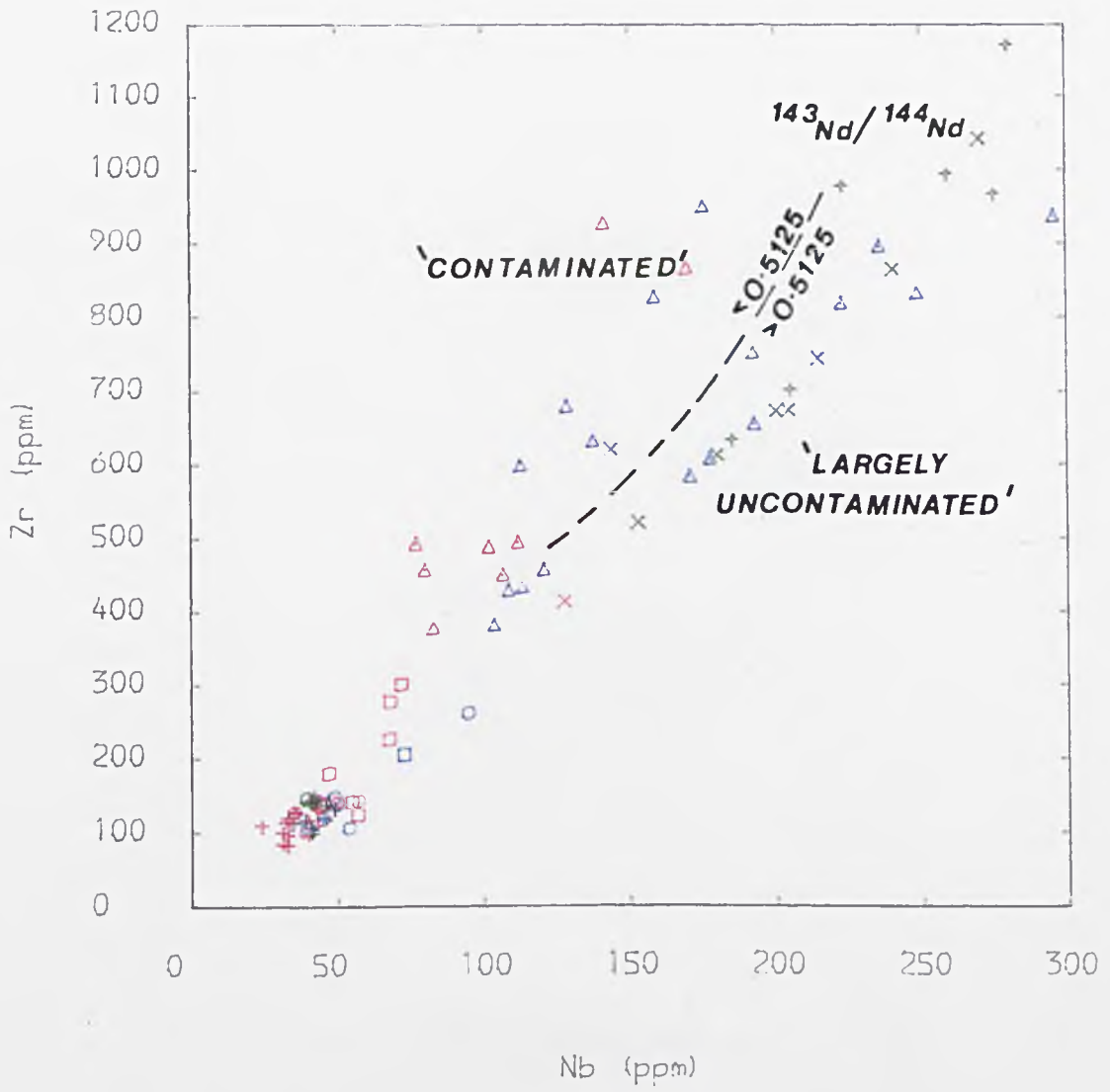
REE's (La, Ce, Nd, Sm, Eu, Gd, Dy, Er and Yb) have been measured on selected samples by stable-isotope dilution (ID) techniques developed by Thirlwall (1981, Appendix E). There are a number of advantages in measuring the abundances of these elements and by the ID method. Firstly, the REE's are geochemically very similar, but vary systematically as the ionic radius decreases from La to Lu for 3+ ions in octahedral co-ordination (this being a function of increasing atomic number). The REE's are characteristically trivalent in most geological situations, except for Ce and Eu which under certain circumstances have different oxidation states and consequently behave anomalously. A further advantage of these elements is that they are relatively immobile under most weathering processes; a





TITLE : Fig : 7.8 Zr vs Nb

BASEMENT ROCKS	= black
NEW SERIES ROCKS	= red
PYROCLASTIC SEQUENCE ROCKS	= green
OLD SERIES ROCKS	= blue



TITLE : Fig : 7.8 Zr vs Nb

- BASEMENT ROCKS = black
- NEW SERIES ROCKS = red
- PYROCLASTIC SEQUENCE ROCKS = green
- OLD SERIES ROCKS = blue

property which is exploited in some Nd isotopic studies. Finally, measurement by the ID method is an extremely precise and accurate analytical technique and its detection limits are well below the ppm level. As a consequence of this, the Kd's of most igneous minerals are relatively well known. The accuracy obtained is particularly important if the Sm/Nd ratio is required for Sm-Nd geochronological studies, where reproducibility better than 0.2% is desirable (Thirlwall, 1982).

In order to offset the Oddo-Harkins effect, REE concentrations are conventionally presented normalised to chondrite, or where it is instructive normalised to primitive basalt. These are plotted on a logarithmic scale against the REE's in order of atomic number. In this thesis chondritic normalising values are taken from Nakamura (1974) and are given in Table E2.

7.5.1 General Features

All the REE patterns for the Jebel Marra volcanics are LREE enriched. The extent of this may be appreciated from the parameter $La/Yb(N)$, which is a measure of the slope of the REE pattern. These are tabulated for all patterns in Table E1. A second general feature is that all the basic rocks have a positive Eu anomaly and all the acidic rocks have a negative Eu anomaly.

7.5.2 New Series Variations

New Series patterns amongst the basic rocks are almost parallel to one another (e.g. Fig. 7.9). A further striking feature, present in all the basic rock patterns, is the positive Eu anomaly. It is often convenient to parameterize the extent of the Eu anomaly by the

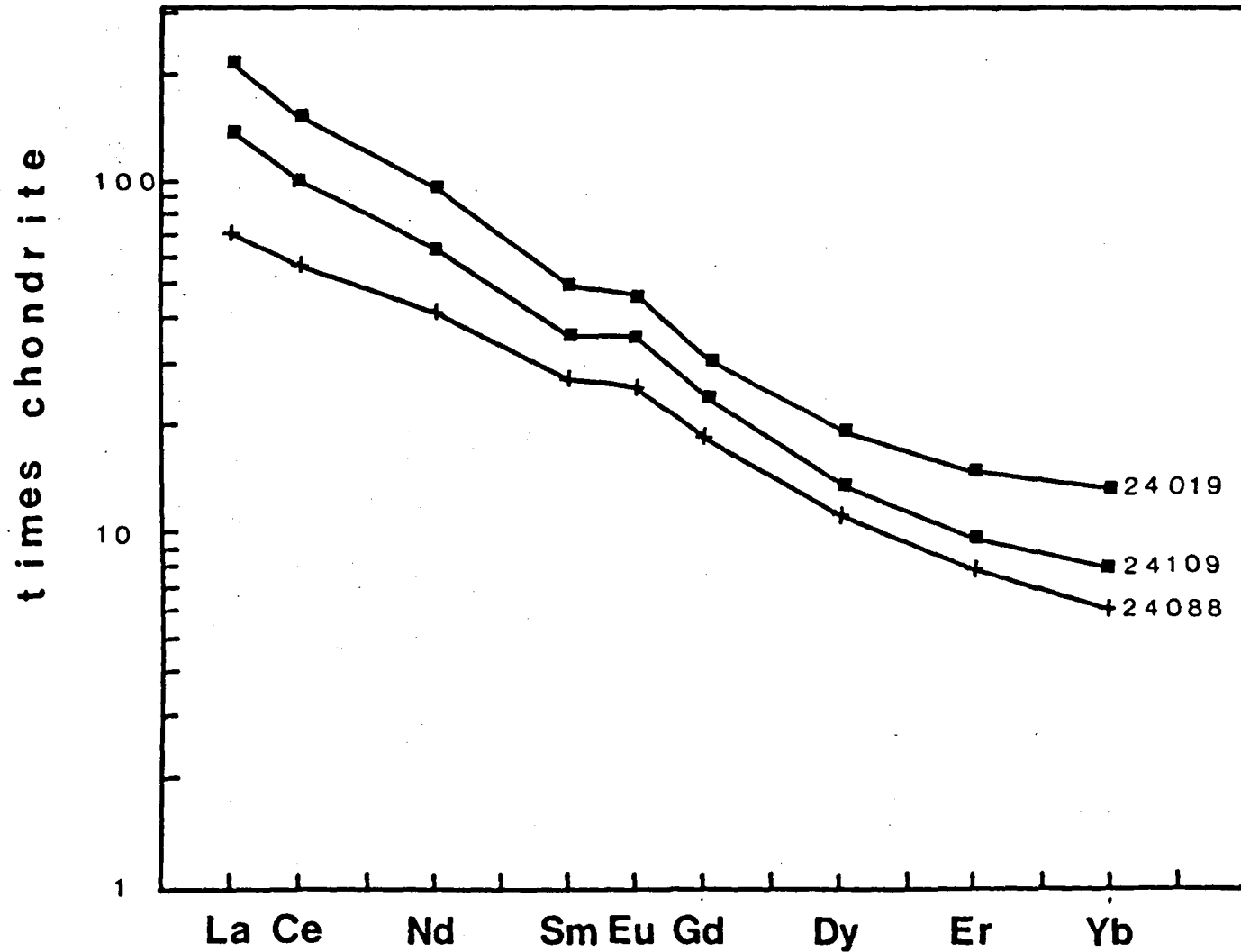


Fig. 7.9 Typical REE patterns for New Series basic rocks.

24088 is a primitive basalt, 24109 is a primitive mugearite and 24019 is an evolved mugearite.

value Eu/Eu^* . This is derived from the interpolation of Sm to Gd and then expressed as a ratio relative to the anomaly, such that positive anomalies are >1 , and negative anomalies are <1 . Eu/Eu^* values are also presented in Table E1 which are obtained from the following expression:-

$$\frac{Eu}{Eu^*} = \frac{Eu}{0.077} \times \frac{(Sm \times Gd)^{-0.5}}{(0.203 \times 0.276)} \quad \text{Eqn. 7.4}$$

There are several ways in which positive Eu anomalies can result. One possibility is that the parental magma from which the fractionates were derived, accumulated plagioclase. This may be invoked because plagioclase preferentially incorporates Eu (strictly Eu^{2+}) relative to the other REE's, particularly under low fO_2 conditions. In the Jebel Marra basic lavas, the accumulation of plagioclase is not supported by petrographic evidence, because in the most primitive basalts plagioclase is an extremely rare phenocryst phase. A more appealing alternative, is one proposed by Leeman (1976) whereby Eu^{2+} is believed to be excluded from residual clinopyroxene in the mantle but is taken up in the partial melt and is thus responsible for the small positive Eu anomalies observed in some basaltic suites. That a positive, and not a negative, Eu anomaly exists further attests to the belief that plagioclase was not significantly fractionated in the basic rocks, assuming that oxygen fugacity is not overly high.

A feature of the transition from basalts to mugearites in New Series rocks is the increasing extent to which the patterns are downwardly bowed. A measure of this effect is given by the parameter $Gd/Gd^*:-$

$$\frac{\text{Gd}}{\text{Gd}^*} = \frac{\text{Gd}}{0.276} \times \frac{(\text{Ce} \times \text{Yb})^{-0.5}}{(0.865 \times 0.22)} \quad \text{Eqn. 7.5}$$

This is effectively an interpolation between Ce and Yb with which the actual Gd content is compared. The values for this are also tabulated in Table E1. It is evident that the extent of bowing systematically increases from basalts to mugearites, as revealed by smaller Gd/Gd* values. In order to explain the bowing by fractionation, a phase is required with a humped Kd-REE pattern corresponding to the middle REE's. Of the major fractionating phases, only clinopyroxene has a humped Kd-REE pattern which could conceivably produce the increased bowing in the basic rocks. Alternatively, fractionation of a minor phase e.g. apatite, amphibole or sphene which also have humped Kd-REE pattern and high Kd's could, with even very small amounts of fractionation, give rise to the observed degree of bowing. A different explanation could be that the magma is being contaminated by a crust with a different REE pattern such that modifications of the contaminated magma's REE pattern will result. In this way the increased bowing of the REE patterns could, in principle, occur. These possibilities will be explored further in Chapter 9.

There is a distinct change in the shape of basic rock patterns to acidic rock patterns (e.g. Figs. 7.9-10). The shape of the patterns for trachytes are gently curved with steep LREE limbs and less steep HREE (heavy rare earth element) limbs which differ from basic REE patterns. Moreover, in the stage from the evolved mugearites to trachytes there is a relative loss in REE's, except in La and Ce, and particularly in the elements Nd, Sm, and Gd. The large negative anomaly in Eu can be explained by plagioclase fract-

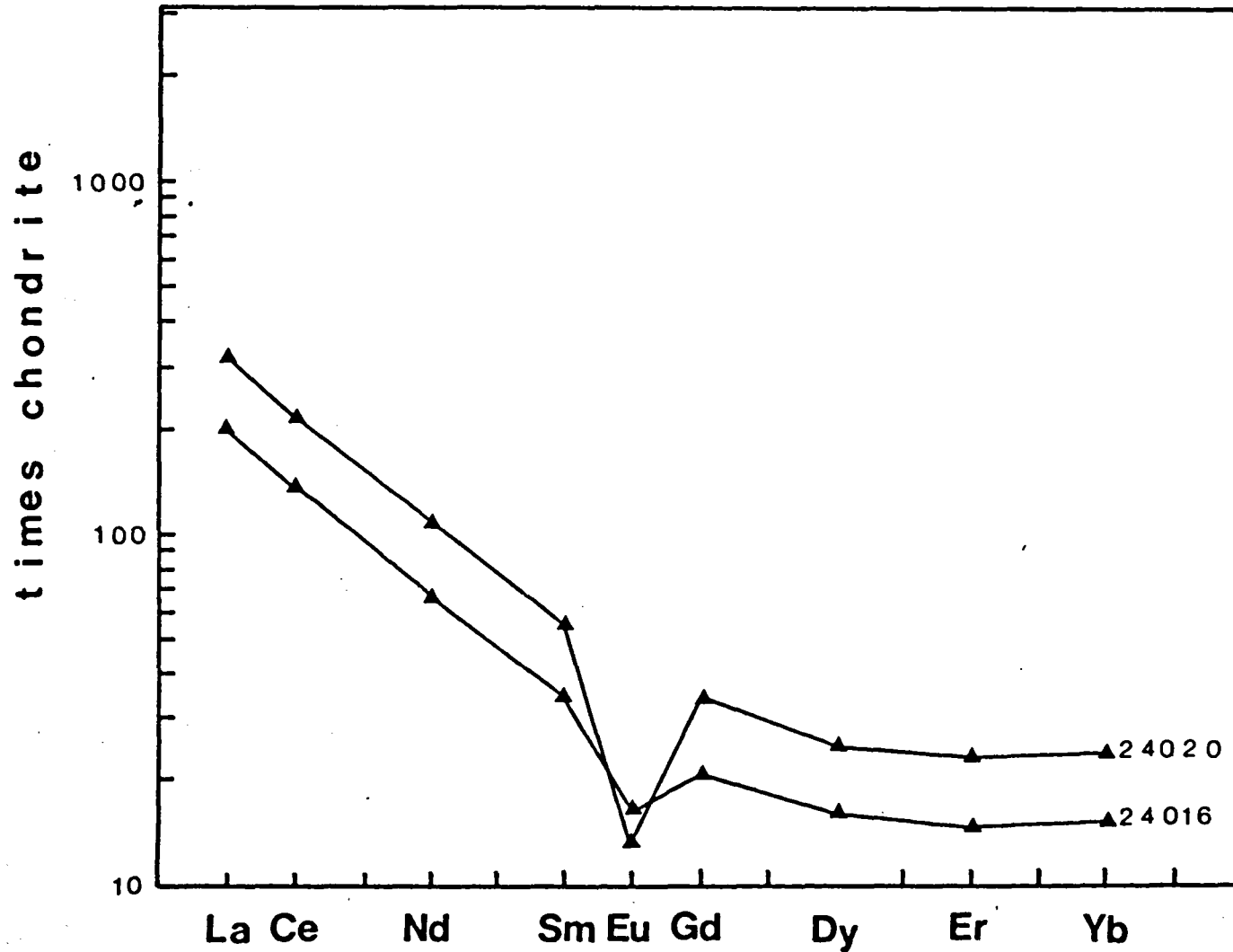


Fig. 7.10 REE patterns for caldera trachytes 24016 and 24020. These differ from basic rock REE patterns by having a marked negative Eu anomaly, a flat HREE section but are similarly LREE enriched.

ionation. The depletions in middle REE's would be difficult to explain by possible dilution effects by contamination. In this instance, it is much more likely to be the result of fractionation. It is clear from the patterns of plagioclase and clinopyroxene (Fig. 9.3: olivine and magnetite have much less REE's) that removal of a olivine-clinopyroxene-plagioclase-magnetite assemblage could only account for the Eu anomaly. In order to explain the deficit in REE's in 24016 by fractionation, a phase with much higher REE abundances and ideally with a humped Kd-REE pattern is required. Possibilities could again include sphene, amphibole or apatite, and their REE patterns are also plotted in Fig. 9.3. Sphene has not been found in any of the specimens and little justification can therefore be found for invoking its removal. Amphibole is present as a minor phase in some mugearites and fractionation could account for the loss of middle REE. However, the weight proportion required to be removed would be of the order of 20% which is in discord with petrographic observations. A more promising alternative is apatite which is present in mugearitic rocks. Moreover, this would be in concordance with the drop in P_2O_5 from evolved mugearites to primitive trachytes. This possibility will again be investigated in Chapter 9.

Plotted in Fig. 7.10 are two trachytes from the series 24016-17. The most obvious difference between these (and all other acid rocks) and the basic rock REE patterns is the appearance of a marked negative Eu anomaly. This has undoubtedly been caused by strong plagioclase fractionation which is in agreement with the conclusion arrived at from the depletion in Sr observed over the same compositional interval. Among the New Series trachytes 24020 is a more evolved and has a pattern parallel to that of 24016, except that it has a larger Eu

negative anomaly. If the two are linked by the same, or a similar, liquid line of descent then the increased negative Eu anomaly can be accounted for by the fractionation of anorthoclase in which Eu has a K_d just greater than 1. This again would tie up with evidence for Ba which is depleted in most of the acidic rocks and strongly suggests fractionation of a potassium feldspar. Also because of the low K_d 's for REE's, other than for Eu, fractionation of anorthoclase will generate evolved liquids with REE patterns which are essentially parallel to the parent. This effect will be modelled in Chapter 9. 24081 and 24087 (Fig. 7.11) are essentially parallel to 24016 although they have smaller negative Eu anomalies.

7.5.3 Old Series Variations

The Old Series basic rocks are similar in pattern to the New Series equivalents. They have comparable abundances, positive Eu anomalies and similar slopes (see Table E1).

The change in shape of the REE patterns from basic to acidic rocks occurs in the Old Series rocks. By analogy with New Series rocks it is considered that this is also the result of apatite fractionation. The Old Series trachytes, as previously outlined, can be divided into those which are 'largely uncontaminated' and those which are 'contaminated' to a varying extent. The former includes the 'silica poor' trachytes, the phonolites from the Pyroclastic Sequence and the Old Series phonolites. Fig. 7.12 depicts REE patterns representative of each group. The latter include the 'silica rich' trachytes and rhyolites. If the contaminant has a REE pattern which is significantly different from those of the magmas it enters then, all other things being equal, it could reveal itself through systematic differences between the REE patterns of 'uncontaminated'

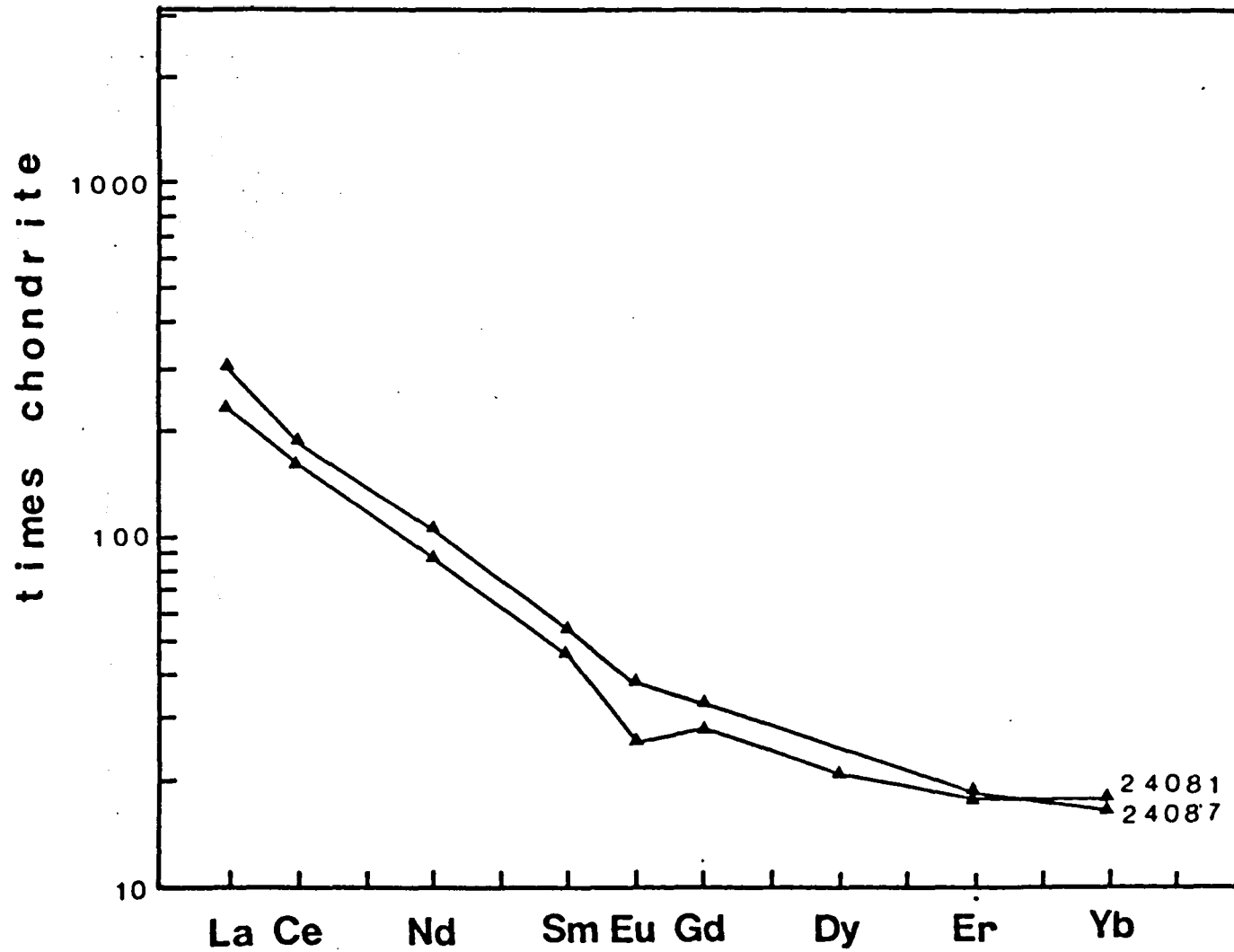


Fig. 7.11 REE patterns for mafic bearing trachytes.

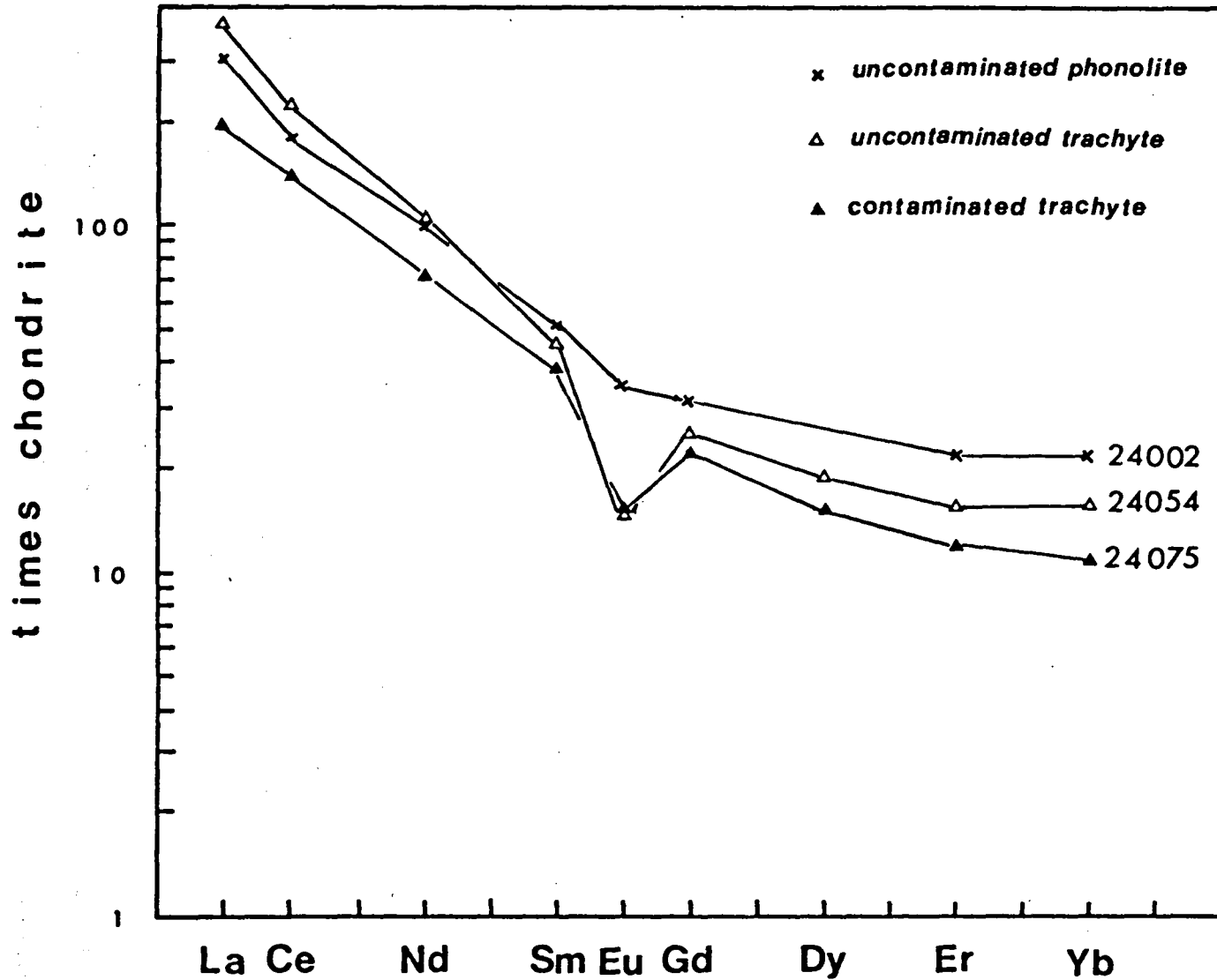


Fig. 7.12 REE patterns for Old Series rocks. Differences in bowing may be related to the degree of contamination suffered.

and 'contaminated' lavas. In Table 7.2 various parameters and values are given which impart information on the form of the REE pattern and its history. Ce concentration provides an indication of how evolved the rock is, while the $^{143}\text{Nd}/^{144}\text{Nd}$ value indicates to what extent it has been contaminated (for the moment a homogenous source close to 0.5129 will be assumed for the lavas). The slope of the REE patterns ($\text{La}/\text{Yb}(N)$) is variable and appears to be largely independent of the amount of fractionation and contamination that has occurred. The negative Eu anomaly is, in general, larger in more evolved rocks though shows little correlation with contamination. The increase in the anomaly is probably a consequence of continued anorthoclase fractionation. A more discerning parameter is Gd/Gd^* , which is a measure of the 'bowedness' of a REE pattern and is given by equation 7.5. It is clear from Table 7.2 that the 'largely uncontaminated' patterns show the greatest amount of bowing while the contaminated patterns are less bowed. If it is accepted, among 'contaminated' and 'uncontaminated' rocks, that the fractionating phases are removed in similar proportions, the shape of the curve is not significantly altered by fractionation and they were derived from comparable parents then the difference between them could be ascribed to the addition of crust. These three assumptions seem reasonable as the probable major fractionating phase in both groups is anorthoclase to which only Eu of the REE's is compatible and that otherwise the two groups are geochemically similar except in SiO_2 content. It is therefore difficult to envisage how they might have had a substantially different history. If this is correct then differences in bowing may be a function of contamination.

In the Old Series the groups as divided in Table 7.2 can mostly

		Ce	La/Yb _(N)	Ce/Yb _(N)	Eu/Eu*	Gd/Gd*	¹⁴³ Nd/ ¹⁴⁴ Nd
'LARGELY UNCONTAMINATED'							
24002	PHONOLITE	172	13.08	8.98	0.8311	0.4569	0.512802
24015	PHONOLITE	287	-	8.08	0.3529	-	0.512632
24114	PHONOLITE	181	11.55	-	-	0.4450	0.512852
24097	PHONOLITE	189	11.15	7.87	0.4419	0.4909	0.512754
24124	PHONOLITE	146	16.23	8.26	0.5237	0.4723	0.512612
24054	TRACHYTE	193	22.21	14.6	0.4437	0.4159	0.512778
'CONTAMINATED'							
24030	TRACHYTE	269	18.52	8.26	.3446	.6590	0.512433
24075	TRACHYTE	128	17.66	12.69	.5109	.5815	0.512405
24130	TRACHYTE	156	16.31	10.59	.4507	.4409	0.512601

Table 7.2 Geochemical characteristics of Old Series trachytes

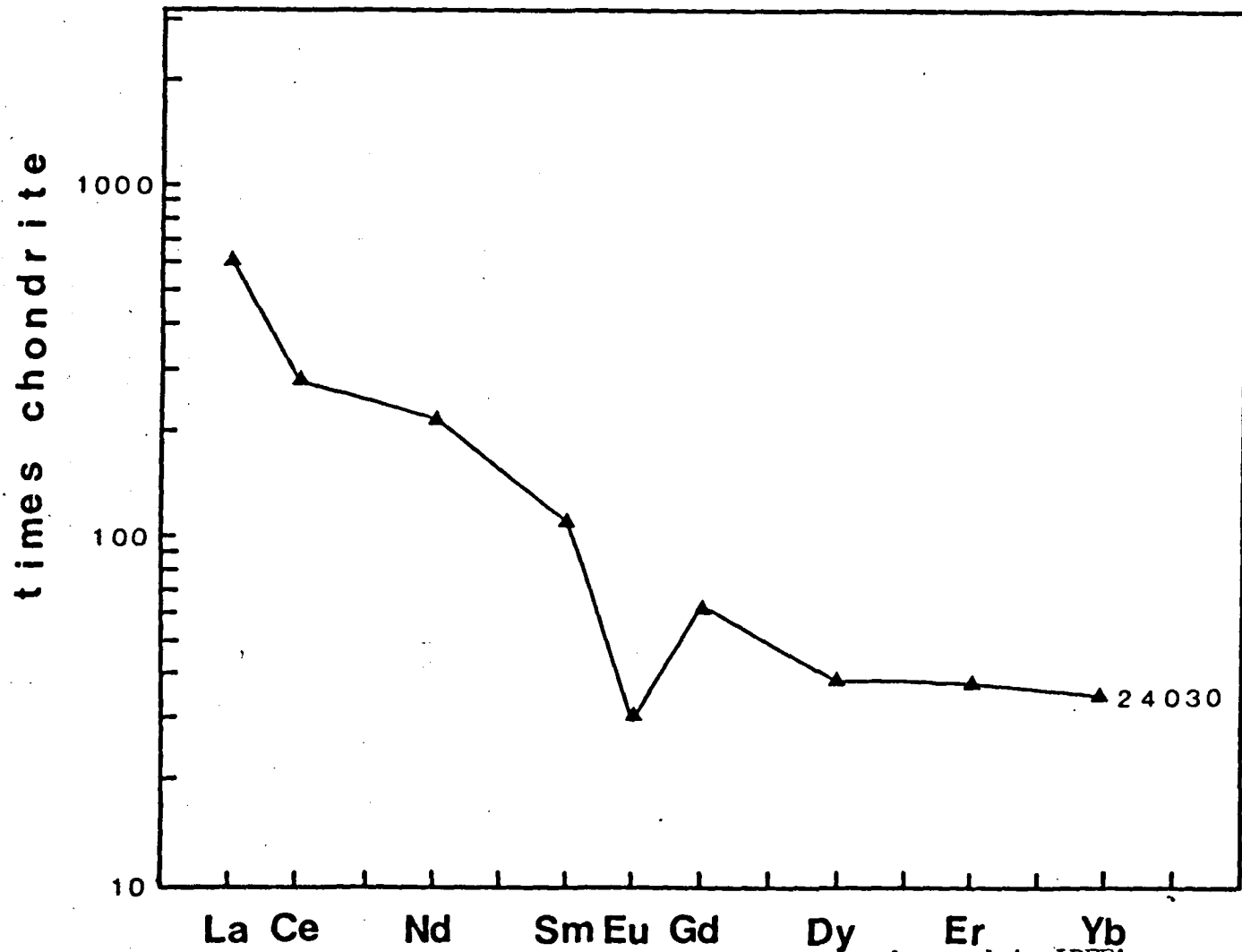


Fig. 7.13 REE pattern for 24030. Anomalies observed in LREE's may be due to the fractionation of minor phases.

be related by fractional crystallisation of an assemblage dominated by anorthoclase. Their patterns in the groups are ostensibly parallel to one another although deviations which occur may be related to other processes such as crustal contamination or fractionation of minor phases. The effect of the latter process is amply illustrated in specimens 24030 (Fig. 7.13) and 24046. Both these samples are highly fractionated as can be seen from their high Zr, Rb, REE etc., abundances. However, both Ce and Th, usually good indices of fractionation are lower than ⁱⁿ rocks of comparable elemental concentrations. The REE pattern for 24030 is kinked at Ce; if the X.R.F. data for Ce is reliable then this effect is even more marked in 24046. Such an effect could be caused by the fractionation of an accessory phase such as allanite in which Ce can be a stoichiometric constituent and in which ThO₂ commonly comprises between 0.35 and 2.23 wt% of the mineral (Deer et. al., 1966).

7.6 Discussion and Conclusions

The trace element behaviour is consistent with the scheme of fractionation suggested from the major element variations in Chapter 6. For example, the depletion in the compatible elements (Ni, Cr, Sc, Sr, Co and Cu) support the fractionation of olivine, clinopyroxene and magnetite in basic rocks. The depletions in Sr and Ba support, respectively, the fractionation of plagioclase and anorthoclase. However, while much of the variation is consistent with fractional crystallisation there are two important features that suggest it did not operate in isolation. Firstly, the degree of scatter is greater than might be expected from a suite which has principally been produced by fractional crystallisation. For example, major and trace element data from East Iceland (Wood, 1978) describe extremely

coherent trends which have been interpreted to be the result, almost wholly, of fractional crystallisation. On the other hand, Cox and Clifford (1982) present data from Mahabaleshwar where the scatter of many of the trends, illustrated by lower correlation coefficients, is greater than for the East Iceland suite. The greater scatter is interpreted as being partly the result of a second order process (crustal contamination) operating upon the first order process of fractional crystallisation (for other contributors to scatter see Section 7.3.). This would be an attractive way to explain some of the relatively high scatter of the Jebel Marra data. Secondly, close examination of variation diagrams involving elements with $D \ll 1$, particularly for the basic rocks, reveals that, in many instances, the extrapolation of the trend does not pass through the origin. Such a relation is not compatible with the operation of fractional crystallisation in isolation. In a theoretical discussion Powell (in press), in its appropriate geological context, interpreted such a feature in terms of combined assimilation and fractional crystallisation. Again this could be an attractive explanation for the Jebel Marra trace element data.

The close parallelism of the REE patterns for basic and acidic volcanics indicates that fractional crystallisation has played an important role in the petrogenesis of these rocks. The depletion of Eu from mugearites to trachytes supports the scheme of plagioclase fractionation. The continued increase in the negative Eu anomaly in acidic rocks supports a scheme of anorthoclase fractionation at this stage. The relative 'loss' of middle REE's from mugearites to trachytes is compatible with the fractionation of apatite. Differences between REE patterns of 'uncontaminated' and 'contaminated'

acidic rocks may be explained by assimilation of crust.

A general conclusion from this Chapter is that fractional crystallisation has clearly played an important role in the variation of the trace elements. Discrepancies which exist from a straight forward fractional crystallisation model are most easily accounted for by crustal contamination. Isotopic evidence in the next Chapter will be drawn upon to evaluate the extent of its involvement.

CHAPTER EIGHTISOTOPIC EVIDENCE8.1 Introduction

A fundamental feature of radiogenic isotopes, as used in petrogenesis, is that they are invariably unaffected by fractionation processes. Consequently, comments regarding the character of mantle sources, for example, can be made with greater certainty as the effects of fractional crystallisation or different degrees of partial melting of a homogeneous mantle can be disregarded. At one time, it was suggested (Sigvaldson et al., 1974; Flower et al., 1975) that isotopic disequilibrium in the mantle could result such that different $^{87}\text{Sr}/^{86}\text{Sr}$ ratios, for example, in melts could be achieved by variable amounts of partial melting if a Rb rich phase such as phlogopite is present. It is now generally agreed following diffusion studies by Hofmann and Hart (1978) and discussions by O'Nions and Pankhurst (1976) that this effect is unlikely. Variations in radiogenic isotope ratios can result if the source region is isotopically heterogeneous or the magmas themselves are variably mixed with material of a different isotopic signature (e.g. continental crust). Nd and Sr isotopic studies are particularly useful in evaluating the extent to which processes such as crustal contamination have occurred, or the effects mantle heterogeneity have had. In order to assess this, Nd and Sr isotopic compositions were analysed on selected samples from the whole suite. These are presented in Appendix D, along with the methods of analysis. Where necessary, $^{87}\text{Sr}/^{86}\text{Sr}$ data have been age corrected for decay of Rb. The results of this are presented in Appendix G. Age corrections to $^{143}\text{Nd}/^{144}\text{Nd}$ are insignificant.

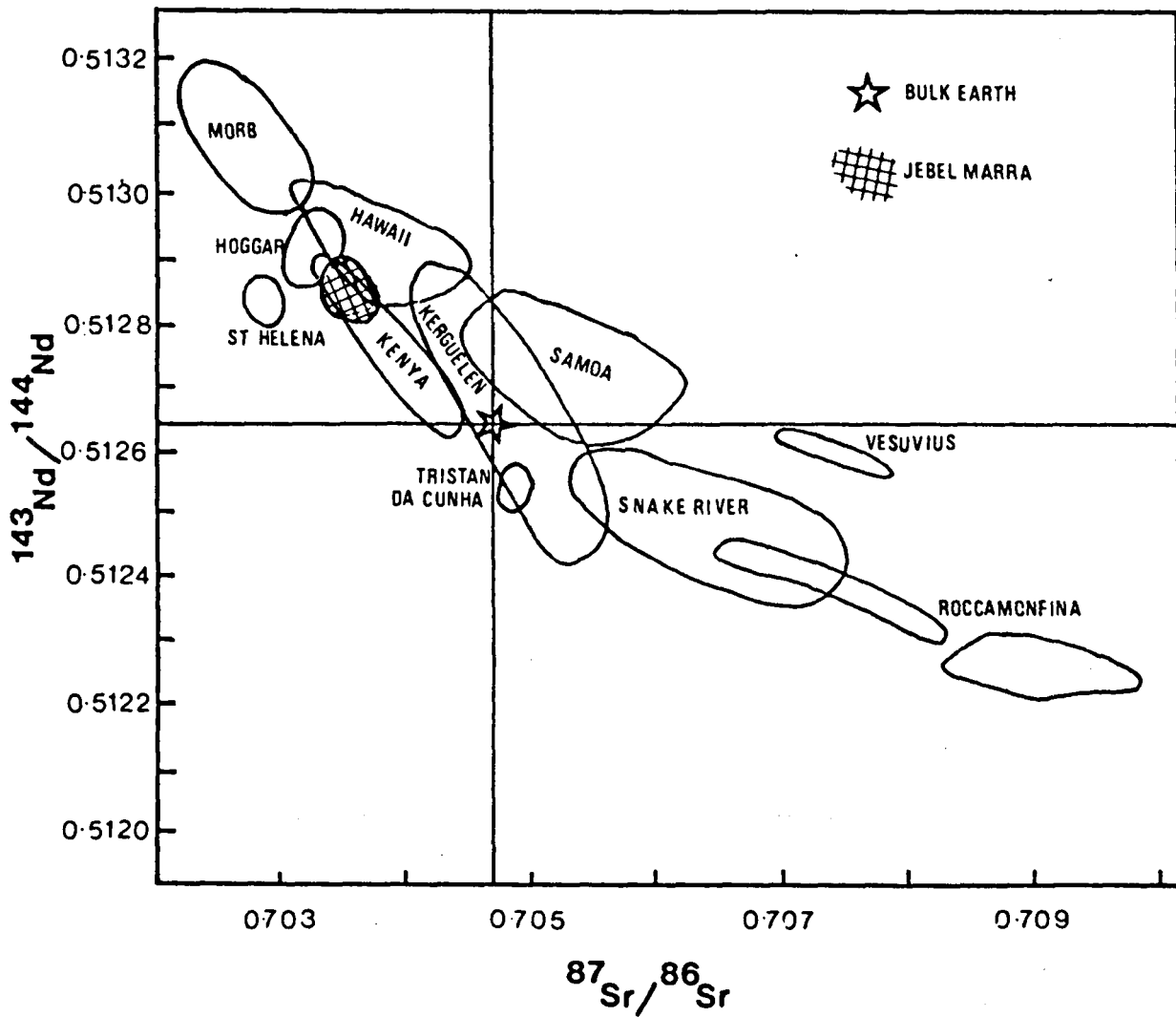
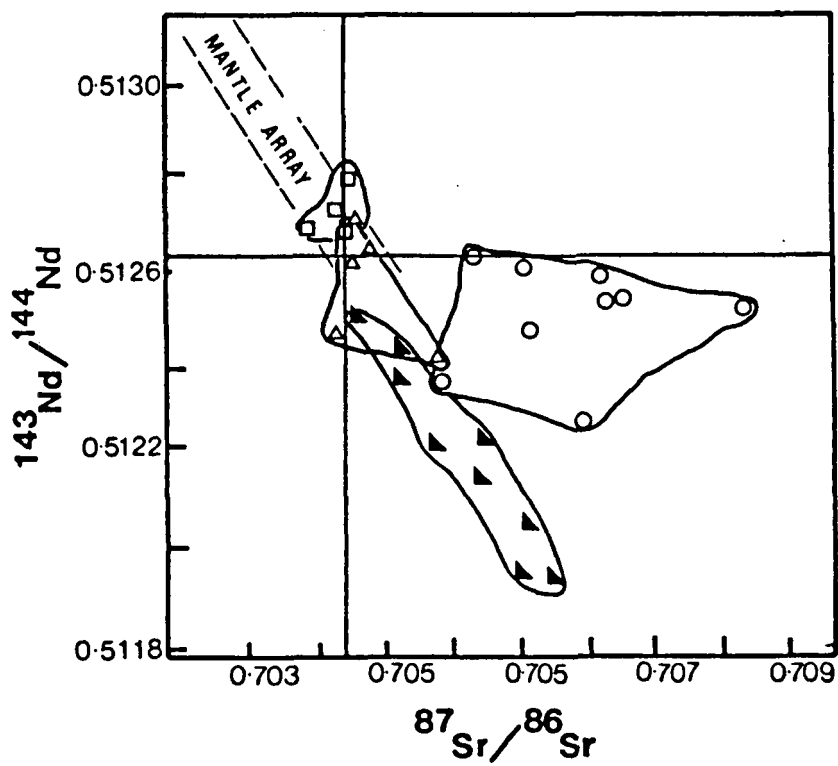


Fig. 8.1a $^{143}\text{Nd}/^{144}\text{Nd}$ vs $^{87}\text{Sr}/^{86}\text{Sr}$ diagram showing fields for several continental and oceanic areas.

Sources: Hawkesworth et al., 1979; Norry and Fitton, 1983; White and Hofmann, 1982.



- △ *Garnet Peridotite & Garnet Phogopite Peridotite*
- *Phlogopite K-Richterite Peridotite*
- ▲ *Diopsides*
- *Kimberlites*

Fig. 8.1b $^{143}\text{Nd}/^{144}\text{Nd}$ vs $^{87}\text{Sr}/^{86}\text{Sr}$ diagram showing range in isotopic composition for mantle samples.

An aim of this Chapter is to demonstrate that the majority of the isotopic variations observed in the Jebel Marra volcanic suite are the result of crustal contamination rather than mantle heterogeneity. Data are presented that suggest that combined assimilation and fractional crystallisation (AFC; DePaolo, 1981) as opposed to other contamination processes, e.g. simple mixing, is largely responsible for both the isotopic and elemental variations. Interpretations of Nd-Sr isotope plots endeavours to place some constraints on the character of the contaminant(s) involved.

Before the variations in Nd and Sr isotopes are studied closely, it is necessary to have a clear idea as to how they may have arisen. Both partial melting of a heterogeneous mantle and crustal contamination can produce major variations in Nd and Sr isotopes. It is their relative roles in petrogenesis which have been the subject of much discussion in recent years (Hawkesworth and Norry, 1983; Hawkesworth and Vollmer, 1979; Norry et al., 1980; Thirlwall, 1982).

8.2 Mantle Heterogeneity

The Earth's mantle, as sampled in oceanic volcanoes and at mid-ocean ridges, is demonstrably heterogeneous in Nd-Sr and other radiogenic isotopes, as is clear from the compilation of data made by White and Hofmann (1982), O'Nions et al., (1979) and Zindler et al., (1982). Most oceanic samples show a good negative correlation between Nd and Sr isotopes, which describe a field known as the 'mantle array', although, recently, oceanic examples have been found which have broadened this array e.g. Samoa and St Helena (White and Hofmann, 1982). On the continents too, where the effects of crustal contamination are negligible, or can be seen through, good cases have

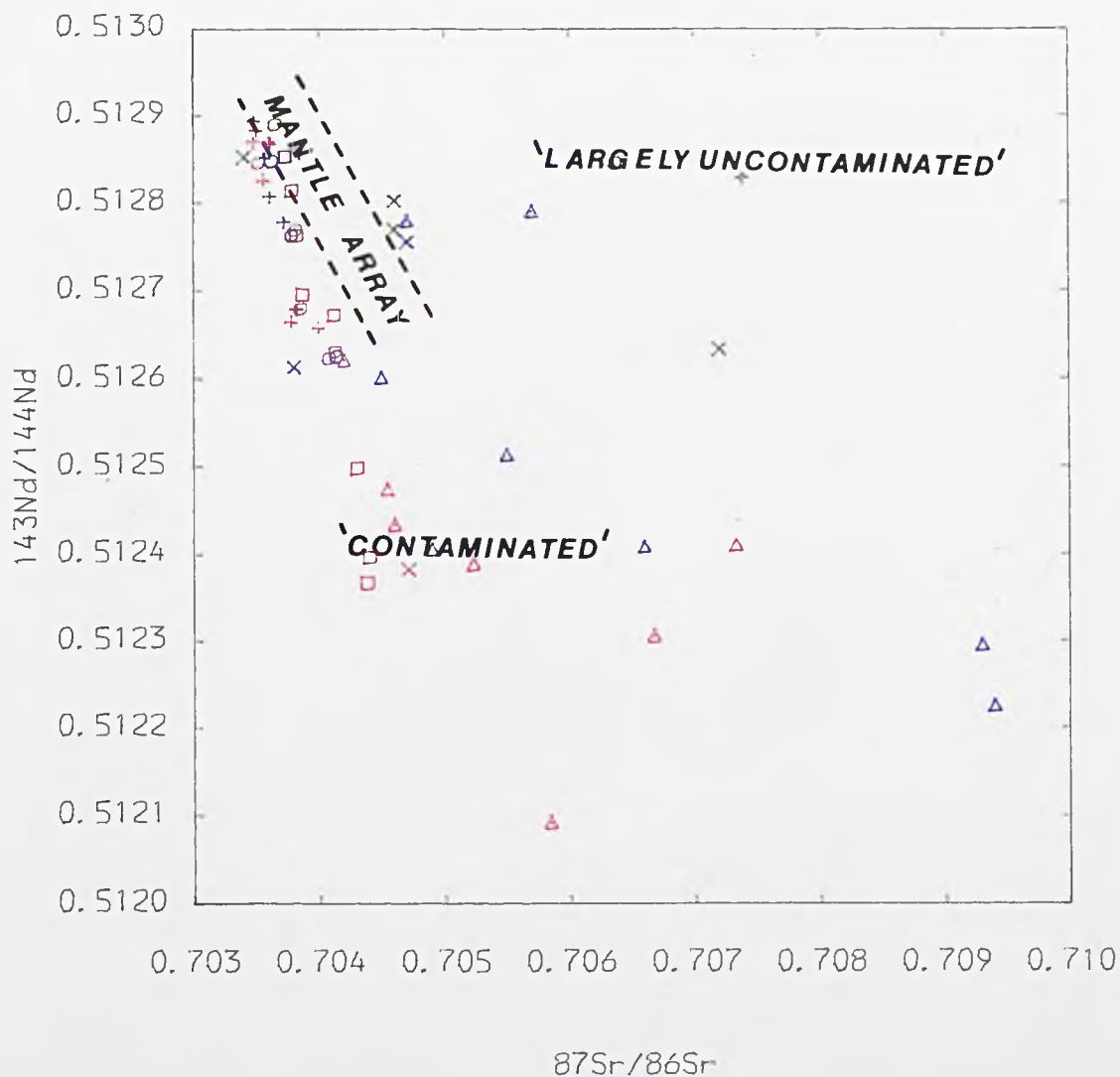
been made for mantle heterogeneity, (Cox, 1983; Hawkesworth and Vollmer, 1979) which with analyses from mantle nodules (e.g. Wass and Rogers, 1980; Menzies and Murthy, 1980; Menzies, 1983; Erlank et al., 1982) have considerably extended the range for mantle samples (Figs. 8.1a-b). The mantle array can therefore be used as a guideline against which the effects of crustal contamination can be assessed. However, it is more dangerous to use the reverse logic to say that because a sample falls within the mantle array, it is uncontaminated.

Fig. 8.2 is a $^{143}\text{Nd}/^{144}\text{Nd}$ vs $^{87}\text{Sr}/^{86}\text{Sr}$ plot for the Jebel Marra volcanics. Most of the data, other than for the primitive basalts, lie outside and to the left of the mantle array. Notwithstanding previous comments, this is the first clue that mantle heterogeneity may not be a major influence on the observed isotopic variations. More convincing than this is the fact that the more evolved the rock is, generally the more radiogenic in $^{87}\text{Sr}/^{86}\text{Sr}$ and less radiogenic in $^{143}\text{Nd}/^{144}\text{Nd}$ it is (see Figs. 8.3 and 8.6). This feature is difficult to reconcile with effects through mantle heterogeneity, as this would also require the isotopic variations in the mantle to be correlated with the extent of partial melting. If different degrees of partial melting, as a process, can be deemed unimportant in the light of isotopic evidence, then the corollary of this is that most of the elemental variations observed within each Series are likely to be the result of fractional crystallisation and crustal contamination rather than through different degrees of partial melting. While discussing this it is appropriate to apply the arguments employed by Thirlwall and Jones (1983). They concluded that because the mantle can only produce melts in equilibrium with Fo88-90,

MANTLE ARRAY

'LARGELY UNCONTAMINATED'

'CONTAMINATED'



TITLE : Fig : 8.2 $^{143}\text{Nd}/^{144}\text{Nd}$ vs $^{87}\text{Sr}/^{86}\text{Sr}$

NEW SERIES ROCKS = red
 PYROCLASTIC SEQUENCE ROCKS = green
 OLD SERIES ROCKS = blue

(using logic from Roeder and Emslie, 1970) which corresponds to high MgO basalts then relatively low MgO rocks, in this context hawaiites and mugearites, are unlikely to be the result of direct mantle melting. In which case they are more likely to be the result of fractionation in or near the crust. Furthermore, the range in $^{143}\text{Nd}/^{144}\text{Nd}$ from basalts to mugearites alone is considerable, and would demand a highly variable mantle beneath Jebel Marra. In conclusion, mantle heterogeneity as a major cause of variations seems unlikely for the Jebel Marra volcanics, although it may be responsible for relatively small variations among the primitive basalts.

In Figs. 8.3 and 8.6 it is seen that isotopic composition correlates very well with indices of fractionation. This important feature of the data is not likely to be a result of mantle heterogeneity. The cause of this effect is much more likely to be linked with the effects of crustal contamination. It is these variations which will be discussed in detail and interpreted primarily in terms of various crustal contamination mechanisms.

8.3 Variations

8.3.1 $^{143}\text{Nd}/^{144}\text{Nd}$ vs $^{87}\text{Sr}/^{86}\text{Sr}$

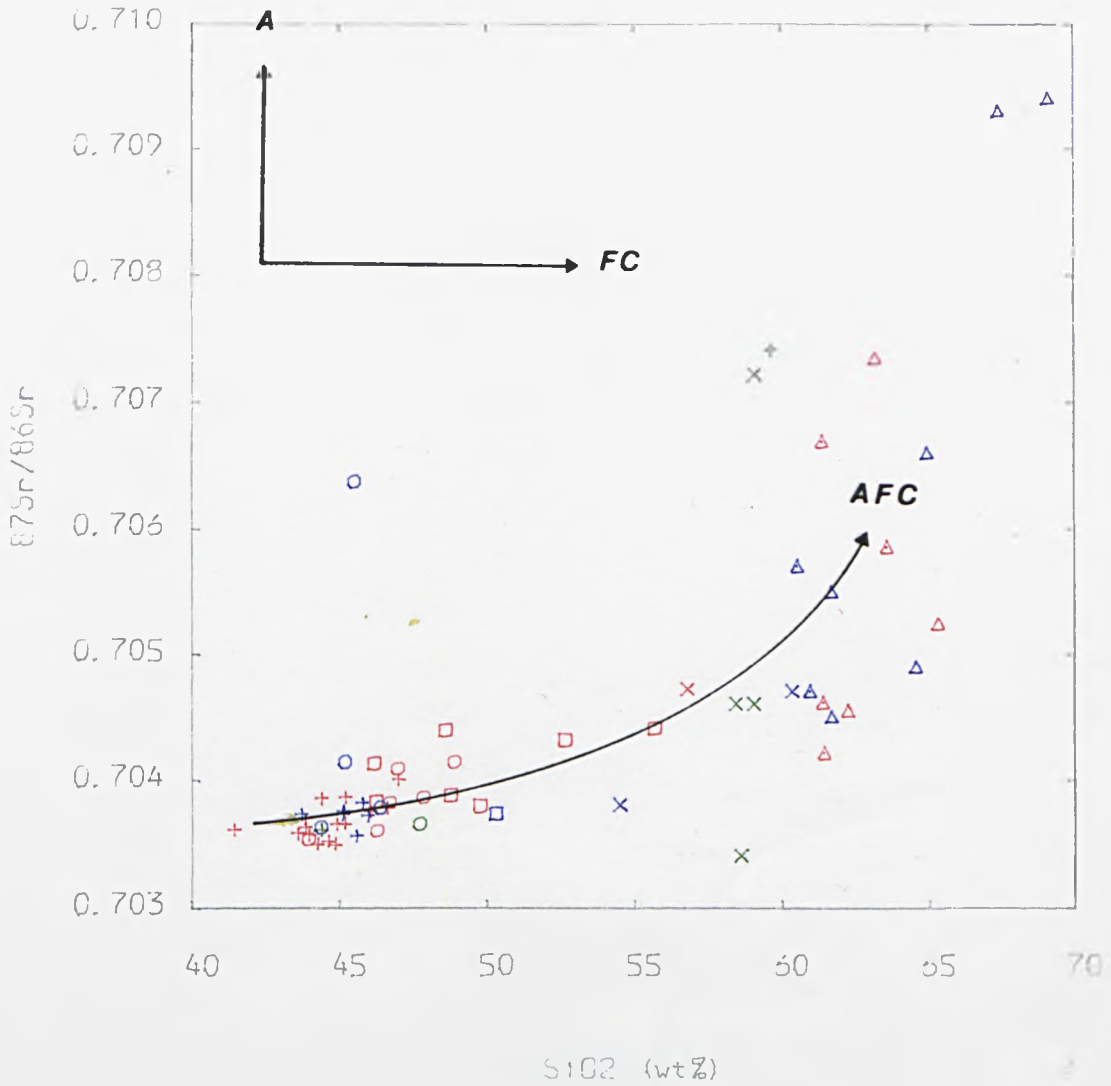
In discussions in Chapters 6 and 7, the data, on the basis of isotopic evidence, were divided into fields described as 'largely uncontaminated' and 'contaminated'. This assertion is partly based on Fig. 8.2 which plots $^{143}\text{Nd}/^{144}\text{Nd}$ vs $^{87}\text{Sr}/^{86}\text{Sr}$ in which the two groups of data are separate. The 'largely uncontaminated' group comprise Old Series acidic rocks and they are described as such because of their high $^{143}\text{Nd}/^{144}\text{Nd}$, compared with the 'contaminated' acidic rocks. This division is indicated in Fig. 8.2 and is clearest

amongst evolved rocks; in the basaltic rocks the division is less discernible. Despite some uncertainty with age corrections, the $^{87}\text{Sr}/^{86}\text{Sr}$ values are, in some cases, high. High $^{87}\text{Sr}/^{86}\text{Sr}$ values in the acidic rocks could result even through small amounts of crustal contamination because these liquids have characteristically high Nd concentrations and low Sr concentrations. The absence of basic rocks along this trend does not contradict a scheme of small amounts of contamination, because high Sr basic rocks would be resistant to such an effect. The increasing magmatic Nd and decreasing Sr resulting from fractionation means that Nd becomes less susceptible and Sr becomes more susceptible to the effects of contamination. This concurs with the conclusion arrived at for an analogous study in Kenya on the Emurangogolak phonolites by Norry et al., (1980). An alternative hypothesis to this is that these samples were affected by hydrothermal fluids. Such a fluid, because of the relatively low solubility of Nd, would have a high Sr/Nd ratio which would tend to shift the isotopic composition of altered lavas in a direction to the right of, and sub-parallel to, the $^{87}\text{Sr}/^{86}\text{Sr}$ axis. The freshness of the phonolites, in particular, would argue against such a process having occurred, however. The data for the 'contaminated' rocks, which include all New Series rocks and some Old Series rocks, are consistent with assimilation of crust with relatively low $^{87}\text{Sr}/^{86}\text{Sr}$ and low $^{143}\text{Nd}/^{144}\text{Nd}$. In this trend, the data are much more coherent and there is a general progression along it from basalts to more evolved rocks.

8.3.2 $^{87}\text{Sr}/^{86}\text{Sr}$ vs Major and Trace Elements

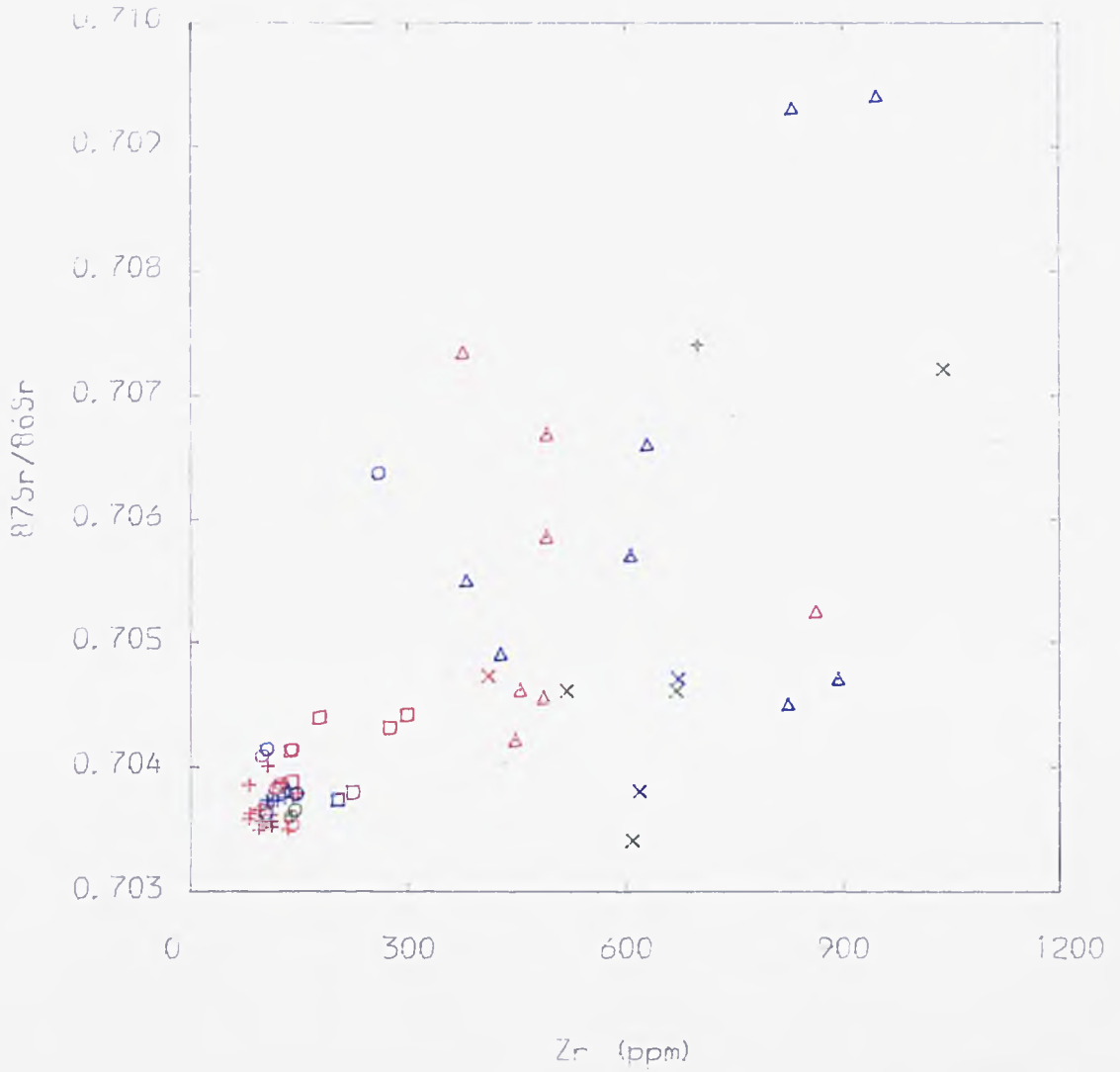
In Figs. 8.3a-c, $^{87}\text{Sr}/^{86}\text{Sr}$ is plotted against SiO_2 , Zr and Nb. The feature prominent in all the diagrams is a general concomitant





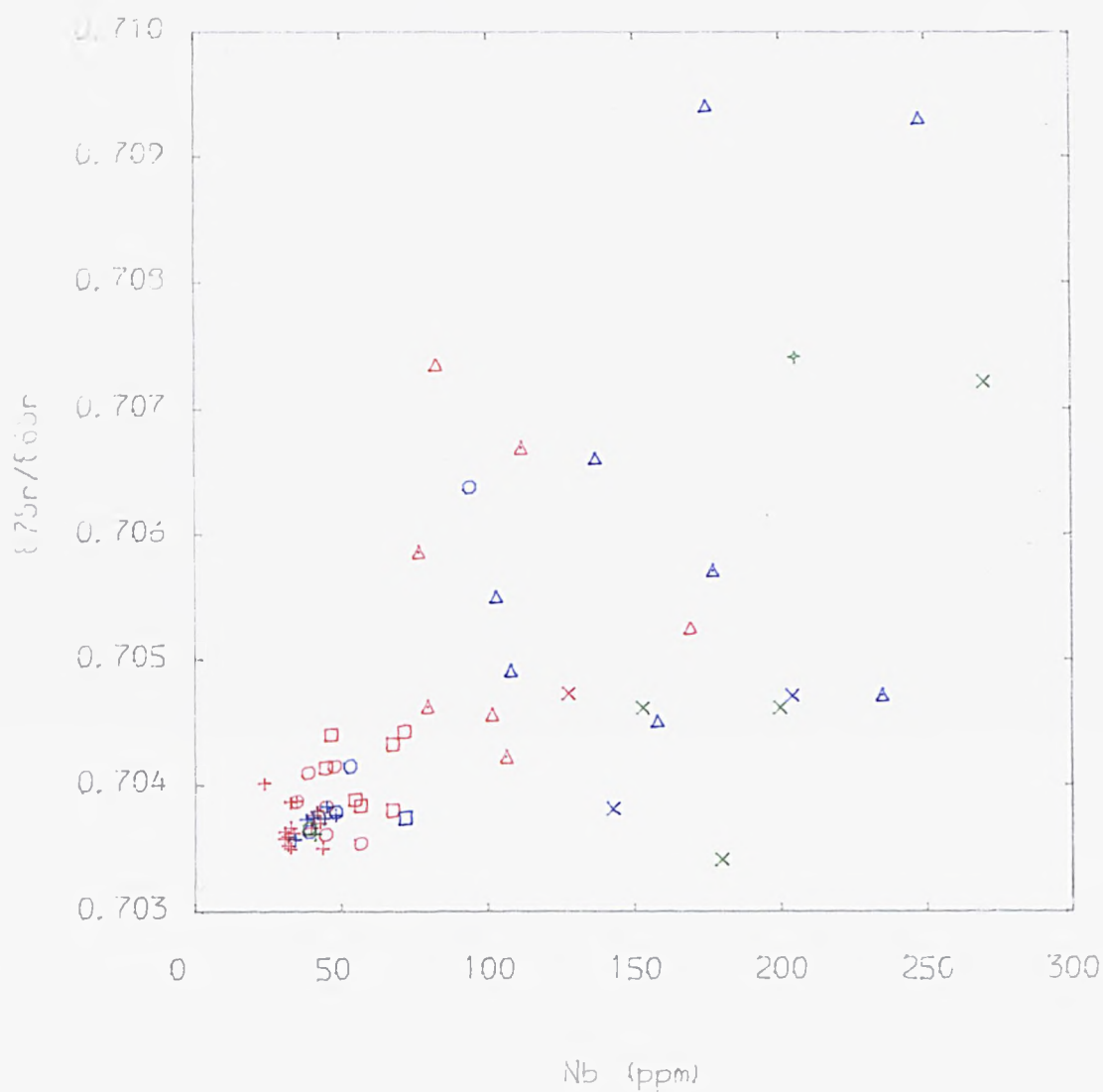
TITLE : Fig : 8.3a $^{87}\text{Sr}/^{86}\text{Sr}$ vs SiO_2

NEW SERIES ROCKS = red
 PYROCLASTIC SEQUENCE ROCKS = green
 OLD SERIES ROCKS = blue



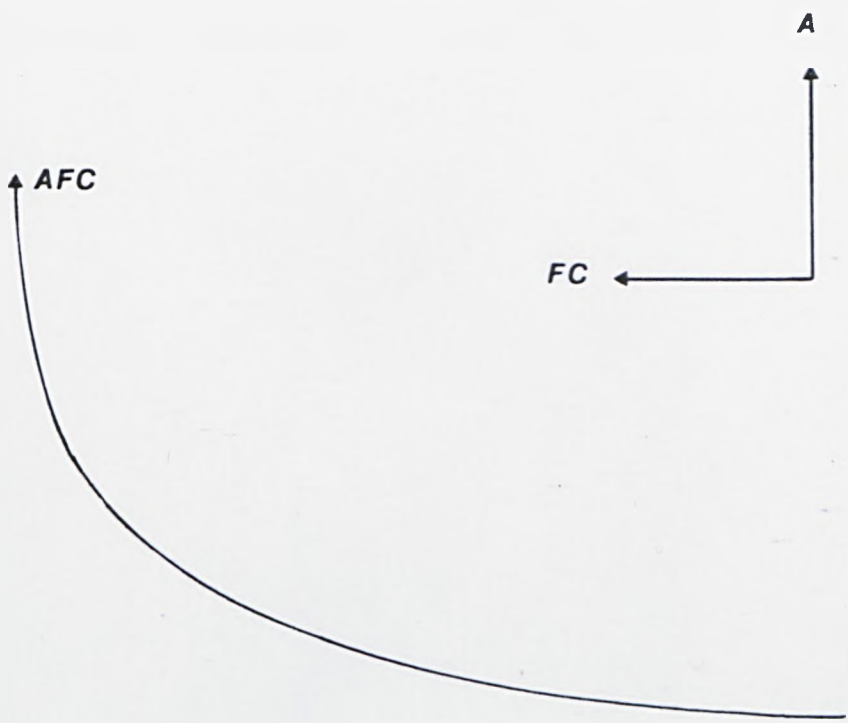
TITLE . Fig . 8.3b $^{87}\text{Sr}/^{86}\text{Sr}$ vs Zr

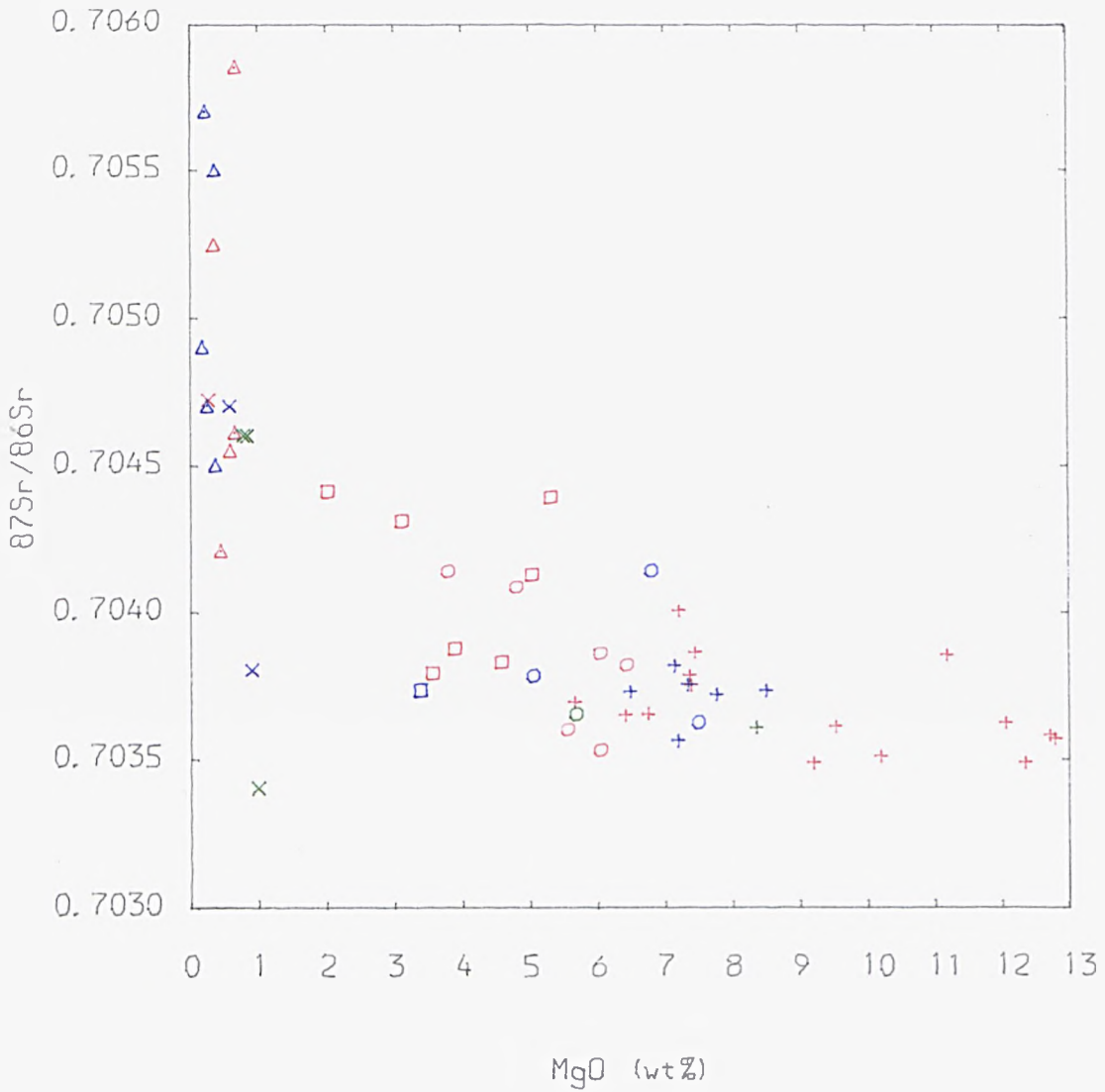
NEW SERIES ROCKS = red
 PYROCLASTIC SEQUENCE ROCKS = green
 OLD SERIES ROCKS = blue



TITLE : Fig : 3.3c $^{87}\text{Sr}/^{86}\text{Sr}$ vs Nb

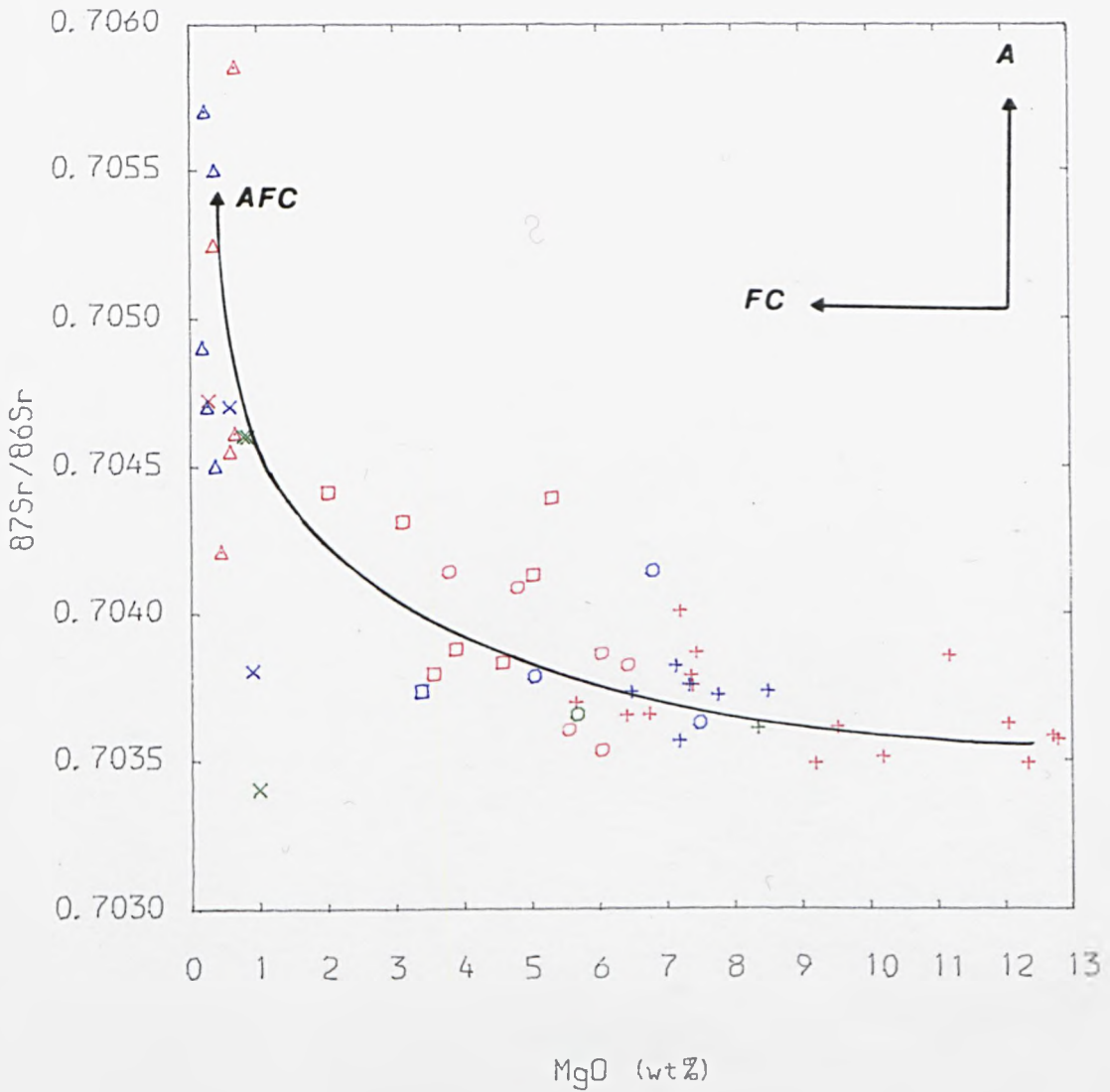
NEW SERIES ROCKS = red
 PYROCLASTIC SEQUENCE ROCKS = green
 OLD SERIES ROCKS = blue





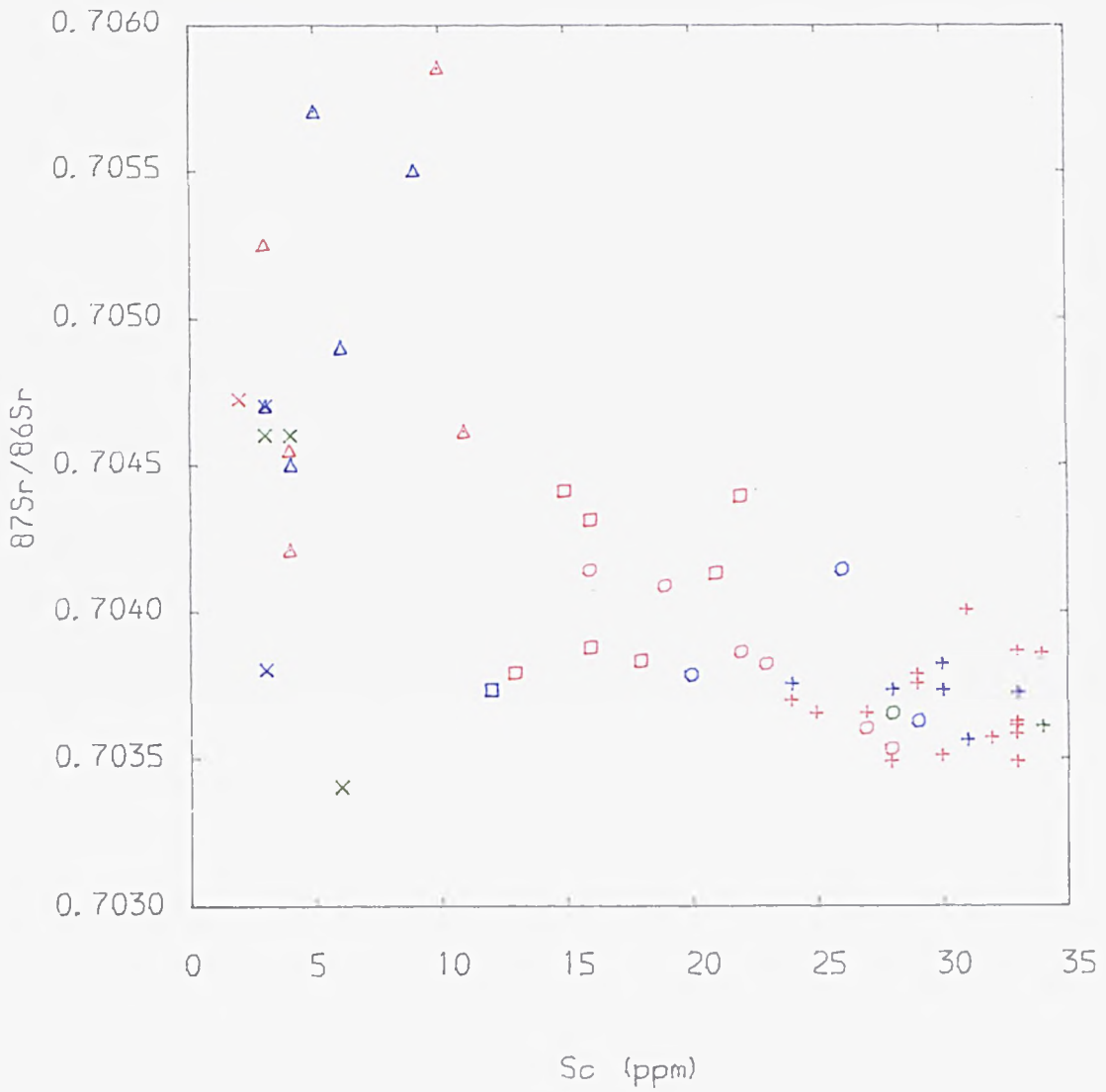
TITLE : Fig : 8.4a $^{87}\text{Sr}/^{86}\text{Sr}$ vs MgO

NEW SERIES ROCKS = red
 PYROCLASTIC SEQUENCE ROCKS = green
 OLD SERIES ROCKS = blue



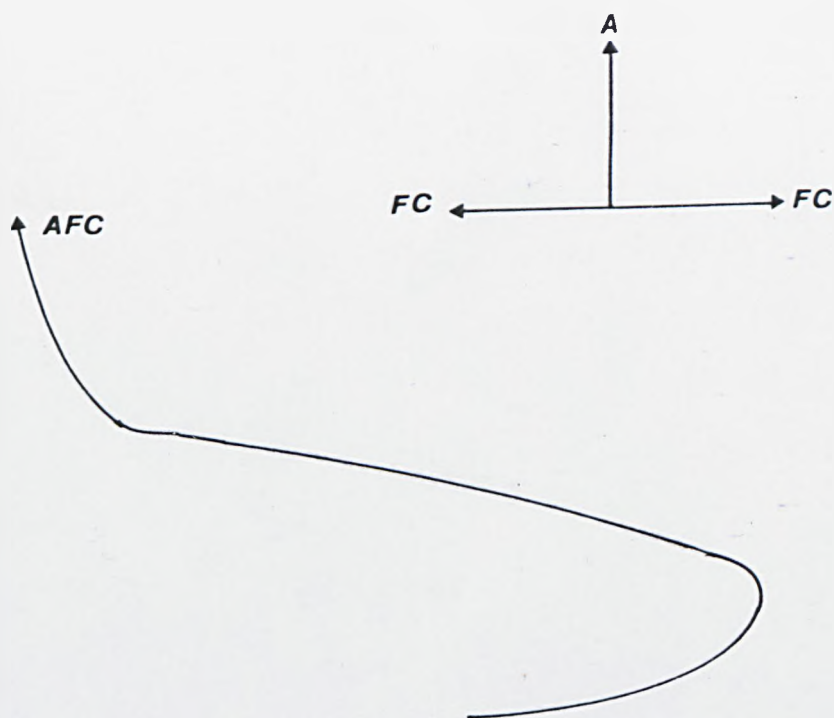
TITLE : Fig : 8.4a $^{87}\text{Sr}/^{86}\text{Sr}$ vs MgO

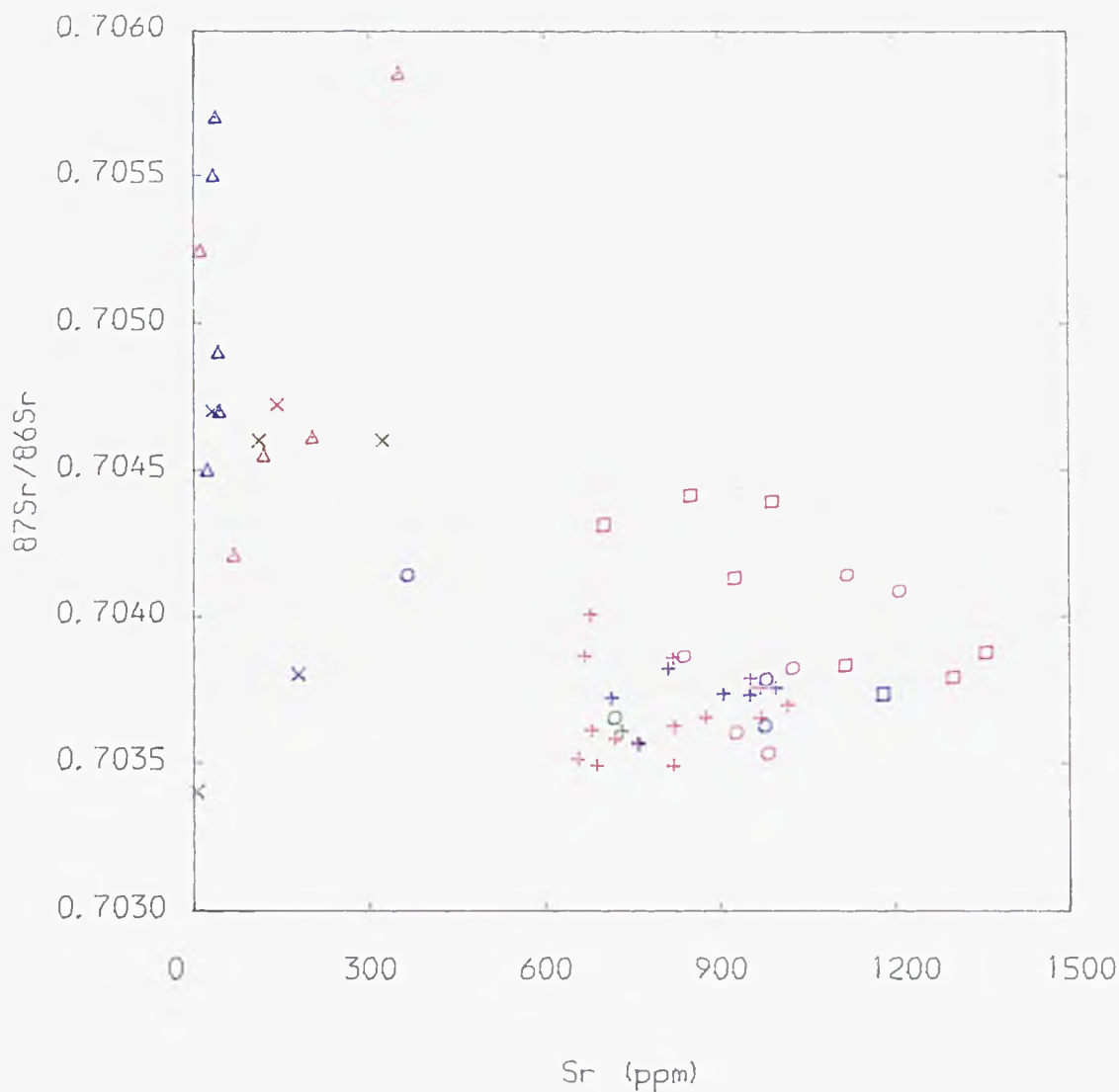
NEW SERIES ROCKS = red
 PYROCLASTIC SEQUENCE ROCKS = green
 OLD SERIES ROCKS = blue



TITLE : Fig : 8.4b $^{87}\text{Sr}/^{86}\text{Sr}$ vs Sc

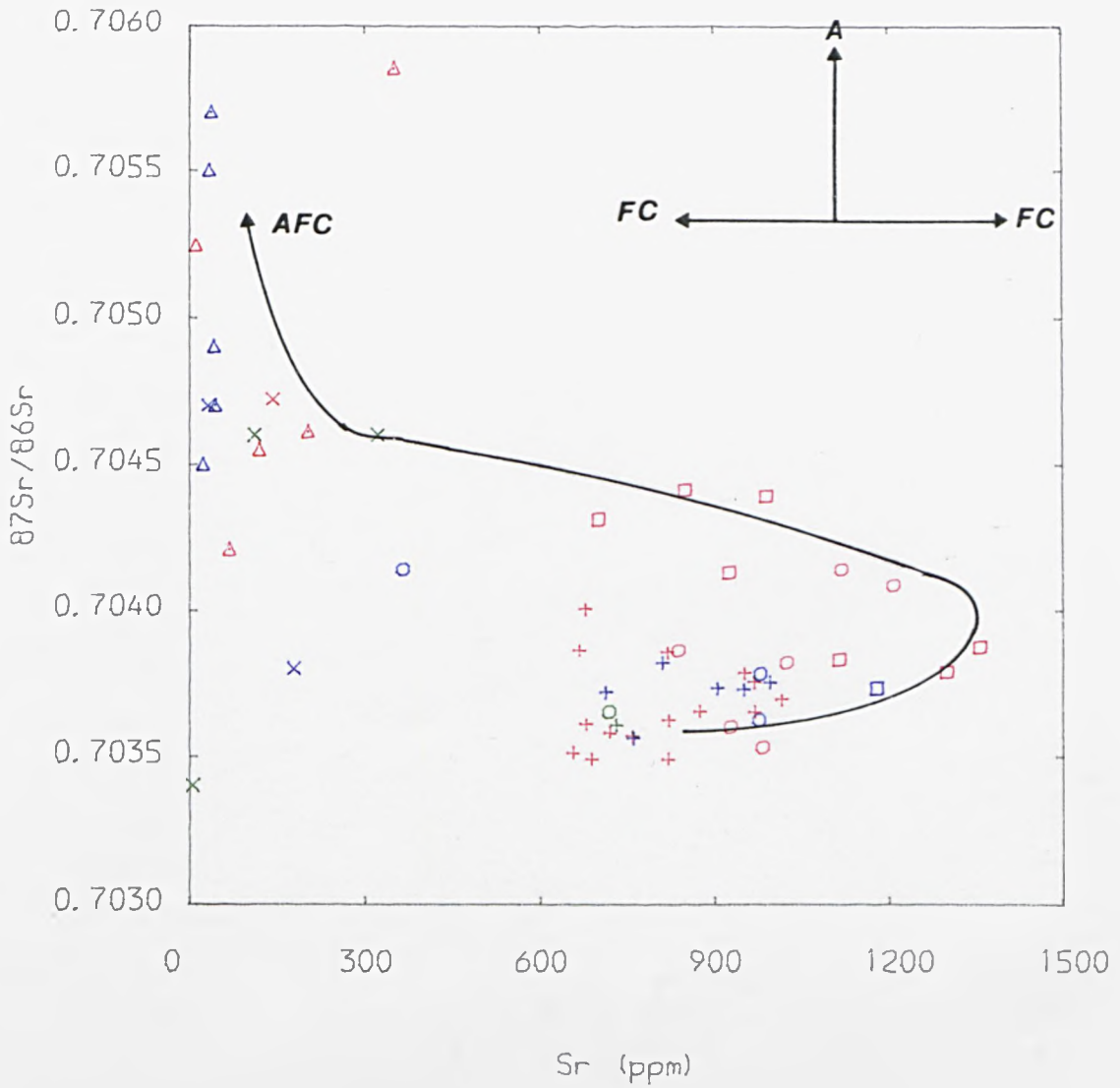
NEW SERIES ROCKS = red
 PYROCLASTIC SEQUENCE ROCKS = green
 OLD SERIES ROCKS = blue





TITLE : Fig : 8.5 $^{86}\text{Sr}/^{86}\text{Sr}$ vs Sr

NEW SERIES ROCKS = red
 PYROCLASTIC SEQUENCE ROCKS = green
 OLD SERIES ROCKS = blue



TITLE : Fig : 8.5 $^{86}\text{Sr}/^{87}\text{Sr}$ vs Sr

NEW SERIES ROCKS = red
 PYROCLASTIC SEQUENCE ROCKS = green
 OLD SERIES ROCKS = blue

increase in $^{87}\text{Sr}/^{86}\text{Sr}$, with increasing SiO_2 and incompatible trace elements. With MgO and compatible trace elements (e.g. Sc) vs $^{87}\text{Sr}/^{86}\text{Sr}$ (Figs. 8.4a-b), there is a concomitant increase in $^{87}\text{Sr}/^{86}\text{Sr}$ with decreases in compatible trace elements and MgO. In Fig. 8.5, $^{87}\text{Sr}/^{86}\text{Sr}$ is plotted against Sr. In this diagram, $^{87}\text{Sr}/^{86}\text{Sr}$ increases as Sr increases, until rocks of roughly mugearitic composition, whereupon Sr decreases, as Sr is removed in plagioclase, while the $^{87}\text{Sr}/^{86}\text{Sr}$ continues to increase. An analogous situation exists for $^{87}\text{Sr}/^{86}\text{Sr}$ vs Ba, which is affected in the same way, but is the result of anorthoclase fractionation.

8.3.3 $^{143}\text{Nd}/^{144}\text{Nd}$ vs Trace Elements

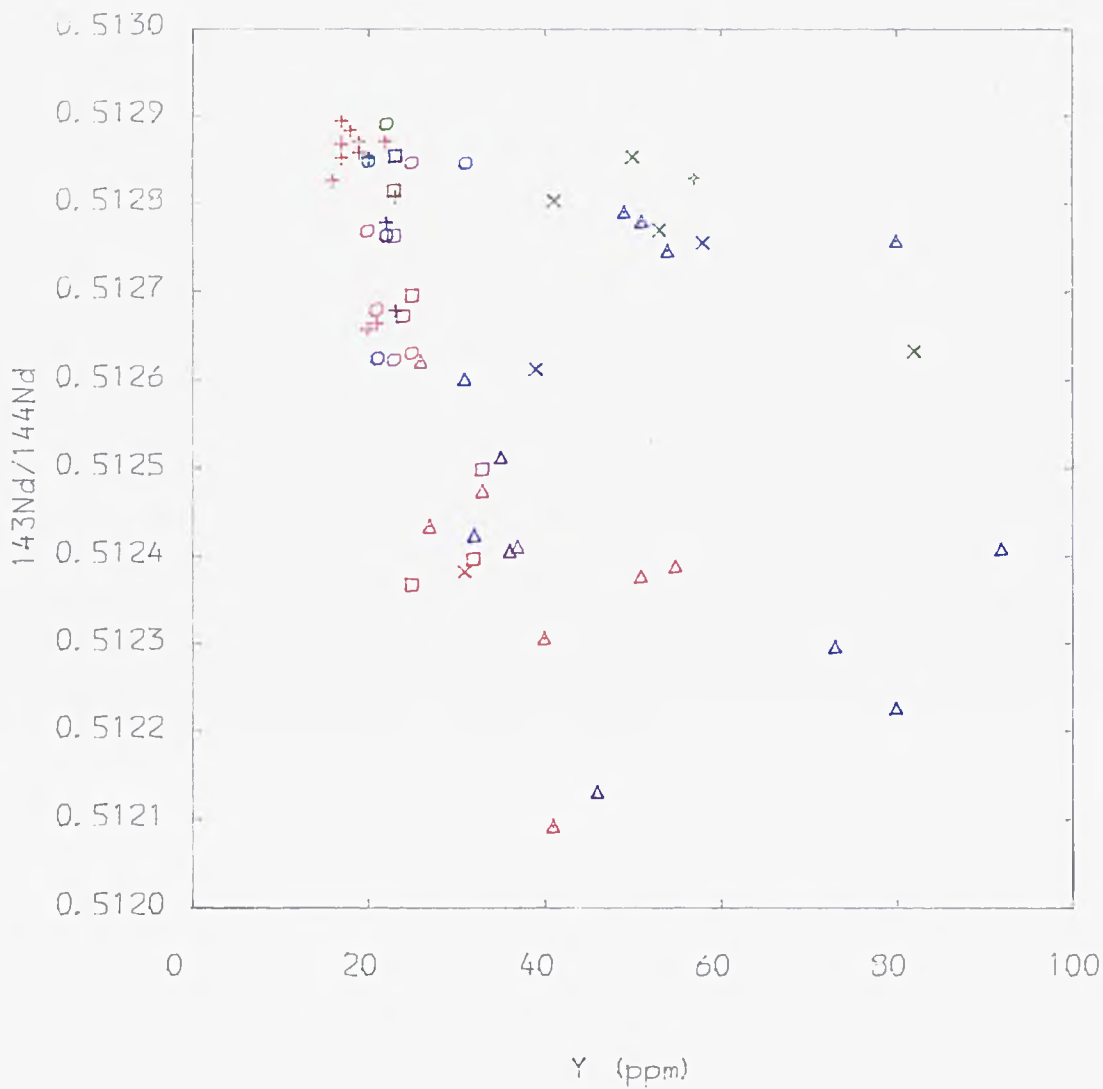
In Figs. 8.6a-g plots of $^{143}\text{Nd}/^{144}\text{Nd}$ vs incompatible elements (Y, Zr, Nb, Th, Rb, La and Ce) show some different features to $^{87}\text{Sr}/^{86}\text{Sr}$ vs incompatible element plots. In all these plots the samples are separated into the two groups previously described; namely, a 'largely uncontaminated' and a 'contaminated' group. Secondly, the basic rocks of the 'contaminated' series show relatively small increases in incompatible elements and large decreases in $^{143}\text{Nd}/^{144}\text{Nd}$ compared with acidic rocks. The fields for 'contaminated' and 'uncontaminated' are indicated in Fig. 8.6a. The 'uncontaminated' group largely parallel variations in acidic rocks of the 'contaminated' series but have a higher $^{143}\text{Nd}/^{144}\text{Nd}$ composition.

8.4 Crustal Contamination

Before discussing the details of the contamination mechanisms it will be useful to collate the information available on the possible magmatic and crustal end-members.

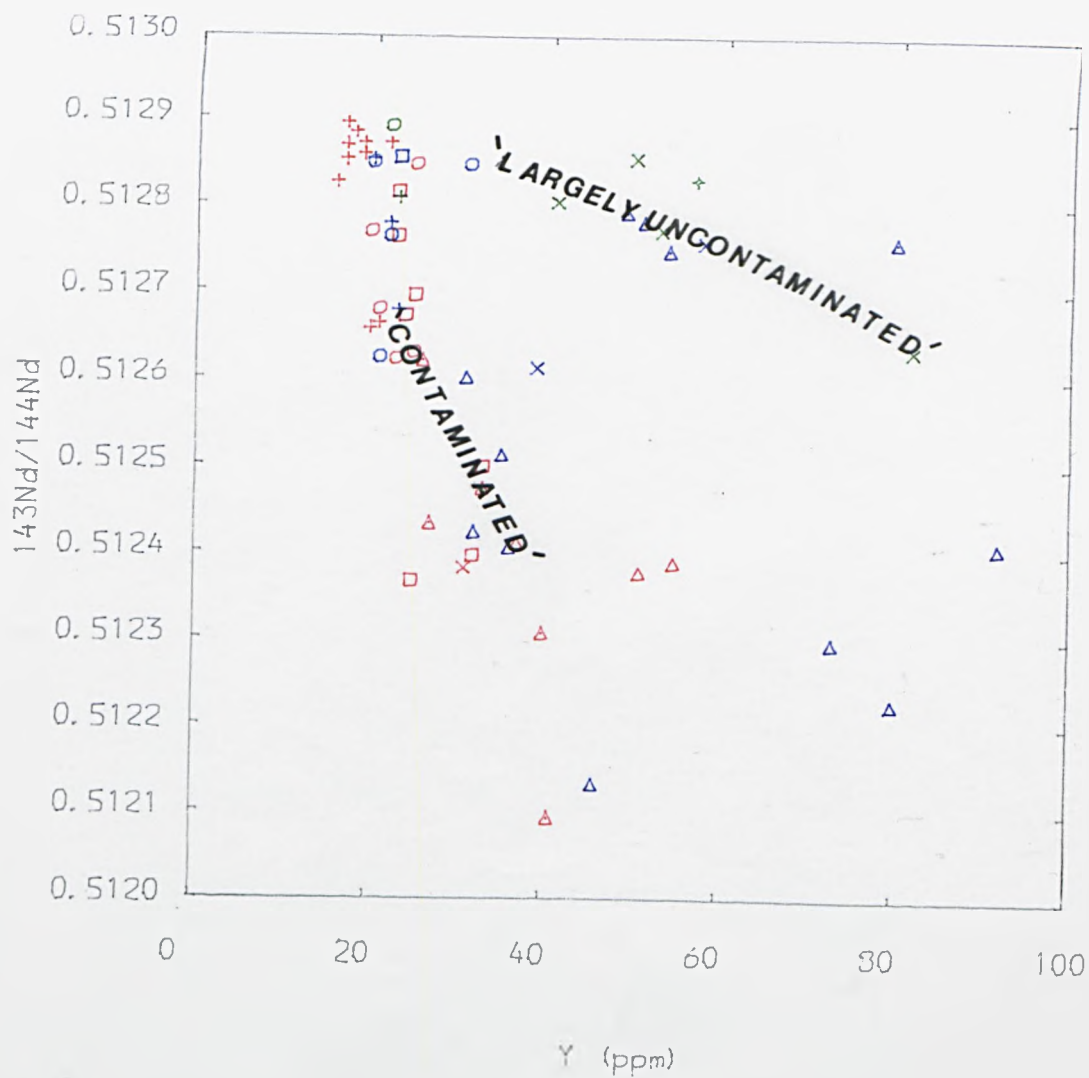
'LARGELY UNCONTAMINATED'

'CONTAMINATED'



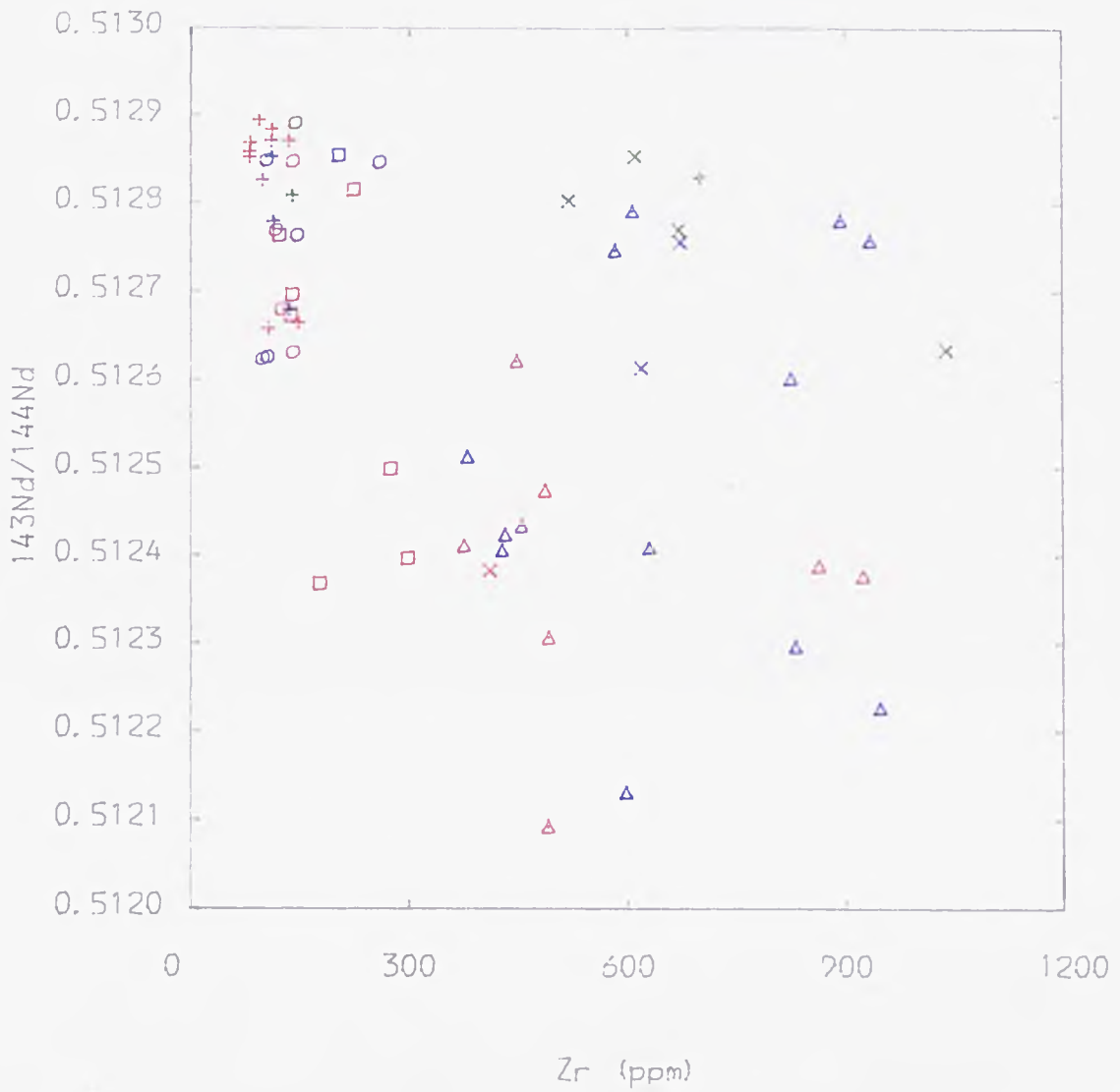
TITLE : Fig : 8.6a-g $^{143}\text{Nd}/^{144}\text{Nd}$ vs Traces

NEW SERIES ROCKS = red
 PYROCLASTIC SEQUENCE ROCKS = green
 OLD SERIES ROCKS = blue



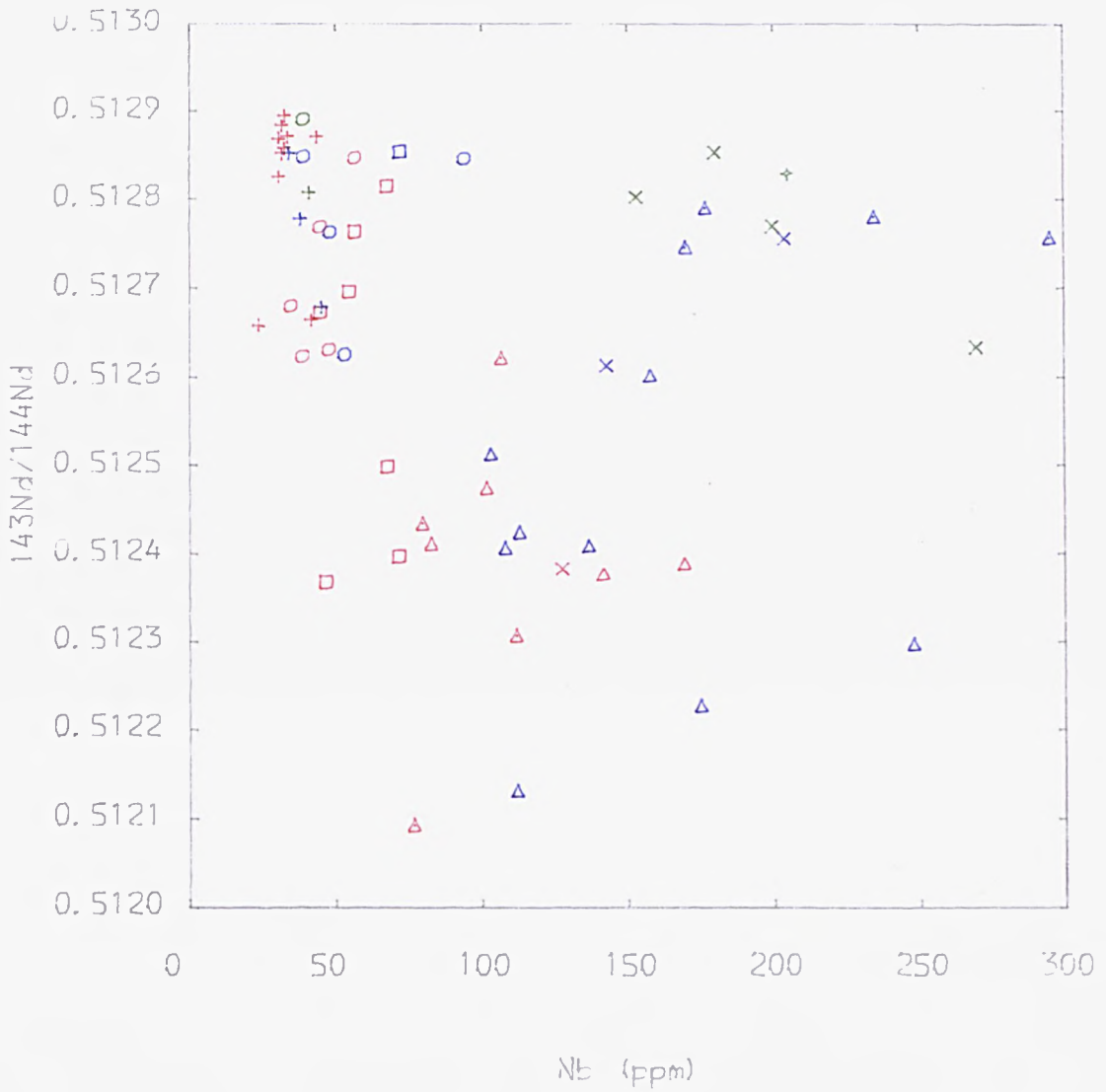
TITLE : Fig. 8. 6a-g $^{143}\text{Nd}/^{144}\text{Nd}$ vs Traces

NEW SERIES ROCKS	= red
PYROCLASTIC SEQUENCE ROCKS	= green
OLD SERIES ROCKS	= blue



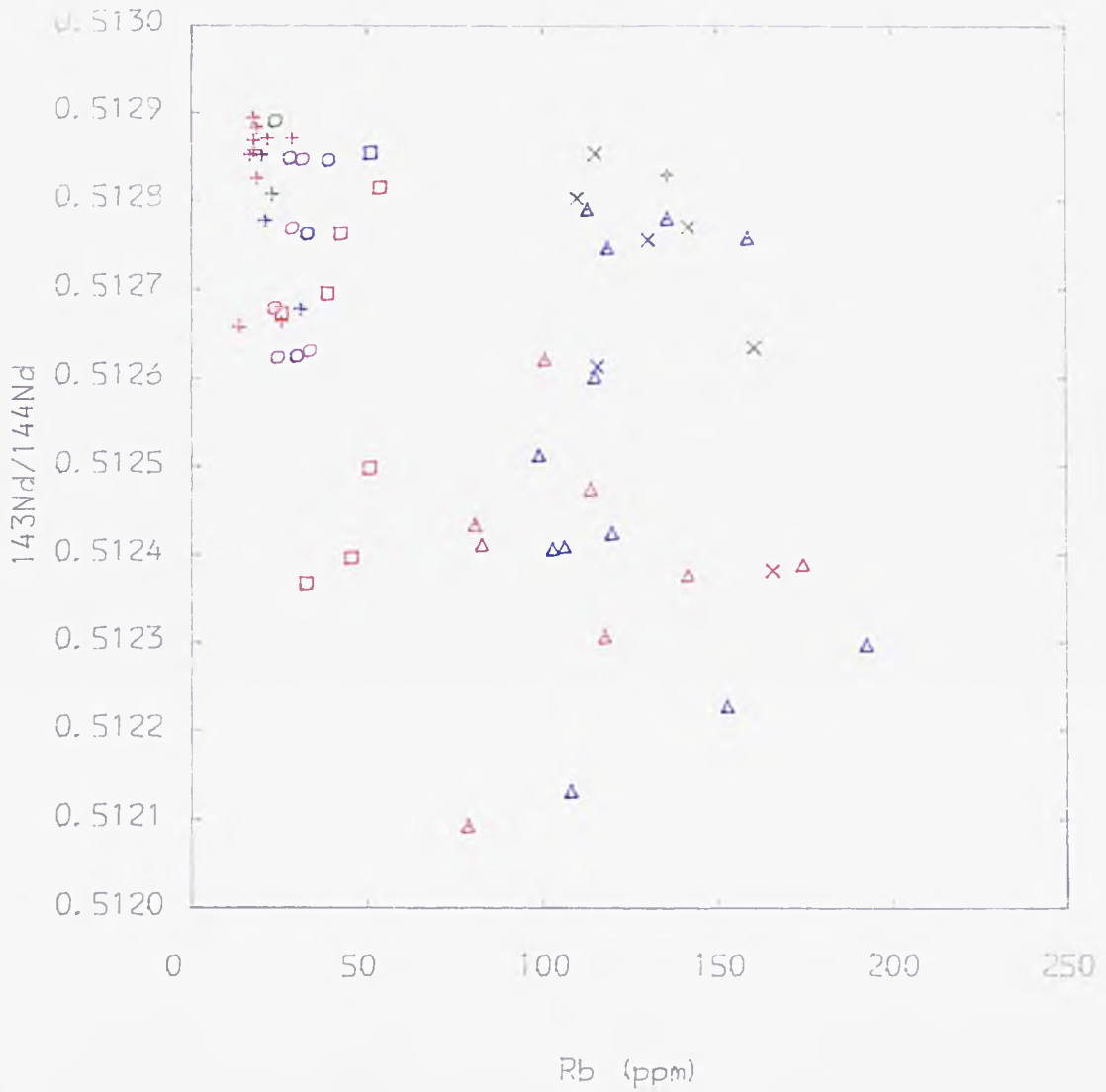
TITLE : Fig : 8.6a-g $^{143}\text{Nd}/^{144}\text{Nd}$ vs Traces

NEW SERIES ROCKS = red
 PYROCLASTIC SEQUENCE ROCKS = green
 OLD SERIES ROCKS = blue



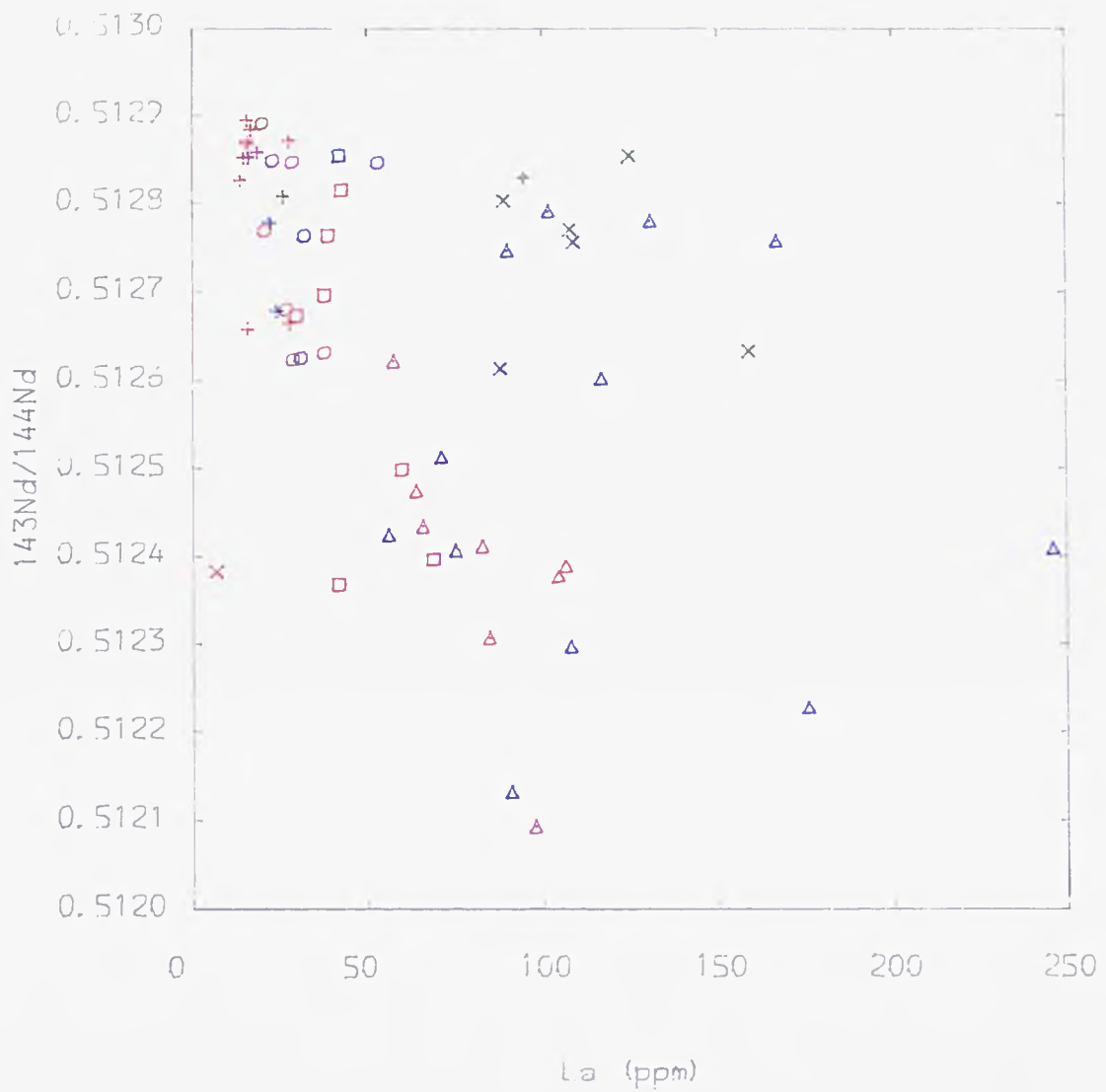
TITLE : Fig : 8.6a-g $^{143}\text{Nd}/^{144}\text{Nd}$ vs Traces

NEW SERIES ROCKS = red
 PYROCLASTIC SEQUENCE ROCKS = green
 OLD SERIES ROCKS = blue



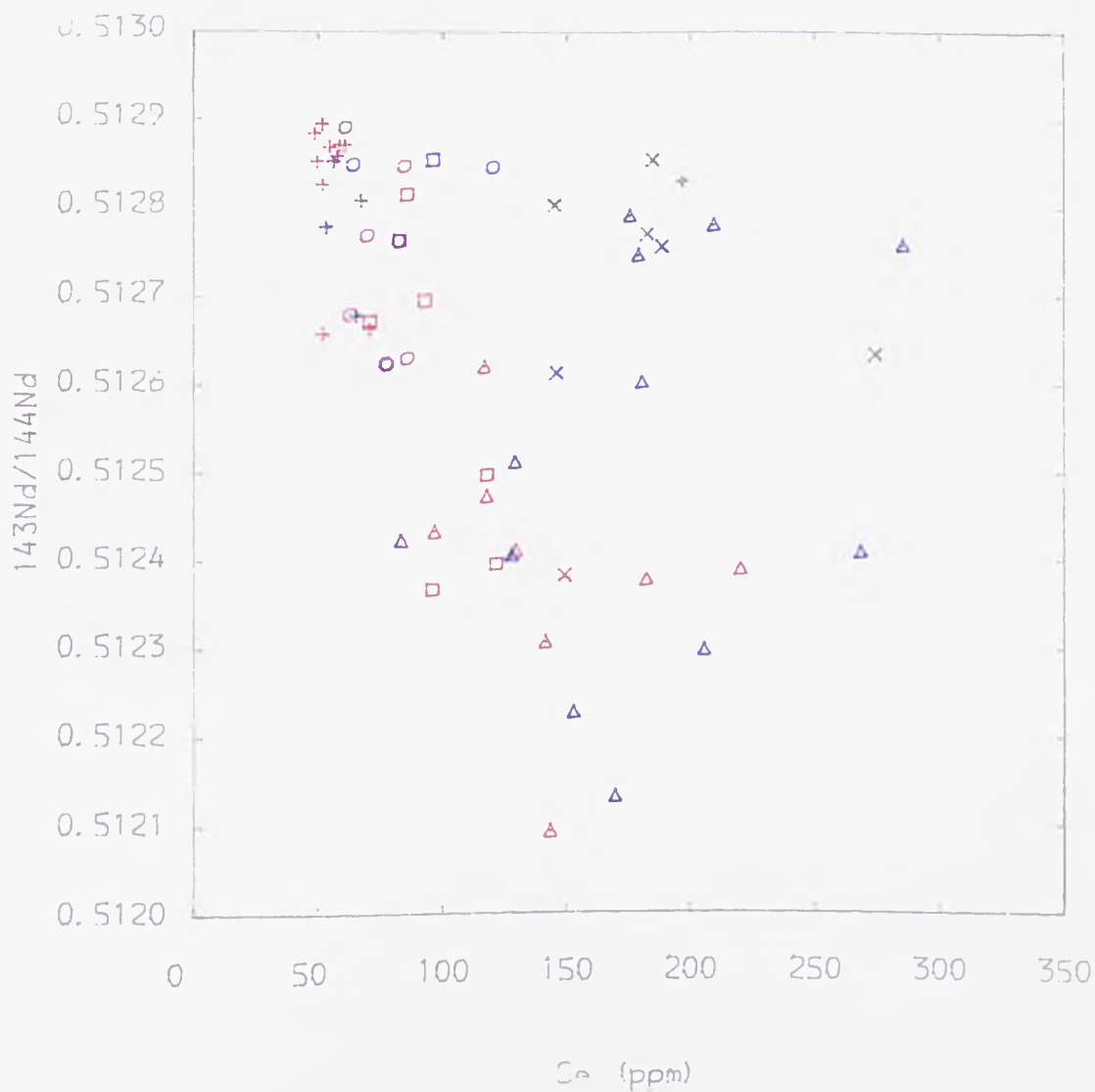
TITLE : Fig : 8. 6a-g $^{143}\text{Nd}/^{144}\text{Nd}$ vs Traces

NEW SERIES ROCKS = red
 PYROCLASTIC SEQUENCE ROCKS = green
 OLD SERIES ROCKS = blue



TITLE : Fig : 8.6a-g $^{143}\text{Nd}/^{144}\text{Nd}$ vs Traces

NEW SERIES ROCKS = red
 PYROCLASTIC SEQUENCE ROCKS = green
 OLD SERIES ROCKS = blue



TITLE : Fig : 8.6a-g $^{143}\text{Nd}/^{144}\text{Nd}$ vs Traces

NEW SERIES ROCKS = red
 PYROCLASTIC SEQUENCE ROCKS = green
 OLD SERIES ROCKS = blue

8.4.1 End-Members

In order to discuss the isotopic data in terms of mixing trends it is important to have a good idea of the isotopic and elemental compositions of the end-members. In practice, rather more is usually known about the end-member corresponding to the primary magma. However, as in this study, for this to be meaningful it is necessary to demonstrate that the effects of mantle heterogeneity are minimal (see Section 8.2).

In Fig. 8.2 the most primitive basalts are those with the highest $^{143}\text{Nd}/^{144}\text{Nd}$ and lowest $^{87}\text{Sr}/^{86}\text{Sr}$ and are also the most primitive elementally (i.e. high MgO, Cr, Ni etc.). They have probably been contaminated to some extent but the basic nature of these samples suggest that this is to a negligible degree and they can therefore be regarded as representative of the primary magma and indeed their source mantle. The elemental concentrations of Nd and Sr are also known from X.R.F. analyses. These abundances are more likely to differ from those of the primary magma (i.e. magmas in equilibrium with its source mantle) as, according to O'Hara (1968), very few primary lavas will ever surface without losing at least 10% olivine en route. For this reason it is considered safer to use the isotopic and elemental compositions of primitive basalts as one end-member rather than that of a primary magma whose composition can only be surmised. However, an important point raised by examination of spidergrams for primitive basalts (see Chapter 9) is that their patterns are very similar to other continental basalts and ocean island basalts which are considered to be largely uncontaminated e.g. Kenya, Cameroons and Azores (Norry and Fitton, 1983).

Table 8.1 End-Member Characteristics

	$^{87}\text{Sr}/^{86}\text{Sr}$	$^{143}\text{Nd}/^{144}\text{Nd}$	Sr	Nd	Sr/Nd	K	R
PRIMITIVE BASALT (A)							
New Series	0.7035	0.5129	650	26	25	-	-
Old Series	0.7034	0.5129	650	26	25	-	-
CRUSTAL ROCKS (B)							
24037 L	0.708633	0.511368	678	34	19.9	1.26	0.80
24135 L	0.730630	0.510747	339	30	11.3	2.17	0.46
24137 L	0.709032	0.511270	802	30	26.7	0.94	1.07
24139 U	0.727068	0.512052	224	21	10.7	2.33	0.43
24036 U	0.764478	0.511398	69	18	3.8	6.57	0.15
24134 U	0.752392	0.511647	102	5	20.4	1.23	0.81
24138 U	0.855156	0.511628	55	35	1.6	15.6	0.06

L = samples with 'lower crustal' characteristics

U = samples with 'upper crustal' characteristics

K = Sr/Nd (A) + Sr/Nd (B)

R = 1/K

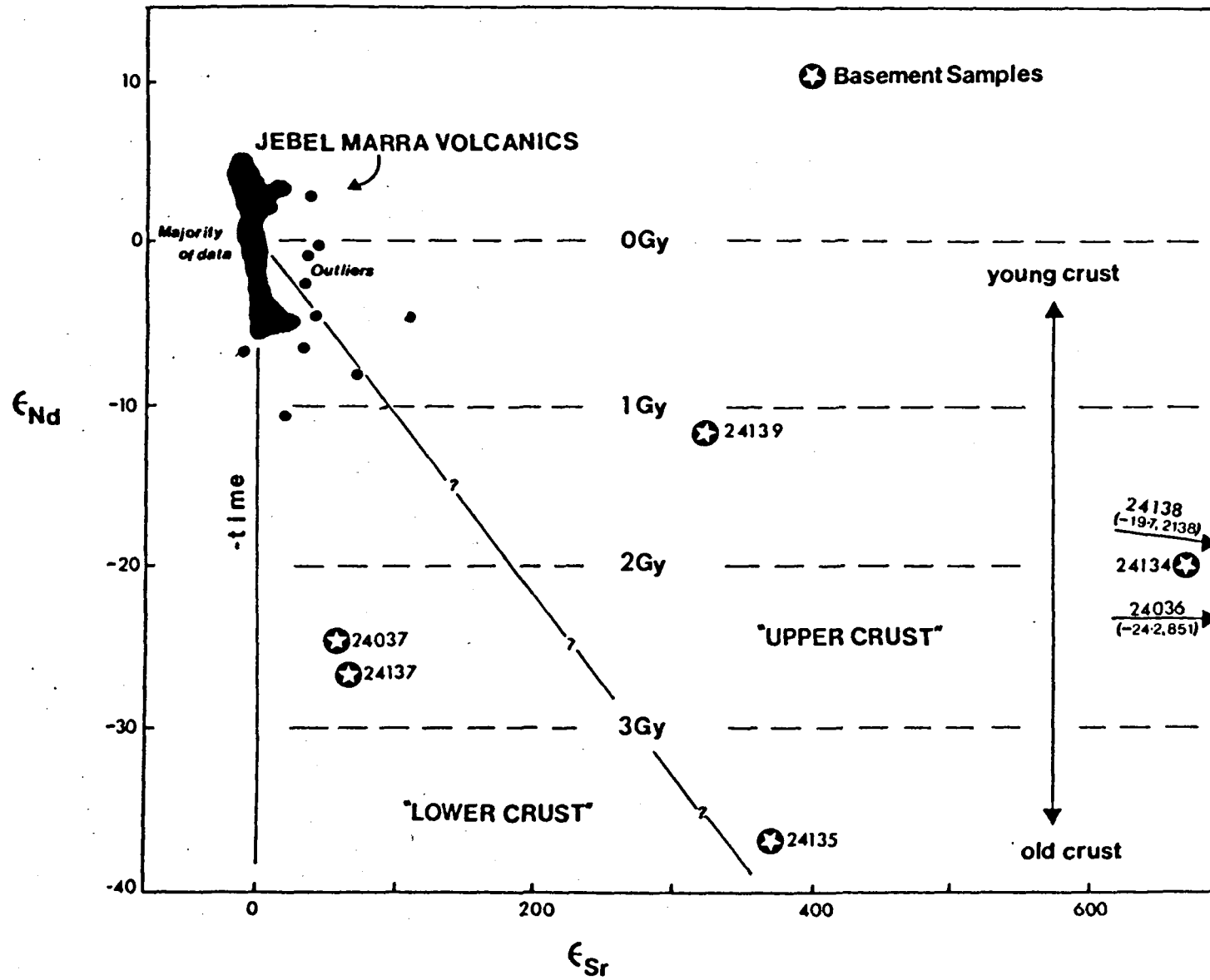
Choice of suitable crustal end-members is considerably more problematical. In a qualitative sense its character can be inferred by extrapolation of isotopic trends such as in Fig. 8.2. From this a crust with low $^{143}\text{Nd}/^{144}\text{Nd}$ and relatively unradiogenic $^{87}\text{Sr}/^{86}\text{Sr}$ might be expected to account for the main trend. Furthermore, the main body of data are roughly described by a straight line which from Eqn. 9.4 would suggest that the Sr/Nd ratio in the primitive magma and in the contaminant were roughly equal. Alternatively, the problem can be approached iteratively by using analyses of crustal samples collected from the basement, as in this study, or from crustal xenoliths (e.g. Hawkesworth et al., 1982; McCulloch et al., 1980). In Table 8.1 the isotopic and elemental compositions of Jebel Marra basement samples are given. The primitive basalt end-member characteristics for each Series are deduced using several primitive basalts. It should be noted that the end-member characteristics of the Old Series are slightly different to the New Series primitive basalts in that they appear to have slightly lower $^{87}\text{Sr}/^{86}\text{Sr}$ ratios.

The crustal samples may be divided into 'lower crustal' and 'upper crustal' samples on the basis of Fig. 8.7 which is explained below.

The isotopic data strongly suggests that the majority of the variations in isotopic composition are the result of varying amounts of crustal contamination. It is also appropriate to discuss the points raised in Section 6.2 concerning the effects of crustal contamination on the extent of over-saturation. Amongst the acidic rocks it is very noticeable that under-saturated rocks (e.g. phonolites) are the least contaminated. Over-saturated rocks (e.g. trachytes), as discussed, are divided into 'contaminated' and 'largely uncontaminated' groups. The existence of over-saturated rocks and under-saturated rocks indicates that the primary magmas straddled the compositions in basaltic rocks lying close to the thermal divide (see Section 6.2) which subsequent differentiation has emphasised. However, the bias towards the contaminated rocks being over-saturated suggests that in all probability some of these evolved from under-saturated parents and were able to transgress the thermal divide by addition of SiO₂ rich crust. The 'largely uncontaminated' trachytes probably evolved from over-saturated parents as they contain little crustal input. A similar conclusion was reached for the oceanic/continental acidic rocks from the Cameroon Line (Norry and Fitton, 1983).

Before interpreting the data further, it is necessary to be aware of the different ways in which crust can be assimilated. This is important as the style of contamination may not only affect isotopic ratios, but may also affect major and trace elements. The mechanisms of crustal contamination can be divided into four categories:-

Fig. 8.7 Basement samples from around Jebel Marra plotted on a ϵ_{Nd} vs ϵ_{Sr} (measured today) diagram after the chemically stratified crustal model of DePaolo and Wasserburg (1979). The displacement with age assuming a constant Sm/Nd is indicated by dashed lines. An estimate of the age of the basement samples can be obtained by reference to these lines. The actual 'model age' depends on the Sm/Nd and $^{143}Nd/^{144}Nd$ ratio of the sample (See DePaolo and Wasserburg 1979). Upper crustal rocks with high Rb/Sr lie to the right of the queried line. The line separating 'lower crust' from 'upper crust' compositions is schematically drawn. Samples 24036 and 24138 lie well to the right of the diagram - their co-ordinates are given in brackets. For reference the Nd-Sr isotopic data for the volcanics are also given.



- a) simple mixing
- b) combined assimilation and fractional crystallisation (AFC)
- c) selective contamination, and
- d) mixing with partial melts from the crust.

8.4.2 Simple Mixing (Bulk Assimilation)

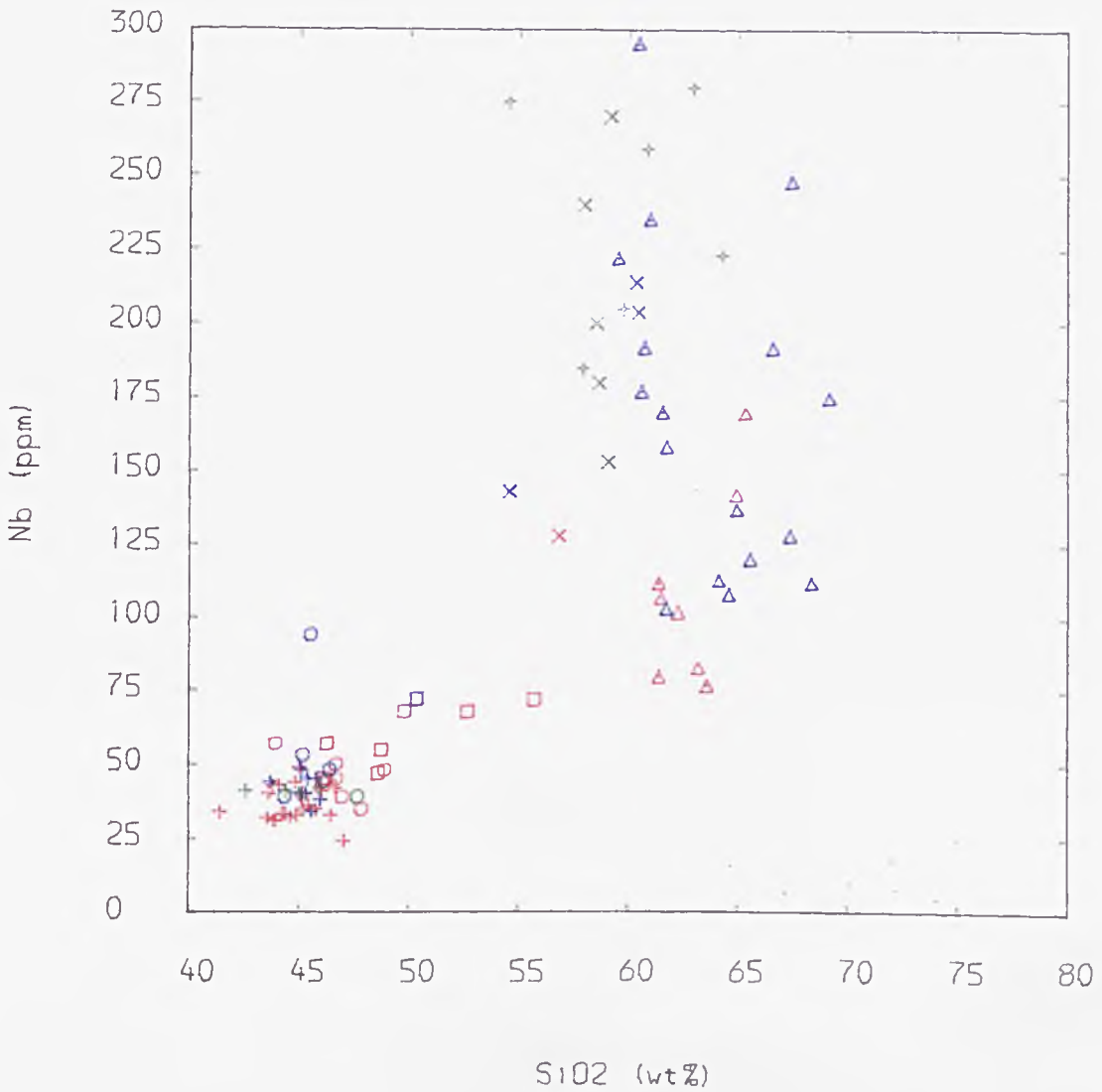
Isotopic variations in $^{87}\text{Sr}/^{86}\text{Sr}$ and $^{143}\text{Nd}/^{144}\text{Nd}$ caused by simple mixing of crust depend on the isotopic composition and the elemental concentration of Sr and Nd in the end-members and the weight proportion of crust assimilated. The equation for simple mixing curves is given in Chapter 9. A feature of the curves is that they all trend towards, and eventually connect with, the end-member contaminant. The isotopic data are presented in Fig. 8.7 on a $\epsilon\text{Nd}-\epsilon\text{Sr}$ diagram after DePaolo and Wasserburg (1979) (explanation of the ϵ notation is given in Chapter 9). In the crustal evolution model of DePaolo and Wasserburg (1979), illustrated in Fig. 8.7, $^{143}\text{Nd}/^{144}\text{Nd}$ is dependent largely on age such that the older the crustal rock is, the lower the $^{143}\text{Nd}/^{144}\text{Nd}$ is. $^{87}\text{Sr}/^{86}\text{Sr}$, however, is dependent on the Rb/Sr which, unlike Sm/Nd, tends to vary significantly between 'lower crustal' rocks, where it is typically lower, and 'upper crustal' rocks where it is typically higher. Low Rb/Sr ratios, with time, will generate relatively low $^{87}\text{Sr}/^{86}\text{Sr}$ ratios. This permits an arbitrary diagonal line to be drawn, dividing the diagram into 'upper' and 'lower crustal' rocks. Granulite facies rocks are often regarded as being a major component of the lower crust and are characterised as having relatively low concentrations of incompatible elements, particularly Th, K and Rb. It is seen that samples 24037, —

24137 and 24135 plot in the area of the diagram where lower crustal rocks would be expected to plot. 24135 is considered to show 'lower crustal' features despite its position on Fig. 8.7. Crustal samples 24036, 24134, 24138 and 24139 have Nd-Sr isotopic characteristics of the upper crust. Furthermore, the diagram can be used to generalise about the age of the 'lower crustal' rocks which, from its $^{143}\text{Nd}/^{144}\text{Nd}$ must be relatively old. Model ages taken from the diagram are of the order of 2.5-3.5 G.yrs.

8.4.3 Qualitative Assessment of Simple Mixing

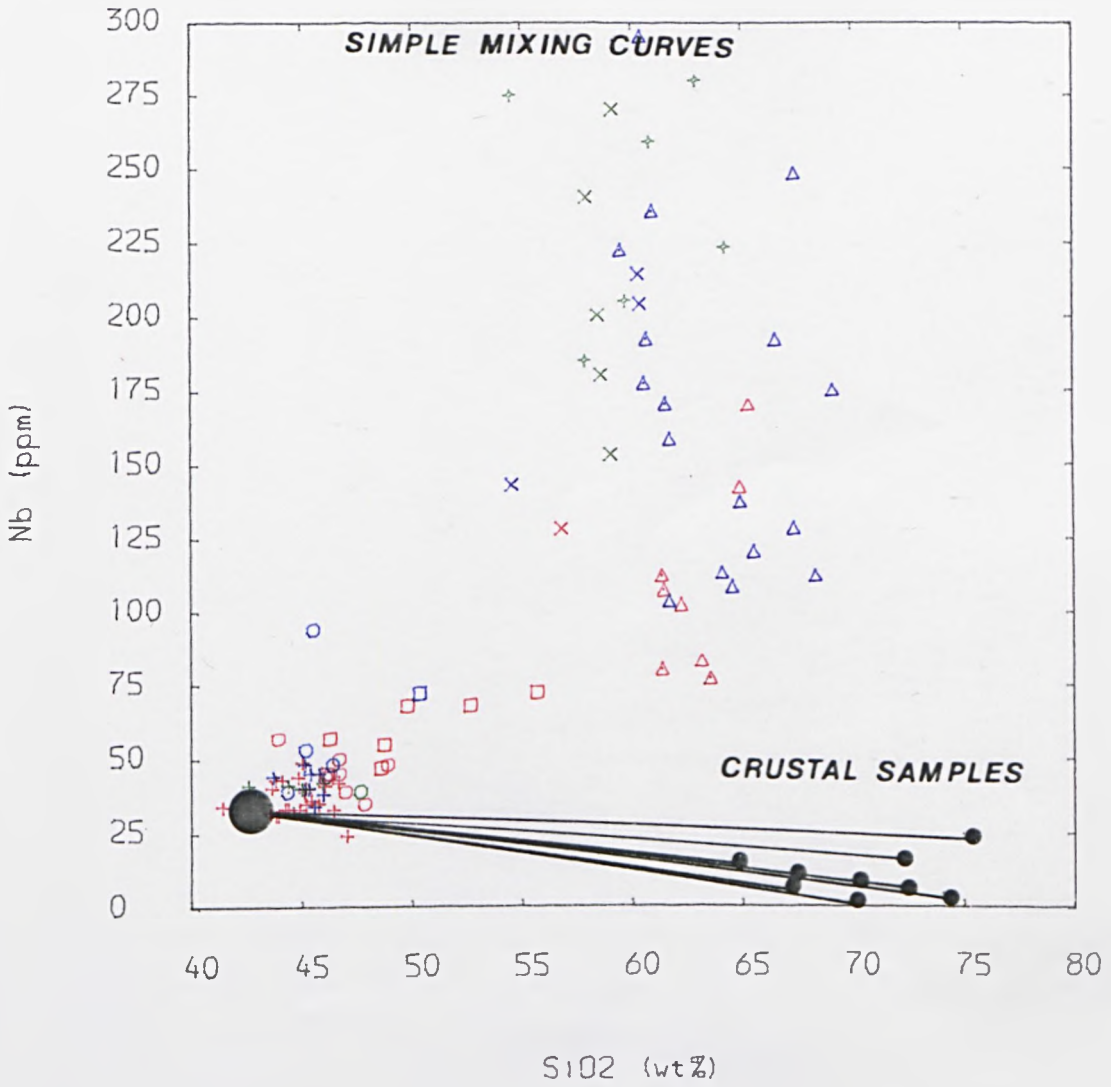
The main body of data in Fig. 8.7 is consistent with simple mixing, in varying proportions, with typical 'lower crustal' rocks. This is indicated by the strong trend towards a contaminant of low $^{87}\text{Sr}/^{86}\text{Sr}$ and low $^{143}\text{Nd}/^{144}\text{Nd}$ which is characterised by lower crustal granulite facies rocks. Similarly, some of the data, which trends to the right of the main data array, is consistent with contamination by typical 'upper crustal' rocks. The simple mixing model can be evaluated further by considering major and trace element data as well. Simple mixing on elemental plots produces straight lines joining the two end-members. To illustrate this, elemental concentrations of 'upper' and 'lower crustal' rocks are used as end-members in Figs. 8.8a-b. Therefore while simple mixing by 'lower crustal' rocks could conceivably account for trends of elements whose concentration in the crust is similar to the concentrations in acidic rocks, such as SiO_2 , Na_2O , Ba, Th, Pb, MgO, Fe_2O_3 etc., it could not account for elements which are markedly different in the crust and the acidic rocks, such as Nb, Y, CaO etc. This is illustrated in Figs. 8.8a-b which shows diagrams of Nb and Y vs SiO_2 in which crustal samples are plotted along with the mixing lines to the primitive magma. The large difference between the mixing lines and the data array is

SIMPLE MIXING CURVES**CRUSTAL SAMPLES**



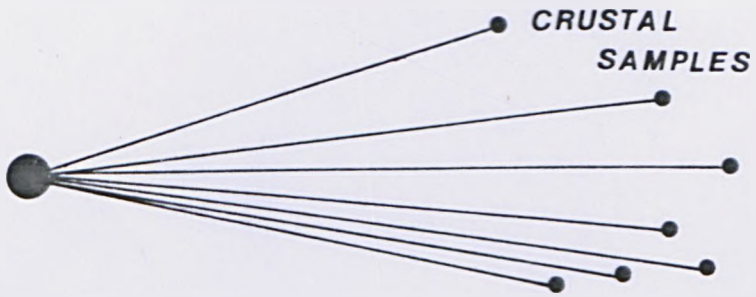
TITLE : Fig : 8.8a Nb vs SiO₂ (Mixing)
(see text for explanation)

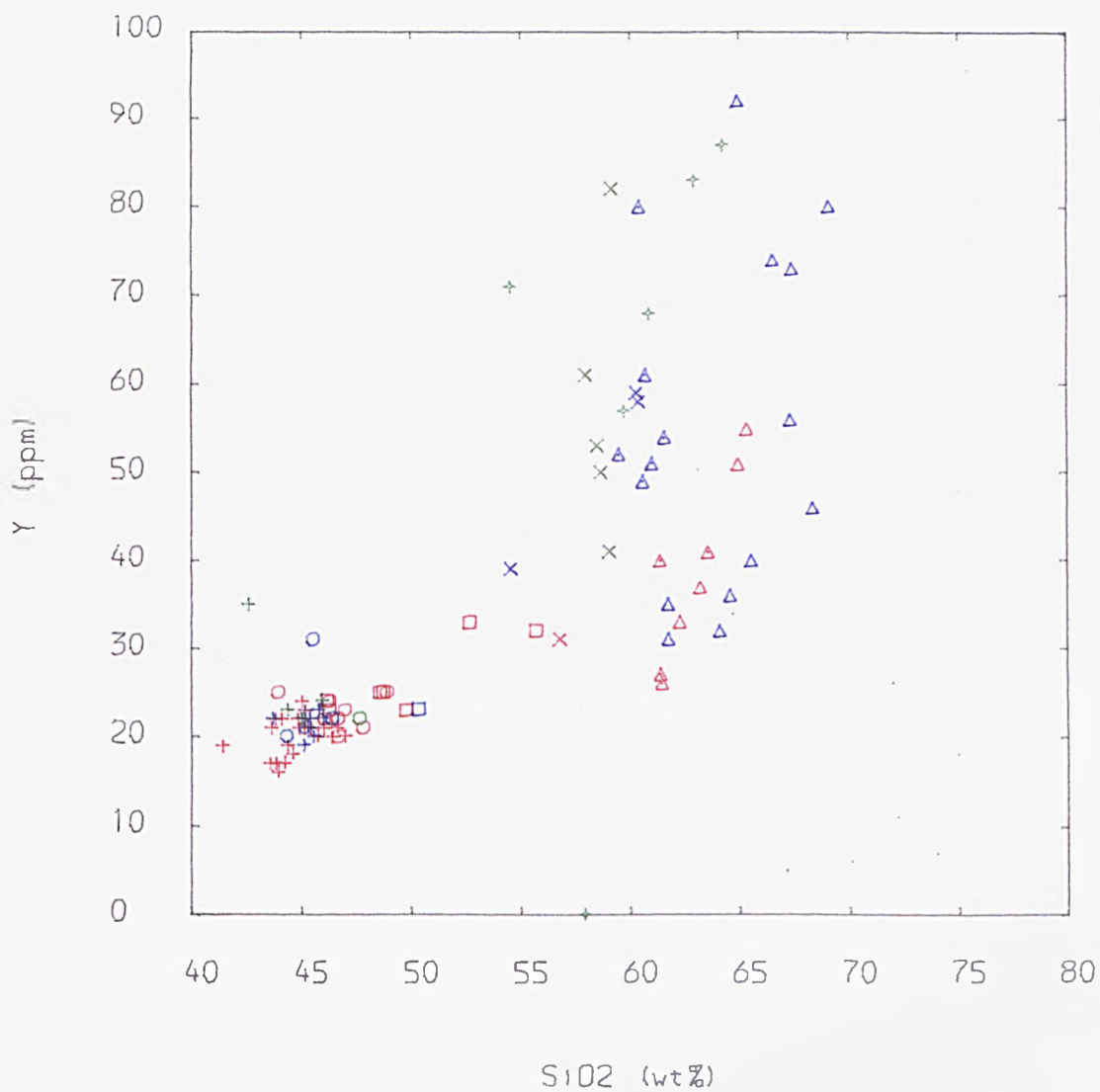
BASEMENT ROCKS	= black
NEW SERIES ROCKS	= red
PYROCLASTIC SEQUENCE ROCKS	= green
OLD SERIES ROCKS	= blue



TITLE : Fig : 8.8a Nb vs SiO₂ (Mixing)
(see text for explanation)

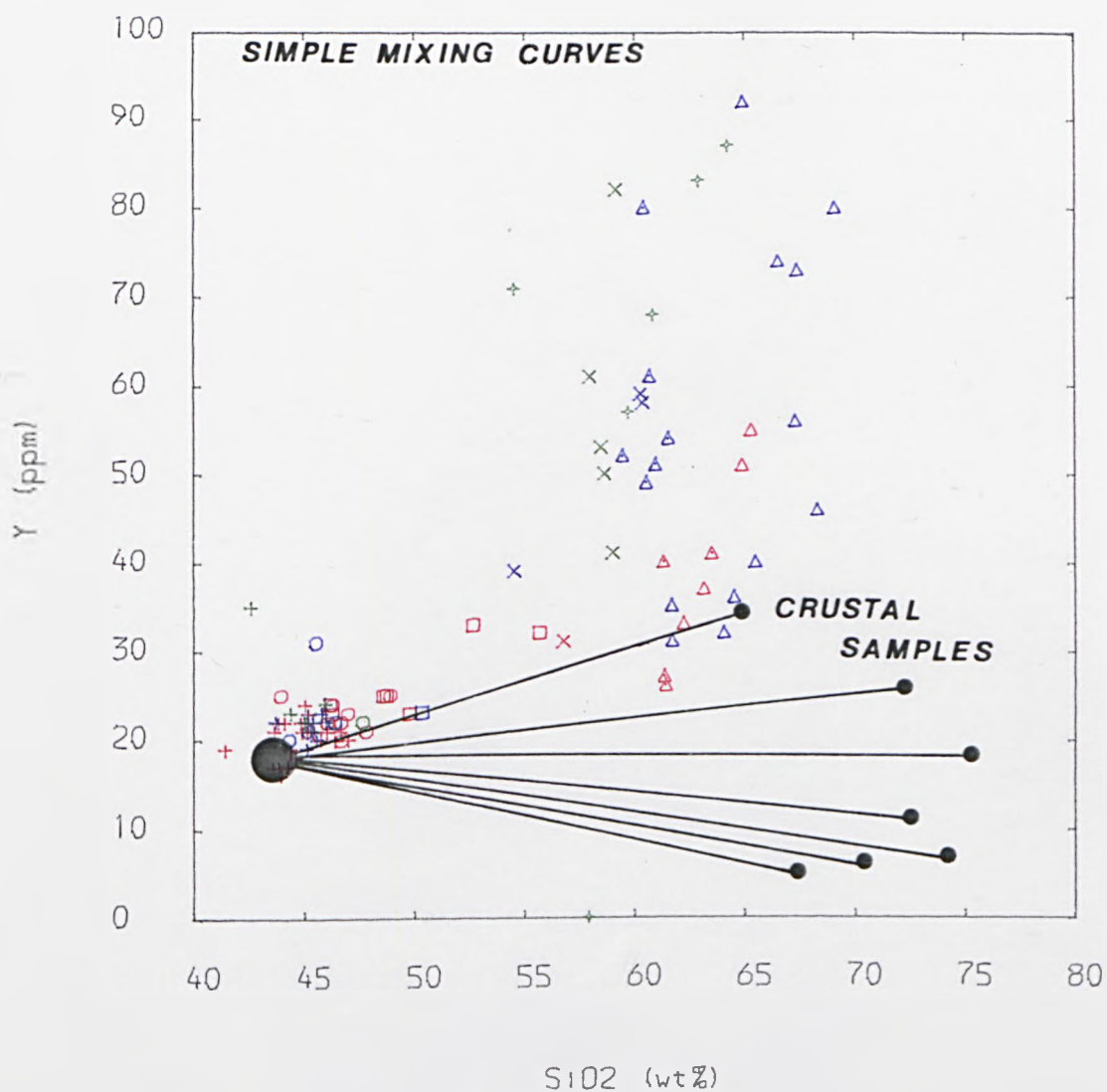
BASEMENT ROCKS	= black
NEW SERIES ROCKS	= red
PYROCLASTIC SEQUENCE ROCKS	= green
OLD SERIES ROCKS	= blue

SIMPLE MIXING CURVES



TITLE : Fig : 8.8b Y vs SiO₂ (Mixing)

BASEMENT ROCKS	= black
NEW SERIES ROCKS	= red
PYROCLASTIC SEQUENCE ROCKS	= green
OLD SERIES ROCKS	= blue



TITLE : Fig : 8.8b Y vs SiO₂ (Mixing)

BASEMENT ROCKS	= black
NEW SERIES ROCKS	= red
PYROCLASTIC SEQUENCE ROCKS	= green
OLD SERIES ROCKS	= blue

evident. The group of rocks previously described as 'largely uncontaminated' in Fig. 8.2, which deviate from the main trend, are consistent with contamination by 'upper crustal' rocks by simple mixing. However, here again, although the isotopic data can be satisfied by simple mixing it is unlikely that the major and trace element data can be. This reasoning is based on the actual contaminant having a similar elemental character to available crustal samples used here. Despite this uncertainty, because much of the elemental variation is explicable by fractional crystallisation and because simple mixing could not explain trends which are substantially curved, for example plots involving Sr, Al_2O_3 , P_2O_5 etc., simple mixing in isolation seems largely untenable. However, its use is still pertinent for modelling of Nd-Sr isotope relationships particularly among the basic rocks (see Chapter 9).

8.4.4 Combined Assimilation and Fractionation (AFC)

Bowen (1928) and more recently Taylor (1980), James (1981) and DePaolo (1981) have pointed out that, in many instances, the processes of assimilation and fractional crystallisation are coupled. This is because the latent heat of assimilation is provided by the heat of crystallisation and therefore the one is a consequence of the other.

The effect of fractionation enriching Sr and Nd in more evolved liquids and therefore making $^{87}Sr/^{86}Sr$ and $^{143}Nd/^{144}Nd$ isotope ratios more resistant to subsequent contamination is well known (e.g. Norry et al., 1980). A quantitative approach to AFC has been addressed by DePaolo (1981) and has highlighted its importance, primarily because departures from simple mixing trends often result. In some

cases, this is mainly reflected in the proportion of crust added, and in other situations radical departures from simple mixing trends occur. In addition, it is important to realise that, in many cases, AFC curves do not necessarily trend towards the composition of the contaminant. If AFC trends, such as these, were interpreted by simple mixing models alone, then erroneous conclusions about the character of the contaminant could be made.

8.4.5 AFC Parameters

The equations for AFC are presented in Chapter 9. The curves produced by AFC (DePaolo, 1981) are dependent on the isotopic and elemental concentrations of the end-members, as well as two additional parameters D and r . D is the bulk distribution coefficient defined in Eqn. 7.2, and r equals the ratio of the rate of assimilation to the rate of fractional crystallisation. In practice, the isotopic and elemental composition of the magmatic end-member (A) is relatively well constrained (Table 8.1). From fractional crystallisation models, it is possible to estimate D reasonably well for a given element, for most stages of fractionation (Chapter 9). Application of the AFC equations are tractable for constant r and D . However, in an evolving system, r is likely to vary, and not necessarily systematically. For example, DePaolo (1981), in discussing his own model, cites a plausible history of an evolving magma body rising through the crust. At deeper levels in the crust, ambient temperatures are higher, such that assimilation of hot crust is likely to promote less crystallisation than would assimilation of cold crust in upper crustal magma chambers. In this situation, all other things being equal, r would be expected to decrease as the magma body approaches the surface. There could also be an increase in r as the magma becomes more viscous as it evolves, because crystals may separate less efficiently from

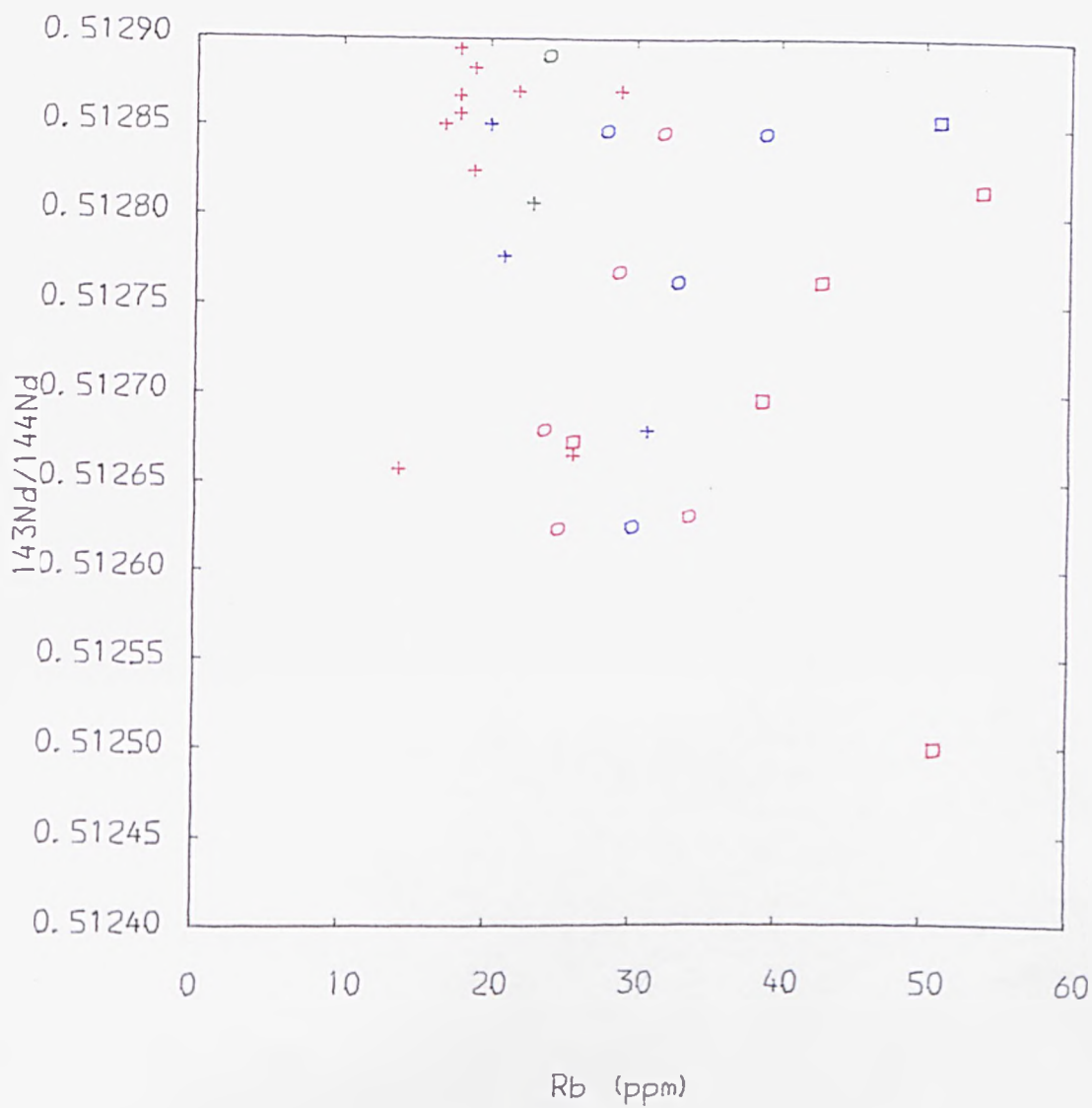
the host liquid. It is demonstrated in Chapter 9, that, for the suite as a whole for most elements, D is not constant with fractionation and for some elements it varies markedly. DSr , in the above situation of an evolving magma body, could easily increase from <1 to >1 , because, as a magma body evolves, significant fractionation of plagioclase at a later stage is usually inevitable. Therefore, a certain amount of care is required when considering AFC, because, in a number of situations, the parameters can vary. This complication is in addition to the uncertainty associated with the composition of the contaminant(s).

8.4.6 Qualitative Assessment of AFC

By looking at selected variation diagrams, the effects of AFC can be assessed. Figs. 8.3 and 8.4 show $^{87}Sr/^{86}Sr$ vs MgO and $^{87}Sr/^{86}Sr$ vs Zr. A vector corresponding to fractionation can be assumed to be parallel to the elemental axis. A contamination vector will tend to be sub-parallel to the isotopic ratio axis, although its actual orientation will depend on the isotopic and elemental composition of the contaminant and will change as fractionation proceeds. The increase in Zr and the decrease in MgO with increasing $^{87}Sr/^{86}Sr$ is consistent with AFC. The other diagrams in Figs. 8.3 and 8.4 can also be explained in this way.

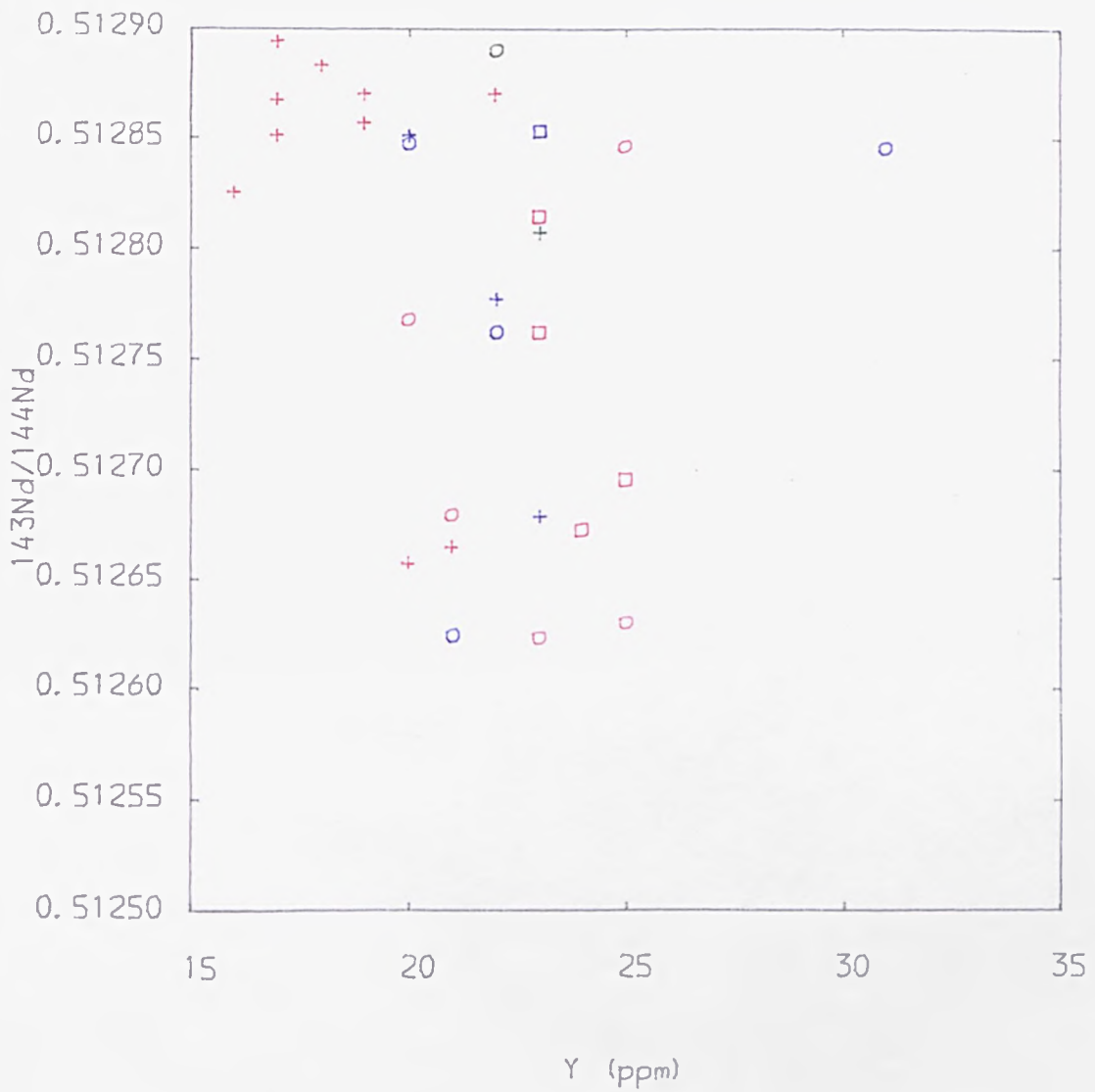
The diagrams involving $^{143}Nd/^{144}Nd$ are even more convincing and also show other features. In Fig. 8.6 for example, the division of data into groups is apparent again. In the New Series basic rocks, there are relatively small increases to incompatible element concentrations with large decreases in $^{143}Nd/^{144}Nd$, compared with evolved mugearites and acidic rocks, where there are small decreases in

$^{143}\text{Nd}/^{144}\text{Nd}$ and large increases in incompatible element concentrations. Because of scale problems the increase in incompatible elements is not altogether clear and so Figs. 8.9a-b illustrates $^{143}\text{Nd}/^{144}\text{Nd}$ vs Rb and Y for example, for basic rocks only. The decrease in $^{143}\text{Nd}/^{144}\text{Nd}$, with increasing incompatible element concentration is consistent with AFC. The differences between the basic and acidic limbs may reflect a decrease in r , a change in contaminant or both. An appealing interpretation of the $^{143}\text{Nd}/^{144}\text{Nd}$ vs incompatible element plots, on the lines of the DePaolo model (1981) (see section 8.4.5), is that the basic limbs represent contamination in a lower crustal environment with a higher r , whereas the acid limbs characterise contamination in an upper crustal environment with a lower r ; whether this is matched by a change in the crustal contaminant is difficult to say. Certainly, granulitic facies type material would account for the Nd and Sr isotopic variations in basic rocks whereas typical upper crustal material probably could not. However, the variations observed in acidic rocks, for the most part, could be brought about by contamination by either typical lower or upper crustal rocks. It is only the samples with very high $^{87}\text{Sr}/^{86}\text{Sr}$ values which require a more radiogenic contaminant than 'normal' lower crustal rocks. It is largely to account for these high $^{87}\text{Sr}/^{86}\text{Sr}$ rocks, that a typical upper crustal contaminant needs to be invoked at all. A further consideration is that with fractionation Nd generally increases and therefore $^{143}\text{Nd}/^{144}\text{Nd}$ becomes progressively more resistant to contamination. Whether this would account for the dog-legs seen in the main data trend is doubtful, although this possibility will be examined more closely in the next Chapter.



TITLE : Fig : 8.9a $^{143}\text{Nd}/^{144}\text{Nd}$ vs Rb

NEW SERIES ROCKS = red
 PYROCLASTIC SEQUENCE ROCKS = green
 OLD SERIES ROCKS = blue



TITLE : Fig . 8.9b $^{143}\text{Nd}/^{144}\text{Nd}$ vs Y

NEW SERIES ROCKS = red
 PYROCLASTIC SEQUENCE ROCKS = green
 OLD SERIES ROCKS = blue

Much of the Old Series data are also characterised by large increases in incompatible element concentrations with small decreases in $^{143}\text{Nd}/^{144}\text{Nd}$ and therefore may share a common history with evolved mugearites and trachytes of the New Series.

In order to illustrate the effects of changing D in the Jebel Marra suite, Fig. 8.5 shows a diagram of $^{87}\text{Sr}/^{86}\text{Sr}$ vs Sr. It can be seen that following progressive enrichment, at the onset of significant plagioclase fractionation at evolved mugearitic compositions, Sr concentration begins to decrease but because of combined assimilation $^{87}\text{Sr}/^{86}\text{Sr}$ continues to increase. This is precisely the result predicted by DePaolo (cf. Figure 3, 1981), for an evolving magma. A similar result is observed for Nd which is temporarily depleted while apatite fractionates from evolved mugearites to primitive trachytes.

One of the features of AFC on a Nd-Sr isotope ratio diagram is that if D_{Nd} and D_{Sr} are of the same magnitude then the AFC trajectories will largely mimic simple mixing curves. This situation can be assumed to apply amongst basic rocks when the D's for Sr and Nd are of similar magnitude. They have been estimated, in Chapter 9, to be 0.15 and 0.13 respectively. This is a useful result because many of the conclusions based on simple mixing curves for $^{143}\text{Nd}/^{144}\text{Nd}$ vs $^{87}\text{Sr}/^{86}\text{Sr}$ are therefore still valid for much of the data while D_{Sr} is approximately equal to D_{Nd} . The onset of significant plagioclase fractionation, as mugearites evolve to primitive trachytes, pushes D_{Sr} to a calculated value of 2.5 but this is matched, to some extent, by D_{Nd} which, because of apatite fractionation, has a calculated D of 1.7 at the same stage (Chapter 9). This explains why there is only a very small shift in $^{87}\text{Sr}/^{86}\text{Sr}$ towards more radiogenic compositions instead of a much larger shift in isotopic compositions, as plagioclase

class becomes a major fractionating phase from evolved mugearites to primitive trachytes, as predicted by DePaolo (1981) on the $^{143}\text{Nd}/^{144}\text{Nd}$ vs $^{87}\text{Sr}/^{86}\text{Sr}$ plot (Fig. 8.2). While the D's are similar, the adherence to the simple mixing curve is maintained. Among the acidic rocks, apatite is no longer significantly involved in fractionation, as only small concentrations of P_2O_5 remain, so that D_{Nd} again becomes <1 whereas the fractionation of anorthoclase ensures that $D_{\text{Sr}} > 1$. It is only now, when $D_{\text{Sr}} \gg D_{\text{Nd}}$, that large displacements sub-parallel to the $^{87}\text{Sr}/^{86}\text{Sr}$ axis in Fig. 8.2 predicted by AFC, can result. Despite a shortage of data for the New Series, this effect appears to occur for the evolved trachytes. In addition, some of the 'contaminated' Old Series trachytes are displaced in this direction and may have also been affected in such a way.

While discussing AFC it is appropriate to make some mention of the features observed in incompatible element trends. Recapitulating, the observation was made that, in incompatible element - incompatible element diagrams, the extrapolation of the trend, most often, did not pass through the origin. Using the model of Powell (in press), this can be interpreted in terms of a second order process, such as AFC. The details of the model are discussed in Chapter 9, where an attempt to quantify r in basic rocks and to establish the composition of the contaminant is made. However, it is possible to use the concept to interpret the two trends observed on the plot for Zr vs Nb (Fig. 7.8). Considering the acidic rocks only, it can be seen that extrapolation of the 'contaminated' group trend would probably intersect the Nb axis close to 50. This effect would be consistent with the effect of AFC on trace elements outlined by Powell (in press). In contrast, the extrapolation of the 'uncontaminated' group trend would

probably pass very close to the origin. This effect requires no second order process and is consistent with fractional crystallisation occurring largely in isolation. This contention is neatly supported by the $^{143}\text{Nd}/^{144}\text{Nd}$ isotopic evidence in which the latter requires only a small crustal input.

From a qualitative standpoint, AFC appears to be an entirely reasonable process to account for much of the observed isotopic and trace element variations. Although it is recognised that there are deviations from the AFC model, it does appear to be consistent with bulk of the elemental and isotopic variations. The AFC features observed at Jebel Marra compare very favourably with other areas where AFC has been invoked and perhaps on less persuasive data e.g. Columbia River (Carlson et al., 1981), Rhum (Palacz, 1983), Cantal (Downes, 1983) and Santorini (Barton et al., 1983).

8.4.7 Selective Contamination

Selective contamination is a process in which certain elements are believed to be selectively enriched into a magma. This may involve equilibration of the magma with a fluid phase or actual contamination by a fluid phase produced by the breakdown of minor phases in the crust. It seems to be most usually invoked in circumstances where a group of elements appear to be anomalously enriched in a magma (Moorbath and Thompson, 1980; Dickin, 1981). In the Jebel Marra suite of volcanics the bulk of the data can be explained by other contamination processes and there is no need to appeal to such a selective process.

8.4.3 Assimilation of Crustal Partial Melts

The first two models are based on the complete assimilation of crust. An hypothesis outlined by Patchett (1980) discusses the circumstances in which a partial melt from the crust could be generated and possibly assimilated by a mafic magma. The model considers the intrusion of a basic magma into the crust in the form of sheets. The model predicts that, in the presence of a fluid phase or hydrous minerals, total melting will only occur close to the conduit, whereas partial melting of the surrounding crust will occur to a much greater extent. Such a partial melt from the crust could then be available for contamination. Consideration of this process is important because the elemental composition of a crustal melt will inevitably differ from the composition of the source and it may even differ in its isotopic composition. Isotopic disequilibrium could occur for $^{87}\text{Sr}/^{86}\text{Sr}$, for example, if Rb rich phases, such as biotite, are preferentially melted in the crust. The model is proposed for an intrusion of mafic magmas into the crust and therefore could apply to the basic rocks in the 'contaminated' group which have been interpreted to have undergone contamination in the lower crust. However, the hypothesis is modelled for basaltic sheets, which will have a high surface to volume ratio. If, rather than sheets, the magma, giving rise to the basic rocks, resides in a 'conventional' magma chamber, then the surface to volume ratio would be much lower. In such a situation the transfer of heat would be less effective and contamination by bulk assimilation, perhaps in the form of stoping, would not be unreasonable. In this way AFC, as outlined by DePaolo (1981), would still be applicable. Secondly, partial melting is facilitated if a free fluid phase, or significant hydrous phases

occur. Such an occurrence would be typical for upper crustal rocks. But if contamination of the basic rocks, as suggested, occurred in a lower crustal environment by typical 'anhydrous' granulite facies rocks then this requirement may not be satisfied. In this event bulk assimilation of the contaminant may again be a more likely mechanism.

From section 8.4.6 there is compelling evidence to suggest that AFC has operated. If contamination by partial melts has occurred to a great extent, then its incorporation has promoted fractional crystallisation in an analogous way to that expected by bulk assimilation. Intuitively however, it would be expected that the incorporation of a partial melt would not be associated with the thermal shock of assimilating material in the way that bulk assimilation, for conventional AFC, does. In turn, crystallisation of phases would be less readily achieved and the effects of AFC would be less noticeable. In which case a circular argument could be used to say that because AFC has been demonstrated to have operated, then the contamination in the form of partial melts is likely to be minimal, especially if the magma resides in magma chambers and assimilates 'anhydrous' granulite.

However, as discussed in Chapter 7, a crustal melt mixing with a basic magma may be required to explain the characteristics of the mafic bearing trachytes. From Figs. 8.6a-g it is evident that the data for the New Series 'contaminated' rocks are divided into two. This division occurs between primitive mugearites and evolved mugearites. While the compositional difference between the mugearites is small, the difference in $^{143}\text{Nd}/^{144}\text{Nd}$ is large from 0.5126-0.5125. A large shift in isotopic composition over a narrow compositional

interval implies, from AFC logic, a significant increase in r . This increase in r may coincide with the change from contamination of basic rocks, interpreted to occur in the lower crust, to the contamination of the evolved mugearites and acidic rocks, interpreted to occur in the upper crust. If this analysis is correct and the basic rocks were contaminated in lower crustal chamber and the acidic rocks were contaminated in upper crustal chambers, then the two environments could be connected by conduits in which contamination by crustal partial melts, with its associated high r , could result. Basic lavas tapped from a possible lower crustal magma chamber may also be affected in this way and may help explain why $^{143}\text{Nd}/^{144}\text{Nd}$ and $^{87}\text{Sr}/^{86}\text{Sr}$ does not correlate perfectly with indices of fractionation. Although speculative, this interpretation does attempt to seek an explanation within the bounds of current contamination models.

8.5 Sources for Alkali Basalts.

The similarity in isotopic and elemental compositions between primitive continental alkali basalts and primitive ocean island alkali basalts (OIB) has been recognised by several workers (Norry and Fitton, 1983; Menzies et al., 1983; Thompson et al., 1983; Hawkesworth, 1981; Allegre, 1981). The elemental similarity is illustrated in Fig. 8.10 where alkali basalts from several continental and oceanic provinces are represented. The similarity is further illustrated in Fig. 8.1a where the Nd-Sr isotopic compositions of various continental basalts and OIB are shown and which commonly plot in the depleted portion of the diagram. The Cameroon Line of intra-plate volcanics lie above both, continental lithosphere which has been affected by the Pan-African event and is therefore at least 600 ma old, and oceanic lithosphere less than 120 ma old. In Fig. 8.10

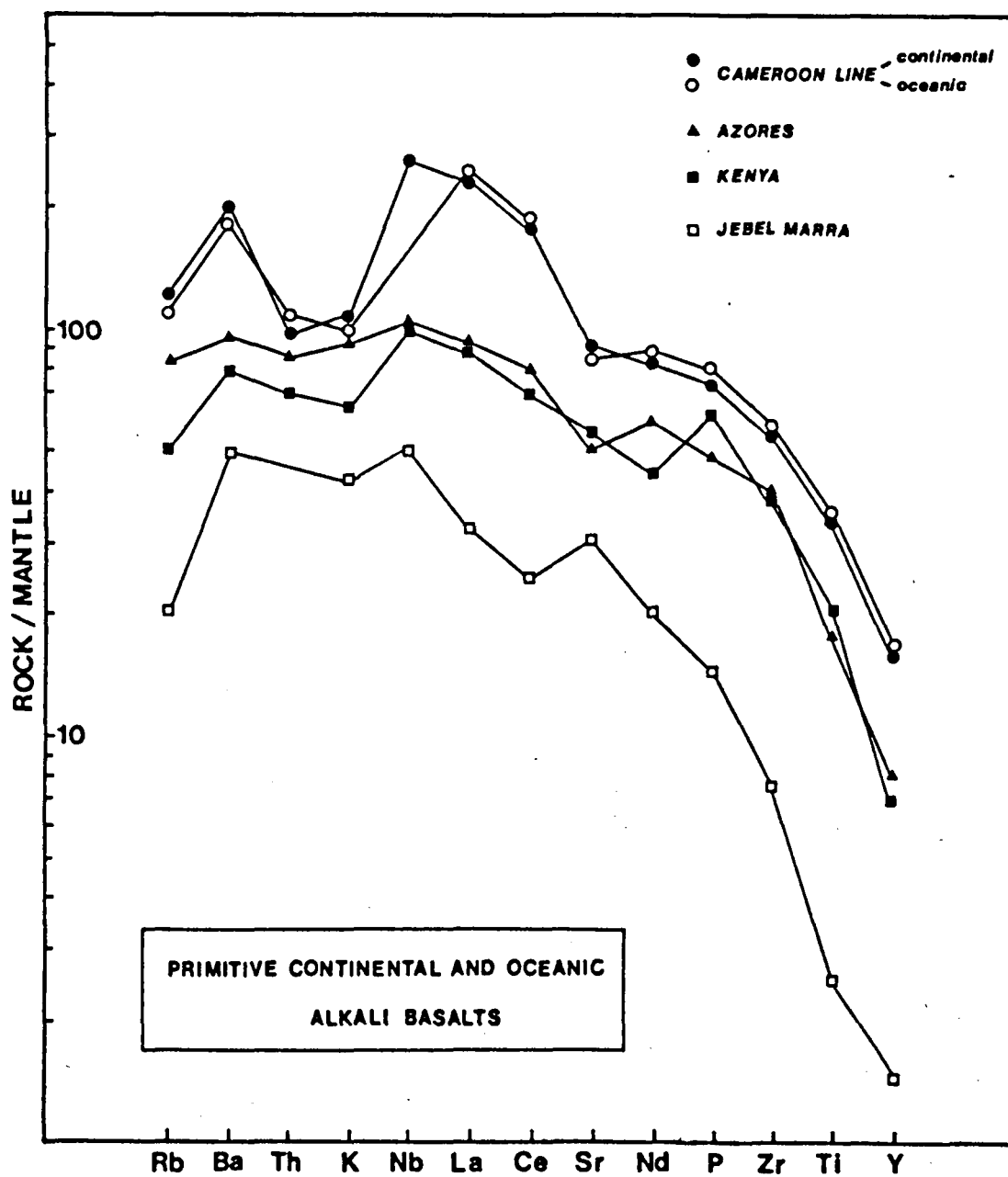


Fig. 8.10 Spidergrams for a selection of continental and oceanic alkali basalts. Note the overall similarity of these patterns which may be indicative of a common source. For compatibility, these values are normalised to Wood's (1979) mantle.

the mantle normalised patterns for basalts from both sections are virtually identical which strongly suggests that, in view of the markedly contrasting lithospheres, the source for the alkali basalts must be sub-lithospheric. The similarity between continental alkali basalts and OIB, and by implication their source is clear. A similar conclusion was reached by Allegre (1981) from comparisons of Hoggar alkali basalts with OIB. A primitive basalt from Jebel Marra is also drawn in Fig. 8.10 and the Nd-Sr compositions illustrated in Fig. 8.1a; the comparison with other continental alkali basalts and OIB are sufficiently close to suggest that the Jebel Marra volcanics also have a similar sub-lithospheric source.

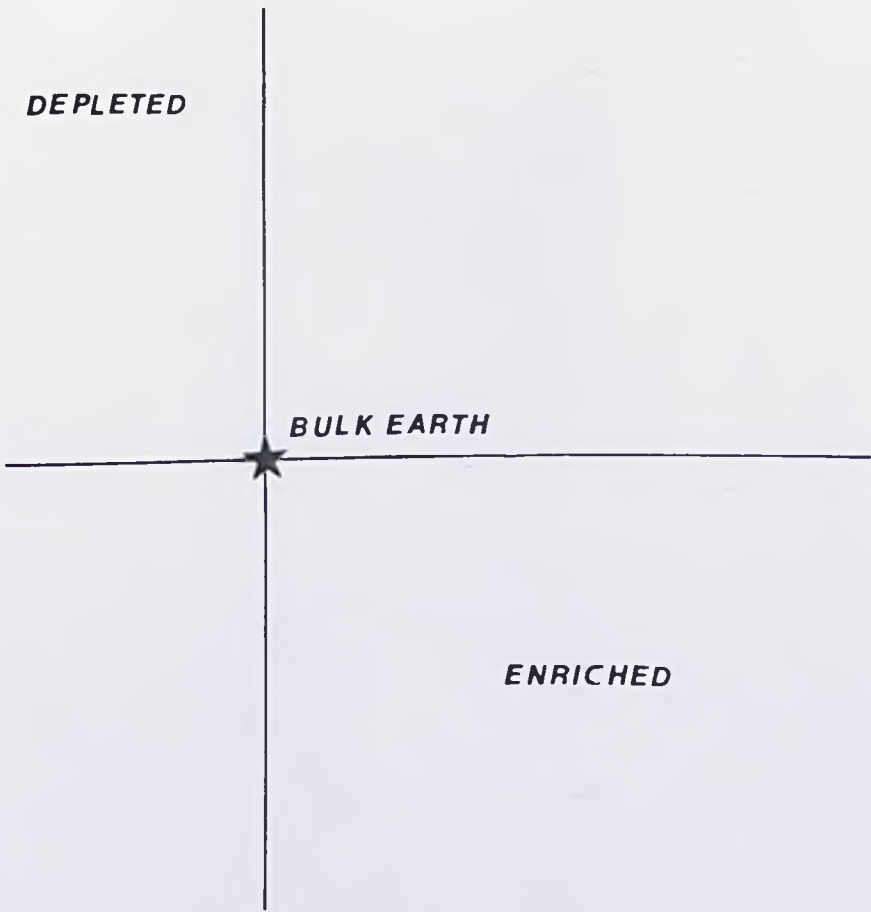
Relative to bulk Earth the Nd-Sr isotopic compositions of the most primitive lavas plot in the 'depleted' quadrant of the diagram (Fig. 8.11). Samples which plot here can be expected to have been derived from a source with time-integrated depletions in Rb and LREE. However, in the conjugate parent-daughter plot (Fig. 8.12, Sm/Nd vs Rb/Sr) the same samples plot in the 'enriched' part of the diagram. If these Sm/Nd and Rb/Sr values have been characteristic of the source for a long time, then the isotopic compositions that Rb and Sm should have generated, would also plot in the same corresponding area in Fig. 8.12. The fact that they do not can be interpreted in two main ways. Either the magmas have been strongly enriched in incompatible elements, including Rb and Nd, by melting processes, or the mantle source has been enriched (metasomatised). Partial melting can, in principle, alter parent/daughter ratios such that values in the source, which are compatible with the observed isotopic ratios, can be fractionated to those now measured in the lavas (Kay and Gast, 1973). The decoupling of Rb/Sr is more difficult but it is possible for Sm/Nd

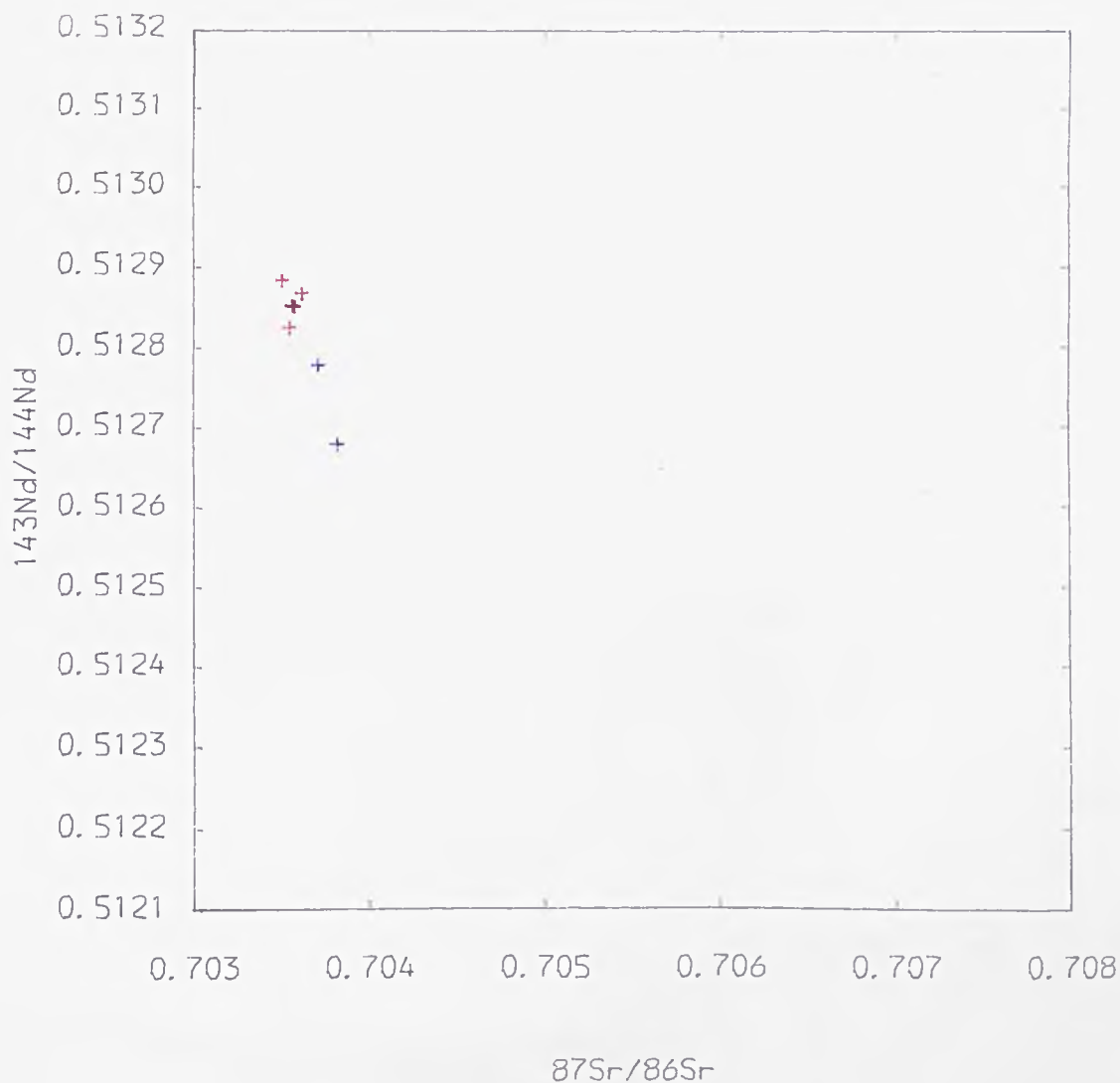
particularly if garnet is residual in the mantle. However, the degree of partial melting calculated (Hawkesworth et al., 1979; Menzies and Murthy, 1980; Norry, 1980) to achieve this is so small, in some circumstances <1%, that perhaps a different process is responsible. A popular alternative explanation is that the source mantle has been metasomatised by a LILE rich fluid prior to melting (Carter, 1978; Hawkesworth et al., 1979; Menzies and Murthy, 1980). The metasomatism must occur shortly before melting otherwise the effects of the decay of Rb and Sm would significantly register in the measured isotopic ratios, as explained above. Mantle metasomatism as a process has long been advocated by many workers to explain physical and chemical features of mantle nodules (Dawson and Smith, 1977; Lloyd and Bailey, 1975; Boettcher et al., 1979). It would also account for the LREE enriched nature of the lavas without again having to appeal to small degrees of partial melting. These apparent geochemical contradictions have been recognised in many areas and is sufficiently common to suggest that a process of mantle metasomatism and subsequent volcanism may have a cause and effect relationship (Futa and Le Masurier, 1983). However, most of the nodules which can be recognised as being metasomatised are thought to be from the lithosphere (Harte, 1983; Menzies, 1983; Hawkesworth et al., 1983). In contrast, alkali basalts are considered to originate from below the lithosphere (Norry and Fitton, 1983; Allegre, 1981; see above) and therefore the relationship between the two must remain equivocal.

A model proposed by Harris (1957) to explain high LREE enrichment in kimberlites, for example, and since used by Norry and Fitton (1983) to account for the above features, is one of zone refining. The advantage of this process is that the strong enrichment of incom-

particularly if garnet is residual in the mantle. However, the degree of partial melting calculated (Hawkesworth et al., 1979; Menzies and Murthy, 1980; Norry, 1980) to achieve this is so small, in some circumstances <1%, that perhaps a different process is responsible. A popular alternative explanation is that the source mantle has been metasomatised by a LILE rich fluid prior to melting (Carter, 1978; Hawkesworth et al., 1979; Menzies and Murthy, 1980). The metasomatism must occur shortly before melting otherwise the effects of the decay of Rb and Sm would significantly register in the measured isotopic ratios, as explained above. Mantle metasomatism as a process has long been advocated by many workers to explain physical and chemical features of mantle nodules (Dawson and Smith, 1977; Lloyd and Bailey, 1975; Boettcher et al., 1979). It would also account for the LREE enriched nature of the lavas without again having to appeal to small degrees of partial melting. These apparent geochemical contradictions have been recognised in many areas and is sufficiently common to suggest that a process of mantle metasomatism and subsequent volcanism may have a cause and effect relationship (Futa and Le Masurier, 1983). However, most of the nodules which can be recognised as being metasomatised are thought to be from the lithosphere (Harte, 1983; Menzies, 1983; Hawkesworth et al., 1983). In contrast, alkali basalts are considered to originate from below the lithosphere (Norry and Fitton, 1983; Allegre, 1981; see above) and therefore the relationship between the two must remain equivocal.

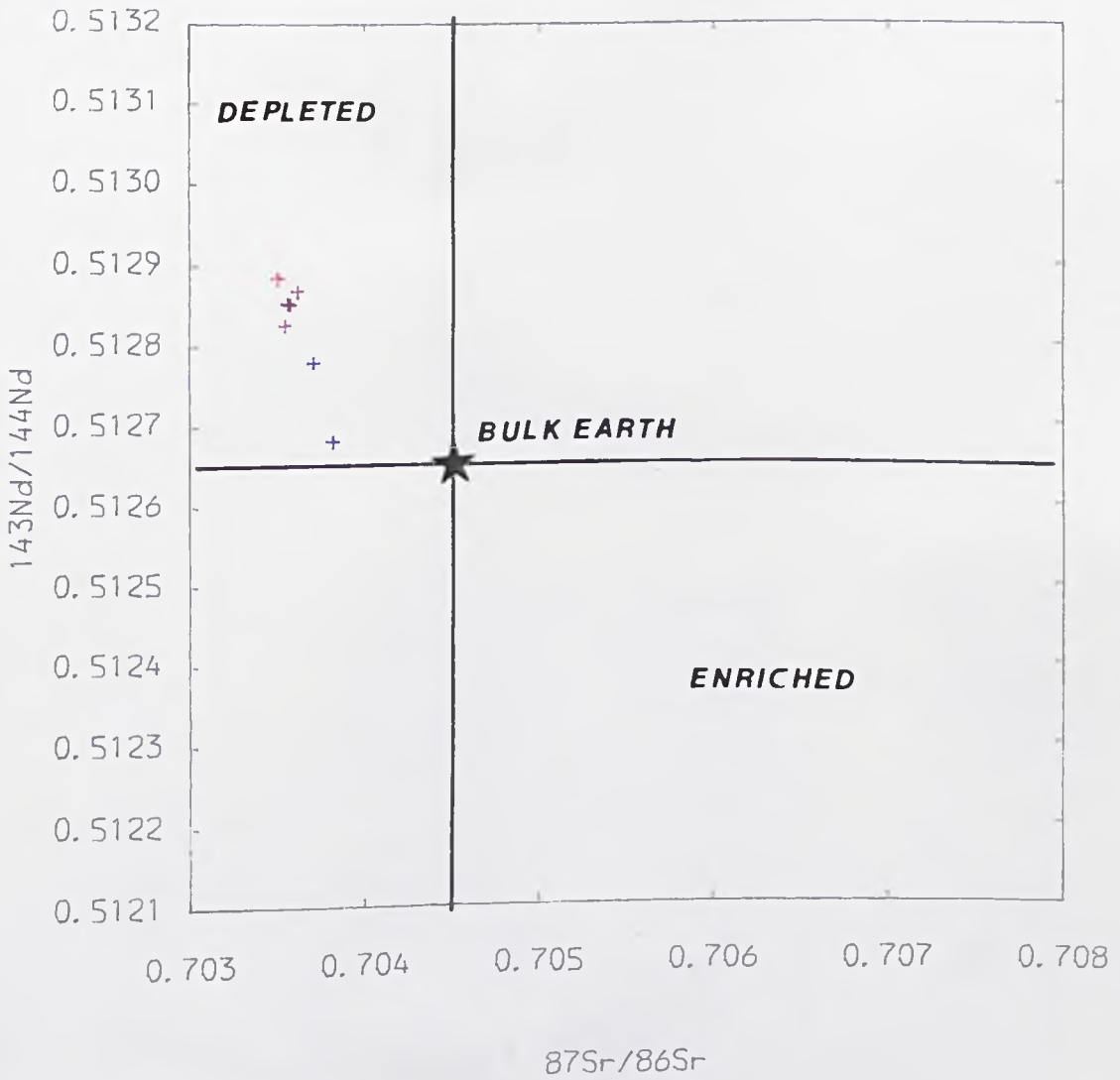
A model proposed by Harris (1957) to explain high LREE enrichment in kimberlites, for example, and since used by Norry and Fitton (1983) to account for the above features, is one of zone refining. The advantage of this process is that the strong enrichment of incom-





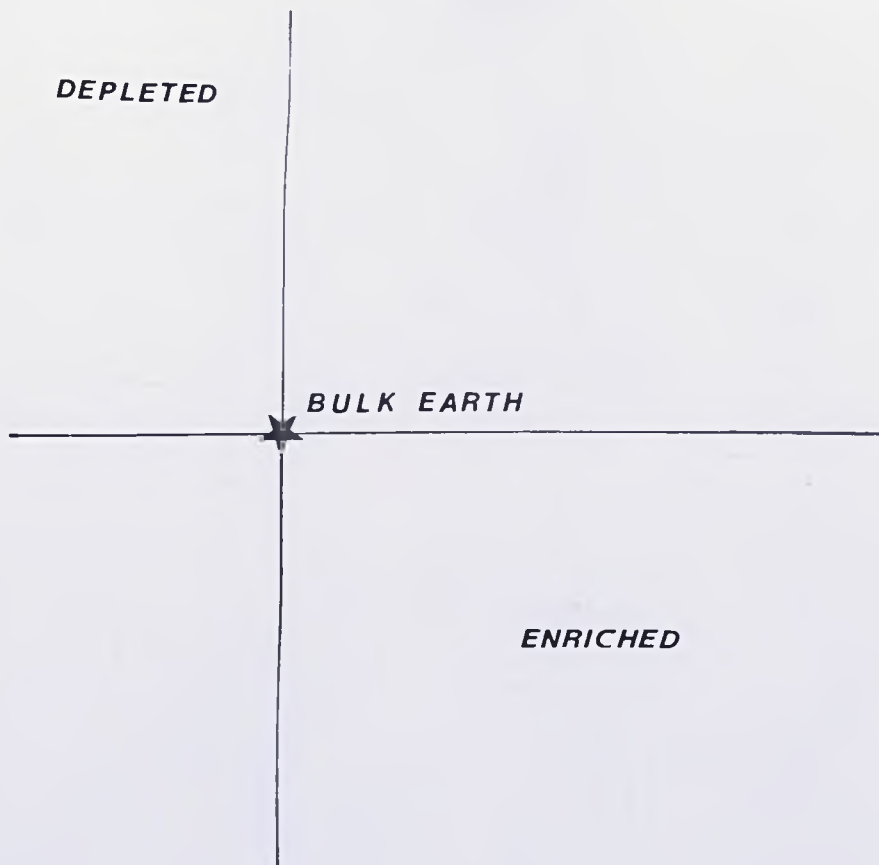
TITLE : Fig : 8.11 $^{143}\text{Nd}/^{144}\text{Nd}$ vs $^{87}\text{Sr}/^{86}\text{Sr}$
 (See text for explanation)

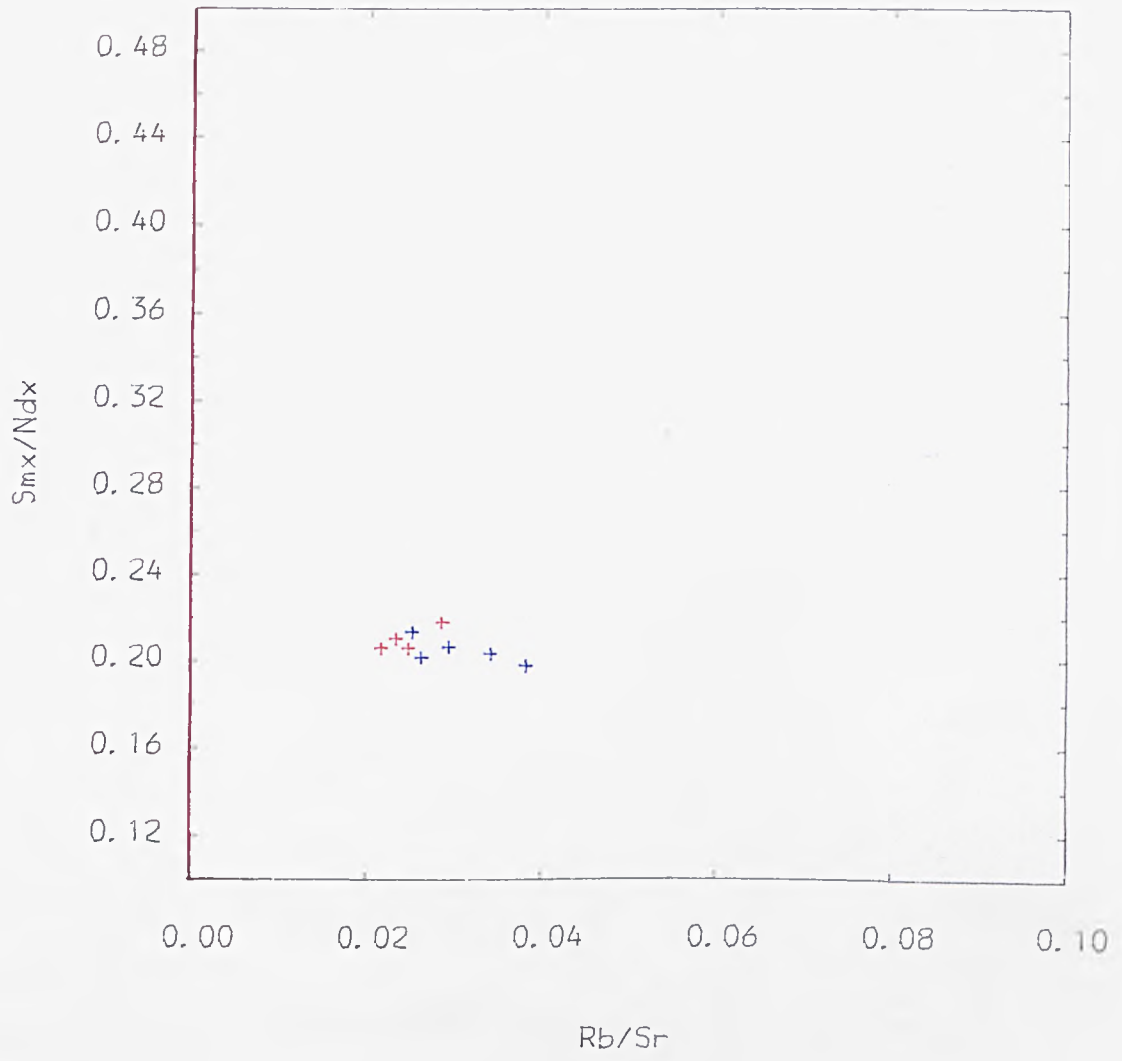
NEW SERIES ROCKS = red
 PYROCLASTIC SEQUENCE ROCKS = green
 OLD SERIES ROCKS = blue



TITLE : Fig : 8.11 $^{143}\text{Nd}/^{144}\text{Nd}$ vs $^{87}\text{Sr}/^{86}\text{Sr}$
 (see text for explanation)

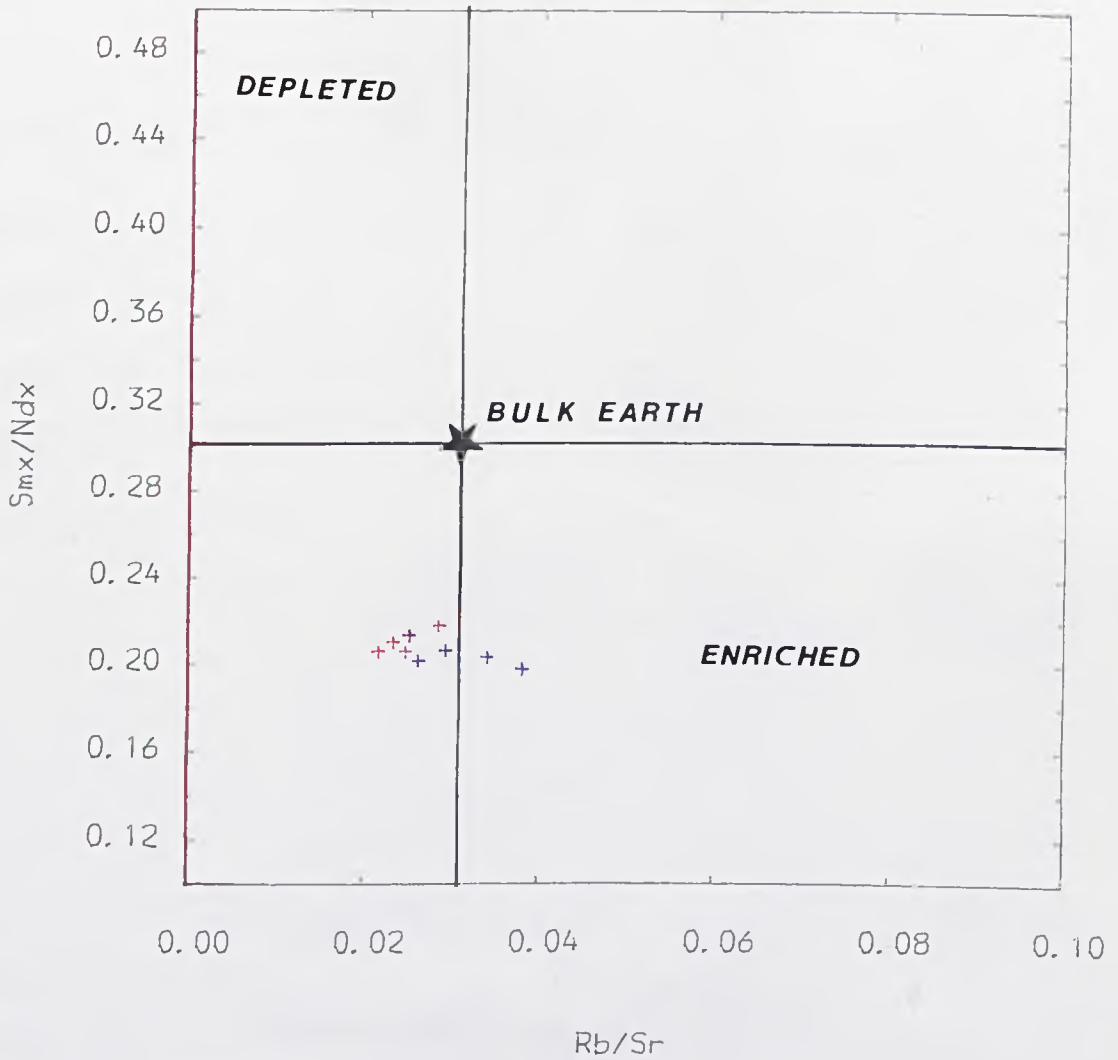
NEW SERIES ROCKS = red
 PYROCLASTIC SEQUENCE ROCKS = green
 OLD SERIES ROCKS = blue





TITLE : Fig : 8.12 Parent/Daughter Plot
(see text for explanation)

- NEW SERIES ROCKS = red
- PYROCLASTIC SEQUENCE ROCKS = green
- OLD SERIES ROCKS = blue



TITLE : Fig : 8.12 Parent/Daughter Plot
(see text for explanation)

NEW SERIES ROCKS	= red
PYROCLASTIC SEQUENCE ROCKS	= green
OLD SERIES ROCKS	= blue

patible elements as well as decoupling incompatible elements from slightly less incompatible elements can result, while more plausible amounts of partial melting are maintained, circa 10%.

There are a number of equations in the literature relating to processes of melting including zone refining. However, our present knowledge of distribution coefficient data for mantle minerals, the modal composition of the source mantle, the proportions of phases melting and the existence or non-existence of minor phases in the mantle is probably not adequate enough to make such calculations worthwhile for the time being (Norry and Fitton, 1983).

In conclusion, two differing processes can in principle generate much of the observed trace element and isotopic variations in the primitive basalts. It may be worthwhile reiterating that on the basis of the spidergram in Fig. 9.5 in Chapter 9 the primitive basalt is consistent with an origin from a depleted source and if the decoupling of Rb/Sr and particularly Sm/Nd can be explained by other processes then the necessity for a recent mantle metasomatic event becomes less compelling.

8.6 Discussion and Conclusions

Nd-Sr isotopic variations are compatible with an hypothesis of crustal contamination. While simple mixing models are able to satisfy Nd-Sr isotopic variations they cannot satisfactorily account for the majority of the elemental variations. The very good correlation between increasing $^{87}\text{Sr}/^{86}\text{Sr}$ and decreasing $^{143}\text{Nd}/^{144}\text{Nd}$ and fractionation indices is strong evidence for the operation of AFC. This is also powerful evidence against mantle heterogeneity being responsible for the majority of the isotopic variations.

Nd-Sr isotopic and $^{143}\text{Nd}/^{144}\text{Nd}$ - incompatible element relationships clearly identify two groups of data. The difference between these two groups may be related to the extent of contamination they have suffered, or more precisely to r , the ratio of the rate of assimilation to the rate of fractional crystallisation. The group with the lower r value, is comprised of Old Series rocks only, and are described as the 'uncontaminated' group. The group with the higher r , is comprised of New Series rocks and some Old Series rocks and is described as the 'contaminated' group. These rocks describe a trend on a diagram of $^{143}\text{Nd}/^{144}\text{Nd}$ vs $^{87}\text{Sr}/^{86}\text{Sr}$, in the basic rocks, which can be accounted for through contamination by 'typical' lower crustal granulites with low $^{143}\text{Nd}/^{144}\text{Nd}$ and $^{87}\text{Sr}/^{86}\text{Sr}$. Furthermore, $^{143}\text{Nd}/^{144}\text{Nd}$ vs incompatible element diagrams indicate that a decrease in r possibly occurred which is interpreted to reflect a change in the contamination environment from lower crust to upper crust. The former situation accounts for the basic rock variations whereas the latter characterises variations in evolved mugearites and acidic rocks. The high $^{87}\text{Sr}/^{86}\text{Sr}$ of some acidic rocks may require a concomitant change in contaminant to one of higher $^{87}\text{Sr}/^{86}\text{Sr}$ composition which is typical of upper crustal rocks. The isotopic trends in the 'uncontaminated' group can be explained, for the most part, by either small amounts of contamination by typical upper crustal or lower crustal rocks, although again high $^{87}\text{Sr}/^{86}\text{Sr}$ acidic rocks may require an upper crustal contaminant.

Field evidence suggests that most of the acidic fractionation and assimilation probably occurred in high level magma chambers as evidenced by the presence of calderas and high level intrusions (Chapter 3). Processes affecting basic rocks must to some extent

occur at greater depths. Therefore the opportunity for assimilation of crust at different depths and of different types is available. In this context geophysical evidence (Chapter 1) supports the existence of a basic body in the lower crust.

The precedent for such a scenario may exist in the British Tertiary Volcanic Province where much of the high level contamination is characterised by amphibolite facies rocks, such as in the Rhum ultrabasic layered intrusion (Palacz, 1983) and the Skye intrusives (Carter et al., 1976) whereas contamination by granulite facies rocks as in Skye Main Lava Series and the Mull Plateau Basalts (Dickin, 1983) may well have occurred at deeper levels in the Earth's crust.

Contamination by partial melts causing AFC effects can not be entirely ruled out, but features are so symptomatic of AFC to make this occurrence for Jebel Marra seem less likely. However, the most recent interpretation of the isotopic and trace element geochemistry of the Skye Main Lava Series (Thirlwall and Jones, 1983), favours a model of contamination by mixing with crustal partial melts. In this example, as well for the Mahabelashwar lavas (Mahoney et al., 1982), the most contaminated samples are elementally the most primitive. The simple explanation offered for this effect (Mahoney et al., 1982) is that the most primitive basalts are the hottest and therefore have a greater capacity for melting country rock. That such stark contrast should exist between assimilation by mixing of partial melts from the crust and AFC, may indicate the importance of such factors, as magma residence time, shape of the magma chamber, nature of the crust etc., on the mechanism of contamination that operates in a given area.

Finally, Nd-Sr isotopic and Sm/Nd-Rb/Sr relationships and LREE enriched REE patterns can be explained by a relatively recent enrich-

ment of the mantle source by a LILE rich metasomatic fluid or by small amounts of partial melting or by a process of zone refining.

An interesting question raised by the division of the two groups, distinguished by the different r's, is how this division should come about. Clearly, the division is related temporarily, as the oldest rocks tend to be the least contaminated. One explanation could be that with time, during volcanism, the crust has become progressively hotter such that it has become more amenable to assimilation. Unfortunately, here again, there are number of reasons which can be advanced to interpret this phenomenon.

CHAPTER NINE

MODELLING

9.1 Introduction

The aim of this Chapter is to verify assertions made from qualitative arguments in Chapters 6, 7 and 8 by quantitative geochemical modelling. In doing this some important parameters will be determined. Models will be developed to determine the effects of fractional crystallisation and combined crustal contamination on the geochemistry of the volcanic rocks.

The modelling is considered in three main parts. Firstly, major elements are used in a least-squares regression approach to ascertain the proportions in which the major phenocryst phases are fractionated to produce the observed geochemical trends. The phases considered in this approach are those which are responsible for the trends in variation diagrams described in Chapters 6 and 7 and which occur as major phenocryst phases in the lavas. Secondly, trace element modelling using the Rayleigh fractionation equation compares calculated trace element concentrations with measured trace element concentrations in the rocks. Differences between the two are often resolved by considering trace element contributions from the crust. Primitive basalt and mantle normalised diagrams are additionally used to demonstrate the effects of fractional crystallisation and contamination. Finally, crustal contamination models are examined using isotope and trace element data and curves are drawn for successful contamination models. These are then compared with observed isotopic and trace element variations.

9.2 Least-Squares Modelling on Major Elements

The coherent variations in major and trace elements described in Chapters 6 and 7 are largely consistent with a process of fractional crystallisation. Major elements can be used to calculate the proportions of phases removed and the extent of fractionation that has occurred (Bryan et al., 1969); the method is described below.

9.2.1 Method

Fractional crystallisation has been examined in a quantitative way, by means of a computer program PETROMIX ALGOL68 (I Luff, unpublished) based on the method of Bryan et al., (1969). The program employs a least-squares regression approach to obtain the 'best fit' between the rocks considered to have parent-daughter relations through the removal (or addition) of phases thought to be involved in fractionation. For example, if it is attempted to produce an hawaiite from a basalt by the removal of olivine, plagioclase, and clinopyroxene then mass balance calculations are performed which give the 'best fit' regression line in terms of the daughter and the proportions of the phases fractionated. The 'best fit' is that which gives the minimum for the sum of the squares of the residuals between the calculated and the measured analyses of the daughter rocks.

The program requires input data for:-

- i) whole rock analyses of rocks thought to be related by fractional crystallisation, and
- ii) analyses of phenocryst phases considered responsible for the fractionation.

There are unfortunately a number of limitations to the technique which have been highlighted by Cox et al., (pp.173-8, 1979) and are documented here.

a) It is assumed in the calculation that the daughter rock originated from the parent rock along a 'liquid line of descent'. In a natural series there is inevitably a certain amount of scatter, of which only a small part can be attributed to analytical error. The implication of this is that not all the rocks are related to one another by exactly the same 'line of liquid descent'. In support of this Cox et al., (pp.36-8, 1979) presents data from Aden, which show that successive eruptive cycles mimic variations in geochemistry seen in other cycles. ("ontogeny recapitulates phyl. ogeny"). It is also the case, as with basic rocks of Jebel Marra, that variations in the Old Series largely parallel variations in the New Series.

Prudence is required in selecting the probable parent-daughter rocks. Here however, there is a wealth of major and trace element, isotopic, field, and thin section data which will indicate the likely paths of evolution.

b) As well as the scatter due to natural variation there is also scatter due to analytical error. This in most cases will be tolerably small, although in oxides such as Ti, Mn and P, in whole rock analyses and similarly in mineral analyses where the range and amounts of a given oxide may also be small, the relative error is magnified.

c) It is possible that other processes such as weathering or differences in the degree of partial melting could blur the effects of fractional crystallisation and lead to erroneous conclusions. If significant assimilation of crust has occurred and is not considered in the calculations, then this can seriously impair the results.

d) Phases, especially olivine and plagioclase exhibit solid solution. Thus, as the composition of the magma changes then the composition of

the crystallising phases will change. This could affect the results if the calculations are made over a very large compositional interval. Also it has been noted (Chapter 5) that many of the phenocrysts are zoned. The subtraction of a phase whose composition was measured at the core of the crystal may not in fact represent the bulk composition of the extracted phase. With regard to this, Zielenski (1975), in his experience, found that the effect on the calculations was minimal.

e) Even though all analyses are approximate, only one, the daughter is considered, to be in error in least-squares.

9.2.2 Results

Despite possible problems, as identified above, the results from least-squares regression approach to fractionation can give useful information. The method can be justified on the following grounds. The calculations make use of all the major element data and do not just consider biaxial plots. The sum of the squares of the residuals can be used as a guideline on the basis of which particularly high values can be disregarded and low ones can be accepted. Finally, the speed of the program enables a large range of permutations to be tested from which the most successful, in terms of low residuals and credibility, can be selected.

In general, it was found from experience that more plausible results were obtained if a reasonably large compositional interval between the parent and daughter existed. However, if the compositional interval became too large then problems arose concerning the choice of suitable extract minerals and also choice of the parent-daughter samples.

On the basis of the temporal divisions made earlier, for both Old and New Series rocks, the data have been independently modelled. The following salient features of the crystallisation history were incorporated in the modelling (Chapter 4). Firstly, olivine is more abundant in the most primitive rocks. Secondly, clinopyroxene is abundant throughout the series except in the most primitive rocks and more evolved basic rocks. Finally, observations from variation diagrams involving Al_2O_3 (Figs. 6.2b and 6.3c) suggest that plagioclase only becomes a significant fractionating phase from evolved mugearite to primitive trachyte compositions.

The first objective of the modelling is to ascertain whether the range in rock compositions can be sensibly produced by fractional crystallisation alone. In general, using this approach, the fit is unacceptably poor. The fit, in the basic rocks for example, is worst for oxides of K and Na, while Mn, P and Ti are also poor. Some of these oxides can be compensated for by selecting phases with differing amounts of the oxide in question, but the problem with K_2O is more acute. In order to balance this component, phase(s) bearing K_2O would have to be extracted which are themselves not present as phenocrysts.

In order to overcome these problems, and in particular the problem of K_2O , an alternative approach is adopted which uses continental crust as an additional component. In fact, it has been shown that (Chapter 8), in the light of isotopic data, the addition of crust becomes a necessary ingredient in the calculations.

1) New Series - The results are presented in Table 9.1 representing a selection of the calculations with the 'best fit'. Four stages in

the fractionation history recognised from elemental variation diagrams were modelled:-

- i) primitive basalt to primitive mugearite
- ii) primitive mugearite to evolved mugearite
- iii) evolved mugearite to primitive trachyte
- iv) primitive trachyte to evolved trachyte.

By using crust as extra component the fit is considerably improved and, in particular, the residual for K_2O is much reduced.

In producing primitive mugearites from primitive basalts, olivine-clinopyroxene-plagioclase-magnetite is removed in the approximate proportion of 30:55:10:5 with the addition of some crust. The exact proportions vary according to the parent and the phases used in the calculation but in most cases results are comparable with one another. 24105, which is representative of primitive mugearites, is selected as the daughter to the basalts because it shows no depletion in Al_2O_3 , CaO or Sr and so may be considered not to have been significantly affected by plagioclase fractionation.

In Table 9.1, 24109 is used as a parent to evolved mugearites which do show the affects of plagioclase fractionation; here, depletions in CaO, Al_2O_3 and Sr are observed. The proportion of plagioclase is increased as is the proportion of crust added. The proportionally greater addition of crust made at this stage is also supported by isotopic evidence (Chapter 8).

In going from evolved mugearites to primitive trachytes the 'best fits' are obtained when olivine-clinopyroxene-plagioclase-magnetite is fractionated in the approximate proportion of 12:12:70:6

NEW SERIES

P	D	SAMPLES						PHASES						WEIGHT PROPORTIONS						SAMPLE NO'S						
		OL	CPX	PLAG	MT	KF	AP	CRUST	Par	Daug	F	SIG	Ol	Cpx	Plag	Mt	KF	Ap	Ol	Cpx	Plag	Mt	KF	Ap		
WITHOUT CRUST - Primitive basalt to primitive mugearite																										
88	109	.354	.655	.210	.125			2.364	1.019	0.431	2.784	26	49	16	9			88	88	91	91					
88	109	.404	.679	.305	.128			2.545	1.029	0.404	3.705	27	45	20	8			91	91	91	91					
88	109	.359	.649	.268	.110			2.400	1.015	0.423	1.164	26	47	19	8			91	91	91	91					
WITH CRUST - Primitive basalt to primitive mugearite																										
88	109	.223	.415	.036	.049		.123	1.696	.996	.520	.043	31	37	5	7			88	88	91	91					
88	109	.244	.413	.082	.045		.134	1.649	1.000	.560	.086	31	33	10	6			91	91	91	91					
88	61	.213	.440	.016	.034		.230	1.469	.997	.588	.103	30	63	2	5			88	88	91	91					
88	123	.234	.471	.049	.033		.166	1.618	.997	.558	.133	30	60	6	4			88	88	91	91					
91	109	.228	.459	.057	.057		.082	1.712	.994	.552	.099	29	57	7	7			91	91	91	91					
91	61	.219	.483	.037	.042		.192	1.585	.995	.558	.075	28	62	5	5			88	91	91	91					
91	123	.268	.523	.134	.040		.134	1.831	1.001	.510	.169	28	54	14	4			91	91	91	91					
67	109	.169	.564	.058	.069		.078	1.778	.996	.532	.121	20	65	7	8			88	88	91	91					
67	109	.191	.572	.121	.069		.090	1.863	1.001	.513	.120	20	60	13	7			91	91	91	91					
93	109	.256	.559	.153	.090		.082	1.973	.997	.484	.182	24	53	14	9			88	88	91	91					
Primitive mugearite to evolved trachyte																										
109	26	+.012	.021	.020	+.023		+.006	.320	.749	1.001	.044								101	101	101				40	
109	26	+.012	.083	.062	+.008		0	.299	.846	.867	.105		55	45						105	105	105				40
109	26	.002	.095	.131			0	.303	.929	1.003	.103	1	42	57					101	101	101					
109	19	.035	.128	.162	.001		.008	.339	1.004	1.009	.738	.756	13	10	71	6			101	101	101	101				
109	19	.026	.131	.134	.011		0	.307	1.010	1.007	.715	.562	9	43	44	4			91	91	91	91				
108	26	.005	.103	.143	.003		0	.324	1.071	1.000	.762	.131	2	41	56	1			101	101	101	101				

Table 9.1 Petromix Results for New Series rocks

NEW SERIES

SAMPLES		PHASES										WEIGHT PROPORTIONS					SAMPLE NO'S									
P	D	OL	CPX	PLAG	MT	KF	AP	CRUST	Par	Daug.	F	SIG	Ol	Cpx	Plag	Mt	KF	Ap	Ol	Cpx	Plag	Mt	KF	AP		
Evolved mugearite to primitive trachyte																										
19	16	.130	.102	.732	.068			.110	1.931	1.010	.497	1.029	13	10	71	6			104	104	104	104				
26	16	.112	.136	.568	.129			.010	1.941	1.009	.516	.022	12	12	67	11			118	118	118	19				
26	16	.150	.584	.116	.117			.048	1.932	1.013	.515	.091	16	20	60	12			104	104	104	104				
109	16	.123	.625	.102			.038	.543	1.535	0.989	.478	.964	11	19	57	9		3	118	118	118	118				40
*26	16	.054	.066	.297	.054			.072	1.948	1.000	.495	.087	12	14	63	11			101	101	101	101				
Primitive basalts to hawaiites																										
91	3	.123	.188		+.004			.081	1.226	.998	.760	.061	40	60					91	91			91			
91	62	.182	.213		.004			.073	1.327	1.001	.694	.082	46	53		1			91	91			91			
91	24	.148	.231		+.001			.106	1.277	1.004	.729	.094	39	61					91	91			91			
Primitive trachytes to evolved trachytes																										
113	87	+0.15	+0.016	.010	+.043	+.461	+.006	.256	.218	1.005		.028							31	31	31	31	81	40		
113	81	0.16	+0.033	.026	+.017	+.141	+.001	.221	.623	1.003		.030							31	31	31	31	81	40		
113	31	+0.007	+0.017	.014	+.013	.205	+.003	.205	.681	1.002		.006							31	31	31	31	81	40		
*16	17		.079		.041	1.314	.004	.322	2.119	1.003	.414	.860		5		3	95	1		2			16	16	40	
16	25		.054		.020	.876	.001	.232	1.721	1.001	.513	.523		6		2	92			2			16	16	40	
16	20		.078		.044	1.345	0	.327	2.147	1.003	.40	.965		3		3	92			2			16	16	40	

Table 9.1 Patromix Results for New Series rocks continued

OLD SERIES

SAMPLES		PHASES										WEIGHT PROPORTIONS						SAMPLE NO'S							
P	D	OL	CPX	PLAG	MT	KF	AP	CRUST	Par	Daug	F	SIG	Ol	Cpx	Plag	Mt	KF	Ap	Ol	Cpx	Plag	Mt	KF	Ap	
Basalt to hawaiite																									
58	90	.106	.252	.092	.017			.051	1.419	1.004	.682	.207	23	54	20	4			88	88	91	91			
23	90	.077	.332	.079	.029			.055	1.465	1.003	.312	.180	15	64	15	6			88	88	91	91			
83	90	.047	.334	.088	.018			.040	1.447	1.000	.672	.130	10	69	17	4			91	91	91	91			
*58	90	.068	.181	.047	.015			.038	1.391	1.000	.700	.110	22	58	15	5			88	88	91	91			
Primitive trachyte to evolved trachyte																									
43	46		.042		.011	.331	.004	.638	0.751	1.000	.010	.010		11		3	85	1		31		31	81	40	
*43	46		.036		.024	.422	.003	.277	1.491	1.000	.566	.021		8		5	87			31		31	81	40	

Table 9.2 Petromix results for Old Series rocks.

Explanation of symbols used in Tables 9.1-2

P = Parent sample no; D = Daughter sample no; OL = olivine; CPX = clinopyroxene
 PLAG = plagioclase; MT = magnetite; KF = potassium feldspar; AP = apatite, F= amount of magma remaining (approximately); SIG = sum of squares of residuals.
 Weight proportions of phases fractionated are given on right-hand side of table;
 sample nos. of analysed phases used in calculation are given on extreme right.
 Average of crustal samples represents composition of CRUST used.

* results from LSQPM: + indicates phases were added.

with the addition of some crust. The importance of plagioclase fractionation at this stage agrees with qualitative observations.

The two trachytes 24016 and 24113 were chosen as the most primitive members of the trachyte groups on isotopic as well as on trace and major element grounds. They were modelled as parents to the two series outlined in Chapter 7. The results are presented in Table 9.1. In the caldera trachytes (24016-25-20-17), anorthoclase is the main fractionating phase in the proportion of 9:1 to clinopyroxene and magnetite. The mafic bearing trachytes (24113-81-31-87) are modelled with a very good fit in which large additions of anorthoclase and crust in the proportions of 2:1 are made while small subtractions of plagioclase also occur. The results of the latter model are in agreement with petrographic observations, interpreted as magma mixing, in which the trachytes contain small modal amounts of olivine and clinopyroxene, usually in a resorbed form, as well as containing plagioclase and anorthoclase.

ii) Old Series - in an identical way to the New Series, the Old Series data have been modelled. However, there are inherent problems because of the smaller size of the data set both with regard to whole rock analyses and the microprobe analyses of the phenocryst phases. Also, the range of composition is reduced due to a much larger 'silica gap' in this series and because the basic rocks begin from less primitive compositions.

Table 9.2 reveals that the proportions in which the phases are fractionating are comparable with the New Series although the amount of fractionation is less which is probably a function of the reduced compositional range.

Attempts to generate the mugearite 24061 from primitive basalts were unsuccessful. In the absence of a suitable parent rock for the trachytes no attempt was made to model this step. However, from comparisons with the New Series trachytes and from trace element data (see Chapter 7), it can be reasonably supposed that the rocks were produced in a closely analogous way, i.e. by relatively large extractions of plagioclase and, in some cases, additions of crust and through small changes in other phases.

The Old Series contaminated trachytes were also modelled (Table 9.2). In these models large additions of crust are required to produce the most evolved rhyolites and trachytes with large subtractions of anorthoclase and smaller subtractions of clinopyroxene and magnetite. No success was achieved in modelling rocks from the 'largely uncontaminated' group.

9.2.3 Assessment of Least-Squares Results

A disturbing feature of the data is the relatively high residual associated with evolved mugearites and trachytes. This is in part due to limitations of the method outlined earlier and other problems which will be addressed specifically. For example, because of the 'silica gap', the compositional range over which the trachytic daughter is expected to be generated from the mugearitic parent in the New Series is much greater than would be normally desirable. In the absence of any micro-probe data, due to the silica gap, problems exist in assessing exactly which mineral compositions are most likely to have been responsible for the fractionation. Also, changes in mineral chemistry in response to changes in magma composition may become important over such a large compositional range. Further

complications surround P_2O_5 . Although it is clear from Fig. 6.21 that fractionation of a P bearing phase, presumably apatite, would account for the depletion of P_2O_5 in the trachytes, it was excluded from the calculations as it tended to upset the results because of very high residuals for P_2O_5 . Similarly, the residuals for MnO and TiO_2 are also high, a feature which can be attributed to the high relative error associated with low concentrations of these oxides recorded in the daughter rocks.

Nevertheless, consistent results concerning the proportions of phases removed have been obtained as well as crude approximations for the amount of magma remaining after fractionation which provide a useful starting point from which the trace elements can be modelled.

9.3 Trace Element Modelling

9.3.1 Introduction

There are a number of trace element models available which attempt to predict the behaviour of trace elements as a result of processes such as partial melting or fractional crystallisation. Rayleigh fractionation is probably the most appropriate for fractional crystallisation of this type and may be expressed as follows:-

$$\frac{C_L}{C_0} = F^{(D-1)} \quad \text{Eqn. 9.1}$$

where C_L = concentration in the daughter liquid

C_0 = concentration in the parental liquid

F = amount of liquid remaining after fractionation

and D = bulk distribution coefficient. D is defined in Eqn. 7.2.

This applies for the case of perfect fractional crystallisation in a closed system where crystals are removed as soon as they are formed. From the form of the equation it is clear that when $D > 1$ (and after some fractionation) the daughter liquid is depleted and when $D < 1$ the daughter liquid is enriched for a given element.

Using some of the results from the least-squares approach it is possible to model the behaviour of trace elements at various stages of fractionation. The least-squares calculations provides the weight proportions of the fractionating phases from which D can be established by using K_d 's from the literature. K_d values used in this study are compiled in Table 9.3. A crude estimate of the amount of fractionation, F , is obtained from the least-squares calculation without using crust as a component. Strictly the F 's of Eqn. 9.1 and the least-squares calculation are only the same when considering incompatible elements with a D of zero (Luff, 1982). C_o and C_L are known from X.R.F. analyses against which a calculated result from the Rayleigh fractionation model can be compared. The results of the calculations presented in Table 9.4 are based on the results of a more sophisticated weighted least-squares program (LSQPM ALGOL68, (R Powell, pers. comm.)). This program differs from the ordinary least-squares program in that the oxides are weighted according to their relative error and their difference from a regression line calculated in PETROMIX. This approach is designed to downgrade the affect of oxides of low concentration or those which, for one reason or another, are off the main trend of data. Inclusion of such data can exert a considerable influence on ordinary least-squares calculations. Unfortunately, the complexity of the program places a large strain on computer resources such that its use had to be restricted.

Table 9.3 Trace Element Kd Data

Basic Rocks

	CPX	CL	PLAG	MT		CPX	OL	PLAG	MT
Ce	0.098	0.0005	0.20	0.005	K	0.02	0.00018	0.2	0.01
Nd	0.21	0.0010	0.14	0.008	Rb	0.011	0.00018	0.07	0.01
Sm	0.26	0.0013	0.11	0.010	Sr	0.007	0.00019	2.2	0.01
Eu	0.31	0.0016	0.73	0.008	Y	0.5	0.01	0.03	0.2
Gd	0.30	0.0015	0.066	0.015	Zr	0.1	0.01	0.01	0.2
Dy	0.33	0.0017	0.055	0.025	Nb	0.1	0.01	0.01	0.4
Er	0.30	0.0015	0.041	0.040	Ba	0.0011	0.00011	0.02	0.01
Yb	0.28	0.0015	0.031	0.070					

Acidic Rocks

	PLAG	CPX	KF	AP		OL	PLAG	CPX	KF	AP	MT
Ce	0.27	0.50	0.044	34.7	K	0.001	0.1	0.04	-	-	0.01
Nd	0.21	1.11	0.025	57.1	Rb	0.001	0.04	0.03	0.4	-	0.01
Sm	0.13	1.67	0.018	62.8	Sr	0.001	4.4	0.50	0.4	-	0.01
Eu	2.15	1.56	1.13	50.4	Y	0.01	0.1	0.40	0.1?	40	2
Gd	0.097	1.85	0.011	56.3	Zr	0.01	0.1	0.60	0.1?	-	0.8
Dy	0.064	1.93	0.006	50.7	Nb	0.01	0.06	0.80	0.1?	-	2.5
Er	0.055	1.66	0.006	37.2	Ba	0.001	0.3	0.13	6	-	0.01?
Yb	0.049	1.58	-	23.9							

No information available for REE's in olivine or magnetite in acidic rocks. Values in basic rocks used instead.

CPX = clinopyroxene; OL = olivine; PLAG = plagioclase; Mt = magnetite; KF = potassium feldspar and AP = apatite. ? refers to values estimated from other elements. Kd data for La assumed to be same as Ce.

Sources: Hanson, (1980); Pearce and Norry, (1979);
Grutzeck et al., (1974); Irving, (1978);
Arth, (1976) and Cox et al., (1979).

Table 9.4 Trace Element Calculations using Rayleigh Equation

NEW SERIES

i) Primitive basalt to primitive mugearite					ii) Primitive mugearite to evolved mugearite						
	F	OL	CPX	PLAG	MT		F	OL	CPX	PLAG	MT
	0.520	31	57	5	7		0762	2	41	56	1
	D	24088	24109		24109		D	24109	24026	24026	
		meas	meas		calc			meas	meas	calc	
Sc	1.8	33	18		20	Sc		18	16	17	
Cr	6.7	655	59		16	Co		36	30	40	
Co	2	61	36		35	Rb		43	51	55	
Ni	5.2	331	33		21	Sr		1118	704	743	
Rb	0.004	17	43		33	Y		23	33	28	
Sr	0.15	723	1118		1260	Zr		123	276	159	
Y	0.30	17	23		27	Nb		57	68	73	
Zr	0.075	82	123		150	Ba		1057	1374	1349	
Nb	0.09	32	57		58						
Ba	0.01	397	1057		758						
iii) Evolved mugearite to primitive trachyte					iv) Primitive trachyte to evolved trachyte						
	F	OL	CPX	PLAG	MT		F	KF	CPX	MT	
	0.495	12	14	63	11		0.86	85	14	1	
	D	24026	24016		24016		D	24016	24017	24017	
		meas	meas		calc			meas	meas	calc	
Sc	1.4	16	4		11	Rb	0.4	114	175	125	
Co	1.03	30	16		29	Sr	3.5	121	13	83	
Rb	0.04	51	114		100	Y	0.6	33	55	35	
Sr	2.8	704	121		198	Zr	0.1	488	865	559	
Y	0.9	33	33		35	Nb	0.15	102	170	116	
Zr	0.3	276	488		452	Ba	5	484	54	265	
Nb	0.4	68	102		104	Pb	0.1	14	28	16	
Ba	0.2	1378	484		2419	Th	0.1	18	32	21	
Pb	0.1	8	14		15						
Th	0.1	10	18		19						

Table 9.4 Continued

OLD SERIES

i) Basalt to hawaiite					ii) Primitive trachyte to evolved trachyte					
	F	OL	CPX	PLAG	MT	F	KF	CPX	MT	
	0.70	22	58	15	5	0.57	88	7	5	
	D	24058	24090		24090	D	24083	24046	24046	
		meas	meas		calc		meas	meas	calc	
Sc	3.2	28	14		13	Rb	0.36	99	162	143
Co	1.5	52	38		44	Sr	3.6	33	8	7
Cr	8.5	211	0		15	Y	0.37	35	80	50
Ni	3.8	130	6		48	Zr	0.13	380	948	624
Rb	0.015	23	39		33	Nb	0.15	103	175	167
Sr	0.35	907	1041		1164	Ba	5.3	794	22	57
Y	0.3	19	31		24	Pb	0.1	15	28	25
Zr	0.07	105	259		146	Th	0.1	15	18	25
Nb	0.08	40	94		131					
Ba	0.04	568	610		800					

Meas = measured abundances; calc = calculated abundances using Rayleigh equation. D = bulk distribution coefficients calculated using Kd data from Table 9.3 and weight proportions, obtained from LSQPM results, listed under mineral species. OL = olivine; CPX = clinopyroxene; PLAG = plagioclase; MT = magnetite and KF = potassium feldspar. F = amount of magma remaining after fractionation; obtained from LSQPM.

For this reason it was only employed for calculations which were to be used for trace element modelling. The method, limitations and statistical details are dealt with by Powell (in press).

9.3.2 Results

The results obtained using Eqn. 9.1 based on data from the weighted least-squares calculations over the whole suite are presented in Table 9.4. The data have been modelled for the four stages of fractionation outlined previously.

The mugearite 24109 which is derived from a primitive basalt (24088) shows remarkably good agreement between the observed and calculated trace element abundances. Amongst the compatible elements, Cr is the most difficult to model successfully. This may be understandable in view of the sensitivity of D to the amount of magnetite fractionation and because D_{Cr} in magnetite is poorly constrained. In Table 9.4 it is seen that both Rb and Ba concentrations are underestimated in the calculated mugearite.

Also presented in Table 9.4 are results involving the step from primitive mugearite to evolved mugearite (24109-24026). The compatible elements have calculated abundances which are higher than the measured abundances whereas Zr has a calculated abundance which falls short of the measured abundance. Cr and Ni are not included in the calculations because their concentrations are too low to be sensibly modelled.

The trace element predictions from the Rayleigh model are also in reasonable agreement with the step from evolved mugearite to primitive trachyte (24026-24016). However, this treatment overlooks

the problem with Ba. Anorthoclase was excluded from least-squares calculations at this stage because of its disruptive effect. But, low Ba concentrations in the trachytes strongly suggests that fractionation of potassium feldspar has occurred, although this is probably at a late stage. Again, Zr falls short of the measured abundance. Also included in the calculations, at this stage, are Pb and Th which in the absence of any Kd data are assigned D's of 0.1. Hitherto, they were excluded because their concentrations were too close to detection limits.

Little success is gained in modelling the New Series trachytes. The least-squares model predicts 80-90% extraction of anorthoclase which agrees fairly well with the marked depletions observed in both Ba and Sr. The least-squares result overall under-estimates the amount of fractionation. An F value closer to 0.47 would be expected to explain the observed enrichment and depletions in the stage from 24016-24017.

Modelling the Old Series data by the same approach has met with some difficulty because the least-squares results are less satisfactory. In the step from primitive basalt to hawaiite the amount of fractionation appears to be under-estimated, particularly for Zr. Amongst the acidic rocks only the silica rich group could be modelled with any degree of success. Here too, the amount of fractionation has been under-estimated in the step from 24043-24046. Once again the proportion of anorthoclase fractionated was around 90%. No trace element calculations for rocks from the Pyroclastic Sequence or rocks from the silica poor series were possible because no sensible results from the least-squares regression were obtained.

9.3.3 Deviations from the Fractional Crystallisation Model

Many of the limitations of the least-squares approach to fractional crystallisation, outlined earlier, can be used to explain the differences between the observed and calculated trace element abundances. Elements such as Rb and Ba which are characteristically enriched in crust commonly have higher measured values than those values calculated using the Rayleigh equation. Similarly, elements, such as Y, have measured values higher than calculated values; Y is typically poor in crustal rocks. Zr has a calculated value higher than the measured value at the primitive mugearite stage but thereafter it is lower than the measured value. These effects are thought to be the result of crustal contamination. The behaviour of Zr will be discussed more fully later.

Special problems occurred in the modelling of the acidic rocks. One of the difficulties may have been due to the fact that the composition of anorthoclase and crust are very similar. In this event, the balance between the two components is critically dependent on compositions used in the calculations. Nevertheless, the proportions in which anorthoclase were subtracted in the calculations were consistently around 80-90%. In fact, the relative constancy of the proportions in which the phases are calculated to be fractionated, even when slightly different parents, daughters or mineral compositions are used, is a feature of other stages of fractionation. This suggests that the values obtained for the proportions in which the phases are removed are reliable, although the amount of fractionation calculated is sometimes variable.

In conclusion, use of Rayleigh fractionation model with crustal assimilation appears to agree with most of the trace element variations.

D's calculated from the least-squares results would seem to be more reliable than F values. Although applying a trace element model to results from least-squares regression has obvious limitations it does appear to crudely identify some characteristics of the possible contaminant, i.e. enriched in certain elements such as Rb and Ba and poor in others such as Y.

9.3.4 Fractionation versus Enrichment/Depletion Diagram:

A convenient visual means of illustrating the behaviour of trace elements with progressive fractionation is to plot fractionation (where fractionation = $1-F$, F = the amount of magma remaining after fractionation) against enrichment, C_L/C_0 (Fig. 9.1). The hyperbolae that are drawn correspond to different D values. The diagram is subject to error, primarily in F, which is itself only a crude estimate based on the weighted least-squares predictions, but also there will be analytical error associated with C_L/C_0 . Notwithstanding these errors, the overall agreement is good. Rb and Ba, in general, plot above the limiting case, when $D=0$. Rb and Ba may be explained as a result of assimilation of basement enriched in these components. Ba is omitted after evolved mugearites because it becomes compatible. Zr only plots above the $D=0$ curve from evolved mugearites onwards. Nb and Y conform characteristically to elements with D values of about 0.25 and 0.5 respectively although the addition of crust poor in these elements will have the effect of elevating D. Y in the stage from evolved mugearite to trachyte shows no increase because of some apatite fractionation (see REE modelling next section). Furthermore, the tenfold enrichment in Rb and Zr is consistent with the D curves, although a much larger margin of error must be allowed for in this region of the diagram because the curves here are asymptotic. The severe depletion in Ni and Cr is evident, while a D of 2 approximates

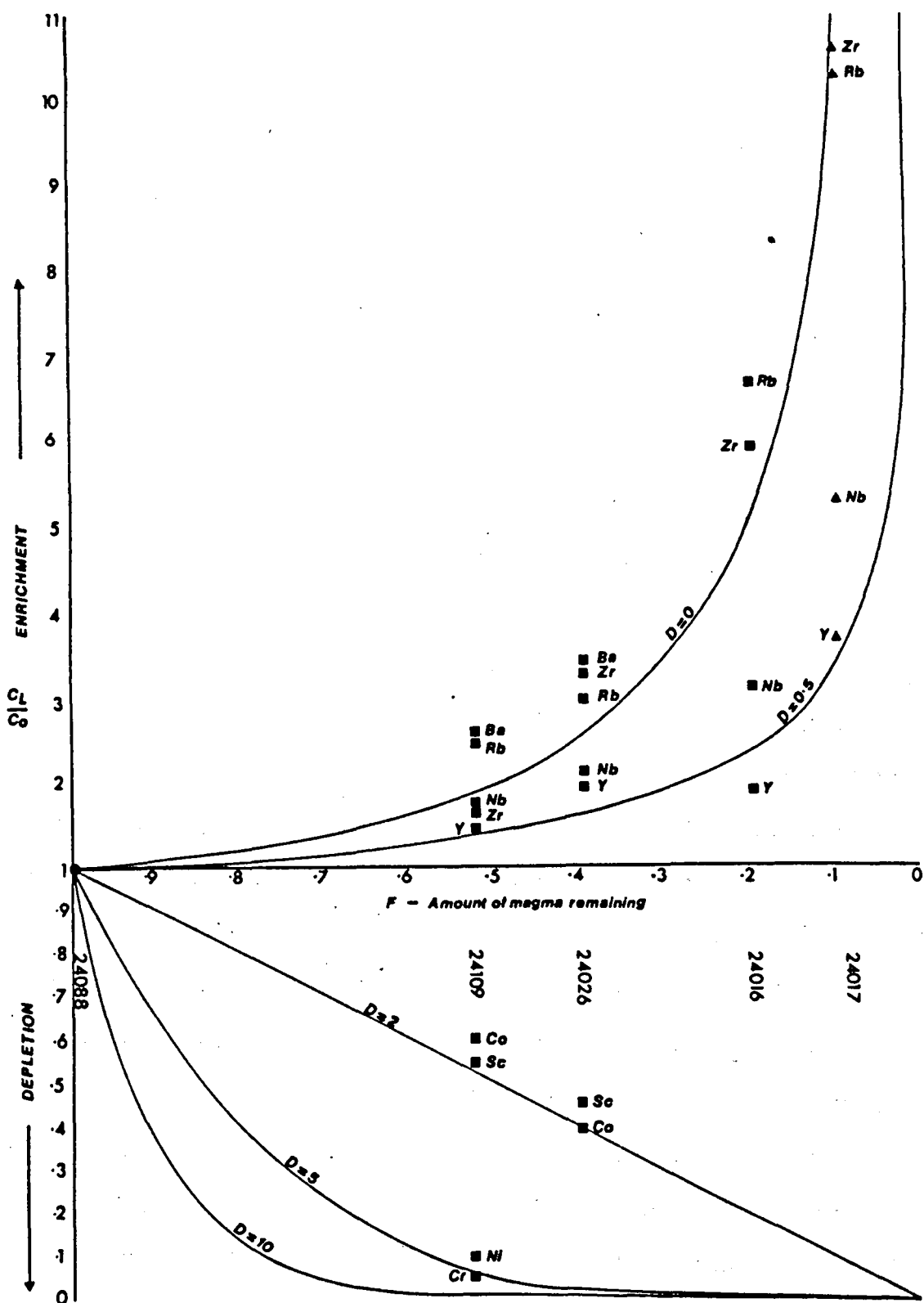


Fig. 9.1 Enrichment/depletion vs F diagram. Samples are plotted normalised to an assumed parent (24088). F values are taken from least-squares results from major elements. D curves are also drawn calculated from the Rayleigh equation. Some elements plot above the limiting curve ($D=0$) which may indicate the operation of a second order process.

to the depletions in Co and Sc. The usefulness of highly compatible elements is limited because they rapidly approach values close to detection limits.

9.3.5 Rare Earth Modelling

In view of the superior accuracy and well constrained Kd data for REE's they should, in principle, provide a good test for evaluating processes of fractional crystallisation and crustal contamination. In this section some of the qualitative assessments will be tested by modelling of the REE's.

Fig. 9.2 shows REE patterns for a primitive basalt (24088) and the calculated REE pattern for 24109 using Eqn. 9.1 based on the weighted least-squares predictions. Also shown is the measured REE pattern for 24109. To a first approximation, the accord between the calculated and the measured pattern for 24109 is good. If it is thought that the amount of fractionation has been over-estimated for the calculated pattern, then employing a higher F value would result in an extremely good match for the HREE's although the mismatch for Nd and, particularly, Ce and La would be increased. A feature of the transition from basalt to mugearites in New Series rocks is the increasing extent to which the patterns are bowed (Eqn. 7.5). It is possible that the downward bowing of REE patterns is the result of fractional crystallisation of a phase relatively rich in middle REE's. Of the major fractionating phases only clinopyroxene has a humped Kd-REE pattern. Humped Kd-REE patterns refer to graphs to which Kd's are plotted against REE's for a given mineral in which the pattern is concave downwards in the MREE region. Clinopyroxene is used in obtaining the calculated pattern for 24109 but from Fig. 9.2 it is

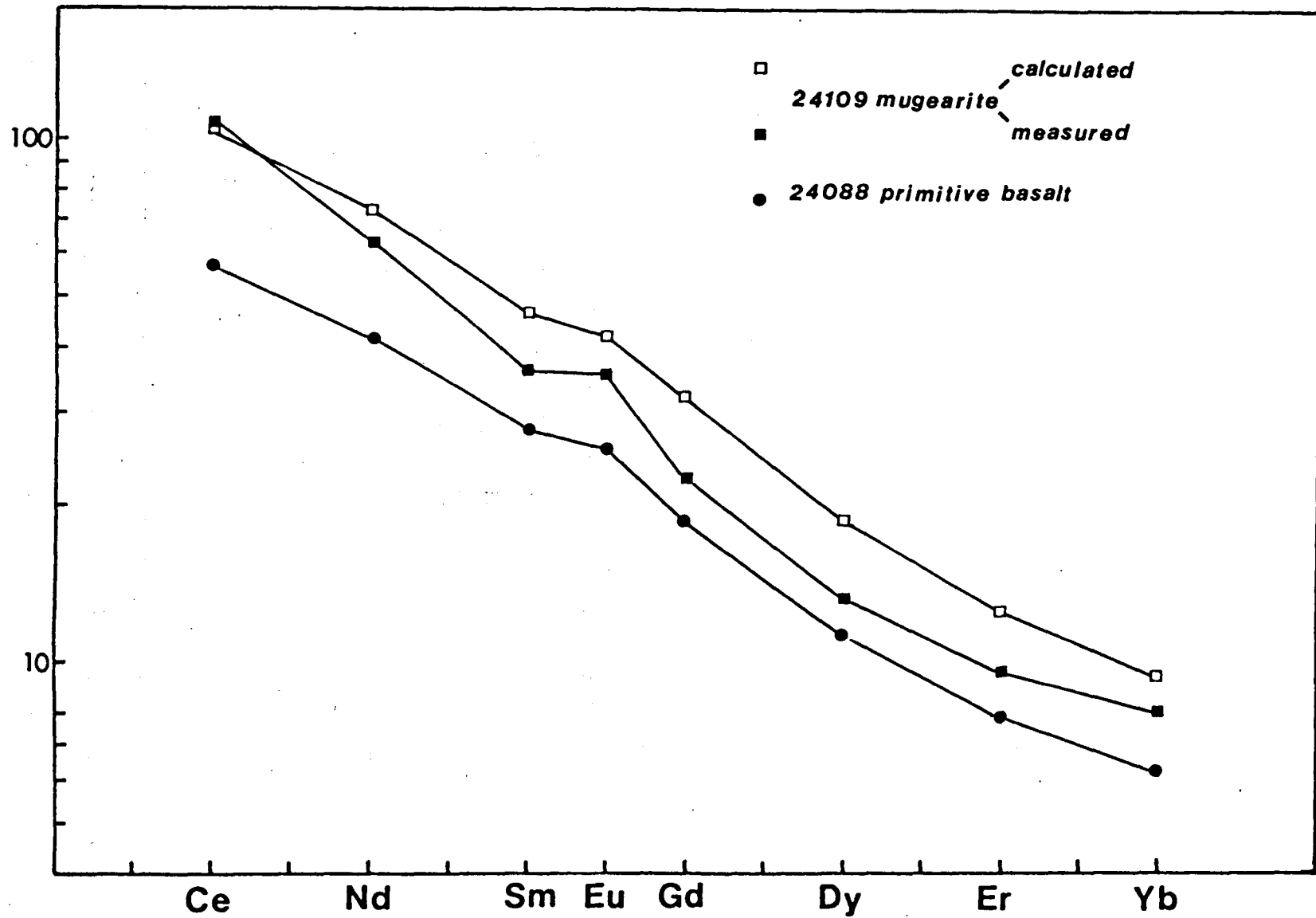


Fig. 9.2 REE patterns for 24088 and 24109 and calculated pattern, from least-squares results, for 24109.

clear that insufficient bowing is produced. This may be reconciled if the clinopyroxenes fractionating from the liquid are relatively more enriched in REE's, and especially middle REE's, than the Kd data suggests. Alternatively, if a minor phase, such as apatite (see later in this section), was fractionated, even by a very small amount, then it is conceivable that the observed bowing could be produced. This notion is largely untestable because apatite is rare in the basalts and hawaiites and also P_2O_5 shows no obvious depletion but the amount of apatite fractionation required to achieve this effect is so small that this possibility cannot be rejected.

Another way to tackle the problem would be to accept the results of the weighted least-squares modelling and to explain the discrepancy by another factor such as assimilation of crust. It can be seen from Table E1 that there is a general correlation between how evolved the rock is, the extent of bowing of the REE patterns (indicated by Gd/Gd^*) and the extent of contamination (indicated by $^{143}Nd/^{144}Nd$). However, it is noted that the hawaiite 24090 appears, from its isotopic characteristics, to be 'largely uncontaminated' but at the same time possesses the bowed REE pattern of other mugearites and hawaiites. This suggests that the increase in bowing from basalts to mugearites is not an effect of contamination and is therefore more likely to be the result of fractionation perhaps of clinopyroxene or very small amounts of apatite.

To account for the relative loss in middle REE's (see section 7.5) in going from evolved mugearites to primitive trachytes by fractionation, a phase with a humped Kd-REE pattern is required. It is unlikely to be caused by possible dilution effects of contamination in view of the relatively large loss of REE's that is involved. The

large negative anomaly in Eu is explained by plagioclase fractionation although it is difficult to quantify the amount of plagioclase fractionation that is required to account for the anomaly as parameters relating to the Kd of Eu in plagioclase are poorly constrained. From the least-squares predictions, for the stage from 24019 to 24016, olivine-clinopyroxene-plagioclase-magnetite were removed in the proportion 13-10-70-7. Plotted in Fig. 9.3 are REE patterns which could be expected for various minerals precipitating in the 24019 liquid as well as for 24019 itself. These are based on the REE concentrations of 24019 and Kd data for REE's for different phases taken from Hanson (1980). By rearranging Eqn. 9.1, a predicted REE pattern for various minerals can be calculated. It is clear from the patterns of plagioclase and clinopyroxene (olivine and magnetite have much less REE's) that removal of the above assemblage could only account for the Eu anomaly. In order to explain the deficit in REE's in 24016 by fractionation, a phase with much higher REE abundances and ideally one with a humped pattern relative to 24019 is required. REE patterns for sphene, amphibole and apatite, obtained as above, are also plotted in Fig. 9.3. In Chapter 7 it was suggested that apatite is the most likely phase to be responsible for the bowing. This would also tie in with the drop in P_2O_5 from mugearites to trachytes which is undoubtedly the result of apatite fractionation. From 24019 to 24016 it falls from 0.75-0.12% which, assuming a P_2O_5 content of 40% in apatite by mass balance, requires the removal of 2.175% apatite. In Fig. 9.3 the measured REE pattern for 24016 and calculated patterns for 24016 based on the least-squares predictions including the removal of 2% and 3% apatite are shown. The patterns produced adequately account for the bowing of the patterns and the 2% apatite pattern is in close agreement with the measured pattern. The assimilation of crust,

Fig. 9.3 Chondrite normalised REE plot showing REE patterns calculated for phases precipitating from a mugearitic liquid (24019). Also shown are the REE patterns of 24019 and 24016 (trachyte). 24019 is considered to be parental to 24016. In order to account for the relative loss of MREE, models in which inclusion of 2% and 3% apatite in the fractionating assemblage are considered.

2% : REE pattern in which 2% removal of apatite is accounted for.

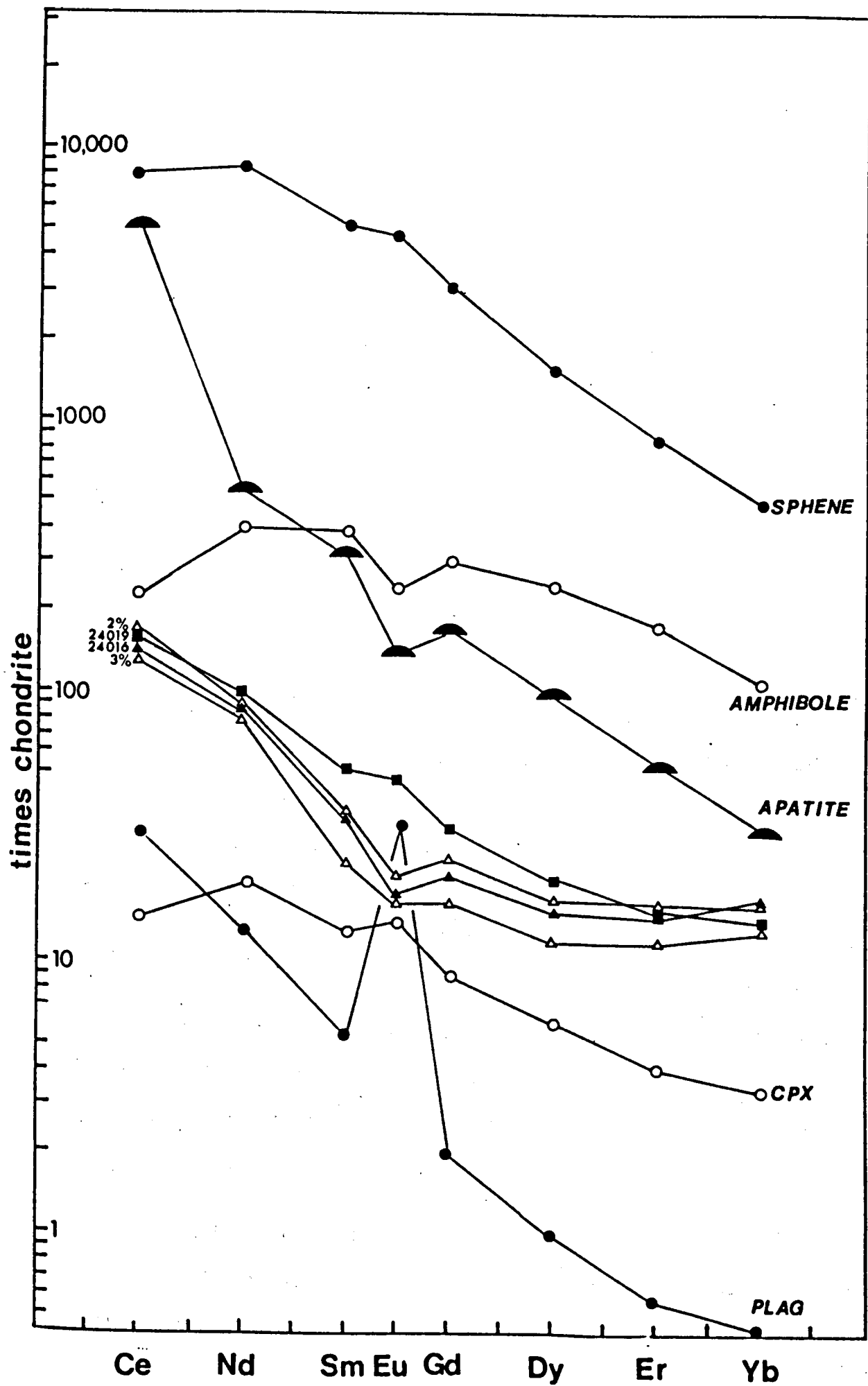
3% : REE pattern in which 3% removal of apatite is accounted for.

Note that 24016 REE pattern agrees reasonably well with the 2% apatite removal pattern.

REE patterns for plagioclase, clinopyroxene, apatite amphibole and sphene are calculated using Kd data from Hanson for respective minerals, REE measured composition of 24019 and by rearranging the equation:-

$$Kd = \frac{\text{concentration in mineral}}{\text{concentration in liquid}}$$

	Kd data used from Hanson (1980)					REE concentrations (ppm) in 24019
	PLAG	CPX	APATITE	AMPH.	SPHENE	
Ce	0.20	0.098	34.7	1.52	53.3	132.18
Nd	0.14	0.21	57.1	4.26	88.3	60.57
Sm	0.11	0.26	62.8	7.77	102	10.45
Eu	0.73	0.31	30.4	5.14	101	3.66
Gd	0.066	0.30	56.3	10.0	102	8.65
Dy	0.055	0.33	50.7	13.0	80.6	6.74
Er	0.041	0.30	37.2	12.0	58.7	3.42
Vb	0.031	0.28	23.9	8.4	37.4	3.02



relatively poor in P_2O_5 , will only alter the amount of apatite fractionation to a small extent. A further obvious feature of the diagram, which should sound as a warning, is the profound differential effect that small amounts of apatite fractionation can have on REE's.

For the New Series trachytes, the step from 24016-24020 overestimates the amount of fractionation. A better estimate for F can be made by assuming the proportions in which the phases fractionate are broadly correct (90% anorthoclase, 5% clinopyroxene and 5% magnetite, in which case the amount of fractionation can be calculated. This can be achieved by taking the enrichments (C_L/C_0) from the measured analyses and D values obtained from the above proportions, and then by rearranging the Rayleigh equation (Eqn. 9.1) in terms of F . The values for F , which are derived for each REE, except Eu, are in very close agreement with one another. The disparity with Eu reflects the uncertainty in K_d for Eu in potassium feldspar. Taking an average for the F values (0.603), a calculated REE pattern for 24020 can be obtained from Eqn. 9.1. Plotted to Fig. 9.4 are the measured patterns for both 24016 and 24020. The measured pattern and the calculated pattern for 24020 are essentially the same except for small differences in Ce, Eu and Gd. In the interests of clarity only these points for the calculated pattern are drawn. The equivalence of the model with the measured pattern is circumstantial evidence that these New Series trachytes evolved, principally, by anorthoclase fractionation.

9.3.6 Normalised Trace Element Diagrams

The advance of rapid trace element analytical techniques coupled with an increased knowledge of trace element K_d 's in mantle material

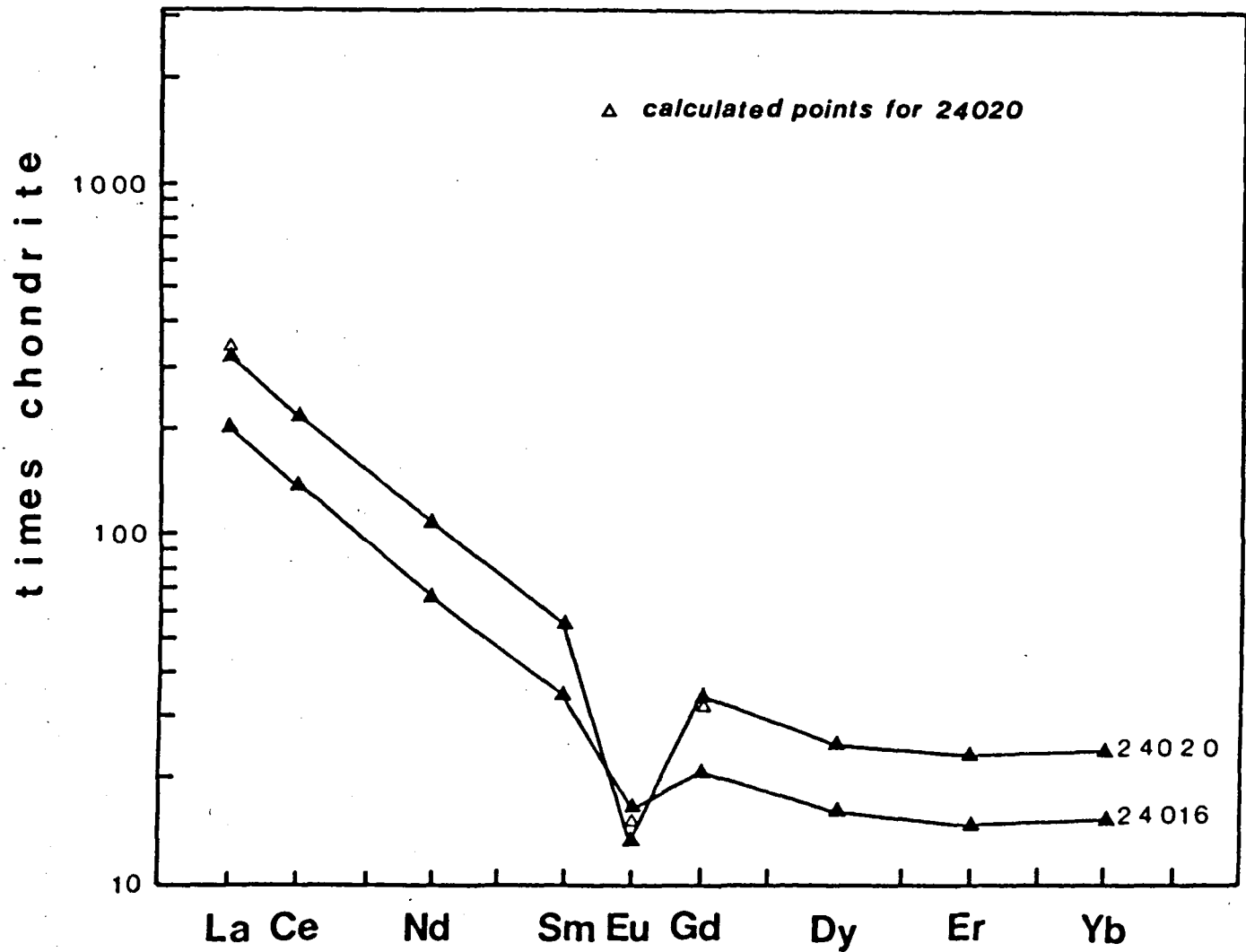
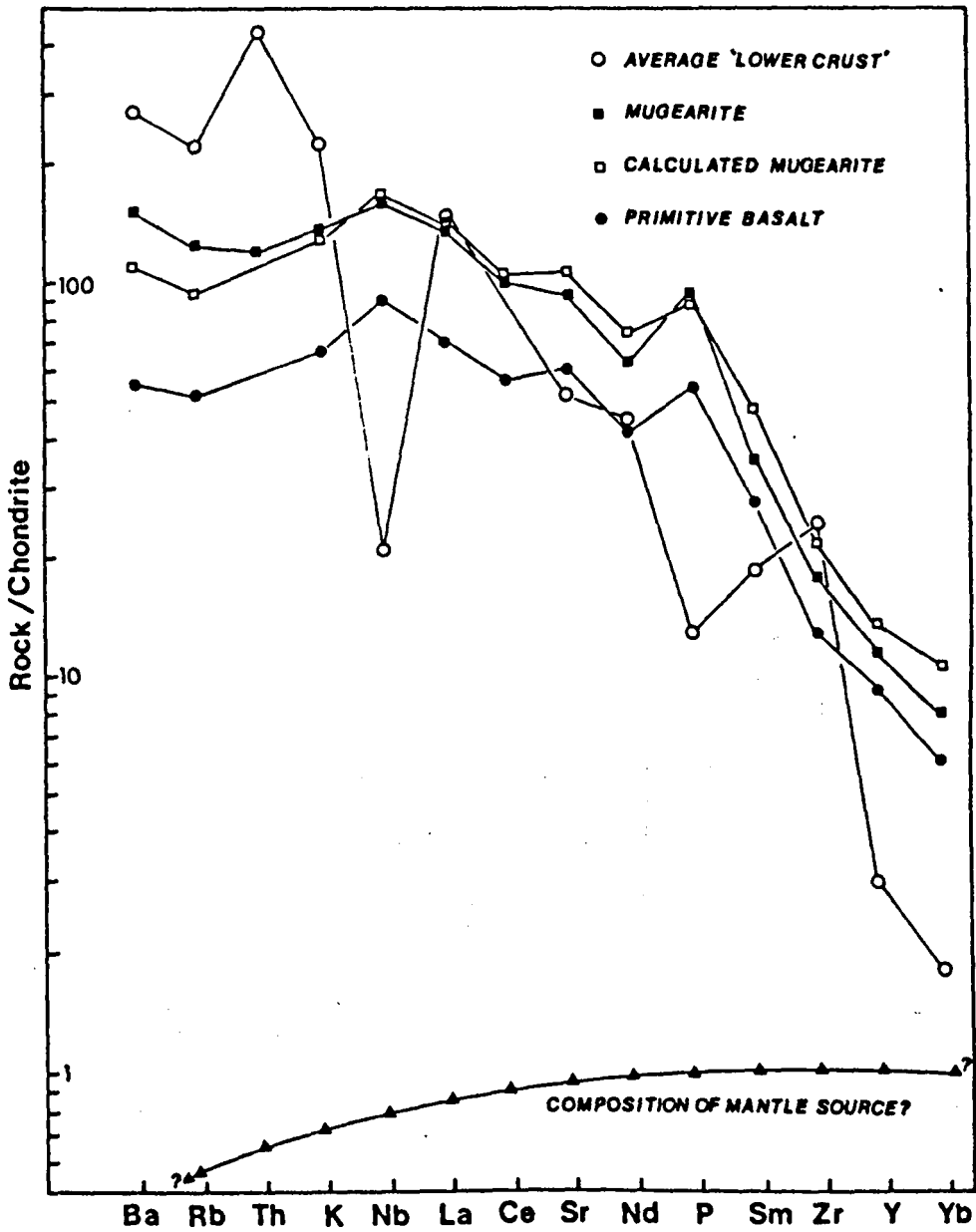


Fig. 9.4 Measured REE patterns for 24016 and 24020. A REE pattern calculated using the Rayleigh equation, for 24020, nearly coincides with the measured pattern. Those points which are appreciably different are indicated by open triangles.

has promoted their representation on 'mantle' normalised graphs (or spidergrams) in the same way as REE's are. This treatment enables the geochemical character of areas, suites or individual rocks to be compared with one another. The normalising values used here are those collated from several sources by Thompson (1983) and are compiled in Table E3. The elements are plotted along the x axis in an order which gives the smoothest curve to the graph and are increasingly incompatible from right to left. Fig. 9.5 shows a spidergram for average primitive Jebel Marra basalts. The pattern is typical of many continental regions e.g. Kenya, Cameroon Line (Norry and Fitton, 1983) Snake River Plain (Leeman and Vitaliano, 1976). The patterns rise gently from Ba to a peak at Nb, before falling to less incompatible elements. In Chapter 8, it was concluded that these are typical patterns for uncontaminated primitive alkali basalts from continental provinces and ocean islands alike. Furthermore, assuming the order of incompatibility is broadly correct, then such a pattern could be produced from source which is depleted, particularly in most incompatible elements, Rb, Ba, K etc., relative to chondrite; this is schematically illustrated in Fig. 9.5. If the source was chondritic then a pattern decreasing from left to right would be anticipated, instead of one that increases from Ba to Nb before decreasing to Yb. The depleted nature of the source is in agreement with isotopic data for primitive basalts (Chapter 8). Also plotted in Fig. 9.5 is the measured pattern for primitive mugearites. Fractionation of olivine and clinopyroxene should not affect the incompatible ratios of most of these elements although from earlier discussions it is clear that some ratios are upset. To illustrate the extent of this deviation, the calculated mugearite pattern from the weighted least-squares results is also plotted. Elements Ba, Rb, Th and K are all higher in

Fig. 9.5 Spidergram showing patterns for primitive basalt, mugearite and average lower crust. Also plotted is the calculated pattern for mugearite. Differences between the measured and calculated patterns for mugearite can often be accounted for by considering a contribution from the crust; only Zr disagrees significantly from this scheme. A depleted source is also represented schematically.



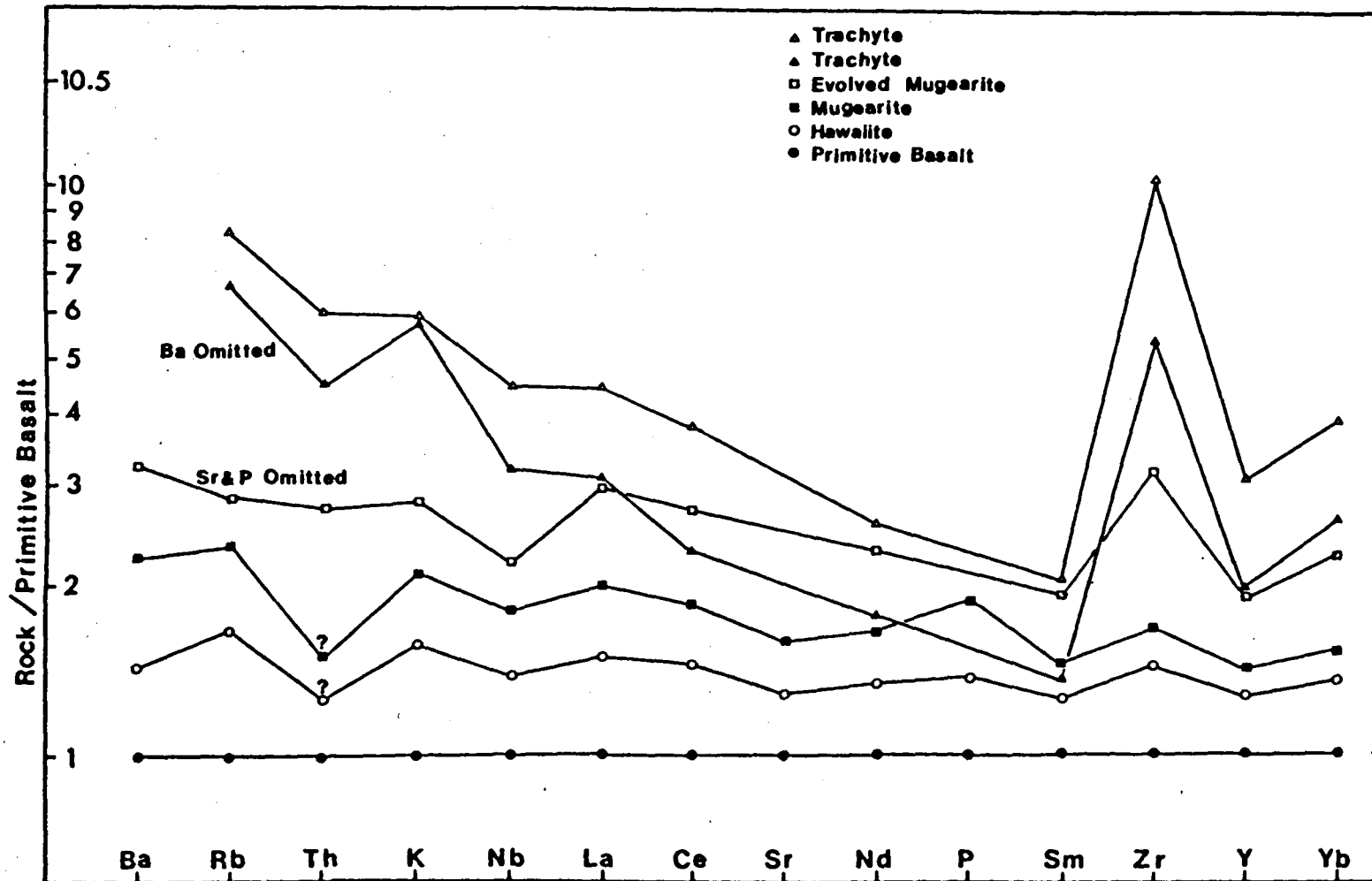
the measured mugearite pattern than the calculated mugearite pattern. Nb, P, La and Ce are approximately equal in this example while Sm, Nd, Zr, Y and Yb are less. In addition average 'lower crust' (average of 24037, 24135 and 24137) is plotted which largely mirrors the deviations fairly closely. That is Ba, Rb, Th, K, La and Zr are all enriched in the crust relative to the calculated pattern whereas Nb, Ce, Sm, P, Y and Yb are all relatively poor in the crust. Only Zr shows any major disagreement with the concentration required from the crustal rock although Nb and Y appear to be much lower in the crustal sample than is indicated by the difference between the calculated and measured patterns.

In order to appreciate the relative effects of fractionation and other processes Fig. 9.6 illustrates patterns for various New Series rocks for incompatible elements normalised to primitive basalt. Many of the features previously pointed out are again present. For example, the greater increase in Ba, Rb, and K, relative to Nb, Sm, Y and Yb is apparent. Imposed on this are effects of fractionation. The depletion in REE's, Y and P due to apatite fractionation from mugearites to trachytes is evident, as is the retardation in Rb and K in trachytes due to anorthoclase fractionation. These effects are in addition to the marked depletions in Ba, Sr and P which are omitted from the diagram as they become compatible in the interests of clarity. Of more interest is the increase in enrichment that occurs to Zr which is discussed below.

9.3.7 Behaviour of Zr

In previous sections, the sudden enrichment of Zr between primitive mugearites and evolved mugearites has been noted (especially

Fig. 9.6 Samples normalised to primitive basalt. Note the sudden enrichment of Zr relative to other elements at the evolved mugearite stage.



evident in Fig. 9.6). This abrupt increase at the evolved mugearite stage in Zr is problematical. It is partly explained by the decrease in D due to less clinopyroxene fractionation but the fact that the increase in Zr is maintained in acidic rocks, and by analogy with Rb and Ba, suggests that a Zr rich crust is assimilated or zircons have been accumulated from the crust. This change in Zr enrichment coincides with the purported change in the contamination environment from lower to upper crust (see Chapter 8) and could possibly be used as evidence for the assimilation of a different contaminant: one which is relatively rich in Zr. Other reasons for the change in behaviour could include a departure from a closed system fractionation model. With regard to the last point, O'Hara (1968) has developed an open system fractionation model in which eruption and input of new magma (not necessarily of the same composition) are taken into consideration. O'Hara (op. cit.) shows that if the number of cycles is great then decoupling of very incompatible elements from incompatible elements can occur; although in this case no other highly incompatible elements appear to be affected in such a way.

9.4 Crustal Contamination

Until now the variations in the data have been viewed from the sense that the overriding process causing elemental variations is fractional crystallisation with an additional contribution from crustal assimilation. It is now appropriate to change the emphasis by examining the effects of contamination in conjunction with fractional crystallisation more closely and assessing its influence on trace elements as well as on isotopic ratio variations.

The isotopic data strongly suggest that the majority of the variations in isotopic composition are the result of varying amounts

of crustal contamination. Given a data set which displays a coherent trend it is often possible, using crustal contamination models, to partially constrain the contaminant(s) and the amount of contamination. The two mixing models which are discussed here are simple mixing (DePaolo and Wasserburg, 1979) and AFC (DePaolo 1981).

9.5 Simple Mixing (Bulk Assimilation)

Isotopic variations in $^{87}\text{Sr}/^{86}\text{Sr}$ and $^{143}\text{Nd}/^{144}\text{Nd}$ caused by simple mixing of crust depend on the isotopic composition and the elemental concentration of Sr and Nd in the end-members and the weight proportion of crust assimilated. Although, in Chapter 8 much of the data was interpreted in terms of AFC, it is useful to discuss simple mixing models, with regard to Nd-Sr isotopic variations, because in basic rocks when DNd and DSr are small and of similar magnitude simple mixing curves closely mimic AFC curves.

The equation of the mixing curve of two components A and B are described by DePaolo and Wasserburg (1979) are formulated using the ϵ notation of DePaolo and Wasserburg (1977). The ϵ notation expresses the departure in isotopic composition of Nd and Sr from "uniform reservoir" values which are assigned ϵ values of zero. They can be calculated for Nd from the following equation:-

$$\epsilon_{\text{Nd}} = \left(\frac{^{143}\text{Nd}/^{144}\text{Nd} \text{ (measured)}}{^{143}\text{Nd}/^{144}\text{Nd} \text{ (CHUR)}} - 1 \right) \times 10^4 \quad \text{Eqn. 9.2}$$

CHUR is the chondritic uniform reservoir and at present (T=0) is taken to be 0.51264. No age correction to $^{143}\text{Nd}/^{144}\text{Nd}$ is necessary.

There is an analogous expression for ϵ_{Sr} but, in this instance, allowance has to be made for data which requires age correction in both $^{87}\text{Sr}/^{86}\text{Sr}$ and $^{87}\text{Rb}/^{86}\text{Sr}$ (UR) values:-

$$6\text{Sr} = \frac{{}^{87}\text{Sr}/{}^{86}\text{Sr} (\text{initial})}{{}^{87}\text{Sr}/{}^{86}\text{Sr} (\text{UR}) - {}^{87}\text{Rb}/{}^{86}\text{Sr}(\text{UR})(e^{\lambda t} - 1)} \times 10^4 \quad \text{Eqn. 9.3}$$

where ${}^{87}\text{Sr}/{}^{86}\text{Sr}(\text{UR})$ is the uniform reservoir

which at present ($T=0$) = 0.7045

${}^{87}\text{Rb}/{}^{86}\text{Sr}(\text{UR}) = 0.0839$

$\lambda = 1.42 \times 10^{-11}$

t = age in years

Using the G notation $G\text{Nd}$ of a mixture $G\text{Nd}(\text{mix})$, of two components A and B is given by the following equation of DePaolo and Wasserburg (1979):-

$$G\text{Nd}(\text{mix}) = \frac{X_A / \text{Nd}/_A (G\text{Nd})_A + (1-X_A) / \text{Nd}/_B (G\text{Nd})_B}{X_A / \text{Nd}/_A + (1-X_A) / \text{Nd}/_B} \quad \text{Eqn. 9.4}$$

where

X_A = weight proportion of component A

$/\text{Nd}/_A$ = concentration of Nd in A

$/\text{Nd}/_B$ = concentration of Nd in B

$(G\text{Nd})_A$ = $G\text{Nd}$ of A

$(G\text{Nd})_B$ = $G\text{Nd}$ of B

The $6\text{Sr}(\text{mix})$ may be obtained from an identical expression in terms of Sr.

The shapes of the curves described by this equation are dependent on the concentrations of Sr and Nd in the end-members which may be expressed by the parameter K:-

$$K = \frac{(\text{Sr}/\text{Nd})_A}{(\text{Sr}/\text{Nd})_B} \quad \text{Eqn. 9.5}$$

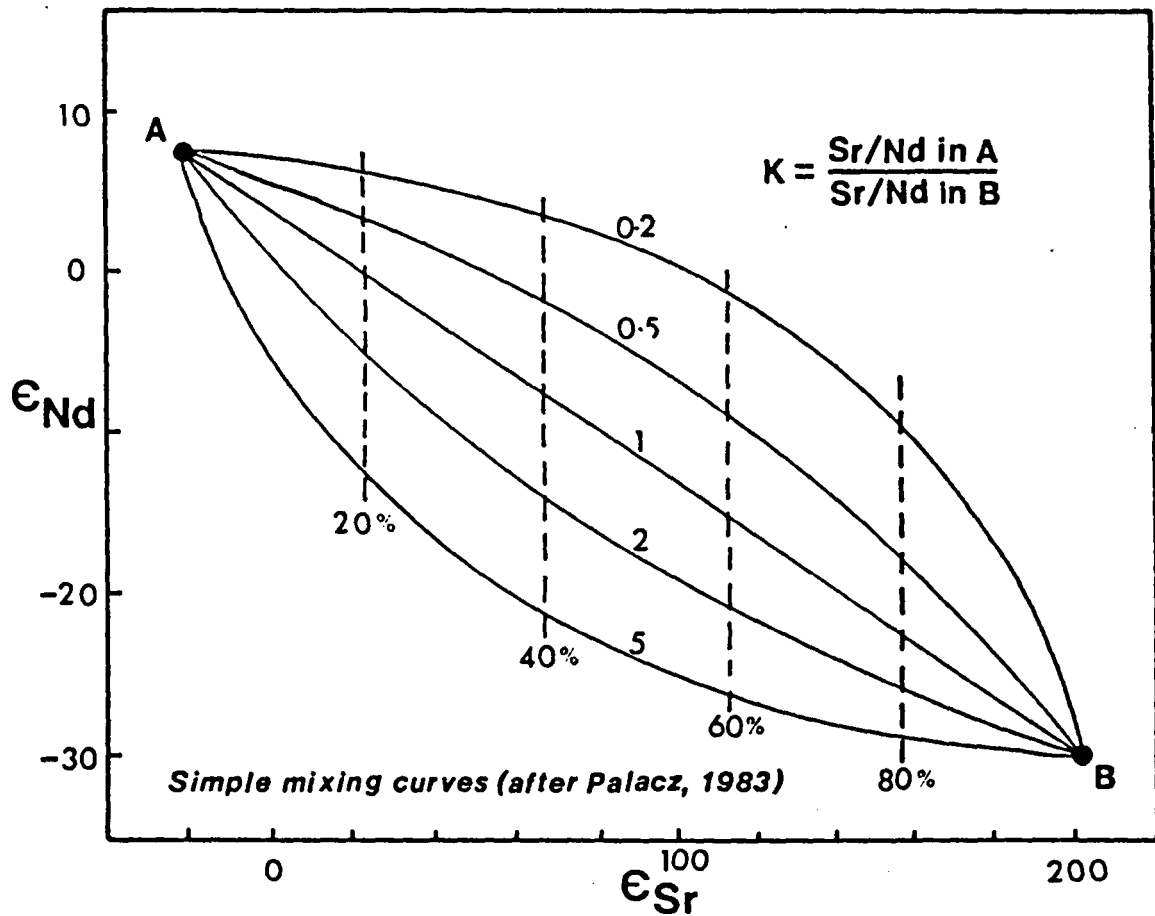


Fig. 9. 7 Range in hyperbolae for simple mixing for two end-members A and B. K values are indicated on the curves. Dashed lines represent amount of B in A. Different K curves are obtained by varying Sr concentration; Nd concentration is kept constant. (redrawn from Palacz, 1983).

The range of hyperbolae expected for different K's are illustrated in Fig. 9.7 (from DePaolo and Wasserburg, 1975, Fig. 1). When $K=1$, a straight line results. In most natural cases $K > 1$ as the Sr/Nd of a basic magma is usually greater than the Sr/Nd of the crust.

9.5.1 Simple Mixing Results

9.5.1.1 New Series

Using Eqn. 9.4, curves for simple mixing are plotted in Fig. 9.8 for crustal samples using the information in Table 8.1. In addition, the isotopic data from the New Series suite are plotted. It is apparent that if simple mixing is the process which caused the isotopic variations then 'upper crustal' rocks (i.e. 24036, 24134, 24138 and 24139; defined in Chapter 8) cannot have been largely responsible. Only 'lower crustal' rocks and principally, 24037 and 24137 have suitable end-member characteristics to account for the data by simple mixing.

It is possible to invert Eqn. 9.4 to contour potential contaminant regions in ϵ_{Nd} and ϵ_{Sr} space in terms of R (Powell, in press), where R is $Sr/Nd(B)/Sr/Nd(A)$ and is thus the reciprocal of K in Eqn. 9.5. This is given by the following equation:-

$$\epsilon_{Nd} = \frac{\epsilon_{Nd_A} (\epsilon_{Sr_B} - \epsilon_{Sr}) - \frac{1}{R} \epsilon_{Nd_B} (\epsilon_{Sr_A} - \epsilon_{Sr})}{(\epsilon_{Sr_B} - \epsilon_{Sr}) - \frac{1}{R} (\epsilon_{Sr_A} - \epsilon_{Sr})} \quad \text{Eqn. 9.6}$$

symbols as before.

In order to do this, it is necessary to specify ϵ_{Sr} in A from which ϵ_{Nd} can be found by calculating a regression line for the data array. From this the slope and axis intercepts can be attained such that:-

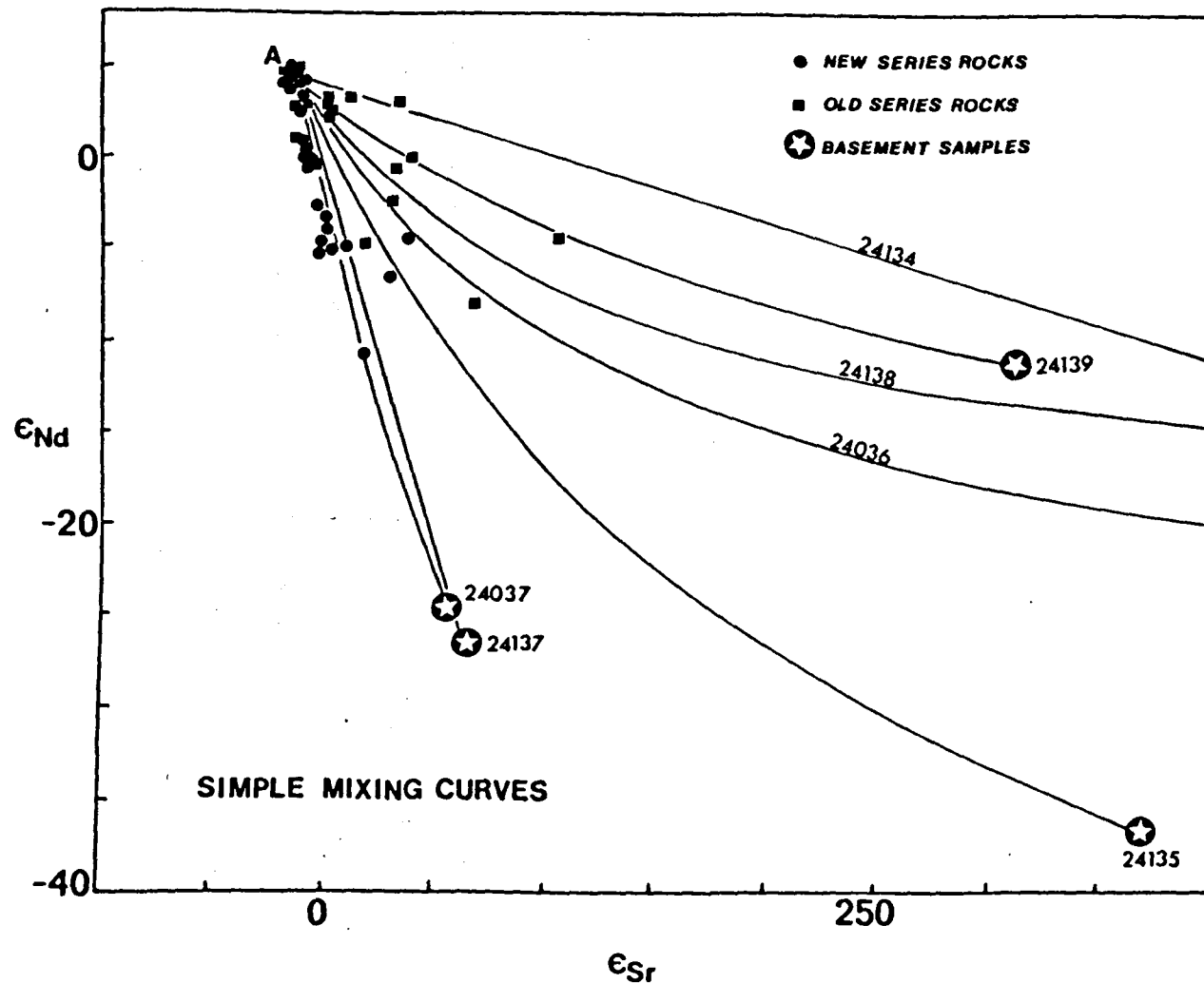


Fig. 9.8 Simple mixing curves drawn using end-member characteristics given in Table 8.1. A represents New Series magmatic end-member.

$$\text{Slope } S = \frac{\delta \epsilon_{Nd}}{\delta \epsilon_{Sr}} = \frac{1}{R} \left(\frac{\epsilon_{Nd}_B - \epsilon_{Nd}_A}{\epsilon_{Sr}_B - \epsilon_{Sr}_A} \right) \quad \text{Eqn. 9.7}$$

symbols as before.

This relies on the data array approximating to a straight line which for Jebel Marra is the case for the majority of the trend. For this reason, the data for more evolved rocks have been omitted as they deviate from the main body of data and, if included in the regression calculation, would significantly alter the slope of the line. Reasons for their departure from the main body of the data have been discussed in Chapter 8.

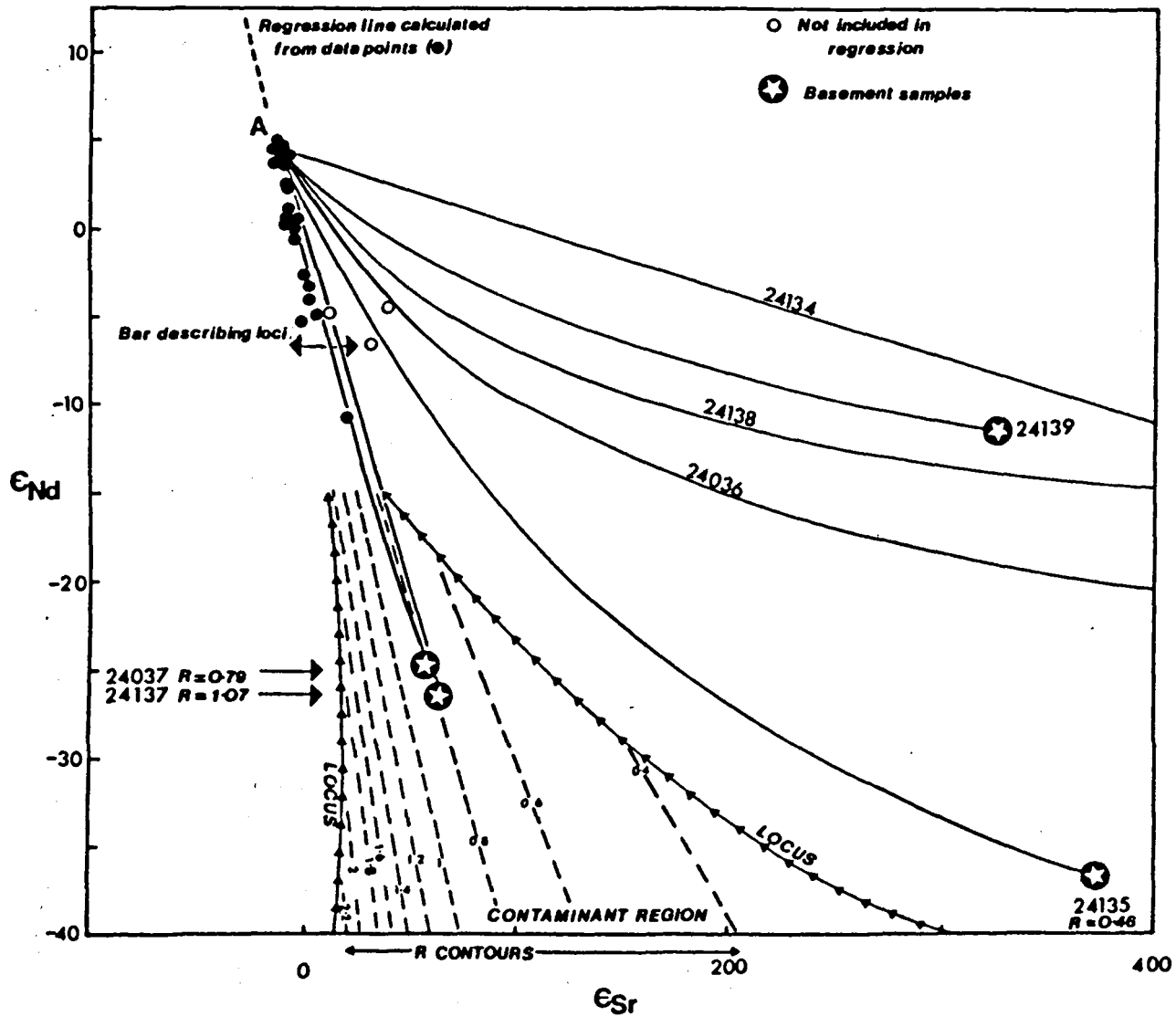
In Fig. 9.9 mixing curves are drawn by CMM ALGOL68 (R Powell, unpub.) for 'lower crustal' samples. Using Eqns. 9.6-7 the contaminant region can be contoured in terms of R. Therefore, crustal samples (possible contaminants) can be plotted and their estimated R values and the contour R values can be compared. From Fig. 9.9 both 24037 and 24137 have R estimated values similar to the contour values whereas the R of 24135 is much different. On this basis, 24135 could be reasonably eliminated as a likely contaminant because only samples with R's close to the R contour values can describe mixing curves which will have slopes in the vicinity of the magmatic end-member close enough to that of the data array.

Some constraint on the size of the contaminant region can be obtained by specifying the maximum departure of the trend in terms of ϵ_{Sr} , simply by erecting a bar at the bottom of the data array. Loci constraining the contaminant region are calculated by combining Eqns. 9.6-7. Only samples which plot within these loci, which have the

Fig. 9.9 Simple mixing curves for New Series rocks
contoured in terms of R

- Filled circles : Samples used in calculation of regression line.
- Open circles : Samples off main trend and not used in calculation of regression line.
- Regression line (thick dashed line) : Calculated from filled circles and by specifying δSr of A.
- A : Magmatic end-member.
- Contaminant region : Area within loci (between barbed lines) which samples of appropriate R value and isotopic composition can describe mixing curves which can satisfy the majority of the data (filled circles).
- Dashed lines : R contours (R values marked) which would describe curves which satisfy most of the data (filled circles). For example 24037 has an R value (0.79) close to the preferred R contour value (0.8) and accordingly describes a curve which satisfies most of the data (filled circles).
- Bar describing loci : At base of data array a bar is erected from which the loci are calculated (see text).

In general, most of the basement samples are unable to generate simple mixing curves which can satisfy the data array. Only samples 24037 and 24137 have the necessary isotopic and Sr/Nd characteristics capable of this.



necessary isotopic characteristics and R values, can possibly generate mixing curves which will pass through the majority of the data. The locii of contaminants are drawn in Fig. 9.9, because 24135 plots outside the locii it can again be eliminated as a likely contaminant.

The three points omitted from the regression line calculation are difficult to explain by simple mixing of the New Series primary magma in view of the position of the locii of reasonable contaminants drawn in Fig. 9.9. An alternative explanation is required to account for these (see Chapter 8).

9.5.1.2 Old Series

The data for the Old Series rocks are less well constrained than the New Series rocks and as a result only semi-quantitative comments can be made. Some of the data follow the trend of the New Series rocks and have presumably been affected in a similar way. Most of the rocks define a broad trend, comprising mainly acidic rocks, towards radiogenic $^{87}\text{Sr}/^{86}\text{Sr}$ compositions. Fig. 9.8 shows that many of these samples lie on mixing curves for 'upper crustal' rocks using the magmatic end-member given in Table 8.1.

Bulk assimilation of crust by a magma can be tested further using major and trace elements. In this instance, simple mixing will produce a straight line between the two end-members from the mass balance equation:-

$$\text{Co mixture} = X (\text{Co in magma}) + (X-1) (\text{Co in crust}) \quad \text{Eqn. 9.8}$$

where

Co = concentration of element or oxide

X = weight proportion of magma

Simple mixing curves have been drawn in Figs. 8.8a-b which suggest that while simple mixing of crustal types like 24037 and 24137 can satisfy the variations in Nd and Sr isotopes they cannot explain the majority of the major and trace element data (see section 8.4.3). Similarly, while assimilation of 'upper crustal' samples can satisfy, in a general way, the isotopic variations observed in many of the Old Series evolved rocks, again there is a discordance with major and trace element concentrations. Therefore it is necessary to interpret the data in terms of a model which can account for both the isotopic and elemental variations by a process involving crustal contamination and fractional crystallisation.

9.6 Combined Assimilation and Fractionation (AFC)

In Chapter 8, the data have been qualitatively interpreted for AFC. It is proposed using the AFC equations to produce models which can be compared with the observed data trends.

DePaolo (1981) has formulated several equations which model the behaviour of trace elements and isotopic ratios for AFC. This model is based on the notion that wall-rock assimilation and fractional crystallisation although commonly treated separately, are from thermal considerations, coupled. This is because the heat required for assimilation is available from the latent heat of crystallisation (DePaolo, 1981; see further discussion in Chapter 8).

9.6.1 AFC Equations

9.6.1.1 Elemental Concentrations

According to DePaolo (op. cit.), the rate of change of an element C_m with respect to time is given by the expression:-

$$\frac{dC_m}{dt} = \frac{M_a^1}{M_m} (C_a - C_m) - \frac{M_c^1}{M_m} (D-1) C_m \quad \text{Eqn. 9.9}$$

where

C_a = concentration of an element in the contaminant

C_m = concentration of an element in the magma

M_a^1 = rate of assimilation

M_c^1 = rate of fractional crystallisation

D = bulk distribution coefficient of the element

M_m = mass of magma

When the rate of assimilation is balanced by the rate of fractionation the equation reduces to:-

$$\frac{dC_m}{dt} = \frac{M_a^1}{M_m} (C_a - DC_m) \quad \text{Eqn. 9.10}$$

This is a situation analogous to zone refining. Usually $M_a^1 \neq M_c^1$, but a more useful equation is obtained by assuming constancy of M_a^1/M_c^1 expressed as r . Using this assumption Eqn. 9.10 can be rewritten as:-

$$\frac{dC_m}{d \ln F} = \frac{r}{r-1} (C_a - zC_m) \quad \text{Eqn. 9.11}$$

Where

$$z = \frac{r + D + 1}{r-1} \quad \text{Eqn. 9.12}$$

$$r = \frac{M_a^1}{M_c^1}$$

M_m^0 = initial mass of magma

Integration of this equation yields the results:-

$$\frac{C_m}{C_m^0} = F^{-2} + \left(\frac{r}{r-1} \right) \frac{C_a}{zC_m^0} (1 - F^{-2}) \quad \text{Eqn. 9.13}$$

Large departures from pure fractional crystallisation can occur when $D \ll 1$ especially when C_a/C_m^0 is large. This commonly applies for the elements Ba, Rb, K, Th and Pb. This departure increases as r becomes larger. For elements with $D > 1$, departures from fractional crystallisation are most apparent when F is small.

9.6.1.2 Isotopic Ratios

For isotopic ratios expressed by δ notation a differential equation can be obtained which on integration give the result:-

$$\frac{\delta_m - \delta_m^0}{\delta_a - \delta_m^0} = 1 - \left(\frac{C_m^0}{C_m} \right) F^{-2} \quad \text{Eqn. 9.14}$$

where

δ_m = isotopic ratio in the magma

δ_m^0 = isotopic ratio in the original magma

δ_a = isotopic ratio in the contaminant

C_m is obtained from Eqn. 9.13

If D_{Nd} and D_{Sr} are of similar magnitude then AFC trajectories will largely mimic simple mixing trajectories. But, if they differ significantly and particularly if one is > 1 then radical deviations from simple mixing may result. In the New Series the shift to radiogenic $^{87}\text{Sr}/^{86}\text{Sr}$ compositions in the evolved trachytes is interpreted to be due to $D_{Sr} \gg D_{Nd}$. Moreover, the K parameter which controls the curvature in simple mixing curves is not the only, and may not be the major, factor controlling curvature in AFC.

9.6.2 AFC Modelling

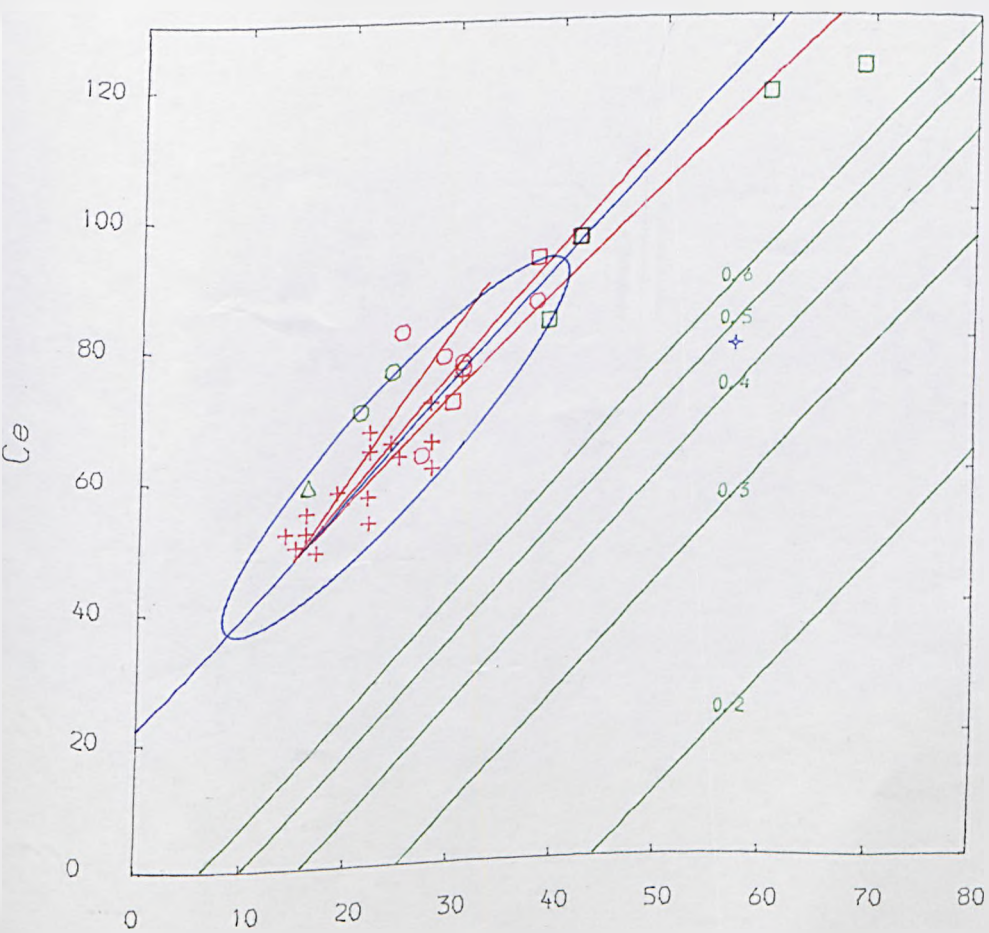
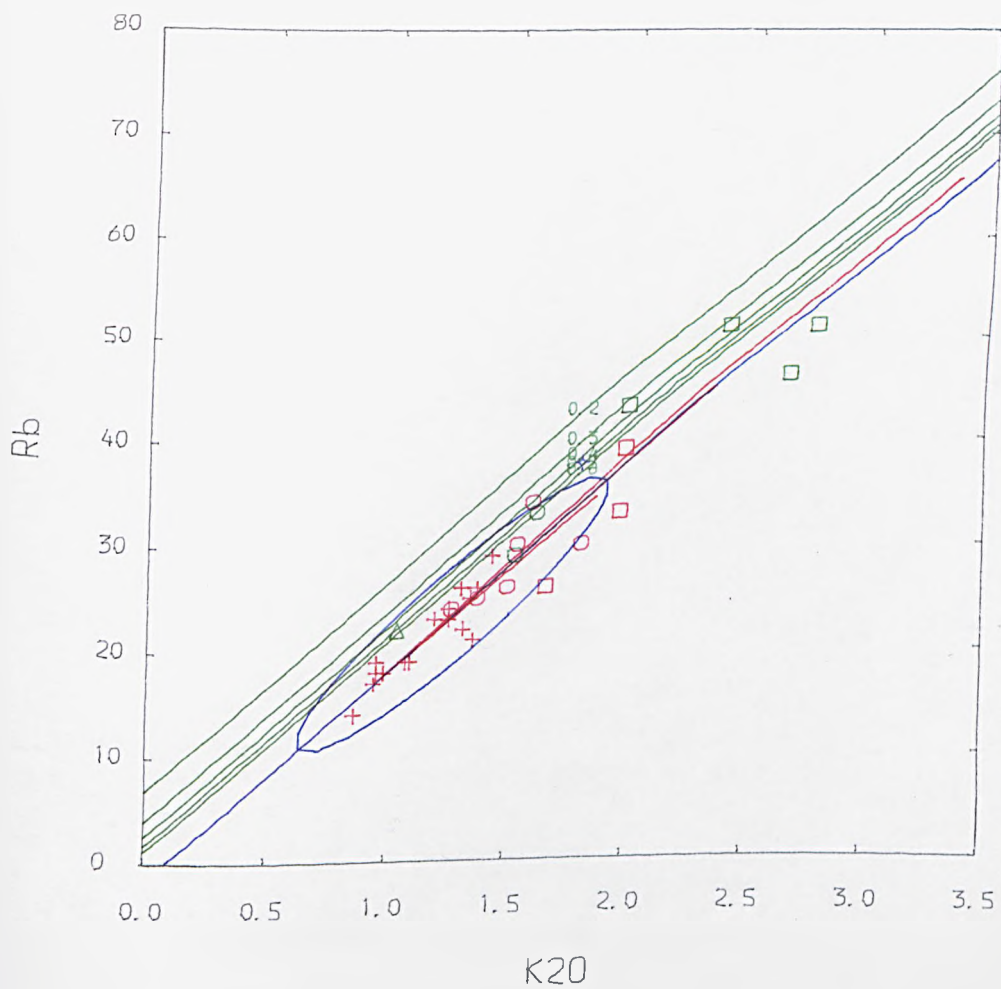
For AFC, two different parameters are introduced which are D and r . D 's can be reasonably estimated from major and trace element models, but r is less tractable. DePaolo (1981), suggests a maximum for r of about 1 in the lower crust, while a maximum value of about 0.3 in the upper crust is suggested by Taylor (1980). Hitherto, likely values for r have been derived using the above guidelines for r or by plotting AFC trends with different r 's to compare with the observed data arrays (e.g. Carlson et al., 1981).

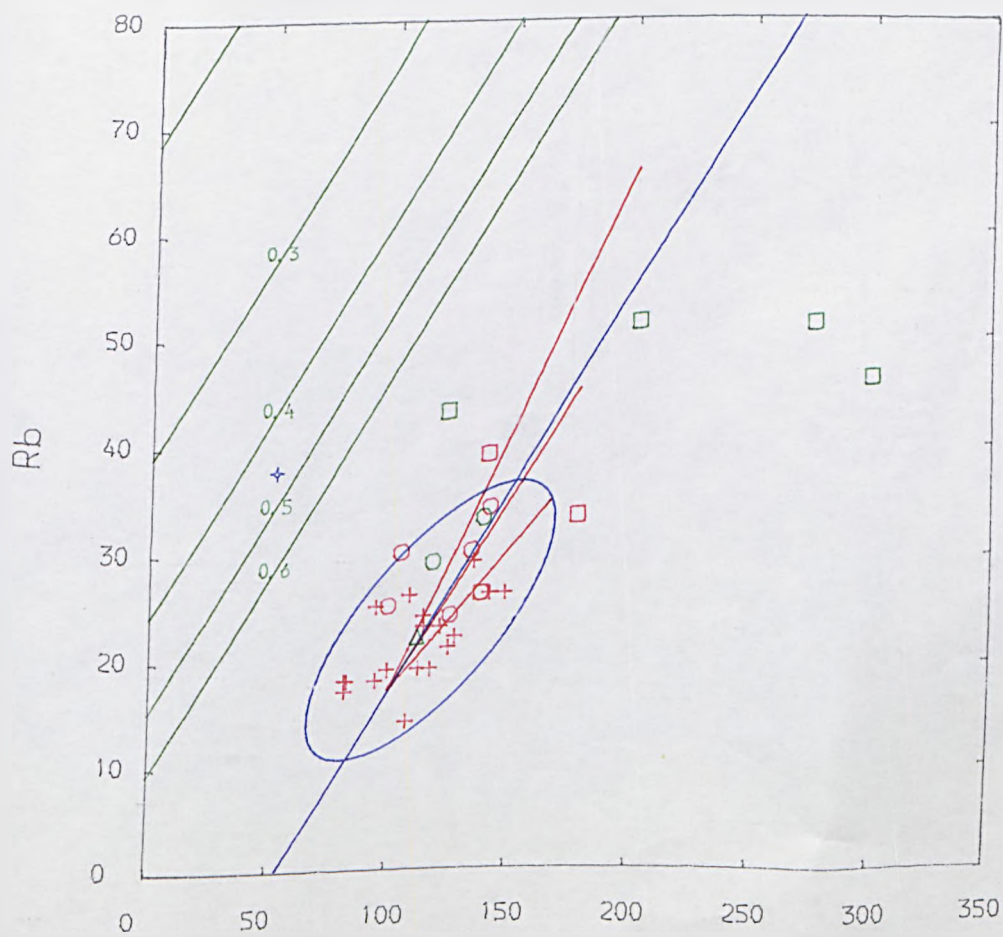
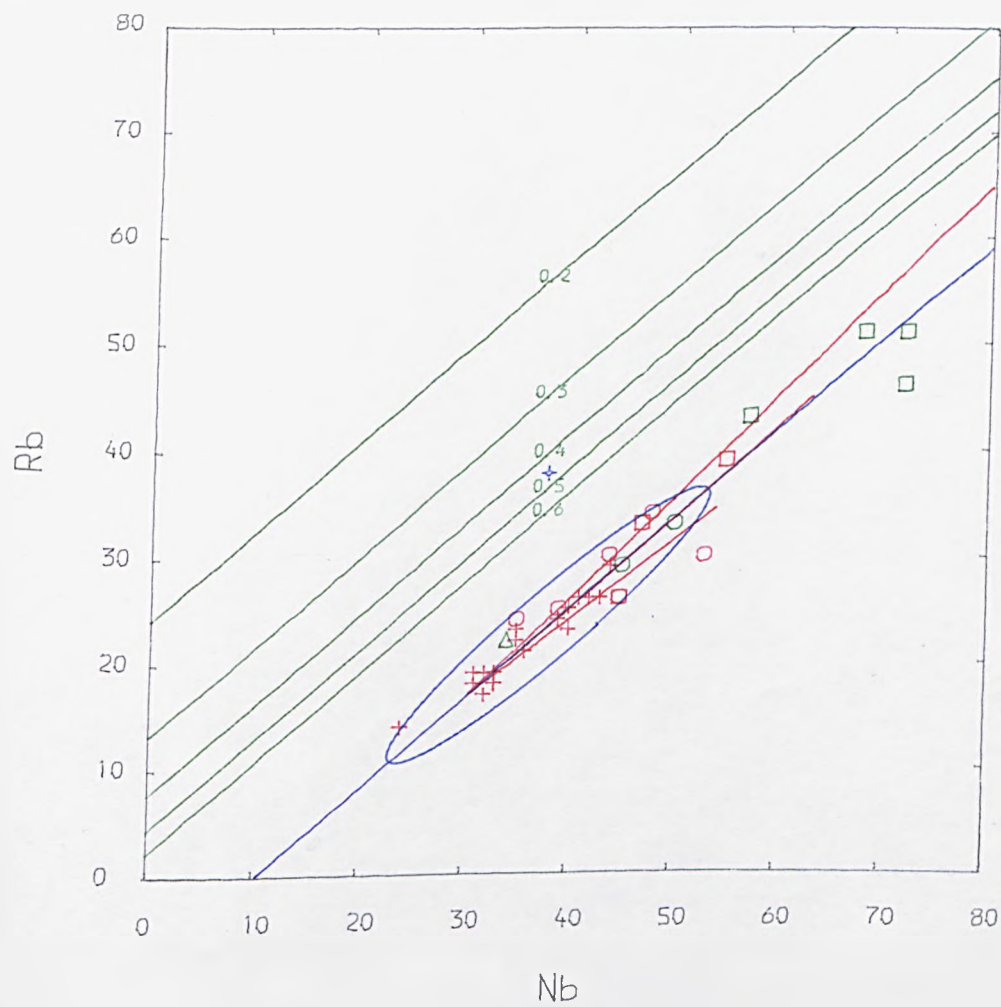
A quantitative approach to ascertain r by Powell (in press), involves considering the effects of AFC on trace element - trace element and isotope ratio - trace element relationships. An illustration of how AFC affects incompatible elements, for example, is shown in Figs. 9.10a-g. It can be seen that, in most cases, a projection of the data array does not intersect with the origin as would be expected if only fractional crystallisation has operated. Many such plots for the basic suite show the same effect. This indicates that a second order process has operated which, in this context, is interpreted to be assimilation occurring concurrently with fractional crystallisation. The problem is tackled quantitatively, by rearranging the AFC equations (DePaolo, 1981, of Eqn. 9.13) and by making use of the fact that in the vicinity of A (primitive magma end-member), the AFC trends are effectively linear. The AFC trends for $r=0.2$, 0.4 and 0.6 are also illustrated in Figs. 9.10a-g as red lines and demonstrate that the amount of curvature is slight. The curvature is dependent on r and the elemental composition of the end-members. The slope of an AFC trend for two elements at A can be obtained, e.g. for Nd and Sr (or any elements i), by combining Eqn. 9.13 for Nd and Sr,

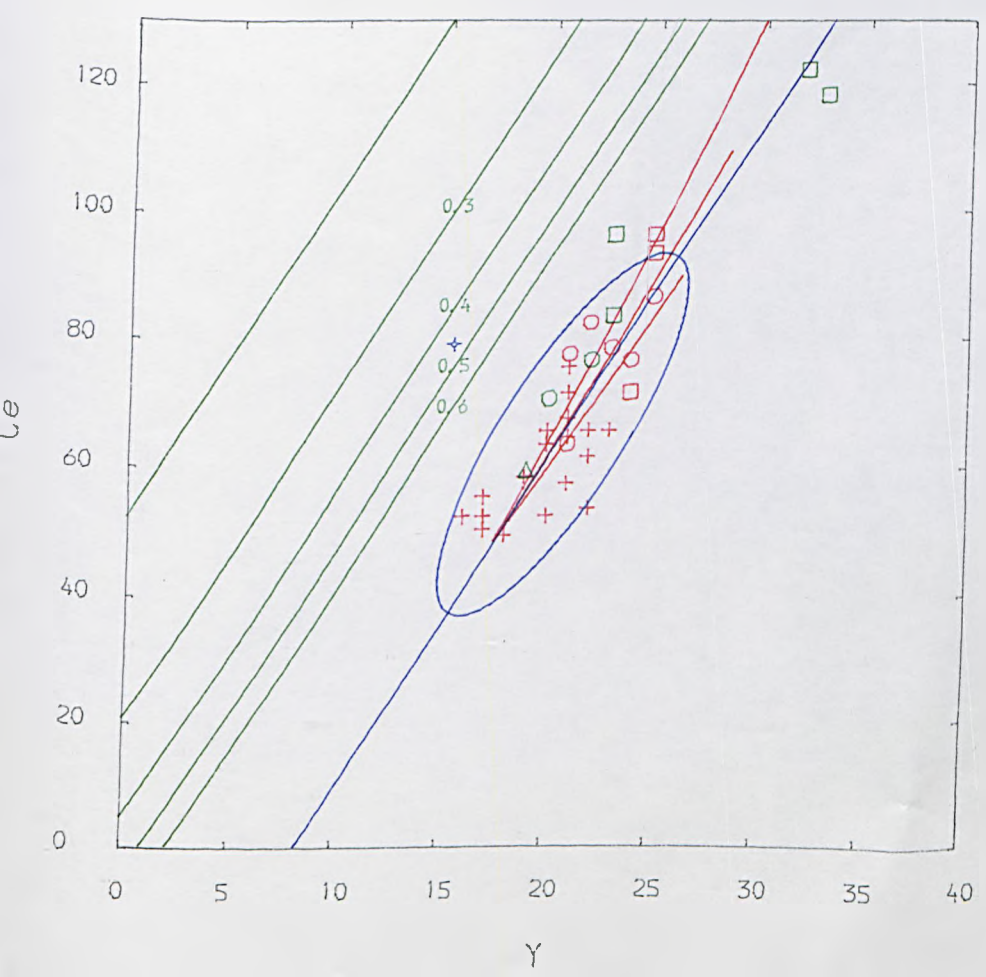
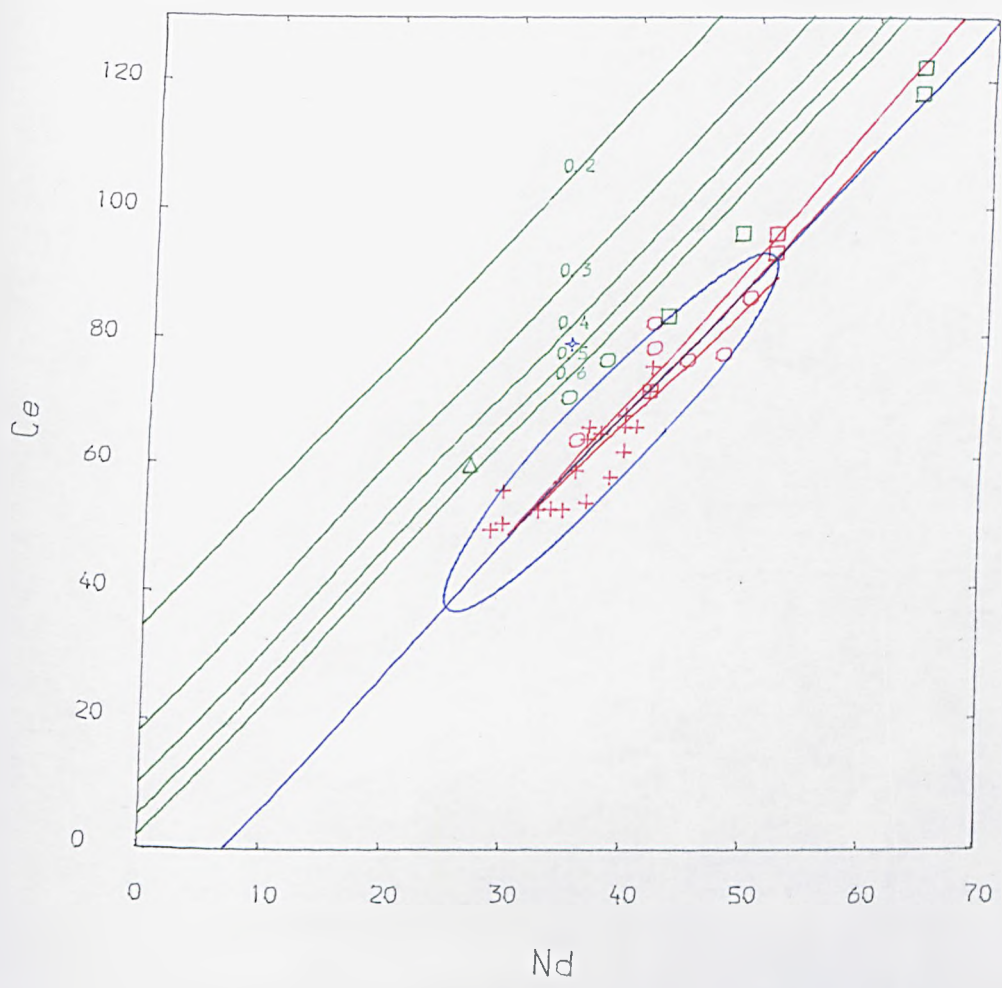
Figs. 9.10a-g AFC plots for selected incompatible elements for New Series basic rocks.

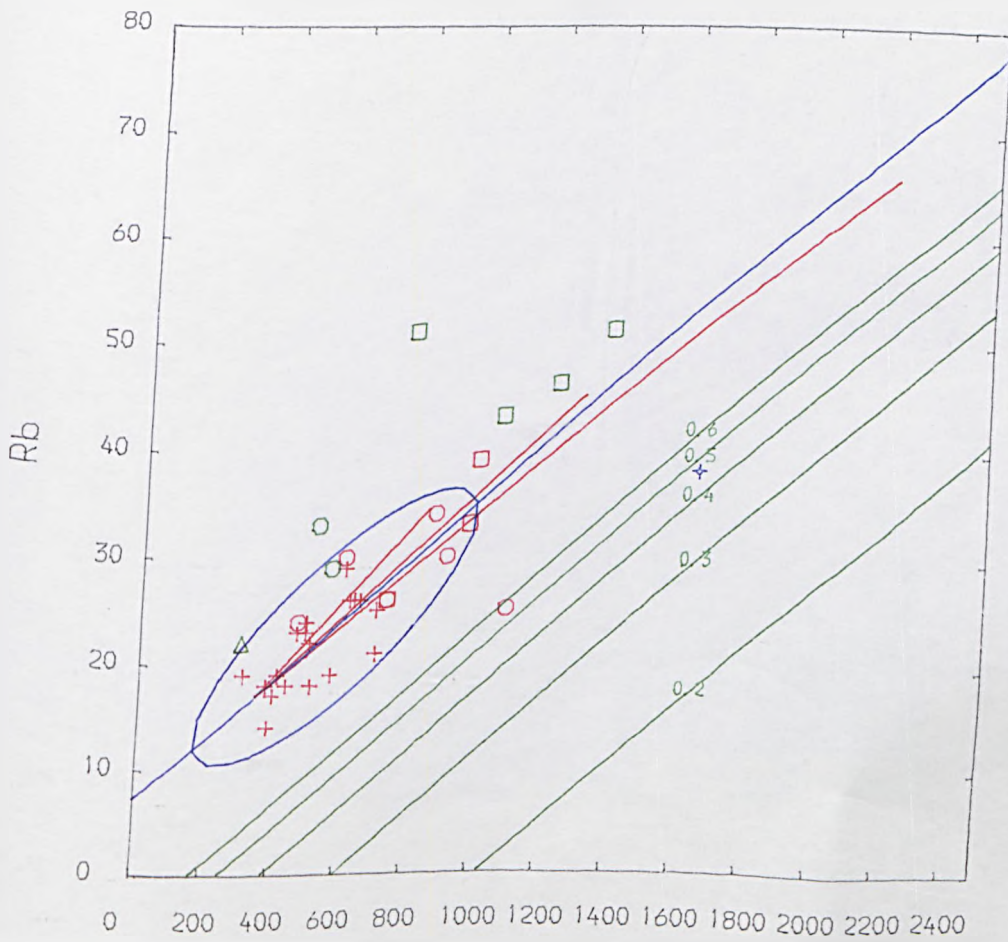
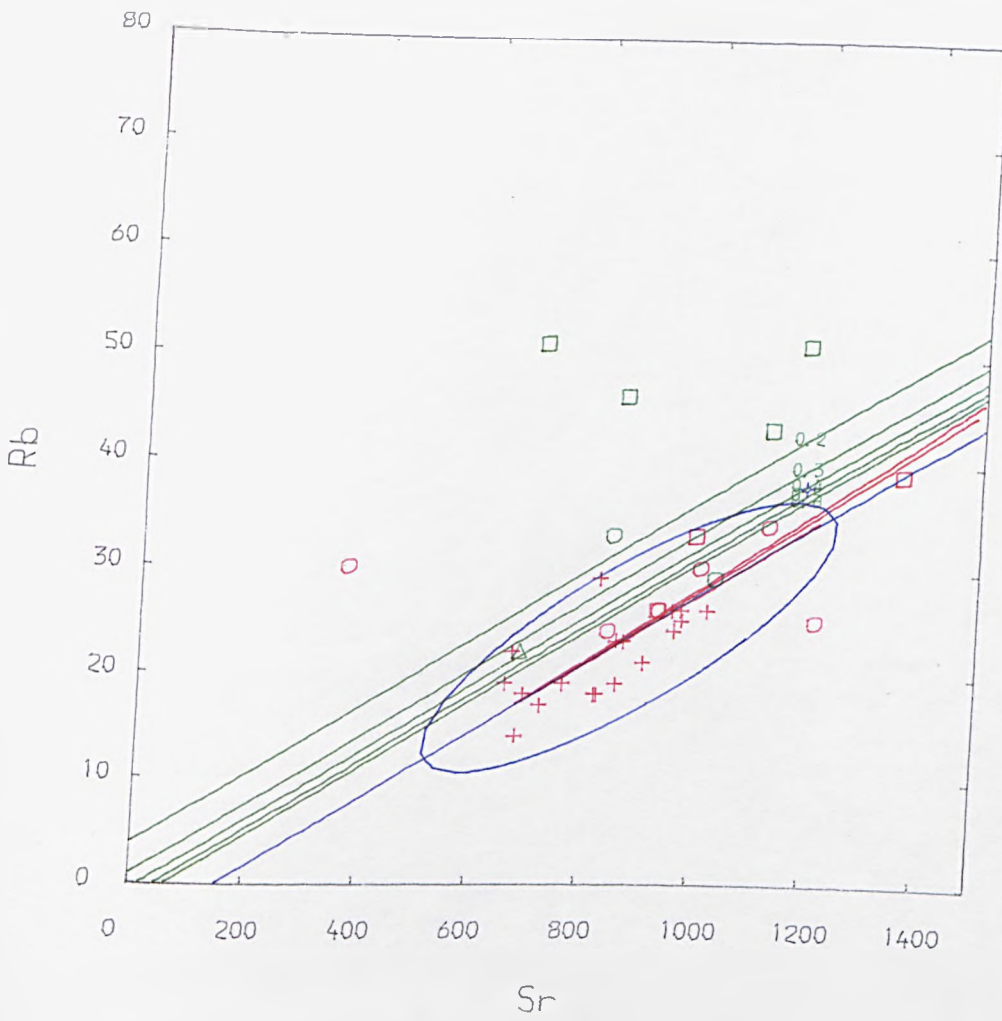
- Red symbols : Symbols as for Fig. 6.2a, cross = basalt; circle = hawaiite; square = mugearite.
- Green symbols : Symbols as above. These represent screened samples which are not included in the calculation of 'best fit' line. Green triangle is sample 24120.
- Blue line : This line represents the 'best fit' line through the data calculated from the robust covariance method. The method has the advantage of downgrading the influence of outliers.
- Blue ellipse : This gives an indication of the correlation and spread of data. Fat ellipses are poorly correlated, tight ellipses are well correlated.
- Red lines : AFC curves for $r = 0.6$ (longest line), $r = 0.4$ (middle size line) and $r = 0.2$ (shortest line). Note that an r curve between 0.4 and 0.6 would be in agreement with the 'best fit' line.
- Green lines : These are the r contours for the contaminant region. r values are indicated by the line. Note parallelism of these lines to 'best fit' line.
- Blue cross : This indicates the position of the model contaminant obtained from NLMLAFC ($r=0.46$). This also provides the composition from which the AFC curves (red lines) are calculated.

The method is based on the observations that the 'best fit' line for many of these plots does not intersect with the origin. Such an effect can be caused by AFC. If this is operating then a region can be contoured, in terms of r , corresponding to the contaminant region using the equations in the text, (method of Powell, in press).









$$\frac{\delta \text{Nd}}{\delta \text{Sr}_A} = \frac{\frac{\text{Nd}/_A}{r} \frac{r-1 + \text{DNd}}{r} - \text{Nd}/_B}{\frac{\text{Sr}/_A}{r} \frac{r-1 + \text{DSr}}{r} - \text{Sr}/_B} \quad \text{Eqn. 9.15}$$

where

$i/$ = elemental concentration in magma

A = magmatic end-member

B = contaminant end-member

D_i = bulk distribution coefficient of an element i

r = the ratio of the rate of assimilation to the rate of fractional crystallisation

Where the symbols are as before, for the actual data trend this slope is denoted by S . Rearranging gives:-

$$\text{Nd}/_B = S/\text{Sr}/_B + \text{Nd}/_A \frac{r-1 + \text{DNd}}{r} - \text{Sr}/_A \frac{r-1 + \text{DSr}}{r} \quad \text{Eqn. 9.16}$$

Thus for known or estimated DNd , DSr , $\text{Nd}/_A$ and $\text{Sr}/_A$ the plot can be contoured for r in the contaminant region. If the projection of the data array intersects the y axis first (if axes from $(0,0)$ are used) then the contaminant must lie below the trend. If two of the three parameters, r , $\text{Nd}/_B$ or $\text{Sr}/_B$ are known, or can be reasonably estimated, then the third is fixed. If a general idea of the elemental composition of the possible contaminant is available the method can provide an estimate of r . From Eqn. 9.16 it is clear that the slope of the contours are the same as the slope at A. Also, when $r=1$, for incompatible elements, the contour passes through the origin.

9.6.3 Application (Determining r)

The New Series basic rocks provide the most coherent data set of the suite and should offer the best chance of acquiring a good estimate of r using the above approach. In this application the elements La, Ce, Nd, Rb, Sr, Zr, Nb, Y and K_2O are used. It is necessary to calculate the slope and axis intercepts for each of the possible 90, two dimensional, plots to obtain the lines which best describe the observed data trends. This can be accomplished for this in dimensional data set using the robust covariance matrix method of Huber (1981), (implemented by a computer program called RCOV ALGOL68, R Powell, unpublished). This has two important advantages for calculating 'best fit' lines over ordinary least-squares methods. Firstly, the errors are not assumed to be all on one axis and secondly, the affect of outliers is downgraded in the calculation of the final slope of the line. The results are more easily visualised if they are projected onto conventional two dimensional plots Figs. 9.10a-g (computer program PAFC ALGOL68, R Powell, unpublished). The blue line represents the 'best fit' line of the trend and defines the major axis about which a 95% confidence ellipse can be drawn. The ellipse gives a measure of the spread and correlation of the data array. Plots involving Sr and Zr, for example, characteristically have ellipses which are 'fat' because they have trends which are less well correlated with other elements. This indicates that the 'best fit' lines in these examples are less reliable as in turn are the r contours which are always parallel to them. Conversely, plots involving REE's, Rb, Ba etc., have tighter ellipses, in general, and therefore have more reliable 'best fit' lines. To further ensure that the robust covariance method gives the best possible 'best fit'

line, the data set has been carefully screened for those samples which consistently lie off the main trend. These samples are indicated by green rock type symbols in Figs. 9.10a-g.

Having information about all the inter-element 'best fit' lines contoured in terms of r makes it possible to estimate r , if a reasonable estimate of the trace element composition of the contaminant is available. Alternatively, if a reasonable estimate of r is available and one of the elemental concentrations of the contaminant is well constrained then the other elemental concentrations can be found. In Figs. 9.10a-g the r contours are drawn. Plotting basement samples, such as 24037, on these diagrams reveals that, while the r values are generally consistent for REE's, Rb and Ba, other elements are consistently different. The concentrations of Y, Sr and Nb are too low whereas the concentrations of K_2O , Rb, and Zr are too high compared with the REE's for 24037. An adjustment of the concentrations of these elements would yield a consistent r value. Such an adjustment of the estimated crustal concentrations is possible using a least-squares regression technique.

The problem is soluble because there are 10 equations involving the trace elements used, and two unknowns, r and F :-

$$\frac{I/B}{r} = \frac{I/A - I/A F_i}{r - 1 + D_i} (1 - f_i) \quad \text{Eqn. 9.17}$$

where $f_i = r - 1 + D_i / r - 1$

A 'best fit' for the trace element concentrations of the contaminant and values of r and F were obtained by a non-linear robust regression program. NLMLAFC ALGOL68 (R Powell, unpublished) based on Huber (1981).

9.6.3.1 Results

The results from NLMLAFC are presented in Table 9.5. The r value obtained is approximately 0.46. This can only be regarded as an estimate for r but is nevertheless a step forward from assuming its value on the basis of pre-conceptions.

Table 9.5 Results for New Series Basic Rocks from NLMLAFC ALGOL68

Concentrations in Crust?

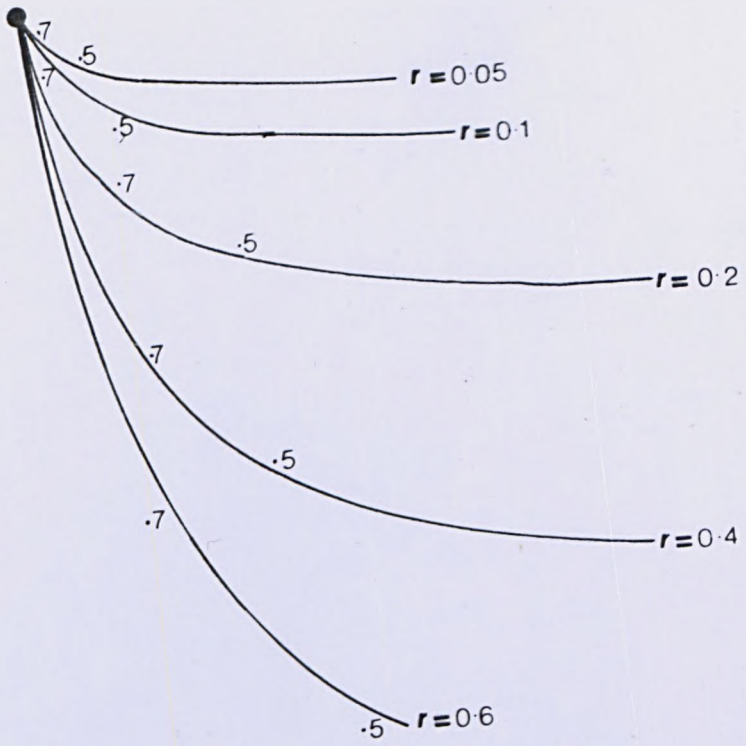
Ba	1646	Zr	51	$r = \frac{\text{rate of assimilation}}{\text{rate of crystallisation}} = 0.46$
Rb	38	Nb	38	
K ₂ O	1.8	Sr	1186	
La	57	Nd	35	
Ce	79	Y	15	

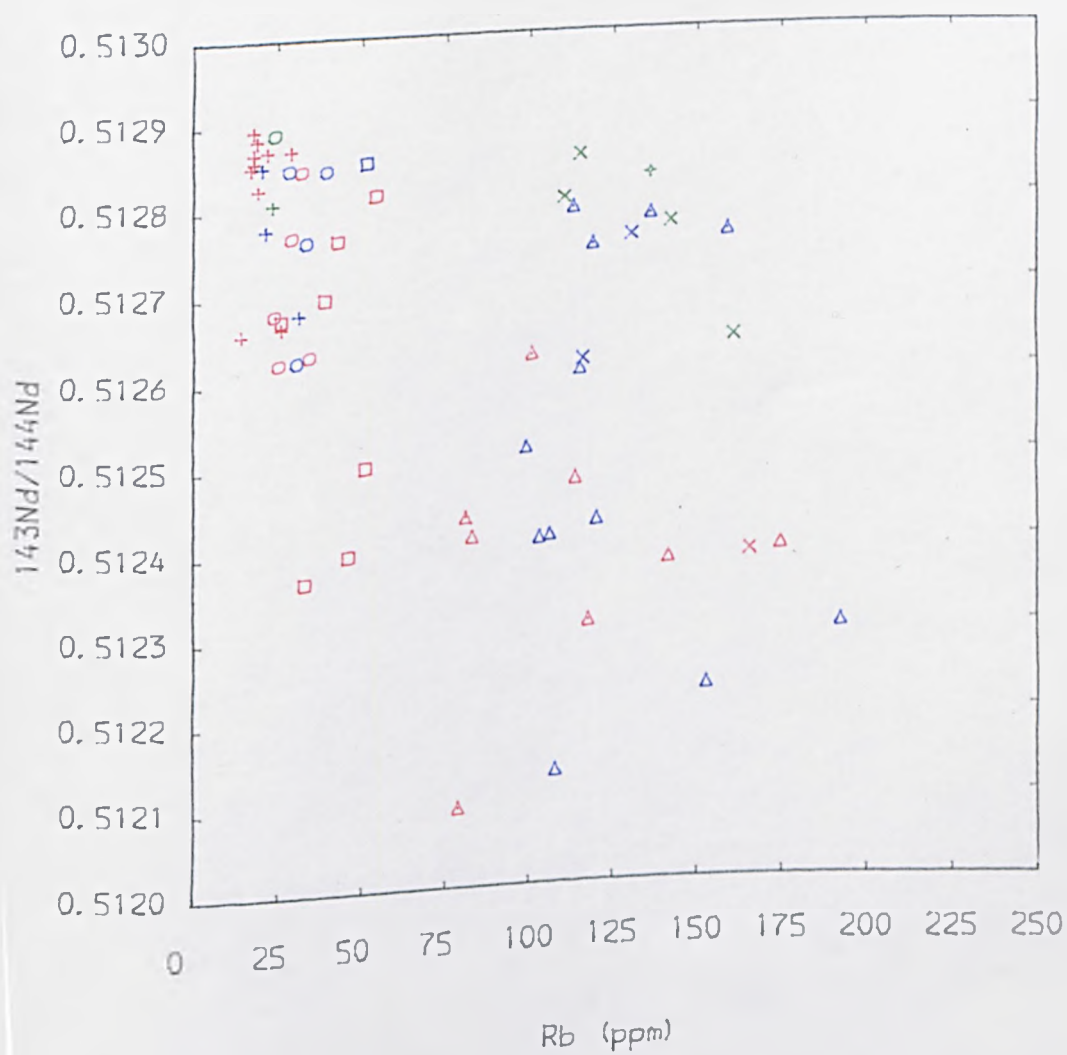
The uncertainty in r is greatest as r becomes larger. This can be seen from the way the r contours become more closely spaced in Figs. 9.10a-g. Similarly, the uncertainty in r increases if the 'best fit' line passes close to the origin as in Fig. 9.10a where Rb is plotted against K₂O. Diagrams in which the 'best fit' line intersects with the origin requires that either fractional crystallisation has operated in isolation or the contaminant lies at some point along the line. Considerable caution should be exercised in interpreting the adjusted contaminant concentrations. For example, for Sr and Zr the confidence ellipses reveal that the correlations are poor for plots involving these elements and so the adjusted crustal concentrations in the contaminant are less reliable. However, it is encouraging to note the adjustments made by NLMLAFC qualitatively agree with the assessments made from examination of the individual plots. Also, the conclusions drawn from the spidergram in Fig. 9.5 suggest that Zr is too high and Nb and Y are too low in the average 'lower crustal' samples (in which 24037 belongs) which is in agreement with the way

9.4.4 $^{143}\text{Nd}/^{144}\text{Nd}$ vs Incompatible Elements

In Chapter 8, Figs. 8.6a-g have been interpreted by AFC with associated variations in r . The 'contaminated' group of rocks are interpreted to have a high r in the basic limb which increases to a smaller r in the acidic limb. This change in r is considered to reflect the change from a lower to an upper crustal environment. The 'largely uncontaminated' rocks are interpreted to have been affected by AFC with a small r . In Figs. 9.11a-c AFC curves for $r=0.6, 0.4, 0.2, 0.1$ and 0.05 are drawn. These curves are constructed using the isotopic and elemental characteristics of the magmatic end-member from Table 8.1 and D values obtained from trace element modelling. The crustal end-member is assumed to have the following characteristics; $\epsilon\text{Sr}=60, \epsilon\text{Nd}=-25, \text{Nd}=35, \text{Sr}=675, \text{Sr}, \text{Nd}, \text{Sr}$ and Nd are based on plausible isotopic and Sr and Nd characteristics of 24037, (Table 8.1). The concentrations for the other elements in the crustal end-member are taken from NLMLAFC results in Table 9.5; the concentrations in the magmatic end-member are estimated from the most primitive basalts in the suite.

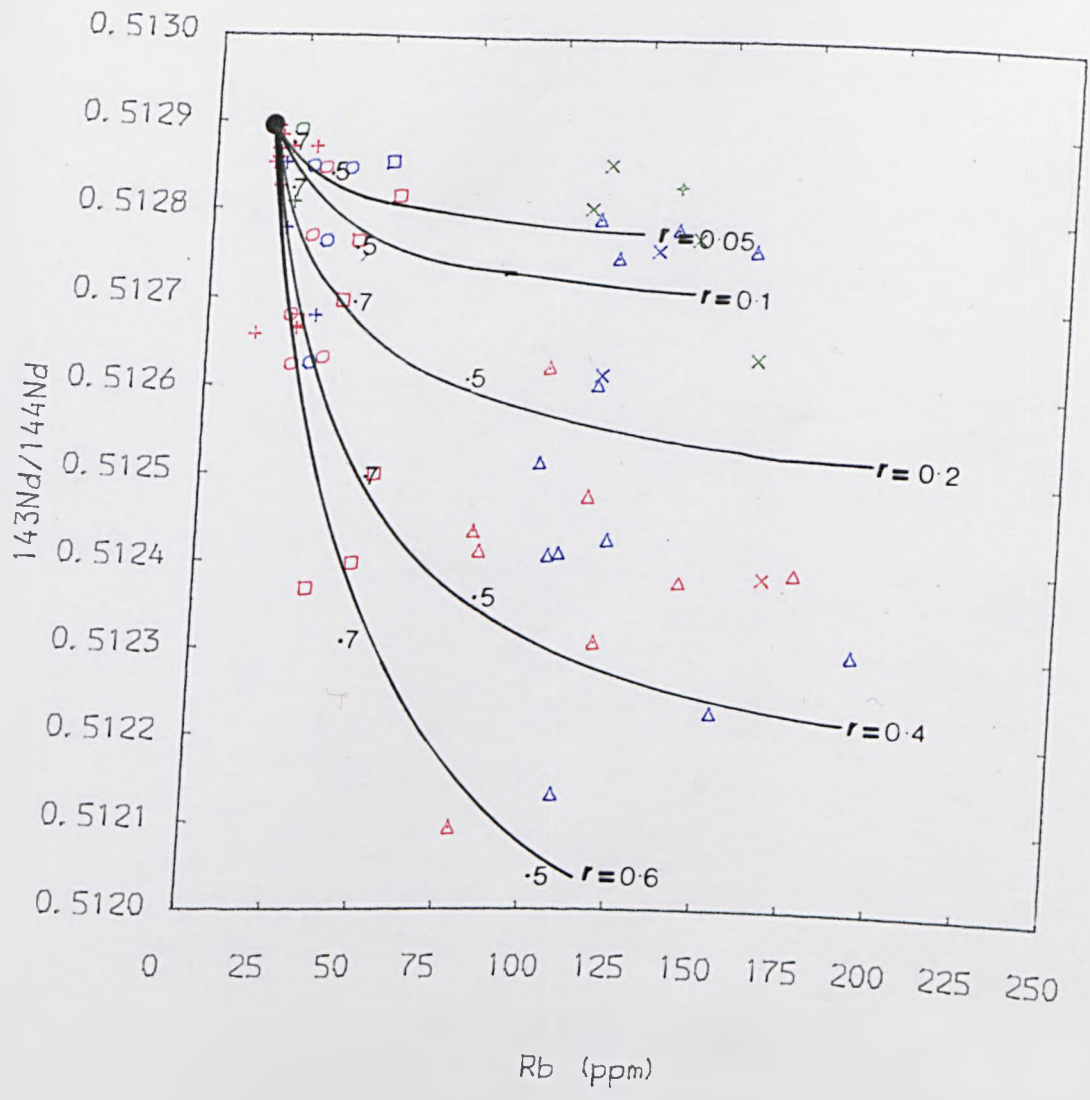
The New Series basic rocks are best explained by an r value of between 0.4 and 0.6 . The agreement between the AFC curves for an r value between 0.4 and 0.6 and the results from NLMLAFC is reassuring. However, the acidic rocks of the New Series are not easily explained by AFC curves with such a high r . Changes in D for these elements, which could be expected would not explain the kink in the trends. The most likely way to explain the change is that a decrease in r occurred at evolved mugearites to about 0.1 . The 'largely uncontaminated' group of rocks on the other hand are consistent with AFC with an r close to 0.05 .





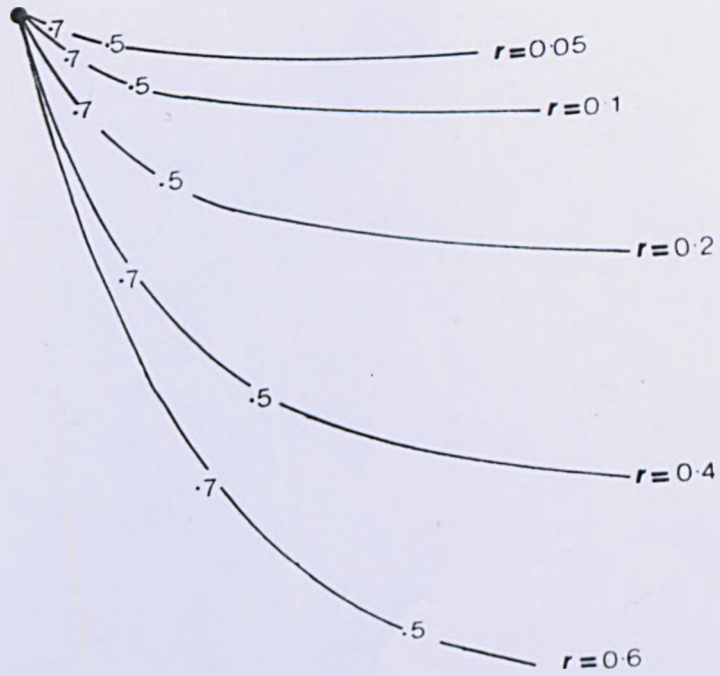
TITLE : Fig : 9.11a $^{143}\text{Nd}/^{144}\text{Nd}$ vs Rb (AFC)

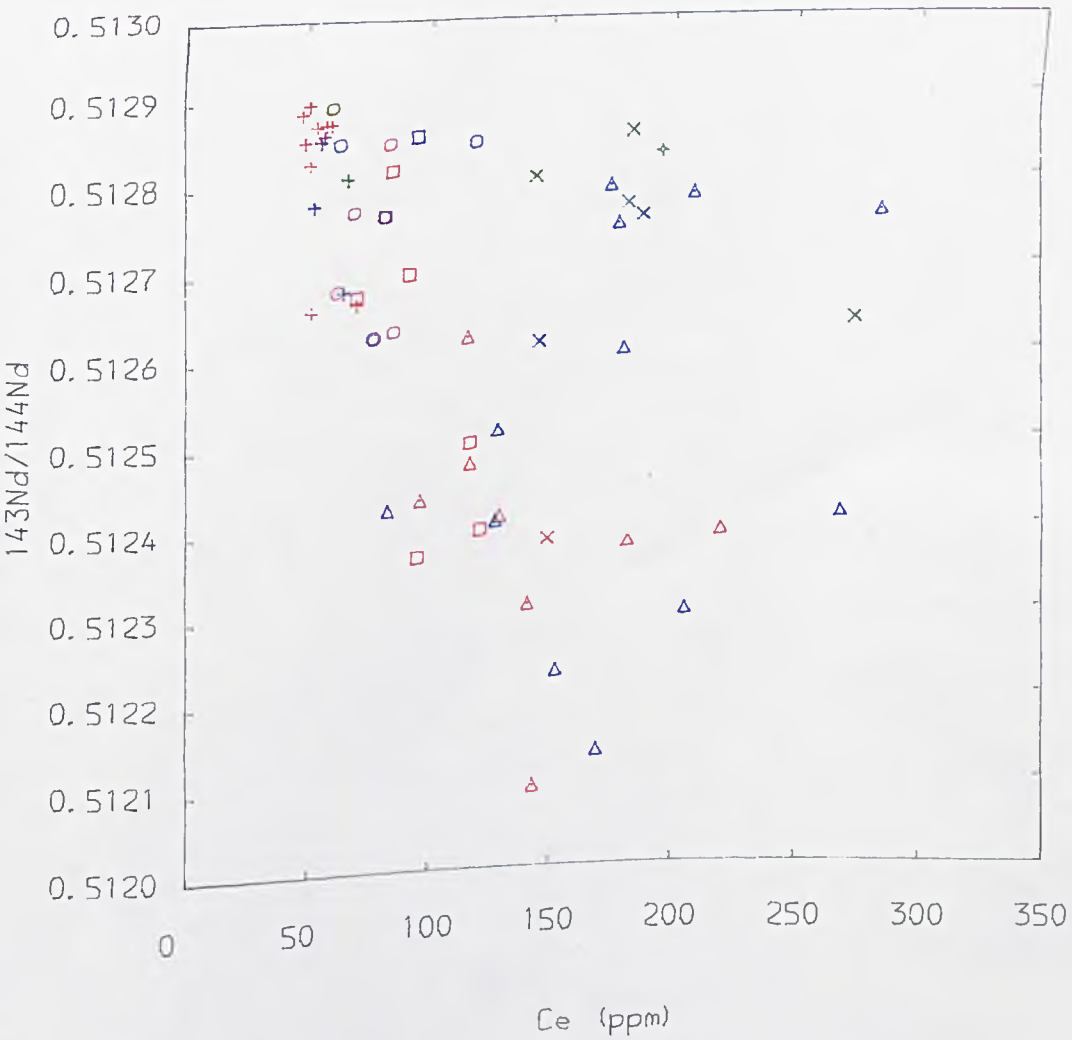
NEW SERIES ROCKS = red
 PYROCLASTIC SEQUENCE ROCKS = green
 OLD SERIES ROCKS = blue



TITLE : Fig : 9.11a $^{143}\text{Nd}/^{144}\text{Nd}$ vs Rb (AFC)

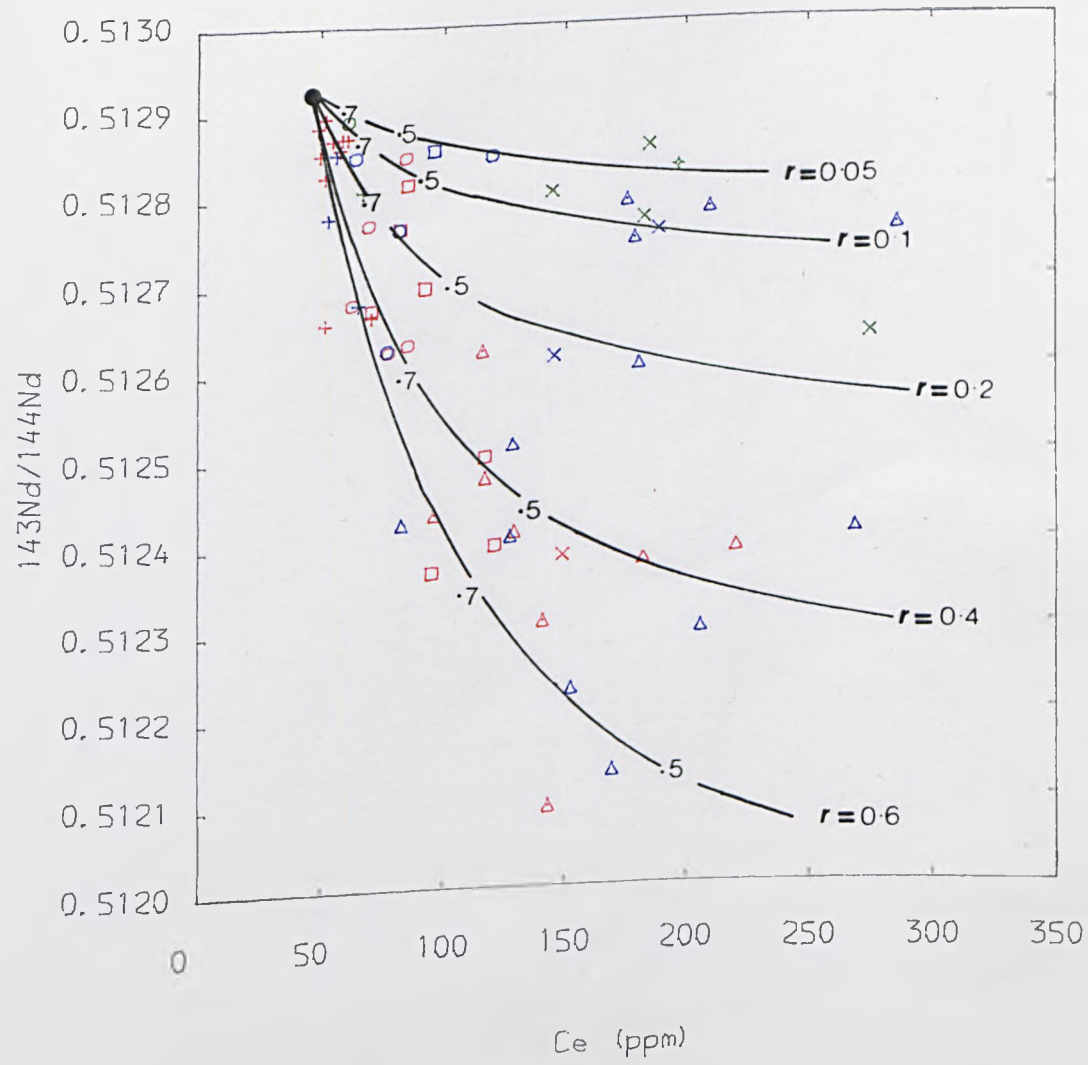
NEW SERIES ROCKS = red
 PYROCLASTIC SEQUENCE ROCKS = green
 OLD SERIES ROCKS = blue





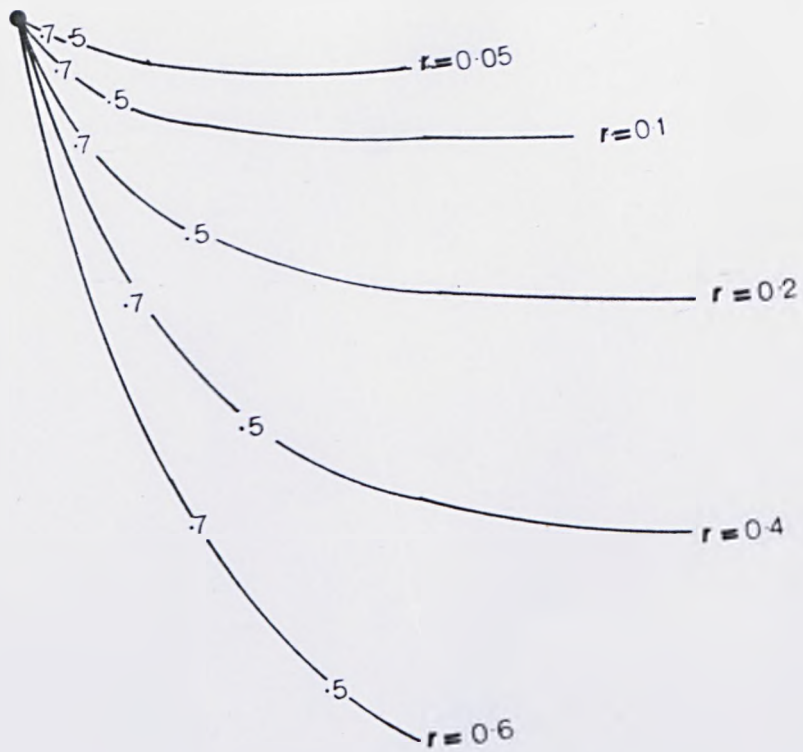
TITLE : Fig . 9.11b $^{143}\text{Nd}/^{144}\text{Nd}$ vs Ce (AFC)

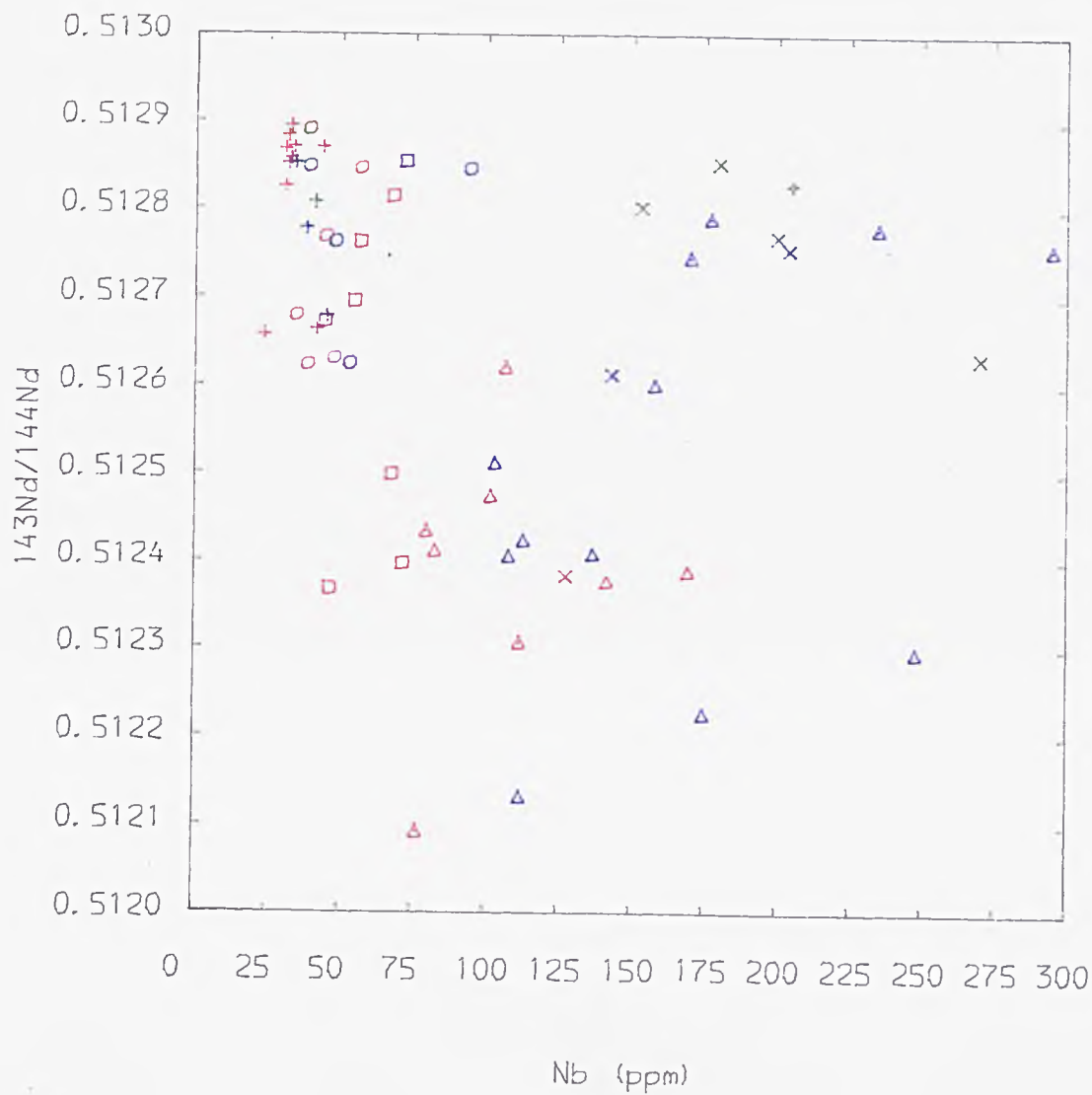
NEW SERIES ROCKS = red
 PYROCLASTIC SEQUENCE ROCKS = green
 OLD SERIES ROCKS = blue



TITLE : Fig : 9.11b $^{143}\text{Nd}/^{144}\text{Nd}$ vs Ce (AFC)

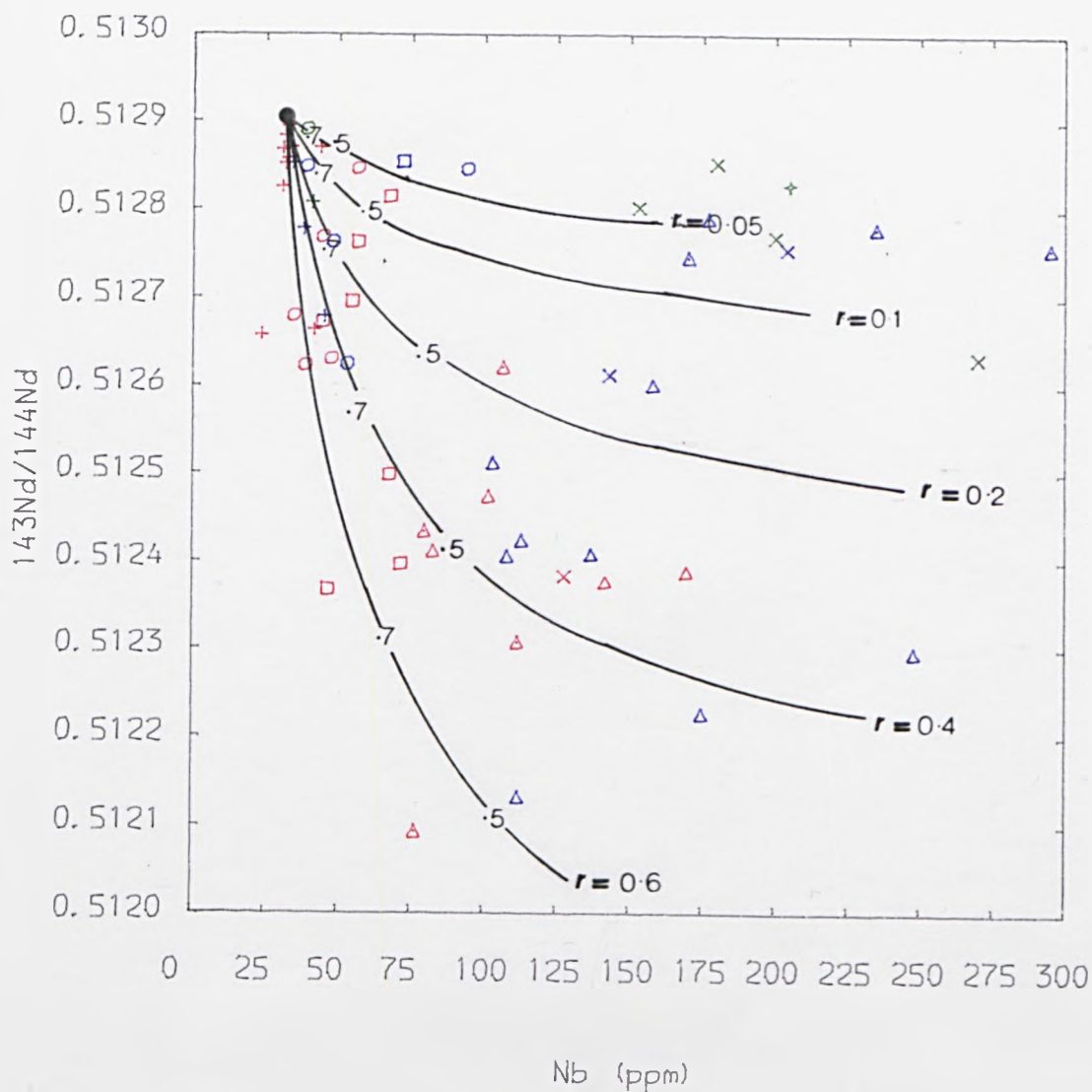
NEW SERIES ROCKS = red
 PYROCLASTIC SEQUENCE ROCKS = green
 OLD SERIES ROCKS = blue





TITLE : Fig . 9.11c $^{143}\text{Nd}/^{144}\text{Nd}$ vs Nb (AFC)

NEW SERIES ROCKS = red
 PYROCLASTIC SEQUENCE ROCKS = green
 OLD SERIES ROCKS = blue



TITLE : Fig : 9.11c $^{143}\text{Nd}/^{144}\text{Nd}$ vs Nb (AFC)

NEW SERIES ROCKS = red
 PYROCLASTIC SEQUENCE ROCKS = green
 OLD SERIES ROCKS = blue

It is possible that much of the scatter in these diagrams is due to non-systematic changes in some of the AFC parameters.

9.6.5 $^{143}\text{Nd}/^{144}\text{Nd}$ vs $^{87}\text{Sr}/^{86}\text{Sr}$

Using information drawn from the previous section and earlier Chapters, it is now possible to construct AFC trends for $^{143}\text{Nd}/^{144}\text{Nd}$ vs $^{87}\text{Sr}/^{86}\text{Sr}$ so that comparisons with observed data trends can be made. These curves are based on the end-member characteristics of Table 8.1 and the additional information which is consistent with isotopic and elemental variations of the respective groups from the previous section. This is summarised below:-

i) 'Contaminated' group

For primitive basalts to primitive mugearites (F=1 to 0.7)

r is approximately equal to 0.5

DSr is approximately equal to 0.15

DNd is approximately equal to 0.13

For evolved mugearites to trachytes (F=0.7 to 0)

r is approximately equal to 0.1

DSr is approximately equal to 2.5

DNd is approximately equal to 0.13

ii) 'Uncontaminated' group

For primitive basalts to primitive mugearites (F=1 to 0.7)

r is approximately equal to 0.05

DSr is approximately equal to 0.15

DNd is approximately equal to 0.13

For evolved mugearites to trachytes (F=0.7 to 0)

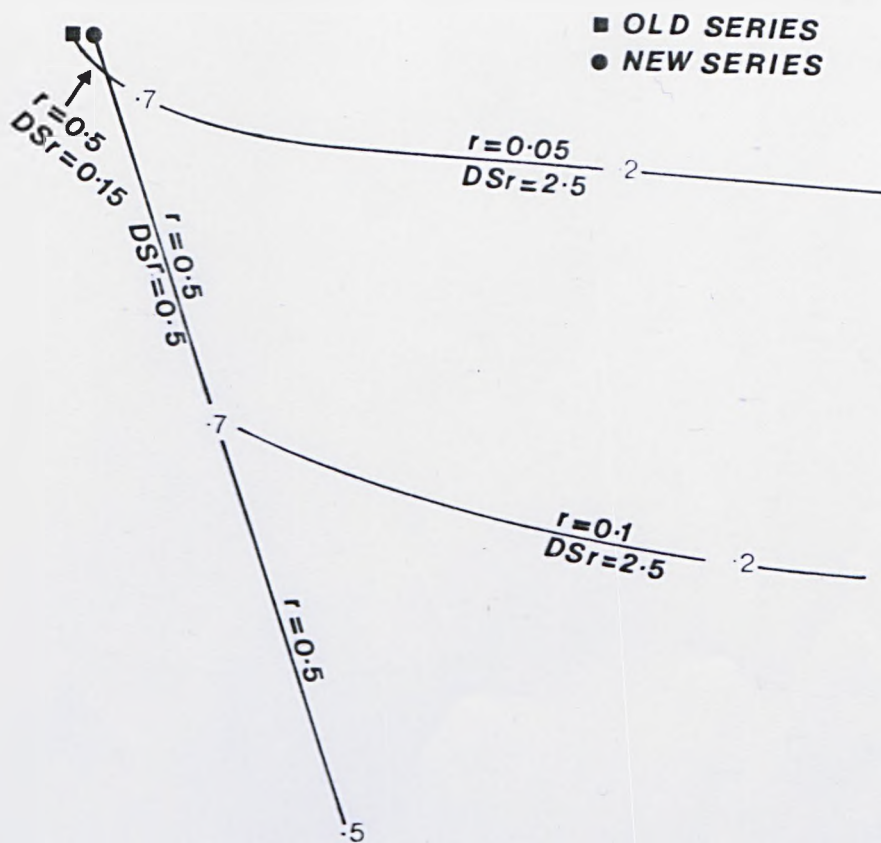
r is approximately equal to 0.05

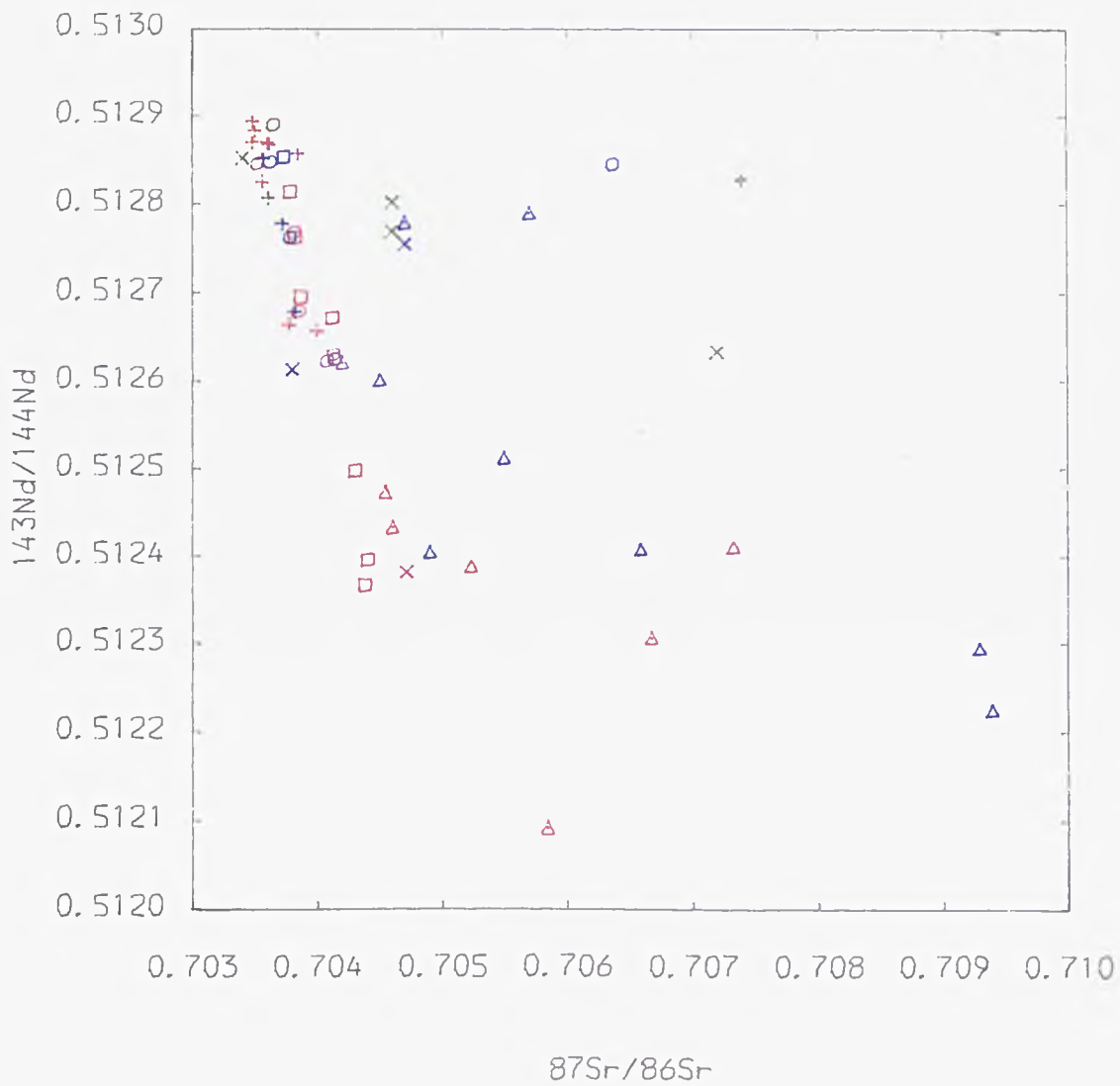
DSr is approximately equal to 2.5

DNd is approximately equal to 0.13

Using this information, various AFC trends are drawn in Fig. 9.12 for $^{143}\text{Nd}/^{144}\text{Nd}$ vs $^{87}\text{Sr}/^{86}\text{Sr}$. The agreement between the AFC curves and the data trends is very good. The effect of changing DSr at the evolved mugearite stage, when $F=0.7$, is to shift the curves dramatically towards radiogenic $^{87}\text{Sr}/^{86}\text{Sr}$ compositions. The r values are based on the result from NLMLAFC and as well as estimates from Figs. 9.11a-c. The values of r for the acidic parts of the limb in particular are only rough approximations.

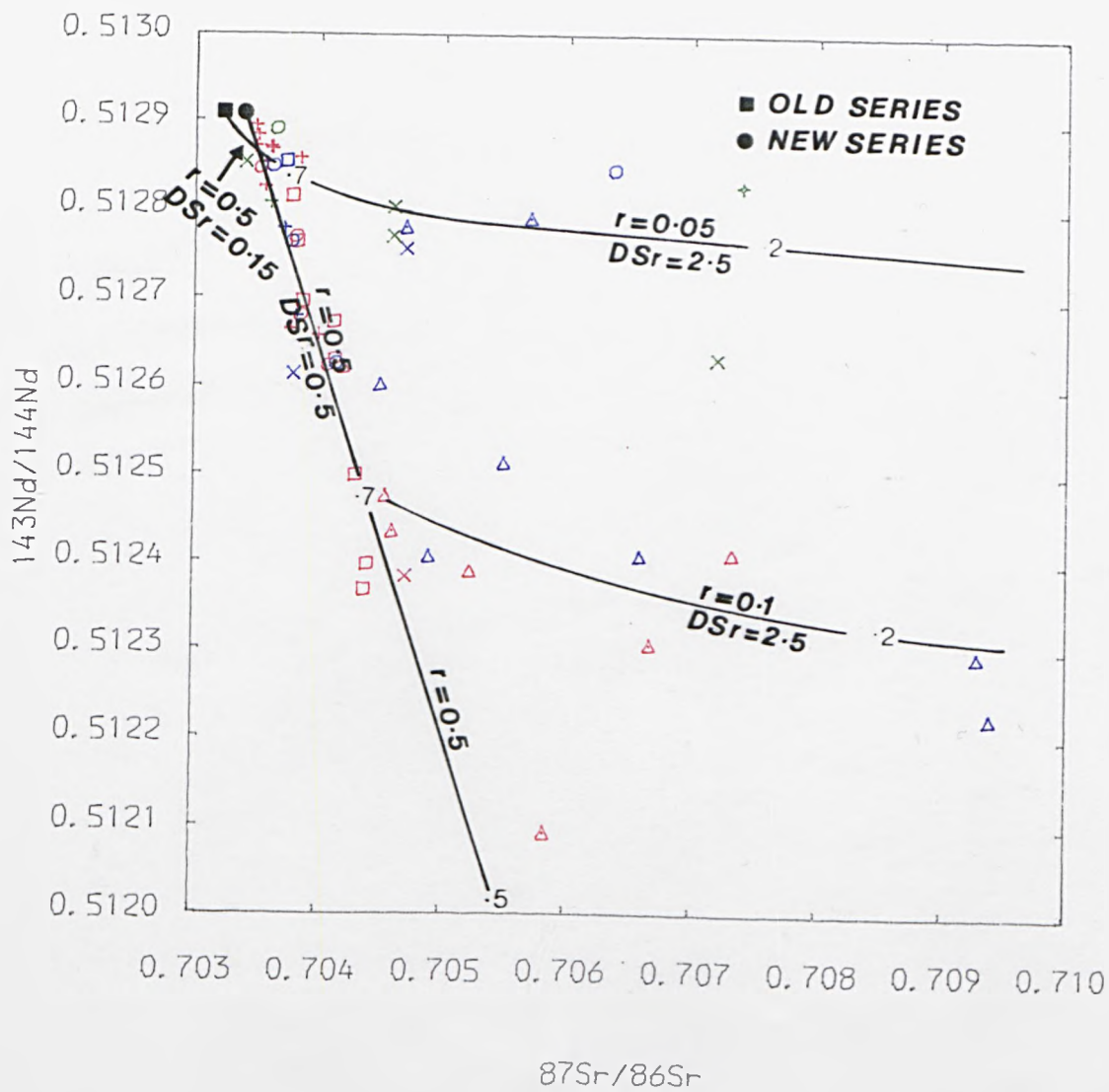
For simplicity, many of the possible complications outlined in Chapter 8 are not accounted for in the construction of these curves. For example, the sudden jump in isotopic composition from primitive mugearites to evolved mugearites is not considered. No consideration, either is given to a possible change in contaminant occurring as r and DSr changes. Furthermore, it is also noted that the data are scattered about these trends which may indicate that variations in D and r , beyond those which have been allowed for, may have also occurred. On top of this are the uncertainties which surround the values for parameters used in the calculations as well as uncertainties in the isotopic and elemental compositions of the end-members that are used which will inevitably differ, to a lesser or greater extent, with the composition of the actual contaminant. Those data points, such as 24087 of the mafic bearing trachytes, lie well off the trends and may require a different explanation. Nevertheless, notwithstanding these limitations, the AFC model, with subtle allowances for major changes in r and DSr, provides plausible quantitative agreement with the majority of the observed isotopic and elemental variations.





TITLE : Fig : 9.12 $^{143}\text{Nd}/^{144}\text{Nd}$ vs $^{87}\text{Sr}/^{86}\text{Sr}$

NEW SERIES ROCKS = red
 PYROCLASTIC SEQUENCE ROCKS = green
 OLD SERIES ROCKS = blue



TITLE : Fig : 9.12 $^{143}\text{Nd}/^{144}\text{Nd}$ vs $^{87}\text{Sr}/^{86}\text{Sr}$

NEW SERIES ROCKS = red
 PYROCLASTIC SEQUENCE ROCKS = green
 OLD SERIES ROCKS = blue

9.7 Conclusions

The main features of fractional crystallisation, identified from elemental variation diagrams, are substantiated by least-squares modelling of the major elements. A much improved 'fit' is obtained if a crustal component is included in the calculations. However, even with the addition of crust, the relatively high residuals suggest that the model is only an approximation to the natural system. Nevertheless, consistent results concerning the proportions in which phases are removed are obtained. The values of F, the amount of magma remaining, that are obtained are less consistent and can therefore only be regarded as first approximations.

Results from trace element calculations based on least-squares results are loosely consistent with observed trace element abundances. The agreement between the two is again improved if consideration of a trace element contribution from the crust is taken into account. Trace element variations reveal a division in acidic rocks into two groups which from isotopic evidence differ in the extent of crustal contamination they have suffered. REE modelling demonstrates that 2-3% fractionation of apatite can account for the increased bowing of REE patterns that occurs between evolved mugearites and trachytes.

Modelling of the isotopic trend of the New Series basic rocks by simple mixing models constrain the isotopic composition of the contaminant to a relatively restricted range characteristic of lower crustal granulite facies rocks. Trends on $^{143}\text{Nd}/^{144}\text{Nd}$ vs incompatible element diagrams suggest that the 'uncontaminated' group of rocks can be satisfied by AFC processes if $r=0.05$. Trends in the 'contaminated' group of rocks can be satisfied by an r value of 0.4 to 0.6 for the basic rocks, followed by a decrease in r to about 0.1 for acidic rocks.

Trace element modelling, independent of isotopic data, gives a value of 0.46 for the basic rocks of the 'contaminated' group. Using the above values, AFC curves can be constructed on a $^{143}\text{Nd}/^{144}\text{Nd}$ vs $^{87}\text{Sr}/^{86}\text{Sr}$ diagram, which incorporate a change of DSr from 0.15 to 2.5 from basic to acidic rocks, which satisfy remarkably well the majority of the observed Nd and Sr isotopic ratio variations. Evidence that the change in contamination from a lower to upper crustal environment is matched by a fundamental change in the contaminant is sparse, but it is supported by the abrupt change in the enrichment of Zr and also by some high $^{87}\text{Sr}/^{86}\text{Sr}$ ratios which may be indicative of assimilation of upper crustal rocks.

CHAPTER TEN

CONCLUSIONS

On the basis of field mapping and photo-interpretation it is possible to divide the Jebel Marra volcanics into Old Series and New Series rocks. The end of the Old Series period of volcanism is marked by a period of intense pyroclastic activity.

In both Series, there is a wide range in composition from basalts through to phonolites, trachytes and rhyolites. There is however, a silica gap present in both groups which corresponds to rocks of benmoreite composition.

There is a close elemental and Nd-Sr isotopic similarity between the Jebel Marra primitive alkali basalts and many alkali basalts from other continental provinces and from ocean islands. The similarity is sufficiently close to postulate a similar source probably located in the sub-lithospheric mantle. Nd and Sr isotopic evidence for these primitive basalts indicates that their mantle source is depleted in Rb and Nd, relative to bulk Earth. In contrast, consideration of Rb/Sr and particularly Sm/Nd ratios indicate that this source is enriched relative to bulk Earth. This apparent paradox can be best resolved by recourse to one of the two following explanations. Either the source has suffered a LILE enrichment event shortly before melting such that this has not yet been registered on the Nd and Sr isotopic signature in the source or alternatively, fractionation of Nd from Sm and Rb from Sr has occurred as a result of melting processes, such as by small degrees of partial melting of a source containing residual garnet or by zone refining methods.

Variations in the degree of partial melting and the effects of a heterogeneous mantle have probably contributed to the scatter observed in geochemical trends but the majority of the elemental and isotopic variations are compatible with processes of combined assimilation and fractional crystallisation.

The phonolites and trachytes are interpreted to be the results of differentiation processes from basaltic precursors. Coherent variations in major and trace elements are consistent with the following fractional crystallisation scheme. Olivine, clinopyroxene and magnetite fractionation in basic rocks, plagioclase and apatite becoming important fractionation phases in the stage from mugearites to trachytes and anorthoclase fractionation occurring in acidic rocks. The presence of both phonolites and trachytes may indicate that they were derived from basaltic parents whose composition spanned the divide between under-saturated and over-saturated liquids. The correlation between less contaminated phonolites and those trachytes which are much more contaminated is not considered to be a coincidence. It is probable that at least some of the contaminated over-saturated trachytes were derived from undersaturated parents but were driven to over-saturation by assimilation of silica rich crust.

Two trends can be clearly recognised on a $^{143}\text{Nd}/^{144}\text{Nd}$ vs $^{87}\text{Sr}/^{86}\text{Sr}$ diagram. The majority of the data describe a strong negative correlation to the left of the mantle array which is interpreted to be the result of assimilation of relatively low $^{87}\text{Sr}/^{86}\text{Sr}$ granulite facies crust. The most evolved trachyte in this trend shows a pronounced shift towards radiogenic $^{87}\text{Sr}/^{86}\text{Sr}$ compositions. This effect is predicted by AFC processes when DSr becomes $\gg \text{DNd}$ which, in

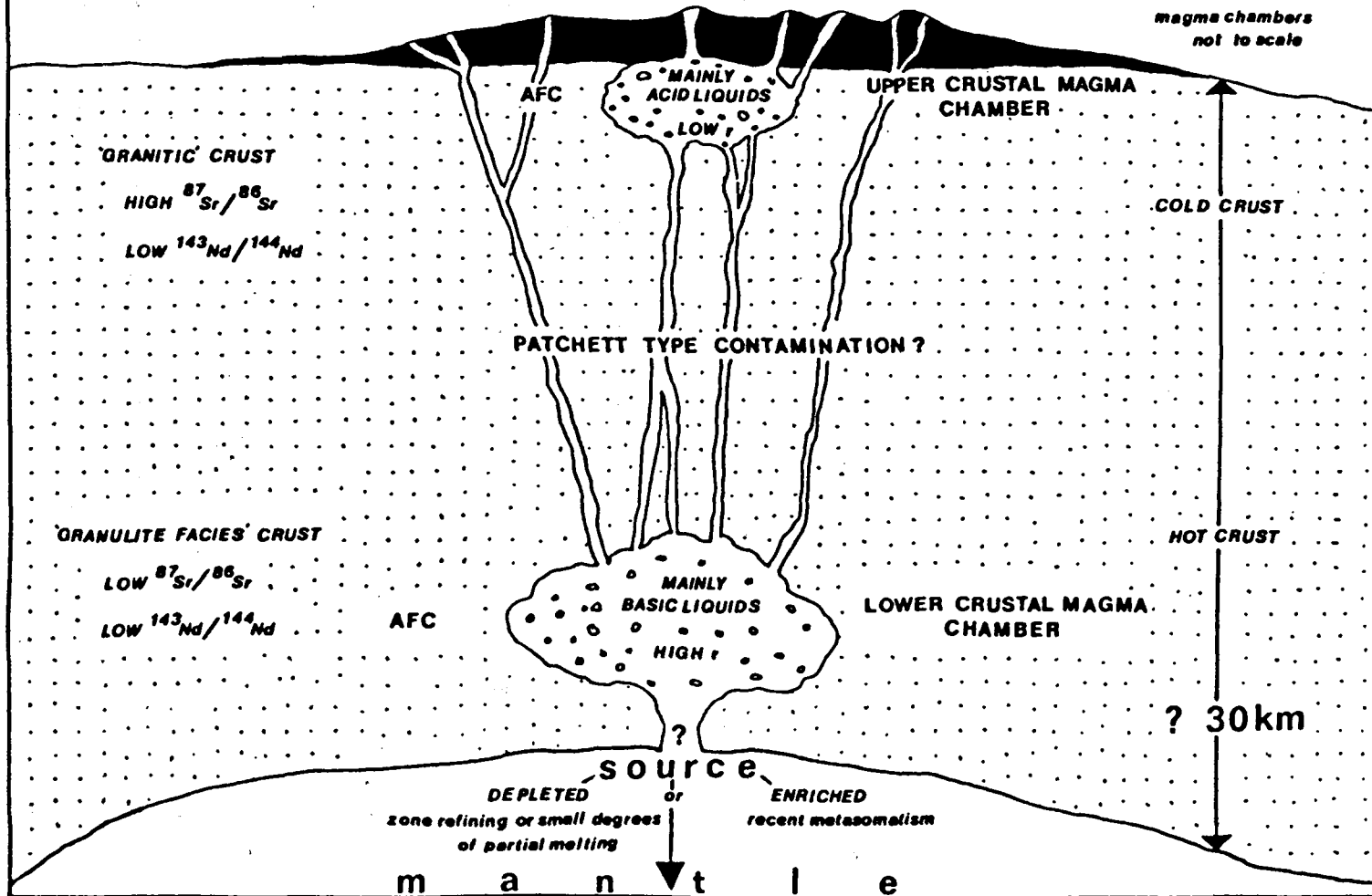
this case, is the result of feldspar fractionation. The second trend is less well defined towards more radiogenic $^{87}\text{Sr}/^{86}\text{Sr}$ compositions. In both trends, there is additionally a strong correlation between decreasing $^{143}\text{Nd}/^{144}\text{Nd}$, increasing $^{87}\text{Sr}/^{86}\text{Sr}$ and increasing fractionation indices. This is interpreted in terms of combined assimilation and fractional crystallisation model (DePaolo, 1981). $^{143}\text{Nd}/^{144}\text{Nd}$ vs incompatible diagrams also show two trends which conform to the trends identified above. In one trend $^{143}\text{Nd}/^{144}\text{Nd}$ decreases relatively more rapidly than the increase in incompatible elements until rocks of evolved mugearite composition where a kink in the trend marks the point at which incompatible elements increase relatively more rapidly than $^{143}\text{Nd}/^{144}\text{Nd}$ decreases. The other trend is largely marked throughout by incompatible elements increasing relatively more rapidly than decreases in $^{143}\text{Nd}/^{144}\text{Nd}$. Consideration of AFC processes suggest that the different trends are the result of differences in r ; the rate of assimilation to the rate of fractional crystallisation. Where increases in incompatible elements occur relatively more rapidly than decreases in $^{143}\text{Nd}/^{144}\text{Nd}$, r is considered to be small, where the reverse situation is observed, r is considered to be large. The kink in the trend noted earlier is thought to be the result of a change in contamination environment from the lower to the upper crust which is likely to have the effect of decreasing r which gives rise to the kinked trends.

The effects of contamination can also be recognised in incompatible inter-element plots. Among basic rocks, extrapolation of trends on these plots rarely intersect with the origin and can be interpreted in terms of a second order affect such as AFC. Among acidic rocks, the more 'contaminated' rocks tend to have a higher

Zr/Nb ratio than less contaminated rocks and this is again likely to represent the effects of crustal contamination. Some of the main points of the conclusions are illustrated in a cartoon in Fig.10.1.

In conclusion, isotopic and elemental variations can be successfully explained by processes of combined assimilation and fractional crystallisation. This is not to say that other processes, such as variable degrees of partial melting, assimilation of partial melts from the crust or effects of a heterogeneous mantle, have not occurred, but rather that their effects on the geochemistry of the Jebel Marra volcanics are less readily detected.

Fig. 10.1 Synthesis of Conclusions



REFERENCES

- Arth, J.G. 1976. Behaviour of trace elements during magmatic processes a summary of theoretical models and their applications. J. Res. U.S. Geol. Survey. 4, 41-47.
- Allegre C.J., Dupre B., Richard P. and Rousseau D. 1982. Sub-continental versus sub-oceanic debate: Lead-neodymium-strontium isotopes from a shield area: Ahaggar suite. C.P.S.L. 52, 85-92.
- Andrew G. 1948. Geology of Sudan, in Tothill J.O. Ed. in: Agriculture in Sudan. University Press, Oxford, 84-128.
- Barton et al
see end.
- Birmingham P.H., Fairhead J.D. and Stuart G.W. 1983. Gravity study of the Central African Rift System: a model for continental disruption. 2 The domal uplift and associated Cainozoic volcanism. Tectonophysics, 94, 205-22.
- Boettcher A.L., O'Neil J.R., Windom J.E., Stewart D.C. and Wilshire H.G. 1979. Metasomatism of the upper mantle and genesis of kimberlite and other volcanics. Eds. Boyd F.R. and Meyer H.O.A., AGU Washington, 173- 182.
- Bowen, N.J. 1928. The evolution of the igneous rocks. Princeton Univ Press. 332p.
- Briden J.C., Rex D.C., Faller A.M. and Tomblin J.F. 1979. K-Ar geochronology and palaeomagnetism of volcanic rocks in the Lesser Antilles island arc. Phil. Trans. R. Soc. Lond., A291, 485-528.
- Bryan W.B., Chayes F. and Finger L.W. 1969. Estimating

- proportions in petrographic mixing equations by least squares approximation. *Science* 163, 926-927.
- Carlson R.W., Lugmair G.W. and MacDougall J.D. 1981. Columbia River volcanism: the question of mantle heterogeneity or crustal contamination. *G.C.A.*, 45, 2483-2499.
- Carter, S.P., Evensen, N.H., Hamilton, P.J., O'Nions, R.K., 1978. Nd- and Sr- isotopic evidence for crustal contamination of continental volcanics. *Science*. 202. 743-747.
- Coomer P.G. and Vail J.F. 1974. 1100 m.y. model age for a Sudan lead deposit. 18th Ann. Rep. African Geol. Univ. Leeds.
- Cooper J.A., Reynolds P.H. and Richards J.R. 1969. Double spiked calibrations of the Broken Hill standard lead. *E.P.S.L.* 6, 467-478.
- Cordell L. and Henderson R.G. 1963. Iterative three dimensional solution of gravity anomaly using a digital computer. *Geophysics*. 33, 596-601.
- Coulon C. and Reyres Y. 1968. Contribution a l'etude du volcanisme posterieur aux Gres de Nubie dans la partie centrale du Darfur (Soudan). *C.R. Acad. Sci. Paris*, 266, 1821-1824.
- Cox K.G. 1983. The Karoo province of southern Africa: origin of trace element enrichment patterns. 139-157. In: *Continental Volcanics and Mantle Samples*. Eds.: Hawkesworth C.J. and Norry M.J. Shiva Press. 272p.
- Cox K.G., Bell J.D. and Pankhurst R.J. 1979. *The interpretation of igneous rocks*. Allen and Unwin.

450p.

- Cox K.G. and Clifford P. 1932. Correlation coefficient patterns and their interpretation in three basaltic suites. C.H.P. 75, 268-278.
- Dawson J.B. 1970. The structural setting of African kimberlite magmatism 321-335. In: African magmatism and tectonics. Eds. Clifford T.N and Gass I.G. Oliver and Boyd, 1970.
- Dawson J.B. and Smith J.V. 1977. The MARID (mica-amphibole-rutile-ilmenite-diopside) suite of xenoliths in kimberlites. G.C.A., 41, 309-323.
- Deer W.A., Howie R.A. and Zussman J 1966. Rock-forming minerals. Longmans. 652p.
- DeLaeter J.R. and Hosie D.J. 1978. The abundance of barium in stony meteorites. E.P.S.L. 38, 416-420.
- DePaolo, D.J. 1981. Trace element and isotopic effects of combined wallrock assimilation and fractional crystallization. E. P. S. L. 53. 189-202.
- DePaolo, D.J. and Wasserburg, G.J. 1976. Nd isotopic variations and petrogenetic models. Geophys. Res. Lett. 3 249-252.
- DePaolo, D.J. and Wasserburg, G.J. 1979. Petrogenetic mixing models and Nd-Sr isotopic patterns. G.C.A. 43. 615-627.
- DePaolo, D.J. and Wasserburg, G.J. 1977. The sources of island arcs indicated by Nd and Sr isotopic studies. Geophys. Res. Lett. 4, 465-468.
- Dickin A.P. 1981. Isotope geochemistry of Tertiary igneous rocks from the Isle of Skye, N.W. Scotland. J. Petrol., 22, 155-189.

- Downes H, 1983. the petrogenesis of co-existing saturated and undersaturated continental alkaline magma series. Leeds Univ. unpub. Ph.D. thesis.
- Druitt T.H. and Sparks R.S.J. 1982. A proximal ignimbrite breccia facies on Santorini, Greece. *J. Volcanol. Res.*
- Erlank A.J., Allsopp H.L., Hawkesworth C.J. and Menzies H.A. 1982. Chemical and isotopic characterisation of upper mantle metasomatism in peridotite nodules from Bulfontein kimberlite. *Terra Cognita*, 2, 216-63.
- Fairhead J.D. 1978. A gravity link between the domally uplifted Cainozoic volcanic centres of North Africa and its similarity to the East African system anomaly. *E.P.S.L.*, 42, 109-113.
- Fairhead J.D., Browne S.E. and Stuart G.W. 1981. Jebel Marra and the Central African Rift system. Abstract submitted in San Francisco to N.A.T.O conference on planetary rifting.
- Flower M.F.J., Schmincke H-U. and R.N. Thompson. 1975. Phlogopite stability and $87\text{Sr}/86\text{Sr}$ step in basalts along the Reyjanes Ridge. *Nature*, 254, 404-6.
- Francis P.W., Thorpe R.S. and Ahmed F. 1973. Setting and tectonic significance of Tertiary-Recent volcanism in the Darfur Province of western Sudan. *Nature* 243, 30-2.
- Futa K. and Le Masurier W.E. 1983. Nd and sr isotopic studies on Cainozoic mafic lavas from west Antarctica: another source for continental alkali basalts. *C.M.P.* 33, 38-44.

- Grutzeck, H.W., Krödelbaugh, S.J., Weill, D.F. 1974. The distribution of Sr and REE between diopside and silicate liquid. *Geophys. Res. Lett.* 1, 273-275.
- Hammerton D. 1968. Recent discoveries in the caldera of Jebel Marra. *Sudan notes and records.* 49, 136-148.
- Hanson G.N. 1980. Rare earth elements in petrogenetic studies of igneous systems. *Ann. Rev. Earth Plan. Sci.*, 3, 371-406.
- Harris P.G. 1957. Zone refining and origin of potassic basalts *G.C.A.*, 12, 195-203.
- Harte B. 1983. Mantle peridotites and processes the kimberlite sample. 46-51. In: In: *Continental Volcanics and Mantle Samples.* Eds.: Hawkesworth C.J and Norry M.J Shiva Press. 272p.
- Hawkesworth C.J. and Vollmer R. 1979. Crustal contamination versus enriched mantle: $^{143}\text{Nd}/^{144}\text{Nd}$ and $^{87}\text{Sr}/^{86}\text{Sr}$ evidence from Italian volcanics. *C.N.P.* 69, 151-169.
- Hawkesworth C.J., Rogers N.W., van Calstren P., Menzies M.A. and Reid D.L. 1982. Nd and Sr isotope studies on crustal xenoliths from the southern Africa. *Terra Cognita, Abs* 2, 236.
- Hawkesworth C.J., Norry M.J., Roddick J.C. and Vollmer R. 1979. $^{143}\text{Nd}/^{144}\text{Nd}$ and $^{87}\text{Sr}/^{86}\text{Sr}$ ratios from the Azores and their significance in LIL-element enriched mantle.
- Hawkesworth C.J. and Norry M.J. 1983. Eds. of *Continental Basalts and Mantle Xenoliths.* Shiva Press 272p.
- Hofmann A.W. and Hart S.R. 1973. An assessment of local and

regional isotopic equilibrium in the mantle.

E.P.S.L., 33, 44-62.

Hooker, P.J., O'Nions R.K., Pankhurst R.J. 1975.

Determination of rare-earth elements by mixed-solvent ion exchange and mass spectrometric isotope dilution. Chem. Geol. 16. 189-196.

Huber, P.J. 1981. Robust statistics. Wiley.

Irving, A.J. 1978. A review of experimental studies of crystal/liquid trace element partitioning. G.C.A. 42. 743-747.

James D.E. 1980. The combined use of oxygen and radiogenic isotopes as indicators of crustal contamination, Ann. Rev. Earth Plan. Sci., 9, 311-44.

Kennedy W.Q. 1965. The structural differentiation of Africa in the Pan African tectonic episode. 8th Ann. Rep. African Geol. Univ. Leeds 48.

Kay R.W. and Gast P.W. 1974. The rare earth content and origin of alkali rich basalts. J. Geol. 81, 653-682.

Lebas M.J. 1971. Per-alkaline volcanism, crustal swelling and rifting. Nature, 230, 85-7.

Lebas M.J. 1980. Alkaline magmatism, and uplift of continental crust. Proc. Geol. Ass. 91, (1&2) 33-38. Lebon J.H.G. and Robertson V.C. 1961. The Jebel Marra, Darfur and its region. Geogr. J. 127, 30-40.

Le Maître R.W. 1976. The chemical variability of some

- common igneous rocks. *J. Petrol.* 17, 589-637.
- Leeman W.P. 1976 Petrogenesis of McKinney (Snake River) olivine tholeiites in rare earth element and Cr/Ni distributions. *Bull. Geol. Soc. Amer.* 87, 1582-6.
- Leeman W.P., Vitaliano C.J. and Prinz H. 1976. Evolved lavas from Snake River Plain: Craters of the Moon national Monument, Idaho. *C.M.P.*, 56, 35-60.
- Leys C.A. 1982. Volcanic and sedimentary processes in phreatomagmatic volcanoes. Leeds Univ. unpub. Ph.D. thesis.
- Lloyd F.E. and Bailey D.K. 1975. Light element metasomatism of the continental mantle: the evidence and the consequences. *Phys. Chem. Earth*, 9, 389-416.
- Luff I.W. 1982. Petrogenesis of the island arc tholeiite series of the South sandwich Islands. Leeds Univ. unpub. Ph.D. thesis.
- Mahoney J., MacDougall J.D., Lugmair G.W., Murali A.V., Sankar D.M. and Gorplan. K. 1982. Origin of the Deccan trap flows of Mahabaleshwar inferred from Nd and Sr isotopic studies. *E.P.S.L.* 60, 47-60.
- Mason B. 1979. Data of geochemistry. Chapter B. Cosmochemistry. Part 1. Meteorites. Prof. Pap. U.S. Geol. Surv. 440-B-1, 1-32.
- McCulloch M.T., Arculus R.J., Chappell B.W. and Ferguson J. 1980. Isotopic and geochemical studies of nodules in kimberlite have implications for the lower continental crust. *Nature* 300, 166-169.
- Menzies M.A. 1983. 46-91. Mantle ultramafic xenoliths in alkaline magmas: evidence for mantle heterogeneity modified by magmatic activity. In:

- Continental Volcanics and Mantle Samples. Eds.: Hawkesworth C.J. and Norry M.J. Shiva Press. 272p.
- Menzies II, and Murthy V.R. 1980. Nd and Sr isotope geochemistry of hydrous mantle nodules and their host alkali basalts: implications for local heterogeneities in metasomatically veined mantle. *E.P.S.L.* 46, 323-334.
- Menzies M.A., Leeman W.P. and Hawesworth C.J. 1983. Isotope geochemistry of Cenozoic volcanic rocks reveals mantle heterogeneity below western USA. *Nature* 303, 205-9.
- Moorbath, S., Thompson, R.N. 1980. Strontium isotope geochemistry and petrogenesis of the Early Tertiary lava pile of the Isle of Skye, Scotland, and other basic rocks of the British Tertiary Igneous Province. *J. Petrol.* 21, 295-321.
- Nakamura, N. 1974. Determination of REE, Ba, Fe, Mg, Na and K in carbonaceous and ordinary chondrites. *G.C.A.* 38, 757-775.
- Norry M.J., Truckle P.H., Lippard S.J., Hawkesworth C.J., Weaver S.D. and Marriner G.F. 1980. Isotopic and trace element evidence from lavas bearing on mantle heterogeneity beneath Kenya. *Phil Trans. R. Soc. Lond.* A297, 259-271.
- Norry M.J and Fitton J.G. 1983. Compositional differences between oceanic continental basic lavas and their significance. In: *Continental Volcanics and Mantle Samples*. Eds.: Hawkesworth C.J. and Norry M.J. Shiva Press. 272p.
- O'Nions R.K., Pankhurst R.J. and Gronvold K. 1976. *Nature*

- and development of basaltic magma sources beneath Iceland and Reykjanes Ridge. *J. Petrol.* 17, 315-8.
- O'Hara, B.J. Mathews, R.E. 1981. Geochemical evolution in an advancing, periodically replenished, periodically tapped, continuously fractionated magma chamber. *J. Geol. Soc. Lond.* 138, 237-277.
- O'Hara M.J. 1968. The bearing of phase equilibria on the origin and evolution of basic and ultrabasic rocks. *Ann. Rev. Earth. Plan. Sci.*, 4, 69-133.
- O'Nions, R.K., Hamilton, P.J., Evensen, N.M. 1977. Variations in $^{143}\text{Nd}/^{144}\text{Nd}$ and $^{87}\text{Sr}/^{86}\text{Sr}$ ratios in oceanic basalts. *E.P.S.L* 34, 13-22.
- Palacz Z.A. 1983. Isotopic evidence for the dynamic behaviour of the Rhum magma chamber. Leeds Univ. unpub. Ph.D. thesis.
- Patchett, P.J. 1990. Thermal effects of basalt on continental crust and crustal contamination of magmas. *Nature*. 283, 559-561.
- Pearce J.A. and Norry M.J. 1979. Petrogenetic implications of Ti, Zr, Y and Nb variations in volcanic rocks. *C.M.P.* 69, 33-47.
- Powell R. 1978 Equilibrium thermodynamics in petrology. An introduction. Harper and Row. 248p.
- Powell R. Inversion of the assimilation and fractional crystallisation (AFC) equations: characterisation of contaminants from isotope and trace element relationships in volcanic suites. In press.
- Roeder P.L. and Emstie R.F. 1970. Olivine-liquid equilibrium. *Contrib. Mineral. Petrol.* 29.

275-289.

- Russell R.D. and Faquhar R.M. 1960. Lead isotopes in geology. Interscience.
- Shaw D.M. 1979. Trace element melting models. Phys. Chem. Earth 11, 577-595.
- Shima Y. 1979. The abundances of titanium, zirconium and hafnium in stony meteorites. G.C.A. 43, 353-362.
- Sigvaldason G.E. 1974. Basalts from the assumed Icelandic mantle plume. J. Petrol. 15, 497-525.
- Sparks R.S.J., Huppert H.E. and Turner J.S. 1983. Fluid dynamic behaviour of magma chambers. Paper submitted to Royal Society of London meeting, 23rd March, 1983.
- Sun S-S. 1980. Lead isotopic study of young volcanic rocks from mid-ocean ridges, ocean islands and island arcs. Phil. Trans. Roy. Soc. Lond. A297, 409-445.
- Sun S-S. and Hanson G.N. 1975. Origin of Ross Island basanitoids and limitations upon the heterogeneity of mantle sources for alkali basalts and nephelinites. C.M.P. 52, 77-106.
- Sun S-S., Nesbit R.W., and Sharaskin A.Y. 1979. Geochemical characteristics of mid-ocean ridge basalts. E.P.S.L. 44, 119-38.
- Taylor, H.P. 1980. The effects of assimilation of country rocks by magmas on $180/160$ and $87\text{Sr}/86\text{Sr}$ systematics in igneous rocks. Earth Planet. Sci. Lett. 47, 243-252.
- Thirlwall M.F. 1982. A triple-filament method for rapid and precise analysis of rare-earth elements by isotope dilution. Chem. Geol. 35 155-166.

- Thirlwall M.F. 1982. Systematic variation in chemistry and Nd-Sr isotopes across a Caledonian calc-alkaline volcanic arc: implications for source materials. *E.P.S.L.*, 58, 27-50
- Thirlwall M.F. and Jones N.W. 1983. 186-201. Isotope geochemistry and contamination mechanisms of Tertiary lavas from Skye, northwest Scotland. In: *Continental Volcanics and Mantle Samples*. Eds.: Hawkesworth C.J. and Norry M.J. Shiva Press. 272p.
- Thompson R.N. 1982. Magmatism in the British Tertiary Volcanic Province (The Carnegie Review Article). *Scott. Jour. Geol.* 18, 45-107.
- Thompson R.N. 1983. Spidergrams rule ok? 158-187. In: *Continental Volcanics and Mantle Samples*. Eds.: Hawkesworth C.J. and Norry M.J. Shiva Press. 272p.
- Thorpe R.S. and Smith K. 1974. Distribution of Cenozoic volcanism in Africa *E.P.S.L.* 22, 91-5.
- Upton B.J.G. 1974. The alkaline province of south-east Greenland. In: *The alkaline rocks*. Ed. H. Sorenson. London J. Wiley 672p.
- Vail J.R. 1971. Geological reconnaissance in part of the Berber district northern Province, Sudan. *Bull. Geol. Sur. Sudan.* 19, 76p.
- Vail J.R. 1972a. Jebel Marra a cormant volcano in Darfur province western Sudan. *Bull. Volcanol.* 36, 251-65.
- Vail J.R. 1972b. Geological reconnaissance in the Zalingei and Jebel Marra areas of western Darfur Province, Sudan. *Bull. Geol. Surv. Sudan.* 19, 50p.

- Vail J.R. and Rex D.C. 1971 Potassium-argon age measurements on pre-Nubian basement complex rocks from Sudan. Proc. Geol. Soc. London. No.1664 205-14.
- Wass S.Y. and Rogers N.W. 1980. Mantle metasomatism - precursor to continental alkaline volcanism. G.C.A. 44, 1811-1823.
- White, W.P., Hofmann, A.W. 1982. Sr and Nd isotope geochemistry of oceanic basalts and mantle evolution. Nature 296. 821-825.
- Williams M.A.J., Adamson D.A., Williams F.M., Horton W.H., and Parry O.E. 1980. Jebel Marra volcano; link between the Nile valley, the Sahara and Central Africa. In: The Sahara and the Nile: Quarternary environments and prehistoric occupation in northern Africa. Eds. A.J Williams and H. Faure, Balkema.
- Wood B.J. and Fraser. D.G. 1976. Elementary thermodynamics for geologists. London, Oxford University Press.
- Wood D.A. 1978. Major and trace element variations in the Tertiary lavas of eastern Iceland and their significance with respect to the Iceland geochemical anomaly. J. Petrol. 19, 393-436.
- Wood D.A. 1979. A variably veined sub-oceanic mantle - genetic significance from mid-ocean ridge basalts from geochemical evidence. Geology. 7, 499-503.
- Zielenski R.A. 1975. Trace element evaluation of a suite of rocks from Reunion Island, Indian Ocean. G.C.A. 39. 713-34.

Zindler A., Jagoutz E. and Goldstein S. 1982. Nd, Sr and Pb isotope systematics in a three component mantle: a new perspective. *Nature* 298, 519-23.

Barton M, Salters VJM and Huijsmans JPP. 1983. Sr isotope and trace element evidence for the role of continental crust in calc-alkaline volcanism on Santorini and Milos, Aegean Sea, Greece. *E.P.S.L.* 63, 273-291.

Poldervaart, A and Hess H H. 1951. Pyroxenes in the crystallisation of basaltic magma. *J. Geol.* 59, 472.

APPENDICES

APPENDIX A - Powder Preparation

Samples chosen for analysis were those which did not show appreciable signs of alteration in thin-section. In practice very few rocks showed any signs of alteration at all. The procedure used to produce powders suitable for analysis was as follows. Firstly, the samples were hand washed to remove adhering surface material and then left to dry. The weight of specimen crushed depended, on the nature of the rock. For example, for aphyric rocks about 400g would be crushed but for porphyritic about twice this sample would be used. The hand specimens were then reduced to chunks less than 3cm cubed in size by means of an hydraulic rock splitter. At this stage all pieces with weathered surfaces were discarded. All the remaining pieces were then reduced to small chips by means of a hand-driven percussion steel mortar. About 100g of the chips were then 'coned and quartered' (so as to obtain a representative sample, T Holder pers. comm.) and ground to a fine flour like consistency. This was achieved by grinding in a tungsten carbide Tema. The resultant powder was stored and labelled in clean glass bottles. Throughout the various stages of the preparation process the equipment was thoroughly cleaned and dried in between samples.

APPENDIX B - Electron Microprobe

The mineral analyses presented in this thesis were measured on the Jeol JXA-50A probe which is fitted with an energy dispersive system (Link 860 Series 2). All ZAF corrections were made on-line. The elements analysed were calibrated to the following standards:-

TABLE B1... CALIBRATION STANDARDS

Si	Wollastonite
Ti	Rutile
Al	Corundum
Fe	Fe metal
Mn	Rhodonite
Mg	HgO
Ca	Wollastonite
Na	Jaedite
K	Orthoclase
P	Apatite

The beam current used was approximately 1 nanoamp, the accelerating voltage was 20kV and the count time was 100 seconds.

Each analysis of major phases that is presented on the following pages represents the average of 3 spots.

clinopyroxene															
	24033	24034	24036	24036	24099	24099	24080	24080	24094	24094	24062	24291	24127	24127	
	CORE	RIM	CORE	PI"	CORE	RIM	CORE	RIM	CCR2	FIM	CCR2	CORE	CORE	RIM	
TiO2	46.73	45.49	46.47	46.65	49.53	47.62	46.06	47.52	49.32	50.35	47.64	47.96	47.95	46.41	
TiO2	1.43	3.32	2.47	2.56	2.07	3.06	2.75	2.64	1.02	1.94	2.17	1.58	1.72	2.13	
Al2O3	5.73	7.39	6.67	5.03	4.02	5.43	3.53	5.68	5.24	3.60	7.41	7.67	7.84	5.36	
Fe2O3	1.56	1.69	1.40	1.39	1.70	1.71	1.79	1.75	1.15	1.76	1.52	1.69	1.46	1.60	
FeO	5.62	6.05	6.24	6.73	6.12	6.15	6.45	6.29	4.15	6.35	5.46	6.07	5.27	5.73	
MnO	0.06	0.12	0.11	0.06	0.15	0.20	0.15	0.09	0.06	0.10	0.16	0.10	0.12	0.04	
MgO	12.95	11.66	12.73	13.05	13.06	12.72	12.19	12.73	14.70	13.46	12.55	13.23	12.89	11.87	
CaO	21.30	23.00	21.49	21.69	22.03	22.25	20.47	22.28	21.82	22.21	22.57	21.54	21.37	21.62	
Na2O	0.74	0.59	0.08	0.11	0.75	0.78	1.05	0.58	1.01	0.11	0.27	0.69	0.33	-	
K2O	0.03	0.03	0.04	-	-	-	0.01	0.01	-	-	-	0.02	0.04	-	
Total	99.70	99.43	99.35	99.21	99.43	99.92	100.45	99.57	96.46	99.91	100.15	100.75	99.00	98.36	
Ti	1.7403	1.7157	1.7660	1.8166	1.9546	1.7830	1.7093	1.7845	1.8434	1.8721	1.7665	1.7697	1.7873	1.7450	
Ti	0.0526	0.0942	0.0698	0.0719	0.0593	0.0862	0.0767	0.0746	0.0287	0.0542	0.0605	0.0438	0.0492	0.0618	
Al	0.3551	0.3378	0.2456	0.2214	0.1775	0.2397	0.4167	0.2515	0.2309	0.1578	0.3239	0.3337	0.3445	0.3334	
Fe3	0.0437	0.0477	0.0338	0.0530	0.0479	0.0432	0.0530	0.0494	0.0324	0.0494	0.0424	0.0462	0.0411	0.0455	
Fe2	0.1747	0.1909	0.2151	0.2119	0.1916	0.1926	0.2000	0.1975	0.1298	0.1975	0.1694	0.1874	0.1643	0.1819	
Mn	0.0019	0.0036	0.0035	0.0019	0.0048	0.0063	0.0047	0.0029	0.0015	0.0031	0.0050	0.0031	0.0038	0.0013	
Mg	0.7190	0.6559	0.7161	0.7262	0.7283	0.7078	0.6738	0.7124	0.6188	0.7470	0.7156	0.7276	0.7160	0.6663	
Ca	0.9491	0.9302	0.8657	0.8674	0.8939	0.8927	0.8135	0.8965	0.8738	0.8849	0.8967	0.8517	0.8535	0.8725	
Na	0.0534	0.0366	0.0058	0.0080	0.0545	0.0566	0.0755	0.0422	0.0732	0.0079	0.0194	0.0637	0.0239	-	
K	0.0014	0.0014	0.0019	-	-	-	0.0005	0.0005	-	-	-	0.0009	0.0019	-	
en	0.4122	0.3671	0.3985	0.4022	0.4039	0.3954	0.3993	0.3944	0.4493	0.4083	0.4016	0.4119	0.4130	0.3872	
fs	0.1093	0.1074	0.1197	0.1173	0.1362	0.1073	0.1195	0.1093	0.0712	0.1080	0.0951	0.1061	0.0948	0.1057	
wo	0.4875	0.5235	0.4818	0.4804	0.4699	0.4973	0.4821	0.4963	0.4795	0.4837	0.5033	0.4821	0.4922	0.5071	
Al,T1	0.4791	0.3593	0.3930	0.3083	0.2773	0.3895	0.4541	0.3922	0.3217	0.3361	0.3832	0.3849	0.3936	0.3740	
Al,T1	0.1299	0.1417	0.1170	0.0917	0.0727	0.1095	0.1459	0.1078	0.0763	0.0639	0.1168	0.1151	0.1064	0.1260	
Al,T1	0.1254	0.0544	0.0616	0.0350	0.0320	0.0227	0.1250	0.0360	0.0742	0.0294	0.0504	0.1034	0.1318	0.1415	
Fe,T1	0.1523	0.1812	0.1892	0.1900	0.1794	0.1799	0.1713	0.1823	0.1183	0.1812	0.1544	0.1651	0.1454	0.1612	
Mg,T1	0.6260	0.6224	0.6266	0.6480	0.6424	0.6630	0.5770	0.6578	0.7463	0.6852	0.6523	0.6405	0.6335	0.5902	
Ca,T2	0.3491	0.3302	0.2657	0.2674	0.2839	0.3229	0.2135	0.2965	0.2738	0.2849	0.2967	0.2517	0.2535	0.2725	
Na,T2	0.0366	0.0265	0.0058	0.0080	0.0545	0.0474	0.0610	0.0337	0.0422	0.0079	0.0194	0.0637	0.0239	-	
Fe,T2	0.0224	0.0093	0.0069	0.0089	0.0122	0.0127	0.0247	0.0152	0.0115	0.0163	0.0150	0.0223	0.0189	0.0204	
Mg,T2	0.0820	0.0335	0.0395	0.0752	0.0464	0.0463	0.0966	0.0547	0.0725	0.0617	0.0634	0.0867	0.0826	0.0761	

clinopyroxene												
	24036	24006	24118	24118	24101	24104	24040	24031	24061	24002	24002	24114
	CORE	PRM	CORE	PRM	CORE	CORE	CORE	GLASS	CORE	CORE	PRM	CORE
SiO2	47.75	48.19	49.13	49.12	47.25	49.90	49.34	52.15	51.01	51.57	51.20	52.50
TiO2	2.15	2.12	1.05	1.71	3.24	1.23	1.63	0.43	0.48	0.40	0.56	0.47
Al2O3	6.20	6.35	3.93	2.64	4.92	6.35	4.74	1.08	0.73	1.38	1.35	0.50
Fe2O3	1.70	1.70	1.71	1.35	2.25	1.24	1.71	2.71	3.44	2.54	2.55	2.73
FeO	6.14	6.11	6.14	6.65	4.10	4.46	6.17	9.75	12.39	9.14	9.30	9.82
MgO	0.04	0.19	0.31	0.33	0.14	0.04	0.22	0.93	0.97	1.00	1.06	1.11
MnO	13.41	13.33	13.14	12.97	11.62	14.02	13.78	12.63	9.64	11.10	10.95	10.77
CaO	21.55	21.50	21.49	22.07	21.33	21.90	21.98	19.48	20.31	21.38	22.54	21.25
Na2O	0.43	0.36	0.76	0.75	0.54	0.45	0.51	0.39	0.15	1.30	1.30	0.90
K2O	-	-	0.04	0.11	0.04	-	-	-	0.07	0.07	0.02	0.99
Total	99.37	100.15	99.30	98.20	99.63	100.09	100.08	99.55	99.40	99.87	100.91	100.13
Si	1.7875	1.7897	1.8611	1.8750	1.7905	1.8286	1.8345	1.9688	1.9654	1.9547	1.9317	1.9865
Ti	0.0605	0.0592	0.0470	0.0491	0.0923	0.0339	0.0456	0.0122	0.0139	0.0114	0.0159	0.0134
Al	0.2736	0.2780	0.1755	0.1188	0.2153	0.2959	0.2073	0.0481	0.0332	0.0617	0.0600	0.0223
Fe3	0.0480	0.0475	0.0487	0.0531	0.0641	0.0342	0.0480	0.0770	0.0956	0.0724	0.0734	0.0777
Fe2	0.1921	0.1898	0.1946	0.2122	0.2566	0.1368	0.1918	0.3079	0.3953	0.2896	0.2936	0.3106
Mn	0.0013	0.0060	0.0059	0.0107	0.0045	0.0012	0.0069	0.0297	0.0317	0.0321	0.0339	0.0356
Mg	0.7441	0.7375	0.7413	0.7379	0.6562	0.7657	0.7636	0.7106	0.5650	0.6270	0.6179	0.6073
Ca	0.8644	0.8675	0.8723	0.9027	0.8661	0.8599	0.8757	0.7880	0.8385	0.8684	0.9112	0.8616
Na	0.0312	0.0259	0.0558	0.0555	0.0617	0.0320	0.0368	0.0285	0.0112	0.0955	0.0951	0.0660
K	-	-	0.0019	0.0054	0.0019	-	-	-	0.0034	0.0034	0.0010	0.0043
en	0.4146	0.4110	0.4101	0.3982	0.3689	0.4345	0.4170	0.3934	0.3134	0.3513	0.3390	0.3413
fs	0.1064	0.1058	0.1076	0.1145	0.1442	0.0776	0.1047	0.1704	0.2215	0.1622	0.1611	0.1746
wo	0.4790	0.4833	0.4823	0.4872	0.4869	0.4879	0.4792	0.4362	0.4651	0.4865	0.4999	0.4842
Si11	0.3937	0.3948	0.3305	0.3375	0.5552	0.9143	0.9172	0.9644	0.9627	0.9774	0.9659	0.9933
Al11	0.1063	0.1052	0.0675	0.0594	0.1043	0.0357	0.0824	0.0156	0.0166	0.0226	0.0300	0.0067
Al211	0.0611	0.0677	0.0366	-	0.0058	0.1246	0.0422	0.0168	-	0.0164	-	0.0088
Fe11	0.1696	0.1690	0.1804	0.2006	0.2355	0.1224	0.1735	0.2703	0.3670	0.2843	0.2933	0.3046
Mg11	0.6607	0.6567	0.6374	0.6373	0.6023	0.6549	0.6907	0.6237	0.5193	0.6155	0.6174	0.5956
Ca11	0.8644	0.8675	0.8723	0.9027	0.8661	0.8599	0.8757	0.7880	0.8385	0.8684	0.9112	0.8616
Na11	0.0257	0.0259	0.0558	0.0555	0.0617	0.0320	0.0368	0.0285	0.0112	0.0955	0.0951	0.0660
K11	0.0000	0.0000	0.0019	0.0054	0.0019	0.0000	0.0000	0.0000	0.0034	0.0034	0.0010	0.0043
Mg12	0.0874	0.0811	0.0844	0.0806	0.0540	0.0808	0.0724	0.0869	0.0116	0.0005	0.0005	0.0111

	feldspar														
	24056 CORE	24056 RIM	24059 GLASS	24060 CORE	24060 RIM	24064 CORE	24064 RIM	24062 GLASS	24291 GLASS	24127 CORE	24127 RIM	24006 CORE	24006 RIM	24113 CORE	
SiO2	50.33	50.06	52.50	50.30	53.44	54.34	53.33	51.22	50.88	56.31	56.30	49.51	49.74	54.85	
TiO2	0.20	0.14	0.27	0.06	0.22	0.16	0.09	0.11	0.17	0.15	20.22	0.15	0.16	0.32	
Al2O3	30.99	31.22	26.27	30.35	28.51	28.29	28.93	30.25	30.42	27.40	27.42	31.23	31.23	25.97	
Fe2O3	0.72	0.34	0.81	0.67	0.59	0.52	0.52	0.53	1.12	0.49	0.50	0.54	0.47	0.41	
MnO	-	0.08	0.01	0.03	0.05	0.03	-	-	-	0.05	-	-	-	-	
MgO	0.15	0.12	-	0.02	0.06	-	-	-	-	0.22	0.04	-	0.02	0.14	
CaO	14.25	14.32	11.86	13.54	11.47	10.54	11.46	13.20	13.46	5.59	5.43	14.88	14.18	5.17	
Na2O	3.03	3.21	4.54	3.55	4.83	5.24	5.02	3.51	3.60	5.85	5.61	3.15	3.18	5.54	
K2O	0.17	0.22	0.36	0.16	0.34	0.45	0.30	0.23	0.21	0.40	0.48	-	-	0.52	
Total	99.32	100.21	99.25	98.70	99.51	99.67	99.65	99.05	99.86	100.46	120.00	99.46	98.98	97.52	
Si	2.3001	2.2841	2.4034	2.3227	2.4344	2.4654	2.4257	2.3456	2.3243	2.5248	2.1656	2.2752	2.2898	2.5333	
Ti	0.0065	0.0043	0.0093	0.0021	0.0075	0.0055	0.0031	0.0038	0.0058	0.0051	0.5849	0.0052	0.0055	0.0320	
Al	1.6677	1.6793	1.5581	1.6524	1.5311	1.5131	1.5513	1.6359	1.6363	1.4484	1.2435	1.6920	1.6949	1.4141	
Fe3	0.0244	0.0250	0.0279	0.0232	0.0202	0.0178	0.0179	0.0184	0.0386	0.0165	0.0145	0.0188	0.0162	0.0143	
Mn	-	0.0031	0.0004	0.0012	0.0019	0.0012	-	-	-	0.0019	-	-	-	-	
Mg	0.0109	0.0092	-	0.0014	0.0041	-	-	-	-	0.0147	0.0023	-	0.0014	0.0096	
Ca	0.6375	0.7001	0.5532	0.6700	0.5599	0.5172	0.5585	0.6488	0.6588	0.4607	0.3687	0.7327	0.6995	0.4533	
Na	0.2632	0.2940	0.4030	0.3179	0.4266	0.4610	0.4427	0.3122	0.3189	0.5086	0.4184	0.2807	0.2838	0.4961	
K	0.0099	0.0123	0.0210	0.0106	0.0198	0.0260	0.0174	0.0135	0.0122	0.0229	0.0236	-	-	0.0306	
an	0.7150	0.7023	0.5790	0.6710	0.5564	0.5151	0.5443	0.6658	0.6655	0.4644	0.4679	0.7230	0.7113	0.4628	
ab	0.2743	0.2949	0.4001	0.3184	0.4240	0.4590	0.4346	0.3204	0.3221	0.5126	0.5037	0.2770	0.2887	0.5060	
or	0.0101	0.0128	0.0209	0.0106	0.0196	0.0259	0.0171	0.0136	0.0124	0.0231	0.0244	-	-	0.0312	
Si,Ti	0.5750	0.5710	0.6008	0.5807	0.6036	0.6163	0.6064	0.5874	0.5811	0.6312	0.5414	0.5686	0.5724	0.6333	
Al,Ti	0.4169	0.4179	0.3405	0.4131	0.3828	0.3753	0.3878	0.4090	0.4096	0.3621	0.3109	0.4230	0.4237	0.3535	
Ca,Fe	0.6975	0.7001	0.5532	0.6700	0.5599	0.5172	0.5585	0.6488	0.6588	0.4607	0.3687	0.7327	0.6995	0.4533	
Na,Fe	0.2642	0.2940	0.4030	0.3179	0.4266	0.4610	0.4427	0.3122	0.3189	0.5086	0.4184	0.2807	0.2838	0.4961	
K,Al	0.0099	0.0123	0.0210	0.0106	0.0198	0.0260	0.0174	0.0135	0.0122	0.0229	0.0236	-	-	0.0306	

feldspar														
	24112	24101	24104	24040	24015	24019	24031	24031	24016	24016	24113	24081	24002	24002
	314	GMASS	GMASS	GMASS	GMASS	GMASS	CORF	FTF	C.FE	FIM	GMASS	CORE	CORE	PIA
SiO2	51.43	52.33	53.63	57.22	59.56	66.09	54.40	64.11	65.90	66.68	66.20	65.95	66.64	65.36
TiO2	0.11	0.12	0.15	0.12	0.22	0.19	0.26	0.09	0.09	0.07	0.13	0.07	0.14	0.23
Al2O3	27.92	29.79	27.83	26.49	23.47	19.58	27.60	20.32	19.40	18.48	19.36	20.59	20.20	19.37
Fe2O3	0.44	0.60	0.49	0.39	0.70	0.54	0.49	0.36	0.22	0.49	0.40	0.50	0.28	0.40
MnO	-	0.04	0.02	0.02	-	0.04	-	0.03	-	0.04	0.03	0.05	-	0.06
MgO	0.43	0.55	0.55	-	-	0.02	-	-	0.02	0.34	-	0.37	-	-
CaO	11.37	12.11	8.31	8.77	5.73	0.76	10.32	1.54	0.80	0.30	0.26	1.96	0.99	0.53
Na2O	4.53	4.19	5.43	6.13	7.03	7.37	5.24	7.56	7.29	7.06	6.57	3.10	8.00	7.63
K2O	0.26	0.29	0.46	0.52	1.13	4.46	0.40	4.73	5.91	6.84	7.57	3.37	4.93	5.65
Total	96.51	99.37	99.37	99.66	97.39	99.57	99.71	98.74	100.13	100.30	100.52	100.57	101.03	99.44
Si	2.4162	2.3974	2.5161	2.5776	2.7155	2.9535	2.4877	2.9023	2.9436	2.9840	2.9622	2.9136	2.9392	2.9312
Ti	0.0039	0.0041	0.0051	0.0041	0.0075	0.0064	0.0089	0.0031	0.0030	0.0024	0.0044	0.0023	0.0046	0.0078
Al	1.5464	1.5274	1.4940	1.4063	1.2615	1.0274	1.4879	1.0845	1.0479	0.9750	1.0213	1.0675	1.0504	1.0505
Fe3	0.0157	0.0205	0.0166	0.0132	0.0240	0.0183	0.0163	0.0121	0.0075	0.0165	0.0135	0.0166	0.0092	0.0135
Mn	-	0.0015	0.0008	0.0009	-	0.0015	-	0.0012	-	0.0015	0.0011	0.0019	-	0.0023
Mg	0.0230	0.0034	0.0034	-	-	0.0013	-	-	0.0013	0.0227	-	0.0046	-	-
Ca	1.5724	0.5333	0.4512	0.4233	0.2799	0.0364	0.5057	0.0747	0.0363	0.0144	0.0125	0.0928	0.0421	0.0279
Na	0.4172	0.3674	0.4762	0.5354	0.6259	0.6906	0.4646	0.6636	0.6314	0.6126	0.5700	0.6939	0.6842	0.6687
K	0.0156	0.0163	0.0265	0.0299	0.0657	0.2543	0.0233	0.2732	0.3366	0.3905	0.4322	0.1900	0.2774	0.3233
an	0.5694	0.6049	0.4730	0.4282	0.2831	0.0371	0.5049	0.0739	0.0380	0.0141	0.0123	0.0950	0.0419	0.0273
ab	0.4151	0.3773	0.4952	0.5416	0.6442	0.7038	0.4676	0.6561	0.6273	0.6021	0.5618	0.7105	0.6817	0.6557
or	0.0155	0.0172	0.0278	0.0302	0.0677	0.2591	0.0235	0.2701	0.3346	0.3838	0.4259	0.1945	0.2764	0.3170
Si71	0.6040	0.5993	0.6290	0.6444	0.6789	0.7334	0.6219	0.7256	0.7359	0.7460	0.7406	0.7284	0.7349	0.7329
Al71	0.3256	0.3968	0.3710	0.3517	0.3154	0.2566	0.3720	0.2711	0.2620	0.2437	0.2553	0.2669	0.2626	0.2626
Ca71	1.5724	0.5333	0.4512	0.4233	0.2799	0.0364	0.5057	0.0747	0.0363	0.0144	0.0125	0.0928	0.0421	0.0279
Na71	0.4172	0.3674	0.4762	0.5354	0.6259	0.6906	0.4646	0.6636	0.6314	0.6126	0.5700	0.6939	0.6842	0.6687
K71	0.0156	0.0163	0.0265	0.0299	0.0657	0.2543	0.0233	0.2732	0.3366	0.3905	0.4322	0.1900	0.2774	0.3233

feldspar		amphibole			biotite	
	24114	24115	24116	24015	24016	24016
	COPE	COPE	ALM	COPE	COPE	ALM
S102	66.95	39.45	39.43	41.02	36.75	36.34
T102	0.02	5.95	5.72	7.73	7.63	7.36
Al2O3	17.26	13.36	13.26	1.92	12.35	12.53
Fe2O3	0.14	2.66	2.75	3.32	3.34	3.33
MnO	0.02	9.55	10.00	31.75	12.03	12.21
MgO	0.01	0.03	0.08	1.52	0.47	0.40
CaO	0.16	12.20	11.41	2.61	13.17	0.64
Na2O	7.23	11.56	11.56	0.76	0.01	0.71
K2O	6.38	3.16	2.74	7.95	0.76	0.71
Total	100.17	101.43	100.43	106.00	100.53	85.46
Si	2.9349	5.7549	5.8173	6.4039	2.7213	3.0957
Ti	0.0007	0.6528	0.6397	0.9076	0.4277	0.4367
Al	1.0123	2.3837	2.3100	0.3534	1.1314	1.2710
Fe3	0.0043	0.2921	0.3095	1.0365	0.1863	0.2145
Mn	0.0006	1.1683	1.2340	4.1457	0.7451	0.8579
Mg	0.0007	0.0099	0.0100	0.2010	0.0295	0.0285
Ca	0.0076	2.6524	2.6189	0.6073	1.4534	0.0601
Na	0.6250	1.3069	1.3276	0.1271	0.0008	0.0639
K	0.3629	0.3933	0.7839	2.4065	0.1091	0.1157
ap	0.0077	0.1731	0.1674	0.0159	0.8343	0.9970
ab	1.6273					
or	0.3645					
Si,T1	0.7462	1.0000	1.0000	1.0000	1.9505	0.0934
Al,T1	0.2531	0.1255	0.1366	0.0244	0.6303	0.7733
Ca,A	0.0076	0.2843	0.2899	0.0036	0.2423	0.2261
Na,A	0.6250	0.9035	0.9133	0.0636	-	0.1834
K,A	0.3629	0.0965	0.0362	0.0379	0.2299	0.4056
		Fe,M2	-	0.7401	0.4434	0.0382
		Mg,M2	-	0.1054	0.2854	0.0407
		Fe2,M3	0.3053	0.3203	0.2722	0.5506
		Mg,M3	0.6842	0.6797	0.1272	0.1540
		Si,A	0.7001	0.6115	1.0000	0.1041
		Na,A	0.1262	0.2141	-	0.1157
						0.9970

Majority:		24015	24019	24020	24049	24062	24071	24127	24006	24118	24101	24104	24090	24019	24031
	CORE	CORE	CORE	CORE	CORE	CORE	CORE	CORE	CORE	COPE	CORE	COPE	CORE	CORE	CORE
S102	0.43	0.44	0.46	0.33	0.37	0.32	0.32	0.31	0.53	0.30	0.35	0.26	0.34	0.41	0.43
T102	22.23	26.31	27.34	27.10	22.33	22.31	22.31	1.02	26.54	26.43	27.84	18.60	13.30	22.43	13.47
A1203	1.73	1.52	1.74	1.65	1.77	3.75	3.75	54.96	1.76	2.53	1.15	6.58	12.55	-	0.43
F203	23.40	17.22	14.56	15.57	23.37	15.56	15.56	10.37	14.74	17.31	14.37	23.75	32.23	25.78	29.13
F20	43.05	52.12	52.12	52.85	49.11	46.45	46.45	17.25	53.00	50.62	53.61	46.59	36.57	43.71	43.61
Y0	0.27	0.76	0.63	0.75	0.21	0.33	0.33	0.12	2.74	1.12	0.10	0.59	0.31	1.22	2.33
Y10	2.14	2.17	2.98	2.30	2.40	2.23	2.23	15.72	0.52	3.23	2.13	0.41	6.33	0.29	0.93
C10	0.22	0.32	0.15	0.03	0.27	0.05	0.05	-	0.17	0.11	5.10	-	-	1.32	0.16
A20	0.26	-	-	-	0.56	0.24	0.24	-	0.12	-	0.42	-	0.39	0.08	-
K20	-	-	-	-	-	-	-	-	-	-	0.02	-	0.05	-	-
Total	37.53	100.29	100.45	100.63	101.66	98.24	98.24	130.35	100.12	102.67	100.79	56.56	102.19	96.30	95.63
S1	0.0143	0.0153	0.0166	0.0138	0.0349	0.0115	0.0115	0.0023	0.0155	0.0106	0.0127	0.0056	0.0113	0.0156	0.0197
T1	0.6160	0.7159	0.7422	0.7387	0.6049	0.6325	0.6325	0.0205	0.7362	0.7046	0.7611	0.5067	0.3331	0.6432	0.5419
A1	0.0353	0.0649	0.0753	0.0705	0.0750	0.1310	0.1310	1.7335	0.0765	0.1061	0.0493	0.2415	0.4928	-	0.0221
F23	0.6473	0.8694	0.3955	0.4246	0.6326	0.5823	0.5823	0.2029	0.4051	0.4611	0.3530	0.6716	0.8093	0.6305	0.2565
F22	1.4773	1.5733	1.5734	1.6021	1.4761	1.4333	1.4333	0.3593	1.6346	1.5073	1.6254	1.4767	1.0165	1.5432	1.4223
X0	0.0271	0.0233	0.0123	0.0230	0.0247	0.0259	0.0259	0.0027	0.0856	0.0336	0.0246	0.0166	0.0047	0.0333	0.0770
Y1	0.1173	0.1172	0.1603	0.1342	0.1235	0.1225	0.1225	0.6264	0.0266	0.1704	0.1154	0.0230	0.3172	0.0164	0.0541
C1	0.0037	0.0124	0.0056	0.0031	0.0104	0.0020	0.0020	-	0.0067	0.0042	0.0035	-	-	0.0033	0.0067
Na	0.0155	-	0.0259	-	0.0390	0.0172	0.0172	-	0.0066	-	0.0246	-	0.0252	0.0059	-
K	-	-	-	-	-	-	-	-	-	-	0.0009	-	0.0021	-	-
ULV	0.6160	0.7169	0.7422	0.7387	0.6049	0.6325	0.6325	0.0205	0.7362	0.7046	0.7611	0.5067	0.3331	0.6432	0.5419
F23	0.2158	0.1555	0.1318	0.1415	0.2109	0.1309	0.1309	0.0646	0.1364	0.1537	0.1310	0.2239	0.2676	0.2268	0.2355
T1	0.2053	0.2330	0.2474	0.2462	0.2016	0.2102	0.2102	0.0064	0.2454	0.2349	0.2537	0.1656	0.1110	0.2144	0.1306
F22	0.4924	0.5264	0.5245	0.5340	0.44520	0.44779	0.44779	0.1331	0.5449	0.5024	0.5433	0.4422	0.3395	0.5164	0.4743

magnetite				ilmenite				nepheline				apatite		
	24016	24113	24114		24113		24016		24113		24040		24113	24040
	COFE	COFE	COFE		COFE		COFE		COFE		COFE		COFE	COFE
SiO2	0.34	0.49	0.32	SiO2	0.30	SiO2	50.34	SiO2	0	SiO2	0	SiO2	0	0
TiO2	1.60	13.13	13.37	TiO2	52.91	TiO2	0.02	TiO2	0	TiO2	0	TiO2	0	0.03
Al2O3	0.01	0.25	0.07	Al2O3	0.43	Al2O3	29.35	Al2O3	0.06	Al2O3	0	Al2O3	0.06	0
Fe2O3	64.44	31.26	42.72	Fe2O3	2.54	FeO	2.05	FeO	0.66	FeO	0.44	FeO	0.66	0.44
FeO	32.44	44.30	40.20	FeO	33.97	TnO	0.23	TnO	0.01	TnO	0	TnO	0.01	0
MnO	0.25	2.38	3.36	MnO	0.99	MjO	0.22	MjO	0.17	MjO	0.36	MjO	0.17	0.36
MjO	-	0.45	0.42	MjO	4.09	Na2O	16.70	CaO	54.03	CaO	54.44	CaO	54.03	54.44
CaO	-	-	0.02	CaO	0.20	K2O	2.62	Na2O	0.48	Na2O	0	Na2O	0.48	0
Na2O	-	-	0.24	Total	101.84	Total	100.35	K2O	0.14	K2O	0.06	P2O5	41.52	40.80
Total	99.06	97.76	101.51	Si	0.0131	Si	1.1729	Total	47.06	Total	56.21			
Si	0.0132	0.0183	0.0119	Ti	0.9520	Ti	0.0004							
Ti	0.0465	0.5237	0.3472	Al	0.0121	Al	0.7925							
Al	0.0005	0.0113	0.0031	Fe3	0.0457	Fe2	0.0333							
Fe3	1.8739	0.9036	1.1931	Fe2	0.9001	Tn	0.0006							
Fe2	1.0516	1.4231	1.2603	Mn	0.0201	Mj	0.0076							
Tn	0.0032	0.0337	0.1056	Mj	0.1452	Na	0.7554							
Mj	-	0.0253	0.0232	Ca	0.0051	K	0.0779							
Ca	-	-	0.0002	ilm	0.6346	ne	0.7554							
Na	-	-	0.0173	Fe3,M1	0.0152	ks	0.0779							
ulv	0.0466	0.5237	0.3472	Ti,M1	0.3173	q	0.1664							
Fe3,M1	0.6266	0.3012	0.3477	Fe,M1	0.2667	Si,T1	0.5865							
Ti,M1	0.0155	0.1746	0.1291			Al,T1	0.3962							
Fe,M1	0.3505	0.4744	0.4231			Na,A	0.7554							
						K,A	0.0779							
						Na,A	0.1664							

APPENDIX C - X.R.F Analysis

Major and trace elements were analysed by x-ray fluorescence using a Phillips PW 1400 spectrometer.

Major Element Analysis

The following elements were analysed at 40kV and 60mA as major elements:-

Si, Ti, Al, Fe, Mn, Mg, Ca, Na, K and P.

Preparation of Glass Discs

0.4g of rock powder was accurately weighed into a platinum crucible. This was diluted, 10:1, by 10g of lithium borate spectroflux (Johnson and Matthey spectroflux 110) which acts as a flux for the rock. The powder and flux were then mixed in the crucible using a Teflon rod. The contents of the crucible, covered by a platinum lid, was then fused in a furnace for 30 minutes at a temperature of 1000 degrees C. After cooling the fusion mixture was reweighed and made up to 10.4g with more flux. The loss in weight was mostly due to water being lost from the hygroscopic flux in the furnace. The fusion mixture was then remelted by an assembly of four bunsen burners. The added flux was stirred into the melt by a platinum wire until homogeneity was attained. The melt was then rapidly cast into a copper ring placed on a steel disc warmed on a hotplate. The disc was made by vigorously depressing the molten blob with an aluminium plunger. Following cooling in an aluminium pen the discs were trimmed, labelled and stored in polythene bags.

Loss on Ignition

A ceramic crucible containing a known weight of powder was placed into the 1000 degrees C furnace for thirty minutes. After cooling the crucible was reweighed to obtain the new weight of the powder. The loss on ignition can be obtained by taking the the difference between the two weights and dividing this by the sample to give an estimate of the proportion of volatiles in the sample.

Trace Element Analysis

The following elements were analysed as trace elements on pressed powder pellets:-

Th, Ga, Nd, Ce, La, Sc, Cr, Co, Ni, Cu, Zn, Rb, Sr, Nb, Pb, and Ba

The operating conditions for Nd, Ce, La and Sc were 50kV and 50mA; the other traces were analysed at 30kV and 30mA.

Preparation of Pressed Powder Pellets

About 15g of rock powder was mixed with 2ml of Moviol agglutinate. The mixture was then compressed in a toughened steel jacket to a pressure of 10 tons per sq. inch for 10 seconds. The resulting pellet was then dried in a low temperature oven for at least 30 minutes prior to being labelled and stored in polythene bags. Shortly before analysis the sample was placed in a vacuum desiccator. The pellets were held in the sample holder by means of 6 micron mylar film which was virtually invisible to the x-ray radiation.

Reduction of Data and Errors

All the data is corrected for mass absorption and matrix affects by computer program. Also the affect of machine drift is compensated for by reference to an internal standard which always occupies one of the four sample positions. A detailed study on reproducibility of major and trace element data and accuracy of major element data on the Leeds X.R.F. was conducted by Downes (1983) and found to be acceptable. The accuracy of some of the trace element data can be gauged from Figs. C1a-e. In table C1 the accuracy for trace elements can be gauged by comparison with international standards.

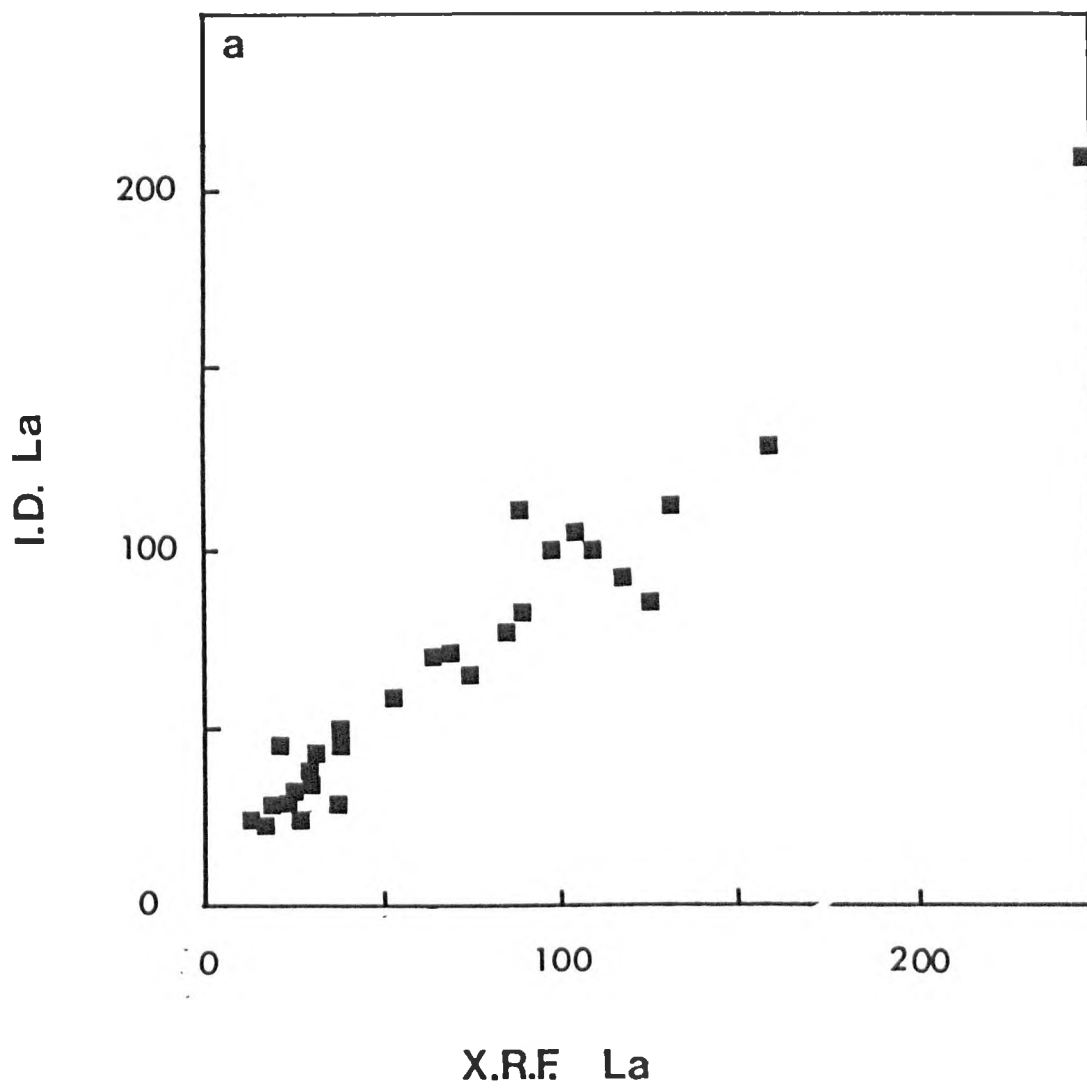
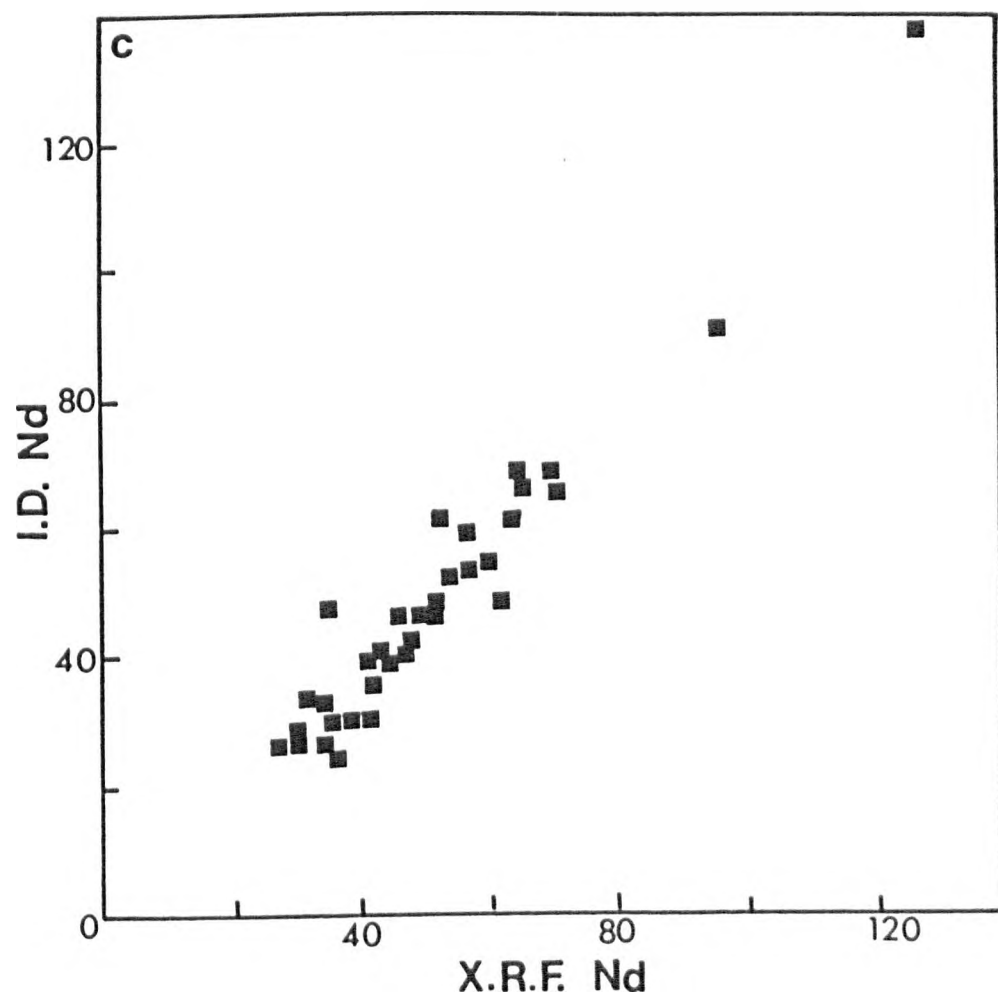
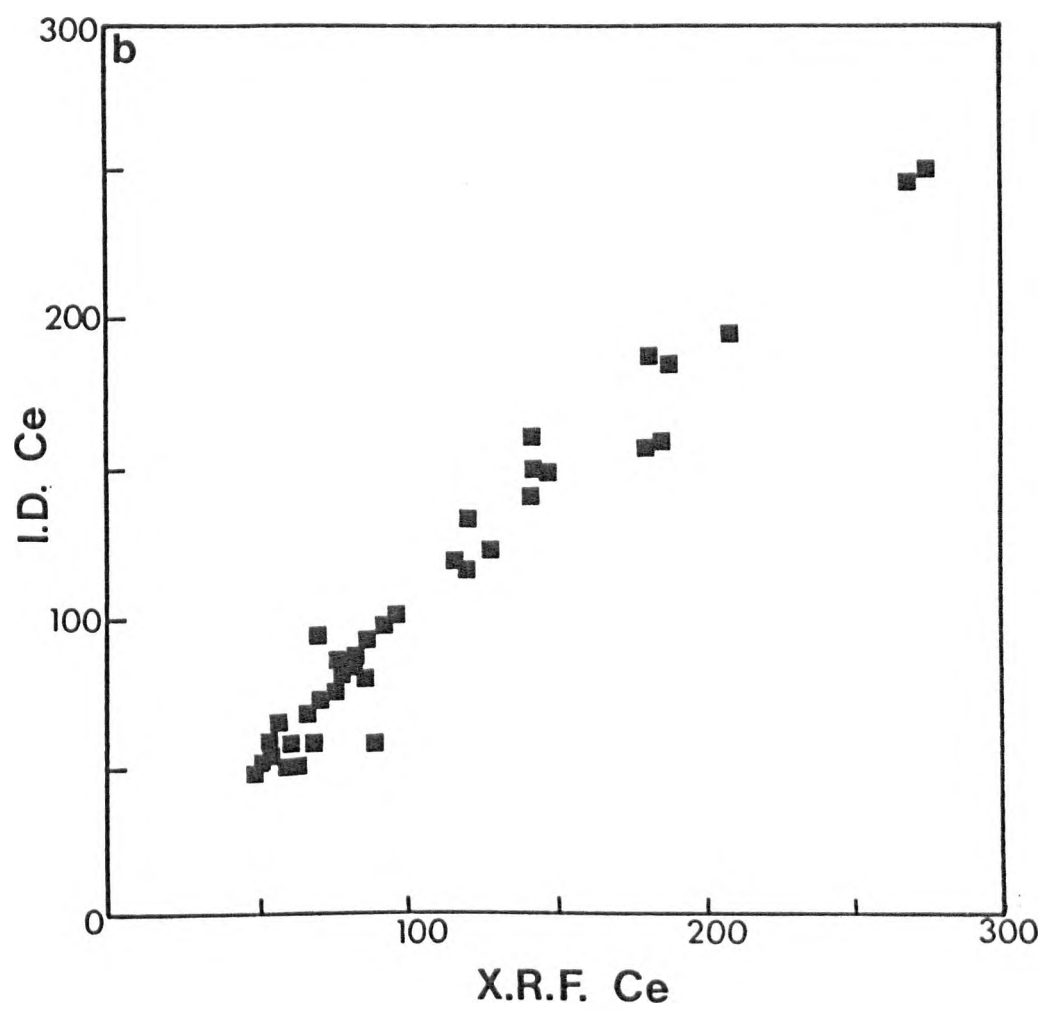
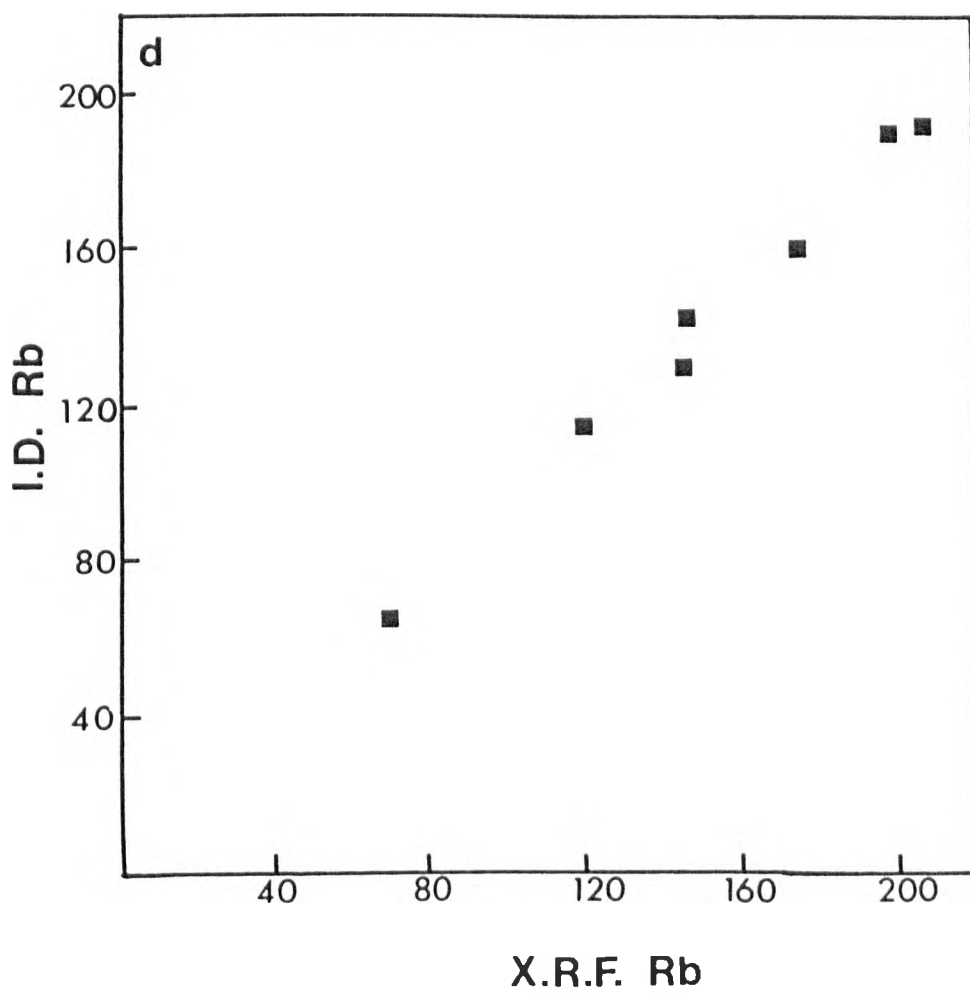


Fig. C1a-e I.D. vs X.R.F. comparisons for La, Ce, Nd, Rb and Sr.





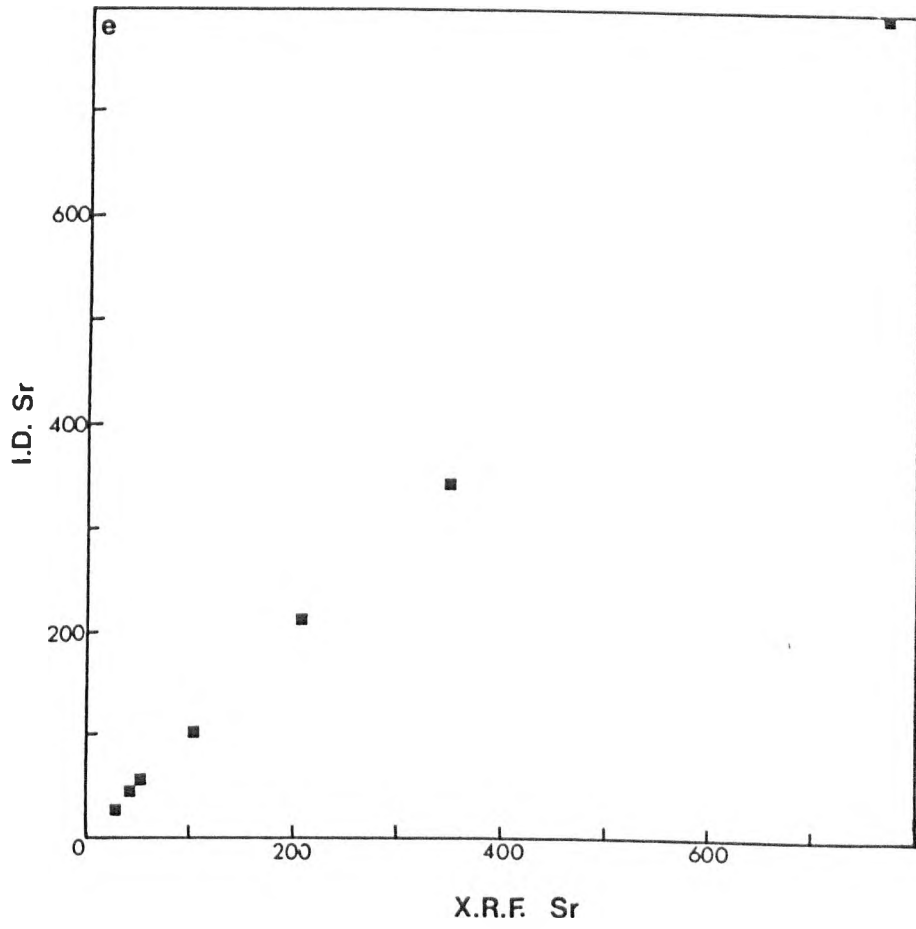


TABLE C1... RESULTS FROM ANALYSES OF INTERNATIONAL STANDARDS

	GRANITE G2 7201	BASALT BCR-1 2318	GRANITE NIM G 1407	NORITE NIM N 1414	SYENITE NIM S 1419
La	86 100	15 25	116 110	15 3	nd
Ce	152 150	54 54	222 200	11 10	nd
Nd	56 60	28 29	66 70	4 2nd	
Th	31 24	7 6	62 53	4 1nd	
Sc	3 4	36 34	<3 1	44 38nd	
Ga	21 23	22 23	32 26	16 16nd	
Cr	3 9	24 16	7 3	34 21	4 13
Co	8 6	43 37	5 2	50 50	6 3
Ni	5 6	13 13	7 8	116 118	6 6
Cu	17 11	26 19	16 12	21 11	24 21
Zn	33 85	101 98	117 123	49 53	54 62
Rb	170 170	46 47	338 330	3 5	540 550
Sr	484 480	325 330	9 10	255 260	61 64
Y	12 12	37 37	146 135	7 7	9 9
Zr	328 300	186 185	289 290	5 22	15 45
Nb	13 14	13 14	66 52	<3 2	<3 4
Pb	30 29	10 15	40 39	<3 6	<3 4
Ba	1774 1850	696 630	107 110	109 110	2613 2600

Values on left mass absorption corrected, values on right preferred values in ppm.

The major and trace element analyses are presented on the following pages.

Table C2... Major and Trace Element Analyses for Volcanic Rocks.

	New Series Basalts									
	24001	24022	24039	24044	24045	24063	24067	24070	24072	24079
SiO2	45.47	45.22	44.89	44.95	45.81	44.00	44.43	46.51	46.70	45.10
TiO2	2.37	2.52	2.39	2.64	2.51	2.25	2.60	2.19	2.36	2.67
Al2O3	15.79	16.99	14.75	15.56	16.23	13.21	13.23	15.62	15.84	15.95
Fe2O3T	11.55	11.72	11.65	12.18	12.26	12.28	12.72	11.57	11.54	12.42
MnO	0.19	0.16	0.20	0.15	0.19	0.19	0.20	0.19	0.16	0.19
MgO	7.43	6.43	9.22	6.76	8.08	12.81	11.20	8.80	7.38	7.93
CaO	9.91	10.21	10.46	10.19	10.16	9.83	11.85	5.20	9.38	10.08
Na2O	3.55	3.75	3.59	4.42	3.67	3.02	3.10	3.69	3.85	3.80
K2O	1.37	1.35	1.44	1.24	1.26	1.08	0.99	1.10	1.31	1.26
P2O5	0.69	0.66	0.68	0.84	0.64	0.61	0.69	0.76	0.66	0.94
LOI	1.21	0.14	0.53	1.34	0.12	0.83	0.13	0.41	0.82	0.09
Th	4	5	4	3	4	4	6	6	6	4
Ga	1	16	13	15	11	12	14	14	13	13
Nd	39	40	40	39	37	34	36	37	42	40
Ce	57	65	61	64	65	52	58	63	71	67
La	22	23	28	23	24	14	19	25	28	22
Sc	28	25	23	27	31	32	34	26	29	27
Cr	216	59	369	183	203	815	646	233	208	162
Co	54	56	57	63	99	71	61	56	55	51
Ni	116	44	181	64	111	342	238	216	111	96
Cu	39	35	46	41	47	49	67	46	42	42
Zn	91	91	98	96	39	90	85	87	87	33
Rb	21	25	29	18	23	19	18	19	26	24
Sr	907	973	823	880	856	762	822	859	956	960
Y	21	23	22	21	20	16	19	20	21	21
Zr	126	95	136	97	122	100	82	118	149	115
Nb	36	40	44	33	35	31	33	33	42	39
Pb	4	3	0	3	6	1	0	1	5	4
δa	701	703	603	536	490	411	506	568	634	493
87Sr/86Sr	0	0.7036	0.7035	0.7036	0	0.7036	0.7039	0	0.7038	0
143Nd/143Nd	0	0	0.5129	0	0	0.5128	0.5129	0	0.5127	0
esr	-10000	-12.06	-14.36	-12.07	-10000	-13.22	-9.155	-10000	-10.15	-10000
end	-10000	-10000	4.487	-10000	-10000	3.609	4.233	-10000	0.4682	-10000
Rb/Sr	0.02315	0.02569	0.03524	0.02045	0.02637	0.02493	0.0219	0.02212	0.0272	0.025
K/Rb	0.05415	0.04482	0.04121	0.05713	0.04547	0.04718	0.04565	0.04805	0.04182	0.04357
Zr/Nb	3.5	2.375	3.051	2.939	3.486	3.226	2.485	3.576	3.548	2.949
alkalis	4.92	5.10	5.03	5.66	4.93	4.10	4.09	4.79	5.16	5.06
Mg/No	61.63	57.64	66.25	57.92	62.35	72.13	68.55	64.54	61.34	61.3
Total	97.56	97.15	99.82	100.27	100.33	100.11	101.14	100.44	100.20	100.51

New Series Basalts										
	24082	24084	24086	24091	24093	24094	24105	24120	24121	24132
SiO2	43.87	44.15	43.62	44.23	43.89	46.10	44.66	43.69	41.46	45.23
TiO2	2.47	2.67	2.49	2.39	2.60	2.34	2.54	2.69	2.33	2.15
Al2O3	16.95	16.43	12.97	13.06	13.35	15.86	13.80	13.61	12.84	15.45
Fe2O3T	11.73	11.80	12.87	12.69	12.86	11.72	12.45	12.36	12.32	10.91
MnO	0.20	0.13	0.20	0.20	0.19	0.19	0.16	0.19	0.18	0.18
MgO	5.63	5.84	12.73	12.36	12.07	7.40	10.21	9.94	9.54	7.46
CaO	10.32	10.26	10.93	10.95	11.25	9.46	9.80	11.36	9.28	10.57
Na2O	3.42	4.00	3.31	3.22	2.90	3.90	3.78	3.58	4.45	3.51
K2O	1.32	1.42	0.95	0.99	0.96	1.32	0.96	1.20	1.04	1.32
P2O5	0.71	0.83	0.57	0.55	0.66	0.90	0.51	0.70	0.50	0.53
LOI	3.72	2.64	0.09	0.08	0.53	1.04	1.10	0.32	1.20	2.28
Th	4	5	4	4	4	5	3	4	4	5
Ga	14	14	13	11	12	14	11	12	15	14
Nd	41	42	30	33	30	42	29	38	27	37
Ce	65	70	50	52	55	75	49	64	59	53
La	28	23	15	16	16	31	17	22	16	22
Uc	24	27	33	33	33	29	30	33	33	33
Cr	23	64	655	736	660	202	320	534	351	214
Co	43	52	61	62	59	56	66	60	67	49
Ni	36	49	331	301	292	107	189	185	201	113
Cu	36	40	62	57	64	42	45	58	46	50
Zn	86	97	87	96	47	87	93	86	105	84
Rb	26	26	17	18	13	26	19	23	22	22
Jr	1013	964	723	692	325	972	659	670	682	670
Y	22	22	17	17	17	21	18	21	19	22
Zr	109	132	82	95	83	143	113	115	112	128
Nb	43	43	32	33	31	41	32	40	34	35
Pb	3	3	4	1	1	1	3	0	3	5
Ba	650	622	397	377	436	620	302	466	298	504
07Sr/86Sr	0.7037	0	0.7036	0.7035	0.7036	0.7038	0.7035	0	0.7036	0.7039
143Nd/143Nd	0	0	0.5129	0.5129	0.5129	0	0.5129	0	0.5129	0
εsr	-11.44	-10000	-13.06	-14.34	-12.45	-10.6	-14.05	-10000	-12.63	-9.042
end	-10000	-10000	4.116	4.955	4.428	-10000	4.74	-10000	4.457	-10000
Nb/Sr	0.02552	0.02697	0.02351	0.02601	0.02132	0.02675	0.02483	0.02644	0.03226	0.03284
K/Rb	0.04405	0.04533	0.04638	0.04565	0.04427	0.04214	0.04194	0.0433	0.03524	0.0498
Zr/Nb	2.535	3.07	2.563	2.879	2.677	3.488	3.531	2.875	3.294	3.657
alkalis	4.40	5.42	4.26	4.21	3.26	5.22	4.74	4.78	5.49	4.83
Σ_40	54.57	55.11	71.04	70.73	69.35	61.03	67.04	66.61	65.76	62.91
Total	100.45	100.23	103.73	100.78	101.32	100.25	99.97	94.86	95.14	99.59

New Series Basalts
24133 24136

S102	45.06	47.09
TiO2	2.64	2.28
Al2O3	15.77	16.01
Fe2O3T	11.46	12.23
MnO	0.20	0.19
MgO	6.88	7.22
CaO	9.90	10.43
Na2O	4.00	3.60
K2O	1.64	0.87
P2O5	0.94	0.57
LOI	1.83	0.21
Th	5	3
Ga	12	15
Nd	51	35
Ce	87	52
La	39	16
Sc	26	31
Cr	181	127
Co	51	59
Ni	94	79
Cu	33	49
Zn	92	98
Rb	30	14
Sr	1094	681
Y	24	20
Zr	134	108
Nb	49	24
Pu	3	1
Ba	969	386
87Sr/86Sr	0	0.704
143Nd/143Nd	0	0.5127
esr	-10000	-7.012
and	-10000	0.3316
Rb/Sr	0.02742	0.02056
K/Rb	0.04537	0.05158
Zr/Nb	2.735	4.5
alkalis	5.64	4.67
Mg/No	59.83	59.42
Total	100.34	100.69

New Series Mugearites							
	24019	24026	24040	24041	24104	24109	24123
SiO2	55.74	52.70	43.69	49.94	46.22	46.31	48.83
TiO2	1.33	1.92	2.35	2.13	2.51	2.13	2.55
Al2O3	17.15	16.72	16.91	17.78	17.29	16.99	17.90
Fe2O3T	9.15	9.66	10.83	9.71	10.73	10.33	11.80
MnO	0.26	0.22	0.16	0.17	0.16	0.20	0.21
MgO	2.04	3.13	5.33	3.58	5.05	4.60	3.91
CaO	3.88	4.96	5.00	6.92	9.47	8.02	7.33
Na2O	6.37	5.27	6.72	5.60	6.82	5.19	5.65
K2O	2.68	2.73	1.98	2.60	1.67	2.00	2.00
P2O5	0.75	1.02	1.05	1.01	0.90	1.00	1.27
LOI	0.45	1.75	0.22	0.82	0.22	0.99	0.21
Th	12	10	5	10	4	5	6
Pa	15	15	15	14	13	14	10
Nd	64	64	52	46	42	43	52
Ce	122	118	96	86	71	83	93
La	69	60	42	43	30	39	38
Sc	15	16	22	13	21	18	16
Cr	0	0	80	3	35	59	0
Co	24	30	42	36	50	36	49
Ni	1	3	41	3	35	33	2
Cu	15	19	29	19	39	31	23
Zn	102	94	85	86	102	89	73
Rb	46	51	33	54	26	43	39
Sr	854	704	993	1303	929	1118	1360
Y	32	33	25	23	24	23	25
Zr	300	276	179	225	139	123	141
Hf	72	63	47	68	45	57	55
Pb	6	3	3	5	4	2	6
delta	1215	1374	970	950	731	1057	990
87Sr/86Sr	0.7044	0.7043	0.7044	0.7038	0.7041	0.7038	0.7039
143Nd/142Nd	0.5124	0.5125	0.5124	0.5128	0.5127	0.5128	0.5127
-sr	-1.274	-2.683	-1.561	-10.08	-5.252	-9.51	-6.857
end	-4.76	-2.77	-5.345	3.394	0.6242	2.38	1.069
Rb/Sr	0.05386	0.07244	0.03323	0.04144	0.02799	0.03946	0.02868
K/Rb	0.94836	0.04524	0.0498	0.03996	0.05331	0.0386	0.04256
Zr/Nb	4.167	4.059	3.409	3.309	3.089	2.158	2.564
alkalis	9.05	9.05	3.70	8.20	8.49	7.19	7.65
137No	35.61	44.56	54.97	47.77	53.86	52.46	45.11
Total	99.50	100.13	102.24	100.16	101.04	97.76	101.66

New Series Hawaiites								
	24003	24024	24049	24062	24101	24111	24118	24127
SiO2	46.10	46.74	43.99	46.31	47.92	46.74	48.94	47.02
TiO2	2.74	2.52	2.65	2.79	2.29	2.52	2.48	2.23
Al2O3	15.78	16.41	16.34	16.73	17.17	17.08	16.78	17.39
Fe2O3T	12.41	12.03	12.19	11.77	11.43	13.17	9.64	10.13
MnO	0.20	0.20	0.20	0.16	0.16	0.20	0.16	0.19
MgO	7.28	6.18	6.06	5.57	6.06	6.45	3.82	4.82
CaO	9.53	9.11	10.64	9.97	9.12	9.61	8.60	8.94
Na2O	4.12	4.19	4.31	4.19	4.44	4.78	4.67	4.47
K2O	1.55	1.62	1.58	1.51	1.27	1.53	1.61	1.38
P2O5	0.92	0.61	0.90	0.88	0.67	0.80	1.10	0.84
LOI	0.21	1.65	1.42	0.73	0.13	0.63	0.21	0.44
Th	4	6	5	4	5	0	6	5
Ga	3	9	18	15	17	0	15	13
Nd	42	38	44	45	36	35	50	42
Ce	32	76	35	76	63	70	66	78
La	25	24	29	31	27	21	36	29
Sc	29	28	28	27	22	23	16	19
Cr	138	36	70	35	70	63	6	71
Co	50	51	53	50	52	47	34	39
Ni	75	54	49	35	55	38	9	34
Cu	38	38	46	39	31	30	23	27
Zn	88	79	94	102	58	82	85	76
Rb	30	33	32	26	24	29	34	25
Sr	1003	841	987	931	842	1027	1123	1212
Y	22	22	25	24	21	20	25	23
Zr	135	139	142	139	126	116	142	100
Mo	44	50	57	45	35	45	48	39
Pb	3	1	6	4	5	4	3	2
da	601	513	575	731	467	557	665	1090
87Sr/86Sr	0	0	0.7035	0.7036	0.7039	0.7038	0.7041	0.7041
143Nd/144Nd	0	0	0.5128	0	0.5127	0.5128	0.5126	0.5126
esr	-10000	-10000	-13.77	-12.78	-9.084	-9.652	-5.11	-5.677
end	-10000	-10000	4.013	-10000	0.7608	2.497	-0.1951	-0.3316
Rb/Sr	0.02991	0.03924	0.03242	0.02793	0.0295	0.02824	0.03028	0.02063
K/Rb	0.04268	0.04075	0.04093	0.0442	0.04392	0.04379	0.0393	0.04582
Zr/Nd	3.064	2.78	2.491	3.029	3.6	2.622	2.958	2.564
alkalis	5.67	5.21	5.69	5.70	5.71	6.31	6.26	5.65
Mg/No	59.27	60.33	55.22	54	56.81	54.85	49.06	54.13
Total	100.54	101.26	109.29	100.61	100.66	102.91	100.41	97.85

New Series Caldera Trachytes

	24016	24017	24020	24025
SiO2	62.29	65.37	64.98	63.26
TiO2	0.55	0.39	0.40	0.44
Al2O3	17.61	15.96	15.77	16.12
Fe2O3T	4.17	4.23	4.02	4.83
MnO	0.13	0.16	0.18	0.23
MgO	0.60	0.36	0.30	0.38
CaO	1.40	0.70	0.34	0.53
Na2O	7.00	7.18	7.12	6.84
K2O	5.46	5.47	5.48	5.54
P2O5	0.12	0.07	0.07	0.09
LOI	0.23	1.38	0.63	1.79
Th	18	32	24	13
Ga	23	21	24	21
Nd	46	76	65	56
Ce	110	221	183	130
La	64	107	105	83
Sc	4	3	6	11
Cr	0	0	0	0
Co	16	23	22	20
Ni	3	3	0	1
Cu	13	13	12	12
Zn	83	118	103	92
Rb	114	175	142	83
Sr	121	13	19	12
Y	33	55	51	37
Zr	488	865	526	377
Yb	102	170	142	83
Pb	14	28	20	14
Ra	464	54	252	211
87Sr/86Sr	0.7045	0.7052	0	0.7073
143Nd/143Nd	0.5125	0.5124	0.5124	0.5124
εsr	0.7097	10.57	-10000	40.31
εnd	-3.253	-4.916	-5.15	-4.487
Rb/Sr	0.9421	13.46	7.474	6.917
K/Rb	0.03975	0.02574	0.03203	0.0554
Zr/Yb	4.784	5.083	6.521	4.542
alkalis	12.46	12.65	12.60	12.38
SiO2/Al2O3	26.3	17.43	15.62	16.33
Total	99.61	101.26	99.79	100.44

New Series Mafic Bearing Trachytes

24031 240E1 24037 24113

SiO ₂	61.43	61.44	63.62	61.51
TiO ₂	0.61	0.62	0.85	0.56
Al ₂ O ₃	17.21	16.32	16.86	16.14
Fe ₂ O _{3T}	4.75	4.70	5.83	4.38
MnO	0.20	0.14	0.14	0.12
MgO	0.67	0.66	0.68	0.46
CaO	1.78	1.97	2.11	1.37
Na ₂ O	6.67	6.33	6.28	7.06
K ₂ O	5.01	4.76	4.08	5.81
P ₂ O ₅	0.21	0.12	0.28	0.15
LOI	1.92	3.03	1.27	0.41
Th	12	20	19	16
Ga	16	20	21	13
Nd	50	60	66	44
Ce	97	142	144	117
La	66	35	98	58
Sc	11	11	10	4
Cr	0	0	0	0
Co	21	19	22	24
Ni	2	3	3	0
Cu	14	11	13	14
Zn	81	99	96	76
Rb	81	118	79	101
Sr	204	207	352	170
Y	27	40	41	26
Zr	456	493	492	449
Nb	80	112	77	107
Pb	3	19	7	9
da	1377	1105	1628	390
87Sr/86Sr	0.7046	0.7067	0.7053	0.7042
143Nd/147Nd	0.5124	0.5123	0.5121	0.5126
ε _{Sr}	1.561	30.94	15.16	-4.131
ε _{Nd}	-4.038	-6.535	-10.71	-0.5901
ε _{Yb}	0.3971	0.57	0.2244	1.443
ε _{Rb}	0.05134	0.03343	0.04237	0.04775
Zr/Hf	5.7	4.402	5.39	4.106
alkalis	11.65	11.93	10.36	12.47
J _{Mo}	25.92	25.83	22.44	20.67
Total	100.46	100.00	102.04	100.05

New Series Phonolites
24089

SiO2	56.67
TiO2	0.25
Al2O3	19.81
Fe2O3T	4.24
MnO	0.24
MgO	0.28
CaO	1.48
Na2O	9.56
K2O	5.62
P2O5	0.03
LOI	0.71
Th	17
Ua	20
Nd	52
Ce	150
La	7
Sc	2
Cr	0
Co	22
Ni	3
Cu	12
Zn	119
Pb	166
Sr	144
Y	31
Zr	412
Mo	128
Pb	23
Ua	685
⁸⁷ Rb/ ⁸⁶ Sr	0.7047
¹⁴³ Nd/ ¹⁴⁴ Nd	0.5124
⁸⁷ Sr	3.123
⁸⁷ Rb	-5.052
Mo/Sr	1.153
K/Rb	0.0281
Zr/Nb	3.217
Alkalis	15.14
J_No	12.55
Total	79.74

Pyroclastic Sequence Basalts

	24005	24010	24011	24060
S102	45.00	42.60	46.01	44.38
T102	2.64	3.29	2.76	2.77
Al2O3	15.84	15.26	16.51	14.67
Fe2O3T	12.40	14.02	10.20	12.20
MnO	0.19	0.20	0.17	0.16
MgO	7.01	6.09	2.98	8.35
CaO	9.72	11.44	12.24	10.66
Na2O	4.25	4.13	3.43	3.31
K2O	1.43	1.25	1.39	1.20
P2O5	0.84	0.62	0.61	0.55
LOI	0.61	1.37	3.21	0.19
Th	4	4	6	5
Ga	13	15	13	14
Nd	43	74	36	39
Ce	78	137	69	67
La	26	56	11	26
Sc	27	26	31	34
Cr	140	13	36	259
Co	60	48	46	52
Ni	73	15	39	93
Cu	39	33	41	46
Zn	88	108	99	93
Nb	27	22	25	23
Sr	972	1080	873	733
Y	22	35	24	23
Zr	140	57	141	139
Nb	40	41	42	41
Pb	3	10	4	3
Ju	577	561	406	398
⁸⁷ Sr/ ⁸⁶ Sr	0	0	0	0.7036
¹⁴³ Nd/ ¹⁴³ Nd	0	0	0	0.5128
esr	-10000	-10000	-10000	-12.67
and	-10000	-10000	-10000	3.258
Rb/Sr	0.02778	0.02037	0.02864	0.03132
K/Rb	0.04396	0.04716	0.04615	0.0433
Zr/Nb	3.5	2.366	3.357	3.39
alkalis	5.69	5.38	4.92	4.51
Tj_No	53.37	51.76	42.02	62.52
Total	99.94	100.92	99.51	98.46

Pyroclastic Sequence Hawaiites
24006

SiO2	47.72
TiO2	2.59
Al2O3	16.53
Fe2O3T	11.00
MnO	0.15
MgO	5.69
CaO	9.35
Na2O	4.51
K2O	1.32
P2O5	0.61
LOI	5.14
Th	6
Sr	17
Nd	36
Ce	61
La	20
Sc	25
Cr	67
Co	50
Ni	44
Cu	41
Zn	90
Rb	24
Sr	720
Y	22
Zr	144
Nb	39
Pb	6
Ba	467
$^{87}\text{Sr}/^{86}\text{Sr}$	0.7036
$^{143}\text{Nd}/^{144}\text{Nd}$	0.5129
δSr	-12.07
δNd	4.877
Rb/Sr	0.03333
K/Rb	0.04565
Zr/Nb	3.682
alkalis	5.33
$\sum\text{No}$	56.2
Total	79.61

Pyroclastic Sequence Phonolites

	24002	24013	24015	24114	24128
Sr102	59.06	58.48	59.13	58.62	57.95
Ti02	0.63	0.56	0.69	0.69	0.73
Al2O3	18.42	18.38	16.06	17.26	15.80
Fe2O3T	4.43	5.11	7.23	5.09	7.22
MnO	0.20	0.24	3.16	0.22	0.13
MgO	0.84	0.79	0.71	1.00	1.02
CaO	1.40	1.67	1.21	1.43	1.68
Na2O	8.05	8.33	7.37	6.98	6.29
K2O	5.15	5.37	5.34	5.25	5.56
P2O5	0.03	0.09	0.06	0.02	0.07
LOI	0.71	1.71	2.53	1.57	3.45
Th	15	19	27	13	24
Ga	26	23	43	7	34
Nd	57	65	96	37	39
Ce	145	183	275	125	257
La	49	103	159	125	128
Sc	4	3	5	6	6
Cr	0	0	0	0	0
Co	20	13	45	14	23
Ni	3	3	3	3	3
Cu	11	12	14	11	12
Zn	135	167	163	174	261
Rb	110	142	161	115	151
Sr	111	322	29	5	5
Y	41	53	62	50	61
Zr	519	671	1040	610	862
Nb	153	200	270	180	240
Pb	14	19	31	18	26
Ba	731	597	0	119	0
⁸⁷ Sr/ ⁸⁶ Sr	0.7046	0.7046	0.7072	0.7034	0
¹⁴³ Nd/ ¹⁴⁴ Nd	0.5128	0.5128	0.5126	0.5125	0
ε _{Sr}	1.419	1.419	33.33	-15.61	-10000
ε _{Nd}	3.16	2.497	-0.1561	4.135	-10000
Rb/Sr	0.991	0.441	5.613	23.02	30.2
K/Rb	0.03846	0.03139	0.02756	0.03796	0.03056
Zr/Nb	3.392	3.355	3.852	3.339	3.592
alkalis	13.20	14.20	12.71	12.23	11.89
U ₂ /No	31.99	27.46	19.59	32.77	25.99
Total	98.94	101.22	100.51	96.13	99.75

Pyroclastic Sequence Ignimbrites

	24012	24018	24103	24110	24115	24119
SiO2	64.23	60.84	62.92	54.51	57.90	59.70
TiO2	0.75	0.51	0.88	0.45	0.67	0.65
Al2O3	15.10	16.92	15.04	16.73	16.39	17.44
Fe2O3T	5.83	3.94	6.12	5.72	5.25	5.71
MnO	0.16	0.05	0.23	0.31	0.30	0.30
MgO	0.63	0.41	0.48	0.31	0.33	0.62
CaO	0.41	0.57	0.46	1.36	1.77	0.83
Na2O	7.56	5.95	7.41	7.35	7.50	9.32
K2O	5.44	5.27	5.47	5.11	5.67	5.31
P2O5	0.07	0.07	0.09	0.05	0.07	0.13
LOI	0.41	5.82	1.21	3.40	3.59	0.56
Th	31	28	35	16	16	20
Pa	30	33	33	23	25	30
Ud	98	98	109	53	86	69
Ce	255	270	328	277	223	197
La	157	148	166	160	168	95
Sc	4	4	7	4	3	4
Er	0	0	0	0	0	0
Co	16	13	22	16	13	25
Ni	3	4	5	2	3	2
Cu	12	11	11	15	9	10
Zn	150	108	194	217	181	196
Ga	173	208	202	200	223	136
Ge	4	37	21	25	217	12
Y	87	68	83	71	0	57
Zr	977	993	1170	765	632	700
Yb	223	259	280	275	185	205
Pb	31	26	37	30	13	20
87Sr/86Sr	0	44	33	67	104	47
143Nd/143Nd	0	0	0	0	0	0.7074
143Nd/143Nd	0	0	0	0	0	0.5128
-sr	-10000	-10000	-10000	-10000	-10000	41.16
end	-10000	-10000	-10000	-10000	-10000	3.667
Ab/Sr	43.25	5.622	9.619	6.877	1.051	11.33
K/Rb	0.0261	0.02103	0.02248	0.02121	0.02064	0.03241
Zr/Nb	4.381	3.834	4.179	3.509	3.416	3.415
alkalis	13.00	11.22	12.66	12.46	13.17	14.63
H2O	21.14	20.52	16.29	26	28.17	21.22
Total	100.64	100.35	100.31	95.40	100.54	100.57

Old Series Hawaiites

	24034	24090	24099	24122
SiO2	46.33	45.51	45.15	44.37
TiO2	2.73	2.25	2.88	2.52
Al2O3	16.96	17.13	15.47	15.45
Fe2O3T	11.67	11.76	12.09	11.77
lnO	0.16	0.23	0.16	0.20
MgO	5.05	3.88	6.80	7.49
CaO	2.76	7.70	8.69	11.37
Na2O	3.96	4.63	4.52	4.64
K2O	1.94	1.86	1.82	1.47
P2O5	0.87	1.04	0.85	0.79
LOI	0.66	1.93	0.43	0.30
Th	4	9	5	5
Pa	16	16	15	10
Nd	47	54	48	42
Sm	82	120	77	64
La	32	53	31	23
Sc	20	14	26	29
Cr	9	0	156	256
Co	43	38	51	64
Ni	21	6	67	44
Cu	31	25	34	47
Zn	94	39	95	33
Rb	33	39	30	28
Sr	980	1041	367	578
Y	22	31	21	20
Zr	146	259	105	104
Nb	43	94	53	39
Pb	3	4	6	0
87Sr/86Sr	0.7034	0.7064	0.7041	0.7036
143Nd/143Nd	0.5123	0.5128	0.5126	0.5124
esr	-10.22	26.5	-5.11	-12.46
end	2.35	3.999	-0.3121	4.04
Rb/Sr	0.03367	0.03746	0.03174	0.02863
K/Rb	0.05005	0.03958	0.05035	0.04357
Zr/Nb	3.042	2.755	1.781	2.667
alkalis	5.95	6.54	6.34	6.11
4J_Ko	51.35	45.01	53.25	61.22
Total	99.46	97.97	99.89	100.37

Old Series Mugearites
24661

SiO2	50.35
TiO2	2.07
Al2O3	18.06
Fe2O3T	10.49
MnO	0.22
MgO	3.38
CaO	6.83
Na2O	5.45
K2O	2.41
P2O5	1.03
LOI	0.21
Th	3
Ua	7
Nd	49
Ce	96
La	42
Sc	12
Cr	0
Co	44
Ni	6
Cu	20
Zn	85
Rb	51
Sr	1181
Y	23
Zr	203
Nb	72
Pb	4
da	760
⁸⁷ Sr/ ⁸⁶ Sr	0.7037
¹⁴³ Nd/ ¹⁴² Nd	0.5129
esr	-10.53
end	4.155
nb/Sr	0.04312
K/Rb	0.03522
Zr/Nb	2.814
alkalis	7.36
ig_no	44.42
Total	100.61

contaminated trachytes - Old Series

	24030	24042	24043	24046	24053	24057	24059	24060	24075	24099
SiO2	64.97	62.37	61.71	69.13	67.36	65.54	64.13	66.53	64.56	67.41
TiO2	0.36	0.45	0.45	0.23	0.34	0.47	0.56	0.42	0.55	0.14
Al2O3	15.99	14.91	15.66	15.02	13.79	17.54	16.92	14.31	16.26	14.25
Fe2O3T	5.45	3.04	5.71	4.34	4.55	5.61	5.14	6.56	4.44	3.34
MnO	0.20	0.04	0.23	0.16	0.19	0.20	0.09	0.31	0.15	0.10
MgO	0.17	0.14	0.36	0.13	0.34	0.32	0.15	0.23	0.18	0.12
CaO	7.13	0.10	0.94	0.25	0.72	0.15	0.30	0.26	0.41	0.53
Na2O	6.83	6.35	6.14	5.24	4.77	6.25	6.52	5.31	6.83	5.90
K2O	5.29	5.02	5.12	5.20	5.09	5.38	5.72	5.21	5.43	4.80
P2O5	0.03	0.04	0.09	0.01	0.06	0.08	0.33	0.04	0.08	0.01
LOI	1.05	0.96	3.23	1.59	2.03	0.26	0.76	0.16	1.04	3.82
Th	20	23	15	13	23	18	18	30	19	42
Ua	29	18	12	9	20	17	19	25	19	30
Ud	127	72	56	39	79	65	40	103	51	64
Ce	267	170	125	153	219	167	83	274	123	206
La	246	91	71	176	99	80	56	147	75	108
Sc	7	10	5	8	6	5	9	5	6	1
Cr	0	0	0	0	0	0	0	0	0	0
Co	14	16	16	21	20	24	30	26	25	23
Ni	3	3	0	5	2	1	1	2	3	3
Cu	12	10	11	12	12	9	12	11	13	13
Zn	121	91	87	139	109	107	89	126	67	159
Rb	107	103	99	153	125	116	120	224	103	193
Sr	4	5	33	8	25	27	8	12	42	8
Y	92	46	35	80	56	40	32	74	36	73
Zr	631	598	350	548	678	456	432	751	428	831
Yb	137	112	103	175	128	120	113	152	108	248
Pb	22	15	15	33	24	17	17	30	13	35
Na	24	644	794	22	61	236	326	49	365	3
87Sr/86Sr	0.7066	0	0.7055	0.7054	0	0	0	0	0.7049	0.7043
143Nd/143Nd	0.5124	0.5121	0.5125	0.5122	0	0	0.5124	0	0.5124	0.5123
εsr	29.81	-10000	14.19	69.55	-10000	-10000	-10000	-10000	5.673	68.13
εnd	-4.526	-9.949	-2.407	-3.055	-10000	-10000	-4.233	-10000	-4.542	-6.73
Rb/Sr	13.31	21.6	3	19.11	5	4.37	15	14.67	2.452	24.37
K/Rb	0.04115	0.03853	0.04293	0.02623	0.0338	0.03784	0.03956	0.0153	0.04376	0.02069
Zr/Yb	4.606	5.337	3.689	5.417	5.297	3.2	3.823	3.911	3.963	3.351
alkalis	12.16	11.37	11.26	10.44	9.66	11.63	12.24	10.52	12.26	10.70
Uj/Mo	7.145	10.25	13.52	6.516	15.64	12.4	6.75	7.556	9.137	8.183
Total	100.59	96.45	94.64	101.29	99.44	101.80	100.62	99.74	99.43	100.42

contaminated trachytes - Old Series

24150

SiO2	61.73
TiO2	2.17
Al2O3	16.59
Fe2O3T	4.82
MnO	0.20
MgO	0.37
CaO	0.53
Na2O	6.73
K2O	5.06
P2O5	0.06
LOI	3.26
In	20
Ca	21
Mg	62
Ce	181
La	117
Sc	4
Cr	0
Co	21
Ni	3
Cu	13
Zn	131
Pb	115
Sr	23
Y	31
Zr	825
Nb	158
Pb	21
Ba	403
$^{87}\text{Sr}/^{86}\text{Sr}$	0.7045
$^{143}\text{Nd}/^{144}\text{Nd}$	0.5126
esr	0
and	-0.7603
Rb/Sr	5.934
K/Rb	0.03649
Zr/Nb	5.222
alkalis	12.05
^{87}Rb	16
Total	99.74

Old Series Uncontaminated Trachytes						
	24047	24052	24054	24071	24073	24125
SiO2	60.69	59.49	60.97	60.41	60.56	61.57
TiO2	0.23	0.21	0.14	0.22	0.28	0.69
Al2O3	16.51	17.42	17.94	16.76	16.78	16.69
Fe2O3T	6.82	5.01	5.08	6.61	5.41	6.26
MnO	0.27	0.19	0.22	0.26	0.15	0.32
MgO	0.24	0.43	0.25	0.33	0.22	0.55
CaO	1.41	1.21	1.43	1.77	1.53	0.93
Na2O	7.14	7.02	6.66	5.92	7.78	6.85
K2O	5.32	5.56	5.31	5.07	4.99	5.61
P2O5	0.04	0.05	0.01	0.03	0.05	0.05
LOI	1.41	2.97	2.07	2.92	2.73	0.60
Th	19	21	23	28	18	17
Ua	20	17	27	30	20	28
Nd	81	80	71	102	67	67
Ce	220	229	210	266	176	179
La	103	117	131	167	102	90
Sc	3	3	3	0	5	5
Cr	0	0	0	0	0	0
Co	17	19	17	21	21	25
Ni	3	2	3	4	3	3
Cu	10	11	12	11	12	10
Zn	152	130	143	203	112	152
Rb	127	142	136	159	113	119
Sr	22	17	44	12	37	15
Y	61	52	51	30	49	54
Zr	654	617	694	935	607	583
Nb	192	222	235	295	177	170
Pb	20	20	21	26	16	16
Ju	28	131	290	0	645	14
87Sr/86Sr	0	0	0.7047	0	0.7057	0
143Nd/143Nd	0	0	0.5128	0.5128	0.5128	0.5127
esr	-10000	-10000	2.939	-10000	17.03	-10000
end	-10000	-10000	2.692	2.263	2.903	2.048
80/8r	5.773	8.353	3.105	13.25	3.054	7.933
K/Rb	0.03477	0.0325	0.03235	0.02647	0.03665	0.03913
Zr/Nb	3.406	3.62	3.004	3.169	3.429	3.429
alkalis	12.46	12.58	11.97	10.99	12.77	12.46
Uj_Th	6.029	17.55	10.68	10.12	9.163	17.49
Total	100.07	99.46	100.68	100.27	100.48	100.12

Old Series Phonolites
 24265 24267 24129

LiO2	60.30	60.39	54.55
Th	1.34	0.72	3.04
Ta	21	21	21
Sr	22	31	22
Yb	32	70	52
Ce	226	163	146
La	112	109	89
Sc	5	3	3
Cr	0	0	3
Co	19	25	25
Mn	2	3	3
Cu	15	11	15
Zn	162	179	121
K2O	135	131	116
Sr	1	32	178
Y	59	58	39
Zr	743	673	619
H2O	219	204	193
Pb	22	13	21
Sum	16	50	141
375F/365F	0	0.7047	0.7038
143Nd/142Nd	?	0.5129	0.5126
Sr	-10000	2.839	-2.536
Sum	-10000	2.224	-0.5462
K2O/Sr	0.03135	4.076	0.6517
K2O	3.472	0.03619	0.03656
Li2O	13.14	3.259	4.327
Al2O3	7.101	13.32	13.55
SiO2	39.5	19.17	20.69
Total	100.40	100.40	97.75

APPENDIX D - Isotopic Analysis

In the following procedures meticulous care was taken to ensure that contamination and cross-contamination was minimised. The equipment was thoroughly cleaned before use, all preparation took place in a 'clean' atmosphere and appropriately pure reagents were used.

Sr and Rb were loaded onto single Ta filaments. Nd and REE's were loaded onto triple filament assemblies consisting of two outer Ta filaments and a centre Re filament. The filaments were outgassed for five minutes in a vacuum to better than 10^{-5} Torr.

Sr Isotope Analysis

Firstly, 30ml Teflon beakers were rinsed for several hours in distilled water and then cleansed in conc. HNO_3 for at least two days. The beakers were then boiled twice in distilled water for 30 minutes. The beakers were then rinsed in s.b. water and dried. To the clean beaker, about 200mg of powder was added and digested overnight in 2ml of conc. HNO_3 and 15ml of 40% HF. After evaporation 2ml of conc. HNO_3 was again added and evaporated. The residue was converted to chloride by adding 15ml of 6M HCl and evaporating. The residue was then just covered with 2.5M HCl and left to dissolve. The solution was then transferred to clean centrifuge tubes and centrifuged to separate out any suspension. 1ml of the solution was then loaded onto the anion exchange column by an auto-pipette. The sample was washed onto the resin bed and eluted by 45ml of 2.5 HCl.

The Sr was collected by washing 12ml of 2.5N HCl onto the column. The sample was then evaporated and stored under Parafilm until required.

Sr was loaded onto a Ta single filament as follows. Firstly, a large drop of H₃PO₄ was placed onto the filament and evaporated until a small amount of it remained. To this a small drop of s.b. water was added containing the dissolved sample. The sample was then evaporated at 1A. Excess H₃PO₄ was liberated by turning the current up to 2.4A for a few seconds. The loaded filaments were now ready for analysis

Sr isotopes measured on both the VG micromass 4430 and the VG isomass 54E. Operating conditions were nominally 2kG and 8 and 8.1 kV for the respective spectrometers. Isotopic peaks switched automatically across masses 88, 97, and 86. Rb interference was monitored and compensated for, at peak 85. The 88 tail was monitored and compensated for, at 87.3. The zero was measured at 84.5. On the MN30, approximately 450 scans were routinely measured with a delay time of 1.5 seconds and a count time 1 second. On the 54E 200 scans were routinely measured using a 2 second delay time and a 5 second count time.

Nd Isotope Analysis

Beaker treatment was the same as for the Sr method. About 150mg of sample was added to the clean beaker and digested overnight in 2ml of conc. HNO₃ and 15ml of 40% HF. After evaporation a further 2ml of conc. HNO₃ was added and evaporated. Approximately 10ml of aqua-regia mixture,

consisting of equal proportions of 6M HNO₃ and conc. HNO₃ was added and evaporated. To the residue 2ml of conc. HNO₃ was added and evaporated, added once more and evaporated to incipient dryness. The residue was taken up in 5ml of 75% 8M CH₃COOH + 25% 5M HNO₃ and left for a day. The extraction of Nd involves the use of three anion exchange columns using Bio-Rad AG 1X8 resin. The first, principally separates the major element cations. The second separates Nd from the other REE's and principally Sm. The final columns clean-up columns, amongst other things, reduces the Ba content in the sample. The solution was then centrifuged and decanted onto the first column set which had been pretreated with 90% 8M CH₃COOH + 10% 5M HNO₃. The sample was eluted with 50ml of 90% 8M CH₃COOH + 10% 5M HNO₃ and collected using 0.05M HNO₃. The sample was then evaporated and taken up in 1ml of 75% MeOH + 10% 8M CH₃COOH + 5% H₂O. This was then loaded onto the second columns pretreated with 75% MeOH + 10% 8M CH₃COOH + 5% H₂O. The separation of the REE's is temperature dependent and this was regulated by water jackets. The sample was eluted with 75% MeOH + 10% 8M CH₃COOH + 5% H₂O at 25 degrees C. Following this the sample was further eluted with 75% MeOH + 5% 8M CH₃COOH + 10% H₂O at 35 degree C before the sample was collected in more of the same solution. After evaporation the sample was taken up in 75% 8M CH₃COOH + 25% 5M HNO₃ and loaded onto the clean-up columns pretreated with 90% 8M CH₃COOH + 10% 5M HNO₃. The sample was eluted with 15ml of 90% 8M CH₃COOH + 10% 5M HNO₃ and then collected with 5ml of 0.05M HNO₃.

The sample was loaded onto the side filaments of a

Re/Ta triple filament assembly and stored for analysis.

All the $^{143}\text{Nd}/^{144}\text{Nd}$ measurements were made on the MM30 at operating conditions of 3kG and 3.0kV accelerating voltage. Peaks were switched automatically across masses 146, 144 and 143. A zero was measured at 146.5 and Sm interference was monitored, and compensated for, at 147. About 700 scans across the mass spectrum were routinely measured. $^{143}\text{Nd}/^{144}\text{Nd}$ was normalised to a $^{146}\text{Nd}/^{144}\text{Nd}$ ratio of 0.7219. As a check for $^{143}\text{Nd}/^{144}\text{Nd}$, $^{148}\text{Nd}/^{144}\text{Nd}$ was additionally measured on some runs. The two ratios are correlated but $^{148}\text{Nd}/^{144}\text{Nd}$ is not affected by radioactive decay of Sm

Results of Standards

These are the mean and 2 standard deviation values of Sr and Nd standards which were measured during the duration of the isotopic study by workers in the Leeds Lab.

Sr Standard NBS987 MM30 0.710279 ± 80 (11 analyses)

Sr Standard NBS987 54E 0.710264 ± 52 (36 analyses)

Nd Standard La Jolla 54E 0.511865 ± 60 (13 analyses)

The $^{87}\text{Sr}/^{86}\text{Sr}$ and $^{143}\text{Nd}/^{144}\text{Nd}$ for the analysed samples are presented in Table D1. The error quoted is to two standard errors. All the $^{87}\text{Sr}/^{86}\text{Sr}$ ratios are present day values.

TABLE D1... 87Sr/86Sr AND 143Nd/144Nd ISOTOPIC DATA

NEW SERIES BASALTS		
24022	0.703649±24	nd
24038	0.703488±23	0.512870±10
24063	0.703569±23	0.512825±11
24067	0.703855±35	0.512857±9
24071	nd	0.512756±6
24072	0.703735±25	0.512664±11
24082	0.703694±30	nd
24088	0.703580±18	0.512851±24
24091	0.703490±25	0.512894±14
24093	0.703623±45	0.512867±9
24094	0.703753±26	nd
24105	0.703513±44	0.512883±8
24121	0.703607±33	0.512870±26
24131	0.703717±32	0.512777±9
24132	0.703863±23	nd
24136	0.704006±47	0.512657±8
PYROCLASTIC SEQUENCE BASALT		
24080	0.703606±38	0.512807±22
OLD SERIES BASALTS		
24021	0.703750±21	nd
24029	0.703817±27	0.512678±13
24044	0.703650±20	nd
24053	0.703730±20	nd
24083	0.703560±19	0.512851±8
24086	0.703727±21	nd
NEW SERIES HAWAIIITES		
24049	0.703530±21	0.512846±8
24062	0.703596±25	nd
24099	0.704138±118	0.512624±9
24101	0.703964±17	0.512679±5
24104	0.704126±38	0.512672±9
24111	0.703821±20	0.512768±36
24118	0.704138±26	0.512630±6
24127	0.704086±104	0.512623±6
PYROCLASTIC SEQUENCE HAWAIIITE		
24006	0.703650±69	0.512890±24
OLD SERIES HAWAIIITES		
24034	0.703779±23	0.512762±13
24090	0.706367±16	0.512867±19
24122	0.703622±25	0.512847±21
NEW SERIES HUGFARITES		
24019	0.704911±22	0.512396±20
24026	0.704311±10	0.512438±13
24090	0.704333±40	0.512366±19
24109	0.703831±35	0.512762±17

24123 0.703876₊₂₆ 0.512695₊₁₂

OLD SERIES MUGEARITES

24041 0.703770₊₇₃ 0.512814₊₉

24061 0.703730₊₂₁ 0.512853₊₁₆

NEW SERIES TRACHYTES

24016 0.704553₊₁₈ 0.512473₊₆

24017 0.705245₊₂₂ 0.512338₊₁₁

24020 nd 0.512376₊₁₆

24025 0.707426₊₂₃ 0.512410₊₁₂

24031 0.704610₊₃₂ 0.512433₊₁₀

24081 0.706675₊₁₀₀ 0.512305₊₆

24087 0.705852₊₁₆ 0.512091₊₁₂

24113 0.704209₊₂₄ 0.512620₊₁₀

OLD SERIES TRACHYTES

24030 0.712050₊₇₇ 0.512408₊₁₄

24042 nd 0.512130₊₅

24043 0.706729₊₂₃ 0.512512₊₂₄

24046 0.717242₊₈₃ 0.512225₊₁₅

24054 0.705944₊₈₆ 0.512778₊₈

24059 nd 0.512423₊₈

24073 0.706994₊₂₅ 0.512789₊₁₁

24098 0.719635₊₁₉ 0.512295₊₂₀

24125 nd 0.512745₊₈

24130 0.706922₊₁₉ 0.512601₊₁₃

NEW SERIES PHONOLITE

24089 0.704720₊₇₅ 0.512381₊₉

PYROCLASTIC SEQUENCE PHONOLITES

24002 0.704693₊₇₀ 0.512802₊₈

24013 0.704636₊₂₃ 0.512768₊₇

24015 0.708161₊₇₀ 0.512632₊₉

24114 0.706278₊₂₄ 0.512852₊₁₇

24119 0.708786₊₁₆ 0.512828₊₁₂

OLD SERIES PHONOLITES

24097 0.706421₊₇₀ 0.512754₊₇

24124 0.704050₊₄₄ 0.512612₊₆

BASEMENT SAMPLES

24037 0.708630₊₃₁ 0.511368₊₃₀

24135 0.730630₊₃₀ 0.510747₊₁₀

24137 0.709028₊₂₀ 0.511270₊₁₂

24036 0.764478₊₂₂ 0.511398₊₄₄

24134 0.752392₊₆₃ 0.511647₊₁₅

24139 0.727068₊₄₂ 0.512052₊₁₆

24138 0.855156₊₁₄ 0.511628₊₈

nd = not determined

APPENDIX E - Isotope Dilution

REE Analysis

Firstly, the Teflon bombs were thoroughly cleaned as for the previous techniques. About 100mg of sample was accurately weighed into the clean dry bombs to which LREE and HREE spike of known weight were also added. The mixture was then digested overnight in 2ml of conc. HNO₃ and 6ml of 40% HF. After evaporation these reagents were added again in the same amounts. The bombs were then loaded into pressure jackets and left for 2 days in an oven at 190 degrees C. This process ensured the complete digestion and equilibration of the sample with the spikes. The solution in the bomb was then evaporated. 2ml of conc. HNO₃ was added and evaporated following which 15ml of 6M HCl was added and evaporated. The treatment with HNO₃ and HCl was repeated until finally conc. HNO₃ was added and evaporated to incipient dryness. The REE's were then taken up in 5ml of 75% 8M CH₃COOH + 25% 5M HNO₃ and left overnight to dissolve. The sample was then run through two sets of columns which correspond to sets 1 and 3 in the Nd separation process. The REE's were loaded onto triple filaments in the same way as Nd.

REE's were measured automatically on the 54E using a method and program written by Dr. M Thirlwall at Leeds (cf Thirlwall, 1982).

The concentrations of REE's are presented in Table E1 for the analysed samples.

TABLE E1... RARE EARTH ELEMENT ANALYSIS

	Basement 24037	24135	24137	24036	24134	24139
La	61.83	46.90	48.35	20.20	4.20	43.38
Ce	95.79	72.60	75.98	36.44	8.07	67.08
Nd	34.19	29.52	29.54	18.50	4.96	21.38
Sm	4.47	4.27	4.43	5.63	1.94	3.66
Eu	1.27	1.07	1.31	0.65	0.42	0.59
Gd	2.46	3.01	2.82	6.05	2.64	2.69
Dy	1.27	1.73	1.49	9.14	3.34	2.10
Er	0.52	0.73	0.64	5.36	1.81	1.09
Yb	0.41	0.57	0.54	5.36	1.62	1.00
(La/Yb) _N	100.8	55.02	59.87	2.52	1.734	29.01
(Ce/Yb) _N	59.42	33.23	37.67	1.729	1.267	17.06
Sm/Nd	0.1307	0.1446	0.148	0.3076	0.3911	0.1712
Eu/Eu*	1.177	0.9175	1.139	0.3406	0.5705	0.578
Gd/Gd*	0.6204	0.7396	0.6782	0.6842	1.154	0.5191
REE(T)	204	163	172	113	31	146

Basalts									
	24021	24029	24063	24083	24086	24088	24293	24105	24121
La	27.56	32.33	24.21	0	27.85	23.45	0	22.26	24.42
Ce	57.66	66.13	50.04	63.97	57.14	48.80	53.31	46.90	49.31
Nd	30.61	32.70	26.10	33.31	29.82	26.43	26.60	25.55	26.29
Sm	6.26	6.46	5.37	6.71	6.36	5.56	5.89	5.57	5.69
Eu	2.36	2.17	1.69	2.36	2.28	1.97	2.10	1.96	1.96
Gd	0	5.90	4.87	6.13	6.04	5.20	5.36	5.27	5.43
Dy	0	4.66	3.68	5.22	4.18	3.83	3.99	4.08	0
Er	0	2.37	1.69	2.50	1.96	1.79	1.83	1.69	2.07
Yb	1.46	2.00	1.28	1.99	1.51	1.35	1.39	1.46	1.57
(La/Yb) _N	12.62	10.81	12.65	0	12.33	11.62	0	10.2	10.4
(Ce/Yb) _N	10.04	8.41	9.943	8.217	9.624	9.194	9.754	8.17	7.988
Sm/Nd	0.2032	0.1976	0.2057	0.2014	0.2133	0.2104	0.2059	0.218	0.2164
Eu/Eu*	0	1.081	1.136	1.131	1.131	1.126	1.149	1.112	1.084
Gd/Gd*	0	0.8109	0.9616	0.8609	1.028	1.013	0.9842	1.007	0.9754
REE (T)	127	159	122	126	141	122	106	118	120

Hawaiites									
	24006	24034	24049	24062	24090	24099	24101	24111	24118
La	28.00	0	39.47	37.34	58.15	42.36	23.40	45.12	45.93
Ce	56.47	62.50	79.27	75.62	115.60	85.42	47.94	93.10	91.53
Nd	29.56	39.79	38.66	38.26	51.59	42.10	23.87	46.86	45.88
Sm	6.34	7.40	7.47	7.49	9.32	7.73	4.63	8.85	8.61
Eu	2.22	2.56	2.49	2.62	2.94	2.77	1.63	3.56	3.06
Gd	0	6.35	6.68	6.77	7.92	6.48	4.16	7.76	7.57
Dy	0	4.78	5.30	5.09	7.22	4.53	2.73	5.87	0
Er	0	2.32	2.56	2.45	3.07	2.06	1.34	2.77	0
Yb	1.77	1.89	2.07	1.94	2.62	1.58	1.10	2.15	2.04
(La/Yb) _N	10.58	0	12.75	12.87	14.84	17.93	14.22	14.03	15.06
(Ce/Yb) _N	8.114	11.1	9.74	9.914	11.22	13.75	11.08	11.01	11.41
Sm/Nd	0.2145	0.186	0.1932	0.1958	0.1807	0.1836	0.154	0.1889	0.1877
Eu/Eu*	0	1.143	1.084	1.131	1.052	1.203	1.142	1.321	1.165
Gd/Gd*	0	0.8038	0.8242	0.8834	0.7193	0.8816	0.9054	0.8669	0.8756
REE (T)	125	152	189	182	264	199	114	221	210

Mugearites					
	24019	24040	24104	24109	24123
La	70.89	0	34.66	45.48	49.53
Ce	132.18	98.88	70.74	86.76	96.45
Nd	60.57	47.71	35.13	40.24	46.48
Sm	10.45	8.65	6.94	7.33	8.37
Eu	3.66	3.09	2.36	2.78	3.14
Gd	8.65	7.31	6.27	6.27	7.09
Dy	6.74	5.30	5.56	4.40	0
Er	3.42	2.57	2.79	2.15	2.00
Yb	3.02	2.10	2.31	1.78	1.97
(La/Yb) _N	15.69	0	10.03	17.09	16.81
(Ce/Yb) _N	11.13	11.98	7.789	12.4	12.45
Sm/Nd	0.1725	0.1813	0.1976	0.1822	0.1801
Eu/Eu*	1.183	1.195	1.1	1.261	1.253
GJ/Gd*	0.6843	0.8018	0.7752	0.7975	0.813
REE(T)	305	180	171	201	220

Trachytes								
	24016	24020	24030	24054	24075	24081	24087	24130
La	69.73	104.37	208.02	111.92	63.91	76.19	96.84	91.45
Ce	117.32	186.20	244.02	193.49	120.78	139.80	159.04	156.15
Nd	45.63	67.33	137.56	64.47	45.77	54.00	65.72	47.48
Sm	7.66	11.26	22.57	9.61	7.88	9.30	10.90	7.03
Eu	1.36	1.03	2.25	1.16	1.17	1.93	2.91	1.01
Gd	5.08	9.59	17.85	6.72	6.29	7.65	8.96	6.75
Cy	10.44	8.57	13.32	6.07	5.27	6.92	0	0
Er	3.99	5.27	8.57	3.42	2.64	3.90	4.01	3.26
Yb	3.52	5.34	7.51	3.37	2.42	3.73	3.64	3.75
(La/Yb) _N	13.25	13.07	18.52	22.21	17.66	13.66	18.16	16.31
(Ce/Yb) _N	8.477	8.868	8.264	14.6	12.69	9.532	11.11	10.59
Sm/Nd	0.1679	0.1672	0.1641	0.1491	0.1722	0.1722	0.1659	0.1461
Eu/Eu*	0.6702	0.3047	0.3446	0.4437	0.5109	0.7034	0.9042	0.4507
Gd/Gd*	0.3751	0.4807	0.659	0.4159	0.5815	0.5295	0.5899	0.4409
REE (T)	270	408	660	407	262	310	361	323

	Phonolites				
	24002	24015	24097	24114	24124
La	32.35	129.21	95.42	95.30	110.93
Ce	148.57	248.32	184.51	156.35	148.36
Nd	53.03	90.35	66.03	55.93	61.31
Sm	8.91	16.13	12.03	9.78	9.70
Eu	2.17	2.01	1.60	2.02	1.48
Gd	7.23	19.01	10.30	0	7.79
Dy	7.13	0	10.37	0	7.41
Er	4.26	0	6.15	0	4.53
Yb	4.21	0	5.56	4.94	4.57
(La/Yb) _N	13.02	0	11.15	11.55	16.23
(Ce/Yb) _N	8.975	0	7.874	8.075	8.257
Sm/Nd	0.163	0.1785	0.1763	0.1747	0.1592
Eu/Eu*	0.8311	0.3529	0.4419	0	0.5237
Gd/Gd*	0.4569	0	0.4909	0	0.4723
RCE(T)	324	521	408	318	363

TABLE E2... CHONDRITE NORMALISING VALUES OF NAKAMURA, 1974

La	-	0.329
Ce	-	0.865
Nd	-	0.630
Sm	-	0.203
Eu	-	0.077
Gd	-	0.276
Dy	-	0.343
Er	-	0.225
Yb	-	0.220

TABLE E3... MANTLE NORMALISING VALUES OF THOMPSON (1982) & WOOD (1979)

	THOMPSON	WOOD
Ba	6.9	7.56
Rb	0.35	0.86
Th	0.042	0.096
K	120	252
Nb	0.35	0.62
La	0.328	0.71
Ce	0.865	1.9
Sr	11.8	23
Nd	0.63	1.29
P	46	90.4
Sm	0.203	0.385 all values in ppm
Zr	6.84	11
Ti	620	1527
Y	2	4.87
Yb	0.22	-

The sources for Thompson's 'mantle' normalising values are Nakamura (1974), DeLaeter and Hoesie (1978), Mason (1979), Shima (1979) and Sun (1980).

Rb and Sr I.D. Analysis

The chemistry used to isolate Rb is similar to that for Sr. A Rb spike is accurately weighed into a beaker with the sample. The column procedure is the same as for Sr except that collection occurred after 25ml elution of 2.5M HCl. Rb was analysed on Ta single filaments at 2kG and 8.0 kV on the MM30. I.D. work for Sr follows the same procedure as for unspiked Sr except again both an accurately weighed Sr spike and sample are weighed into the beaker. Figs. C1a-e are graphs which compare I.D. data with X.R.F. data for La, Ce, Nd, Rb and Sr. Rb and Sr I.D. data are presented in Table E4.

TABLE E4... Rb and Sr I.D. DATA

Rock	Rb(ppm)	Rock	Sr(ppm)
24015	160.8	24015	28.65
24020	130.6	24054	43.63
24054	143.9	24097	32.02
24075	103.0	24130	55.02
24097	130.5	24134	101.7
24098	192.6	24135	339.3
24114	115.1	24137	802.5
24130	115.3	24139	223.5
24139	190.7		

APPENDIX F - K-Ar Dating

The samples dated were primarily for the purposes of correcting Sr isotope data for the decay of Rb. The samples were prepared in the following way. Excess chips from the powder preparation method were crushed by the percussion mortar until a size fraction of $-60+90$ was obtained. It was necessary to be as coarse as this so that the vacuum under which the analyses were measured was not impaired. The argon analyses were performed by Mr D.C. Rex by a method detailed in Briden et al. (1979). The results are presented in Table 3.2.

APPENDIX G Age Corrections to $^{87}\text{Sr}/^{86}\text{Sr}$

Because of the long half life of ^{147}Sm and the low Sm/Nd of all the samples no age correction was necessary for $^{143}\text{Nd}/^{144}\text{Nd}$ results. The effect for rocks of 12 ma was only <1 in the sixth place. For basic rocks with low Rb/Sr and younger than 3 ma the effect was <1 in the fifth place. Old Series acidic rocks with high Rb/Sr have been corrected for the radioactive decay of Pb . Some rocks have been corrected to an age known from K-Ar dating. Other rocks have been corrected to an age based on field evidence correlated with rocks of known age. This approximation was considered adequate for the purposes of petrogenetic modelling. Initial and present day $^{87}\text{Sr}/^{86}\text{Sr}$ values are given in Table C2; initial $^{87}\text{Sr}/^{86}\text{Sr}$ values were given in Table G1.

TABLE G1... $^{87}\text{Sr}/^{86}\text{Sr}$ RATIOS CORRECTED FOR DECAY OF Rb

	AGE(ma)	Rb/Sr	$^{87}\text{Rb}/^{86}\text{Sr}$	$^{87}\text{Sr}/^{86}\text{Sr}$	$^{87}\text{Sr}/^{86}\text{Sr}(\text{initial})$
PYROCLASTIC SEQUENCE PHONOLITES					
24002	3.0	0.931	2.866	0.704692	0.7046
24013	2.50*	0.441	1.275	0.704686	0.7046
24015	4.35*	5.631	16.24	0.708161	0.7072
24114	3.00*	23.02	66.59	0.706278	0.7034
24119	3.0	11.33	32.79	0.708786	0.7074
OLD SERIES PHONOLITES					
24097	10.3*	4.076	11.79	0.706421	0.7047
24124	10	0.6517	1.885	0.704050	0.7038
OLD SERIES 'LARGELY UNCONTAMINATED' TRACHYTES					
24054	10	3.105	8.992	0.705944	0.7047
24073	10	3.054	8.835	0.706994	0.7057
OLD SERIES 'CONTAMINATED' TRACHYTES					
24030	10	13.31	38.48	0.712050	0.7066
24043	10	3	8.678	0.706729	0.7055
24046	10	19.11	55.34	0.717242	0.7094
24075	10	2.452	7.093	0.705911	0.7049
24098	10	24.08	69.73	0.719635	0.7093
24130	11.6*	5.004	14.48	0.706922	0.7045

* represents a K-Ar age data,

Only rocks with relatively high Rb/Sr ratios have corrected for decay of Rb. Corrections to basic rocks are insignificant to four decimal places. The $^{87}\text{Sr}/^{86}\text{Sr}$ ratios are only corrected to four decimal places because of the uncertainty in Rb and Sr concentrations, which were mostly measured by X.R.F. analysis, and the uncertainty in the estimated ages. K-Ar dates are available for a few samples but for the majority an estimate of the age based on comparable samples of known age was used. Also where available Rb and Sr I.D. data have been used in the correction.

APPENDIX H - Thin-Section Description

The following Table compiles the essential details of the petrography of individual sections. The Phenocryst Mode, is a rough visual estimation of the modal proportions of the phenocrysts present. Content indicates a rough ratio of phenocrysts to groundmass. The groundmass tends to be less variable than the phenocrysts and largely conforms to details given in the main text and is not described.

Abbreviations - px=clinopyroxene, pg=plagioclase, ol=olivine, mt=titanomagnetite, kf=anorthoclase, bi=biotite, ae=aeenigmatite, ka=kaersutite. ne=nepheline, meg=megacryst, ig. lam=igneous lamination (i.e. preferred orientation usually in feldspars), c.g.=coarse grained groundmass.

TABLE H1... THIN-SECTION DESCRIPTION

No	DESCRIPTION	PHENOCRYST MODE						CONTENT	REMARKS
		ol	pl	px	kf	mt	?		
24001	Basalt	25	30	45	--	--	--	25:75 Zoning, Ig. Lam.	
24002	Phonolite	--	--	--	95	mt	bf	30:70 Some kf crystals partly resorbed	
24005	Basalt	33	--	65	--	mt	--	15:85 Some meg px, badly altered	
24006	Hawaiite	20	60	18	--	mt	--	27:75 Clear and resorbed pg	
24008	Ignimbrite	--	--	--	100	--	--	5:95 Some good flame	
24009	Ignimbrite	--	--	--	95	--	bf	15:35 Contains trachyte fragments	
24010	Basalt	20	75	5	--	--	--	5:35 Badly altered	
24012	Ignimbrite	--	--	--	95	--	bf	5:95 Haematite rimmed vesicles - altered	
24013	Phonolite	--	--	3	95	--	bf	20:30 Ig. Lam. rounded kf phen's	
24014	Basalt	25	70	5	--	--	--	25:75 Macrophyric, badly altered	
24015	Phonolite	neph=100	--	--	--	--	ae	15:85 Late stage aenigmatite	
24016	Trachyte	--	--	4	95	mt	bf	20:30 Macrophyric	
24017	Trachyte	Anorthoclase phyric glass							
24019	Fuogearite	--	--	--	--	--	--	0:100 Felsic matrix, Ig. Lam.	
24020	Trachyte	--	--	4	95	1	--	35:65 Ig. Lam. macrophyric	
24021	Basalt	5	70	20	--	--	--	20:80 Zoning, some ol altered	
24022	Basalt	50	35	15	--	--	--	30:70 Px zoned, sub-ophitic texture	
24025	Trachyte	--	--	--	97	mt	--	3:92 C.g. matrix	
24026	Fuogearite	--	50	50	--	--	Ne	5:95	
24029	Basalt	15	--	95	--	--	--	7:93 Macrophyric, some ol altered	
24030	Trachyte	--	--	--	100	--	--	3:97	
24031	Trachyte	5	--	4	95	mt	--	40:60 Plaj cores with kf rims	
24034	Basalt	20	60	20	--	--	--	10:90 Ig. Lam.	
24040	Fuogearite	17	65	13	--	mt	--	35:65 Macrophyric, ka & ap present	
24041	Fuogearite	5	95	--	--	--	--	5:35 Ig. Lam.	
24044	Hawaiite	20	30	50	--	--	--	20:90 Ig. Lam., zoning	
24045	Basalt	60	15	35	--	--	--	10:90 Macrophyric, much resorption	
24046	Rhyolite	--	--	--	100	--	--	5:95 Trachytic texture	
24049	Basalt	85	--	15	--	--	--	10:90 Ig. Lam., elongate pg	
24052	Trachyte	--	--	--	--	--	--	0:100	
24054	Trachyte	--	--	--	100	--	--	10:90	
24053	Basalt	3	2	95	--	--	--	10:90	
24057	Trachyte	--	--	--	95	mt	--	20:80 Macrophyric, Ig. Lam.	
25061	Fuogearite	--	40	--	--	--	ka	20:90 Cumulate ka?	
24062	Basalt	20	60	20	--	--	--	5:95	
24063	Basalt	30	2	60	--	mt	--	25:75 Macrophyric	
24067	Basalt	60	--	40	--	--	--	15:95 Vesicular	
24070	Basalt	30	20	50	--	--	--	10:90 Macrophyric, ragged ol's	
24071	Trachyte	30	--	--	--	mt	--	10:90 Ig. Lam.	
24072	Basalt	10	20	70	--	--	--	10:90 Vesicular	
24073	Trachyte	--	--	--	--	--	--	0:100 C.g.	
24075	Trachyte	--	--	--	95	mt	--	15:85 Microphyric	
24078	Ignimbrite	5	--	--	90	mt	bf	10:90 Contains trachyte/phonolite clasts	
24079	Basalt	--	--	100	--	--	--	5:95 Microphyric, vesicular	
24080	Basalt	30	2	3	--	--	--	35:65 Meg px	
24081	Trachyte	5	30	5	--	--	--	30:70 Macrophyric, some phen's resorbed	
24082	Basalt	20	10	70	--	--	--	20:30 Zoning, c.g., vesicular	
24083	Basalt	10	--	70	--	--	--	10:90 Sub-ophitic	
24084	Basalt	25	65	10	--	--	--	10:90 Some resorbed pg	
24086	Basalt	40	40	20	--	--	--	5:95	
24087	Trachyte	20	75	5	--	--	--	35:65 Macrophyric	
24089	Basalt	10	--	90	--	--	--	15:35	

No	DESCRIPTION Rock Type	PHENOCRYST MOD.						CONTENT	REMARKS
		ol	pg	px	kf	mt	?		
24089	Phonolite	--	--	--	--	--	--	0:100	
24090	Hawaiite	--	--	--	--	--	--	0:100	
24091	Basalt	10	--	??	--	--	--	10:90	Orange rinds to cl's
24093	Basalt	35	--	65	--	--	--	20:80	Macrophyric
24094	Basalt	--	3	97	--	--	--	5:95	Ig. Lam.
24097	Phonolite	3	--	--	96	--	bl	10:97	Macrophyric
24099	Basalt	20	5	75	--	--	--	5:95	Meg px
24101	Basalt	--	75	25	--	--	--	5:95	Sub-ophitic
24103	Igneimbrite	--	--	--	100	--	--	10:90	
24104	Basalt	13	75	5	--	mt	--	25:75	Resorbed pg and px
24105	Basalt	--	--	100	--	--	--	15:95	
24109	Mugearite	20	75	5	--	--	--	15:85	
24110	Igneimbrite	--	--	--	100	--	--	5:95	Contains trachyte/phonolite clasts
24111	Hawaiite	10	10	80	--	--	--	5:95	Microphyric
24112	Hawaiite	10	80	10	--	--	--	20:80	Pg resorbed
24113	Phonolite	5	--	--	95	--	--	25:75	Px light green
24114	Phonolite	--	--	--	97	mt	--	25:75	Rounded kf
24115	Phonolite	--	--	--	100	--	bl	10:90	
24119	Hawaiite	5	85	10	--	--	--	25:75	Macrophyric
24120	Basalt	5	--	95	--	--	--	10:90	Ig. Lam.
24121	Basalt	--	--	--	100	--	--	10:90	
24122	Basalt	65	25	10	--	--	--	15:95	
24123	Mugearite	5	80	15	--	--	--	15:95	Ig. Lam.
24124	Phonolite	50	--	--	50	--	--	5:95	
24127	Hawaiite	7	90	3	--	--	--	25:75	Macrophyric, meg cpx
24130	Trachyte	--	--	--	100	--	--	5:95	
24131	Basalt	35	30	35	--	--	--	10:90	Orange rinds to some ol's
24133	Basalt	35	30	35	--	--	--	20:90	Macrophyric
24136	Basalt	20	70	10	--	--	--	15:85	Microphyric

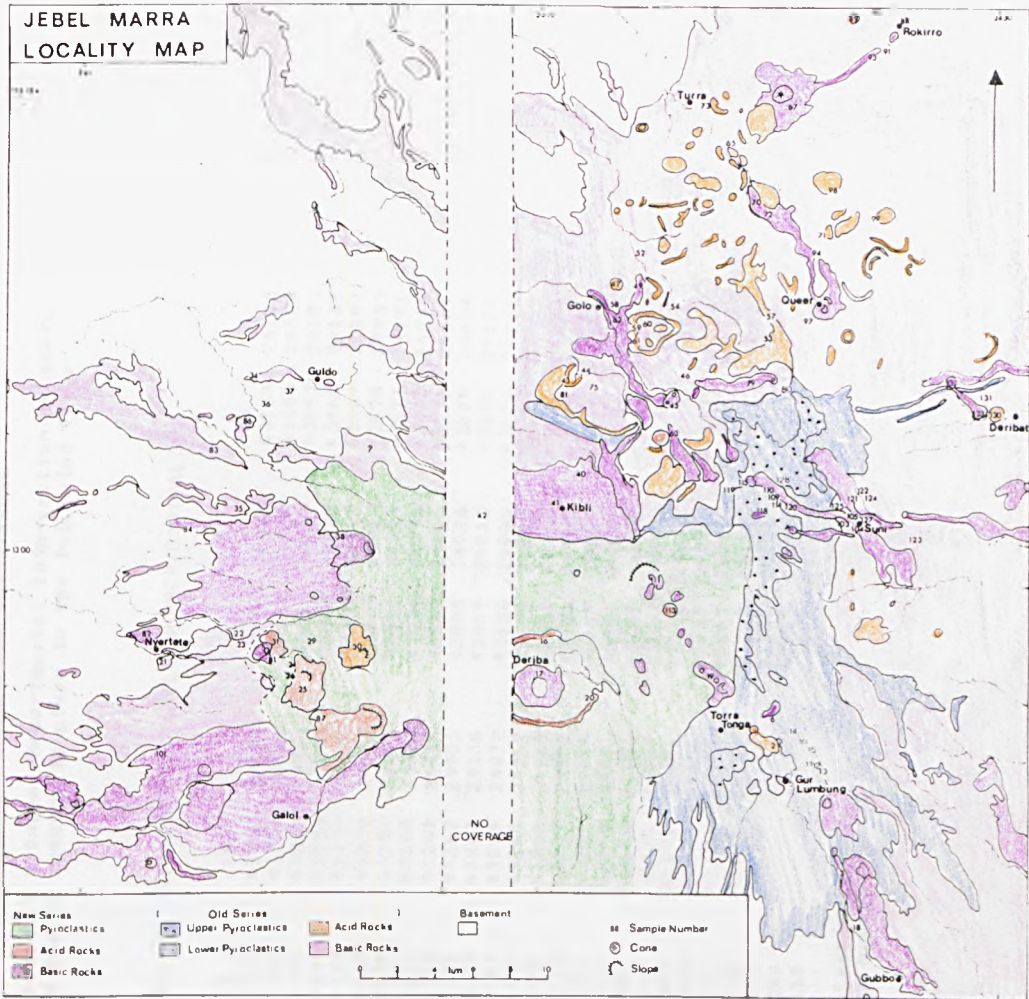


Fig. 11 Sample-locality map.

APPENDIX J Thin-Section = Sample No. Equivalence

The equivalence between departmental thin-section numbers and field sample numbers is given in the following Table.

TABLE J1 THIN-SECTION/SAMPLE NUMBER EQUIVALENCE

TS	S	TS	S	TS	S	TS	S
43227	24013	43253	24057	43839	24009	43865	24126
43229	24012	43254	24073	43840	24031	43866	24094
43229	24015	43255	24121	43841	24009	43867	24103
43230	24134	43256	24075	43842	24225	43868	24131
43231	24135	43257	24029	43843	24020	43869	24097
43232	24117	43258	24058	43844	24014	43870	24133
43233	24030	43259	24099	43845	24019	43871	24191
43234	24113	43260	24124	43846	24028	43872	24045
43235	24010	43261	24119	43847	24005	43873	24131
43236	24127	43262	24081	43848	24026	43874	24094
43237	24109	43263	24138	43849	24036	43875	24120
43238	24111	43264	24072	43850	24065	43876	24092
43239	24101	43265	24062	43851	24022	43877	24059
43240	24104	43266	24080	43852	24061	43878	24123
43241	24130	43267	24022	43853	24086	43879	24001
43242	24041	43268	24016	43854	24067	43880	24136
43243	24044	43269	24037	43855	24063	43881	24122
43244	24021	43270	24002	43856	24072	43882	24074
43245	24087	43271	24089	43857	24084	43883	24093
43246	24054	43272	24006	43858	24070	43884	24090
43247	24040	43273	24108	43859	24078	43885	24110
43248	24137	43274	24139	43860	24071	43886	24111
43249	24105	43275	24108	43861	24112	43887	24083
43250	24052	43276	24115	43862	24091	43888	24088
43251	24046			43863	24049		
43252	24114			43864	24106		

TS = Thin-Section Number
S = Sample Number

APPENDIX K COMPUTER PROGRAMS USED IN THIS THESIS

The following programs have been used in the production of Tables and diagrams in this thesis.

Written by R Powell

COR ALGOL68: Calculates correlation coefficients and plot variation diagrams for geochemical data sets.

REC ALGOL68: Recalculates mineral analyses.

PAFC ALGOL68: Calculates and plots AFC curves.

CMM ALGOL68: Draws simple mixing curves and contours contaminant region in terms of R.

LSQPM ALGOL68: Weighted least-squares approach to calculating proportions of phases fractionating.

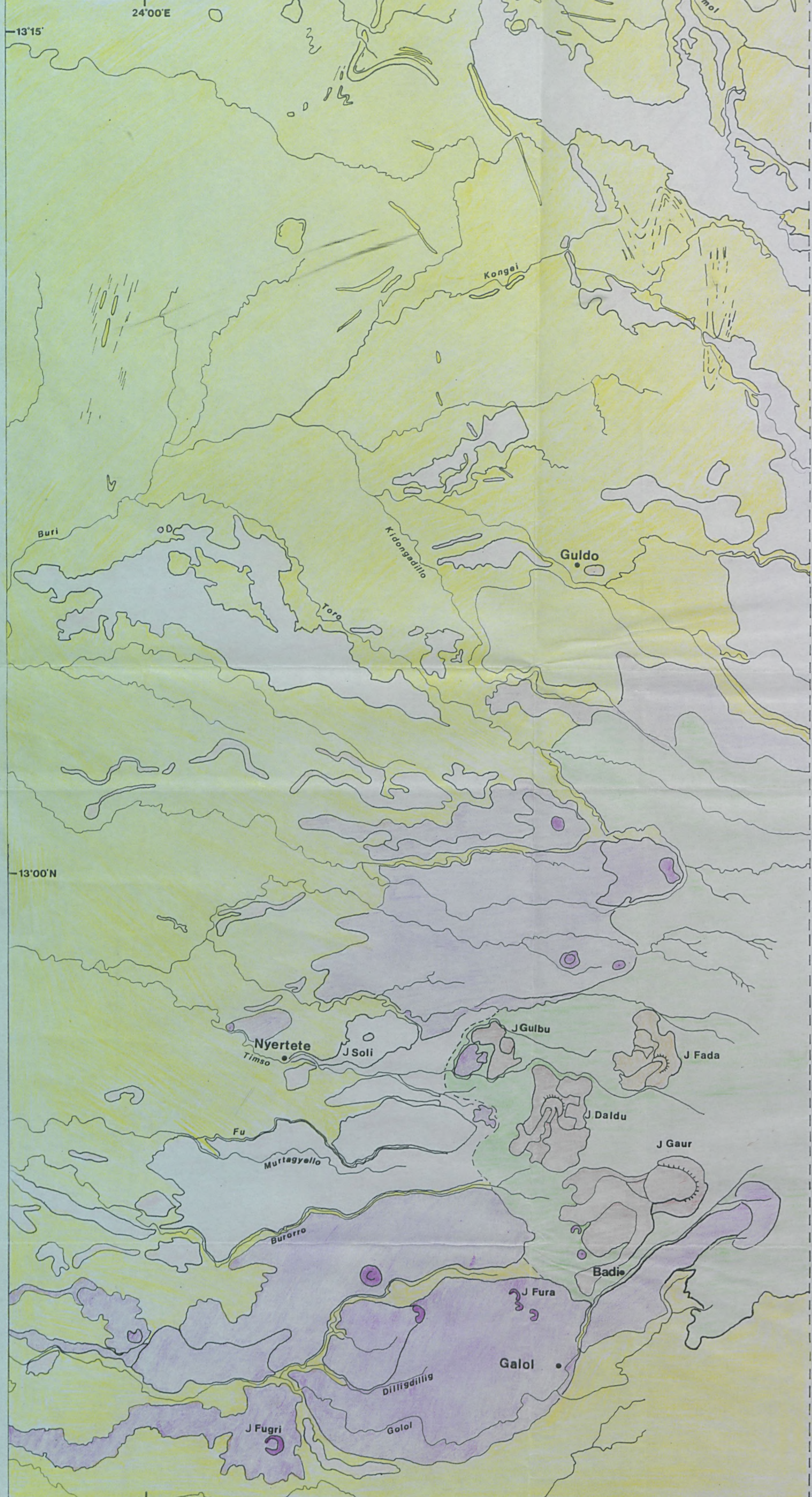
Written by I Luff

PETROMIX ALGOL68: Ordinary least-squares approach to calculating proportions of phase fractionating.

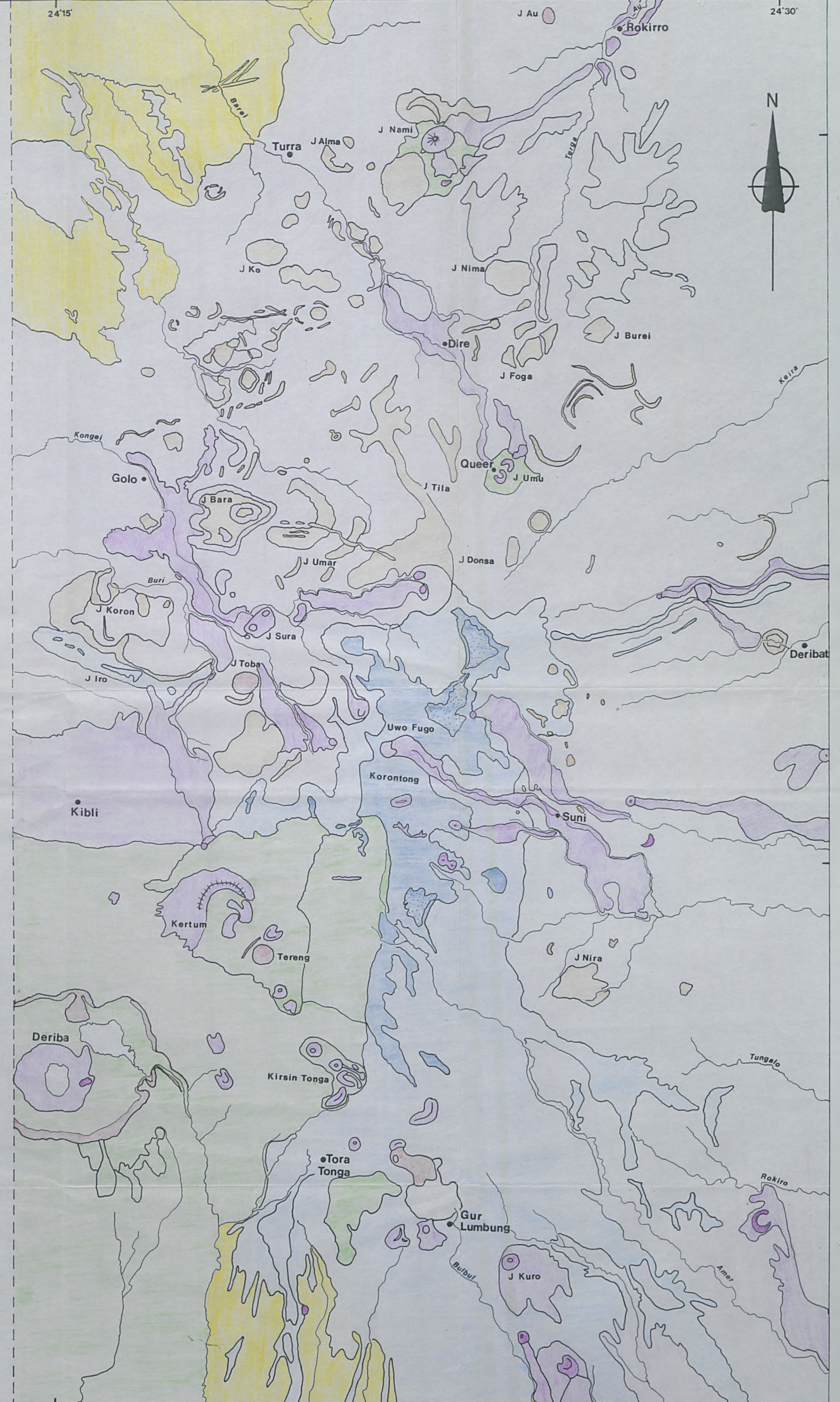
Written by M.F Thirlwall

L5REERAT: Plots chondrite-normalised graphs.

JEBEL MARRA SUDAN



Aerial photographs unavailable



KEY

<p>New Series</p> <ul style="list-style-type: none"> Pyroclastics – mainly airfall deposits Trachyte flows and domes –rare phonolites Basic flows 	<p>Old Series</p> <ul style="list-style-type: none"> Trachyte intrusions or flows Basic flows 	<p>Basement</p> <ul style="list-style-type: none"> Granitic gneisses with some amphibolites Bedding in basement rocks 	<p>Symbols</p> <ul style="list-style-type: none"> Formational boundary Cinder cone Villages Slope indication on volcano Drainage Lake
--	--	---	--

Scale = 1:70 000